Age and the microbiota-gut-brain axis: a non-human primate model of human ageing

Catherine Elin Purse

Submitted for the degree of Doctor of Philosophy

University of East Anglia

Quadram Institute

September 2024

Abstract

Age-associated changes to the intestinal microbiome, and its impact on the gut-brain axis, are increasingly being linked to the development of inflammageing and neurodegenerative disease. To study the interactions of the microbiota-gut-brain axis, it is important to find a suitable animal model for studies of human ageing. Here, the impact of ageing on the microbiota-gut-brain axis is assessed in a cohort of healthy, captive-bred cynomolgus macaques of differing ages. Using whole-genome sequencing (WGS) and internal transcribed spacer 1 (ITS1) amplicon sequencing methods, age-associated changes in taxonomic composition and metabolic potential were assessed in multiple spatial regions of the intestine, from duodenum to distal colon. Alpha and beta diversity metrics revealed distinct prokaryotic composition profiles in the small and large intestine, but relative invariance of taxonomy and metabolic potential was observed with age. 108 putative novel prokaryotic genomes were also identified. The predominant fungus in all regions and at all ages was *Arxiozyma pintolopesii*. Closely related *Arxiozyma* species have been implicated as potential intestinal pathobionts, however, *A. pintolopesii* did not appear to exhibit pathogenicity in an *in vitro* model of the intestinal epithelial barrier. Parallel work in germ-free mice showed that orally delivered *Candida albicans*, a human pathobiont, can translocate from the gut to the brain, inducing an inflammatory response. Accumulation of age-associated brain pathology, including iron deposition in the substantia nigra, was observed in cynomolgus macaques ≥13 years. However, this did not correlate with increased microglial cell density, as assessed by ionized calcium binding adaptor molecule 1 (Iba1) expression compared to young animals. Indications of an age-associated increase in systemic inflammation and intestinal permeability were studied via the quantification of blood-based biomarkers and histological examination of intestinal tissue. This work establishes a foundation for further study of the impact of ageing on the microbiota-gut-brain axis in this important animal model.

Table of Contents

List of Figures

List of Tables

List of Appendices

Abbreviations

AD	Alzheimer's Disease
AEBSF	4-(2-aminoethyl)benzenesulfonyl fluoride hydrochloride
ANOVA	Analysis of variance
APC	Antigen presentation molecules
ASV	Amplicon sequence variant
BBB	Blood brain barrier
BH	Benjamini-Hochberg
BLAST	Basic local alignment search tool
BMEC	Brain microvascular endothelial cells
CA	Cornu ammonis
CD	Cluster of differentiation
CFU	Colony forming unit
CI	Confidence interval
CNS	Central nervous system
CoPM	Copies per million
COVID-19	Coronavirus disease 2019
CPM	Copies per million
CRP	C-reactive protein
DAB	3,3'-diaminobenzidine
DC	Dendritic cell
DG	Dentate gyrus
DNA	Deoxyribonucleic acid
DSS	Dextran Sulphate Sodium
EDTA	Ethylene diamine tetra-acetic acid
FABP2	Fatty acid binding protein 2
FITC	Fluorescein isothiocyanate
FMT	Faecal microbial transplant
FTH	Ferritin heavy chain
FTL	Ferritin light chain
GF	Germ-free
GTDB	Genome taxonomy database
GTDB-Tk	Genome taxonomy database toolkit
H&E	Haemosiderin and eosin
H_2O_2	Hydrogen peroxide
I-FABP	Intestinal fatty acid binding protein

Iba1	Ionized calcium binding adaptor molecule 1
IBD	Inflammatory bowel disease
IBS	Irritable bowel syndrome
IEC	Intestinal epithelial cell
Ig	Immunoglobulin
IL	Interleukin
ITS	Internal transcribed spacer
JAM	Junctional adhesion molecule
K3EDTA	Tripotassium ethylene diamine tetraacetic acid
LAL	Limulus Amebocyte Lysate
LBP	Lipopolysaccharide binding protein
LPS	Lipopolysaccharide
MAG	Metagenome assembled genome
MAMPs	Microbe associated molecular pattern molecules
MHC-II	Major histocompatibility complex class II
MRI	Magnetic resonance imaging
mRNA	Messenger RNA
NBF	Neutral buffered formalin
NCBI	National Center for Biotechnology Information
NCYC	National Collection of Yeast Cultures
NHP	Non-human primate
NMDS	Non-metric multidimensional scaling
NVU	Neurovascular unit
OD	Optical density
PBS	Phosphate-buffered saline
PD	Parkinson’s Disease
PERMANOVA	Permutational multivariate analysis of variance
PET	Polyethylene terephthalate
PET	Position electron tomography
PFA	Paraformaldehyde
PRR	Pattern recognition receptor
RNA	Ribonucleic acid
ROI	Regions of interest
rRNA	Ribosomal RNA
SASP	Senescence associated secretory phenotype
SCFA	Short chain fatty acid

SD	Standard deviation
SGB	Species-level genome bin
SN	Substantia nigra
SPF	Specific pathogen free
SRA	Sequence read archive
TBS	Tris-buffered saline
TBS-T	Tris-buffered saline with Tween® 20 Detergent
TEER	Transepithelial electrical resistance
TH	Tyrosine hydroxylase
TMAO	Trimethylamine-*N*-oxide
TNF	Tumour necrosis factor
UK	United Kingdom
UKHSA	UK Health Security Agency
USA	United States of America
VTA	Ventral tegmental area
WGS	Whole genomic sequencing
YM	Yeast malt
ZO	Zonula occludin

Acknowledgements

This thesis would not have been possible without the efforts and guidance of my supervisory team. Their expertise, thoroughness, and generosity made this thesis much better, but they shouldn't be held responsible for any of its failings. First and foremost, I am extremely grateful for the knowledge and counsel of my primary supervisor, Professor Simon Carding, during the last four years. His honest opinions, astute observations, and, perhaps, a love of Gantt charts made this work possible. I am also thankful to my secondary supervisor, Dr Simon Funnell, whose intelligent advice guided this thesis, and without whom this project would not have come to fruition. I am constantly in awe of his unwavering enthusiasm and dedication to his work. Finally, I am almost certain I could not have completed this project without Dr Aimée Parker and Dr Steve James. I will be forever grateful for their kindness, humour, intelligence, and belief in my abilities. It has been a privilege to know them.

Everyone in the Carding group has helped me in some way, big or small, during this project. To Dr Regis Stentz, Dr Ariadna Miquel Clopés, Dr Rik Haagmans, Dr Rokas Juodeikis, Anne Jordan, thank you. Thank you especially to Dr Emily Jones and Victoria White, for their work on cell culture experiments presented in this thesis. A special thanks to Dr Katherine Seton and Rosie Young for their friendship and moral support.

There are many at the Quadram Institute who have provided help or support during my PhD. I would especially like to thank Dr Andrea Telatin, Dr Sumeet Tiwari, Dr George Savva, Cath Booth, Dr James Lazenby, Dave Baker, Cara-Jane Moss, and Rhiannon Evans, for their help, support, and guidance. I am equally grateful to those at UKHSA who have supported this project: Dr Francisco Javier Salguero Bodes, Alison Bird, Chelsea Kennard, Laura Hunter, James Durham, Steve Lawrence, Mike Dennis, Dr Kevin Bewley, Dr Naomi Coombs, Conner Norris, Karen Gooch. They made this work possible.

Thank you to my friends in Norwich and elsewhere for their encouragement. To Lucy and Emily, for their unconditional love and support from afar.

To Joe, always. To Mum and Chris, always. To Dad, always.

Contribution Statement

Some of the work that appears in Chapter 5 is an adaptation of published work and appears with permission [3, 4].

The UK Health Security Agency (UKHSA) managed the colony of cynomolgus macaques, sample collection from these animals, and delivery of samples to the Quadram Institute.

Chapters 3 and 6 features collaborative work with the histology department at UKHSA. Alison Bird and Chelsea Kennard sectioned cynomolgus macaque intestinal tissue samples for histological staining and carried out H&E and PAS staining on these sections. Dr Francisco Javier Salguero Bodes carried out transection of cynomolgus macaque brains. Alison Bird and Chelsea Kennard prepared the brain tissue samples for histology and immuno-histochemistry (IHC) and carried out H&E staining on tissue sections from these samples.

Chapters 4 and 5 features collaborative work with researchers at the Quadram Institute. Dr Steve James, Dr Aimée Parker, and I extracted DNA from intestinal luminal content and faecal samples for WGS and ITS1 sequencing. David Baker, Rhiannon Evans, and Cara-Jane Moss performed library preparation for these samples. Dr Andrea Telatin analysed the ITS1 sequencing data for samples from both mice and cynomolgus macaques. He and Dr Steve James created the taxonomic profile data for the mouse mycobiome. Dr Emily Jones and Victoria White carried out the Transwell system assays, IHC staining of the Transwell system membranes, and analysis of the associated data. Administration of *Candida albicans* to mice, collection of murine samples, and quantification of *C. albicans* in vibratome brain sections were carried out by Dr Aimée Parker. Fungal cell culture, counts of colony-forming units, and fungal phenotypic analysis were carried out by Dr Steve James.

1.0. Chapter 1: Introduction

1.1. Introduction

The proportion of the global population aged 65 or over, defined as older adults by the United Nations, is expected to double by 2050. The number of elderly people, aged 80 or over, is projected to rise even faster, with the population estimated to triple in the same timeframe compared to numbers in 2021 [5]. This presents several societal and medical challenges due to a high prevalence of one or more age-associated chronic illnesses within these populations [6, 7]. Of particular concern is the increasing prevalence of neurodegenerative diseases with advancing age, disorders characterised by the progressive and irreversible degeneration of the central nervous system (CNS), which severely impacts quality of life [8]. No cure exists for these diseases, and their complex aetiology and pathogenesis impedes the development of new and effective treatments [9]. Recognition that the intestinal microbiome may play a role in neurodegenerative disease has, however, opened new avenues for research and potential therapy [10].

The human intestinal tract is colonised by a multitude of microorganisms including bacteria, viruses, fungi, and archaea, collectively called the microbiota [11]. These microorganisms produce a variety of microbial metabolites and other products which can have varied effects on the immune system. This includes modulation of both the innate and adaptive immune response, often resulting in systemic effects at sites distal to the intestine [12]. With age, the composition of the intestinal microbiota changes, altering the profile and production of microbial metabolites [13-22]. These changes correlate with age-associated declines in immune function, suggesting that the age-associated remodelling of the intestinal microbiota may contribute to this deterioration [23].

Inflammageing refers to the low-grade, chronic, systemic inflammation that develops with age in the absence of overt infection. It is a strong risk factor for frailty, defined as an increased risk for poor health outcomes resulting from age-associated functional decline that is often characterised by decreased muscle strength and fatigue, as well as morbidity and mortality in older adults [24-29]. The concept of inflammageing was originally described by Franceschi *et al.*, who proposed that the immune response is continually provoked by antigenic load and stress, eventually reaching a pro-inflammatory threshold with an increased risk of disease [30]. A significant source of this antigenic load was later proposed to be the intestinal microbiome, owing to the production of microbial antigens, metabolites, and other microbial products which may trigger an immunogenic response [31]. Age-related changes in the intestinal microbiome may also exacerbate the physiological stresses typically associated with ageing. These

stresses are driven by molecular, cellular, and systemic processes that are hallmarks of the ageing process [32].

The intestinal microbiota communicates with the CNS through complex bi-directional communication pathways, referred to as the microbiota-gut-brain axis. These include neural, endocrine, and immunological signalling pathways [10, 33]. Evidence from animal models suggests that the intestinal microbiota is able to influence aspects of disease pathogenesis in the CNS [34-38]. In humans, distinct intestinal microbial profiles are associated with neurodegenerative diseases such as Alzheimer's disease (AD) and Parkinson's disease (PD) [39-47]. While it is unclear whether these compositional profiles are causal, there is evidence to suggest that they may exacerbate symptoms and influence disease progression [10]. This raises the question of whether intestinal microbiome-based interventions or therapies may be used to alleviate the symptoms of ageing and age-associated disease.

Much of the characterisation and mechanistic investigation of ageing and the microbiota-gut-brain axis is based on small animal models, particularly rodents [48]. For studies of ageing, rodents have the benefit of a reduced lifespan in comparison to humans, but do not closely recapitulate the genetic profiles and physiology of humans and may not accurately model human responses [49]. In comparison, non-human primates (NHPs) have a much closer similarity to humans, especially regarding brain architecture and cognitive function [49, 50]. Due to this similarity, they represent an important animal model for human studies of ageing. In this chapter, I explore how ageing affects the microbiota-gut-brain axis and discuss the key mechanisms connecting inflammageing to age-related changes in the intestinal microbiome. When reviewing the intestinal microbiome, particular focus is given to studies on humans and macaques, Old World NHPs which are commonly used in biomedical research, emphasising the similarities between the species. The suitability of NHPs as models for humanageing is also explored. Additionally, the effect of age on intestinal fungi and their immunomodulatory capacity, which has been relatively understudied compared to their bacterial counterparts, is considered.

1.2. The intestinal microbiome

The symbiotic relationship between the host organism and the intestinal microbiota is reliant on the maintenance of several complex homeostatic interactions between the microbiota and the host immune system [12]. The composition of the intestinal microbiota can be influenced by a variety of factors, including diet, behaviour, medications, oral cavity health, and age-associated physiological decline [32, 51-54]. Intestinal dysbiosis, defined as an altered composition of the intestinal microbial community relative to the community found in healthy individuals, has now been recognised as a hallmark of ageing [32, 55]. Age-related alterations

to the intestinal microbiota may therefore disrupt the homeostatic interactions between the microbiota and the host, with implications for overall health.

1.2.1. Age-related influences on the intestinal microbiome

In infancy, the intestinal microbiota has a low level of microbial diversity compared to adults in both humans and NHPs [56, 57]. The human infant intestinal microbiota is dominated by the bacterial phyla Actinomycetota (formerly known as Actinobacteria) and Pseudomonadota (formerly known as Proteobacteria), with the former dominated by the genus *Bifidobacterium*. The progression of the human infant intestinal microbiota toward an adult-like microbial composition happens in the first 2-3 years of life, following weaning and consumption of solid foods [56, 58]. In NHPs, studies of the intestinal microbiota pre-weaning are scarce. However, one study of captive cynomolgus macaques shows that infants (aged 1-3 months) had an increased relative abundance of Actinomycetota and Bacteroidota (formerly known as Bacteroidetes), and a reduced abundance of Bacillota (formerly known as Firmicutes), compared to other age groups (aged >2 years). As in humans, *Bifidobacterium* were the dominant genera within the Actinomycetota phylum [57].

The adult intestinal microbiota in both humans and NHPs is primarily composed of bacteria from the Bacteroidota and Bacillota phyla [15, 57, 59-65]. Taxa from both phyla are key contributors to the production of short-chain fatty acids (SCFAs), including acetate, propionate, and butyrate, from the degradation of dietary fibre [66]. Alterations to the Firmicute:Bacteroidota ratio in the elderly may be relevant as SCFA production, particularly of butyrate, has been shown to have beneficial effects on intestinal health and immune function [67-69]. Some human studies have observed an altered Bacillota:Bacteroidota ratio with age in healthy subjects, although the direction of change is inconsistent across studies. In a Ukrainian population, an increased Bacillota:Bacteroidota ratio was associated with age, while in other populations the ratio was reduced in the elderly compared to adults [15, 63, 65]. This discrepancy may be a result of environmental and geographical influences on the intestinal microbiota. Conversely, a separate study of captive cynomolgus macaques found an increased Bacillota:Bacteroidota ratio in middle-aged and elderly animals compared to young adults, while no change was observed in captive rhesus, captive cynomolgus, or wild Assamese macaques [57, 59, 61, 64, 70].

Age-related changes to the intestinal microbiota are not uniform across individuals. This can be attributed to personal, environmental and behavioural factors, including diet, disease, social relationships, and medication [71-74]. For example, adherence to a Mediterranean diet, characterised by a high consumption of vegetables, fruits, fish, legumes, and nuts, is associated with retention of beneficial microbial taxa in older adults, including *Faecalibacterium*

prausnitzii, *Roseburia hominis,* and *Bacteroides thetaiotaomicron*. These taxa were positively associated with measures of improved cognitive function and negatively associated with measures of frailty and inflammation [75]. Antibiotic and non-antibiotic drugs have also been associated with changes to the intestinal microbiome, which can mediate indirect effects on the host. Metformin, for example, an anti-hyperglycaemic drug commonly used in the treatment of the age-associated disease type 2 diabetes mellitus, drives changes to the composition of the intestinal microbiota [76, 77]. It is thought that these compositional changes are responsible for reduced liver gluconeogenesis, previously supposed to be a direct action of metformin [76].

Age-associated factors affecting the intestinal microbiome may also impact the microbiome of the oral cavity [78]. Oral microbes, carried by saliva or food, can colonise the intestinal tract, meaning that oral cavity health has a direct influence on the intestinal microbiome [79, 80]. With age, increasing frailty is associated with reduced oral hygiene, resulting in an increased incidence of dental caries and periodontal diseases [81]. Microbial taxa associated with poor oral cavity health may also translocate to the intestinal tract. For example, dissemination of the periodontopathic bacterium *Porphyromonas gingivalis* to the intestinal tract disturbs the intestinal microbiota, induces intestinal and systemic inflammation, and increases intestinal barrier permeability in mice [82]. Oral administration of the bacterium to a mouse model of PD resulted in degeneration of dopaminergic neurons and microglial activation in the substantia nigra (SN), potentially linking intestinal colonisation by oral *P. gingivalis* to the pathogenesis of PD [83].

Separating the effect of age from the variety of factors which may affect intestinal microbiome composition in older adults a complex task, especially as many factors are interlinked. Geographical and residential location, and the associated differences in diet and other cultural factors, are known to effect intestinal microbiome composition, as does ethnicity [58, 84, 85]. The cross-sectional design of studies investigating the effect of age on the intestinal microbiome also often makes it difficult to determine whether changes to intestinal microbiota composition are a cause or effect of potentially modulatory factors [86].This is exemplified in a study of older adults and elderly people, where intestinal microbiome composition in adults in long-term residential care was distinct from those who were community-dwelling. Both residence and dietary pattern were found to be contributing factors to this discrepancy. Several markers of age-associated inflammation and poor health were also significantly correlated with changes in microbiome composition in those in long-term residential care, with blood C-reactive protein (CRP), interleukin (IL)-6, and tumour necrosis factor (TNF)-α significantly higher than in community dwellers [52]. The cross-sectional nature of the study, however, means it is

difficult to make conclusions on whether residence, and the associated differences in factors such as diet, may promote or prevent health deterioration in the elderly.

Despite considerable inter-individual variance, broad taxonomic and diversity changes to the intestinal microbiota are associated with both healthy and unhealthy ageing in humans. In unhealthy ageing, defined as ageing accompanied by age-associated declines in health, several species belonging to the *Clostridium* genus have been positively associated with multiple diseases and increased frailty with age. In healthy ageing, age-associated declines in health are delayed. In these individuals, genera including *Akkermansia*, *Odoribacter*, *Butyricimonas* are increased with age, while those such as *Roseburia*, *Prevotella*, and *Bifidobacterium* are decreased with age [13, 14]. Alpha diversity is a measure of species diversity within a defined community. Shannon diversity, an alpha diversity metric evaluating species richness (*i.e.* the number of species), has also been negatively associated with unhealthy ageing, while measures of uniqueness (an increase in rarer taxa in relation to abundant and/or highly prevalent taxa) are positively associated [14]. Increased uniqueness has been observed in adults from approximately 50 years of age, suggesting that age-associated changes to the intestinal microbiome may start in middle-age [87]. These changes have been positively associated with intestinal microbial metabolites which are associated with immune regulation, inflammation, and longevity, including toxins *p*-cresol sulfate and phenylacetylglutamine, which are linked to cardiac dysfunction in kidney disease patients and cardiovascular disease, respectively [14, 87-89].

Age related changes to the intestinal microbiota in macaques differ between studies (Table 1.1). Most previous studies of the effect of age on the intestinal microbiota in macaques have utilised 16S ribosomal RNA (rRNA) gene sequencing to assess bacterial taxonomy only [57, 59, 61, 64, 70, 90-92]. This contributes to differing taxonomic resolution across studies, making it difficult to identify trends and patterns [93]. Between studies of the same macaque species, factors including differing sample sizes, age ranges, methodologies, environmental factors (including geographical location and whether animals are wild or captive), and exposure to medications all likely contribute to the inconsistencies in the findings. Findings in macaques also show inconsistencies with human studies, which is likely partially attributable to species-specific effects [13, 14].

The composition of the intestinal microbiota may be distinct in centenarians and extremely long-lived individuals (≥ 90 years old) compared to older adults. In humans, studies across multiple geographic regions have consistently shown an increase in opportunistic pathogens, also known as pathobionts, alongside a decline in SCFA-producing bacteria in the intestinal microbiota [15-22]. However, the findings are often inconsistent, with conflicting trends in the

Table 1.1. Studies investigating intestinal microbiota alterations in older macaques

Study (cohort size)	Species (wild/ captive)	Molecular technique (sample type)	Main microbiome alterations in older macaques
Sadoughi *et al.* [61] (41 – 97)	Assamese macaques (wild)	16S (faecal)	↑ *Anaerosporobacter, Cellulosilyticum, Alistipes, Ruminococcaceae CAG-352, Acholeplasmataceae EMPG18, Spirochaetaceae GWE23110* ↓ *Eubacterium eligens*, *Lachnoclostridium*, *Fusicatenibacter, Bifidobacterium, Ligilactobacillus, Collinsella*
Wei *et al.* [70] (104)	Cynomolgus macaques (captive)	16S (faecal)	(In males) Beta diversity, ↑ Bacillota:Bacteroidota ratio ↑↓ genera from the Ruminococcaceae family (including ↓ *Faecalibacterium, Fournierella)* ↓ *Roseburia*, *Alloprevotella*
Duan *et al.* [64] (16)	Cynomolgus macaques (captive)	16S (faecal)	(In females) ↑ Veillonellaceae, Coriobacteriaceae, Succinivibrionaceae ↓ Ruminococcaceae, Rikenellaceae
Yang *et al.* [57] (41)	Cynomolgus macaques (captive)	16S (faecal)	(In females) No significant differences
Adriansjach *et al.* [59] (40)	Rhesus macaques (captive)	16S (faecal)	↓ Bacilli
Janiak *et al.* [91] (105)	Rhesus macaques (wild)	16S (rectal)	↓ *Bifidobacterium*, Betaproteobacteriales
Pallikkuth *et al.* [94] (12)	Rhesus macaques (captive)	WGS (rectal)	↑ species belonging to the Pseudomonadota phylum ↓ species belonging to Bacillota phylum
Sang *et al.* [90] (49)	Rhesus macaques (captive)	16S (faecal)	Beta diversity, ↓ Bacteroidota, *Faecalibacterium, Roseburia, Coprococcus, Prevotella, Prevotellamassilia*
Chen *et al.*, 2018 [92] (174)	Rhesus and rhesus/ cynomolgus macaque hybrids (wild)	16S (rectal)	(In males) Beta diversity, ↑ *Prevotella*, *Prevotellamassilia, Ruminococcus, Roseburia, Faecalibacterium, Phascolarctobacterium, Propionspira, Succinivibrio, Clostridium, Eubacterium, Oscillobacter, Blautia*, Bacteroidaceae, Porphyromonadaceae ↓ *Heliobacter*

16S = 16S rRNA sequencing; WGS = Whole genome sequencing

abundance of genera such as *Bifidobacterium* and *Akkermansia* [15-22]. The inclusion of individuals with co-morbidities within several of these studies may explain these differing results, highlighting that not all individuals who live to extreme old age will necessarily maintain their health.

A key limitation of studies of the impact of age on the intestinal microbiota is their cross-sectional design, making it impossible to determine whether microbial taxa found in each age cohort are retained through life, or are acquired and established in the host at specific life-stages. Another limitation is the use of stool samples as a proxy for intestinal luminal content to characterise the intestinal microbiota. The stool microbiota most closely resembles the colonic microbiota and is not indicative of the microbial composition of the entire intestine, and especially not of the small intestine [95].

To my knowledge, there are no studies in NHPs investigating the effect of age on the small intestinal microbiome. In humans, the composition of the duodenal microbiota has been investigated in patients aged between 18-80 years who underwent esophagogastroduodenoscopy for gastrointestinal diseases or symptoms, including irritable bowel syndrome (IBS), Crohn's disease, abdominal pain, and anaemia. The dominant phylum was Bacillota, with the relative abundance of Pseudomonadota increasing with age, becoming the second most abundant phylum in older adult (aged 66-80 years) patients. Age, the number of concomitant diseases, and number of medications were all factors associated with a negative correlation between age and alpha diversity, and an altered abundance of several bacterial genera. Enrichment of the genera *Escherichia*, *Lactobacillus*, and *Enterococcus* was associated solely with chronological age and increased in older adults [96]. The microbial composition of the duodenum was also found to be highly divergent from that of the faecal microbiota [95]. These findings highlight the differences which exist between the microbial communities in the small intestine and the faeces, and that the composition of the duodenal microbiota may be affected by age in humans. However, the use of samples from patients with gastrointestinal disorders or diseases means that the observed microbial profiles may significantly diverge from those in healthy individuals. Factors such as diet and frailty were also not assessed [95, 96]. Further studies investigating the small intestinal microbiota in healthy individuals would be beneficial.

1.3. Immunomodulatory role of the intestinal microbiota

In early life, interaction between the intestinal microbiota and the immune system is essential for education and maturation of the adaptive immune system [97]. Evidence for this comes from examination of germ-free (GF) mice, who are born and raised in sterile conditions and therefore lack a microbiota. GF mice exhibit defective intestinal-associated lymphoid tissues, reduced

intestinal lymphocytes and innate immune defences, and increased susceptibility to infection [98-101]. During ageing the intestinal microbiota and the immune system continue to interact through bi-directional crosstalk [12]. Factors such as diet, antibiotics, geographical location, infections, ethnicity, urbanisation, and lifestyle are major factors which impact the composition and function of the intestinal microbiota and are potential triggers for inflammation and inflammatory disease [84, 102-107].

1.3.1. Homeostatic interactions of the intestinal microbiota and the host immune system

1.3.1.1. Host mediation of intestinal homeostasis

Ordinarily, a variety of homeostatic mechanisms maintain immune tolerance to the intestinal microbiota in healthy individuals. One of the methods by which this is accomplished is the maintenance of a sterile mucus layer to spatially separate the commensal microbes from the intestinal epithelium and underlying tissue (Figure 1.1). The mucus layer is formed of mucins secreted by specialised intestinal epithelial cells (IECs) known as goblet cells. In the small intestine, goblet cells in the crypts release a non-attached, loose, discontinuous layer of mucus. In the large intestine, which houses a significantly increased number of goblet cells in the

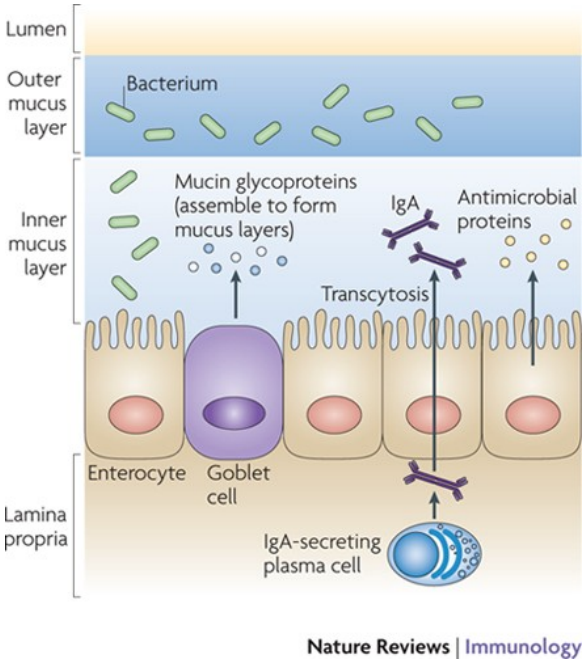

Figure 1.1. The mechanisms maintaining spatial segregation between the IEC surface and the intestinal microbiota. Goblet cells release mucins that assemble into a mucus layer. In the colon there are two distinct mucus layers: a dense, sterile inner layer and a loose, outer layer that provides a habitat for microbial commensals. IECs and IgA^+ B cells (plasma cells) release anti-microbial proteins and IgA, respectively, to help limit microbial incursion through the mucus layer and prevent their penetration of host tissues. This figure was sourced from Hooper and Macpherson (2010) [2].

crypts, there are two distinct mucus layers. The inner layer is dense, highly polymerised, and devoid of microbes. The outer layer is looser and relatively porous, providing a habitat for microbial commensals [108].

The production of the antibody immunoglobulin A (IgA) by IgA^+ B cells residing in the lamina propria plays an important role in controlling the composition and localisation of the microbiota. IgA deficient individuals have an altered intestinal microbiota in comparison to healthy individuals [109]. Dendritic cells (DCs) in the lamina propria and resident beneath Peyer's patches actively sample the small number of bacteria that reach the apical surface of IECs, leading to the induction of commensal-specific B cell responses and secretion of IgA across the epithelial barrier [110-113].

Anti-microbial proteins are also produced by IECs, including enterocytes, goblet cells, and Paneth cells, either constitutively or in response to activation of pattern recognition receptors (PRRs) via interaction with highly conserved microbe associated molecular pattern molecules (MAMPs) expressed by microbes [2, 114-116]. Both IgA and anti-microbial proteins are retained in the mucus layer, preventing microbial incursion through the mucus and IEC layer, and helping to maintain homeostasis while retaining the ability to respond to pathogenic invasion [117-120].

1.3.1.2. The role of the microbiota in immune homeostasis

The intestinal microbiota is also involved in maintaining immune tolerance. Several intestinal microbiota-derived metabolites, including SCFAs, intermediate bile acid metabolites, amino acid-derived metabolites, and membrane associated lipids, have homeostasis-promoting, immunomodulatory effects [121]. For example, the SCFAs acetate, propionate, and butyrate are a crucial energy source for IECs, contributing to the maintenance of intestinal tight junction proteins and helping to prevent an increase in intestinal barrier permeability [67]. Antibiotic-treated specific pathogen free (SPF) mice have a reduced proliferation of IECs in the small intestine compared to controls. Administration of Gram-positive commensal bacteria or a mixture of acetate, propionate, and butyrate alone promoted increased turnover of IECs [122]. Butyrate administration also promoted IEC barrier integrity *in vivo* through enhancement of tight junction protein transcription [123]. Other microbial metabolites, such as tryptophan derivatives, have also been shown to regulate intestinal barrier integrity [124].

SCFAs may also have a role in immune suppression. SCFAs, especially butyrate, can act as an epigenetic regulator by inhibiting histone deacetylases, enzymes that are involved in regulating gene expression [68, 69, 125, 126]. Uptake of butyrate into IECs reduces expression of pro-inflammatory cytokines and chemokines *in vitro*, linking SCFAs to anti-inflammatory effects. Different histone deacetylases inhibitors could replicate this effect, suggesting that this

may be the mechanism of action of butyrate [69]. This aligns with findings in mice, where it has been shown that butyrate and propionate can be taken up into colonic DCs, resulting in histone deacetylase inhibition and inducing production of immunosuppressive enzymes. This favours the ability of DCs to convert naïve T cells to immunosuppressive regulatory T cells, rather than a pro-inflammatory phenotype [68]. Butyrate can also reduce production of pro-inflammatory mediators in macrophages, rendering them hyporesponsive to the microbiota [125]. Conversely, butyrate has also been shown to drive monocyte to macrophage differentiation through histone deacetylase inhibition *in vitro*, enhancing anti-microbial activity, thus amplifying anti-microbial host defences [126].

Other microbial metabolites also mediate immune homeostasis. Microbiota-derived bile acid derivatives, including lithocholic, 3-oxo-lithocholic, and 3β-hydroxydeoxycholic acids, have been shown to potentiate colonic regulatory T cell populations *in vivo* and in mice [127, 128]. Lipid metabolites, such as conjugated linoleic acids and all-*trans* retinoic acid, also have immunomodulatory effects. They induce regulatory T cell differentiation, as well as potentiate a $CD4^+$ intraepithelial lymphocyte population that plays an essential role in dietary tolerance [129, 130].

Beyond the intestinal tract, microbial products and metabolites have systemic effects, influencing immune responses in distal sites such as the bone marrow and brain [121]. GF mice or antibiotic treated SPF mice are more susceptible to extra-intestinal infections, which may be related to the role of products and metabolites of the intestinal microbiota in priming innate and adaptive immune defences [131-133]. For example, the PRR Nod1, expressed on neutrophils, recognises intestinal microbiota-derived peptidoglycan. Peptidoglycan levels in the blood sera were shown to correlate with bone marrow neutrophil function in mice. Depletion or absence of the intestinal microbiota was also associated with reduced neutrophil function [131]. Antibiotic-treated mice have impaired innate and adaptive anti-viral immune responses, including defective responses in macrophages. Genes involved in viral detection, inhibition of viral replication, and interferon responses were downregulated in antibiotic-treated mice compared to controls [133]. Overall, these data provide evidence that the intestinal microbiota is crucial for both local and systemic immune system function, conferring benefits for the host during periods of homeostasis.

1.4. Dysregulation of intestinal immune-microbiome interactions in ageing and the contribution of intestinal dysbiosis to inflammageing

Inflammageing is characterised by an increase in systemic inflammation and elevated blood inflammatory markers, with pro-inflammatory mediators such as IL-6, TNF-α, and CRP being upregulated with age [134-136]. Characterisation of the immune system across the lifespan

has also shown that frequency and functional capacity of multiple immune cell subsets is altered with age in humans, although there is a high level of individual variability in this trajectory [23, 137-139].

During homeostasis, the intestinal microbiota can positively influence host health and immunity, as discussed previously. Increasing age is associated with alterations in microbial community composition, referred to as microbial dysbiosis, which may have detrimental effects on systemic immunity and contribute to inflammageing. Age-associated changes in intestinal microbial composition have also been correlated with markers of systemic inflammation in young and elderly rhesus macaques, including elevated TNF-α, CRP, and IL-6 [94]. GF mice are protected from inflammageing, displaying reduced levels of circulating pro-inflammatory cytokines compared to SPF mice, suggesting the intestinal microbiota is implicated in driving inflammageing. Co-housing of GF mice with aged mice, a method of intestinal microbiota transfer, drives systemic inflammation in GF mice [140].

Further evidence for the role of the intestinal microbiota in inducing inflammageing comes from microbiota transfer studies in mice. Young mice receiving an aged donor microbiota show an increased concentration of blood-based biomarkers of systemic inflammation and intestinal permeability [34]. Conversely, exposure of aged mice to used bedding from young mice stimulated maturation of M cells, antigen uptake, and IgA responses [141]. Health span, lifespan, and increased viability of intestinal function have also been observed in aged mice receiving a young microbiota [140, 142, 143].

Changes to the composition of the intestinal microbiota occur in conjunction with a number of physiological stressors associated with age, including cellular senescence, mitochondrial dysfunction, dysregulated nutrient sensing, loss of proteostasis, epigenetic alterations, telomere attrition, genomic instability, altered intercellular communication, and stem cell exhaustion [32, 51]. In particular, cellular senescence is likely to contribute to the systemic elevation of inflammatory markers due to secretion of a distinct set of pro-inflammatory cytokines, chemokines, growth modulators, angiogenic factors, and matrix metalloproteases by senescent cells, termed the ‘senescence associated secretory phenotype’ (SASP) [144]. While senescent cells can be beneficial in some circumstances, during the ageing process they appear to become resistant to cell death and accumulate, resulting in the secretion of large quantities of SASP proteins implicated in various age-related pathologies [145].

Several metabolites of the intestinal microbiota have been implicated in the promotion of SASP secretion. Deoxycholic acid is an obesity associated metabolite produced by the intestinal microbiota that causes DNA damage and can induce cellular senescence and promote SASP

secretion in murine hepatic stellate cells *in vitro* [146]. Microbial metabolism of choline and phosphatidylcholine produces trimethylamine, which can be further metabolised to trimethylamine-*N*-oxide (TMAO). TMAO can induce cellular senescence by causing mitochondrial damage, leading to secretion of SASP [147]. Altered levels of circulating TMAO has also been linked to the development of several diseases, including cardiovascular disease, PD, and AD [147-152].

The age-associated accumulation of SASP-producing senescent cells may negatively impact intestinal homeostasis. The absence of an intestinal microbiota in GF mice protects them from the accumulation of senescent B cells in intestinal germinal centres in old age. In comparison, B cell senescence in SPF mice leads to a decline in intestinal IgA production and diversity. This reduction, in turn, contributes to age-associated changes in the composition of the intestinal microbiota [153]. Age-dependent increases in intestinal cellular senescence has been observed in intestinal tissues in mice and humans [154-156]. In mice, cellular senescence has also been linked to alterations in intestinal barrier permeability, immune activation, and intestinal microbiota composition [156]. It is possible that a positive feedback loop exists, where the intestinal microbiota influences the development of cellular senescence and SASP secretion, while SASP secretion potentiates age-associated changes to the intestinal microbiota.

1.4.1. Intestinal permeability

An increase in intestinal barrier permeability, leading to an increased translocation of microbial antigens across the intestinal barrier, may be a driver of inflammageing. Evidence supporting this hypothesis comes from animal models, including rodent and NHP studies [34, 140, 157-160]. For example, increased translocation of a fluorescent tracer molecule to the bloodstream was observed in aged mice compared to young mice following administration by oral gavage [140]. In baboons, transepithelial electrical resistance (TEER), an electrophysiological measure of permeability, and expression of tight junction proteins zonula occluden (ZO)-1, occludin, and junctional adhesion molecule (JAM)-A were decreased in colonic tissue from older baboons (>18 years) compared to young animals [161].

Work in humans has been contradictory, with no definitive evidence for an age-associated increase in intestinal permeability in healthy humans [162-166]. In healthy older adults (65-75 years), *in vivo* intestinal permeability was not increased compared to young adults (18-40 years) when assessed by urinary sugar excretion tests. Intestinal permeability of *ex vivo* sigmoid colon biopsies, assessed by TEER measurements and translocation of a fluorescent tracer molecule, was similar between age groups. Expression of genes related to formation of tight junction proteins and immune responses (AMPs, cytokines, and PRRs) were also

unaffected by age [163]. Conversely, in ileal tissue biopsies, age was associated with increased permeability to solutes, although not macromolecular particles. This did not correspond with altered expression of tight junction proteins, ZO-1, occludin, and JAMA-1, but was correlated with increased IL-6 expression in ileal tissue from older adults (67-77 years) [162]. Although evidence for altered intestinal permeability in healthy older adults and the elderly is inconclusive, intestinal permeability is increased in patients with IBS and type 2 diabetes independently of age [163, 164]. This suggests that age-associated factors, such as co-morbidities, may affect intestinal barrier function.

In animal models, increased intestinal permeability is linked with age-associated alterations to the intestinal microbiota, with work in mice providing evidence that the intestinal microbiota may at least partially drive these changes. Intestinal fatty acid binding protein (I-FABP) and lipopolysaccharide binding protein (LBP), surrogate biomarkers of intestinal permeability, were elevated in young mice following the transfer of an aged donor microbiota via faecal microbial transplant (FMT). This also resulted in elevated circulatory IL-6 [34]. Additionally, a study which co-housed GF mice with aged SPF mice found that the intestinal paracellular permeability of GF mice was increased. This effect was not seen when GF mice were co-housed with young mice. Intestinal barrier permeability was also elevated in aged TNF knock-out mice compared to wild-type controls, and anti-TNF treatment in older mice led to alterations in microbial community composition. [140]. In simian immunodeficiency virus-infected pig-tailed macaques, reduction of circulating levels of lipopolysaccharide (LPS) by sequestration with the drug sevelamer was shown to reduce intestinal permeability and systemic inflammation, providing evidence that translocation of bacterial products into the bloodstream is a driver of inflammation and intestinal permeability [167]. Together, these findings further support a connection between age-related inflammation, intestinal permeability, and microbial dysbiosis.

1.5. The intestinal mycobiome

1.5.1. The composition of the intestinal mycobiome

Fungi are components of the intestinal microbiota, though the community structure and function of fungal commensals, known as the ‘mycobiome,’ are less understood than that of their bacterial counterparts. In healthy humans, fungal abundance and diversity in the human intestinal tract is lower than that of bacteria [168]. Despite this, there is evidence that they interact with other members of the commensal microbiota as well as the host immune system [169].

The fungal mycobiome of healthy humans is composed of taxa mainly from the Ascomycota and Basidiomycota phyla, although composition and diversity vary according to geographical location [168, 170]. A meta-analysis of the intestinal mycobiome from several populations has,

however, shown broad structural and compositional patterns that are common across studies and geographical regions. This led to the definition of four enterotypes that all individual mycobiome datasets could be assigned to. The enterotypes are characterised by an abundance of *Saccharomyces* (mainly *Saccharomyces cerevisiae*), *Candida* (*Candida albicans*), and *Aspergillus*. The fourth enterotype was dominated by an Ascomycota phylum that was unclassified at the genus or species level [170]. Notably, although it is a benign commensal in the majority of healthy individuals, *C. albicans* is an opportunistic pathogen, capable of causing disease in primarily immunocompromised individuals [171].

A separate study of the faecal mycobiome in a Chinese cohort found several genera, including *Saccharomyces*, *Candida*, *Aspergillus*, and *Malassezia*, were highly prevalent within the population. The prevalence of these genera remained stable during a period of over 3 years, suggesting that they represent core fungal taxa. Associations between human metabolic health outcomes and fungal genera were also explored. *Blastobotrys* was positively associated with increased levels of low-density lipoprotein. *Malassezia* and *Kazachstania* (a genus which has since been taxonomically revised [172]) were found to be positively associated with fasting glucose and waist circumference, respectively, while *Saccharomyces* was inversely associated with fasting glucose. *Saccharomyces* was also positively associated with bacterial alpha-diversity, while *Candida* was negatively associated [173].

There are a limited number of studies investigating the intestinal mycobiome of NHPs, but existing research suggests similarities to humans at the phylum level. As in humans, a study of the wild and captive cynomolgus and Tibetan macaques faecal mycobiome found that it is dominated by Ascomycota and Basidiomycota [174, 175].

1.5.2. The immunomodulatory role of the intestinal mycobiome

Several studies have provided evidence of the immunomodulatory role of intestinal fungi [176-178]. Fatal susceptibility to colitis and influenza-A virus infection in mice whose intestinal bacteria had been eradicated with antibiotics is rescued by mono-colonisation with *C. albicans* or *S. cerevisiae*. Administration of a fungal cell wall component, mannan, also improves survival, suggesting that it is responsible for mediating these effects [176]. Disruption of intestinal fungal communities using anti-fungal drugs elicits fungal dysbiosis, increased severity of acute and chronic models of colitis, and exacerbated allergic airway disease in mice [177]. This is suggestive that commensal fungi protect against infection and intestinal injury, and that fungal dysbiosis may influence peripheral immune homeostasis. These outcomes were also associated with decreased relative abundance of specific bacterial taxa, including *Bacteroides*, *Clostridium*, and *Lactobacillus* species [177]. This indicates the presence of inter-kingdom interactions, with the disruption of either community impacting the other. Evidence of these

interactions were further demonstrated in a study where both bacterial and fungal community structure was impacted by co-colonisation, compared to colonisation by bacteria or fungi alone [178]. As previously discussed, microbial colonisation in early life is known to be important for immune system maturation. Fungal colonisation in early life also induced changes in local and systemic immunity in GF mice, providing evidence that fungal taxa can stimulate immune responses. Co-colonisation with bacteria resulted in the greatest changes, compared to bacteria or fungi alone, showing a larger shift in abundance of splenocyte populations and cytokine production [178].

The immunomodulatory capabilities of intestinal fungi may explain their possible role in the exacerbation of several human diseases, including inflammatory bowel disease (IBD), coronavirus disease 2019 (COVID-19), disease progression of chronic hepatitis B virus infection, Hirschsprung-associated enterocolitis, graft-versus-host disease, colorectal cancer, and AD [179-189]. Some fungal species are directly implicated in disease genesis, such as pathobionts within the *Candida* genus, for which a link has been shown between their expansion in the intestine and candidemia, an invasive *Candida* infection in the bloodstream [190]. *C. albicans* is the most common cause of candidiasis, a broad term for *Candida* infection of any organ or tissue, due to its high pathogenicity. However, infections caused by species including *Candida glabrata*, *C. tropicalis*, *C. parapsilosis* and *C. krusei* also rank in the top five *Candida* species causing disease globally [171, 191]. The pathogenicity of *Candida* species is mediated by their ability to adhere to host tissues, evade host defences, and produce hydrolytic enzymes, including proteases, phospholipases, and haemolysins [192]. Several Candida species are capable of growing elongated, filamentous cells known as pseudohyphae if they have constrictions between cells, or hyphae if there are no constrictions [193]. Only *C. albicans* and *Candida dubliniensis* produce hyphae, which are key for invasion of host tissue and mediating cell damage [194]. Some *Candida* species, notably *C. albicans* but also *C. tropicalis* and *C. dubliniensis*, also produce candidalysins, cytolytic peptide toxins, which are potent inducers of cell damage and cytokine responses [195, 196].

1.5.3. The intestinal mycobiome in ageing

Recent studies have explored the characteristics of the age-associated intestinal mycobiome in humans. The largest of these, incorporating data from >3000 faecal samples from multiple geographical locations, found that the *Candida* and Ascomycota enterotypes were enriched in participants >60 years, while *Saccharomyces* and *Aspergillus* enterotypes were enriched in participants <30 years. Certain genera, including some which contain opportunistic pathogens, were also positively associated with age, including *Cutaneotrichosporon* and *Candida.* The

Candida enterotype was also significantly associated with patients with chronic diseases such as type 2 diabetes and AD [170].

A separate study which investigated the mycobiome of a Chinese cohort, including centenarians, (n=311) similarly found age was associated with an increased abundance of an enterotype characterised by a dominance of *Candida*. The number of observed taxa was also significantly reduced with age, suggesting a decrease in microbial diversity, aligning with the findings of Lai *et al.* [170, 197]. The *Candida* enterotype was associated with a bacterial enterotype characterised by an abundance of *Bacteroides* in both young and long-lived individuals, suggesting that the mycobiota of centenarians is characterised by its similarity to that of younger populations. Importantly, participants with chronic diseases, acute intestinal diseases, impaired cognition, malignant neoplasia, or acute infectious disease were excluded from the study, indicating that the centenarian mycobiome in this cohort is associated with healthy ageing [197]. Additionally, this association with health may be at least partially mediated by inter-kingdom interactions between fungal and bacterial species.

Together, these studies provide evidence for age-associated changes to the intestinal mycobiome. In a subset of individuals, alterations to the intestinal mycobiome occur which is characterised by an enrichment of pathobionts, including *Candida,* which may be associated with increased risk of age-associated morbidities [170]. The immunomodulatory capacities and inter-kingdom interactions of specific fungal commensals may determine whether these changes lead to health or disease-associated outcomes.

1.6. The role of the intestinal microbiota in age-associated neuroinflammation

1.6.1. The microbiota-gut-brain axis in ageing

The microbiota-gut-brain axis comprises the bi-directional communication pathways between the intestinal microbiota and the CNS. This includes signalling via intestinal microbial metabolites and products which can influence the CNS through both direct and indirect mechanisms. The metabolites include or modulate the production of host neurotransmitters, hormones, and amino acids, which may act through the immune system, the enteric nervous system, the neuroendocrine system, or the circulatory system to influence the CNS [10].

One of the key ways in which the microbiota-gut-brain axis facilitates communication between its organ systems is through immunological signalling via the intestinal and peripheral immune system. As Powell, Walker, and Talley [198] note, there are three ways in which the immune system may achieve communication with the brain. Firstly, through bloodborne cytokines produced by immune cells in the intestinal tract or the periphery, or other humoral factors such

as hormones and bacterial lipopolysaccharide. Secondly, through immune cells triggering signals in afferent sensory fibres and/or enteric nerves which are then relayed to the brain via neurons. Lastly, through the trafficking of circulatory immune cells to the brain, thus allowing the release of inflammatory mediators close to the relevant brain structures. As previously discussed, the intestinal microbiota has significant impacts on the development and function of host immunity. Age-associated intestinal dysbiosis may therefore render the CNS vulnerable to changes in host immune function.

FMT studies have demonstrated the impact that the intestinal microbiota can have on CNS inflammation and function. For example, young mice receiving a microbiota transplant from aged donors exhibit increased retinal and CNS inflammation, impaired spatial learning and memory, and reduced microbial SCFA production [34, 35]. The SCFA butyrate has an inhibitory effect on inflammatory responses in *in vitro* cultures of CNS cells and *ex vivo* tissue samples, suggesting a mechanistic link between reduced SCFAs and CNS impairment [199]. In another study, GF mice transplanted with the microbiota of aged mice showed decreased spatial learning and memory, along with diminished SCFA levels, compared to those receiving transplants from young donors [36]. These studies provide evidence that the aged microbiota alone is sufficient to induce CNS inflammation and cognitive decline in rodents, and that this effect may be linked to reduced SCFA production. This prompts the question of whether the intestinal microbiota could play a role in regulating age-related inflammation in the CNS.

1.6.2. Microglia

Microglia, the brain's resident immune cells, are key regulators of neuroinflammation, and their activation is a hallmark of neurodegenerative disease [200]. The age-associated increase in neuroinflammation has primarily been attributed to persistent changes in microglial functional profiles and morphology. Microglia play essential roles in maintaining brain homeostasis, including monitoring and pruning neuronal synapses, driving oligodendrocyte differentiation, and phagocytosis [201]. In their resting state, under homeostatic conditions, microglial cells are ramified cells with long, thin, motile processes and a small cell soma. These processes continuously sample the brain parenchyma, allowing the cells to respond to changes in homeostasis [202].

In neuroinflammation, however, microglia become dysregulated. This results in synaptic loss and accumulation of cellular debris as their phagocytic capacity becomes overwhelmed [201]. In response to inflammatory stimuli, resting microglia transition to an activated, or disease-associated, morphology [203]. Activated microglial processes are greatly enlarged, becoming shorter and thicker, as is the cell soma. Functional changes also occur, with activated microglia

expressing an increased number of activation markers and producing pro-inflammatory cytokines, chemokines, and reactive oxygen species [204].

Microglial cells in the aged human brain are associated with dystrophic morphology, characterised by de-ramified processes, meaning the fine cytoplasmic processes seen in resting microglia become shorter, thicker, and often fragmented [205, 206]. The cell soma is enlarged as in the activated phenotype, and accumulates lipofuscin with age, a degraded phagocytic material which appears as a brown pigment [203, 205-207]. Dystrophic microglia are associated with a primed phenotype, characterised by upregulation of antigen presentation molecules (APCs) (*e.g.* major histocompatibility complex class II (MHC-II)), expression of pro-inflammatory mediators, and downregulation of regulatory molecules (*e.g.* CX3C chemokine receptor 1 (CX3CR1)) [208-212]. Upregulation of molecules associated with antigen presentation, including MHC-II and cluster of differentiation (CD) 86, has been associated with ageing in rodents, humans and NHPs [208, 213-215]. Rodent studies provide evidence that primed microglia exhibit an exaggerated, prolonged response to inflammatory stimuli [210, 215, 216]. In aged mice administered with LPS, prolonged sickness, increased pro-inflammatory cytokine expression in the brain, and enhanced inflammatory gene expression in microglia were seen compared to adults [215]. A separate study also found increased pro-inflammatory cytokine expression in microglia in old compared to young mice, which was further potentiated upon exposure to LPS [210]. Exposure of microglia from aged rats to LPS induced increased pro-inflammatory cytokine expression compared to microglia from young animals. Gene expression of microglial activation markers CD11b, ionized calcium-binding adaptor molecule 1 (Iba1), and MHC-II was significantly increased in microglia from aged rats regardless of exposure to LPS [216]. Increased $Iba1^+$ immunoreactivity has also been observed in the brains of mice challenged with LPS [217]. Primed microglia also show functional deficits, including decreased phagocytic capacity and reduced speed of migration to inflammatory sites [203, 218].

Mouse studies provide evidence for the role of the intestinal microbiota in regulating microglia. In GF mice microglial cells display an immature phenotype, and their function is impaired compared to those of SPF mice. These defects were partially rescued by either restoration of the intestinal microbiota or administration of a mixture of SCFAs (propionate, butyrate, and acetate) [219]. Administration of a broad-spectrum antibiotic cocktail in early life to mice also resulted in altered microglial morphology, accompanied by anxiety-like and compulsive-like behaviours in adolescence [220]. Prolonged antibiotic treatment in mice has been associated with subtle morphological changes associated with an activated morphology, increased

expression of activation markers CD40 and MHC-II, and an increased number of Iba1^{+} cells in the hippocampus [221].

1.6.3. Blood-brain barrier

The blood-brain barrier (BBB) is a semi-permeable membrane which separates the circulatory system and the CNS and helps to control the brain microenvironment. It consists of tightly sealed brain microvascular endothelial cells (BMECs) that form the walls of cerebral blood vessels. Microglia, astrocytes, neurons, the extracellular matrix, and pericytes, help to regulate the BBB in a structure known as the neurovascular unit (NVU) (Figure 1.2). Tight junction proteins are a key component of the BBB and are composed of three types of molecules: occludins, claudins, and JAMs [222]. These proteins form a continuous band around cerebral blood vessels, restricting the entry of most blood-borne substances into the CNS, including pathogens [222, 223]. The BBB also regulates immune cell trafficking into the CNS under homeostatic conditions [224]. However, the expression of tight junction proteins can be reduced during heightened inflammation. This may increase the accessibility of microbial and immune factors to the brain, resulting in increased neuroinflammation [225].

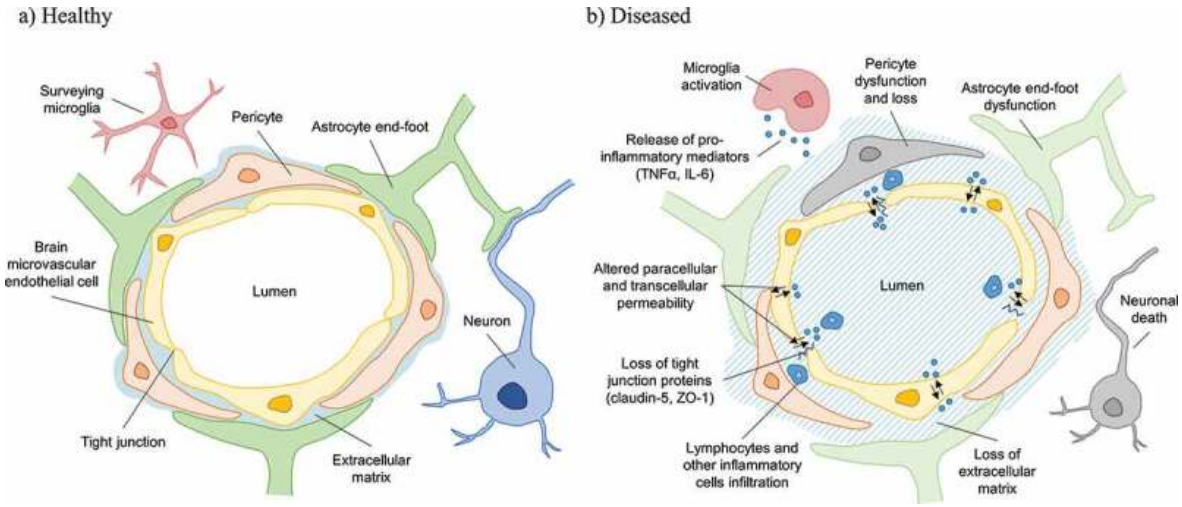

Figure 1.2. The human blood-brain barrier (BBB) neurovascular unit (NVU) in (a) healthy and (b) diseased states. Increased permeability in the diseased state is associated with increased inflammation due to infection or injury, resulting in altered BBB and NVU structure and function. Infiltration of blood-borne immune cells and inflammatory mediators, including cytokines, chemokines, microbes, and microbial products into the brain microenvironment enhances local inflammation, leading to dysfunction and loss of extracellular matrix, astrocytes, neurons, and microglia. This figure was sourced from Parker, Fonesca, and Carding (2020) [1].

Several studies in rodents have demonstrated the link between the intestinal microbiota and BBB permeability. It should be noted that while the BBB is structurally similar in rodents to humans, differences, including increased expression of tight junction and transporter protein expression, are seen in the rodent BBB [226, 227]. Rodents also display differences in

astrocyte morphology, including the structure of astrocytic end-feet, and lack interlaminar astrocytes, a cell type which is specific to primates and may help regulate the BBB in the cortex [228, 229]. Reduced tight junction expression in the BBB and a corresponding increase in BBB permeability was observed in GF mice compared to SPF mice, suggesting that the microbiota has a role in maintaining BBB integrity. The study also showed that BBB integrity may be specifically linked to SCFA production by the intestinal microbiota. Administration of the butyrate producer *Clostridium tyrobutyricum* or oral administration of sodium butyrate upregulated BBB tight junction proteins and decreased BBB permeability in GF mice [230]. Butyrate and propionate administration has also been found to have a protective effect on the induction of neuroinflammation, both in ageing mice and an *in vitro* human brain endothelial cell culture model [231, 232]. Conversely, high levels of the neurotoxic microbial tryptophan derivative, quinolinic acid, negatively impact BBB integrity, by enhancing plasma protein extravasation from the circulatory system to the brain in rats [233]. Human *ex vivo* and *in vitro* studies have shown that high levels of circulating microbes or microbial products, as might occur following a breakdown in intestinal epithelial barrier integrity, are associated with decreased BBB integrity [234, 235]. Post-mortem samples of patients with fatal sepsis found a decreased expression or absence of tight junction molecules, including occludin and claudin-5 [234]. Exposure of human BMECs to LPS *in vitro* was also associated with decreased tight junction protein expression [235].

1.7. Intestinal microbiota in neurodegenerative diseases

Intestinal dysbiosis and inflammageing have been implicated in the development of neurodegenerative diseases, with AD and PD being the most common [39-47, 236-238]. FMT studies in rodent models using faecal material from patients with neurodegenerative diseases have partially recapitulated disease pathology and symptoms [37, 38]. This is suggestive of a causal relationship between intestinal dysbiosis and disease progression that is mediated by the microbiota-gut-brain axis. Although the precise mechanisms are not yet fully elucidated, the known role of the intestinal microbiota in AD and PD is briefly outlined here.

1.7.1. AD

AD patients have an altered intestinal microbiota composition compared to heathy, elderly controls. However, the changes observed in AD patients are not common to all studies, making it difficult to define a compositional shift, or microbial signature, associated with AD [39-41]. In a study of 43 AD patients and an equal number of age-matched controls, the proportion of Bacteroidota was significantly reduced in AD patients, while Actinomycetota were increased [39]. In contrast, Vogt *et al.* found that Actinomycetota and Bacillota were decreased in 25 AD patients, while Bacteroidota were increased. They found that *Bifidobacterium* and *Adlercreutzia*

were significantly decreased at the genus level, accounting for the decrease in Actinomycetota. Within Bacteroidota, *Bacteroides* and *Alistipes* were increased [40]. Liu *et al.* also observed reduced levels of Bacillota and Bacteroidota in AD patients, in addition to an increased abundance of Pseudomonadota. Commensal diversity, as assessed by Shannon and Simpson indices but not Chao1, was reduced in AD patients [41]. These discrepancies may be due to different patient populations, lifestyle, study design, and methodological factors. Notably, in the study conducted by Liu *et al.* alterations in the intestinal microbiota composition were seen in patients with mild cognitive impairment, a pre-dementia stage of AD, suggestive that intestinal dysbiosis arises at an early stage of the disease. A progressive increase in the class *Gammaproteobacteria*, the order *Enterobacteriales*, and family *Enterobacteriaceae* in patients with mild cognitive impairment and AD compared to healthy controls was also seen, suggestive of a link between these taxa and AD progression [41].

The pathological hallmarks of AD include accumulation of Aβ pathology and neurofibrillary tangles, microglial activation, and neuron and synapse loss. The appearance of disease-associated pathology precedes clinical symptoms, which is characterised by memory loss and cognitive decline [239]. In addition to studies in humans, rodent models provide some evidence of a link between compositional changes in the intestinal microbiota and AD symptoms and pathology. Notably, antibiotic-treated young rats receiving a microbiota from a human AD patient resulted in cognitive deficits and impaired adult hippocampal neurogenesis [37]. This indicates a causal role for the intestinal microbiota in AD pathogenesis. Abnormal production of phenylalanine and isoleucine by the intestinal microbiota has also been observed in an 5xFAD transgenic mouse model of AD, which was shown to induce the expression of peripheral Th1 cells. Subsequently, the Th1 cells infiltrate the brain and trigger neuroinflammation, which is ablated in response to treatment with antibiotics, indicating a role for the intestinal microbiota in driving peripheral immune cell infiltration to the brain in AD [240].

Additionally, several studies have shown that manipulating the intestinal microbiota impacts the severity of Aβ pathology and neuroimmune activation in genetic mouse models of AD. Cox *et al.* reported a sex-specific age-related increase in *Bacteroides* in female mice compared to wild type mice in a mouse model of AD. Elevated *Bacteroides* abundance was shown to strongly correlate with Aβ plaque formation. Administration of *Bacteroides fragilis* to young, female APP/PS1 mice, a separate mouse model of AD, was also shown to drive Aβ formation [241]. An independent study of APP/PS1 mice showed a sex-specific decrease in Aβ deposition, microglial morphology, and peripheral inflammatory biomarkers in male mice treated with antibiotics to deplete the intestinal microbiota [242]. A subsequent study by the same group found that short-term antibiotic treatment in APP/PS1 male mice in early life (2-3 weeks)

reduced Aβ pathology and microglial activation at 9 weeks. Microglial depletion mitigated these protective effects, suggesting microglia may be essential for driving these antibiotic-mediated effects [243]. Together these studies indicate that there may be sex-specific mechanistic links between intestinal microbiota composition and AD progression. A decrease in the Firmicute:Bacteroidota ratio and *Akkermansia* abundance in conventionally colonised APP/PS1 mice has also been observed when compared to wildtype controls. The abundance of *Akkermansia* also negatively correlated with Aβ42 deposition in the brain. Subsequent generation of GF APP/PS1 mice was associated with a reduction of Aβ deposition in the brain, as well as a decrease in microglial activation and levels of neuroinflammatory cytokines [244]. A separate study of antibiotic exposure in APP/PS1 mice resulted in reduced Aβ plaque deposition in the brain and altered populations of blood-circulating and brain-residing lymphoid cell populations, further indicating a link between the intestinal microbiota and AD pathogenesis [245].

1.7.2. PD

Intestinal symptoms are common in PD patients, often preceding clinical manifestations of the disease, with increased inflammatory and intestinal permeability markers seen in PD patients compared to age matched controls [237, 246]. An increased incidence of symptoms such as constipation are observed in patients who go on to develop PD up to a decade before diagnosis [246]. Alterations to the intestinal microbiota have also been observed in patients with PD, suggesting the involvement of the microbiota-gut-brain axis in PD development [42-47]. As with AD, the microbial alterations vary across studies, making it difficult to define a PD-associated microbial signature. However, a recent meta-analysis of ten studies investigating the PD-associated intestinal microbiome using 16S rRNA gene sequencing found enrichment in the genera *Lactobacillus*, *Akkermansia*, *Hungatella*, and *Bifidobacterium* to be common across studies when the datasets were pooled. Depletion of the SCFA producers *Faecalibacterium* and bacteria in the *Lachnospiraceae* family was also observed [47]. The depletion of these genera aligns with studies that link low levels of faecal acetate, propionate, and butyrate, speculated to be mediators of microbiota-gut-brain axis crosstalk, to PD [45, 247, 248]. Microbial richness was also observed to be increased in PD patients. When studies were considered individually, however, the number of taxa found to be significantly different between PD patients and healthy controls varied. Changes in diversity indices also varied. These discrepancies highlight the effect that different study populations, study methodology, and analysis methods may have on the results of cross-sectional studies of commensal microbiome communities and structure [47].

A meta-analysis of six studies investigating the PD-associated intestinal microbiome using shotgun metagenomic sequencing, in contrast, found that alpha diversity, assessed with Shannon index, was increased across all datasets in PD patients. As in studies using 16S rRNA sequencing, genera such as *Akkermansia*, *Bifidobacterium*, and *Hungatella*, but not *Lactobacillus*, were enriched in PD patients. *Faecalibacterium*, however, was depleted. At species level, *Akkermansia muciniphila* was significantly enriched, while *Roseburia intestinalis* and *F. prausnitzii* were depleted. The study also identified a significant decrease in riboflavin and biotin biosynthesis pathways, which was correlated with decreased faecal SCFA concentration [249]. Therapeutic administration of riboflavin and biotin are associated with amelioration of neuroinflammation and neurotoxicity, respectively, and treatment with riboflavin has been linked with improved motor function in PD [250-252].

Mouse studies provide evidence for a link between the intestinal microbiota and PD-associated pathology [38, 253]. The pathological hallmark of PD is the intracellular aggregation of α-synuclein in the brain, which is associated with neuronal cell death and neuroinflammation. Both α-synuclein pathology and microglial activation were found to be exacerbated in SPF α-synuclein-overexpressing mice, compared to their GF or antibiotic-treated counterparts. An FMT in GF mice from PD human patient donors was also shown to induce PD-associated pathology and motor deficits, suggesting a causal role of the PD-associated intestinal microbiota in disease pathogenesis [38]. Further evidence comes from a separate, chemically induced, mouse model of PD, in which a FMT from wild-type mice ameliorated PD-associated pathology, reducing glial activation, intestinal inflammation, neurotransmitter abnormalities, and motor deficits. A FMT from the same mouse model also induced PD-associated pathology in wild-type, healthy mice [253].

1.8. Intestinal microbiome as a therapeutic target

Growing awareness of the intestinal microbiota's influence on immunity and disease progression has led to its recognition as a promising therapeutic target. Recently, FMT has been the subject of several clinical trials for the treatment of PD, with the results suggesting that it is a safe, well-tolerated, and beneficial treatment for patients with early to mid-stage PD [254-256]. A small trial of FMT in patients with early-stage PD (*n*=46) found beneficial effects on motor symptoms that continued to be observed until the 12-month follow-up [254]. A second trial (*n*=12) found temporary improvements in motor symptoms, but found that the FMT alleviated gastrointestinal symptoms, including constipation, intestinal transit times, and intestinal motility [255]. An 11-month trial of patients with mild-moderate PD (*n*=52) who were given an FMT via an oral capsule also reported improved motor and gastrointestinal symptoms [256]. These trials demonstrate that the use of FMT is clinically feasible and effective for the

treatment of early-mid stage PD. Whether FMT would be effective in patients in advanced stages of the disease is unknown.

Although no clinical trials on FMT in AD patients have yet been carried out, a case report of an 82-year-old man showed rapid improvement in their AD symptoms following FMT treatment for recurrent *Clostridioides difficile* infection. At 2 and 6-month follow ups the individual displayed significant improvements in their cognition and mood [257]. Although the exact mechanisms of FMT in these cases are unknown, the results of these trials and case reports show that FMT for neurodegenerative disease may be an effective treatment with minimal side effects. In addition, they add to the evidence of a causal link between intestinal dysbiosis and neurological dysfunction in humans, aligning with what has been found in animal models.

Similar beneficial effects have been observed following FMT for the treatment of other chronic inflammatory conditions, including IBD [258]. FMT in rhesus macaques infected with simian immunodeficiency virus was also found to be well tolerated and enhanced the frequency of beneficial immune cell populations [259]. These findings, along with, as previously discussed, results from animal studies linking intestinal dysbiosis to inflammageing and immunosenescence, suggest that FMT and other microbiota-modulating methods, such as antibiotic or probiotic treatments, may positively impact neuroinflammation and systemic inflammation

1.9. The suitability of NHPs as models for human ageing

The use of animal models in research enables researchers to elucidate disease mechanisms by performing experiments which are not ethically possible in humans. It also allows researchers to control many environmental variables that could influence study outcomes in humans and may not be fully accounted for through statistical analysis [260]. While rodent models are valuable for research, the translational gap between findings in rodents and humans, particularly in studies of neurodegenerative disease, underscores the limitations of relying solely on rodent research [261-263]. NHPs, and particularly Old World NHPs, are genetically and physiologically similar to humans, and their outbred nature allows validation of research findings that goes beyond what can be proved in principle by genetically inbred rodent models maintained under tightly controlled environmental conditions [49]. NHPs may be particularly valuable for ageing research due to their similar ageing process to humans and their brain structure, which more closely resembles that of humans compared to rodents. They are also susceptible to age-related chronic diseases, and their immune responses are analogous to humans, suggesting that immunosenescence may also develop similarly [264, 265]. As in humans, NHPs experience age-related declines in sensory, motor, and cognitive

function, as well as changes in social interactions [266, 267]. Aβ pathology and tau aggregation are also found to naturally occur in elderly NHPs [260, 267].

As exemplified by much of the research discussed here, our understanding of how ageing effects communication in the microbiota-gut-brain axis and the development of inflammageing relies heavily on rodent studies. The benefits of using rodents in research compared to NHPs includes their short lifespans, relatively low cost of managing and maintaining aged populations, and availability of genetically modified strains [263]. The long lifespan of NHPs, in comparison, makes ageing research using these animal models challenging from a cost and planning perspective, and their use is associated with a number of ethical implications [268]. If the use of NHPs in a research project is deemed necessary, selection of the particular species used also requires careful consideration.

The use of New World NHP models in ageing research may be preferable due to their smaller size and relatively shorter lifespan, which helps reduce housing costs and improves the feasibility of longitudinal studies [269, 270]. The common marmoset, for example, which has recently been established as a valuable model for ageing research, has an average lifespan of five to seven years and a maximum lifespan of 16½ years [271]. Further advantages of New World species include a high reproductive efficiency, reduced floor space requirements, and, for pharmacological studies, reduced compound synthesis requirements compared to larger Old World species. The smaller size of New World species also makes handling and husbandry comparatively easier [269, 270]. However, their reduced evolutionary proximity to humans compared to Old World species may make them less an attractive option, depending on the needs of the study [270]. All these factors should be considered when determining the suitability of a particular NHP species.

Despite the high costs and ethical implications associated with their use, the high translational value of NHPs to humans make them an attractive model for ageing research. This may be especially true for studies investigating the efficacy of microbiome-targeted therapies, where potential negative health consequences may render human trials inappropriate.

1.10. Conclusions

There is ample evidence that the intestinal microbiome undergoes age-associated alterations in humans, NHPs, and rodents. Numerous, primarily rodent, studies also show that modulation of the intestinal microbiota can alter immune function, potentially linking age-associated intestinal dysbiosis to inflammageing. Although the bacterial component of the intestinal microbiota receives more attention, there is evidence that fungal commensals could also play a role in inflammageing. Fungi have immunomodulatory effects, and the composition of the

intestinal mycobiome has been shown to change with age in humans. Modulation of the intestinal microbiome is associated with inflammatory disease-associated pathology in the intestine and the brain, which is likely mediated by the microbiota-gut-brain axis. Early phase clinical trials have shown that microbial modulation of the intestinal microbiome via FMT may be a safe and effective treatment option for inflammatory diseases, including neurodegenerative disease. Inflammageing is a common factor in the development of age-associated functional decline and diseases. Further research is needed to confirm the role of the intestinal microbiota in driving inflammageing, clarify the mechanisms linking intestinal dysbiosis to its development, and assess whether modulating the microbiome could be an effective treatment for inflammageing. Given the translational gap between rodent models and humans, NHPs may serve as a more relevant animal model for studying age-related vulnerabilities of the microbiota-gut-brain axis.

1.11. Aims

The cynomolgus macaque, an Old World NHP, is a commonly used model in biomedical research. However, in comparison to the closely related rhesus macaque, the characterisation of the structures which form the microbiota-gut-brain axis has been limited. The aim of this thesis was to determine the relevance of cynomolgus macaques as a model for studying the effect of ageing on the microbiome-gut-brain axis and inflammageing in humans. It addresses the hypothesis that the microbiota-gut-brain axis is analogously affected by age in cynomolgus macaques and humans. To test this hypothesis, the effects of ageing on the brain, the intestinal tract, and the composition of both the prokaryome and mycobiome across multiple regions of the intestinal tract, from duodenum to the distal colon, were characterised in a cohort of healthy, captive-bred cynomolgus macaques of differing ages. Specifically, the main objectives were:

- To investigate the effect of age on intestinal morphology and goblet cell density in small and the large intestinal tissue samples (Chapter 3).
- Determine the concentration of blood inflammatory and intestinal barrier permeability markers across the lifespan (Chapter 3).
- To conduct a taxonomic and functional survey of the intestinal prokaryome in six regions of the intestinal tract (duodenum, jejunum, ileum, caecum, proximal colon, and distal colon), and assess the effect of age on its composition, diversity, and function (Chapter 4).
- To conduct a taxonomic survey of the intestinal mycobiome in the same six intestinal regions and assess the effect of age on its composition and diversity (Chapter 5).

- To characterise the accumulation of age-associated brain pathology in ageing macaques in the midbrain, SN, hippocampus, and cerebellum, as well as to assess the relationship between brain iron accumulation and microglial activation (Chapter 6).

2.0. Chapter 2: Materials & Methods

2.1. Animals

2.1.1. NHPs

All animal procedures required for these studies were conducted by UK Health Security Agency (UKHSA) staff, approved by the UKHSA Porton Down Establishment Animal Welfare and Ethical Review Body (Project License: PD28B8ED5) and authorised under a UK Home Office license to breed, supply, and use macaques for scientific research (Establishment license: XBF9440B0). All animals used in this study were required to be euthanised as part of colony management requirements. Animals enrolled onto this study were culled for reasons separate to the study objectives, such as ex-breeder status designation, diagnosis of non-infectious disease or illness, or abnormal or aggressive behaviour. Samples from 40 cynomolgus macaques were included in this study, ranging in age from 0-20 years old. Samples were collected on an *ad hoc* basis, with the aim to collect brain tissue, intestinal tissue, plasma samples, and intestinal luminal/faecal content from each animal, although this was not possible for all animals. The animals were categorised into three age groups, young (< 7 years), adult (8-12 years), and aged (> 13 years). All animals were housed and captive-bred at a UKHSA facility and are derived from either Mauritian or South-East Asian origin. No new animals have been introduced to these colonies since 2004. The breeding colonies were, and continue to be, maintained to the highest standard in terms of animal welfare, health status, genetic profile, and behavioural compatibility, compliant with the UK Home Office Code of Practice for the Housing, and Care of Animals Bred, Supplied or Used for Scientific Purposes, 2014. Animals were housed in compatible social groups, either in harem breeding groups, or single sex, aged-matched holding groups. Their accommodation consisted of climate controlled, multiple room, solid floor caging systems, with a floor of deep litter in the largest rooms to allow foraging and access to a non-climate controlled external 'extension' pen which is open to the elements. Additional complex enrichment was provided to fulfil the behavioural needs of the animals. Water and a complete primate diet was provided *ad libitum*, and supplemented daily with fruits, vegetables, and pulses. None of the animals included in the present study had been used previously for experimental procedures.

2.1.2. Mice

All murine experimental work and sample collections were carried out by Dr Aimée Parker. Male and female SPF (C57BL/6-SPF) mice aged 3 months or 24 months, and male GF (C57BL/6-GF) mice aged 3 months, were maintained in individually ventilated cages (SPF) or in sterile isolators (GF) in adjacent rooms of the Quadram Institute Germ-Free mouse facility within the University of East Anglia Disease Modelling Unit. All mice received autoclaved water and were

fed RM3 (SPF) or RM3-(Autoclavable) (GF) diet (Special Diets Services). All mice were maintained under 12-hour light-dark cycle. All mouse experiments were conducted in full accordance with EU and United Kingdom Home Office Legislation, and the Animals (Scientific Procedures) Act, 1986 (UK). The study was approved by the University of East Anglia Animal Welfare and Ethical Review Body. All procedures were conducted under the authority and in compliance with UK Home Office project license number P723E9201.

2.2. Fungal administration for *in vivo* mouse experiments

Administration of *C. albicans* to mice was carried out by Dr Aimée Parker. *C. albicans* cells were administered to GF mice by oral gavage at doses of 2.5×10^5 (n = 5) or 5.0×10^5 (n = 5) in a volume of 200 µL in phosphate buffered saline (PBS) or 2.5×10^4 cells in a volume of 100 µL in PBS via intravenous tail vein injection (n = 2). Control mice received 200 µL PBS only (n = 2). SPF mice (n = 16, 8 females and 8 males) were pre-treated for four days with either PBS (n = 8) or a cocktail of broad-spectrum antibiotics (VMNA, 0.5 mg/mL vancomycin, 1 mg/mL metronidazole and 1 mg/mL neomycin delivered in 200 µL sterile water by daily oral gavage, and 1 mg/mL ampicillin delivered via drinking water, available *ad libitum*) (n = 8). Following a 24-hour washout period, 5×10^5 *C. albicans* cells in PBS were administered by oral gavage in a volume of 200 µL. Mice were then maintained in individually ventilated cages until sacrifice.

2.3. Sample collection

2.3.1. NHPs

A redacted copy of the original study plan is available in Appendix 1. Autopsy of all NHPs and NHP sample collections were carried out by UKHSA-based technical staff. Animals were initially sedated with ketamine hydrochloride (Ketaset, Fort Dodge Animal Health Ltd., UK) at a dose of 10 mg/kg and exsanguinated. Animals were then euthanised by intracardial injection with sodium pentobarbital (140 mg/kg, Vetquinol UK Ltd., UK). Samples were collected immediately after confirmation of death, as described in the following sections. All procedures were conducted under the authority and in compliance with a UK Homes Office License.

2.3.2. Plasma sample collection

During exsanguination, blood from each NHP was collected into a blood collection tube containing Tripotassium ethylene diamine tetraacetic acid (K3EDTA) (BD Vacutainer, BD, USA). Samples were subsequently placed in a centrifuge operated at 1000-2000 x g for 10 minutes. The resulting plasma supernatant was drawn off and aliquoted into clean Eppendorf tubes, before being snap frozen on dry ice and subsequently stored at -70ºC.

2.3.3. Brain tissue collection

Upon autopsy, the brain of each animal was removed and flushed through with cold protease inhibitor buffer (4-(2-aminoethyl)benzenesulfonyl fluoride hydrochloride (AEBSF) 2 mM, Aprotinin 3 µM, Bestatin 130 µM, Ethylene diamine tetra-acetic acid (EDTA) 1.0 mM, E-64 14µM, Leupeptin 1 µM, Sodium Fluoride 2 mM, Sodium Pyrophosphate 10 mM. All prepared in PBS and stored between 0-4ºC and held in an ice bath before use), then cold 10% neutral buffered formalin (NBF). The two hemispheres of the brain were separated and placed into 10% NBF (Surgipath® Prefilled Specimen Jars, Leica) for 5 days, before being placed in 70% v/v ethanol in water and stored at 4ºC until further processing.

2.3.4. Intestinal tissue collection

Two sets of intestinal tissue samples were collected from the duodenum, ileum, jejunum, proximal colon, and distal colon. One set of samples was snap frozen and subsequently stored at -70ºC until further processing. The second set of samples were fixed by immersion in 10% NBF for 24 hours before being placed in 70% v/v ethanol in water and stored at 4ºC until further processing.

2.3.5. Luminal content and faecal sample collection

Luminal content samples from macaques were collected from the duodenum, jejunum, ileum, caecum, proximal colon, and distal colon upon autopsy. Faecal samples were collected from freshly dropped faeces and were either immediately snap frozen upon collection or collected using OMNIgene-GUT collection tubes (DNA Genotek Inc.) at room temperature. All samples were later stored at -70ºC.

2.3.6. Mice

Sample collection from mice was carried out by Dr Aimée Parker. Brains and caecal content were harvested from GF and SPF mice administered with *C. albicans* at day 5 post-inoculation and used for downstream analysis. A separate group of 3 and 24-month SPF mice (n = 10/group) were temporarily singly housed and faecal pellets collected from their cages using sterile picks and sterile RNA-DNA-free microtubes. Caecal content was transported at 4 ºC and used fresh for plating for fungal colonies. Faecal pellets were frozen on dry ice at point of collection and stored at -80ºC until use. Tissues were collected into 4% paraformaldehyde (PFA) and fixed overnight. I then formalin-fixed and paraffin embedded the tissues. Blocks were stored at 4ºC until sectioning.

2.4. Yeast strains and growth conditions

Yeast cell culture was carried out by Dr Steve James. Yeast strains were provided by the National Collection of Yeast Cultures (NCYC) (Norwich, United Kingdom). *C. albicans* strain

(NCYC 3115) is a human clinical isolate from patient faeces collected in a United Kingdom hospital. *Arxiozyma pintolopesii* (formerly *Kazachstania pintolopesii*) strain (NCYC 4417) was originally isolated from a faecal sample obtained from an aged cynomolgus macaque by Dr Steve James. For inoculum preparation, stocks were cultured in yeast malt (YM) liquid medium (10g/L glucose, 3g/L malt extract, 5g/L peptone, 3g/L yeast extract) at 30°C or 37°C for 48h with shaking (200 rpm) or 72h statically. Cells were collected by low-speed centrifugation (3,000 rpm, 5 min), washed twice in sterile PBS and re-suspended in PBS at ambient room temperature prior to delivery to mice.

2.4.1. Assessment of CFUs

Fungal colonisation of mice administered with *C. albicans* was assessed by measuring colony forming units (CFUs) of *C. albicans* in the caecum of each mouse. 50mg caecal content was mechanically homogenised in PBS to 100 mg/mL, serially diluted, and plated onto YM agar plates. All agar plates were incubated anaerobically at 37°C for 48 hours. Colony counts were assessed, and morphology determined by visual inspection. Colonies of differing morphology (morphotypes) were selected for additional phenotyping. YM broth cultures derived from two morphotypes (white and domed vs. darker and flattened) were incubated statically at 37°C for 72 hours. The presence/absence of hyphal and pseudohyphal morphology was assessed by standard light microscopy. Confirmation of species identity was carried out by standard colony PCR using *C. albicans* specific primers, and by ITS1 sequencing using the primers in Table 2.1.

Table 2. 1. Primer sequences used for confirmation of C. albicans identity

Primer	Sequence	Use	Amplicon Size (bp)	Reference
SACALF	TTTATCAACTTGTCACACCAGA	*C. albicans*-specific detection	~354	[272]
SACALR	GGTCAAAGTTTGAAGATATACGT			
pITS1F	CTTGGTCATTTAGAGGAAGTAA	Amplification of fungal ITS1 region	257*	[273, 274]
pITS2	GCTGCGTTCTTCATCGATGC			

* ITS1 amplicon size for *C. albicans* type strain (NCYC 597)

2.5. Human cell lines

2.5.1. Mammalian cell culture

Cell culture of human cell lines was carried out by Dr Emily Jones and Victoria White. Briefly, the human colonic epithelial cell line Caco-2 (ECACC 86010202) and HT19-MTX-E12 (ECACC 12040401) were cultured in Eagle's Minimal Essential Medium (EMEM) with 1% non-essential

amino acids (M5650; Merck) supplemented with 2 mM L-glutamine (G7513; Merck), 10% fetal bovine serum (FBS; F9665, Merck) and penicillin-streptomycin (P4333; Merck) at passage 21 and 64 respectively. During passage, each cell line was split sub-confluently (70-80%) 1:2 to 1:8 using 0.05% trypsin.

2.5.2. Yeast Transwell system assay

The following yeast transmigration assay was conceptualised by Dr Steve James and I and carried out by Dr Emily Jones and Victoria White. Caco-2/HT29-MTX-E12 cells were cultured at a 9:1 ratio on the apical compartment of 0.4 µm transparent polyethylene terephthalate (PET) membrane inserts in a 24-well plate Transwell system (Greiner, Austria) for 14 days or until a confluent, polarised monolayer was formed. This was confirmed by performing a TEER measurement, described below, every 2-3 days until a reading of >3000 Ω/cm² was reached. To quantify the number of yeast cells required for inoculation, the optical density (OD) was measured at 600 nanometres (nm) (OD_{600}) on a spectrophotometer (BMG Spectrostar Nano). Cells were diluted to a final OD of approximately 1.0 in PBS. Using the Transwell system, confluent Caco-2 monolayers were treated with 30 µL culture containing 5.0 x 10^4 *K. pintolopesii*, 5.0 x 10^4 *C. albicans*, or 5.0 x 10^4 *A. pintolopesii* and 5.0 x 10^4 *C. albicans* cells in a total of 300 µL cell culture medium.

2.5.2.1. TEER measurements

TEER measurements were recorded using an EVOM^2 epithelial voltmeter with chopstick electrode (World Precision Instruments Inc., USA) by Dr Emily Jones and Victoria White. Measurements were taken every 3-4 days while Caco-2 cells were reaching confluence as well as prior to administration of DSS, yeast cultures, and following completion of the assay. Resistance was calculated by the following equation, where R = resistance, TR = total resistance, and Membrane Area = 0.336cm^2:

$$R\ (\Omega cm^2) = TR\ (\Omega) - Blank\ Resistance\ (\Omega)\ x\ Membrane\ Area\ (cm^2)$$

2.5.2.2. FITC-dextran translocation

After inoculation with yeast cultures, the apical compartment of a separate plate was treated with 1 mg/mL 3–5 kDa fluorescein isothiocyanate (FITC)–dextran (Sigma-Aldrich, USA) in the cell culture medium for 24 hours. Translocation of fluorescent FITC–dextran into the basal media compartment was recorded using a FLUOStar OPTIMA (BMG Labtech, Germany) at excitation 485 and 520 nm emission. Treatment of Caco-2 monolayers with FITC-Dextran and spectrophotometry was carried out by Dr Emily Jones and Victoria White.

2.5.2.3. DSS assay

Using the Transwell system described above, the apical compartment of a separate plate was treated with 2% w/v 40 kDa dextran sulphate sodium (DSS) in cell culture medium at 37ºC and 5% CO_2 for 24 hours. As described below, media was collected from the apical and basal compartments of the Transwell systems, inoculated into YM liquid medium and incubated at 30ºC.

2.5.2.4. Yeast growth measurement

100 µL of the apical and basal media obtained from the Transwells was added to 900 µL of YM media in a clear 48-well plate and incubated at 37ºC for 72 hours. Yeast growth was assessed by measuring the OD_{600} (BMG Spectrostar Nano).

2.6. Sample preparation for histology and IHC

2.6.1. NHP brain tissue

Dr Francisco Javier Salguero Bodes, a veterinary pathologist at UKHSA, carried out the following transection of the NBF-fixed brain tissue samples. One hemisphere of each NHP brain was transected using a semi-horizontal plane parallel to the long axis of the SN pars reticulata to provide an area the SN, as well as portions of the midbrain, cerebellum, hippocampus, choroid plexus and blocked at the level of the PONS [275]. Brains were formalin-fixed and paraffin-embedded, before being sectioned at 5µm using a microtome by Alison Bird and Chelsea Kennard, members of the Pathology Department at UKHSA. One section per individual was taken for haemosiderin and eosin (H&E) staining. I prepared at least 6 further sequential 5µm sections for further staining methodologies from young and aged individuals. Every second section and a total of 3 sections were selected for Perl's Prussian Blue staining, while the remaining sections were stained using IHC methods.

2.6.2. Mouse brain tissue

I formalin-fixed, paraffin-embedded, and sectioned at 5 µm GF and SPF mouse brains. Starting at the midline of the left hemisphere, five sections were taken from each brain sample of *C. albicans*-colonised GF mice (n = 5 mice), non-colonised control GF mice (n = 3 mice) and from *C. albicans*-colonised SPF mice receiving either antibiotic or PBS only pre-treatment (n = 8 mice/group). I and Dr Aimée Parker prepared sagittal vibratome sections of 100 µm thickness from PFA-fixed whole brains embedded in low-melt agarose, a method adapted from Snippert *et al.* (2011) [276]. The sections were cleared post-staining and prior to mounting using RapiClear (CamBioscience, UK).

2.6.3. NHP intestinal tissue

NHP NBF-fixed intestinal tissue samples were formalin-fixed and paraffin-embedded. Alison Bird and Chelsea Kennard sectioned the samples at 5µm, taking one section per spatial region as necessary for each staining protocol described in Section 2.7.

2.7. Histological staining

2.7.1. H&E

H&E staining of both brain and intestinal NHP tissue sections was carried out by Alison Bird and Chelsea Kennard. Briefly, the sections were deparaffinised, rehydrated using an alcohol gradient, and rinsed in distilled water, before staining using Hematoxylin solution. Samples were thoroughly rinsed in distilled water before counterstaining with Eosin Solution, dehydration using an alcohol gradient, and mounting.

2.7.2. Perl's Prussian blue

Perl's Prussian Blue staining methodology was carried out using an Iron Stain Kit (ab150674; Abcam, UK). Slides were stained according to manufacturer's guidelines. Briefly, sections were deparaffinised, rehydrated using an alcohol gradient, and rinsed in distilled water, before being placed in a 1:1 solution of potassium ferrocyanide and 2% hydrochloric acid solution for 3 minutes. Slides were rinsed thoroughly in distilled water before counterstaining with Nuclear Fast Red solution for 5 minutes. Slides were again rinsed thoroughly in distilled water before being dehydrated in 95% ethanol followed by 100% ethanol. Slides were cleared in Histo-Clear II (National Diagnostics, USA) before being mounted using DPX (Agar Scientific, UK).

2.7.3. PAS

Periodic-acid Schiff (PAS) staining was carried out on a further set of colonic tissue samples by Alison Bird on one section per intestinal spatial region per animal. Briefly, sections were deparaffinised, rehydrated using an alcohol gradient, and rinsed in distilled water, before oxidisation in 0.5% Periodic Acid solution for 5 minutes. The sections were again rinsed in distilled water before being placed in Schiff's reagent for 15 minutes, rinsed, then counterstained with Mayer's haematoxylin for 1 minute. Samples were thoroughly rinsed in distilled water before dehydration using an alcohol gradient and mounting.

2.8. IHC

2.8.1. NHP brains

2.8.1.1. Iba1

For all antibody dilutions tris-buffered saline (TBS) with 0.05% w/v Tween® 20 detergent (TBS-T) was used as an antibody-diluent. Iba1 was visualised in NHP brain sections using IHC staining with a fluorescent secondary antibody. Briefly, formalin-fixed paraffin embedded brain

sections were deparaffinised, rehydrated using an alcohol gradient, and rinsed in distilled water. Heat induced antigen retrieval was carried out using 10 mM sodium citrate, pH 6. Sections were rinsed in distilled water followed by TBS-T, then incubated overnight at 4ºC with rat monoclonal antibody to Iba1 (1:2000; ab283346; Abcam, UK) diluted in TBS-T with 10% goat serum. The slides were rinsed in TBS-T before application of the secondary antibody, goat anti-rat IgG Alexa Fluor® 568 (1:1000; ab175476; Abcam, UK), and Hoescht 33258 (1:1000) as the nuclear stain. Slides were incubated for 1 hour at room temperature before being mounted using Fluoroshield (Sigma-Aldrich, USA). Negative controls, where the primary antibody solution was replaced with TBS-T with 10% goat serum only, were included in each run to evaluate non-specific binding.

2.8.1.2. TH

Tyrosine hydroxylase (TH) was visualised in NHP brain sections using IHC staining with a 3,3'-diaminobenzidine (DAB) chromogen. Formalin fixed paraffin sections were deparaffinised, rehydrated using an alcohol gradient, and incubated in 1% v/v hydrogen peroxide (H_2O_2) in methanol to block endogenous peroxidases, before being rinsed in distilled water. Heat induced antigen retrieval was carried out using 10 mM Sodium citrate, pH6. Sections were washed in TBS-T before being incubated overnight at 4ºC with rabbit polyclonal antibody to TH (1:100; orb770260, BioOrbyt, UK) diluted in TBS-T with 10% goat serum. Slides were washed in TBS-T before being incubated with HRP-conjugated goat anti-rabbit IgG (1:500; ab6721, Abcam, UK) for 40 minutes at room temperature. Slides were again washed with TBS-T and then incubated with DAB staining solution (DAB Peroxidase Substrate Kit, SK-4100, Vector Laboratories, USA). Slides were counterstained with Haematoxylin Harris Acidified solution (APC Pure, UK) for 3 minutes, rinsed in distilled water, placed in 1% v/v HCl in 70% v/v ethanol in water for 15 seconds, again rinsed in distilled water, and incubated in 0.1% w/v sodium bicarbonate for 1 minute. Slides were thoroughly rinsed in distilled water before being dehydrated using an alcohol gradient, cleared in xylene and mounted in DPX (Agar Scientific, UK).

2.8.2. Mouse brains

I carried out the following IHC staining methodology on mouse brain sections using the same antigen retrieval method as described above for NHP samples. *C. albicans* was visualised in mouse brain sections using a rabbit polyclonal anti-*C. albicans* antibody (1:100 v/v; NB100-64750, Novus Biologicals, USA). Activated microglia/macrophages were visualised using rabbit anti-Iba1 (1:100 v/v; Abcam, UK). For single staining, ab178846 was used; for co-staining, ab150167. Secondary antibodies used were goat anti-rabbit IgG Alexa Fluor-594 (1:100 v/v; A11012, Invitrogen, USA), Goat Anti-Rat Alexa-647 (1:500 v/v; ab150167, Abcam, UK) or

donkey anti-rabbit IgG Alexa Fluor 488 (1:500 v/v; A21206, Invitrogen). Nuclei were stained with Hoechst 33258 (1:1000 v/v).

2.8.3. Transwell system membranes

Staining of the Transwell system membranes was carried out by Dr Emily Jones and Victoria White. Caco-2/HT29-MTX-E12 cells cultured on Transwell membrane inserts were fixed in 4% (v/v) PFA (ThermoFisher Scientific), washed twice in PBS pH 7.4, and incubated in blocking buffer (1% w/v bovine serum albumin (BSA) (Merck) and 10% goat serum (Merck) in PBS) at 20ºC for 1 hour. To visualise the interactions of yeast with Caco-2/HT29-MTX-E12 cells, inserts were incubated with a non-specific anti-yeast antibody (rabbit polyclonal anti-*C. albicans* antibody; 1:200; ab53891, Abcam) diluted in blocking buffer at 4ºC for 16 hours. After incubation, cells were washed 3 times with wash buffer (PBS with 0.05% Triton-X100; Merck) for 5 minutes on a rocking platform then incubated at 20ºC for 1 hour with goat anti-rabbit IgG AlexaFluor 647 (1:2000 v/v; A21244, Invitrogen) diluted in PBS. The secondary antibody solution was aspirated off, and the membranes were incubated with Hoescht 33342 (1:2000 v/v; ThermoFisher) and Alexa-488 Phalloidin (1:1000 v/v; ab176753, Abcam) in PBS for 30 minutes. Cells were washed 3 times with PBS. Transwell membranes were mounted using Fluoromount-G mounting medium (SouthernBiotech) and high precision coverslips (IBIDI). Membranes were imaged using a Zeiss LSM880 confocal microscope equipped with 63x/1.4 oil DIC objective and Zen black software (Zeiss) by Dr Emily Jones. Fluorescence was recorded at 405 nm (blue), 488 nm (green) and 647 nm (far-red). Images were analysed using ImageJ/FIJI v1.52p.

2.9. Image analysis

2.9.1. Mice

Images of IHC-stained brain tissue samples were collected and analysed using a Zeiss LSM880 confocal microscope and ZEN 2010 software (Zeiss, Germany), and FIJI/ImageJ v2.1.0 [277] by Dr Aimée Parker and myself. Dr Aimée Parker carried out manual quantification of *C. albicans* cells within 100 µm sagittal vibratome sections of the brain. Cells were not included in counts if they were obviously within vessels or were on the periphery of the section and therefore considered to not be truly within the brain tissue.

2.9.2. NHPs

2.9.2.1. Crypt/villi measurements

Whole brightfield slide scans were taken of the stained slides using a NanoZoomer S360 Digital Slide Scanner (Hamamatsu Phonics, Japan). All slide scans were initially evaluated using NDP.view2 software (v2.9.29) (Hamamatsu Phonics, Japan). Quantitative measurements of

villi height, mucosal tissue depth, and goblet cell area fraction was carried out using NIS Elements BR Software (Nikon, Tokyo, Japan). Quality of the tissue samples was variable, likely as a result of variation in the speed of post-mortem tissue sampling. Measurements were therefore only carried out in areas of well orientated tissue, where villi and crypts did not exhibit bending, evidence of tissue autolysis, or mechanical damage. For measurements of villi and mucosal tissue depth, samples were only included if at least 5 or 10 measurements per section could be taken, respectively.

2.9.2.2. Goblet cells

Whole slide scans were taken as described in section 2.9.2.1. In PAS-stained proximal colonic tissue samples, goblet cells were colour picked and regions of interest (ROI) were drawn around well-orientated crypts using NIS Elements BR Software. The software then determined the ratio between the two areas, hereafter referred to as goblet cell area fraction. Goblet cell area fraction was determined by measuring the ratio of goblet cell area to colonic crypt area. For goblet cell analysis, images were only included if at least 5 measurements per tissue section could be taken.

2.9.2.3. Age-associated brain pathology

Whole brightfield slide scans were taken of H&E-stained tissue sections as described in section 2.9.2.1. All slide scans were visually assessed using NDP.view2 software (v2.9.29).

2.9.2.4. Brain iron deposits

Whole brightfield slide scans were taken of Perl's Prussian blue-stained tissue sections with an Olympus VS200 Slide Scanner using the X20 objective. All slide scans were initially evaluated using Olympus VS200 Desktop (v4.0). Image regions containing the SN were extracted and cropped to a new image to enable further analysis. Images were imported into QuPath (v0.4.3). To evaluate the number of iron deposits within the SN, four square ROIs (500 x 500 µm) were created and manually placed within the SN. Iron deposits were manually counted using the "Point" tool, with annotation points added to the image to mark each positive iron deposit. The results exported to Excel (Microsoft). Four regions of interest per image, per section, per brain were analysed. Results were visualised in R (v4.3.2) using RStudio (v2024.04.2).

2.9.2.5. Iba1^{+} brain cells

Whole fluorescent slide scans were taken of Iba1 stained tissue using an Olympus VS200 Slide Scanner using the X20 objective. Fluorescence was recorded using the DAPI (blue) and Cy3 (orange) filter cubes. All slide scans were initially evaluated using Olympus VS200 Desktop (v4.0). Regions of Cy3 channel images containing the SN and the hippocampus were extracted and cropped to a new image to reduce image size and enable further analysis. Images were

analysed using ImageJ/FIJI using a custom macro (see Appendix 2) to assess Iba1$^+$ cell density. Briefly, using images of the Iba1 channel only, background pixel noise was reduced using the “Despeckle” function. The threshold was set using the same values for all images and images made binary. Four circular ROI of a specified size were placed to encompass as much of the tissue section as possible within the brain region being assessed. The “Analyse particles” function was used to count Iba1$^+$ particles within the four regions, and the results exported to Excel (Microsoft). Four regions of interest per image, per section, per brain were analysed. Images were excluded from the analysis if deemed to contain staining artefacts. Results were visualised in R (v4.3.2) using RStudio (v2024.04.2).

2.10. DNA extraction

2.10.1. Extraction of NHP luminal content/SPF mouse faecal pellets for ITS1 sequencing

Total microbial DNA was extracted from NHP luminal content by Dr Steve James and I using the QIAamp PowerFecal Pro DNA Kit (Qiagen, Germany), following manufacturer’s instructions. Dr Steve James and Dr Aimée Parker carried out microbial DNA extraction from faecal pellets collected from singly housed SPF mice. Approximately 200 mg of luminal content (NHP) or 50 mg faecal (mouse) samples were weighed out into Lysing Matrix E tubes (MP Biomedicals, USA) and homogenised using a FastPrep-24 benchtop tissue homogeniser (MP Biomedicals, USA) at 6.0 m/s for 1 min as an additional preliminary step to aid fungal cell wall disruption and improve fungal DNA recovery. Extracted DNA was quantified, and quality checked using the Qubit 3.0 fluorometer and associated Qubit dsDNA BR Assay Kit (Invitrogen, USA). DNA samples were stored at −20 °C prior to library preparation and further analysis. An empty bead-beating tube underwent the same steps as tubes containing luminal content within the DNA extraction protocol, serving as an extraction control.

2.10.2. Extraction of NHP luminal content for WGS

Total microbial DNA was extracted from NHP luminal content by Dr Aimée Parker, Dr Steve James, and I using the FastDNA^{TM} Spin Kit for Soil DNA Extraction (MP Biomedicals), following manufacturer’s instructions. Approximately 200 mg of luminal content (NHP) samples were used for DNA extraction. Extracted DNA was quantified, and quality checked using the Qubit 3.0 fluorometer and associated Qubit dsDNA BR Assay Kit (Invitrogen, USA). DNA samples were stored at −20 °C prior to library preparation and further analysis. An empty bead-beating tube underwent the same steps as tubes containing luminal content within the DNA extraction protocol, serving as an extraction control.

2.11. ITS1 amplification, library preparation, and sequencing

2.11.1. NHPs/ Mice

ITS1 amplification by PCR from genomic DNA extracted from NHP luminal content and murine faecal pellets was carried out by Dr Steve James. The fungal ITS1 region was amplified from 100 ng of template DNA by PCR using the ITS1F and ITS2 primer set [273, 274], with each primer modified at the 5′ end to include an Illumina adapter tail using the following amplification conditions: 94 °C for 5 min; 35 cycles of 92 °C for 30 s, 55 °C for 30 s, and 72 °C for 45 s; and a final extension of 72 °C for 5 min. Amplification reactions were set up in duplicate for each faecal DNA sample, and positive (50 ng *K. telluris* DNA) and negative (microbial DNA-free H_2O) controls were also included in each PCR run. The extraction control was included within the initial PCR run.

Following ITS1 PCR, library preparation was carried out by David Baker. A 0.7× SPRI purification using KAPA Pure Beads (Roche, Wilmington, MA, USA) was performed and the purified DNA was eluted in 20 µL of EB buffer (10 mM Tris-HCl). In a second PCR, library index primers were added using a Nextera XT Index Kit v2 (Illumina, UK) and amplified using the following conditions: 95 °C for 5 min: 10 cycles of 95 °C for 30 s, 55 °C for 30 s, and 72 °C for 30 s; and a final extension of 72 °C for 5 min. Following PCR, libraries were quantified using the Invitrogen™ Quant-iT dsDNA high sensitivity assay kit (Thermo Fisher, USA) and run on a FLUOstar Optima plate reader (BMG Labtech, UK). Libraries were pooled following quantification in equal quantities. The final pool was double-SPRI size selected between 0.5x and 0.7x bead volumes using KAPA Pure Beads (Roche), then quantified with a Qubit 3.0 fluorimeter and processed on a D5000 ScreenTape (Agilent), using the Agilent Tapestation 4200, to determine the final library pool molarity. The pool was then run at a final concentration of 8 pM, on an Illumina MiSeq instrument using the MiSeq® v3 (2× 300 bp) Kit (Illumina, UK) at the Quadram Institute Bioscience, Norwich. The raw data were analysed using MiSeq reporter. For NHP sequences, a mean sequence depth of 123,710 reads/sample was achieved; samples with fewer than 10,000 filtered sequences were excluded from further analysis. Libraries were also prepared from the DNA extraction control and from single fungal species DNAs (*C. albicans* and *K. telluris*) and were used as pipeline controls in the downstream bioinformatic analyses.

2.12. Mycobiome characterisation

2.12.1. NHPs

Dr Andrea Telatin, Head of Bioinformatics at QIB, carried out the characterisation of ITS1 sequencing reads. Illumina MiSeq reads were analysed using the automated pipeline Dadaist2, a dedicated workflow for ITS profiling [278]. The quality profile of the raw reads (in FASTQ

format) was assessed using SeqFu 1.9.3 [279], followed by primer removal using Cutadapt 3.5 [280] and quality filtering via Fastp 0.20.0 [281]. Locus-specific primers and conserved flanking regions were removed using ITSxpress [282]. The identification of representative sequences was performed using DADA2 [283], to produce a set of amplicon sequence variants (ASVs), and their taxonomic assignment was determined using the UNITE Fungal ITS database (release 8.3) [284]. The multiple alignment of the representative sequences was performed using ClustalO [285] and the guide tree was produced using FastTree [286]. Data normalisation and diversity were produced using the Rhea scripts [287].

Dr Steve James carried out further investigation of several of the ITS1 sequences using the National Center for Biotechnology Information (NCBI) Basic Local Alignment Search Tool (BLAST).

2.12.1.2. Data availability, analysis, and visualisation

I carried out data analysis and visualisation in R (v4.3.2) using RStudio (v2024.04.2) [288]. Custom scripts are available from the Github repository https://github.com/Cat-Elin/0924_Thesis_RScripts (September 2024).

The raw Illumina ITS1 sequence data produced by the present study have been deposited at the European Nucleotide Archive (EBI), under the Project accession number PRJEB54860. Metadata and supporting scripts are available from the GitHub repository https://github.com/quadram-institute-bioscience/nhp-gut (22nd July 2022).

2.12.2. Mice

Illumina MiSeq reads derived from mouse samples were analysed as above, except that locus specific primer removal was carried out using SeqFu (v1.8) [279]. The output feature table, taxonomic classification, phylogeny and metadata files were exported and further analysed using MicrobiomeAnalyst [289] and the built-in plotting provided by Dadaist2 by Dr Andrea Telatin and Dr Steve James. Every ASV with a zero count in all samples was removed to assess alpha diversity measures.

2.13. WGS library preparation and sequencing

2.13.1. NHPs

Library preparation was carried out by David Baker, Rhiannon Evans, and Cara-Jane Moss. Genomic DNA was quantified using the Qubit dsDNA BR Assay Kit and Qubit 3.0 fluorimeter (Invitrogen) and normalised to 5 ng/μL. Library preparation was carried out using the Illumina Nextera DNA Flex Library Prep Kit (Illumina). Genomic DNA was first tagmented by mixing 2.0μL of normalised DNA (10ng) with 0.5 μL Tagmentation Buffer 1 (TB1), 0.5 μL bead-linked transposomes (BLT) and 4.0 μL PCR-grade water per sample in a chilled 96-well plate.

Samples were heated to 55 °C for 15 minutes. The Kap2G Robust PCR kit (Merck) was combined with P7 and P5 Nextera XT Index Kit v2 index primers (Illumina), along with tagmentation mix, and amplified through PCR with the following cycling parameters: 72ºC for 3 minutes, 95 ºC for 1 minute, 14 cycles of 95 ºC for 10 s, 55 ºC for 20 s and 72 ºC for 3 minutes. Libraries were quantified using the Quant–iT dsDNA Assay high-sensitivity kit (Invitrogen), and the readings were taken by a GloMax® Explorer Multimode Microplate Reader (Promega). Following quantification, the libraries were pooled in equal quantities. The final pool was double-SPRI size selected between 0.5x and 0.7x bead volumes using KAPA Pure Beads (Roche), then quantified with a Qubit 3.0 fluorimeter and processed on a D5000 ScreenTape (Agilent), using the Agilent Tapestation 4200, to determine the final library pool molarity. PBS controls (which were processed using the same DNA extraction method as all samples) were included within the library preparation procedure. These samples failed due to low input of genomic material, suggesting no or minimal DNA contamination. Illumina sequencing was carried out on the libraries using the NovaSeq 6000 or NovaSeq X system by SourceBio (UK).

2.14. Prokaryome characterisation

2.14.1. Taxonomic and functional profiling

Raw sequence reads were trimmed to a quality of phred 30, and adapters were removed using Fastp (v0.23.1) [290]. Host reads were determined and removed by mapping reads to the cynomolgus macaque genome (*Macaca fascicularis* MFA1912RKSv2, reference genome as of March 2023) using BBmap from BBTools (v38.79) (sourceforge.net/projects/bbmap). Calculation of raw sequence reads before and after removal of contaminating reads was carried out using SeqFu (v1.17.0) [279].

Taxonomic profiling was performed on the filtered reads using MetaPhlAn (v4.1), including estimation of the unknown fraction (parameter: $--unclassified\_estimation$) with the database mpa_vJun23_CHOCOPhlAnSGB_202307 [291]. Functional read profiling was performed using HUMAnN3 (v3.9) with DIAMOND (v2.1.9) and MetaPhlAn (v4.1), using the mpa_vJun23_CHOCOPhlAnSGB_202307 and uniref90 (v201901b) databases [291-293]. Annotated reads were assigned to Metacyc pathways. Abundances of taxonomic and functional annotations were normalised using copies per million (CoPM) reads before statistical analysis.

2.14.2. Genome reconstruction and clustering

Metagenome assembled genomes (MAGs) were reconstructed from trimmed and decontaminated reads using the pipeline MetaWRAP (v1.2.1) [294]. I used a single-sample approach for metagenomic assembly and contig binning. Raw reads were assembled using MEGAHIT (v1.2.9) [295], and summary statistics of the assembly were generated using QUAST [296]. Contigs were then binned using MetaWRAP's binning module, using MetaBAT2

(v2.15) [297], Maxbin2 (v2.2.6) [298], and Concoct (v1.1.0) [299] with default settings. The results of the three different binning software were consolidated into one using MetaWRAP's bin_refinement module, with completion and contamination parameters set as 50% and 10% respectively. Bins were dereplicated using dRep (v3.4.3), yielding 1077 medium quality MAGs (completion > 50% and contamination < 10%), and 358 high quality MAGs (completion > 90% and contamination < 5%), assessed using CheckM (v1.2) [300, 301].

After metagenomic assembly and binning, MAGs were clustered at 5% genetic distance using dRep (v3.4.3) [300]. Overall, 534 species-level genome bins (SGBs) were obtained, and taxonomy assigned to each using the Genome Taxonomy Database Tool Kit (GTDB-Tk) (v2.4.0) and GTDB release 220 [302-305]. 108 SGBs were undefined at species level, representing putative novel taxa. The abundance of each SGB was quantified using MetaWRAP's quant_bin module. Abundance was normalised to copies per million (CPM).

2.14.3. Data availability, analysis, and visualisation

I carried out data analysis and visualisation in R (v4.3.2) using RStudio (v2024.04.2) [288]. Custom scripts are available from the Github repository https://github.com/Cat-Elin/0924_Thesis_RScripts (September 2024).

The raw Illumina ITS1 sequence data produced by the present study have been deposited at the NCBI Sequence Read Archive (SRA), under the Project accession number PRJNA1164203 (30th September 2024).

2.15. Alpha and beta diversity analyses

Species relative abundances were obtained from MetaPhlAn (v4.1) and DADA2, imported into R, and manipulated using the *phyloseq* package (v1.48.0) [288]. Three measures of alpha diversity were calculated (Chao1, Shannon's index, and Inverse Simpson's index) using the *alpha* function from the *microbiome* package (v1.24.0) [306]. Statistical comparisons of alpha diversity values were carried out to assess differences between intestinal regions with a linear mixed effects model (lme) using the *nlme* package (v3.1.163) in R [307]. The model specification was as follows:

$$lme(diversity \sim type,\ random\ =\ \sim 1\ |ID,\ data\ =\ data,\ method\ =\ "REML")$$

"ID" refers to each animals' unique identification code. Random effects (~1|ID) were included to account for intra-subject correlations in diversity measurements obtained from intestinal regions within the same animal. The intestinal region ("type") was included as a fixed effect to assess the relationship between the intestinal region and alpha diversity. The model is fit by maximising the restricted log-likelihood (method = "REML"). The Benjamini-Hochberg (BH) procedure was applied to the raw p-values to control for multiple comparisons and adjust for

the false discovery rate (FDR). Statistical comparisons were then carried out between age groups. Kruskall-Wallis test was used for comparisons between three age groups and the unpaired two-samples Wilcoxon test for comparisons between two age groups. Multiple pairwise comparisons were performed using Wilcoxon rank sum test with BH corrections for multiple comparisons where necessary.

To assess beta diversity, a non-metric multidimensional scaling (NMDS) ordination based on Bray-Curtis dissimilarities was performed using the *phyloseq* package. Statistical differences between age groups and intestinal regions were assessed by performing a permutational multivariate analysis of variance (PERMANOVA) with 999 permutations using the function *Adonis2* from the R package *Vegan* (v2.6.6.1) [308]. Multiple pairwise comparisons were performed using the function *pairwise.adonis2* from the package *pairwiseAdonis* (v0.4.1) [309] with BH corrections for multiple comparisons where necessary. Permutations were constrained within samples obtained from the same animal to account for intra-subject correlations in diversity measurements.

2.16. Differential abundance analyses

To assess associations between the relative abundance of taxa/ Metacyc pathways with increasing age, the prokaryotic taxonomic and functional read profiles obtained from each intestinal region were analysed individually using MaAsLin2 [310]. Continuous age was defined as a fixed effect. The following parameters were used in each analysis: $min\_prevalence = 0.4$, $max\_significance = 0.2$, $normalisation = "NONE"$, $transform = "none"$, $analysis\_method = "LM"$, $correction = "BH"$.

2.17. Plasma marker assays

Due to the opportunistic approach to NHP sample acquisition, varying numbers of samples were available for analysis throughout the period of data collection, which is reflected in the varying number of samples utilised in each plasma-based assay.

2.17.1. Chromogenic endotoxin quant kit

The concentration of bacteria; endotoxin, or lipopolysaccharide (LPS), in a cohort of cynomolgus macaques was determined in blood plasma samples using a PierceTM Chromogenic Endotoxin Quant Kit (Thermo Scientific; A39552/S), which utilises limulus amebocyte lysate (LAL) to detect bacterial endotoxins, following manufacturer's instructions.

2.17.2. ELISA

In cynomolgus macaques, the concentration of CRP, LBP, and I-FABP were determined in blood plasma samples using Monkey CRP ELISA Kit (Abcam; ab260062), a Monkey LBP Elisa Kit (Novus Biologicals; NBP2-75369), and a Monkey fatty acid binding protein 2/ I-FABP

(FABP2/I-FABP) ELISA Kit (Novus Biologicals; NBP2-82219) respectively, following manufacturer's instructions.

2.18. Statistical analysis

Unless otherwise specified, all statistical analysis was carried out in R (v4.3.2) using RStudio (v2024.04.2). Where appropriate, a value of $p < 0.05$ was considered statistically significant. Statistical analysis of microbial diversity was performed as described above in section 2.15., "Alpha and beta diversity analysis". Statistical analysis of taxa and pathway differential abundance was performed as described above in section 2.16., "Differential abundance analyses".

The correlation between age and the results of all plasma biomarker assays, intestinal crypt/villi measurements, and goblet cell area fraction was tested using the Pearson Correlation Coefficient. Where appropriate, outliers were determined using Dixon's Q test or Generalised Extreme Studentised Deviate Many-Outlier Test, using the *outliers* (v.0.15) and *PMCMRplus* packages in R, respectively [311, 312].

For all Transwell assays, statistical analysis was carried out in GraphPad Prism 5 software (version 5.04) by Victoria White and Dr Emily Jones. All data was presented as mean ± standard error of the mean (SEM). For TEER and FITC-Dextran assays, p-values were calculated using one-way analysis of variance (ANOVA) with Dunnett's multiple comparisons to determine statistical differences between groups.

Statistical analysis of NHP brain Iba1$^+$ cell counts and iron counts were carried out with a linear mixed-effects model, using the *lme4* (v1.1.35.5) package in R [313]. The model specification was as follows:

$$lmer(Count \sim AgeGroup + (1|ID), \quad data = data)$$

"ID" refers to each animals' unique identification code. Random effects (1|ID) were included to account for intra-subject correlations for repeated measurements per ROI per section per animal. Age group was included as a fixed effect to assess the relationship between the number of Iba1$^+$ cells/ iron deposits and age.

3.0. Chapter 3: Intestinal ageing and inflammageing

3.1. Introduction

Intestinal motility deteriorates with age, coinciding with age-related changes to the intestinal microbiota, the immune system, and the enteric nervous system [314-316]. These age-related changes may contribute to age-associated increases in intestinal inflammation and permeability, as well as systemic inflammation [140, 317, 318].

Histological studies have linked intestinal inflammation with altered intestinal morphology, such as a reduction in goblet cells, goblet cell mucin production, and villus and crypt distortion [319, 320]. Similar changes have also been observed in studies of ageing, although the results are often conflicting. In mice, ageing has been associated with longer villus length, a reduction in the numbers of crypts and villi, and thickening of the muscular layer [321-323]. Morphological changes to the small intestine have also been observed in multiple senescence accelerated mouse strains, although the specific alterations differed depending on the strain of mice [324]. In rats, ageing has been associated with villus blunting in the jejunum and ileum, and an increased number of goblet cells in the jejunum [158, 325]. Another study of rats found no age-associated change in duodenal or jejunal villus height, but found a reduction in ileal villus height in aged rats. Conversely, a significant age-associated increase in crypt depth was found in the duodenum and jejunum, but not ileum [326]. In humans, few studies have investigated intestinal morphology and those which exist contain small sample numbers. Two studies reported no significant morphological changes associated with age in the small intestine, while another reported that ageing is associated with blunted villi in the jejunum [327-329].

The physical separation of the microbiota from the intestinal epithelium by the mucus layers represents an important mechanism of host defence against microbiota-resident pathobionts [330]. Studies of goblet cells or the mucus layer is limited in humans, likely owing to the difficulty of obtaining samples, but one study of biopsy samples suggests that no significant thinning of the duodenal mucus layer is found to occur with age [331]. In mice the number of viable goblet cells and the thickness of the mucus layer significantly reduced with age in the colon. These changes were correlated with age-associated alterations to the faecal microbiota and a decline in expression of genes related to mucus biosynthesis, as well as increased bacterial penetration of the aged mucus layer [321, 332]. Ageing was also associated with a decline in genes encoding immune function, including those needed for T cell marker, chemokine, and immunoglobulin expression [321]. A reduction in goblet cells numbers has also been found in the ageing mouse ileum, suggesting a reduction in the mucus layer [321]. Together these findings suggest an age-related decline in gut barrier function, which may result in an increased

or dysregulated immune response to the intestinal microbiota and contribute to systemic inflammageing.

It is often hypothesised that an outcome of intestinal senescence is an increase in intestinal permeability. Supporting evidence comes from studies of mice, rats, and NHPs, and has been linked to faecal microbial dysbiosis [34, 140, 158-160, 333]. Ileal biopsies from healthy subjects ranging in age from 7-77 years also showed an age association with increased intestinal permeability to solutes, but not macromolecular particles, despite no apparent change in tight junction protein expression [162]. In contrast, sugar excretion tests have provided little evidence of increased intestinal permeability in elderly, healthy humans, although permeability has been found to be increased in elderly patients with IBS and non-insulin dependent type 2 diabetes [163-166].

Cynomolgus macaques, due to their genetic and intestinal anatomical and physiological similarities to humans present a promising model for characterising changes in morphology and barrier function in the ageing intestine [334]. An investigation of the impact of age on their intestinal tissue morphology and barrier function has, to my knowledge, not been attempted previously. In this chapter, I aim to address the hypothesis that ageing is associated with altered tissue morphology and goblet cell number in a cohort of healthy, cynomolgus macaques of differing ages. The correlation between age and concentration of multiple blood-based biomarkers relating to intestinal barrier function is also evaluated. To my knowledge, this study represents the first phenotypic characterisation of the ageing intestine in healthy cynomolgus macaques.

3.2. Results

To investigate the effect of age on intestinal tissue architecture, intestinal barrier permeability, and systemic inflammation in cynomolgus macaques, samples were collected from a subset of the cohort of cynomolgus macaques described in Section 2.1.1. All cynomolgus macaques were aged between 4-20 years and were defined as young (4-7 years), adult (8-12 years), or aged (13-20 years). All cynomolgus macaques included within the analysis in this chapter were healthy. As a result of the *ad hoc* nature of sample collection for this study, the number of animals included in each of the analyses described in this chapter ranged from 9-18 animals. The number of animals included from each age group also differed in each set of analysis. Animals from each age group are therefore represented using different colours in each plot to indicate the number of animals per group.

3.2.1. Age-associated changes to intestinal tissue architecture

First, the impact of age on mucosal tissue architecture was investigated in the intestinal tract of a cohort of cynomolgus macaques of differing ages. A classical method of determining morphological changes to the intestine is measurement of villi height and crypt depth. In this study, mucosal tissue depth is taken as a proxy for crypt depth in the large intestine. Villi height was measured in H&E-stained intestinal tissue sections taken from jejunal and ileal tissue samples, with a significant positive association between villi height and age observed in the ileum ($p=0.009$) (Figure 3.1C and 3.1D). No significant relationship was observed between mucosal tissue depth in the distal colon (Figure 3.1F). However, in the proximal colon, intestinal tissue depth was positively associated with age ($p = 0.017$) (Figure 3.1E)

Goblet cells are specialised intestinal epithelial cells which produce mucins that form the mucus layer, helping to spatially separating the intestinal microbiota from boundary epithelial cells. Here, changes in goblet cell number with age in the proximal colon were investigated by determining the goblet cell area fraction per colonic crypt, defined as the area of goblet cells in each colonic crypt divided by the area of the crypt itself. No significant change in the goblet cell area fraction of colonic crypts was observed to occur with age (Figure 3.2).

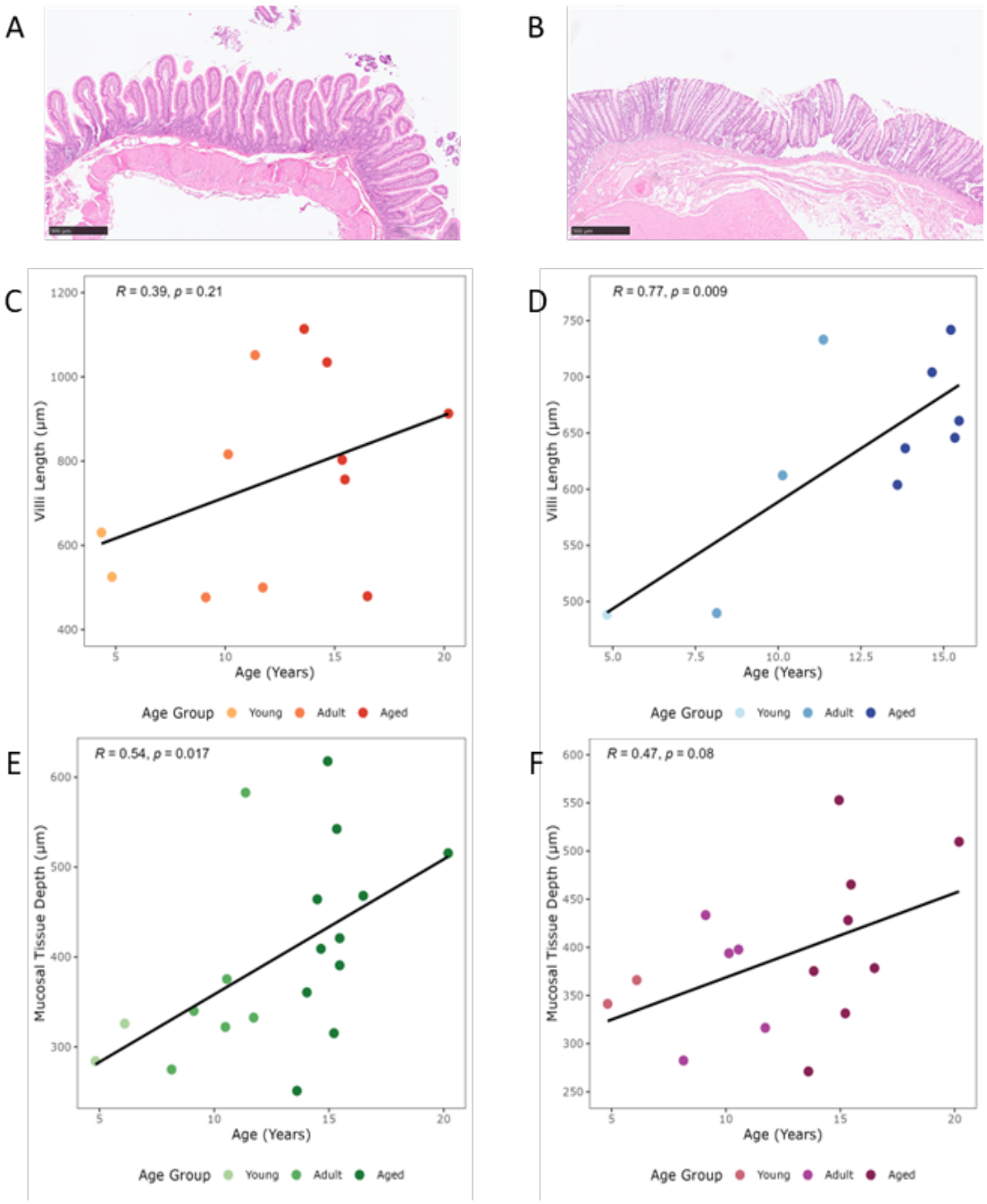

Figure 3.1. The effect of age on villi length and mucosal tissue depth in a cohort of cynomolgus macaques. Representative images of H&E-stained tissue sections from (A) small intestinal and (B) colonic tissue samples are shown. Small intestinal villi length and colonic mucosal tissue depth were measured in H&E-stained sections (minimum of 5 measurements per section/ 1 section per cynomolgus macaque in the small intestine; minimum of 10 measurements per section/ 1 section per cynomolgus macaque in the large intestine) in samples obtained from captive, healthy cynomolgus macaques aged between 4-20 years. Villi measurements were obtained in the (C) jejunum and (D) ileum. Mucosal tissue depth measurement were obtained in (E) the proximal colon and (F) the distal colon. Statistical comparisons were carried out with Pearsons Correlation Coefficient ($p < 0.05$). Image analysis was carried out using NIS Elements BR software. Scale bars = 500 µm.

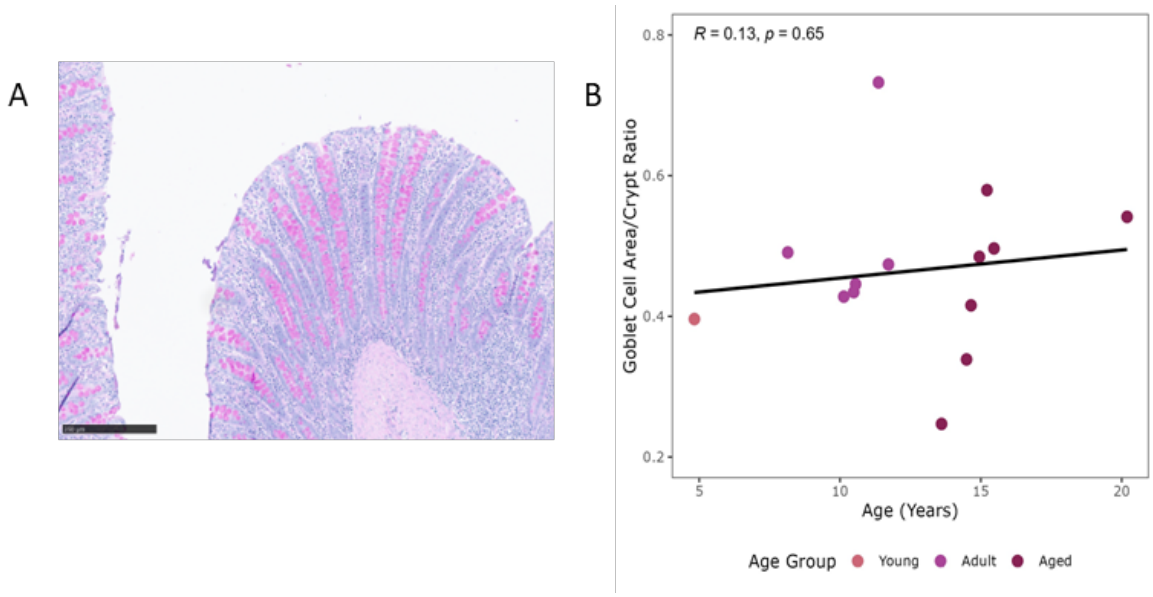

Figure 3.2. The effect of age on goblet cells located in colonic tissue crypts in a cohort of cynomolgus macaques. (A) A representative image of a colonic Periodic acid-Schiff (PAS)-stained tissue section is shown. Goblet cells are indicated by PAS staining. (B) Ratio of goblet cells to colonic crypt area shown for young, adult, and aged animals. Goblet cell area fraction determined by measuring ratio of goblet cell area to colonic crypt area in samples obtained from captive, healthy cynomolgus macaques aged between 4-20 years. The statistical association between goblet cell area/ crypt ratio and age was carried out with Pearson Correlation Coefficient ($p < 0.05$). Image analysis was carried out using NIS Elements BR software. Scale bar = 250μM.

3.2.2. Correlation between age and biomarkers of intestinal permeability and systemic inflammation

In clinical settings, the concentration of the acute phase protein CRP in the blood is a biomarker for systemic inflammation, with increased levels also associated with advancing age in humans [335-338]. In this study population of cynomolgus macaques no significant association between plasma CRP concentration and advancing age was observed (Figure 3.3A).

LBP, an acute phase protein produced primarily by hepatocytes, binds to and mediates the innate immune response to LPS in the bloodstream [339]. It is also considered to be a biomarker for intestinal permeability, as it binds LPS which may in part derive from translocation from the intestine [340]. In the present study, a positive association was observed between advancing age and LBP concentration in the blood (p = 0.042) (Figure 3.3C). Conversely, no significant association was observed between age and LPS concentration in the blood (Figure 3.3B).

Finally, I-FABP, a biomarker of intestinal barrier dysfunction, was measured. I-FABP is an intracellular protein expressed in intestinal epithelial cells that is released into the circulation as a result of damage to the intestinal mucosa. In the present cohort, plasma levels of I-FABP were not significantly associated with age (Figure 3.3D).

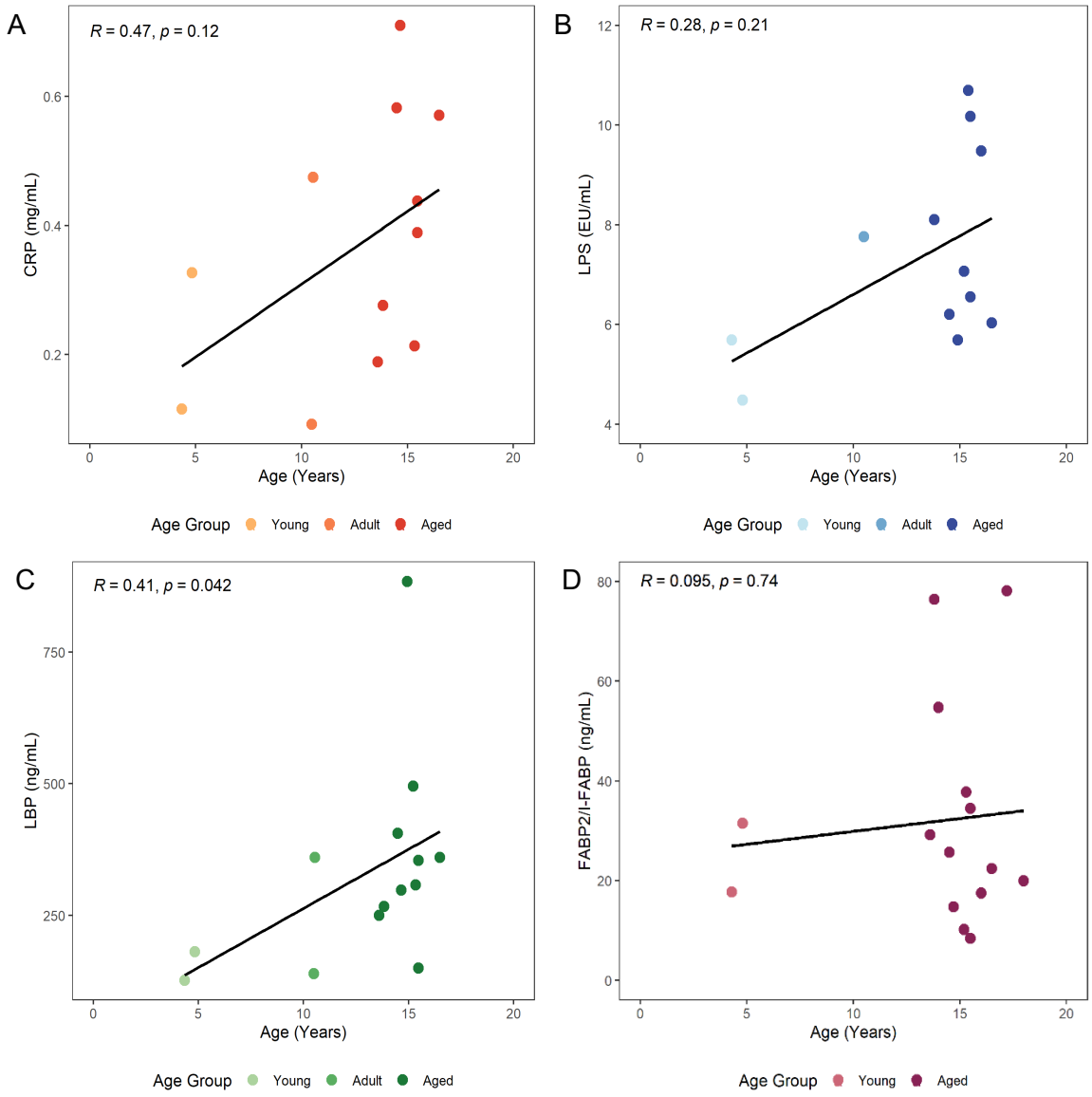

Figure 3.3. The effect of age on blood (A) C-reactive protein (CRP), (B) lipopolysaccharide (LPS), (C) plasma lipopolysaccharide binding protein (LBP) and (D) intestinal fatty acid binding protein (FABP2/I-FABP) concentration in a study population of captive, healthy cynomolgus macaques aged between 4-20 years. Statistical comparisons were carried out with Pearsons Correlation Coefficient ($p < 0.05$).

3.3. Discussion

An overview of the findings of the present study and previous human and animal studies of the effect of age on intestinal morphology and goblet cell density discussed in this chapter can be seen in Table 3.1. In this cohort of cynomolgus macaques, age was positively associated with a significant increase in mucosal tissue depth in the proximal colon. No previous studies measuring the changes in mucosal tissue depth, or crypt depth, with age in the colon exist in humans or NHPs. However, in mice colonic crypt depth, and thus mucosal tissue depth, has been described as increasing in line with severity of chronic inflammation in colonic tissues [319]. Therefore, these findings may indicate an ongoing low-grade inflammatory response in the proximal colon, resulting in an age-associated elongation of colonic crypts in this region.

Chronic inflammation is also associated with goblet cell loss in mice [319]. Goblet cell loss and decreased mucus layer thickness has been observed in the colon of ageing mice, however, no indication of goblet cell loss in the proximal colon was observed with age in the present cohort of cynomolgus macaques, despite the observed increase in mucosal tissue depth in this region [321, 332]. Overall, these findings indicate that there might be an increase in inflammatory status in the proximal colon based on tissue morphology, but it is not severe enough to impact goblet cell numbers. Further investigation of inflammatory cell infiltrates and, if samples allow, the mucus layer may be helpful in future studies to confirm age-related changes in inflammatory status in the intestine.

In the small intestine, a significant positive association was seen between age and ileal villus height in the cynomolgus macaque intestinal tract. Contrary to previous reports of villus blunting with age in rats and humans, which is often linked to chronic inflammation, our findings more closely align with a study in mice showing that ageing is associated with longer villi in the ileum [321, 325, 329]. A separate study also found a positive relationship between villus height and food intake in the jejunum of mice, with villus height being longest in mice fed a high-fat diet [341]. The authors note that this may be due to fructose content of the high-fat diet. Fructose consumption has separately been linked to improved survival of intestinal cells and increased villus height in mice [342]. This altered morphology expands small intestinal surface area, increasing nutrient absorption, and exacerbated weight gain in mice fed a high-fat diet. In the present study, the cynomolgus macaques' diet included daily fortification with fruits and vegetables. As the macaques are also housed in social groups, where hierarchical structures often influence distribution of resources, social hierarchy might result in older, higher-ranking macaques accessing more 'high value' food items, such as fruit, resulting in an increased fructose intake and accounting for the observed increase in villus height with age [343]. Study of dietary behaviour and intake in cohorts of cynomolgus macaques, as well as the impact of

increased fructose consumption on intestinal morphology in non-human primates would be required to confirm this hypothesis.

Table 3. 1. Studies investigating the effect of age on intestinal tissue morphology and goblet cell density

			Observation		
Study	Species (Cohort Size)	Age range (Sex)	Villus height	Colonic mucosal tissue or crypt depth	Goblet cell density
Present study	Cynomolgus macaques (9 – 18)	4 – 20 years (MF)	↔* jejunum, ↑ ileum	↑ proximal colon, ↔ distal colon	↔
Hassan *et al.* [325]	Rats (30)	6 – 24 months (M)	↓ jejunum	-	-
Ren *et al.* [158]	Rats (24)	3 – 24 months (M)	↓ ileum	-	-
Holt, Pascal, and Kotler [326]	Rats (24 – 28)	4 – 27 months (M)	↔ duodenum, jejunum, ↑ ileum	-	-
Sovran *et al.* [321]	Mice (10)	10 weeks – 19 months (M)	↑ ileum	↔	↓ ileum, colon
Martin, Kirkwood, and Potten [322]	Mice (38)	7 – 32 months (M)	↔ proximal small intestine, ↑ distal small intestine	-	-
Webster and Leeming [329]	Humans (16)	13 – 90 years (not reported)	↓ jejunum	-	-
Lipski, Bennett, and James [327]	Humans (47)	46 – 89 years (MF)	↔ duodenum	-	-
Corazza *et al.* [328]	Humans (38)	15 – 82 years (not reported)	↔ jejunum	-	-

M, male; F, female; MF; mixed-sex group
* ↔ indicates no change

To my knowledge, no observational studies of the impact of age on intestinal barrier permeability in cynomolgus macaques have previously been carried out. In this study, the integrity of the intestinal barrier, as well as systemic inflammation, was assessed using blood-based biomarkers (for an overview of the findings of the present study and previous human and animal studies discussed in this chapter, see Table 3.2). Specifically, the associations between age and blood concentration of LPS, LBP, CRP, and I-FABP were tested. However, LBP was the only biomarker whose concentration was observed to significantly increase with age. This is in agreement with previous findings in rhesus macaques and humans, where a positive association between blood LBP concentration and age was observed [159, 344, 345]. In humans, LBP levels have been correlated with factors such as obesity, glucose metabolism, liver function, thyroid function, and iron metabolism, among others, suggesting that heightened LBP levels might be a common factor in the development of multiple diseases [344].

Although no other significant associations between age and blood-based biomarkers were observed in the present study, a significant increase in serum CRP concentration with age has previously been observed in a cohort of captive baboons [346]. In humans, CRP has similarly been associated with increasing age, but has also been associated with increased frailty independent of age, thus decoupling chronological age from clinical metrics of inflammation [335-338]. As all animals included in the present study were healthy, this may explain why a significant association was not observed between CRP and age in this cohort of cynomolgus macaques.

A significant age-associated increase in I-FABP has also been observed in rhesus macaques [159]. I-FABP concentration was not observed to significantly increase with age in the present study, however, the disagreement between these findings may be related to the inclusion of animals of more extreme ages (> 25 years) in the study of rhesus macaques, a larger study population, methodology, and/or a species-specific effect.

An age associated increase in intestinal barrier permeability, resulting in increased translocation of bacterial LPS from the intestinal microbiome to the circulation, is postulated to be the cause of heightened LBP levels with age [340]. Supporting this theory, higher levels of inflammation and increased circulating LPS have previously been associated with age in mice [347, 348]. In the present study, the lack of a significant correlation between age and plasma LPS, despite the significant positive association between age and plasma LBP, is therefore conflicting. This inconsistency may reflect that the sample size of the present study was insufficient to fully discern the effect of age on the presence of these biomarkers in the circulation. Alternatively, the inability to discern the effect of age on LPS in the blood circulation may be related to the detection method. Under certain conditions, the LAL assay, used in the

present study to detect LPS, is known to inaccurately detect the quantity of LPS in a sample due to a masking effect [349]. While all samples were prepared and treated equally, it's possible that variations in protein or lipid content in the blood plasma may have interfered with the LAL assay, impacting the results. A third possibility is the development of an age-dependent dysregulated immune response. The reactions of mice challenged with an acute or repeated dose of LPS has suggested that the immune responses of older mice are more sensitive to LPS exposure [350, 351]. It is possible that in aged macaques, production of LBP is enhanced as a result of increased sensitivity to LPS, compared to young animals.

Table 3. 2. Studies investigating the effect of age on blood biomarkers of systemic inflammation and intestinal permeability

			Observation			
Study	Species (Cohort size)	Age range (Sex)	LPS	LBP	CRP	I-FABP
Present study	Cynomolgus macaques (9 – 18)	4 – 20 years (MF)	↔*	↑	↔	↔
Walker *et al.* [159]	Rhesus macaques (14 – 18)	15 – 27 years (MF)	-	↑	-	↑
McFarlane *et al.* [346]	Baboons (120)	2 – 26 years (MF)	-	↑	-	-
Fuke *et al.* [344]	Humans (896)	≥ 20 years (MF)	-	↑	-	-
Gonzalez-Quintela *et al.* [345]	Humans (420)	18 – 92 years (MF)	-	↑	-	-
Puzianowska-Kuźnicka *et al.* [335]	Humans (3632)	≥ 65 years (MF)	-	-	↑	-
Baumann *et al.* [347]	Mice (19)	2 – 30 months (M)	↑	-	-	-
Kim *et al.* [348]	Mice (16)	4 – 18 months (M)	↑	-	-	-

M, male; F, female; MF; mixed-sex group
* ↔ indicates no change

3.3.1. Limitations

The cohort size and number of samples available was a significant limitation. In the studies of intestinal morphology, sample size was further reduced due to tissue autolysis or mechanical trauma of intestinal tissues, limiting the collection of informative histology. Sampling procedures for future studies of the cynomolgus macaque intestinal tract should prioritise the quick removal and preservation of intestinal tissue to minimise tissue autolysis. Gut sections were also not derived from the exact same location in each animal, potentially introducing additional variability that could obscure the effect of age on intestinal morphology in each region. Future studies should include precise guidelines on sampling procedures to prevent this. Additionally, the number of samples included may not have been sufficient to account for biological variation in the morphology of the intestinal tract or biomarker expression, obscuring more subtle age-related changes [352]. Also unaccounted for are dietary factors and the time of day that the animals were euthanised. Both factors are linked to diurnal oscillations in the intestinal microbiome and the immune system and might affect the concentration of circulating immune and microbial biomarkers [353, 354]. For the analysis described here, a confirmatory study with a larger cohort of cynomolgus macaques would help reveal which associations are significant and improve confidence in the findings.

Due to the necessity of keeping cynomolgus macaques in social groups and providing a varied diet, in addition to the use of foraging for food as an enrichment activity, it is not possible to fully control their dietary intake on an individual basis. This might lead to variations in diet that are dependent on factors such as age, social hierarchy, preference, or chance. Of particular relevance to the present study, these variations might also lead to consumption of differing levels of fructose, likely due to variable fruit intake, of which increased consumption has previously been found to have an impact on intestinal morphology and nutrient absorption in mice [342]. It would be interesting to examine whether fructose consumption in cynomolgus macaques has the same effect on the intestine as in mice, as it would suggest whether this is a broader phenomenon across primates and would help to disentangle the effects of diet and age on the intestine.

Lastly, a study in ageing humans has suggested that markers of intestinal permeability and inflammation are not increased with ageing *per se* but are associated more strongly with age-related disease [163]. In this Chapter, animals with morbidities were excluded from the analysis, but this does not exclude the possibility that animals at an early stage of disease development were missed, contributing to any observations linked to increase in inflammation or intestinal permeability.

3.4. Conclusions

The findings presented here provide the first insight into the relationship between ageing and intestinal health in cynomolgus macaques, although further research is needed to clarify the impact of age on intestinal inflammation and permeability. Morphological examination showed thickening of the mucosal tissue layer in the proximal colon with age, which could be indicative of an increase in colonic inflammation. The age-associated increase in blood LBP concentration is also suggestive of age-specific changes in inflammatory status and intestinal barrier integrity, meriting further investigation. If cynomolgus macaques are to be used in studies of ageing and the microbiome-gut-brain axis, establishing the baseline level of variation in these and other measures of inflammation is both important and necessary.

4.0. Chapter 4: The intestinal prokaryome

4.1. Introduction

Microbial products and metabolites influence host hormonal, immune, and neural signalling networks which can facilitate bi-directional communication between the gut and the brain [1]. Studies of the human intestinal microbiota have demonstrated age-dependent changes in both microbial taxonomy and function [15, 17, 355, 356]. These alterations have been linked to compromised immunity, the development of neuroinflammation, and the onset of neurodegenerative diseases [34, 39, 40, 140, 357, 358]. However, few studies have directly linked age-associated pathophysiology to specific changes in microbial metabolism, partially due to the difficulty in defining what constitutes a healthy microbiome [13]. It is important therefore to characterise the intestinal microbiota in healthy ageing, both in humans and animal models, to better understand its impact on host immunity and age-related diseases.

Cynomolgus macaques, due to their genetic and physiological similarities to humans, represent an important animal model for the study of the intestinal microbiome and its role in the ageing microbiota-gut-brain axis [49, 359]. Previous studies that have isolated both microbial genes and genomes isolated from the wild cynomolgus macaque intestinal microbiome have demonstrated that it is distinct from the human microbiome, particularly that of Westernised populations, although both diet and captivity can increase their similarity [60, 360, 361].

Three studies have previously investigated the impact of age on the captive cynomolgus macaque intestinal microbiota using 16S rRNA sequencing of faecal samples [57, 64, 70]. Wei *et al.* [70] found that the Bacillota:Bacteroidota ratio was significantly increased in individually caged, captive middle-aged (7-10 years) and elderly (>13 years) male macaques compared to young adults (4-6 years). No significant change in alpha diversity was seen with age. However, beta diversity, an approach used to measure of the dissimilarity between microbial communities, differed significantly in faecal samples from middle aged and elderly macaques compared to those from young adults and infant macaques (1-2 years). Several phyla, including Bacteroidota and Fusobacteria, and genera, including those from the Ruminococcaceae, Lachnospiraceae and Prevotellaceae family, were found to be negatively associated with age. Other phyla, including Bacillota and Actinomycetota, and genera, including 6 from the Ruminococcaceae family, were positively associated with age.

Duan *et al.* [64], examined macaques aged 2-20 years and found no significant changes in faecal microbiota alpha diversity or beta diversity with age. However, they detected significant age-related shifts in the relative abundances of certain bacterial families, including a decrease in Ruminococcaceae, which has also been observed to decline with age in humans [17]. In

contrast, Yang *et al.* [57], studying macaques aged 2-15 years, reported no age-related changes in diversity or taxon abundance, except in infants (1-3 months old) who showed reduced alpha diversity and significant changes at the family and genus levels.

Yang *et al.* also found that the faecal microbiota from middle-aged (12-15 years) animals was significantly enriched in metabolic pathways related to carbohydrate, vitamin, and cofactor metabolism, as well as cellular signalling, compared to adults (7-10 years). However, no other changes in microbial community function were observed except for in infants [57]. All three studies primarily reported taxonomy at the family and genus levels, reflecting the limited taxonomic resolution of 16S rRNA sequencing. Additionally, all studies targeted the V4 region of the 16S gene, which has been found to have reduced taxonomic accuracy [93].

Reduced sequencing costs has enabled shotgun metagenomic sequencing to become an accessible alternative to 16S rRNA sequencing, with the added benefit that microorganisms from multiple taxonomic kingdoms, as well as functional potential, can be profiled from the same dataset. When analysing metagenomic datasets, there are two different strategies to classify sequencing reads to taxa. The first is taxonomy dependent, or reference-based, which compares individual sequencing reads to reference databases. The second strategy is taxonomy-independent, assembly-based methods, which rely on *de novo* assembly and do not use any reference databases [362]. Assembly-based methods require that unassembled sequencing reads are assembled into contiguous sequences (contigs). Those contigs are then grouped into distinct clusters, known as bins, which are assumed to have originated from the same population. Bins can then be taxonomically classified, after which they may be defined as a metagenome assembled genome (MAG).

Most previous shotgun metagenomic sequencing studies of the NHP intestinal microbiome have relied on assembly-based methods as the reference databases utilised in supervised strategies are not comprehensive, especially for uncultured taxa in little characterised environments or microbiomes, such as the NHP intestinal microbiota [361]. However, the reference database of MetaPhlAn4, a reference-based computational tool for assigning taxonomy to metagenomic datasets, has recently been expanded to include a much broader variety of genomes. This includes those retrieved from NHP metagenomes, which now makes the use of a reference-based classification approach feasible for studies of the NHP microbiome, even if it is still not fully comprehensive [291].

In this Chapter, I have employed both reference-based and assembly-based approaches to characterise the prokaryotic microbiota in multiple spatial regions of the intestine (from ileum to distal colon) in captive-bred cynomolgus macaques, as well as in faecal samples from a

small subset of obese and age-matched controls. The impact of age on taxonomy and functional profiles was assessed. The study provides the first characterisation and spatial analysis of the age-associated changes to the microbiota in the small and large intestine of cynomolgus macaques [57].

4.2. Results

4.2.1. Taxonomic and functional profiling of the intestinal microbiome in ageing cynomolgus macaques

To assess the impact of age on the prokaryotic intestinal microbiota, 109 samples from 6 regions of the intestine (from duodenum to distal colon) obtained from 25 cynomolgus macaques were analysed. All cynomolgus macaques were aged between 4-20 years and were sorted into three age groups, defined as: young (4-7 years; n = 4), adult (8-12 years; n = 6), and aged (13-20 years; n = 15). All animals included in this analysis were healthy except for two animals (M1464F and I153CE), who had high blood glucose levels indicative of diabetes prior to culling. These animals did not receive specific treatment for diabetes and were culled within a short time-period following diagnosis. For a detailed overview of the samples and individuals included in this analysis see Appendix 3.

After removing reads mapping to the host genome and retaining only samples with greater than 1 million reads, the final dataset comprised 65 intestinal microbiome samples from 23 cynomolgus macaques, ranging in age from 4-20 years (the number of sample reads pre- and post- filtering for host reads can be seen in Appendix 4). The dataset included samples from 4 young, 4 adult, and 15 aged macaques. These samples represented the jejunum, ileum, caecum, proximal colon, and distal colon.

Four microbiome summary statistics were first calculated at the species level. This included three measures of alpha diversity, namely Chao1, Inverse Simpson's index, and Shannon diversity. Regional-specific assessments of the relationship between age and alpha diversity were carried out (Appendix 5). An increase in microbial diversity in the distal colon of the aged cohort, as assessed by the Inverse Simpson's index, was seen compared to the young cohort ($p = 0.04$). No other significant differences were observed. For a summary of the results of the statistical tests see Appendix 6.

Following assessment of the effect of age on alpha diversity, I then compared the alpha diversity of each intestinal region (Figure 4.1A-C). These metrics revealed that both species richness and evenness were significantly increased in the caecum, the proximal colon, and the distal colon compared to the jejunum and ileum. Richness and evenness in the caecum were also significantly lower than in the proximal and distal colon (Figure 4.1D). For a summary of the results of the statistical tests see Appendix 7.

Beta diversity at the species level was assessed using an NMDS ordination plot based on Bray-Curtis community dissimilarities (Figure 4.1E). Statistical analysis indicated that there were no significant differences in community composition between age groups. However, distinct

clustering patterns were observed across different intestinal regions. The ileum and jejunum exhibited similarities in their microbial communities and formed a distinct cluster, as did the proximal and distal colon ($p<0.05$). The caecum also formed a separate cluster from all other regions ($p<0.05$). For a summary of the results of the statistical tests see Appendix 8.

Taxonomic profiles of the 65 intestinal samples were created using reference-based taxonomic profiling methods. This revealed that a large proportion of microbial genomes in these samples were uncharacterised (average relative abundance of uncharacterised taxa = 49.3% ± 13.2%) (Figure 4.2). Archaea were identified in 28 samples. Within these samples, the average relative abundance of archaea was 0.6% (± 0.6%), and the highest percentage of taxa in any sample assigned to archaea was 2.3%.

Table 4. 1. The number of prokaryotic taxa found at each taxonomic rank in the cynomolgus macaque intestinal tract

Kingdom	Phylum	Class	Order	Family	Genus	Species
Bacteria	18	297	309	331	762	1109
Archaea	2	2	2	2	6	8

Bacterial taxonomy was assessed in samples from each intestinal region. The number of taxa present at each taxonomic level can be seen in Table 4.1. Overall, the three most abundant phyla were Bacteroidota (19.7%), Bacillota (20.4%), and Pseudomonadota (7.4%), with Bacillota dominating in the small intestine (26.7%) (Figure 4.3A). At the class level and order level, Bacteroidia (18.0%) and Bacteroidales (18.0%) respectively dominated in the large intestine (Figure 4.3B and Figure 4.3C). At the family level, Clostridiaceae (17.7%) and Prevotellaceae (17.7%) were dominant in regions of the small and the large intestine, respectively (Figure 4.4A). *Segatella*, a recently defined genus derived after the division of *Prevotella* into seven distinct genera, was dominant in all large intestine at the genus level (14.4%), while *Sarcina* was dominant in the small intestine (17.4%) (Figure 4.4B) [363]. At the species level, 7 of the 10 most abundant taxa belonged to the *Segatella* genus or were candidate species belonging to the *Segatella* genus. Conversely, samples from regions of the small intestine were dominated by *Sarcina ventriculi*, an anaerobic, Gram-positive, spore-forming bacterium in the *Clostridiaceae* family, the only species belonging to the genus *Sarcina* in the present dataset (Figure 4.4C) [364]. No age-associated changes in the abundance of bacterial taxa at any taxonomic level were observed in any region.

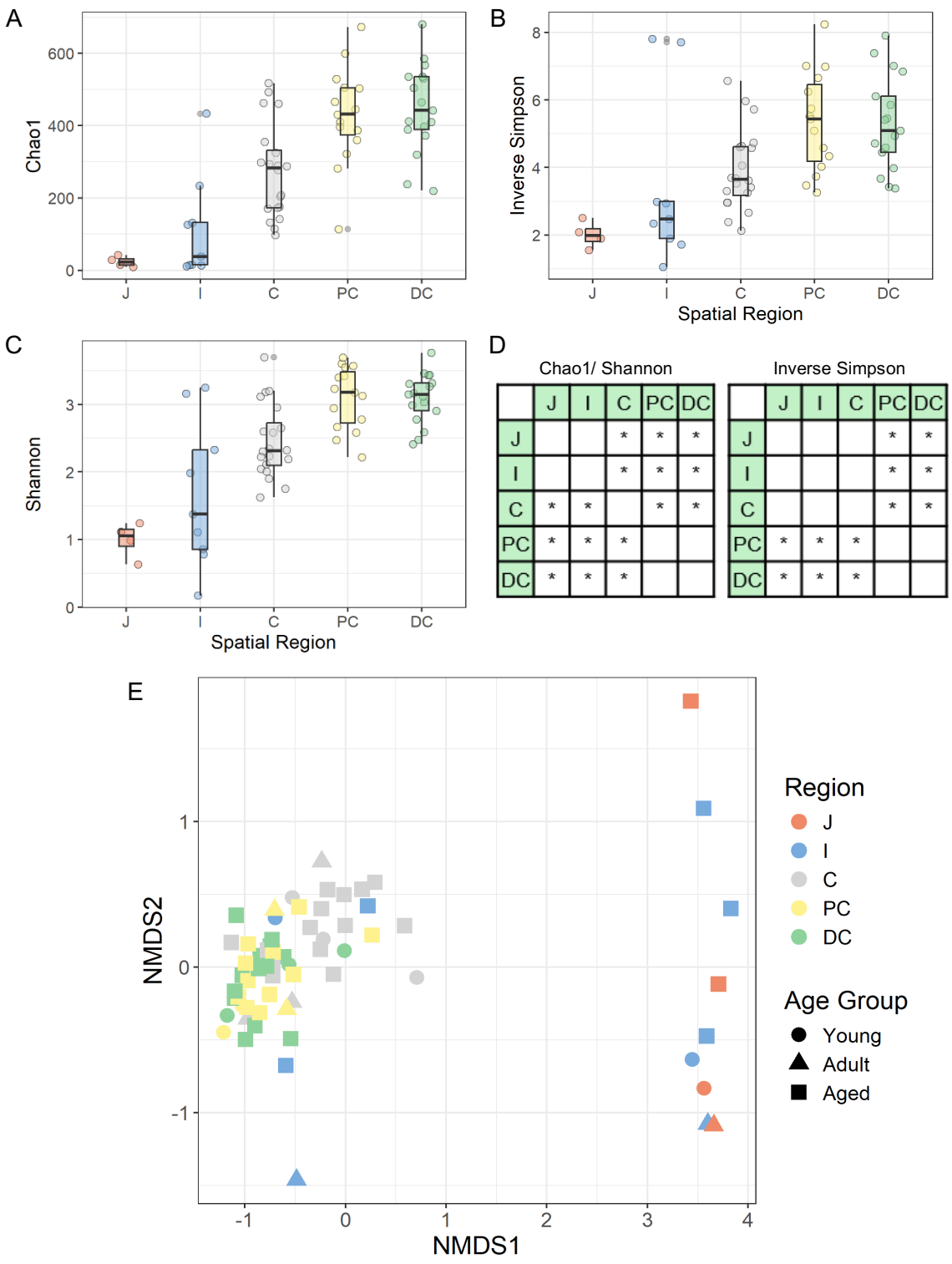

Figure 4.1. Species-level alpha and beta diversity measures of the intestinal microbiota across different regions of the intestinal tract in a group of healthy cynomolgus macaques of differing ages. Alpha diversity is assessed using three metrics: (A) Chao1 index (B) Inverse Simpson's index (C) Shannon's index. (D) Tables summarizing statistically significant differences in alpha diversity between intestinal regions (* = $p < 0.05$). (E) NMDS plot based on Bray-Curtis dissimilarity, showing the clustering of samples by intestinal region and age group. Animals were classified as young (4-7 years), adult (8-12 years), or aged (13-20 years).

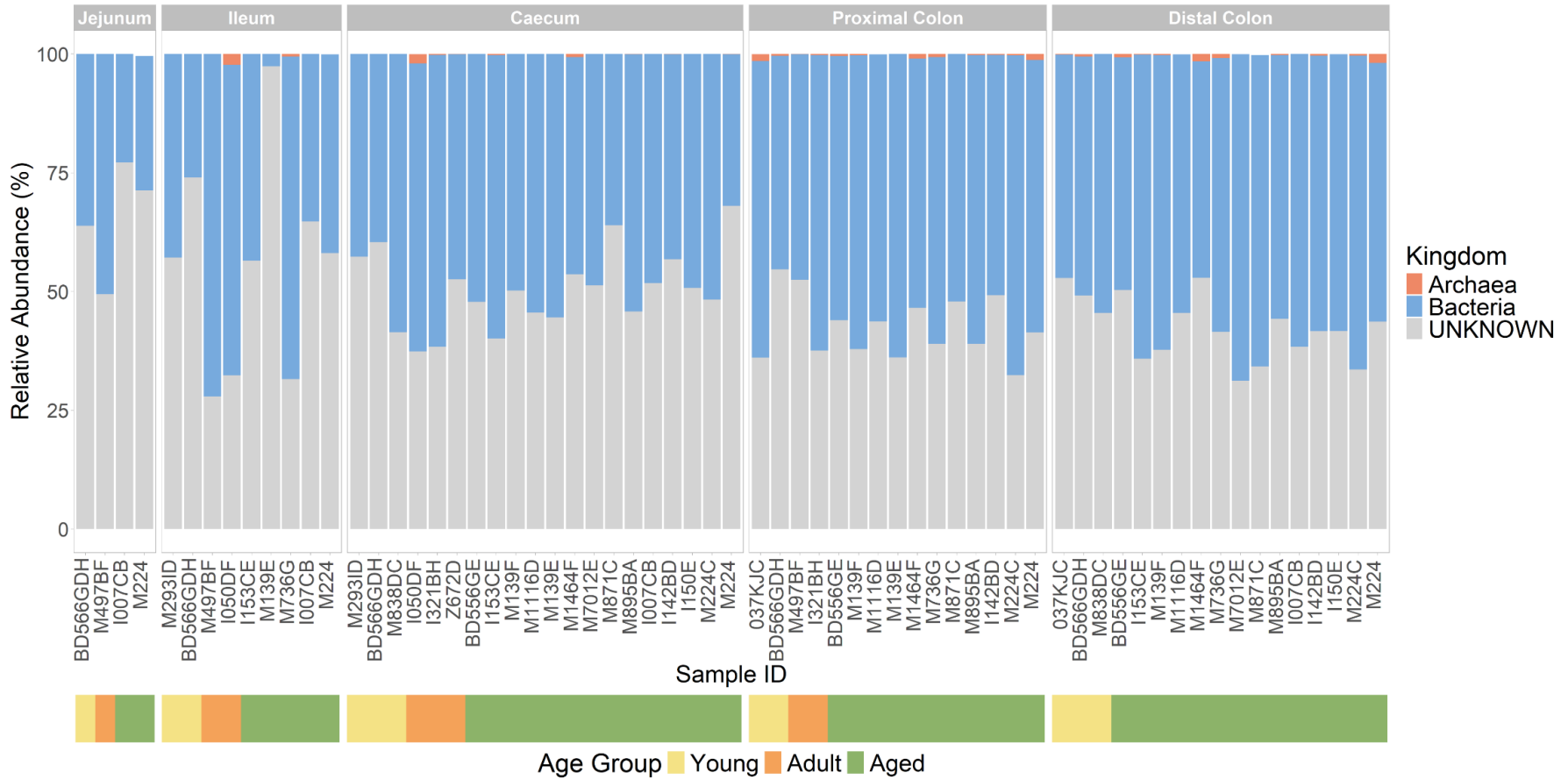

Figure 4.2. Relative abundance of microbial taxa at the kingdom level across different regions of the intestinal tract in a group of healthy cynomolgus macaques of differing ages (4-20 years). Within each facet, individual bars represent samples from different animals, arranged in order of ascending age from left to right. Animals were classified as young (4-7 years), adult (8-12 years), or aged (13-20 years). Classification is indicated by the coloured bar at the base of the plot.

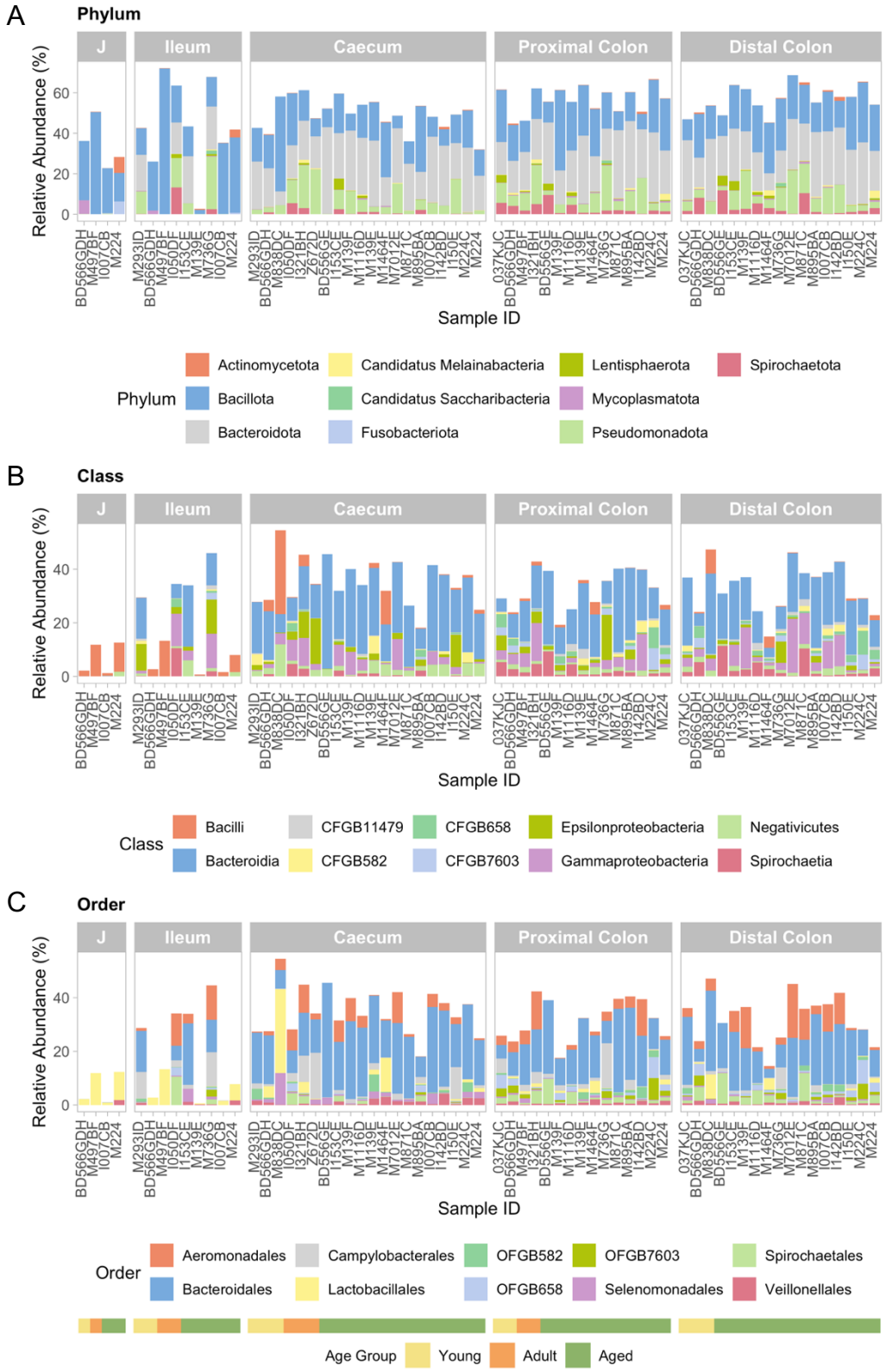

Figure 4.3. Relative abundance of the top 10 most abundant bacteria in the intestinal microbiota at the (A) phylum (B) class and (C) order level across different regions of the intestinal tract in a group of healthy cynomolgus macaques of differing ages (4-20 years). Within each facet, individual bars represent samples from different animals, arranged in order of ascending age from left to right. Animals were classified as young (4-7 years), adult (8-12 years), or aged (13-20 years). Classification is indicated by the coloured bar at the base of the plot. J = Jejunum.

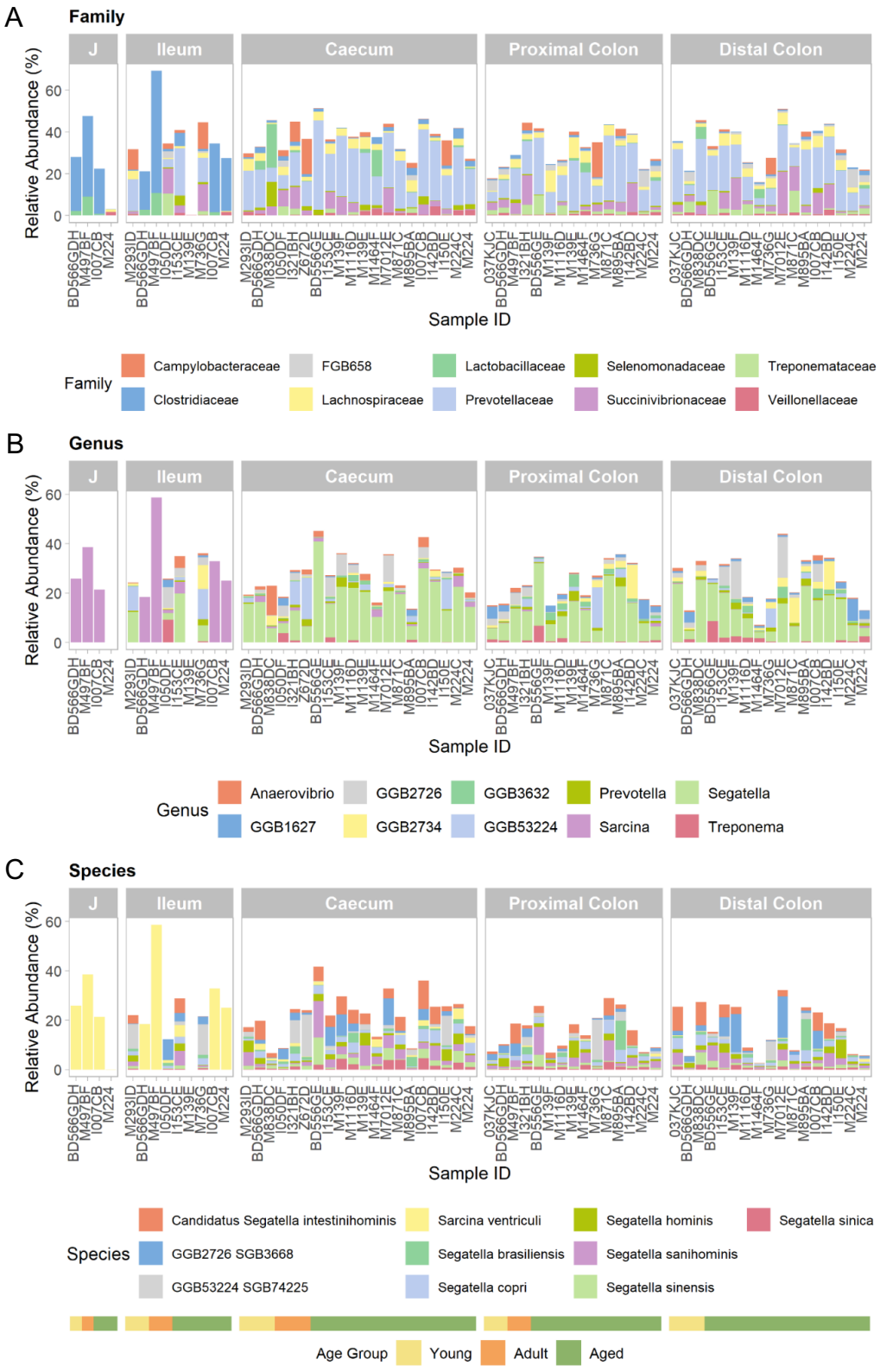

Figure 4.4. Relative abundance of the top 10 most abundant bacteria in the intestinal microbiota at the (A) family (B) genus and (C) species level across different regions of the intestinal tract in a group of healthy cynomolgus macaques of differing ages (4-20 years). Within each facet, individual bars represent samples from different animals, arranged in order of ascending age from left to right. Animals were classified as young (4-7 years), adult (8-12 years), or aged (13-20 years). Classification is indicated by the coloured bar at the base of the plot. J = Jejunum.

Due to the prevalence of *Segatella* at both the genus and species level, I investigated the number and relative abundance of all *Segatella* species across all samples at >0.1% relative abundance (Figure 4.5). *Segatella* was identified in 86% samples and in samples from all regions except the jejunum, with ten *Segatella* species or candidate *Segatella* species identified. Additionally, *Candidatus (Ca.) Segatella albertsiae* was identified at less than 0.1% abundance in a single proximal colon sample. *Segatella* species were broadly distributed across all surveyed regions.

Two archaeal phyla were seen in all surveyed intestinal regions except the jejunum: *Candidatus* Thermoplasmatota (formerly part of the Euryarchaeota phylum, but recently proposed as a novel phylum [365]) and Euryarchaeota (Figure 4.6A). No association between age and relative abundance was seen for either phylum. At the class level, these phyla were represented by Thermoplasmata and Methanobacteria (Figure 4.6B). At the order level, they were classified as Methanomassiliicoccales and Methanobacteriales (Figure 4.6C), and at the family level as *Candidatus* Methanomethylophilaceae and Methanobacteriaceae (Figure 4.7A), respectively.

Six taxa were identified at the genus level, the most dominant of which was *Methanobrevibacter* (0.3%) (Figure 4.7B). At a species level eight archaeal taxa were identified, three of which belonged to the *Methanobrevibacter* genus (Figure 4.7C). No age-associated changes in the abundance of archaeal taxa at any taxonomic level were observed in any region.

HUMAnN3, a pipeline for profiling microbial metabolic pathways, was used to predict the metabolic potential of the microbial communities in each intestinal region and produce the relative abundance of MetaCyc pathways based on the composition of microbial communities in each sample. Identified MetaCyc pathways were sorted into broader classes of higher-level organisational terms, with the resulting profiles found to be similar across all samples (Figure 4.8). For each intestinal region, the associations between MetaCyc pathway abundance and age were assessed. The only significant association found was ‘PWY.1861: Formaldehyde assimilation II (Ribulose monophosphate (RuMP) Cycle)’ in an unclassified prokaryote in the proximal colon (Coefficient = -9.03; SD = 1.60; n = 14; p = 0.00011; q = 0.19). This pathway describes the assimilation of formaldehyde in cellular biosynthesis pathways in methanotrophic bacteria [366].

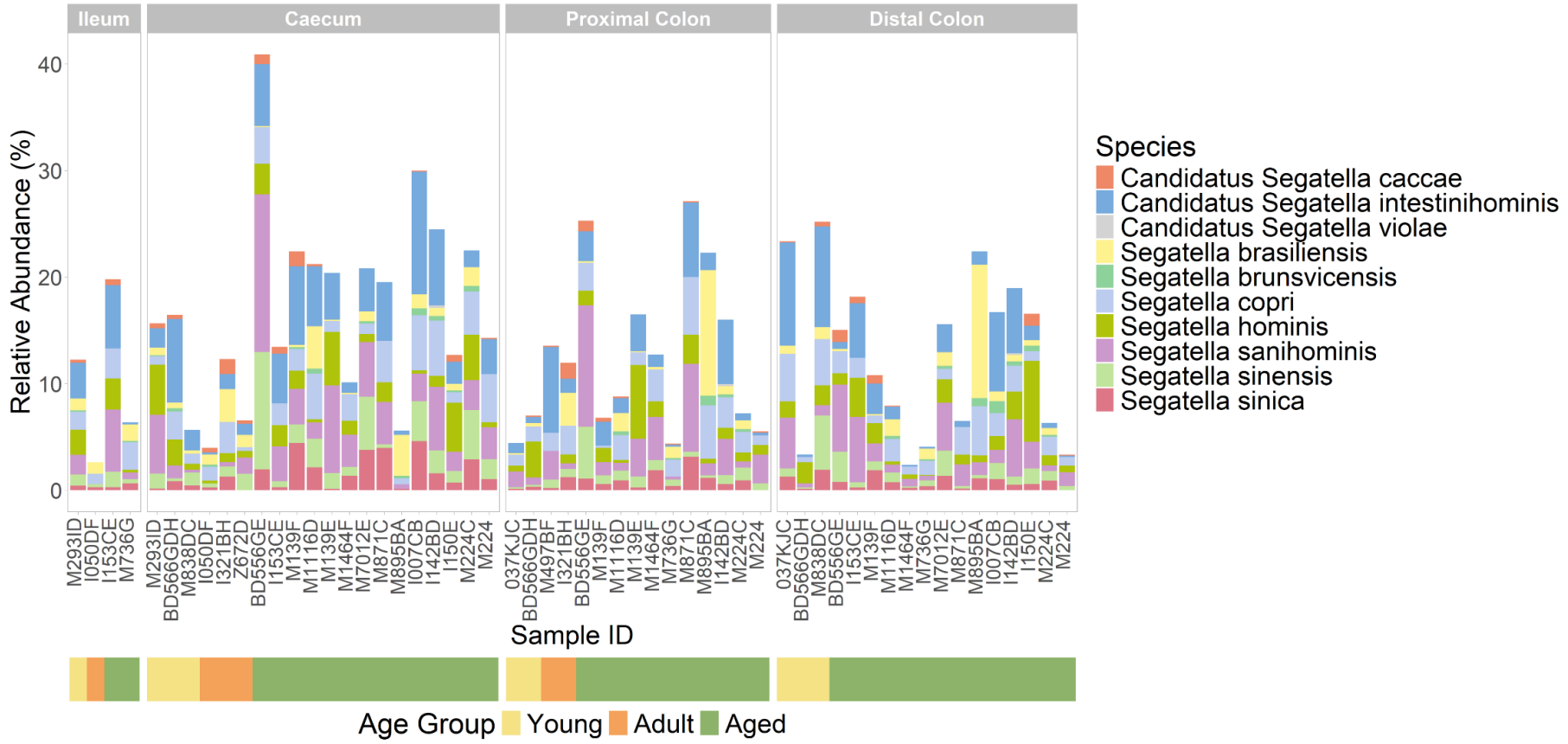

Figure 4.5. Relative abundance of *Segatella* species in the intestinal microbiota across different regions of the intestinal tract in a group of healthy cynomolgus macaques of differing ages (4-20 years). Only samples with greater than 0.1% relative abundance of *Segatella* are shown on the plot. Within each facet, individual bars represent samples from different animals, arranged in order of ascending age from left to right. Animals were classified as young (4-7 years), adult (8-12 years), or aged (13-20 years). Classification is indicated by the coloured bar at the base of the plot.

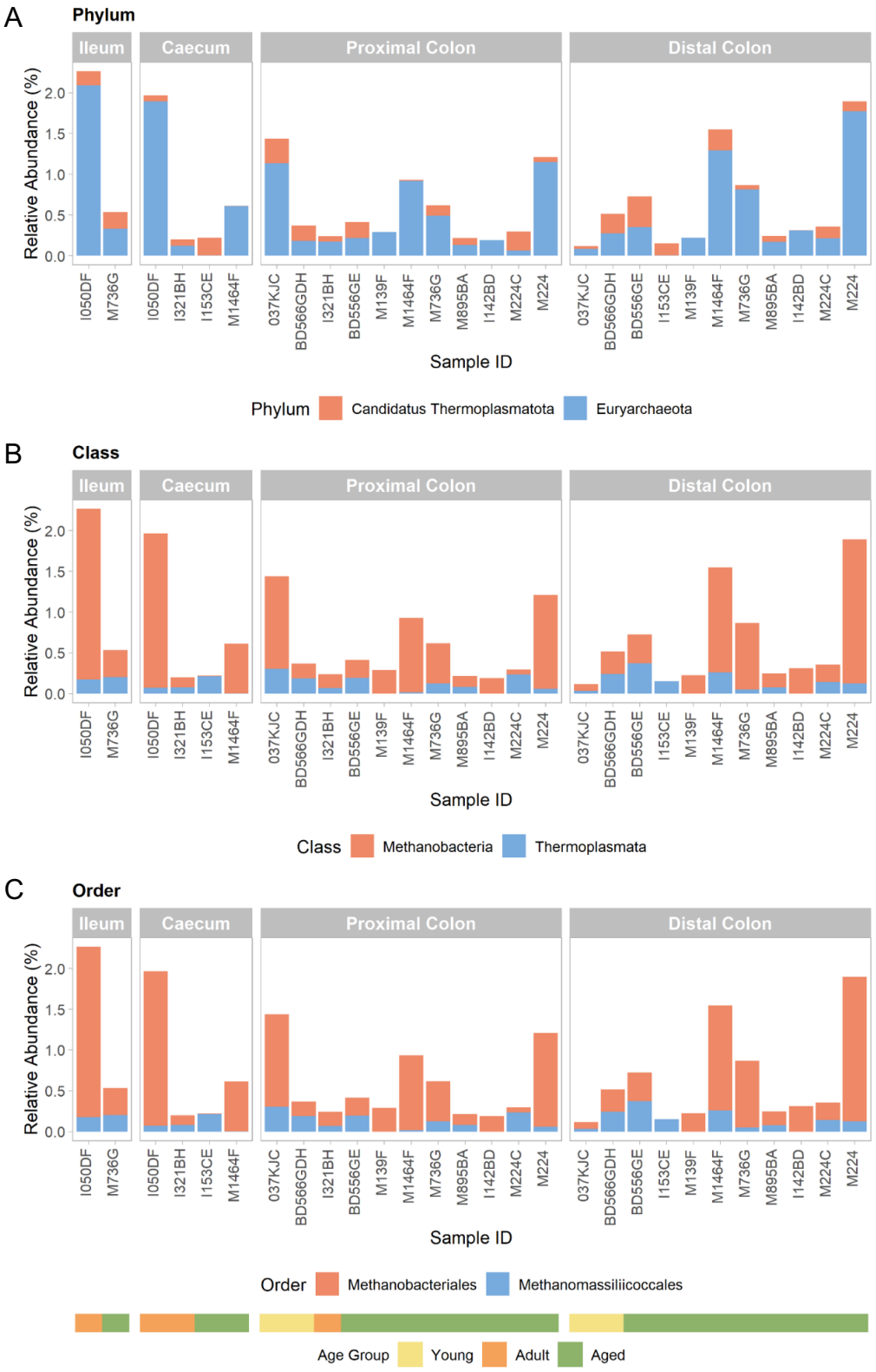

Figure 4.6. Relative abundance of the top 10 most abundant archaea in the intestinal microbiota at the (A) phylum (B) class and (C) order level across different regions of the intestinal tract in a group of healthy cynomolgus macaques of differing ages (4-20 years). Within each facet, individual bars represent samples from different animals, arranged in order of ascending age from left to right. Animals were classified as young (4-7 years), adult (8-12 years), or aged (13-20 years). Classification is indicated by the coloured bar at the base of the plot.

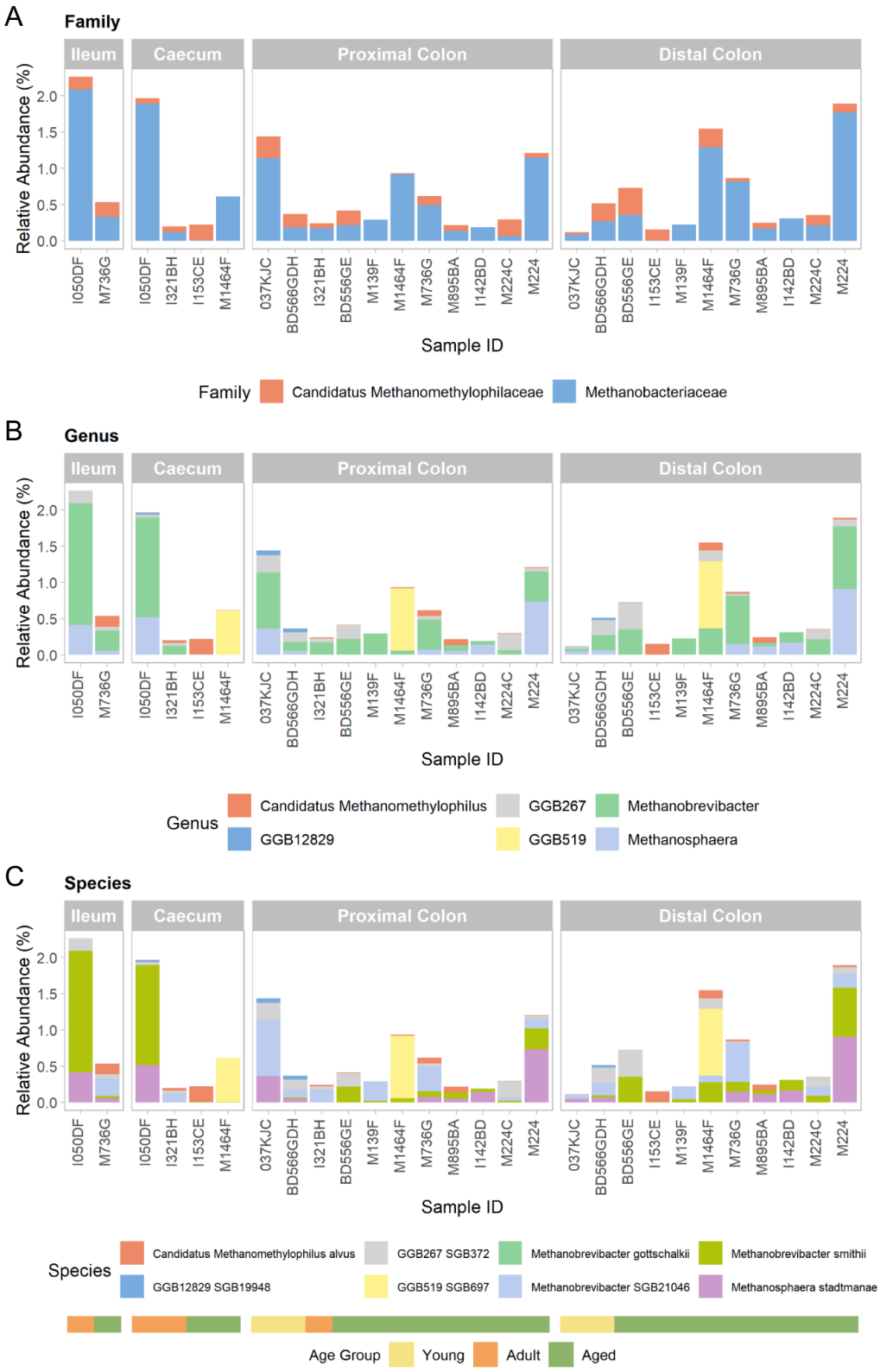

Figure 4.7. Relative abundance of the top 10 most abundant archaea in the intestinal microbiota at the (A) family (B) genus and (C) species level across different regions of the intestinal tract in a group of healthy cynomolgus macaques of differing ages (4-20 years). Within each facet, individual bars represent samples from different animals, arranged in order of ascending age from left to right. Animals were classified as young (4-7 years), adult (8-12 years), or aged (13-20 years). Classification is indicated by the coloured bar at the base of the plot.

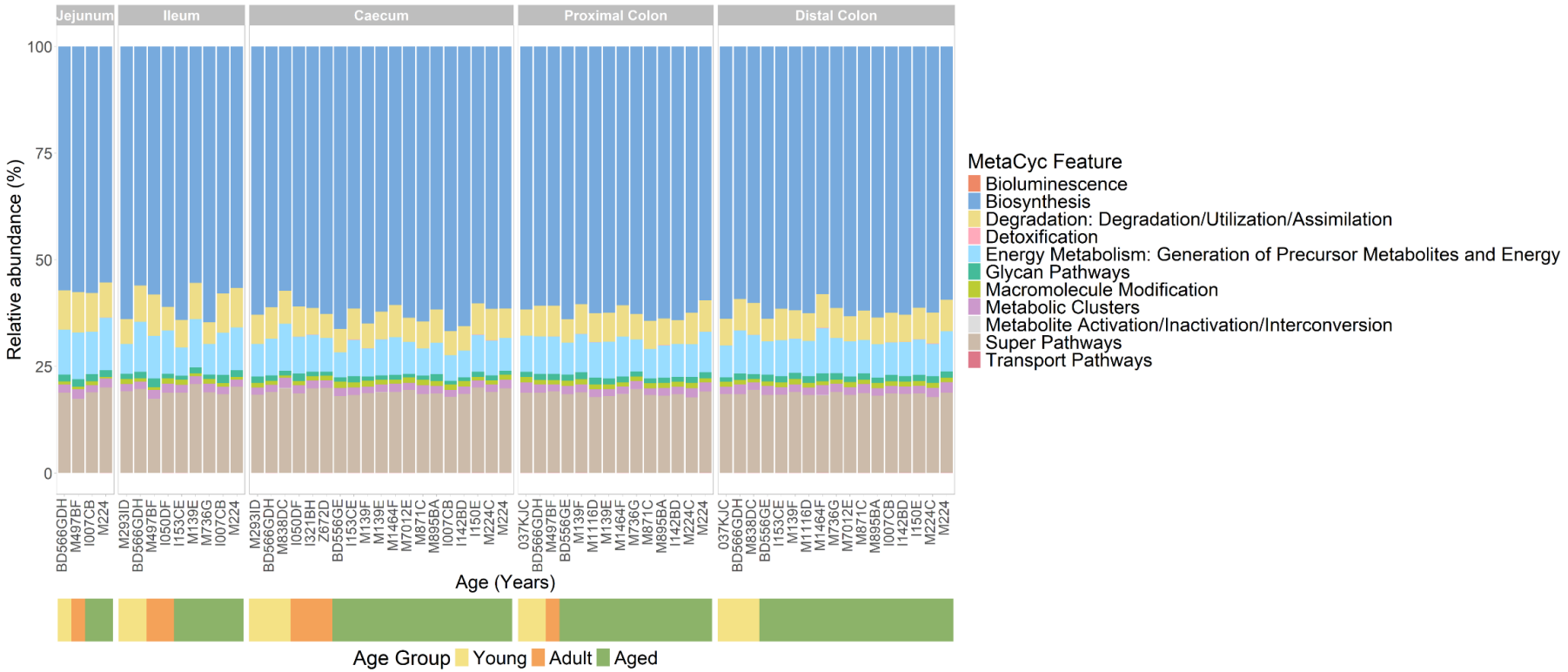

Figure 4.8. Relative abundance profiles of MetaCyc pathways across samples from different regions of the intestinal tract in a group of healthy cynomolgus macaques, aged 4-20 years. Pathways are categorised into higher-level organisational terms. Within each facet, bars represent individual samples from different animals, arranged by ascending age from left to right. Animals were classified as young (4-7 years), adult (8-12 years), or aged (13-20 years). Classification is indicated by the coloured bar at the base of the plot.

4.2.2. A taxonomic survey of the faecal microbiota of obese cynomolgus macaques

In addition to the samples collected to assess the impact of age on prokaryotic taxonomy and function in the intestinal tract, faecal samples were obtained from an obese mother (M972-AB) and daughter (M972H-AB), aged 19 and 10 years, respectively. The cause of obesity was unknown in these animals, as they were not part of any experimental trials and were not kept separate from the larger colony at the time. For comparative analysis of microbial composition, faecal samples were also obtained from healthy animals of a normal weight, matched as closely as possible by age (G30 = 10-year-olds, MHC2 = 15–16-year-olds).

Alpha diversity measures indicated that faecal samples from the obese individuals had an increased level of species richness compared to age-matched controls (Figures 4.9A-C). Beta diversity at the species level was assessed using an NMDS ordination plot based on Bray-Curtis community dissimilarities, but no clustering of samples was apparent because of age or obesity status (Figure 4.9D).

Taxonomic profiles were created using reference-based taxonomic profiling methods. As in intestinal samples, a large proportion of microbial genomes in the faecal microbiota remained uncharacterised (average relative abundance of uncharacterised taxa = 45.0% ± 7.9%). On average, bacteria accounted for 54.6% (±7.9%) of taxa, while archaea accounted for 0.4% (±0.3%). For both obese individuals and age-matched controls, the number of taxa present at each taxonomic level can be seen in Table 4.2.

Table 4. 2. The number of prokaryotic taxa found at each taxonomic rank in faecal samples from obese and non-obese cynomolgus macaques

Health Status	Kingdom	Phylum	Class	Order	Family	Genus	Species
Obese	Bacteria	17	257	260	277	608	814
	Archaea	2	2	2	2	4	5
Healthy	Bacteria	16	252	260	278	626	871
	Archaea	2	2	2	2	6	7

Overall, the three most abundant phyla were Bacteroidota (21.3%), Bacillota (24.4%), and Pseudomonadota (2.5%). In the obese animals the proportion of Bacillota was expanded compared to the age matched controls (35.9% versus 14.4%, respectively) (4.10A). At the class and order level, Bacteroidia and Bacteroidales respectively dominated in both age groups (Figures 4.10B-C). At the family level, Prevotellaceae dominated, although the abundance was reduced in the obese animals (average abundance = 4.8% and 18.5% respectively in obese

animals and age-matched controls) (Figure 4.11A). A similar reduction in *Segatella* abundance was observed at the genus level, where the average abundance of *Segatella* was 2.7% and 13.1% in obese animals and age-matched controls, respectively (Figure 4.11B). As in the intestinal microbiota, a large proportion of the top 10 most abundant species in the faecal microbiota of the obese animals and age-matched controls were *Segatella* species (Figure 4.11C). However, the overall relative abundance of all *Segatella* species of >0.1% abundance was reduced in obese animals compared to age-matched controls (2.5% and 11.4%, respectively). Archaeal taxa were the same as observed in intestinal microbiota of the ageing cohort, and no apparent changes were observed between obese animals and age-matched controls (Figures 4.12A-C & 4.13A-C).

As in intestinal tract samples, the relative abundance of MetaCyc pathways in faecal samples was assessed (Figure 4.14). While the profiles were generally consistent with those observed in the intestine, there was a small increase in the relative abundance of ‘Energy Metabolism’ pathways in obese animals, accompanied by a decrease in ‘Biosynthesis’ pathways.

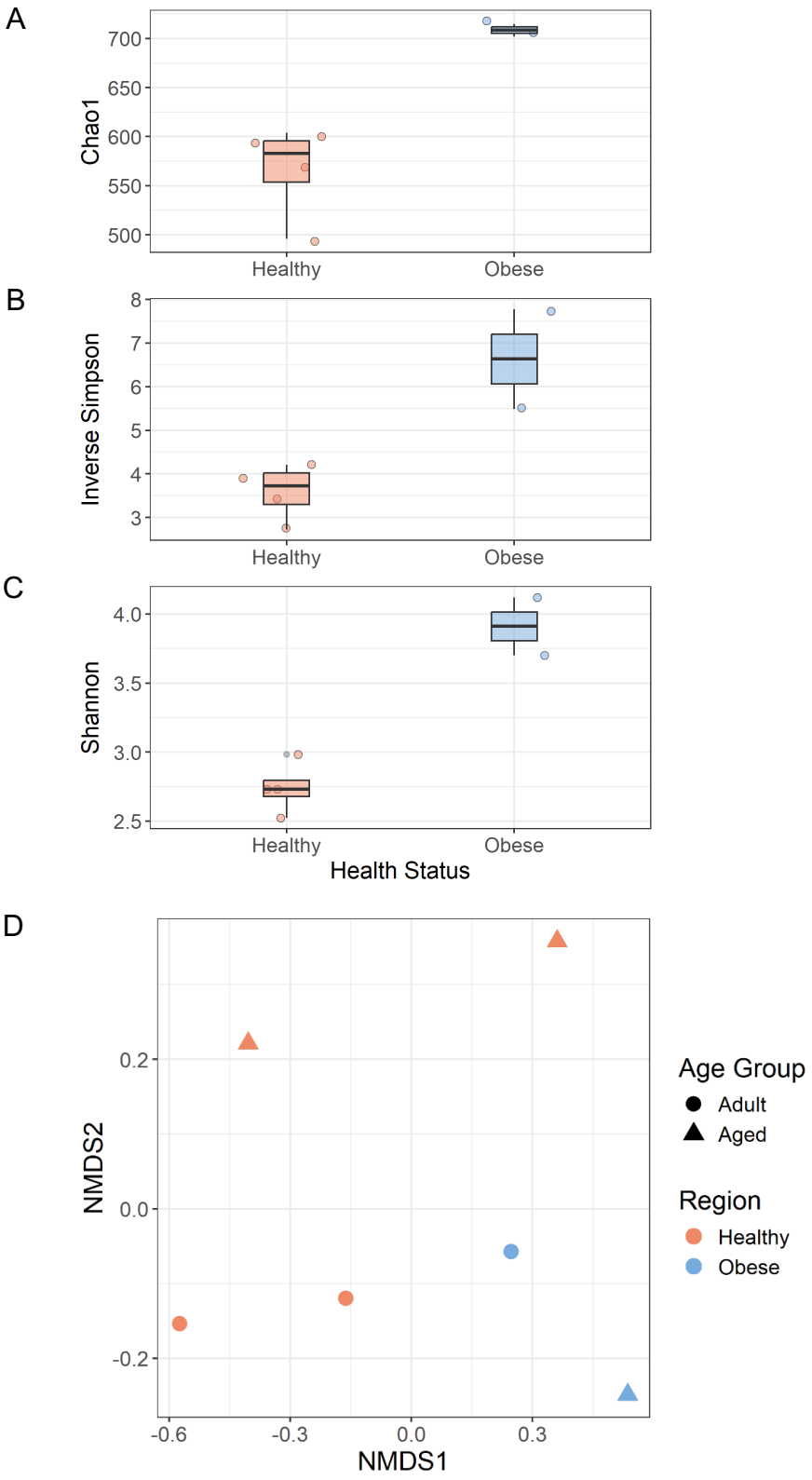

Figure 4.9. Species-level alpha and beta diversity measures of the faecal microbiota in obese cynomolgus macaques and closely age-matched controls. Alpha diversity is assessed using four metrics: (A) Chao1 index (B) Inverse Simpson's index (C) Shannon's index. (D) NMDS plot (Bray-Curtis) depicting clustering of samples by sampling region and age group. Obese animals were a mother (M972-AB, 19 years) and daughter (M972H-AB, 10 years). Animals were classified as adult (8-12 years) or aged (13-20 years).

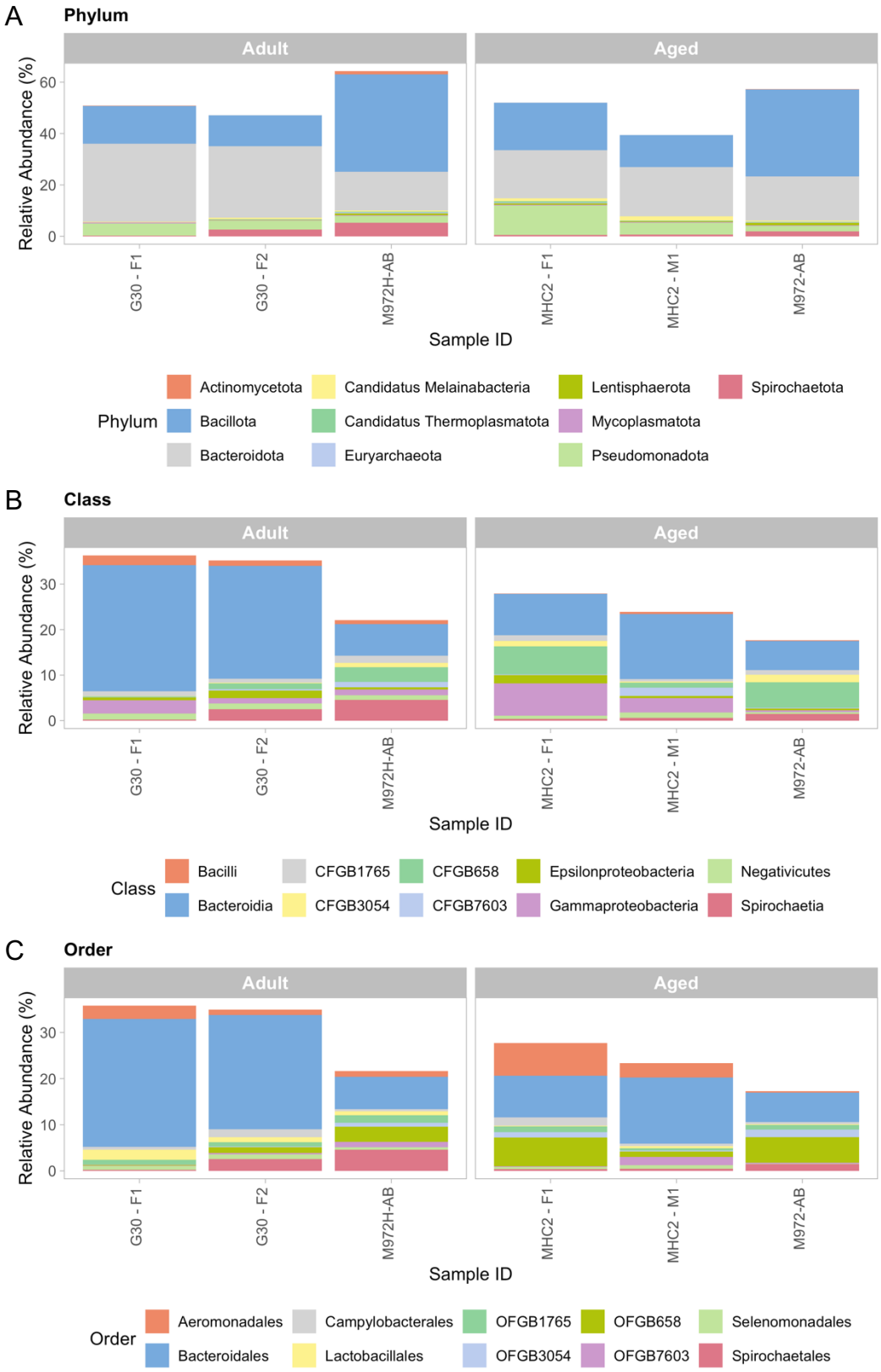

Figure 4.10. Relative abundance of the top 10 most abundant bacteria in the faecal microbiota at (A) phylum (B) class and (C) order level in obese cynomolgus macaques and closely age-matched controls. Obese animals were a mother (M972-AB, 19 years) and daughter (M972H-AB, 10 years). Animals were classified as adult (8-12 years) or aged (13-20 years).

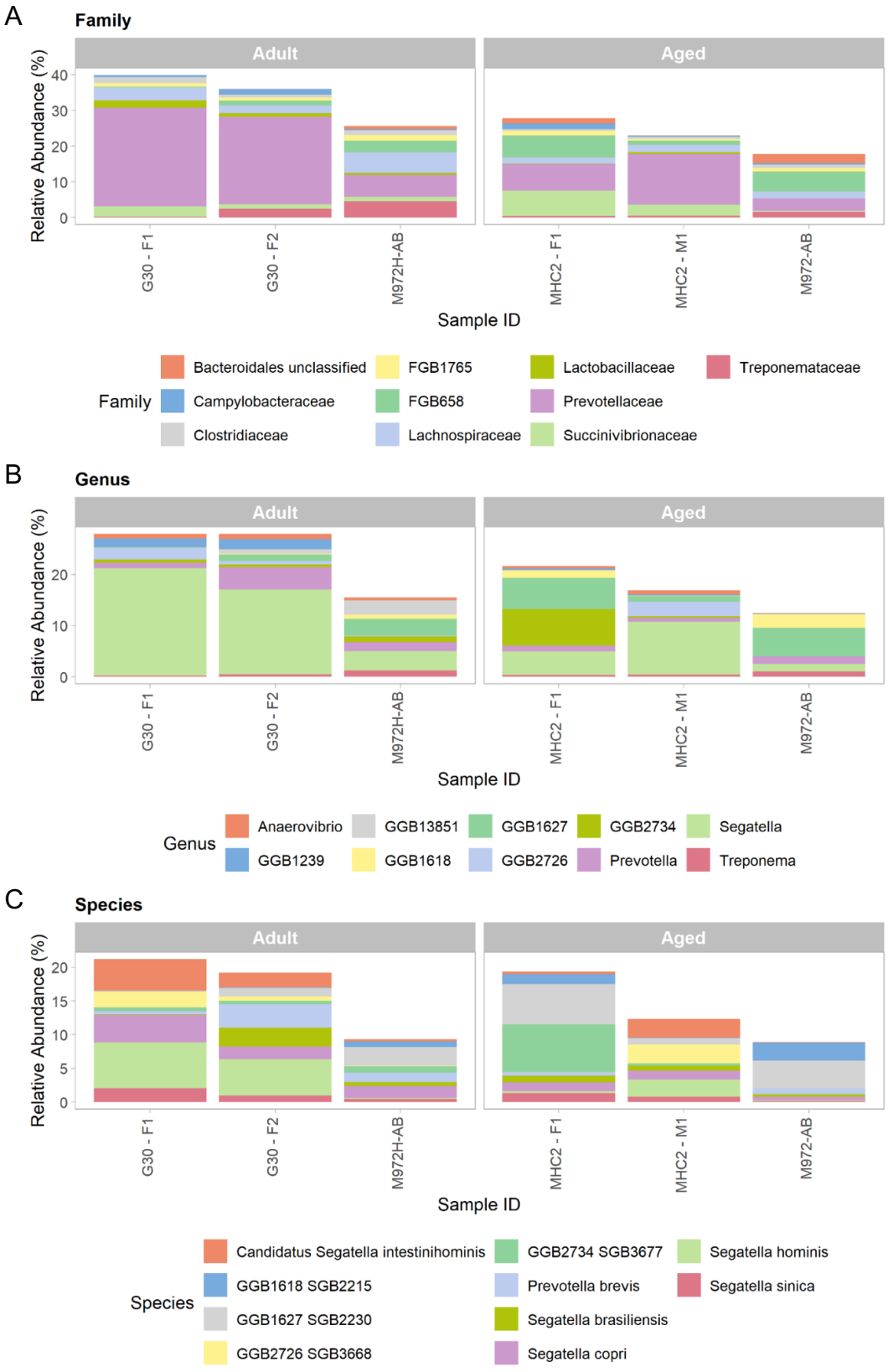

Figure 4.11. Relative abundance of the top 10 most abundant bacteria in the faecal microbiota at (A) family (B) genus and (C) species level in obese cynomolgus macaques and closely age-matched controls. Obese animals were a mother (M972-AB, 19 years) and daughter (M972H-AB, 10 years). Animals were classified as adult (8-12 years) or aged (13-20 years).

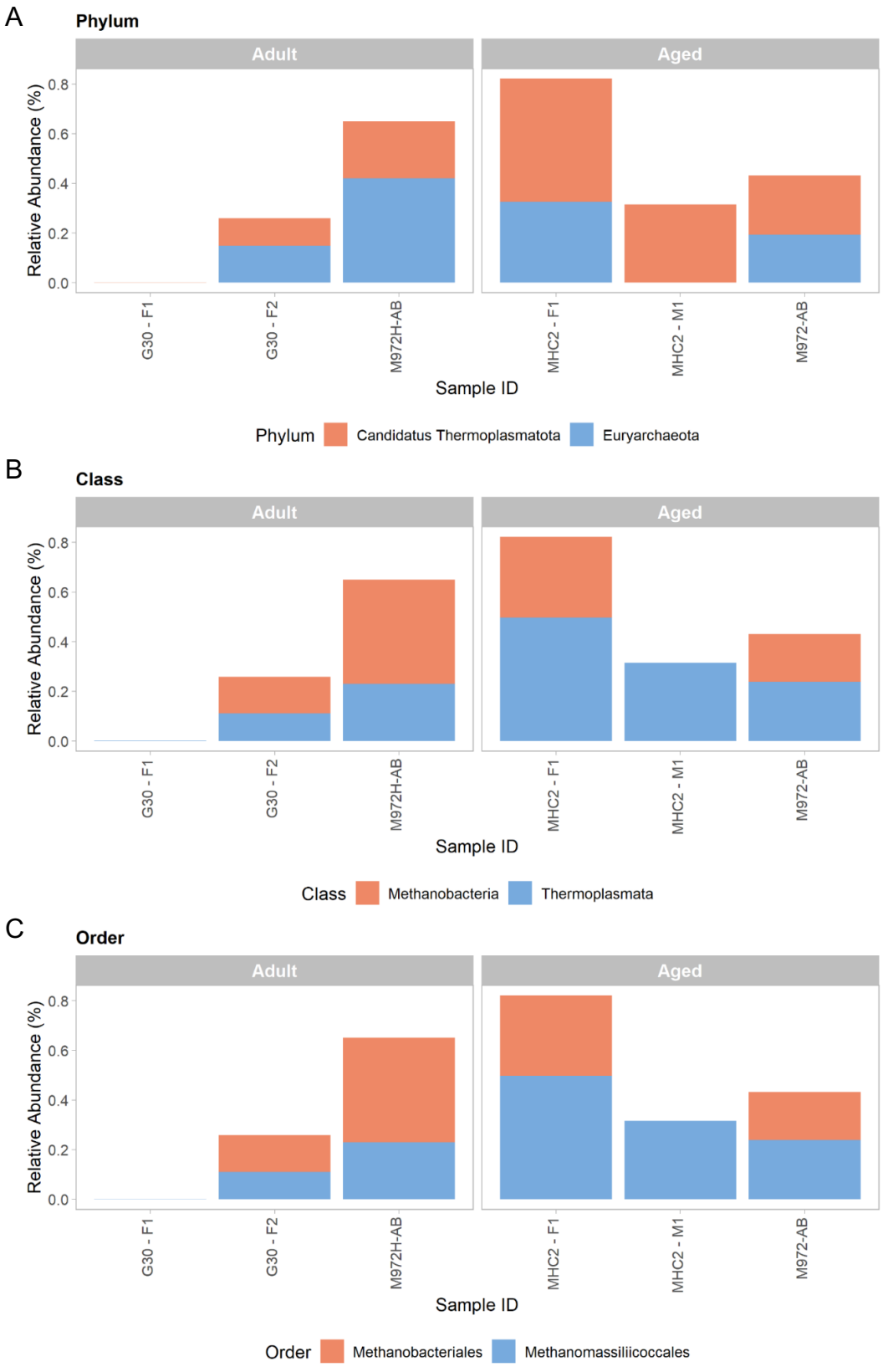

Figure 4.12. Relative abundance of the top 10 most abundant archaea in the faecal microbiota at (A) phylum (B) class and (C) order level in obese cynomolgus macaques and closely age-matched controls. Obese animals were a mother (M972-AB, 19 years) and daughter (M972H-AB, 10 years). Animals were classified as adult (8-12 years) or aged (13-20 years).

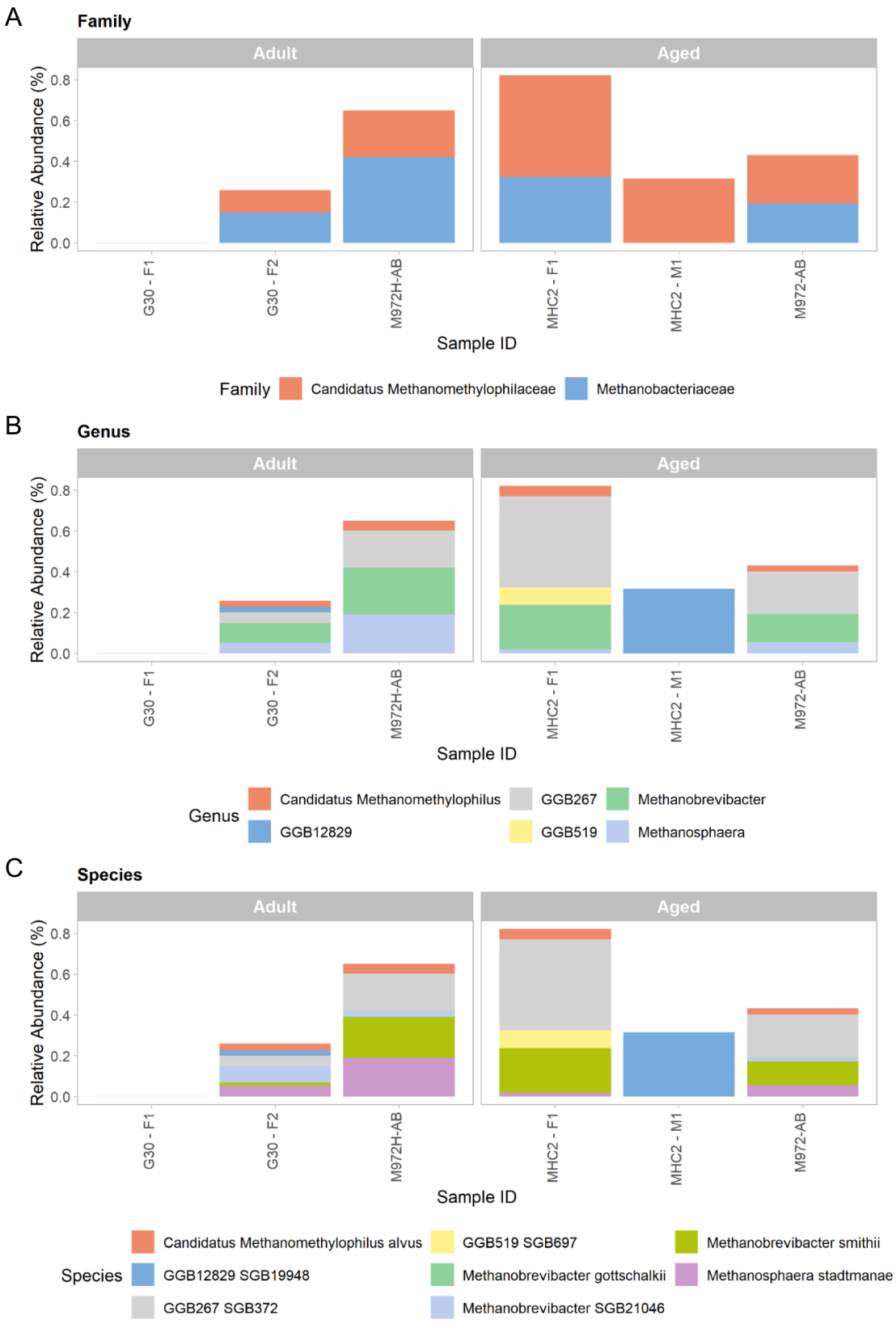

Figure 4.13. Relative abundance of the top 10 most abundant archaea in the faecal microbiota at (A) family (B) genus and (C) species level in obese cynomolgus macaques and closely age-matched controls. Obese animals were a mother (M972-AB, 19 years) and daughter (M972H-AB, 10 years). Animals were classified as adult (8-12 years) or aged (13-20 years).

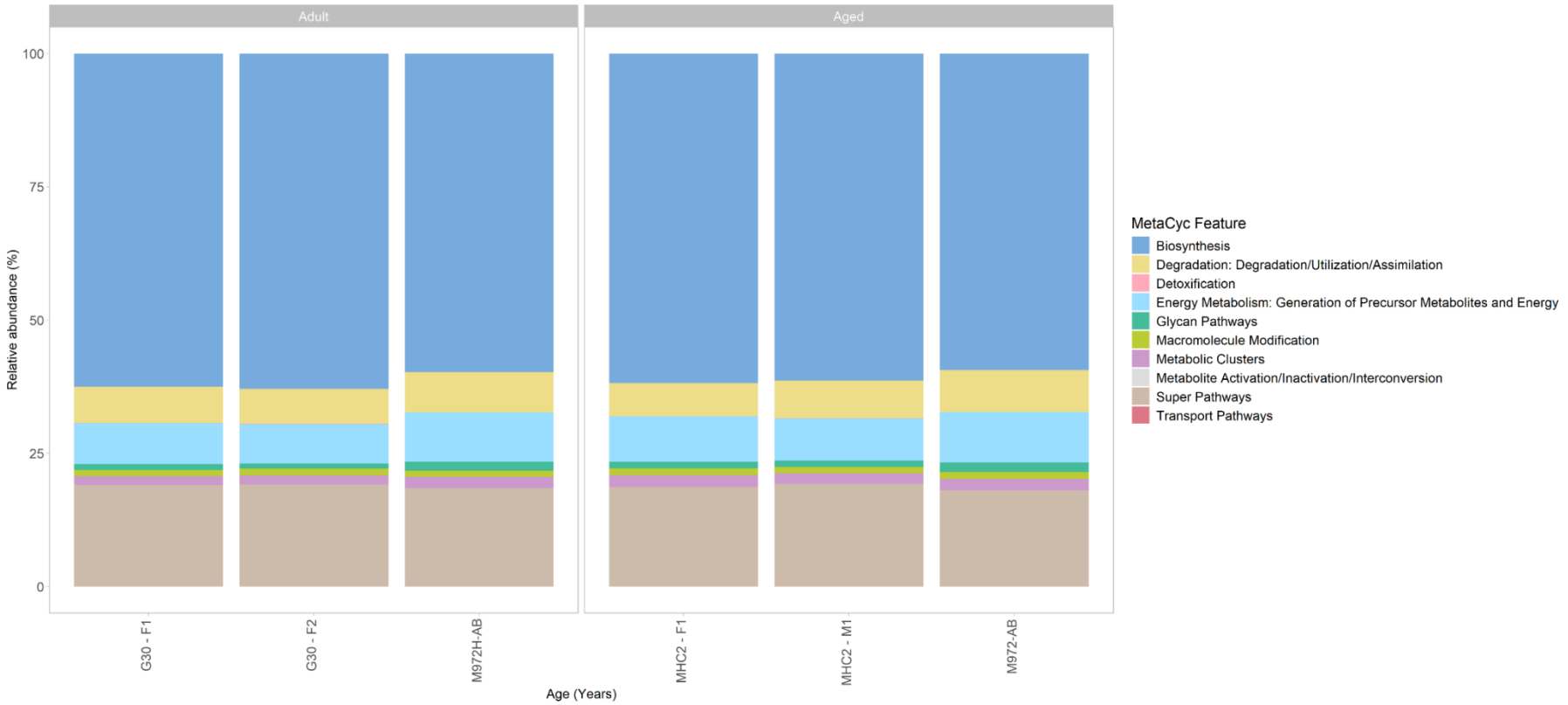

Figure 4.14. Relative abundance profiles of MetaCyc pathways in faecal samples from obese cynomolgus macaques and closely age-matched controls. Pathways are categorised into higher-level organisational terms. Obese animals were a mother (M972-AB, 19 years) and daughter (M972H-AB, 10 years). Animals were classified as adult (8-12 years) or aged (13-20 years).

4.2.3. Reconstruction of 108 putative novel genomes from cynomolgus macaque intestinal tract microbial metagenomes

A large proportion of reads remained unclassified when carrying out reference-based taxonomic profiling, highlighting the relative scarcity of microbial genomes representative for the cynomolgus macaque intestinal microbiota. Therefore, I employed an assembly-based approach to reconstruct bacterial and archaeal genomes *de novo* in all available metagenomic samples, including those from both the intestinal tract and faecal sampling. After individual sample assembly and contig binning of the 119 samples considered, 1,435 MAGs were retrieved that met the criteria of completeness > 50% and contamination < 10%, previously defined as medium quality draft genomes [367]. Of these, 358 had completeness > 90% and contamination < 5%, defined as high quality draft genomes [367].

MAGs were clustered at 95% ANI to obtain 534 species-level genome bins (SGBs), which were composed of 526 bacterial SGBs and 8 archaeal SGBs. Of SGBs not defined to species level, 106 bacterial SGBs (19.9% total bacterial SGBs) and 2 archaeal SGBs (25% total archaeal SGBs) had an average nucleotide identity of <95%, representing potentially novel species.

Taxonomic labels for all putative novel genomes were determined to genus level using the GTDB database. It should be noted that this database differs from the one used previously for reference-based profiling of intestinal microbial taxonomy, which may result in different taxonomic naming conventions. At a phylum level, 69 (65.1%) of all identified bacterial SGBs belonged to the Bacillota phylum, while the two archaeal SGBs belonged to the phyla Methanobacteriota and Thermoplasmatota (Figure 4.15A). 58 of the 69 SGBs assigned to Bacillota were represented at a class level by Clostridia. At the order level, the majority of bacterial SGBs were represented by Lachnospirales (30.2%) and Oscillospirales (17.0%), both belonging to the class Clostridia (Figure 4.15B). At a family level 29.2% bacterial SGBs were represented by taxa belonging to the Lachnospiraceae (Figure 4.15C). The two archaeal genomes were assigned to the families Megasphaeraceae and Methanobacteriaceae. At a genus level, the prevalence and abundance of all potential novel genomes in all available intestinal and faecal metagenomes was assessed (Figure 4.16). The abundance and distribution of these previously uncharacterised SGBs was relatively homogenous among faecal and large intestinal samples but appeared largely absent in samples from the small intestine.

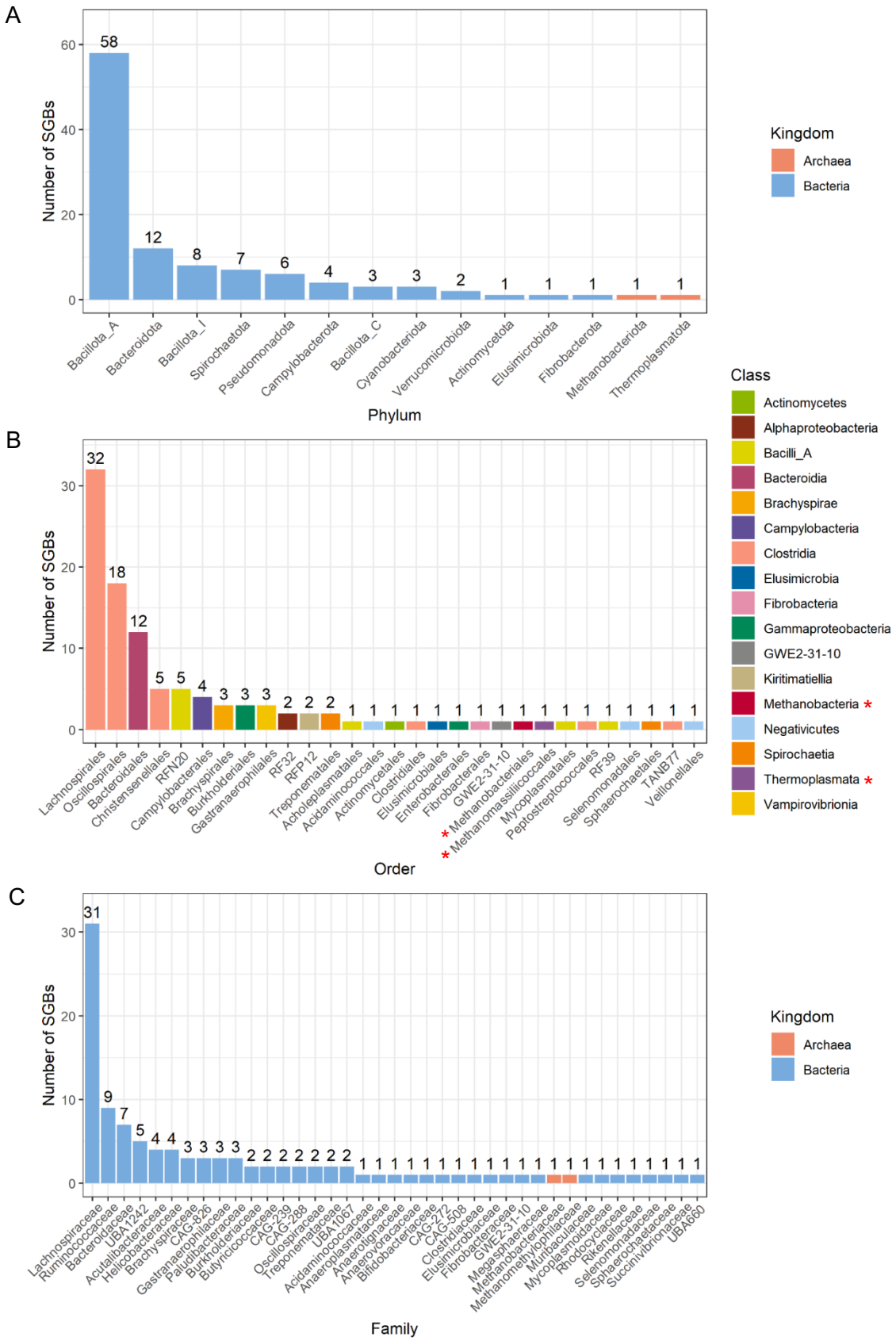

Figure 4.15. Taxonomic labels of SGBs from cynomolgus macaque intestinal and faecal metagenomes at (A) kingdom and phylum level (B) class and order level and (C) family and kingdom level. Red asterisks in (B) denote archaeal taxa.

Figure 4.16. Relative abundance of SGBs constructed from cynomolgus macaque intestinal and faecal metagenomes at genus level. Within each facet, each labelled column represents an individual sample from different animals. Abundance values are Log10 transformed. Grey represents absent taxa.

4.3. Discussion

4.3.1. Captivity may have altered the cynomolgus macaque microbiota

Taxonomic profiling of bacteria in the intestinal microbiota of cynomolgus macaques of differing ages revealed that Bacteroidota, Bacillota, and Pseudomonadota were the most abundant phyla, although the proportion of Pseudomonadota was reduced compared to the other two phyla. This aligns with previous studies of cynomolgus macaques, but contrasts with a study comparing the faecal microbiota in humans, wild rhesus macaques, and wild hybrids of rhesus and cynomolgus macaques, which found approximately equal proportions of Bacteroidota, Bacillota, and Pseudomonadota in the macaque microbiota [57, 64, 70, 92]. In comparison, human samples were dominated by Bacteroidota and Bacillota, with less than 5% Pseudomonadota, more closely aligning with the findings in the present study [92]. Previous studies have shown that captivity causes shifts in the faecal microbiota of NHPs, with a survey of the faecal microbiota in both captive and wild douc langurs and howler monkeys finding that captivity causes their microbiota to become more similar to the modern human microbiota [60, 368]. Here, therefore, the reduced proportion of Pseudomonadota in cynomolgus macaques may be a result of captivity, although species-specific differences may also play a role.

The genus *Segatella* was notably abundant in the bacterial intestinal microbiota in the caecum, proximal colon, and distal colon in healthy animals of the present cohort. Further investigation of the prevalence of all *Segatella* species at >0.1% abundance revealed a broad distribution of ten *Segatella* species from the ileum to the distal colon.

Before the *Prevotella* genus was divided into seven distinct genera, including *Segatella*, an increased abundance of *Prevotella* was reported to be associated with the microbiomes of non-Westernised human populations, or those which typically follow plant-based, low-fat, high-fibre diets, such as the Mediterranean diet [58, 369-373]. Many of these studies could only assign taxa to genus, not species, level, although two studies did specifically identify *P. copri* within the *Prevotella* genus [58, 372]. These studies were conducted prior to the taxonomic revision and expansion of *S. copri* into a complex encompassing thirteen distinct and genetically diverse species, so it remains unclear whether the species identified as *P. copri* would now correspond to one or more *Segatella* species. The taxonomic reclassification of *S. copri* utilised genomes identified from both human and NHP metagenomes [374]. This previously unrealised diversity in *S. copri* may account for why it's presence in the intestinal microbiota has previously been linked to both positive and negative health outcomes, as different species may exert distinct effects in the intestinal microbial community and on the host [375-380]. However, none of the thirteen identified *Segatella* species were found to be associated with age, BMI, or disease [374].

Four of the thirteen new *S. copri* species were primarily retrieved from NHP metagenomic datasets (*Ca. S. intestinihominis, Ca. S. violae, Ca. S. mututuai,* and *Ca. S. papionsis*). However, of these, only *Ca. S. violae* was identified in the present study [374]. The remaining nine species were primarily retrieved from human metagenomes and were all present in the current dataset. Blanco-Míguez *et al.* subsequently investigated the human metagenomes from which these nine human-associated *Segatella* genomes were originally isolated. Consistent with previous studies, they found that the prevalence and diversity of these species were higher in non-westernised human populations [374, 375]. *S. copri, S. brunsvicensis, S. sinensis*, and *S. brasiliensis* were also prevalent in 20-25% of ancient metagenomes. Human-associated *Segatella* genomes were also prevalent in faecal metagenomes from a cohort of captive cynomolgus macaques, aligning with the present study's findings [374].

In the present study, the prevalence of *Segatella* across the lifespan in healthy cynomolgus macaques mirrors the levels observed in non-Westernised human populations. This similarity is likely a result of the macaques' plant-based, high-fibre diet, supporting the hypothesis that a low-fibre Western diet may drive the loss of *Segatella* in the intestinal microbiome [58, 369-373]. Interestingly, the colonic microbiota of wild-born cynomolgus macaques housed in captivity showed an enrichment in *S. copri* after one year, as well as a reduction in alpha diversity [60]. The database used for bacterial classification in this study precedes the reclassification of *S. copri* into thirteen distinct species, so it is unknown which species in the *S. copri* complex are referred to in this study. As the authors note, the reduction in *S. copri* (complex) may be a result of differences in diet and environment, as well as an increase in human contact. In the present study, the prevalence of human-associated *Segatella* species in healthy cynomolgus macaques raises the question of whether their prevalence and abundance are linked to the colony's captivity and interaction with human handlers, altering their intestinal microbiota composition from what it would be in their natural environment [374]. In future work, it would be interesting to profile the intestinal microbiome of a similar cohort of captive cynomolgus macaques and their human handlers to assess the overlap between their microbial communities. This may be achieved via classification of metagenomes obtained from faecal samples at sub-species or strain level. An increased proportion of strains shared between the two groups would be indicative of direct transmission occurring as a result of social interactions [381, 382]. However, a previous study of strain transmission in a wild baboon population identified that shared environmental characteristics were also a significant factor that resulted in increased strain sharing between individuals, even in animals that did not interact directly, obscuring the ability to identify socially-determined transmission networks [382]. To determine whether a transmission network exists between captive-bred cynomolgus macaques and their

human handlers, it may therefore be beneficial to incorporate longitudinal sampling into the study design to assess recently acquired strains in each group, as well as strain persistence.

4.3.2. A microbial signature for obesity in cynomolgus macaques?

In faecal samples from obese animals, differences in microbial taxonomy were evident when compared to non-obese age-matched controls. Most notably, this included an expansion of the Bacillota phylum, a reduction in the abundance of *Segatella* species, and an increase in alpha diversity in the obese faecal microbiota. This increase in alpha diversity contrasts with previous findings in humans, which have reported reduced diversity in the faecal microbiota of obese individuals [383]. The reduction in *Segatella* species abundance both aligns and contradicts with previous studies of *Prevotella* abundance in obese individuals. As described above, this discrepancy may be explained by these studies preceding the reclassification of *Prevotella* to multiple genera, including *Segatella*, and *S. copri* to a clade comprising of thirteen distinct species [363, 374, 384, 385]. Other variables, such as ethnicity, diet, and socioeconomic status, have also been shown to affect the relationship between obesity, alpha diversity and the relative abundance of *Prevotella*/*Segatella*, which likely also contributes to the lack of consensus of the relationship between these variables [385].

A higher Bacillota:Bacteroidota ratio aligns with previous findings in obese animal models, although evidence in mice suggests that an increased proportion of Bacillota is more strongly associated with diet-induced obesity rather than genetic obesity [386, 387]. In humans, the relationship between the Bacillota:Bacteroidota ratio and obesity is less clear, with studies reporting positive, negative, or no association between the two variables [383, 388-392]. In studies that found a positive association, this was primarily due to a reduction in Bacteroidota rather than an expansion of Bacillota [383, 389]. The faecal microbiome has also been shown to alter in cynomolgus macaques fed with different human-like dietary patterns, with the Bacillota:Bacteroidota ratio increasing in macaques fed a diet mimicking a typical Western diet [393]. However, the obese animals in this study followed the same dietary pattern as all other animals in the study. The reason for their obesity may therefore be due to genetic or behavioural factors, for example, exhibiting more sedentary behaviours. As discussed in Chapter 3, another potential cause may be social hierarchical factors, meaning they may have consumed more food compared to others in the colony as a result of their social standing. It may also reflect an increased capacity for energy harvest by the obese intestinal microbiota, as is found in studies of both obese mice and humans [394, 395]. This hypothesis is consistent with the modest increase in the relative abundance of energy metabolism pathways seen in the present study.

More recent studies of the intestinal microbiota and obesity have also questioned the existence of an obese 'signature' in the human intestinal microbiota, suggesting that previous studies may have had insufficient sample sizes to accurately identify such a signature due to the high levels of inter-individual variation in microbial composition [392, 396]. Inter-individual variation may also explain the differing taxonomy observed in the obese cynomolgus macaques in the present study. Additionally, a study of baboons found intestinal microbiome phenotypes to be significantly heritable, which may contribute to the similarity observed in the faecal microbiome profiles of the obese mother and daughter [397]. Alternatively, the similarity between the obese animals may be a result of grooming behaviours, which has been found to promote intestinal microbiome similarity in other NHP species [381, 398-400]. Therefore, although the findings indicate potentially heritable or socially transferable differences in faecal microbial taxonomy in the obese animals, the limited number of samples available is insufficient to determine whether a distinct microbial signature for obesity exists in cynomolgus macaques.

4.3.3. First characterisation of the small intestinal microbiota in cynomolgus macaques

In the small intestine of healthy macaques, *S. ventriculi*, a Gram-positive, spore-forming, anaerobic bacterium, was the most dominant species identified. *S. ventriculi* cells are cuboidal and form into a tetrad arrangement, aiding the identification of their presence through histological methods [401]. *S. ventriculi* has previously been identified in faecal samples from a number of apparently healthy mammals, including a number of Old World NHPs, suggesting that it may be a common (shared commensal) intestinal microorganism in the present cohort of cynomolgus macaques [402, 403]. A previous study of human faecal samples, published in 1971, also indicated that it is a common commensal in vegetarians living in Uganda, India, and London, although nearly absent in meat-eaters [404]. Conversely, in more recent case studies, *S. ventriculi* is often reported to be a pathogen, capable of exacerbating pre-existing gastrointestinal conditions and implicated as a potential cause of emphysematous gastritis, gastric perforation, and gastric ulcers [405, 406]. These contradictory findings suggest that *S. ventriculi* may be an opportunistic pathogen in humans, and that its identification may be rare in studies of the human intestinal microbiota because it resides in the small intestine—a region that is both difficult to sample and poorly characterised in humans [407].

It is unclear, however, whether *S. ventriculi* also represents an opportunistic pathogen in NHPs. A case study describing the sudden death of a cynomolgus monkey who had recently undergone an FMT found gastric dilation and rupture upon autopsy, coinciding with a high abundance of *S. ventriculi* in the duodenum [408]. This association does not, however, provide definitive evidence that *S. ventriculi* was the causative agent. A closely related, highly virulent,

species of *Sarcina*, which forms a similar tetrad arrangement of bacterial cells to *S. ventriculi*, was recently identified and closely associated with a lethal neurological and gastrointestinal syndrome affecting chimpanzees in an animal sanctuary in Sierra Leone [409]. The authors speculate that previous documented cases of *S. ventriculi* infection based on morphology alone may have been caused by a closely related, but more virulent, *Sarcina* species. 16S rRNA gene sequencing also indicated substantial variation between cultured strains of *S. ventriculi*, suggesting strain variation may account for the apparent lack of pathogenicity in NHPs [402]. Alternatively, tolerance for *S. ventriculi* colonisation in NHPs may stem from differences in physiology or microbial community interactions. The asymptomatic presence of *S. ventriculi* in cynomolgus macaques may prove useful in studies aiming to understand the aetiology and pathogenesis of *S. ventriculi* infection in humans. However, it's prevalence also highlights the potential differences between the human and macaque intestinal microbiota, emphasising the need for caution when extrapolating findings from animal models to humans.

4.3.4. High prevalence of methanogenic archaea in the cynomolgus macaque microbiota

The overall observed percentage of archaea in the present cohort (both healthy and obese cynomolgus macaques) was 0.5%, lower than what has been reported in humans (approximately 1.2%) [410]. The archaea identified were all methanogens within the Euryarchaeota and the *Candidatus* Thermoplasmatota (formerly Euryarchaeota) phylum, closely aligning with findings in the human intestinal tract [411]. The most prevalent archaea in humans are of the order Methanobacteriales and Methanomassiliicoccales, both of which were detected in the present cohort at a prevalence of 56.5% [410]. The abundance of archaea has been positively correlated with dietary fibre content in NHPs and their prevalence in the present cohort of cynomolgus macaques is therefore likely a result of diet [412].

Breath methane content is often taken as a proxy for the presence of methanogens, as intestinal methane is solely produced by this subpopulation of archaea [413-415]. High-methane emission has been correlated with a more complex intestinal microbiome, suggesting that the presence of methanogens might influence or be influenced by overall diversity of the intestinal microbiome [413]. Methane emissions have also been positively associated with age in humans, suggesting that the abundance of methanogens in the intestinal microbiota increases with age [414, 415]. No association between methanogen abundance and increasing age was seen in this cohort of cynomolgus macaques. It is possible that this may be related to methodological limitations. The protocol used for DNA isolation in the present study was not optimised for extraction of DNA from archaea, potentially limiting the ability to determine full archaeal diversity of the intestinal microbiota in this cohort of cynomolgus macaques [410].

Further work should consider the use of DNA isolation protocols which have previously been determined to most effectively isolate DNA from both bacteria and archaea [416].

4.3.5. Limited changes to intestinal microbial taxonomy and function with age

The present study found that there was significant regional heterogeneity in the composition of the cynomolgus macaque intestinal microbiota. Microbial richness and evenness were increased in the caecum and the colon compared to the small intestine. Observed species richness (Chao1), and the proportional distribution of the most common species (Simpson) and the rarest species (Shannon), increases progressively along the intestinal tract, from jejunum to distal colon. These findings align with a previous study on microbial community structure along the intestinal tract in mice [417]. However, while that study found no significant change in alpha diversity between the caecum and the colon, my findings show that the caecum is distinct from both the small intestine and the colon in cynomolgus macaques.

In contrast, the present study found no associations between age, beta diversity, or the abundance of specific bacterial or archaeal taxa along the intestinal tract. This conflicts with the findings of several studies investigating the effect of age on the intestinal microbiota in captive and wild cynomolgus and rhesus macaques (Table 1.1). In a study of captive, male cynomolgus macaques conducted by Wei *et al.*, microbial profiles were distinct in different age groups in faecal samples taken from infant (1-2 years), young adult (4-6 years), middle-aged (7-10 years), and elderly (≥13 years) macaques [70]. The discrepancy between the findings of this study and my own may be due to differences in cohort size (the study by Wei *et al.* included samples from >100 macaques), distribution of ages, methodology, and environment. The animals within the present cohort were captive-bred, co-housed animals from a UK colony with a high health status. In comparison, the animals within the study conducted by Wei *et al.* were individually caged and never mixed for co-housing [70]. This does not reflect the social dynamics of wild populations of cynomolgus macaques and may have influenced the ability of the authors to determine significant effects of age on intestinal microbial composition. Additionally, the study by Wei *et al.* was conducted on male animals only [70]. A separate study of wild rhesus macaques and rhesus/cynomolgus macaque hybrids also found age-related shifts in the anal microbiota in male, but not female, animals [92]. This raises the question of whether age-associated changes to the intestinal microbiota are sex-dependent. With only a small proportion (5/23) of male animals in the present study, examining sex-based associations was not feasible. Future work investigating the effect of age on the intestinal microbiome in cynomolgus macaques may benefit from including an equal number of animals of each sex.

With one exception, age also did not have a significant effect on intestinal region-specific measures of alpha diversity, which included metrics of both microbial richness and evenness.

This aligns with previous findings in adult cynomolgus macaques (Table 1.1) [57, 64, 70]. While sex-based differences in age-related effects on the intestinal microbiota might explain their absence in the present study, it is likely that the small sample size and uneven age distribution in the cohort may have limited the statistical power to detect such changes and could have increased the likelihood of false positives. Therefore, the results should be interpreted with caution. The large percentage of host-genomic DNA contamination in many of the samples, especially those obtained from the small intestine, further reduced the size of the dataset. It is also possible that age-related shifts are only seen in more elderly cynomolgus macaques (>20 years), which were not included in the present study. Studies reporting taxonomy shifts in elderly humans generally only find them in the oldest individuals, with most changes reported to occur after 70 years of age [15, 355]. Well-designed studies encompassing a broader range of ages are needed to establish the effect of ageing on the intestinal microbiota in cynomolgus macaques.

Of the functional pathways identified in this dataset, a single metabolic pathway, describing the assimilation of formaldehyde in an intracellular metabolic pathway found in methanotrophic bacteria, in the proximal colon was identified to be negatively associated with age. Methanotrophs are Pseudomonadota that can assimilate methane as their sole carbon source, therefore belonging to a phylum which has been reported to account for a significant proportion of functional variability in the intestinal microbiota [366, 418]. Using reference-based profiling methods, the taxa that this pathway belongs to was unable to be identified, highlighting the large proportion of microbial reads classified as ‘Unknown’ in this study. As age did not appear to influence microbial taxonomic profiles, the lack of age-associated effects on functional profiles was not unexpected. Functional similarity in animals of different ages may be promoted by factors such as co-housing, grooming behaviours, and similarities in diet [381, 398-400, 419]. Due to the fibre-rich diet of cynomolgus macaques, in future work it may be interesting to focus functional analyses on genes encoding carbohydrate-active enzymes (CAZymes), which include glycoside hydrolases and polysaccharide lyases [420]. In humans, representation of glycoside hydrolase genes in the intestinal microbiome has been associated with intake of dietary fibre [421]. Investigating the association between dietary preferences, which may be influenced by social hierarchy, and representation of CAZymes in captive cynomolgus macaques may therefore provide insights into how diet influences microbiome structure and function. It may also provide insights into why age-associated changes in structure and function are limited in the present cohort.

4.3.6. Expansion of the cynomolgus macaque intestinal microbiota genome catalogue

Although the MetaPhlAn4 reference database has recently been expanded for previously little characterised microbiomes, including NHP microbiomes, it is not fully comprehensive, likely explaining the characterisation of only approximately half of taxa in the current datasets [291]. This highlights both the limited overlap between human and NHP microbiomes, as well as the limitations of the findings of the present study. Without knowledge of the entirety of the microbial community composition, it is impossible to know which taxa are truly the most abundant, or whether there are age-associated changes in taxonomy that would be apparent if a larger fraction of the microbial community could be identified.

I attempted to explore the uncharacterised portion of the present metagenomic dataset by undertaking an assembly-based approach to identify putative novel genomes. This revealed 108 potentially novel bacterial and archaeal SGBs, all of which could be classified down to genus level. Notably, the majority of these SGBs belong to the Lachnospiraceae family, which comprises a diverse range of anaerobic, fermentative genera capable of metabolising dietary polysaccharides [422]. Within the Lachnospiraceae family several genera, including *Roseburia*, *Coprococcus*, and *Lachnospira*, all of which are butyrate producers, were identified [423-425]. Butyrate is known for its beneficial effects on immune cells and intestinal barrier function and may play a key role in the microbiota-gut-brain axis, influencing communication through immune, hormonal, and neuroendocrine signalling pathways [426]. The identification of a number of putative novel SGBs in the cynomolgus macaque intestinal microbiome suggest that it may be a source of previously unrealised diversity among numerous taxa. Future work should include functional characterisation of these SGBs to develop a deeper understanding of their function within the intestinal microbial community.

A previous study that isolated MAGs from both wild and captive NHP metagenomic datasets found that approximately three-quarters of the MAGs from captive NHP metagenomes were shared with those isolated from human metagenomes, while only a small percentage of those from wild NHPs could be found in human datasets [361]. It would be interesting to replicate this analysis with the present dataset, which would give an indication of how similar the intestinal microbiota of cynomolgus macaques in long-term captivity is to humans.

The majority of putative novel SGBs are absent in small intestinal samples, although they are relatively evenly distributed across large intestinal and faecal samples. The absence of the SGBs in the small intestine may be reflective of an uneven distribution between the small and the large intestine. It may also be a result of the lower sequencing depth in samples obtained from the small intestine, discussed in greater detail in the following section.

While the ability to assemble MAGs has significantly advanced knowledge of microbial diversity in a large diversity of environments, it is important to note that MAGs can contain assembly and binning errors [427]. Draft MAGs should therefore be considered in conjunction with genomes obtained from single isolate sequencing to ensure accuracy in genomic studies. If this is not possible, and as concluded by Chen *et al.*, recovery and curation of complete genomes from metagenomic datasets should be attempted in major lineages to provide high-quality references for the identification of novel genomes [427]. Future work utilising any of the putative novel genomes presented here should consider implementing these approaches so as not to risk propagating errors arising from the assembly process, including misbinning. Additionally, although the GTDB is regularly updated (the database used in the present analysis was released in April 2024), it may not include the most recently identified taxa, or accommodate all recently proposed naming conventions [428]. This is exemplified by, as of August 2024, the continued use of *Prevotella* as the genus name for *Segatella copri.*

4.3.7. Limitations of metagenomic analysis and potential host DNA interference

Mapping metagenomic samples to the cynomolgus macaque genome revealed a high proportion of host DNA in the samples (Appendix 4). The presence of host DNA can reduce sequencing sensitivity, thereby decreasing the ability to detect low-abundance species due to reduced sampling depth of microbial reads [429]. Consequently, only samples with >1 million reads were included in the present taxonomic analysis using reference-based profiling methods. This threshold has previously been found to be sufficient for achieving <1% dissimilarity to the full taxonomic composition of metagenomic samples [430]. Most notably, this criterion led to a reduced number of small intestinal samples included in the reference-based taxonomic profiling, with no duodenal samples included, which meant that characterisation of all six intestinal sampling regions could not be carried out. Based on observations at the time of sample processing for DNA extraction, small intestinal samples contained a substantial amount of mucus and little faecal material, which likely accounts for the high proportion of host DNA in these samples. Further characterisation of the small intestinal microbiota in cynomolgus macaques is desirable.

As with inference of taxonomy in metagenomic datasets, a drawback of functional annotation is that the results are limited by the completeness and accuracy of the database used. Misannotations in public databases are thought to be increasing, partially due to a reliance on homology-based inference to predict function [431]. This can result in over-annotation, where a gene is assigned an incorrect function, which may lead to incorrect assumptions about the role of a microbe within the intestinal microbiome and their interactions with the host [431, 432]. In the present study, it is possible that functional assignment was affected by the presence of

errors in the databases used. Another drawback of functional profiling of metagenomes is that the method only quantifies the changes in abundance of metabolic pathways in the microbial community, not changes in activity. As microbial metabolites are key for activation of gut-brain-axis signalling networks, it would be interesting to include metabolomic profiling in future work to investigate how the metabolic capacity of the intestinal microbiota alters with age [433].

4.3.8. Health status of NHPs

In humans, the composition of the faecal microbiome is altered in those with type II diabetes compared to healthy controls [434-437]. Two aged cynomolgus macaques within this cohort had high blood sugar levels, indicative of diabetes, which may impact on the composition of the intestinal microbiota. However, this analysis did not reveal evidence of a distinct microbiota composition in these animals.

4.4. Conclusions

The present study represents the first characterisation of the intestinal microbiota in both the small and large intestine across the lifespan in a cohort of captive-bred cynomolgus macaques. Species-level taxonomy and function of prokaryotic communities was investigated along the intestinal, as well as in the faecal microbiota in a small subset of obese animals. While, with one exception, no significant relationships were found between age, taxonomy, and function, the study raises awareness of the potential effects of long-term captivity on the cynomolgus macaque intestinal microbiome. The study's use of both reference- and assembly-based methods demonstrated the differing taxonomy of the cynomolgus macaque intestinal microbiota in the small and the large intestine, while still exemplifying the need for further characterisation of the NHP intestinal microbiome. The catalogue of putative novel genomes retrieved from the present dataset provides a resource that will contribute to better understanding of the diversity of the cynomolgus macaque intestinal microbiota.

5.0. Chapter 5: The intestinal mycobiome

5.1. Introduction

Fungi are a recognised but under-characterised constituent of the mammalian intestinal microbiota. Fungal taxa regulate and interact with the host immune system and other residents of the intestinal tract microbiota [438]. While fungi are estimated to account for a relatively small proportion of the intestinal microbiota, contributing only 0.1% total gene content in the faecal microbiome, their larger cell size means they likely represent a significant share of biomass [439]. In humans, fungal commensals maintain a stable population over years [173]. They have also been implicated in the aetiology and/or exacerbation of several human diseases, including age-related conditions, such as IBD, colorectal cancer, and AD [182-187, 190, 440-442].

Only recently has the effect of age on the intestinal mycobiota started to be elucidated in humans, where it is recognised to be a driving factor in changes to fungal community composition [18, 170, 173, 197]. A meta-analysis of intestinal mycobiome study data defined four distinct enterotypes at genus level in which *Candida*, *Saccharomyces*, *Aspergillus*, and an unknown genus belonging to the Ascomycota phylum dominated. *Candida* and the unclassified genus were most abundant enterotypes and were significantly enriched in elderly participants (>60 years) [170].

The *Candida* genus is one of the most abundant within the intestinal fungal community of healthy humans, comprising multiple human-associated commensals, including *C. albicans* [18, 168, 170, 197]. *Candida* species typically reside as harmless commensals on mucosal surfaces in the majority of individuals, but at least 15 distinct *Candida* species are pathobionts with the majority of infections caused by five species: *C. albicans*, *C. glabrata*, *C. tropicalis*, *C. parapsilosis* and *C. krusei* [171, 443]. These species can cause infections ranging in severity from mild mucosal surface infections to life-threatening bloodstream infections and candidemia [444, 445]. Recent global estimates suggest there are >1.5 million cases annually of candidemia and invasive candidiasis [446]. The most prevalent disease-causing *Candida* species in both adult and paediatric populations is *C. albicans*, although non-*C.albicans Candida* species are increasing in prevalence [447]. *C. albicans* is a dimorphic yeast species, which means it can switch between a unicellular yeast and a multicellular filamentous morphology, the yeast and hyphal forms. Its pathogenicity is associated with this ability, with the latter form linked to virulence and tissue invasion [443].

Intestinal fungal pathobionts can disseminate from the intestinal tract to the bloodstream and other organs, including the brain. For example, clinical evidence suggests that expansion of *C. albicans* and *C. parapsilosis* within the intestinal microbiota precedes translocation and

infection of the bloodstream in patients with candidemia [190]. Fungal antigens from *Candida* species have also been detected within the serum of AD patients [186]. Examination of the brains of AD patients post-mortem has revealed fungal DNA, proteins, and cell bodies from multiple fungal species, including *Candida* [182-185]. As no fungal material is detectable within healthy brains, these findings suggest that a set of circumstances arise within AD patients allowing for dissemination of fungi from other body sites, such as the intestinal tract, following compromisation of the immune system and/or integrity of epithelial/endothelial barriers. While fungal infection of the human brain is uncommon, *Candida* meningitis can occur as a complication of candidemia. Neonates and premature neonates are particularly susceptible to this infection, although candidemia does not always precede manifestation of *Candida* infection [448-450]. Whether or not fungal brain infection is a contributor to the aetiology of AD or a sign that AD patients have an increased susceptibility to fungal infections is, however, unclear. There is significant opposition to the theory that links the development of neurodegenerative disease to a microbial aetiology [451]. However, it is possible that during ageing the presence of immunosenescence, inflammageing, intestinal microbial dysbiosis, and increased likelihood of co-morbidities, could create a set of circumstances allowing for disseminated mycoses.

Previous studies investigating the relationship between age and the intestinal mycobiota in humans collected extensive demographic data, highlighting the challenge of attributing changes in the intestinal microbiota solely to ageing [18, 170, 173, 197]. Numerous confounding factors, such as age-related shifts in lifestyle and behaviour, must also be considered. These co-variables are minimised in animal studies, where both environmental conditions and diet can be controlled. Cynomolgus macaques offer a promising animal model for studying age-related changes in the mycobiota due to their significant physiological similarities to humans, combined with the ability to control their environment and diet [49].

Before the present study, only one previous study of the intestinal mycobiome in cynomolgus macaques had been carried out, surveying the faecal mycobiota in cohorts of both wild and captive macaques of a similar age. The study found that in both populations the faecal mycobiota was dominated by Saccharomycetales at order level, and by *Kazachstania* (a genus which has since been taxonomically revised) at the genus level [174]. Only a limited number of taxa were identified to species level, so it is unclear which species account for the abundance of *Kazachstania*. However, the authors speculate that it may be a closely related species to *Kazachstania* (*Arxiozyma*) *sloofiae*, a common intestinal commensal in pigs [452-454].

In this chapter, we employ ITS1 sequencing to characterise the intestinal mycobiota in multiple spatial regions of the intestine (from duodenum to distal colon) in a cohort of healthy cynomolgus macaques in long term captivity. We also assess the ability of both *C. albicans*, a

common human intestinal commensal and known pathobiont, and *Arxiozyma pintolopesii*, a putative commensal of the cynomolgus macaque intestinal tract with potential pathogenicity, to translocate across an IEC barrier *in vitro*. Finally, we used a mouse model to assess the ability of a human-derived clinical isolate of *C. albicans* to traverse both the intestinal and the blood-brain barriers and translocate to the brain.

5.2. Results

5.2.1. Characterisation of the intestinal mycobiome in cynomolgus macaques

The work in this section (5.2.1) is an adaptation of previously published work which I contributed to and is reproduced here with permission of the co-authors (Appendix – Publications) [4].

Fungal community profiling was conducted on the luminal contents from six distinct intestinal spatial regions, spanning the duodenum to the distal colon, in a cohort of 16 cynomolgus macaques (a subset of the cohort described in Chapter 4). The macaques, aged between 4 and 20 years, were categorised into three age groups: young (4-7 years; n = 3), adult (8-12 years; n = 6), and aged (13-20 years; n = 7). All animals included in this analysis were healthy except for two animals (M1464F and I153CE), who had high blood glucose levels indicative of diabetes prior to culling. These animals did not receive specific treatment for diabetes and were culled within a short time-period following diagnosis. A detailed overview of the samples and individual animals included in this analysis is provided in Appendix 9. Profiling was achieved through ITS1 amplicon sequencing, employing a DNA extraction protocol previously optimised for mycobiome characterisation in preterm human infants as described by James *et al.* [455]. Over 700 amplicon sequence variants (ASVs) across 56 samples were identified, with 684 classified as fungal and 649 identified to at least Phylum level.

The number of unique taxa present at each taxonomic rank can be seen in Table 5.1. For ASVs with an average abundance exceeding 0.01% across all samples, we assessed the distribution of ASVs across the different age groups (Figure 5.1). Out of 127 ASVs identified, 108 (85.0%) were shared between two or more age groups, and 83 (65.4%) were shared by all age groups.

Table 5. 1. The number of fungal taxa found at each taxonomic rank in the cynomolgus macaque intestinal tract

Phylum	Class	Order	Family	Genus	Species
7	26	62	135	227	353

Analysis of the non-filtered dataset at the species level revealed no significant differences in alpha diversity between age groups within specific regions, measured by Chao1, Inverse Simpson's index, and Shannon’s index (Appendix 10). However, regional comparisons showed that Chao1, which measures species richness, was increased in all intestinal regions compared to the duodenum ($p < 0.05$) (Figure 5.2A). A summary of the results of the statistical tests is provided in Appendix 11. In contrast, no significant variation in Inverse Simpson’s or Shannon’s index, which consider both species richness and evenness, were seen across the different regions ($p > 0.05$) (Figure 5.2A).

Beta diversity at the species level was assessed using an NMDS ordination plot based on Bray-Curtis community dissimilarities (Figure 5.2B). Statistical analysis indicated samples did not cluster according to intestinal region or age group.

Taxonomic profiles showing the top 10 most abundant fungal taxa were created at each taxonomic rank. At the phylum level, 96.9% of ASVs were classified. Of these, Ascomycota (84.2%) and Basidiomycota (14.7%) represented over 99% of all classified taxa, with only one ASV classified as Mucoromycota (Figure 5.3A). At class and order levels, Saccharomycetes (78.5%) and Saccharomycetales (78.5%) were the most abundant taxa respectively (Figure 5.3B-C).

At a family level, Debaryomycetaceae (23.1%) and Saccharomycetaceae (54.4%) accounted for the majority of taxa (Figure 5.4A) which were represented by *Debaryomyces* (23.1%) and *Arxiozyma* (54.3%) at the genus level (Figure 5.4B), and an unclassified *Debaryomyces* species (23.1%) and *Arxiozyma pintolopesii* (formerly *Kazachstania pintolopesii* [172]) (54.2%) at the species level (Figure 5.4C). Both species were found in every macaque regardless of age. The remaining 0.1% of *Arxiozyma* species were represented by *A. telluris* (formerly *Kazachstania telluris*).

Further taxonomic investigation of the ITS1 sequence variant belonging to the unclassified *Debaryomyces* species, using NCBI BLAST, suggested it belongs to *Debaryomyces prosopodis*, *D. fabryi*, or *D. hansenii* (synonym *Candida famata*). The fungal ITS gene sequence has limited divergence between some closely related species, resulting in an inability to distinguish them [456, 457]. All three species have identical ITS1 sequences and therefore cannot be differentiated using this ITS region. *D. prosopodis* has previously only been isolated from mesquite trees, making this designation unlikely [458]. *D. fabryi* and *D. hansenii* are closely related species (previously both designated as *D. hansenii*). The majority of *D. fabryi* isolates are from human skin infections, while *D. hansenii* is widespread in nature and commonly found in food products including meat and cheese [459]. Due to its prevalence, we have tentatively designated this *Debaryomyces* species as *D. hansenii* and will refer to it as such, though we acknowledge that this classification may be incorrect.

Candida species are common commensals in the human intestinal tract. In the present cohort of cynomolgus macaques, the *Candida* genus accounted for 0.34% of overall relative abundance. Five species were identified with an overall abundance of >0.01%, of which three (*C. albicans*, *C. parapsilosis* and *C. tropicalis*) are considered fungal pathobionts in humans. The remaining species (*C. anglica* and *C. saitoana*) are unable to grow above 30ºC and were therefore considered transient species in the intestinal tract. Of the three pathobionts, *C.*

parapsilosis was the most abundant species, with 0.19% overall abundance, followed by *C. albicans* (0.07%) and *C. tropicalis* (0.01%) (Figure 5.5).

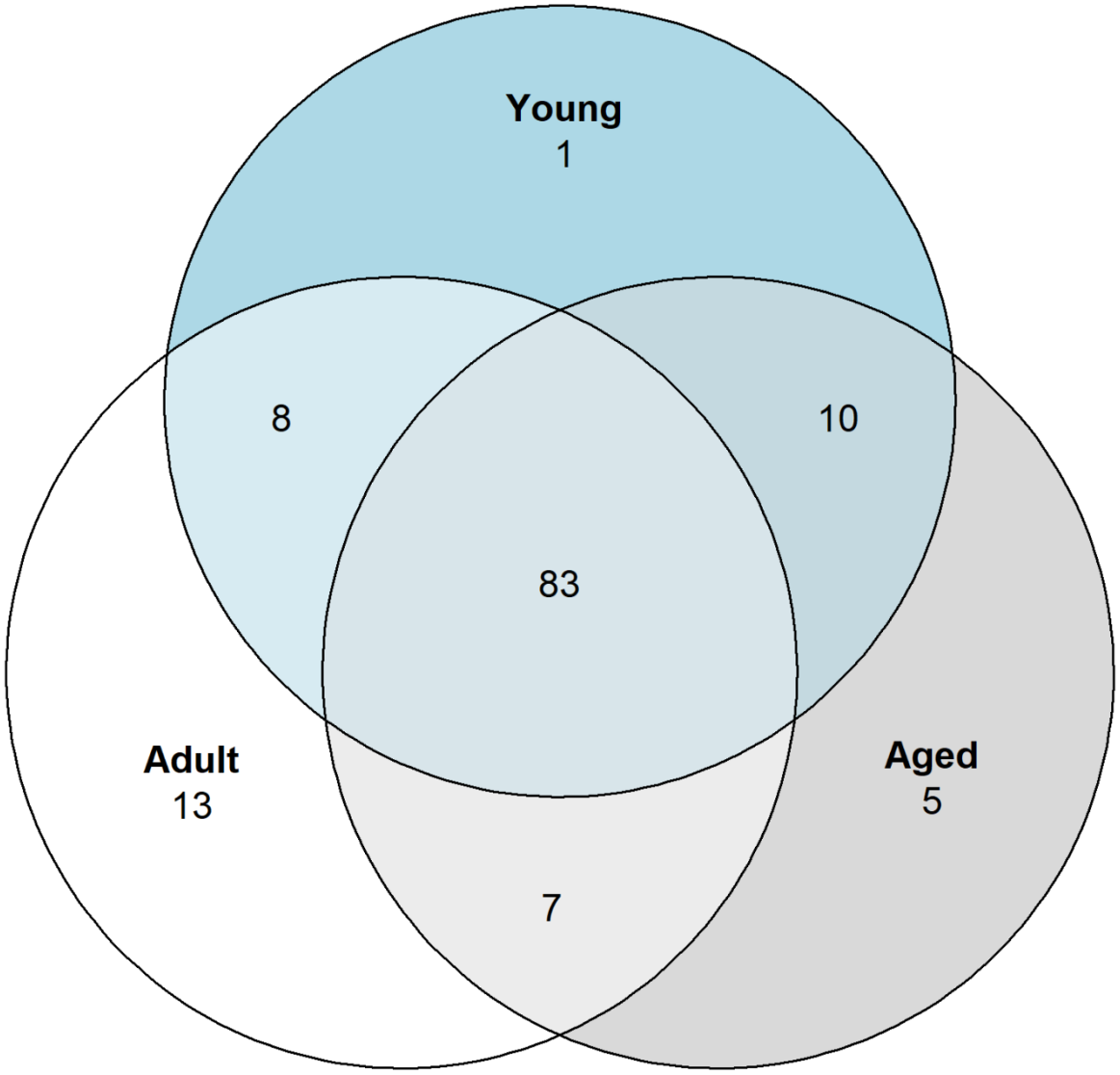

Figure 5.1. Venn diagram of the number of fungal ASVs (with >0.01% overall abundance) observed in the cynomolgus macaque intestinal tract found in different age groups. Animals were classified as young (4-7 years), adult (8-12 years), or aged (13-20 years).

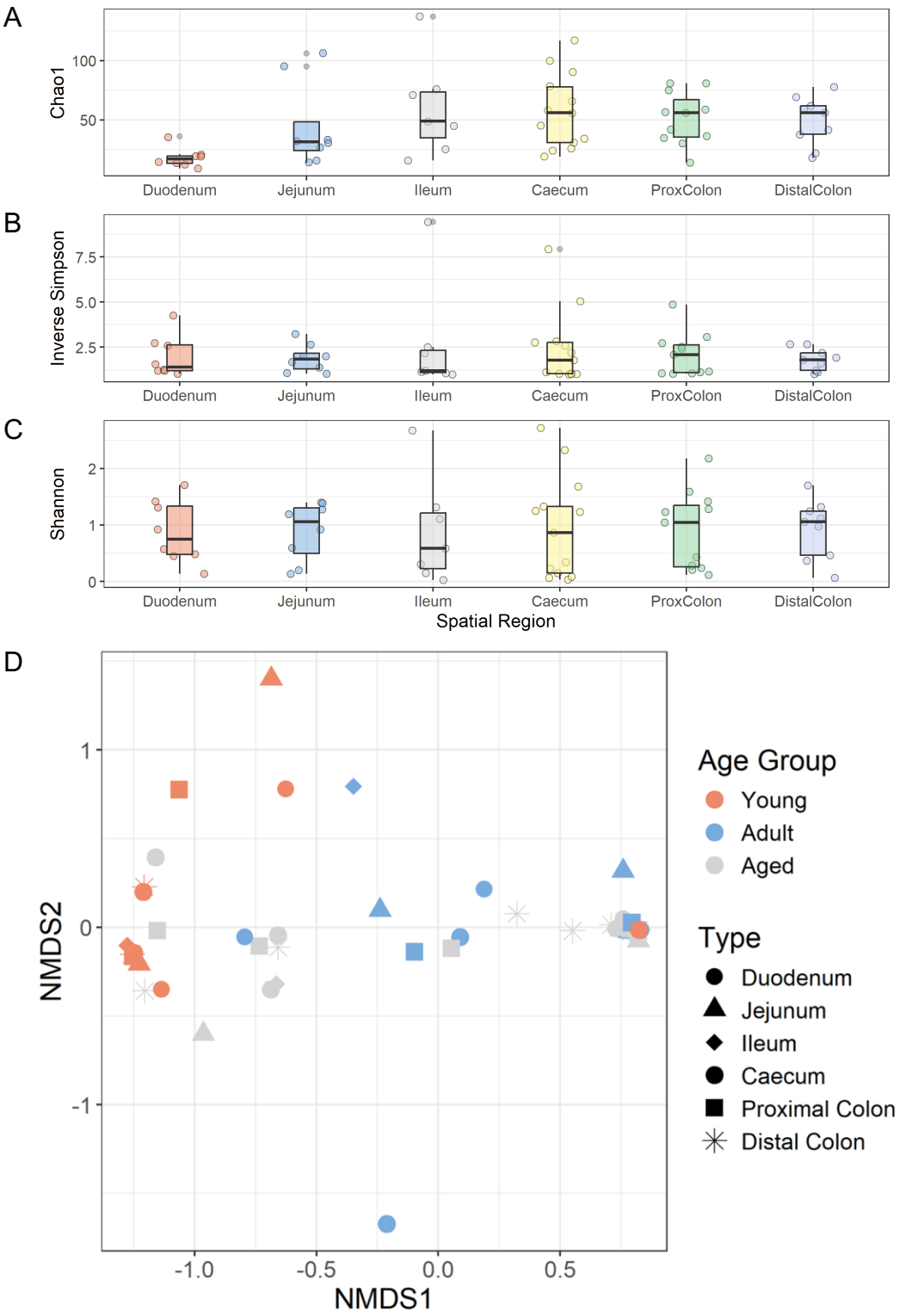

Figure 5.2. Species-level alpha and beta diversity measures of the intestinal mycobiota across different regions of the intestinal tract in a group of healthy cynomolgus macaques of differing ages. Alpha diversity was assessed using three metrics: (A) Chao1 index (B) Inverse Simpson's index (C) Shannon's index. The letter "d" above the boxplots indicates statistical significance from the duodenum ($p<0.05$). (D) NMDS plot based on Bray-Curtis dissimilarity, showing the clustering of samples by intestinal region and age group. Animals were classified as young (4-7 years), adult (8-12 years), or aged (13-20 years).

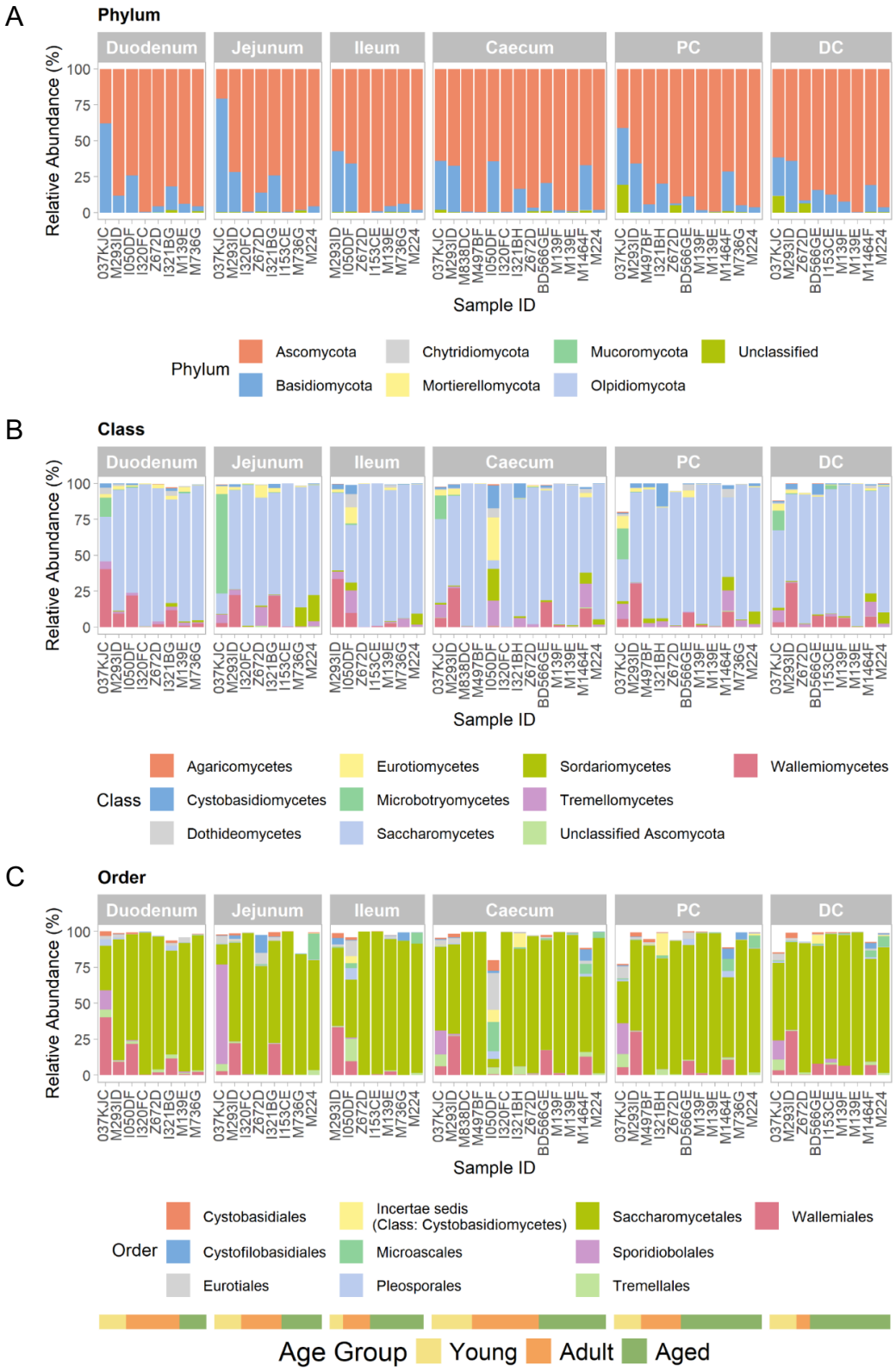

Figure 5.3. Relative abundance of the top 10 most abundant fungal taxa in the intestinal mycobiota at the (A) phylum (B) class and (C) order level across different regions of the intestinal tract in a group of healthy cynomolgus macaques of differing ages (4-20 years). Within each facet, individual bars represent samples from different animals, arranged in order of ascending age from left to right. Animals were classified as young (4-7 years), adult (8-12 years), or aged (13-20 years). Classification is indicated by the coloured bar at the base of the plot.

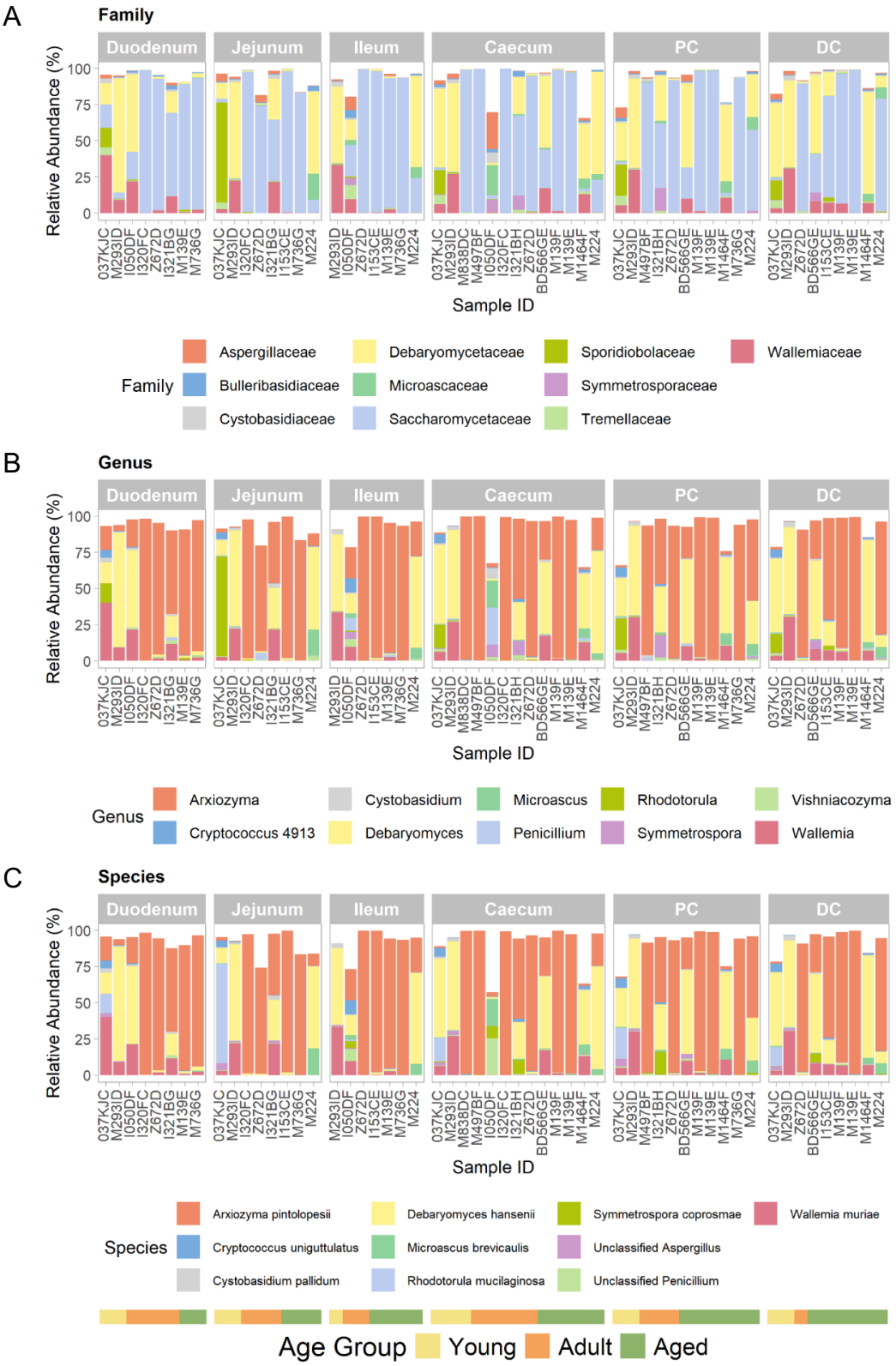

Figure 5.4. Relative abundance of the top 10 most abundant fungal taxa in the intestinal mycobiota at the (A) family (B) genus and (C) species level across different regions of the intestinal tract in a group of healthy cynomolgus macaques of differing ages (4-20 years). Within each facet, individual bars represent samples from different animals, arranged in order of ascending age from left to right. Animals were classified as young (4-7 years), adult (8-12 years), or aged (13-20 years). Classification is indicated by the coloured bar at the base of the plot.

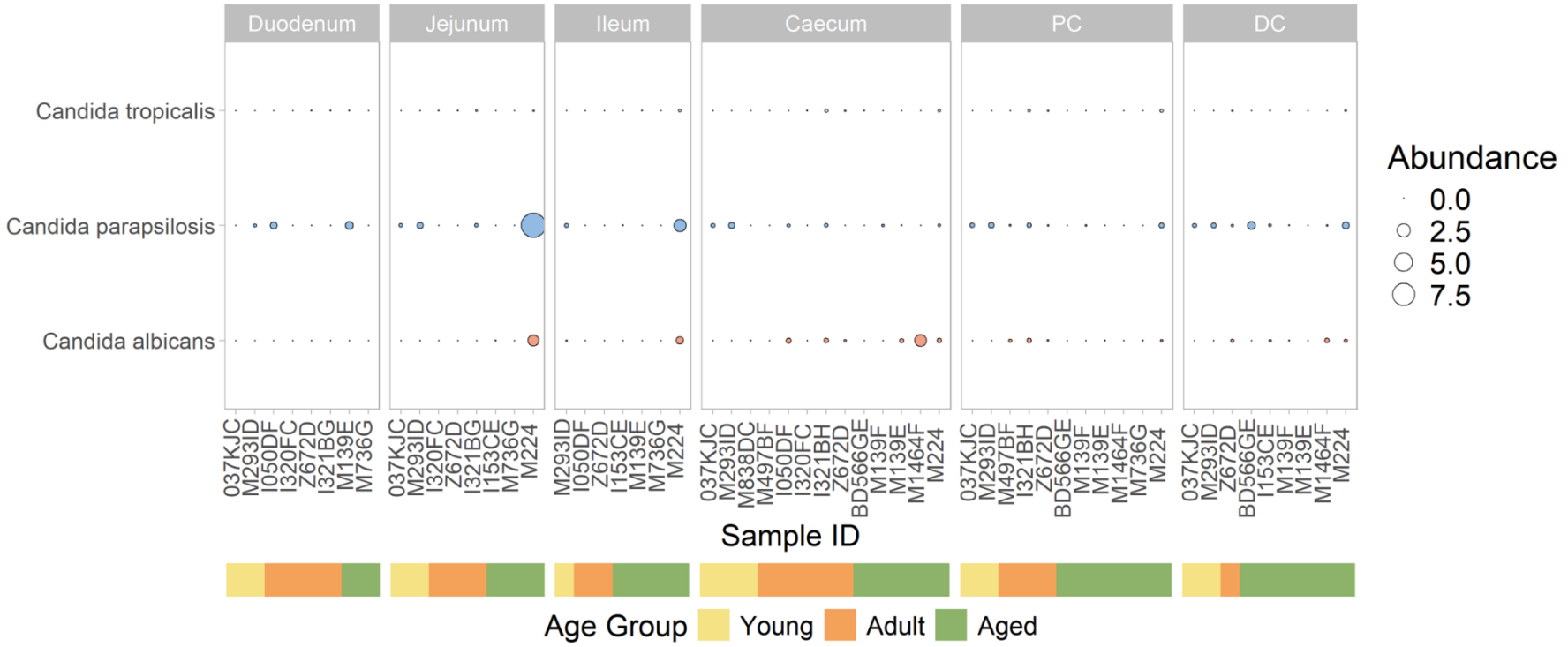

Figure 5.5. Relative abundance of three human-associated *Candida* pathobionts across different regions of the intestinal tract in a group of healthy cynomolgus macaques of differing ages (4-20 years). Within each facet, species abundance is indicated by the size of the circle and animals are arranged in order of ascending age from left to right. Animals were classified as young (4-7 years), adult (8-12 years), or aged (13-20 years). Classification is indicated by the coloured bar at the base of the plot.

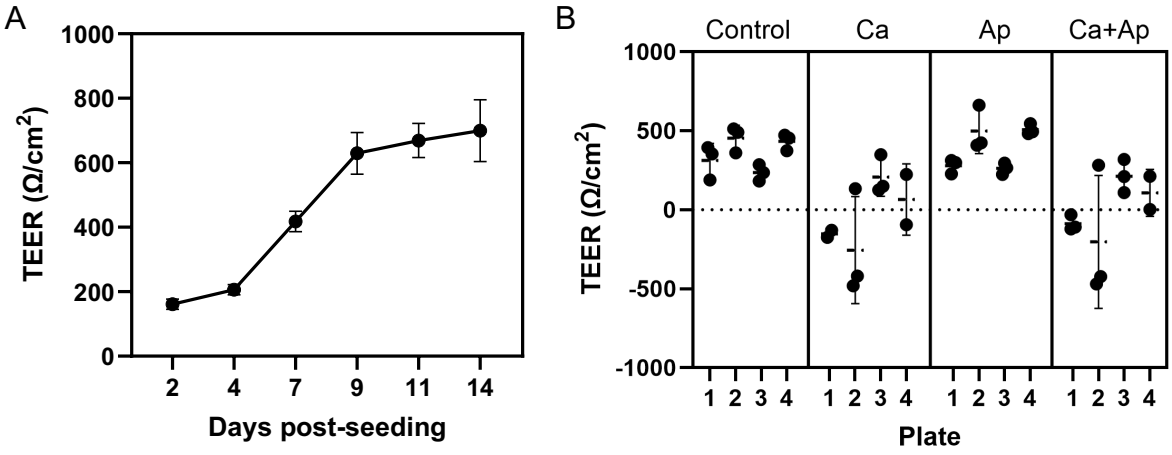

Figure 5.6. *A. pintolopesii* and *C. albicans* do not affect IEC barrier integrity *in vitro*. (A) Mean TEER measurements recorded during Caco-2/HT-29-MTX cell maintenance and (B) the change in TEER measurements following inoculation with blank media (Control), *A. pintolopesii* (Ap), *C. albicans* (Ca), or a combination of both yeast species (Ca + Ap). Results depict the measurements from four independent plates with three technical replicates per treatment group. Error bars depict mean ± SD.

A. pintolopesii has previously been linked to a fatal gastrointestinal infection in mice, raising the question of whether it may be an intestinal pathobiont, analogous to *C. albicans* in humans [460]. In addition, closely related species have been linked to exacerbation of a *Heliobacter suis*-associated infection in Mongolian gerbils, as well as a fatal *Escherichia coli* infection of a white-handed gibbon [461, 462]. Together, these studies suggest that *Arxiozyma* species (formerly known as the *Kazachstania telluris* species complex) may be opportunistic pathogens in polymicrobial infections.

Given these associations, we investigated the impact of *A. pintolopesii*, as well as the human pathobiont *C. albicans*, on IEC barrier integrity using an *in vitro* two-cell culture model. The effects of each yeast species were examined in isolation as well as in combination, given that previous reports suggest that closely related *Arxiozyma* species may be associated with co-infections [461, 462]. Colonic enterocyte-like Caco-2 and the mucus-secreting goblet cell-like HT29-MTX IEC lines were grown on the apical side of the porous membrane of a Transwell insert model consisting of two chambers separated by a porous membrane. Three Transwell systems per experimental condition were set up on each of four separate plates. To confirm IEC polarisation and tight junction barrier formation, TEER measurements were taken every 2-3 days post initial seeding until the IECs formed an intact monolayer (Figure 5.6A). The TEER values observed here were consistent with those reported previously in a co-culture of Caco-2 and HT29-MTX cells [463]. *A. pintolopesii* and *C. albicans* were then introduced to the apical chamber either in isolation, or in combination, and TEER measurements were taken to assess

the impact of the yeast on IEC barrier integrity (Figure 5.6B). Control Transwell systems were inoculated with sterile media only. Post-inoculation, Transwell cultures inoculated with *C. albicans* and *C. albicans* in combination with *A. pintolopesii* exhibited an average decrease of 392.6 Ω/cm^2 and 219.8 Ω/cm^2, respectively, in TEER measurements after 24 hours. This decrease was, however, not significant ($p > 0.05$).

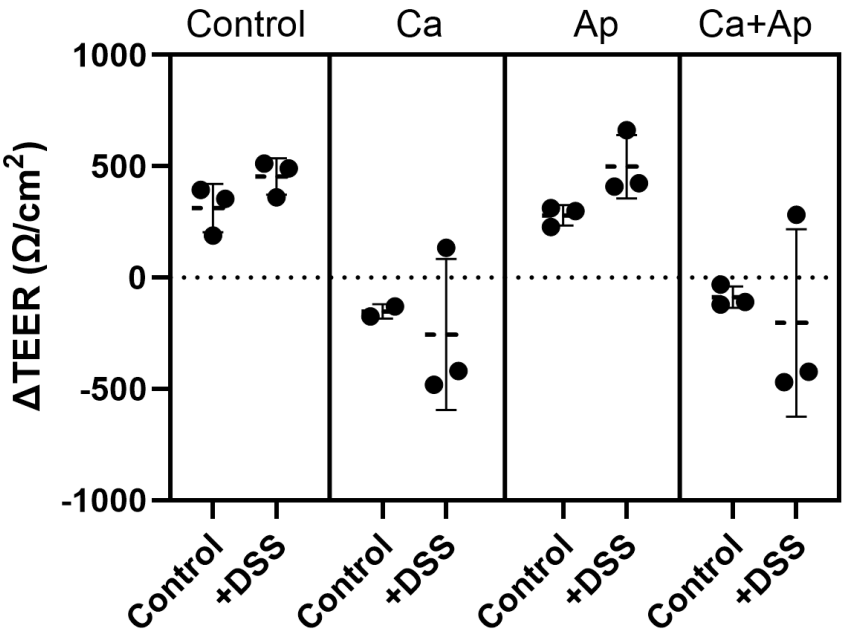

Figure 5.7. *A. pintolopesii* and *C. albicans* do not affect DSS-treated IEC barrier integrity *in vitro.* The change in TEER measurements of a co-culture of Caco-2/HT-29-MTX cells prior to and following inoculation with blank media (Control), *A. pintolopesii* (Ap), *C. albicans* (Ca), or a combination of both yeast species (Ca + Ap). Transwell systems were either untreated (Control) or treated with DSS (+DSS), which is indicated on the x-axis. Three technical replicates were performed for each treatment group. Error bars depict mean ± SD.

We hypothesised that an inflammatory state may be required to trigger the virulence mechanisms of the yeast, such as the formation of invasive hyphae in *C. albicans*. The experiment was therefore repeated adding 2% (w/v) DSS to half the Transwell systems for each condition. Although this concentration of DSS has previously been shown to significantly impact the permeability of Caco-2 monolayers in Transwell systems, we did not observe a decrease in TEER measurements in response to DSS treatment (Figure 5.7) [464]. DSS-treated Transwell systems inoculated with *C. albicans* and *C. albicans* in combination with *A. pintolopesii* exhibited a non-significant average decrease of 103.4 Ω/cm^2 and 116.2 Ω/cm^2, respectively, compared to non-DSS-treated controls ($p > 0.05$).

In addition to TEER measurements, FITC-dextran permeability assays were conducted. Post-inoculation with fungal cells, no significant changes to the concentration of FITC-dextran were observed in the apical chamber after 24 hours (Figure 5.8A). In the basal chamber, a significant

increase in FITC-dextran was observed in non DSS-treated Transwell systems inoculated with *C. albicans* in combination with *A. pintolopesii* (p = 0.0092), and in DSS-treated Transwell systems inoculated with *C. albicans* (p = 0.03), confirming that the IEC barrier was compromised (Figure 5.8B). Non-significant increases in the concentration of FITC-dextran in the basal media were seen in all other conditions compared to controls (p > 0.05).

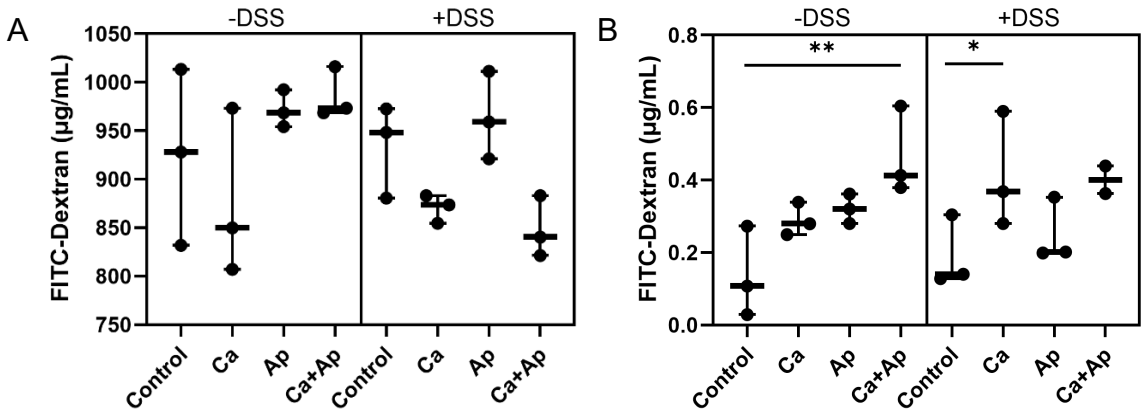

Figure 5.8. Concentration of FITC-Dextran in (A) the apical and (B) the basal compartments of Transwells inoculated with either blank media (Control), *A. pintolopesii* (Ap), *C. albicans* (Ca), or a combination of both yeast species (Ca + Ap). Transwell systems were either untreated (-DSS) or treated with DSS (+DSS). 3-5 kDa FITC-Dextran (1 µm/ mL) was added to the apical compartment of the Transwell inserts 24 hours before inoculation of yeast. Three technical replicates were performed for each treatment group. Error bars depict mean ± SD.

Following completion of the FITC-dextran permeability assay, media from the apical and basal chamber of each Transwell were collected and assessed for the presence of yeast using OD measurements (Figure 5.9). In Transwell systems inoculated with one or both yeast species OD measurements showed a high concentration of yeast only in the apical chamber. OD measurements of the basal media were comparable to those seen in the controls, confirming that no yeast were able to pass through the IEC barrier. It was determined that this was due to the 0.4 µm pore size of the Transwell membrane used in this model, which was too small for the yeast to pass through.

Confocal microscopy analysis was used to visualise the interactions of yeast with the IEC barrier (Figure 5.10). *C. albicans* was seen in both yeast and hyphal forms close to the apical side of the IECs, in one instance appearing between adjacent IECs, although no hyphae were observed to be actively invading the IEC layer (Figure 5.11B). *A. pintolopesii* was similarly observed on the apical side of the IEC layer, although the cells were observed to be noticeably higher above the IEC layer than *C. albicans*, indicating they may be residing in the mucus layer (Figure 5.11A). Blue puncta reminiscent of bacterial morphology were observed in the basal media, indicating the possible presence of a low level of bacterial contamination of the cell culture medium (data not shown).

We attempted to repeat the assay with Transwell systems containing a permeable membrane with a larger pore size (8 µm), which would allow yeast to transmigrate through the IEC layer. Attempts to grow a confluent cell layer were, however, unsuccessful (data not shown).

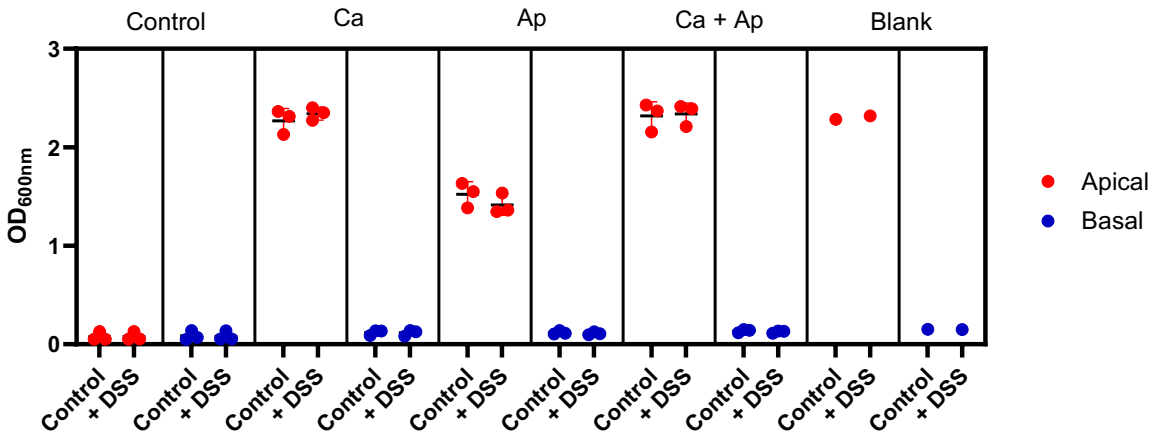

Figure 5.9. Optical density readings of media from the apical and basal compartments of Transwell systems after 72 hours of subculture. Transwells were inoculated with either blank media (Control), *A. pintolopesii* (Ap), *C. albicans* (Ca), or a combination of both yeast species (Ca + Ap). Systems were either untreated (-DSS) or treated with DSS (+DSS). 'Blank' Transwells refer to inserts without IECs. Three technical replicates were performed for each treatment group. Error bars depict mean ± SD.

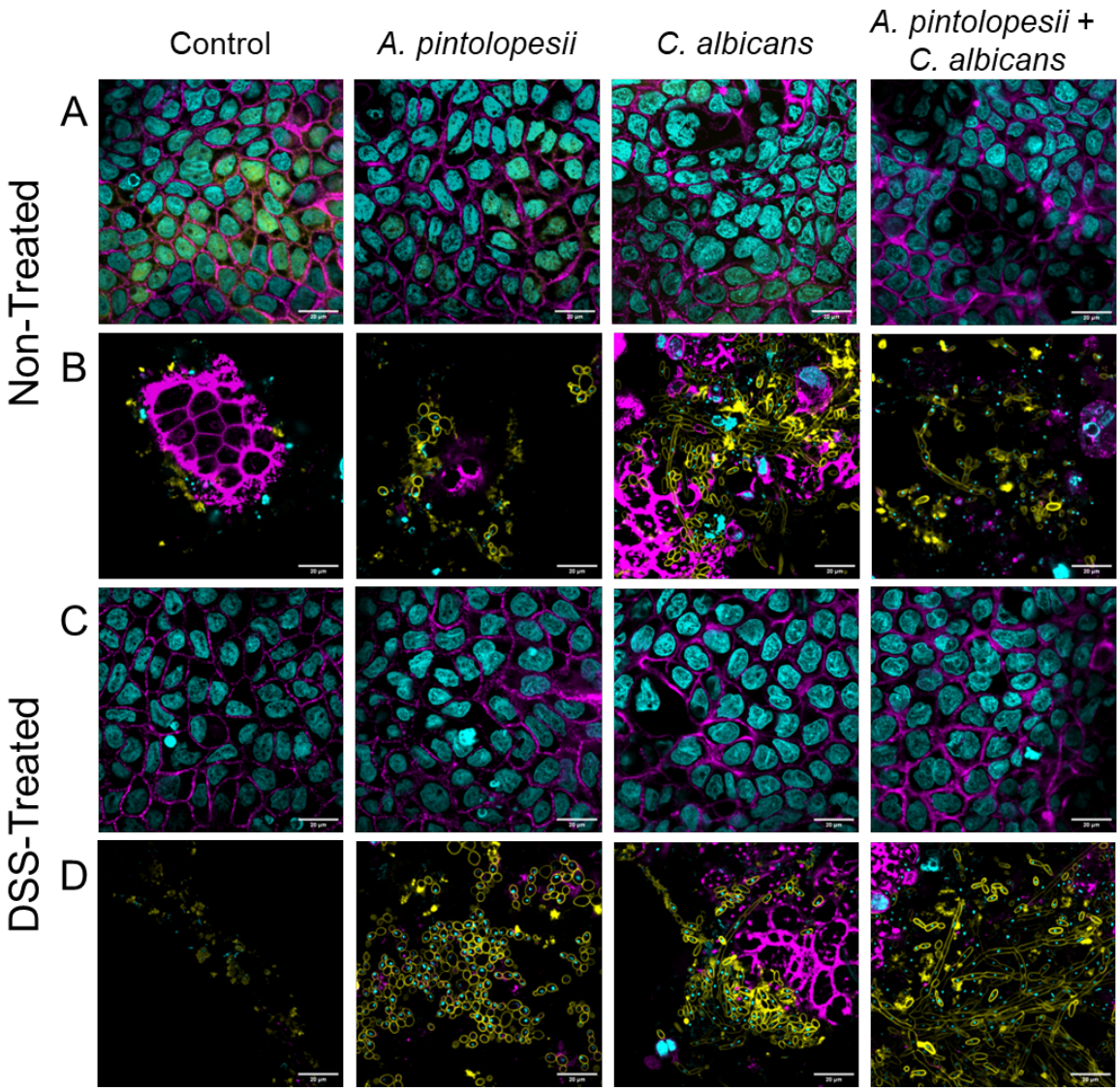

Figure 5.10. Representative images of IECs grown on Transwell inserts following 24-hour inoculation with either blank media (Control), *A. pintolopesii*, *C. albicans*, or a combination of both yeast species. Transwell systems were either (A & B) untreated (Non-Treated) or (C & D) treated with DSS (DSS-Treated). Images were captured either at the plane of the IECs (A & C) or at the yeast level (B & D). In all images, yellow indicates yeast, purple indicates Phalloidin staining, and blue represents nuclei (Hoechst). Scale bar = 20 μm. Images were taken by Dr Emily Jones and appear here with permission.

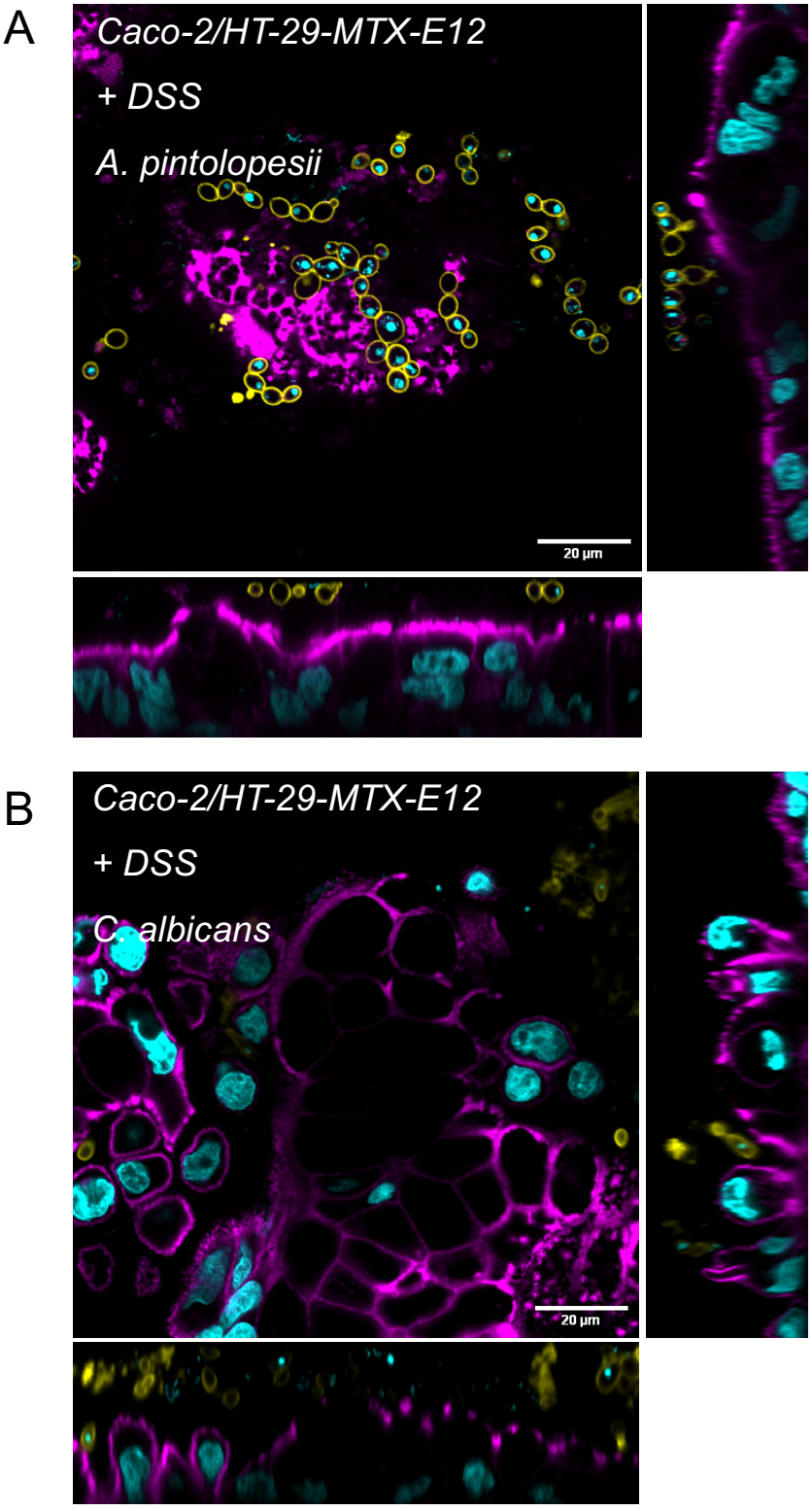

Figure 5.11. Representative z-stack images of IECs grown on DSS-treated Transwell inserts following 24-hour inoculation with (A) *A. pintolopesii* or (B) *C. albicans*. Main image panels depict merged XY images, side panels depict XZ and YZ z-plane orthogonal views. In all images, yellow indicates yeast, purple indicates Phalloidin staining, and blue represents nuclei (Hoechst). Images were taken by Dr Emily Jones and appear here with permission.

5.2.3. Fungal gut to brain translocation of the human pathobiont C. albicans in GF mice

The work in this and the following section (5.2.3 & 5.2.4) is an adaptation of previously published work to which I contributed and is reproduced here with permission of the co-authors (Appendix – Publications) [3].

To assess whether fungal cells can traverse both the intestinal IECs and BBB *in vivo*, we administered a human clinical isolate of *C. albicans* (NCYC 3115) by oral gavage to two groups of GF adult C57BL/6 mice at doses of either 2.5×10^5 (low dose, LD) or 5×10^5 (high dose, HD) cells. A third group received an inoculum of 2.5×10^4 cells via tail vein injection, a dose previously shown to result in non-lethal fungal translocation to the brain [465]. Control mice were administered PBS alone by oral gavage.

Both intravenous and oral delivery methods led to colonisation of the murine intestinal tract, as shown by CFU counts recovered from caecal contents collected five days after administration (Figure 5.12A). Caecal CFU counts in LD mice ranged from 1×10^5 to 1×10^7 CFU, and 6.2×10^6 to 2.2×10^7 CFU in HD mice. Mice that received *C. albicans* intravenously had caecal CFU counts ranging from 8×10^5 to 3×10^6. No fungal colonies were recovered from control mice receiving PBS only. Standard colony PCR was performed to confirm species identity of colonies with *C. albicans*-specific primers [272].

To test whether depletion of the intestinal bacterial community was necessary for expansion of *C. albicans* in the intestinal tract, SPF mice were treated with a short course of broad-spectrum antibiotics prior to delivery of *C. albicans* at a dose of 5×10^5 cells (SPF + Abx). A second group of SPF mice were administered PBS alone in place of antibiotic treatment, prior to administration of the same dose of *C. albicans* cells as SPF + Abx mice (SPF + PBS). Caecal CFU counts in SPF + Abx mice were increased compared to SPF + PBS mice but were at much lower levels compared to LD or HD mice (Figure 5.12B).

Two distinct *C. albicans* morphotypes were retrieved from the caecal contents: a white, domed morphotype resembling the wild-type cells prior to passage, and a darker, flatter morphotype resembling the previously described Gastrointestinally indUced Transition (GUT) phenotype, which is associated with commensalism [466] (Figures 5.12C-F). Unlike wild-type cultures, cells resembling the GUT phenotype did not produce hyphae, on either solid or in liquid media, when grown at 37ºC. Approximately 66% colonies recovered from the mouse caecal content resembled the GUT phenotype.

Five days post-inoculation, GF mice were sacrificed, and brain tissue was collected for analysis. Immunostaining of the brain tissue with an anti-*C. albicans* antibody revealed that *C. albicans*

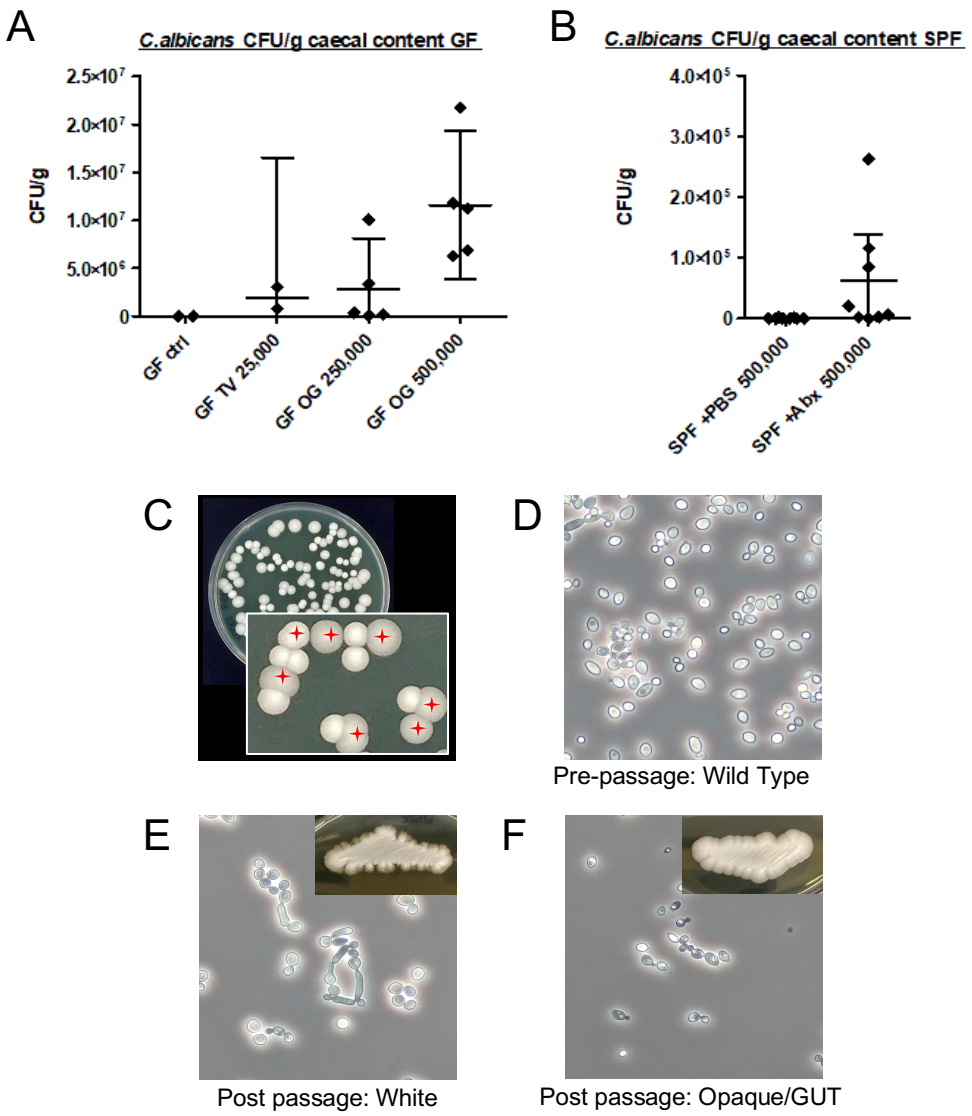

Figure 5.12. Colonisation of the mouse caecum by *C. albicans* NCYC 3115. (A) CFU recovered from caecal content following delivery of *C. albicans* NCYC 3115 to germ-free mice (GF) or (B) specific pathogen free (SPF) mice. No colonies were present in the caecal content of germ-free control mice administered PBS alone (GF ctrl). TV = tail vein, OG = oral gavage. Numbers on x-axis labels denote amount of *C. albicans* cells administered, error bars denote 95% CI. (C) Example YM agar plate with zoom inset showing two phenotypically distinct *C. albicans* colony morphotypes recovered from caecal contents. White and domed morphotype and darker and flattened/GUT morphotype (red crosshairs). (D-F) Photomicrographs of pre-passage wild type cells (D), post-passage white phenotype cells (E), and post-passage darker/GUT phenotype cells (F), all grown at 37°C for 3 days in YM broth. This figure also appeared in Parker, James *et al.* (2022) and is reproduced with permission.

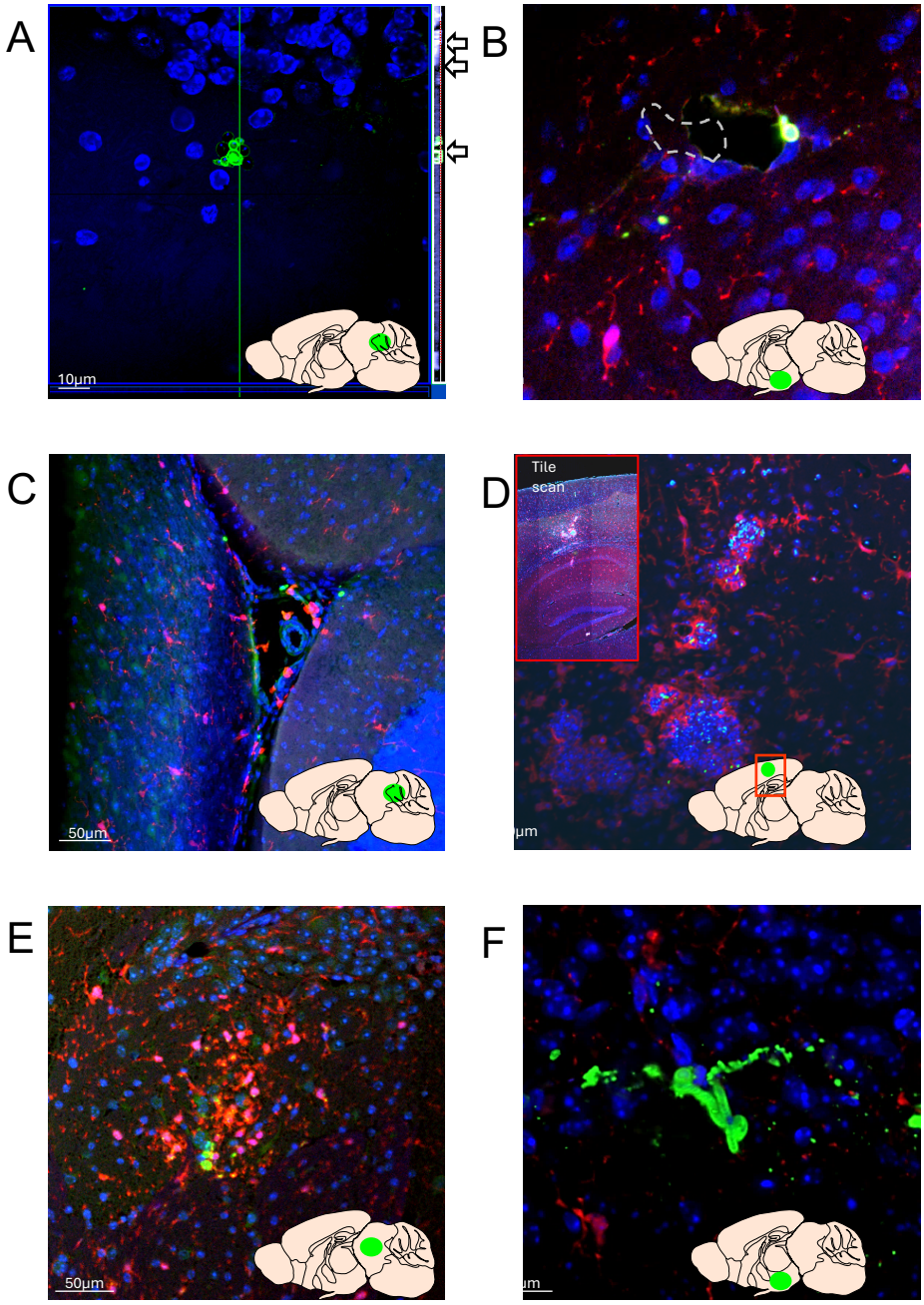

Figure 5.13. *C. albicans* can disseminate from the intestinal tract to the brain and can grow in invasive hyphal form within brain tissue. In all images, blue = nuclei (Hoechst), green = *C. albicans*, red = Iba1^{+} microglia/macrophages. Green area in inset brain schematic indicates approximate position of image. (A) *C. albicans* cells are detectable within cerebellar brain tissue at 5 days post-colonisation. Z-stack orthogonal view (side bar and arrows) shows *C. albicans* cells are in the same plane as brain cell nuclei. Orthogonal side bar brightness and contrast has been enhanced here for visibility. (B) *C. albicans* cells in proximity to a hypothalamic blood vessel (dashed outline). (C) *C. albicans* cells and Iba1^{+} macrophages within the cerebral aqueduct (lobule II granule layer visible as dense Hoechst-stained area bottom right of image). (D) Foci of clustered Iba1^{+} cells (red) around *C. albicans* cells (green) within the posterior parietal association area of the cortex. Inset box shows overview tile scan of the cortex and hippocampus. (E) Cluster of Iba1^{+} cells around *C. albicans* cells within the midbrain (F) Entwined hyphal *C. albicans* hyphae within the hypothalamus. This figure also appeared in Parker, James *et al.* (2022) and is reproduced with permission.

cells were present in the brain of LD and HD mice (Figure 5.13A-F). Both individual cells and clusters of cells were found throughout the brain, in the ventricular spaces, cerebellum, hypothalamus, midbrain, and cortex. These were confirmed to be in the plane of the brain tissue through z-stack imaging (Figure 5.13A). *C. albicans* cells and cell clusters were frequently found in or adjacent to blood vessels (Figure 5.13B), and within the ventricular spaces, including the cerebral aqueduct (Figure 5.13C). Fungal cells were also frequently surrounded by $Iba1^+$ cells resembling both resident microglia and infiltrating macrophages, indicating a localised inflammatory response (Figure 5.13E). In one mouse, granuloma-like clusters of yeast and $Iba1^+$ cells were observed in the posterior parietal cortex, a brain region crucial for spatial awareness and orientation (Figure 5.13D). In one instance a hyphal formation was also observed. The yeast to hyphal morphological transition is linked to virulence and pathogenicity in *C. albicans*, suggesting the cells are viable and capable of actively invading the brain tissue (Figure 5.13F) [443]. No fungal cells or $Iba1^+$ cell clusters were observed in PBS-administered control mice, or SPF + PBS and SPF + Abx mice, either by staining specifically for *C. albicans* or by using a non-specific fungal cell wall stain (example staining of a positive control shown in Appendix 12).

Visualisation of fungal cells in 5 μm sections was infrequent in LD and HD mice, with fungal cells not always observed in each section. The frequency of fungal cells in the brain was therefore manually quantified in five sequential midline sagittal 100 μm whole-brain sections taken from a second cohort of HD mice (n = 5) (Figure 5.14). The average number of cells observed per section per individual was between 2.8 and 7.2 cells, with an average of 4.6 cells per section observed across the cohort. This suggests that while *C. albicans* was capable of translocating from the intestinal lumen to the brain across the cohort, the frequency of this occurrence varied between individuals.

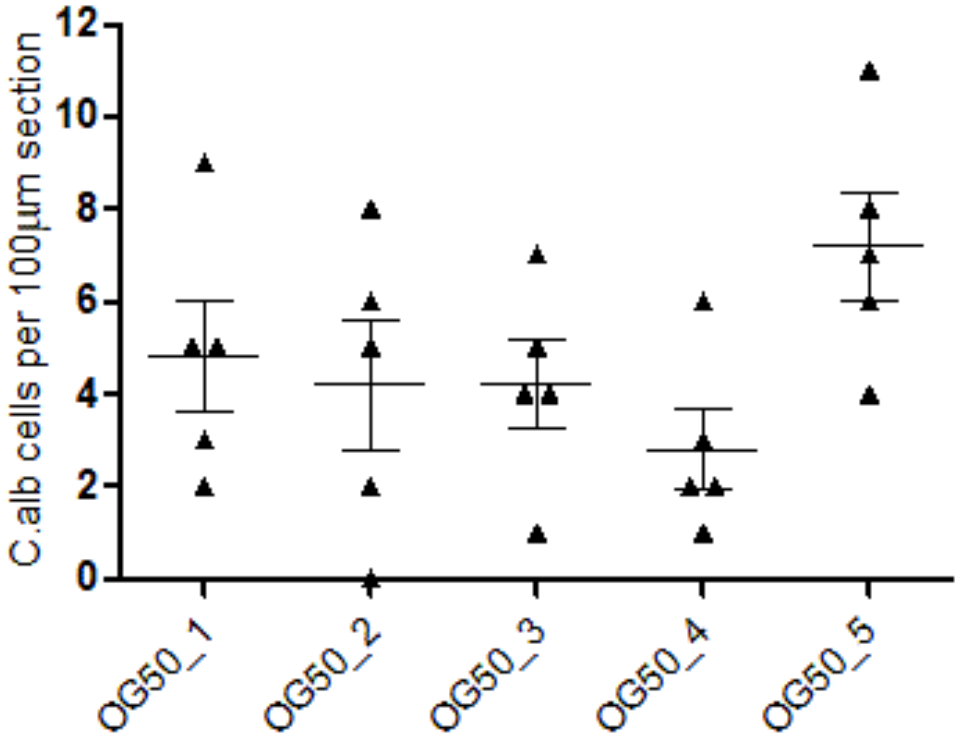

Figure 5.14. Quantification of *C. albicans* cells detected in 100 µm vibratome whole-brain sequential sections, shown as cells per whole 100 µm section. Five midline sagittal sections were taken per brain hemisphere per mouse (n = 5). Each mouse (OG50_1-5) was administered 5 × 10^5 *C. albicans* cells by oral gavage. This figure also appeared in Parker, James *et al.* (2022) and is reproduced with permission.

5.2.4. Characterisation of the faecal mycobiome in young vs aged SPF mice

ITS1-based fungal community profiling was performed on faecal samples collected from young (3-month) and aged (24-month) SPF mice. The dominant taxa at the phylum level were Ascomycota and Basidiomycota, with Basidiomycota being the most abundant in both age groups.

The taxonomic profiles of genera with an overall relative abundance greater than 1% (representing over 80% of all ITS1 reads) were similar between age groups, with no significant differences in mean relative abundance observed (Figure 5.15A) (Table 5.2). *Vishniacozyma* was the most abundant taxa at genus level. Although the reduction was not statistically significant, *Candida* and *Holtermanniella* were, on average, about half as abundant in aged mice compared to young mice (Table 5.2). Genus-level alpha diversity was also assessed in each age group, with no significant differences observed between them (Figure 5.15B).

Table 5. 2. The mean relative abundance of the most abundant fungal genera in faecal samples from young and aged SPF mice.

Genus	Phylum	Mean rel. abundance		T-test (CLR)
		Young	Aged	*P* value
Vishniacozyma	Basidiomycota	52.15%	53.12%	0.66469
Alternaria	Ascomycota	10.16%	12.11%	0.27966
Sporobolomyces	Basidiomycota	7.28%	6.09%	0.72700
Candida	Ascomycota	4.76%	2.35%	0.99092
Holtermanniella	Basidiomycota	3.20%	1.84%	0.20797
Cladosporium	Ascomycota	2.37%	2.14%	0.47865
Wallemia	Basidiomycota	1.69%	1.78%	0.07468
Aspergillus	Ascomycota	1.43%	1.83%	0.42524
Davidiella	Ascomycota	1.38%	1.18%	0.38557
Fusarium	Ascomycota	1.09%	1.02%	0.91780

Among the taxa resolved to the species level, only six were identified as candidate intestinal commensals based on their ability to survive and proliferate at 37ºC (Figure 5.16A). These species were *Aspergillus aflatoxiformans*, *Aspergillus chevalieri*, *C. albicans*, *C. parapsilosis*, *A. pintolopesii*, and *Saccharomyces cerevisiae*. Of these, *C. albicans* was the most prevalent and abundant species. Although its abundance decreased in aged mice, this reduction was not statistically significant (Figure 5.16B). *A. pintolopesii* was detected in only one young and one aged mouse, with a relative abundance of approximately 1% in each case.

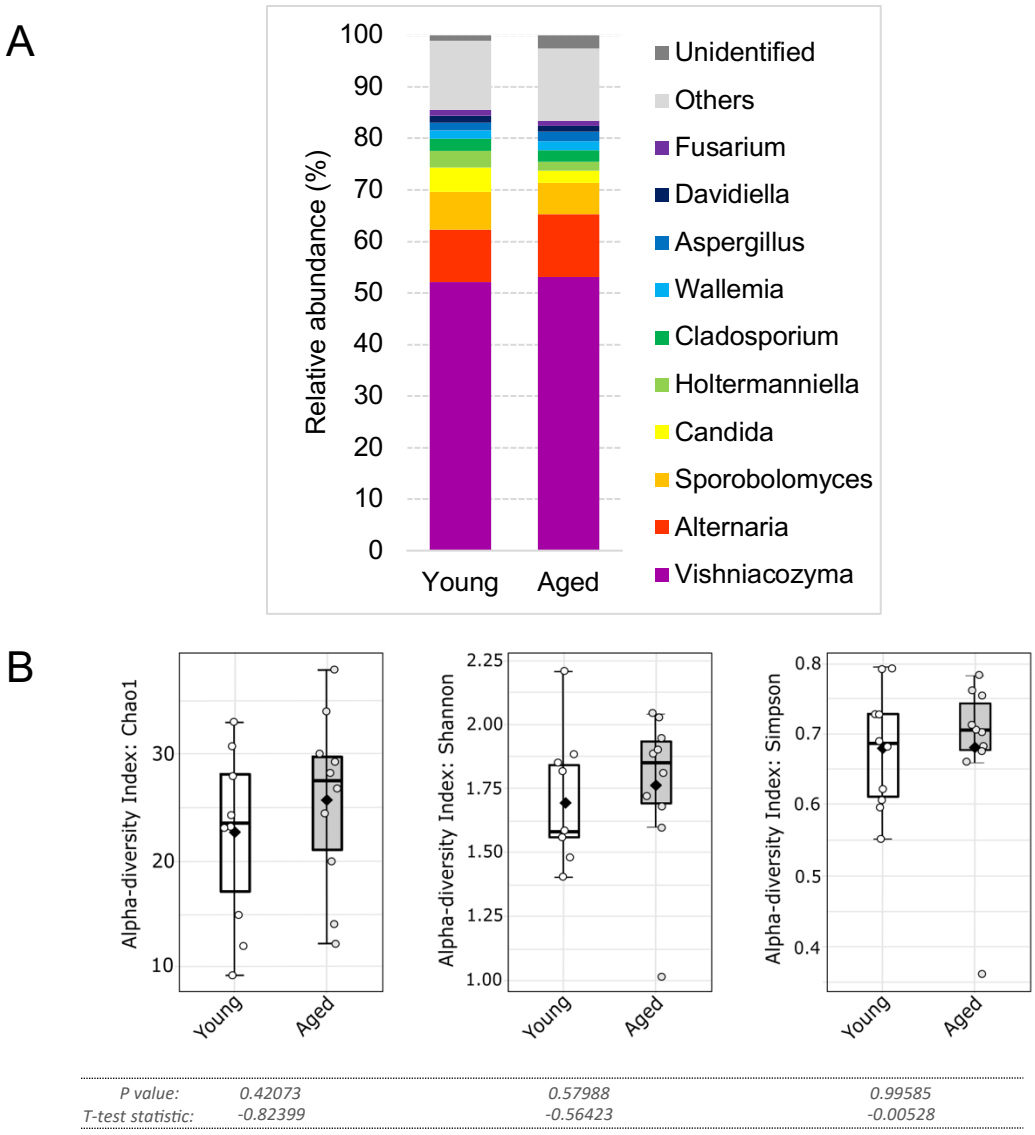

Figure 5.15. Faecal fungal diversity and top ten genera in aged vs. young SPF mice. (A) Top ten most abundant genera (percentage mean relative abundance) in faecal samples of young vs. aged SPF mice (n = 10/group). (B) Alpha diversity (L-R: Chao1, Shannon, and Simpson indices) of faecal fungal composition of young vs. aged SPF mice (n = 10/group), whiskers show spread of data across all mice, solid black dot indicates the mean, horizontal line indicates the median. Dr Aimée Parker and Dr Steve James carried out this work. This figure also appeared in Parker, James *et al.* (2022) and is reproduced with permission.

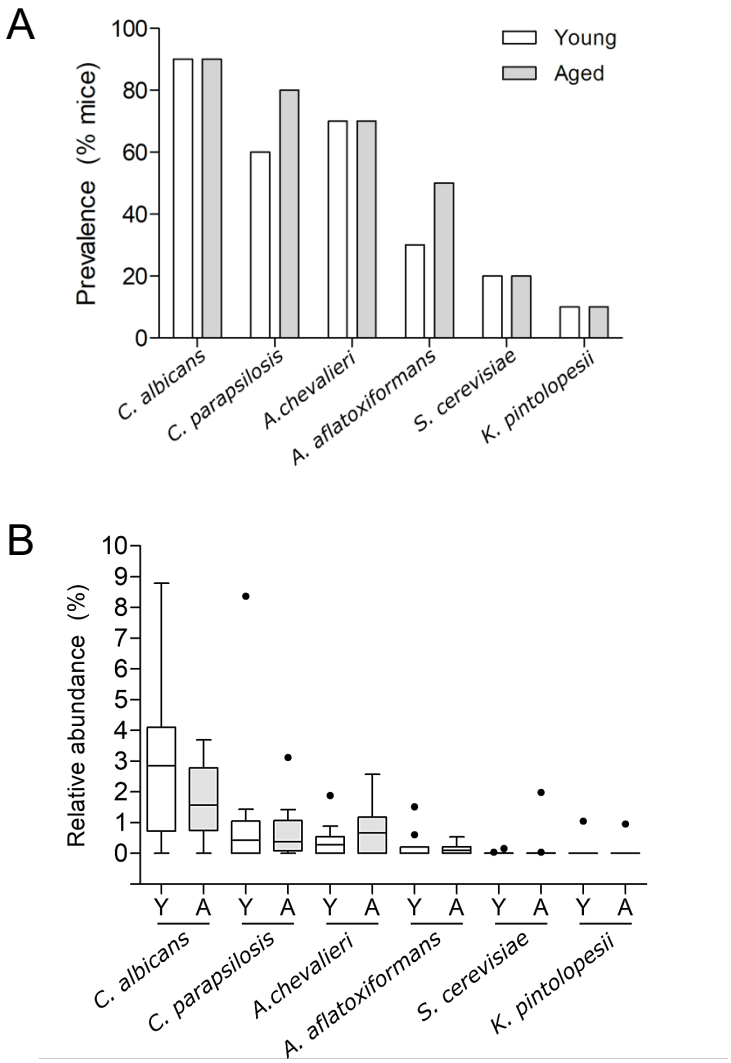

Figure 5.16. Prevalence and relative abundance of putative intestinal commensal fungal species in faecal samples of young vs. aged SPF mice. (A) Prevalence of putative gut commensal fungal species *Candida albicans*, *Candida parapsilosis, Aspergillus chevalieri*, *Aspergillus aflatoxiformans*, *Saccharomyces cerevisiae*, and *Kazachstania pintolopesii* (subsequently renamed *Arxiozyma pintolopesii*) in faecal samples from groups of young and aged SPF mice (n = 10/group), percentage of mice harbouring each species displayed as % prevalence. (B) Percentage relative abundance of those same species in faecal samples from aged (A) vs. young (Y) mice (n = 10/group), Tukey whiskers, horizontal bars show the mean, outliers displayed as round points. Dr Aimée Parker and Dr Steve James carried out this work. This figure also appeared in Parker, James *et al.* (2022) and is reproduced with permission.

5.3. Discussion

5.3.1. Characterisation of the cynomolgus macaque intestinal mycobiota revealed a high abundance of a potential pathobiont

Here, taxonomic profiling of the cynomolgus macaque intestinal mycobiome revealed that it is almost exclusively populated by fungi of the Ascomycota and Basidiomycota phyla, with Ascomycota dominating in all sampled regions. This aligns with findings in both wild and captive cynomolgus macaques, as well as the human intestinal mycobiota [168, 174].

Species richness, measured by the Chao1 index, was broadly similar across all intestinal regions except for the duodenum, in which richness was significantly decreased compared to all other regions. However, the results of both Inverse Simpson's and Shannon's index, which take into account both species richness and evenness, were consistent across regions. The discrepancy between these indices and Chao1 suggests that while the duodenum harbours the lowest number of species among the intestinal regions examined, the evenness of species distribution of both the most common species (Simpson) and the rarest species (Shannon) remains relatively consistent throughout the intestine [467].

No significant associations were seen between age and fungal alpha or beta diversity in this cohort of cynomolgus macaques. It should be noted that the small cohort size, along with unequal group sizes when assessing both age and intestinal region, may impact the reliability of the statistical tests in detecting any true biological differences.

At genus level, *Debaryomyces* and *Arxiozyma* were the most abundant taxa in the intestinal mycobiota of the present cohort. This differs from reports in humans, where *Saccharomyces*, *Malassezia*, *Candida*, and *Aspergillus* are among the most abundant genera, although proportionality varies according to geographical location [168, 170]. In comparison to *Arxiozyma*, *Debaryomyces* represents a smaller proportion of genera, although on average it still represents nearly a quarter of total abundance. At species level, the *Debaryomyces* taxon was, given the limitations of ITS1 sequencing to resolve taxa at species level, tentatively identified as *D. hansenii*. *D. hansenii* is a species widely distributed in nature and a common food-borne dairy-associated yeast that appears to be a prevalent commensal in the human intestinal tract [168, 455, 468, 469]. In some studies, *D. hansenii* is associated with IBD and colorectal cancer [470-472]. However, as it can typically only grow in temperatures up to 35ºC, lower than the core body temperature of cynomolgus macaques (37-39ºC), we question whether it can be considered a true intestinal commensal [473, 474]. Some strains of *D. hansenii* also appear to be capable of producing myocins that kill *C. albicans*, although not all at physiologically relevant temperatures [475, 476]. Although we do not attempt to link its

abundance to the relative scarcity of *C. albicans* here, it may be interesting to explore their relationship in the intestinal mycobiota in future studies.

Arxiozyma was the most abundant taxa at genus level, totalling greater than 50% average abundance over all samples surveyed, and exceeding 90% in some samples. This is almost entirely attributable to *A. pintolopesii*, with A*. telluris* contributing less than 0.1% total abundance. *Arxiozyma* was recently reclassified as distinct from the genus *Kazachstania*, which was previously found to be the most abundant genus in both captive and wild cynomolgus macaques [174]. *Arxiozyma* comprises a clade of five thermotolerant yeast species *(A. telluris*, *A. bovina*, *A. heterogenica*, *A. pintolopesii*, and *A. slooffiae*), which are phylogenetically distinct from other genera within *Saccharomycetaceae* [172, 477]. They are characterised by their ability to grow at 37ºC, with some strains of *A. pintolopesii* capable of surviving at temperatures as high as 42ºC, a rare physiological trait in yeasts [477]. To date, most *Arxiozyma* strains have been isolated from the nasal passages and intestinal tracts of birds and mammals [452, 460, 477-479]. Only one species, *A. heterogenica*, has been previously identified in NHPs, having been implicated as a co-infectious agent in a fatal *E. coli* infection of a white-handed gibbon [462]. Prior to this study, *A. pintolopesii* has mainly been isolated from the intestinal tract of wild and captive mice [460, 477, 478]. However, it's prevalence and abundance in the present macaque cohort, in addition to its ability to grow at and above 37ºC, suggests it may also represent a commensal in the NHP intestinal tract.

Having identified *A. pintolopesii* as a potential commensal organism, we sought to determine its role within the intestinal microbiome. A close relative, *A. slooffiae*, also a member of the *Arxiozyma* complex, is the predominant fungal species in the porcine intestinal tract post-weaning and persists through adulthood [452-454]. *A. slooffiae* is believed to play a beneficial role in piglet weaning, growth and development, showing a strong positive association with beneficial, health-promoting bacterial species like *Lactobacillus* and, before its reclassification (discussed in detail in Chapter 4), *Prevotella*, both of which have been linked to improved health outcomes in piglets [452, 454, 480, 481].

C. albicans has also been positively associated with these two bacterial species in pigs [452, 480]. However, compared to *Arxiozyma*, the presence of *Candida* species in the current dataset was extremely limited. Three of the *Candida* species identified, *C. albicans*, *C. tropicalis*, and *C. parapsilosis*, are well-known human-associated pathobionts. The genetic similarity of *Candida* and *Arxiozyma*, along with the dominance of *A. sloofiae* and the paucity of *Candida* species has led to the suggestion that the role of *Arxiozyma* species in the porcine intestinal microbiota is analogous to that of *Candida* in humans [452, 460]. This parallel extends to the present study, with *A. pintolopesii* in place of *A. sloofiae* representing the dominant fungus in

the intestinal mycobiota of cynomolgus macaques. However, reports linking *Arxiozyma* species to the exacerbation of bacterial infections in both rodents and NHPs also raise the question of whether *A. pintolopesii* can act as an opportunistic pathogen (pathobiont), as certain *Candida* species are known to be in humans [460-462]. Unlike *C. albicans*, however, *A. pintolopesii* appears to incapable of producing hyphae, a key virulence factor of *C. albicans* [460]. The potential virulence factors of *A. pintolopesii*, therefore, remain unclear.

As highlighted by our tentative designation of *D. hansenii*, one of the main limitations of the taxonomic survey of the cynomolgus macaque intestinal mycobiome is the reliance on ITS1 sequences as a DNA barcode for fungal taxonomic classification. The ITS region is well-represented in fungal databases, while fungal genome sequences are relatively scarce in comparison to bacterial genome sequences, making this method of taxonomic characterisation preferable to WGS methods due to the higher diversity of available references [482]. However, the ability to distinguish closely related species with limited divergence in their ITS region, which can be similar to the intragenomic variation within some species, remains limited [456, 457]. To circumvent this issue, the inclusion of a secondary barcode marker to improve the taxonomic resolution of ITS could be adopted in future studies [482]. As sequencing technologies improve and costs reduce, increased fungal genome sequencing may also result in more widespread adoption of WGS methods for characterising the diversity of the mycobiome in the future, thereby improving taxonomic resolution [457].

5.3.2. A. pintolopesii does not appear to effect IEC integrity in vitro

To assess the virulence of *A. pintolopesii* in the intestinal tract, we evaluated its effect on human intestine-derived IECs in an *in vitro* two-cell culture model. As the presumed virulence of *A. pintolopesii* has previously been linked to polymicrobial infections, we also inoculated Transwell systems concurrently with *C. albicans*. For comparison, we also inoculated the system with *C. albicans* alone. TEER measurements of Transwell model systems inoculated with *A. pintolopesii*, *C. albicans*, and both species in combination revealed no significant decrease in TEER values.

We hypothesised that to trigger the pathogenicity of the yeast species, an inflammatory environment may be required. We therefore repeated the assay, incubating half of the Transwell models with 2% (w/v) DSS for 24 hours prior to addition of yeast. However, no significant decrease in TEER measurements was seen post-addition of DSS that would indicate any change to the integrity of the IEC barrier, regardless of inoculation with *C. albicans* and/or *A. pintolopesii*. This indicates that the concentration of DSS may not have been sufficient for the induction of inflammation in co-cultured Caco-2/HT-29 cells, despite falling within the range (1-5%) often used to elicit inflammation and mucosal damage in mouse models of colitis *in vivo*

[483]. In the FITC-dextran assay, an increase in FITC-dextran in the basal chamber was observed in non-DSS-treated Transwell systems inoculated with both yeast species, and in DSS-treated Transwell systems inoculated with *C. albicans* alone. As addition of DSS alone did not affect barrier integrity, this suggests that the addition of *C. albicans*, whether alone or with *A. pintolopesii*, may impact IEC barrier integrity *in vitro*, leading to increased epithelial permeability and enhanced translocation of FITC-dextran across the chambers. *C. albicans*, however, appears to be the primary driver of this effect.

A link between *C. albicans* and compromised IEC integrity aligns with previous findings [484-486]. Here the effect of *C. albicans* on the IEC barrier appears to be relatively small, however, and not all measurements reach significance. These inconsistencies may be accounted for by our use of a Transwell system that utilises a membrane with a small pore size. As hyphae formation and translocation of *C. albicans* has previously been found to be key for epithelial damage and loss of epithelial integrity, the Transwell membrane's small pore size likely prevented the disturbance of the IEC barrier that would otherwise be caused by translocation of *C. albicans* cells [484]. Hyphal invasion is thought to create an 'invasion pocket', an invagination of the epithelial cell membrane that allows an accumulation of candidalysin, a toxin produced by *C. albicans* that helps mediate epithelial cell damage and fungal translocation [196, 484]. In the present study, release of candidalysin or the formation of invasion pockets may contribute to the compromising of the IEC barrier, resulting in increased translocation of FITC-dextran from the apical to the basal chamber. However, while *C. albicans* hyphae may have been able to partially penetrate the IEC barrier, full translocation from the apical to the basal chamber would have been prevented by the presence of a non-traversable membrane, thought to be required for full damage potential. *C. albicans* cells measure approximately 5-6 µm in their yeast form, although hyphae can extend to over 100 µm in length, while spherical *A. pintolopesii* cells have been reported to measure 2.1-6 µm in diameter [460, 487]. Although we attempted to repeat the experiment with a Transwell system with an 8 µm pore size, which would allow us to investigate the ability of both yeast species to translocate through the IEC barrier, attempts to grow the Caco2/HT-29-MTX to confluence within the available timeframe were unsuccessful.

Immunostaining revealed that the spatial distribution of *C. albicans* cells was close to the IEC barrier. In comparison, *A. pintolopesii* cells appeared to be present at a greater distance from the IEC layer, suggesting that *A. pintolopesii* may have been confined to the mucus layer produced by HT-29-MTX cells, although staining for the mucus layer would be required to confirm this. This close presence of *C. albicans* to the IEC layer could be attributed to *C. albicans*' ability to adhere to and degrade the mucus layer using mucinolytic enzymes. Once

C. albicans penetrates the mucus layer, it can adhere to IECs and initiate mechanisms for invasion, including a switch to the hyphal form and the release of candidalysin [488, 489]. These findings imply that *A. pintolopesii* may lack similar mucinolytic enzymes, although a full genome annotation for this species has not yet been completed. However, we have recently published the first draft genome sequence for a primate isolate of *A. pintolopesii* (Appendix - Publications) [490]. Future research should focus on completing a full genome annotation to further explore the potential pathogenic traits of this yeast species. Immunostaining also revealed the presence of possible bacterial contamination in all Transwells used for immunostaining, which may have had unknown effects on the integrity of the IEC barrier in addition to the presence or absence of fungi. The experiment would benefit from being replicated to remove the potential effects of bacterial contamination.

A limitation of our experiment was the use of human cell lines, which may not allow for the replication of species-specific interactions between *A. pintolopesii*, a hypothesised NHP intestinal commensal, and the NHP intestinal tract. An *in vitro* system also offers limited complexity compared to an *in vivo* system and does not resemble physiological tissue organisation or the full complexity of the intestinal microbiota. Despite these limitations, our experiment shows that while *C. albicans* may be able to affect IEC integrity *in vivo*, both with and without *A. pintolopesii*, no similar indications were found that *A. pintolopesii* was capable of the same. While this may be a result of the spatial restriction of *A. pintolopesii* to the mucosal layer, it is also possible that *A. pintolopesii* requires a different microbial consortium to initiate an opportunistic infection. In previous co-microbial infections involving *Arxiozyma* species, the corresponding co-infection has been bacterial [461, 462]. Replicating the experiment with a bacterium previously associated with *A. pintolopesii* co-infection may offer insights into the pathogenicity of *A. pintolopesii*. Additionally, although we did not see an effect of *A. pintolopesii* on IEC integrity, previous work has shown that lysates of *A. pintolopesii* isolated from a mouse model of sepsis induce enhanced cytokine production by Caco-2 cells *in vitro*, warranting further investigation of the potential immunogenic effects of *A. pintolopesii* on IECs [491]. As the addition of DSS did not have a noticeable effect on IEC barrier integrity, future work should also include optimisation of DSS concentration and incubation times on Caco-2/HT-29-MTX co-cultures.

To explore the interactions of *A. pintolopesii* within the context of the microbiota-gut-brain axis, we initially planned to use the A172 glioblastoma cell line on a cover slip placed in the basal chamber of Transwells with an 8 µm pore-size membrane. This setup would allow us to observe yeast interactions with the glioblastoma cells in the event they traverse the IEC barrier, and could be incorporated into future work.

5.3.3. Translocation of C. albicans from the intestine to the brain in GF, but not SPF, mice

Fungal cells, including *C. albicans*, have previously been found in the brains of AD patients [183-185]. We hypothesised that the presence of these fungi may arise due to dissemination from the intestinal mycobiota, raising the question of whether pathobionts such as *C. albicans* are capable of crossing multiple barrier sites to translocate from the intestinal tract to the brain.

We demonstrated in GF C57BL/6 mice that a human clinical isolate of *C. albicans* can traverse both the intestinal and blood-brain barriers. We also observed an inflammatory response characterised by $Iba1^+$ cells surrounding invading fungal cells, consistent with previous studies of mouse models of candidiasis [465, 492]. Hyphal projection in the brain tissue showed that the fungus maintained its invasive state in the brain in at least one instance, which has not been observed previously. Whether this could be a result of the use of alternate *C. albicans* strains, or the differences between GF and SPF mice is unknown.

Wild-type *C. albicans* switched to a GUT phenotype post-passage through the murine intestinal tract, which is reported to be a commensal cell type. The GUT phenotype is incapable of hyphal growth at body temperature, suggesting attenuation of *C. albicans'* invasive ability, whereas the wild-type phenotype retains this capability. Thus, continual exposure to the intestinal tract may be required to maintain the GUT phenotype, which explains the presence of both the wild-type and GUT phenotypes post-passage reported here [466]. This suggests that for *C. albicans* to exhibit pathogenicity in the host, switching to the wild-type phenotype might be required. The trigger and conditions required for this phenotypic switch should be the subject of further investigation.

Administration of *C. albicans* to SPF mice treated with a short course of antibiotics results in an expansion of *C. albicans* in the intestinal microbiota, however, we did not visualise any fungal cells in the brains of these mice. This may be due to differences in immune responses, epithelial and/or endothelial barrier integrity, and intestinal mucus layer composition in SPF versus GF mice, effecting hyphal formation and persistence of *C. albicans*, as all are influenced by intestinal microbiota composition [230, 493-496]. It may also be related to length of antibiotic exposure. A previous study has shown that chronic antibiotic exposure in mice (>4 weeks) with a systemic *C. albicans* infection results in bacterial dissemination to other organs. In humans, antibiotic exposure for >7 days greatly increases the risk of invasive candidiasis [497]. The mice in our study were only exposed to antibiotic treatment for 4 days, which may be too short a timeframe to find evidence of fungal dissemination. Additionally, the presence of other fungal species in the intestinal tract may inhibit *C. albicans*' ability to invade. Toxins produced by several fungal species, including *D. hansenii*, have broad activity against a variety of

pathogenic fungi at 37ºC *in vitro*, including *C. albicans* [476]. Although *D. hansenii* was undetectable in the mycobiota of these mice, it is possible that other fungi may similarly restrict *C. albicans* virulence. It is also important to note that *C. albicans* is not a natural coloniser of the murine intestinal tract, and specific host-species interactions may exist which provide resistance to fungal infection by this species [498].

5.3.4. The murine intestinal mycobiome is stable over time

A potential trigger for the translocation of microbes from the intestinal tract to the brain is intestinal microbial dysbiosis which can occur with age. We therefore investigated alterations to the composition of the intestinal mycobiota with age in SPF mice.

In comparison to the dominance of Ascomycota in cynomolgus macaques and humans, discussed above, our findings suggest that while both dominate in SPF mice, the most abundant phylum is Basidiomycota. This may not be the same in all mouse strains, as a previous study of a strain of mice generated by inter-crossing MRL/MpJ, NZM2410/J, BXD2/TyJ, and Cast/EiJ mice found that Ascomycota comprised >90% taxa in mice fed according to multiple dietary patterns [499].

In the present study, the most abundant genus in the murine faecal microbiota was *Vishniacozyma* with a small proportion of *Candida*. *C. albicans*, *C. parapsilosis*, and *A. pintolopesii*, all known murine pathobionts, were found within the cohort, although no significant change in their abundance was observed between age groups. No evidence of significant fungal dysbiosis was observed to occur with age, suggesting that, in mice, ageing alone is unlikely to be a trigger for microbial dissemination from the intestine. However, this does not exclude the possibility that other triggers, such as changes in diet, medications, infection status, or immune status, may result in changes that permit fungal translocation from the intestinal tract to the brain.

5.3.5. Health status of NHPs

In humans, the composition of the faecal mycobiome is altered in those with type II diabetes compared to healthy controls [500-502]. Two aged cynomolgus macaques within this cohort had high blood sugar levels, indicative of diabetes, which may impact on the composition of the intestinal mycobiota. However, this analysis did not reveal evidence of a distinct microbiota composition in these animals compared to healthy animals.

5.4. Conclusions

Our study enhances the basic knowledge of the cynomolgus macaque mycobiome and contributes to the understanding of potential mechanisms of pathogenicity by NHP and human fungal pathobionts. The key finding is that the dominant fungal species in captive-bred, healthy

cynomolgus macaques is *A. pintolopesii*, a putative intestinal commensal and potential pathobiont, although we found no evidence of pathogenicity by this species in an *in vitro* model of IEC barrier disruption. We did however show the major human fungal pathobiont *C. albicans* is able to cross multiple barrier sites and translocate from the intestinal lumen to the brain in GF mice, inducing cerebral inflammation. Our finding that *Candida* pathobionts did not constitute a significant proportion of the intestinal mycobiome in cynomolgus macaques highlights that while the cynomolgus macaque may be a genetically and physiologically relevant animal model for humans, there are species-specific differences in the composition of the microbiota with implications for host health and disease development.

6.0. Chapter 6: The ageing brain

6.1. Introduction

To understand how ageing contributes to the development of neurodegenerative disease, it is important to first characterise normal age-related brain pathology in the absence of disease. This is challenging in humans due to the scarcity of relevant samples, making well characterised animal models essential. The use of macaques in brain ageing research has been said to be indispensable, however, current literature suggests that research has primarily been carried out in rhesus macaques [50]. A comprehensive survey of normal age-related brain pathology in cynomolgus macaques throughout the lifespan has, to my knowledge, not been attempted. This is crucial if they are to be used to help characterise how age-related changes may affect the microbiota-gut-brain axis, and how this might contribute to neurodegenerative disease.

The study of age-related brain pathology in cynomolgus macaques could provide valuable insights into various physiological changes that contribute to brain ageing. This includes brain iron accumulation, which is a significant feature of ageing and is potentially linked to neurodegenerative disease [503, 504]. Iron is essential for many physiological processes in the brain, including myelin synthesis, neurotransmitter synthesis, and metabolism [503]. In the CNS iron is largely stored by ferritin, an iron storage protein composed of both light chain (FTL) and heavy chain (FTH) subunits, as well as other molecular storage forms (including neuromelanin, haemosiderin, and transferrin) [505]. Ageing is accompanied by accumulation of iron in specific regions of the brain, most notably in the SN [506-508]. Why iron levels heterogeneously increase in the brain with age is unknown but could be related to increased BBB permeability and inflammation, redistribution of iron between different molecular storage forms, and changes in iron homeostasis [503].

During ageing, histopathological findings in the brain of NHPs and humans commonly include lipofuscin, haemosiderin, neuromelanin [507-512]. Haemosiderin and neuromelanin are both iron storage molecules which are associated with iron accumulation in the ageing brain [507, 508]. Neuromelanin is a metabolic by-product found in catecholamine-producing neurons, including dopaminergic neurons, which chelates potentially damaging redox-active metals such as iron [513]. Neuromelanin accumulates with age in humans and some NHP species [507, 509]. The abundance of dopaminergic neurons in the SN, a region heavily affected in PD, has led to speculation about the role of neuromelanin in neurodegeneration [513, 514]. Notably, rodents produce no or very small amounts of neuromelanin, indicating that mechanisms of iron homeostasis in the brains of these commonly used animal models differ from primates [513,

515]. This positions NHPs, including cynomolgus macaques, as valuable models of iron homeostasis in the brain and ageing.

Haemosiderin deposition is a common finding in the brains of ageing humans and mammals, although, to my knowledge, its presence has previously not been characterised in ageing cynomolgus macaques [509-512, 516, 517]. It is hypothesised that haemosiderin accumulates as a result of cerebral microbleeds and that brain-resident macrophages phagocytose extravasated erythrocytes, becoming overloaded with iron, which is stored as haemosiderin [518-521]. This hypothesis is supported by findings that link the presence of perivascular macrophages to haemosiderin deposition in a study of elderly humans [511]. Cerebral microbleeds might occur as a result of age-associated disruption to the BBB, which in turn is associated with sustained systemic low-grade inflammation, as occurs in inflammageing [225, 522, 523]. An alternative theory links the presence of haemosiderin to indicators of small vessel ischaemia, such as microinfarcts and arteriosclerosis, and ischaemic stroke [511, 524]. It is hypothesised that ischaemic damage to the brain tissue causes the release of iron from ferritin-containing cells, which is then engulfed by phagocytic cells and stored as haemosiderin due to a reduced number of healthy, ferritin-containing, brain cells.

Iron and ferritin accumulation in the brain has also been associated with increased occurrence of both activated and dystrophic microglial cells, the resident immune cells of the brain [206, 525]. Compared to resting microglia, dystrophic microglia are characterised by an altered, dystrophic, morphology and express increased numbers of activation markers, including APCs, and pro-inflammatory cytokines [203, 212]. Previous work in mice, NHPs, and humans has indicated that activated and dystrophic microglia are present under normal ageing conditions [205, 206, 526-532]. Persistent microglial activation can have major implications for the development of neuronal dysfunction and degeneration and underlies the pathology of several neurodegenerative diseases [533].

Here, I have undertaken the characterisation of age-related pathology in the cynomolgus macaque by describing gross histopathology in young (0-5 years) versus ageing (13-20 years) animals in specific brain regions, including the midbrain, SN, hippocampus, and the cerebellum. I have also evaluated the relationship between age, iron accumulation, and microglial activation in these two cohorts. These findings provide a basis for characterisation of age-related pathology in the cynomolgus macaque brain, benefiting any future studies assessing the impact of age on the microbiota-gut-brain axis in this animal model.

6.1. Results

6.1.1. Histopathologic findings in the brains of ageing cynomolgus macaques

To assess the impact of age on accumulation of age-associated brain pathology and microglial activation in cynomolgus macaques, brain tissue samples were collected from a subset of the cohort of cynomolgus macaques described in Section 2.1.1. The animals included within this analysis were defined as young (0-5 years; n=3) or aged (13-20 years; n=13). Within this cohort of cynomolgus macaques, prior to being culled, one young animal experienced recurrent diarrhoea, while two aged animals had high blood sugar, indicative of diabetes. All other animals were healthy.

I focused my analysis on a specific brain subsection containing areas of the hippocampus, the midbrain (containing the SN), the cerebellum, and the pons (Figure 6.1). The location of the SN within the midbrain was confirmed by identifying dense regions of dopaminergic neurones using an anti-TH antibody and DAB staining (Figure 6.2). The main subdivisions of the macaque hippocampal formation are indicated in a representative H&E-stained section shown in Figure 6.3. Subdivisions were labelled according to those previously described by Kondo *et al.* [534] in the macaque hippocampus, with the exception of the cornu ammonis (CA) 3 subregion, which was further divided into CA2/3 and CA4, as described by Bachstetter *et al.* [535].

In the present study, brain sections from young (n=3) and aged (n=13) cynomolgus macaques were stained with H&E to check for the presence of age-related pathology, which is summarised in Table 6.1. No pathology reminiscent of AD or PD was observed, including neuron loss, Lewy bodies, or plaques, in macaques of either age group. Neuromelanin, a dark brown pigment comprising of melanin, lipid, and protein, was observed within neurons of the SN in aged macaques but was absent in the young cohort (Figure 6.4A). Perivascular and/or neuropil haemosiderin, appearing as a dark brown pigment, was observed in the SN in 77% of aged animals, but not in young animals (Figure 6.4A). Neuropil and perivascular haemosiderin were observed in the midbrain and the hippocampus of the aged cohort, although they were frequently sparse (Figure 6.4B). Perivascular haemosiderin was observed in the midbrain of one young animal. Scattered neuropil and perivascular haemosiderin were detected in the cerebellar grey matter in 85% of aged animals, with a few foci seen in one young animal, predominantly close to or within the Purkinje cell layer (Figure 6.4C). In the hippocampus, haemosiderin was most frequently observed in the CA1 subfield, where it was seen in 75% of sections from aged animals (Figure 6.4D). One aged animal displayed haemosiderin in the CA2/3 subfield, and one young animal displayed heavy neuromelanin deposition in an adjacent region to the CA2/3 subfield of the hippocampus.

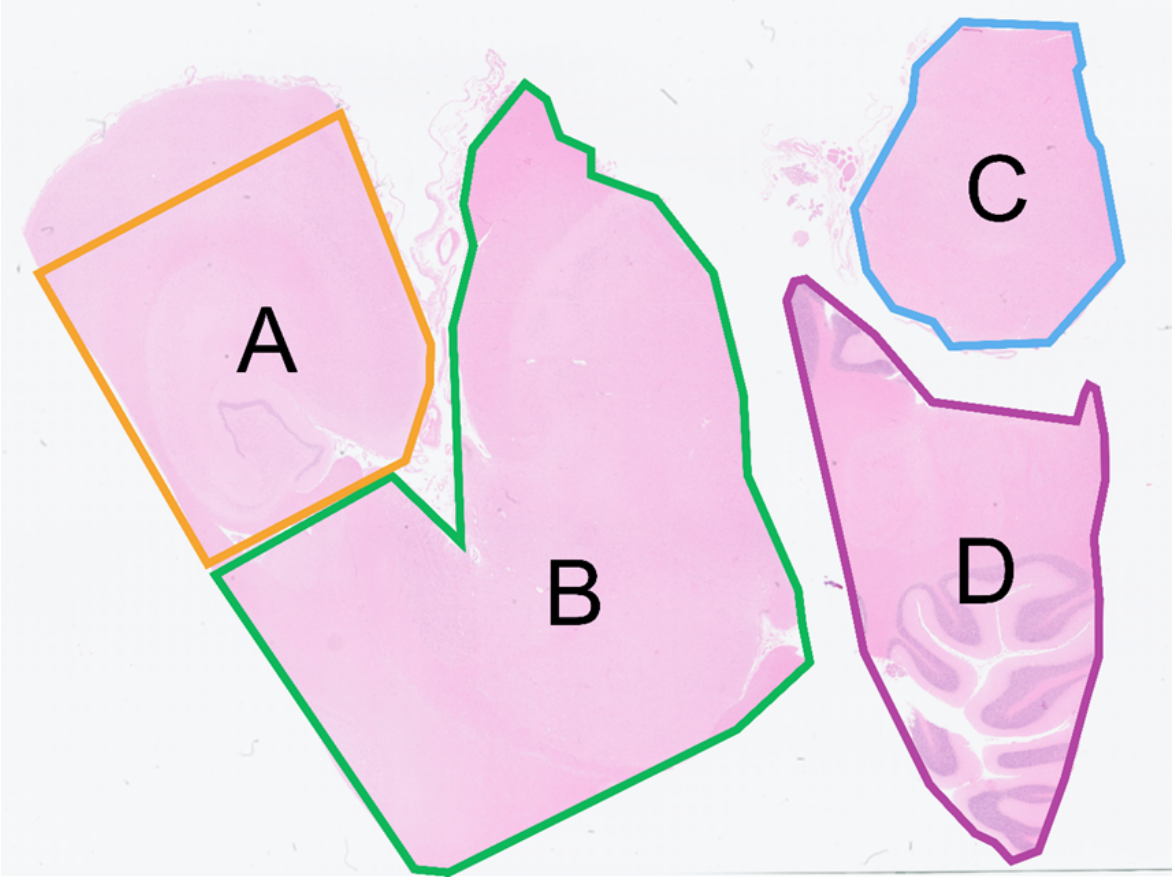

Figure 6.1. Example overview of ROIs used for analysis of the NHP brain on a H&E-stained tissue section. The outlines illustrate the boundaries used in identifying the areas of each tissue section containing the following brain regions: (A) hippocampus, (B) midbrain, (C) pons, (D) cerebellum. The ROIs shown in the figure are not the actual ROIs used for analysis.

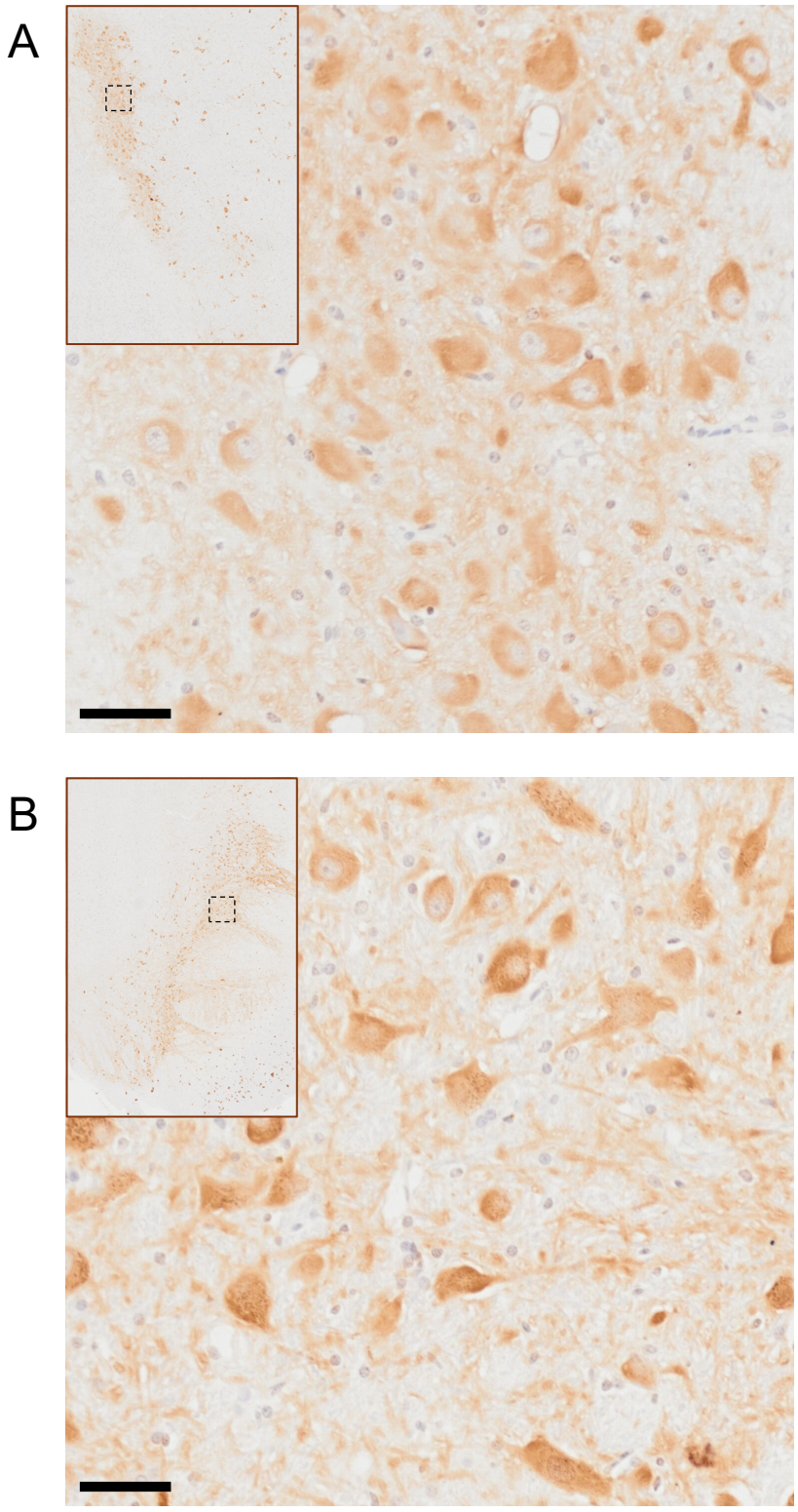

Figure 6.2. The location of the SN was confirmed by immunostaining for TH-containing neurons in cynomolgus macaques. In both images the inset box shows overview of the SN. Within the inset the dashed square indicates approximate location of the magnified image. (A) Representative image from a young cynomolgus macaque. (B) Representative image from an aged cynomolgus macaque. Scale bar = 50μm.

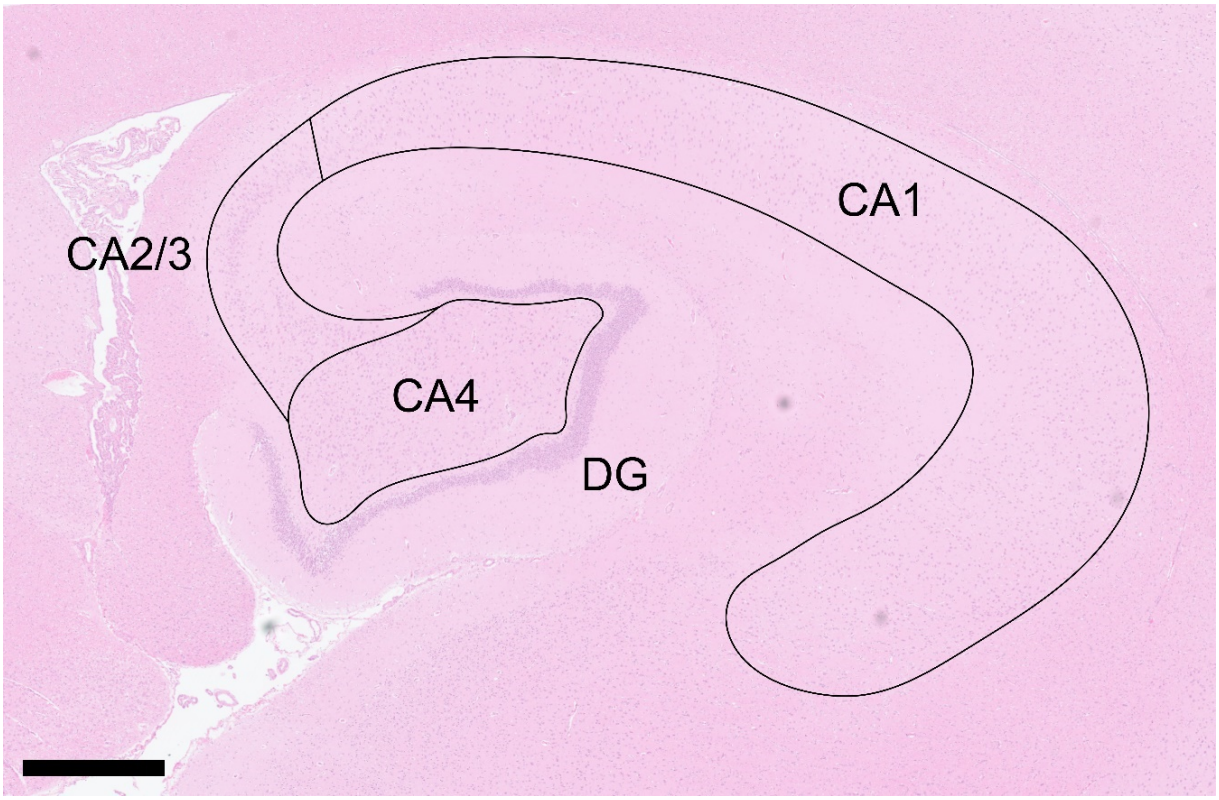

Figure 6.3. H&E-stained tissue section of the cynomolgus macaque hippocampal formation. Line drawings illustrate the cytoarchitectural divisions within the hippocampal formation. CA1, CA2, CA3, CA4, subfields of the hippocampus; DG, dentate gyrus. Scale bar = 1 mm.

Table 6.1. Main histopathologic findings in the brains of cynomolgus macaques

Histopathologic finding	Description (H&E)	Intracellular or extracellular	Special Stain	Commonly affected brain regions per cohort	
				Young	Aged
Haemosiderin	Dark yellow-brown pigment	Extracellular and intracellular (macrophages)	Perls' Prussian Blue	Midbrain	Hippocampus, Midbrain, SN, Cerebellum (Grey Matter)
Neuromelanin	Brown pigment	Intracellular		Hippocampus, Midbrain	Hippocampus, Midbrain, SN, Cerebellum (Grey Matter)

To confirm the presence of ferric iron in the brain tissue, sections obtained from young and aged animals were stained using Perls' Prussian blue methodology (Figure 6.5A). Visible iron deposits may represent either haemosiderin or ferritin, with haemosiderin deposition in the H&E-stained sections indicating that it may contribute at least partially to these deposits. Iron deposits were observed in the cerebellar grey matter, midbrain, and hippocampus in H&E-stained sections. The location of these deposits matched the location of haemosiderin-rich areas seen in H&E-stained sections from the same animals. In the hippocampus, iron deposits were mainly limited to the CA1 subfield, appearing in 92% of samples from aged animals. Iron deposits appeared to be present in both cell bodies and neuropil. A small number of iron deposits were also seen in the CA1 subfield in one young animal, although this was in close proximity to a blood vessel.

In the SN, significant iron deposition was routinely observed in aged animals, while none were seen in young animals. Consequently, the number of iron deposits were quantified across both age cohorts using a manual image analysis. No iron deposits were observed in the SN in young animals, while aged animals showed between 1 and 133 deposits per ROI (Figure 6.5B). No significant association was found between age and iron deposition in the SN, however.

6.1.2. The effect of age on microglial cell density in the hippocampus and the SN of cynomolgus macaques

Next, I sought to determine whether microglial activation was affected by age in the SN. Activated microglia were quantified using the cell surface marker Iba1 in sequential sections taken from young and aged macaques. Elevated Iba1 expression is associated with microglial activation, although it is constitutively expressed by all microglial cells and is not thought to be

restricted to an activated subset [536]. No significant difference in Iba1$^+$ microglial cell densities were observed between the two age groups (Figure 6.6).

Iba1$^+$ microglial cell density was also evaluated in the CA1, CA2/3 and CA4 subfields of the hippocampus, a region where an increase in activated microglia has previously been associated with ageing in humans (Figure 6.7) [537]. Iba1$^+$ microglial cell densities were comparable in the two groups in all subfields.

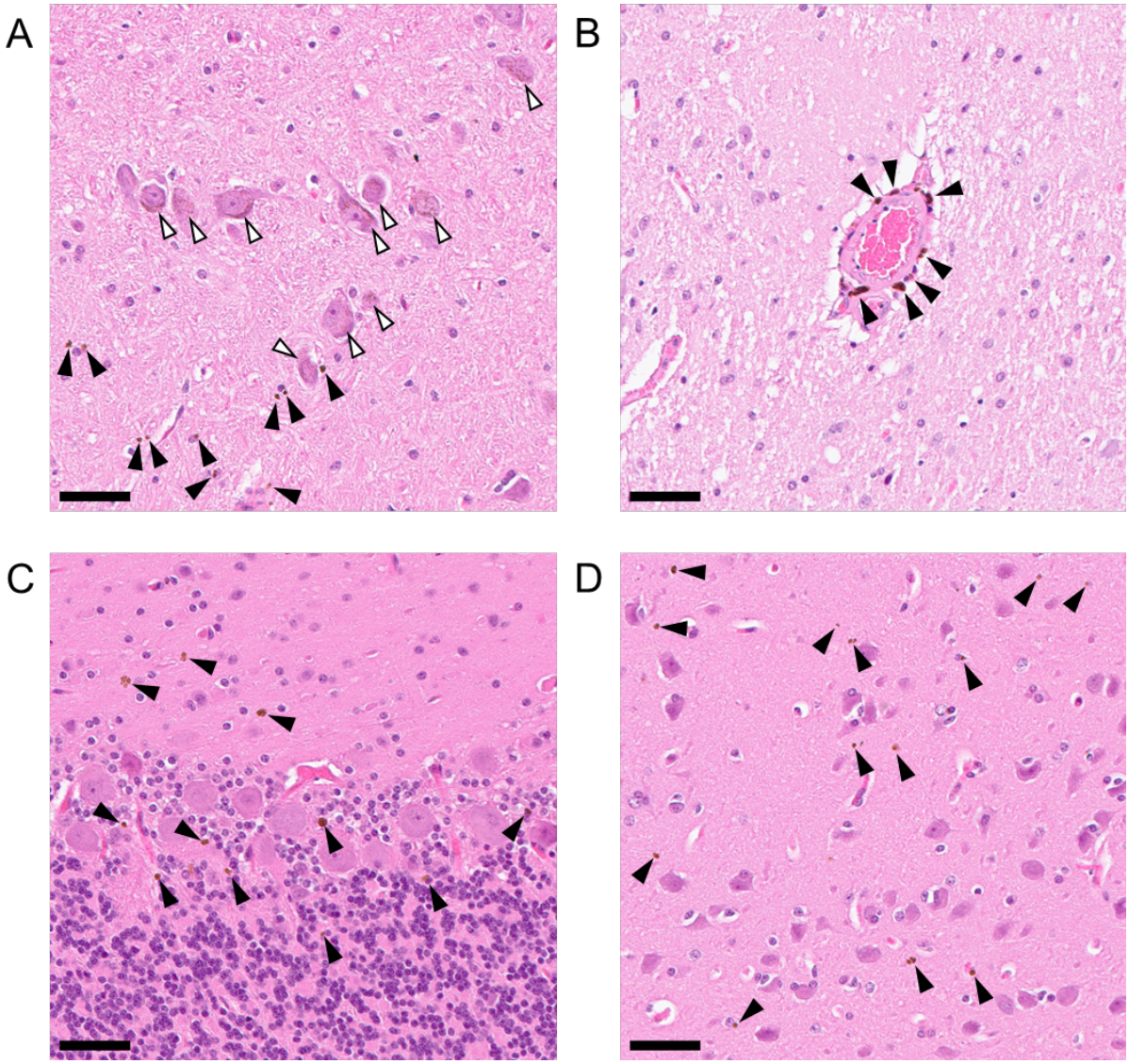

Figure 6.4. Age-related histopathology identified in H&E-stained brain tissue of cynomolgus macaques. (A) Neuromelanin and haemosiderin in the SN. (B) Perivascular haemosiderin. (C) Haemosiderin in the cerebellar grey matter and Purkinje cell layer. (D) Haemosiderin in the CA1 subfield of the hippocampus. All images taken on a 20X magnification. In all images black arrows indicate haemosiderin and white arrows with black borders signify neuromelanin. Scale bar = 50µm.

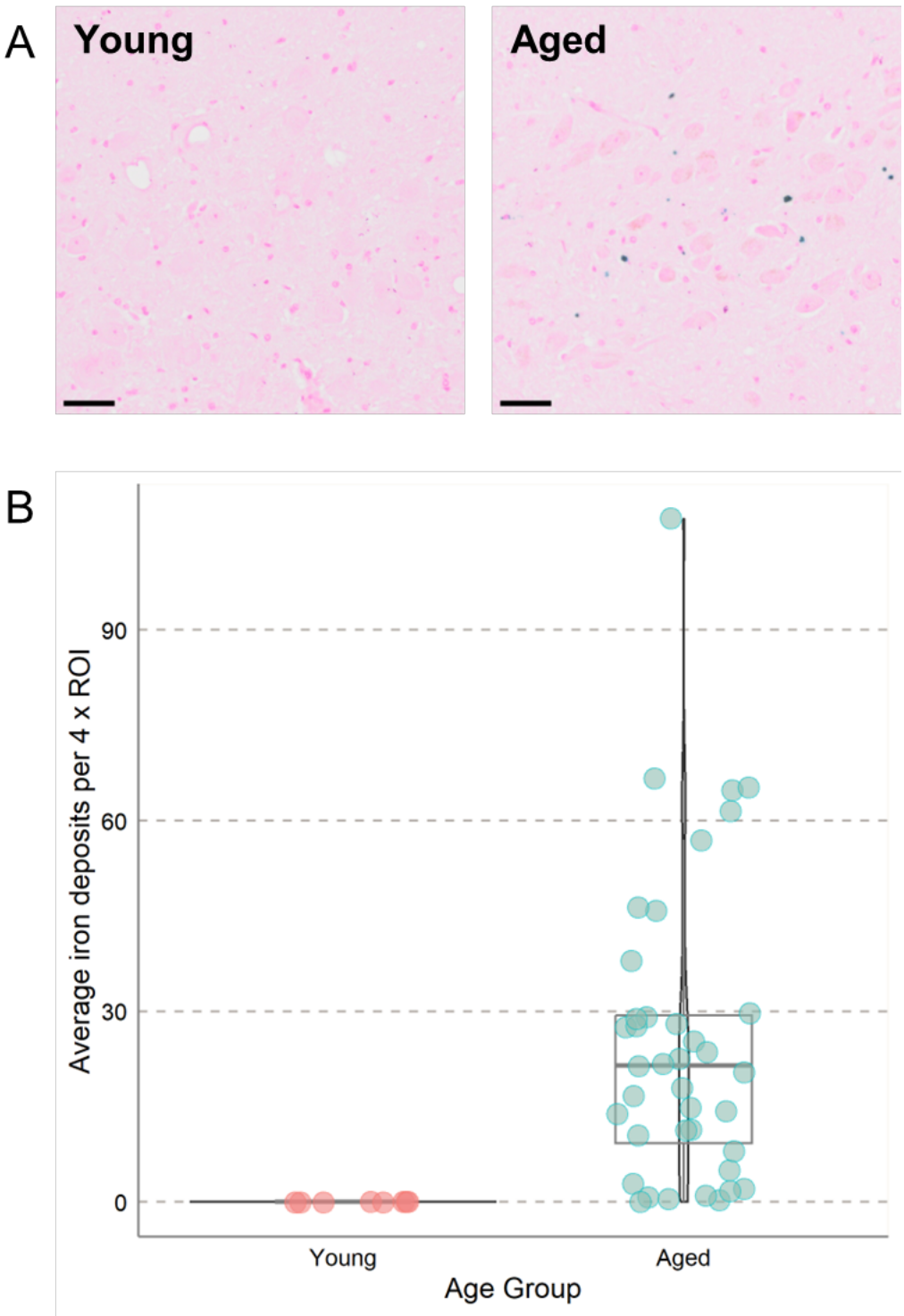

Figure 6.5. Quantification of iron deposits in the SN in Perls' Prussian blue-stained brain tissue sections from cynomolgus macaques. (A) Representative images of sections from young (0-5 years; n=3) and aged (13-20 years; n=13) cynomolgus macaques are shown. (B) Quantification of iron deposits in the SN. Each data point displayed in the figure represents the average number of Iba1^{+} cells across 4 ROIs in one tissue section. Measurements were taken from three sequential tissue sections for each cynomolgus macaque in each age group. Statistical analysis between the groups was carried out by fitting a linear mixed model. 95% CI and p-values were computed using a Wald t-distribution approximation. The effect of age group was found to be statistically non-significant and positive (95% CI [-2.92, 53.74], t(43) = 1.81, p = 0.077). Scale bar = 50µm.

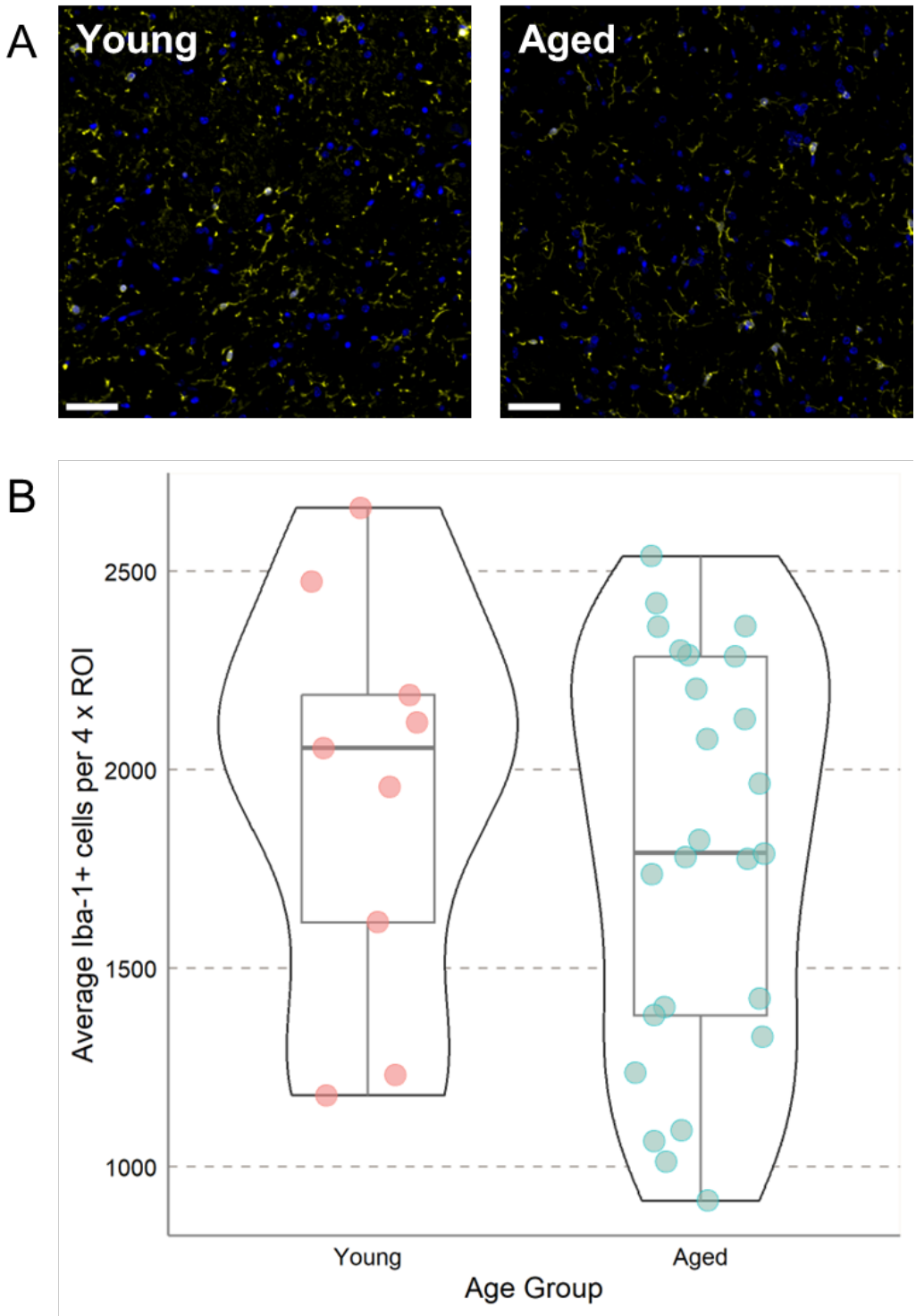

Figure 6.6. Iba1$^+$ microglial cell density is unaffected by age in the cynomolgus macaque SN. (A) Iba1$^+$ microglial cells were identified by immunostaining (yellow) and nuclei were counterstained with Hoechst (blue). Representative images of microglia in young (0-5 years; n=3) and aged (13-20 years; n=13) cynomolgus macaques are shown. (B) Quantification of Iba1$^+$ microglial cells was carried out in the SN. Each data point displayed in the figure represents the average number of Iba1$^+$ cells across 4 ROIs in one tissue section. Measurements were taken from three sequential tissue sections for each cynomolgus macaque in each age group. Statistical analysis between the groups was carried out by fitting a linear mixed model. 95% CI and p-values were computed using a Wald t-distribution approximation. The effect of age group was found to be statistically non-significant and negative (95% CI [-774.06, 540.30], t(30) = -0.36, p = 0.719). Scale bar = 50μm.

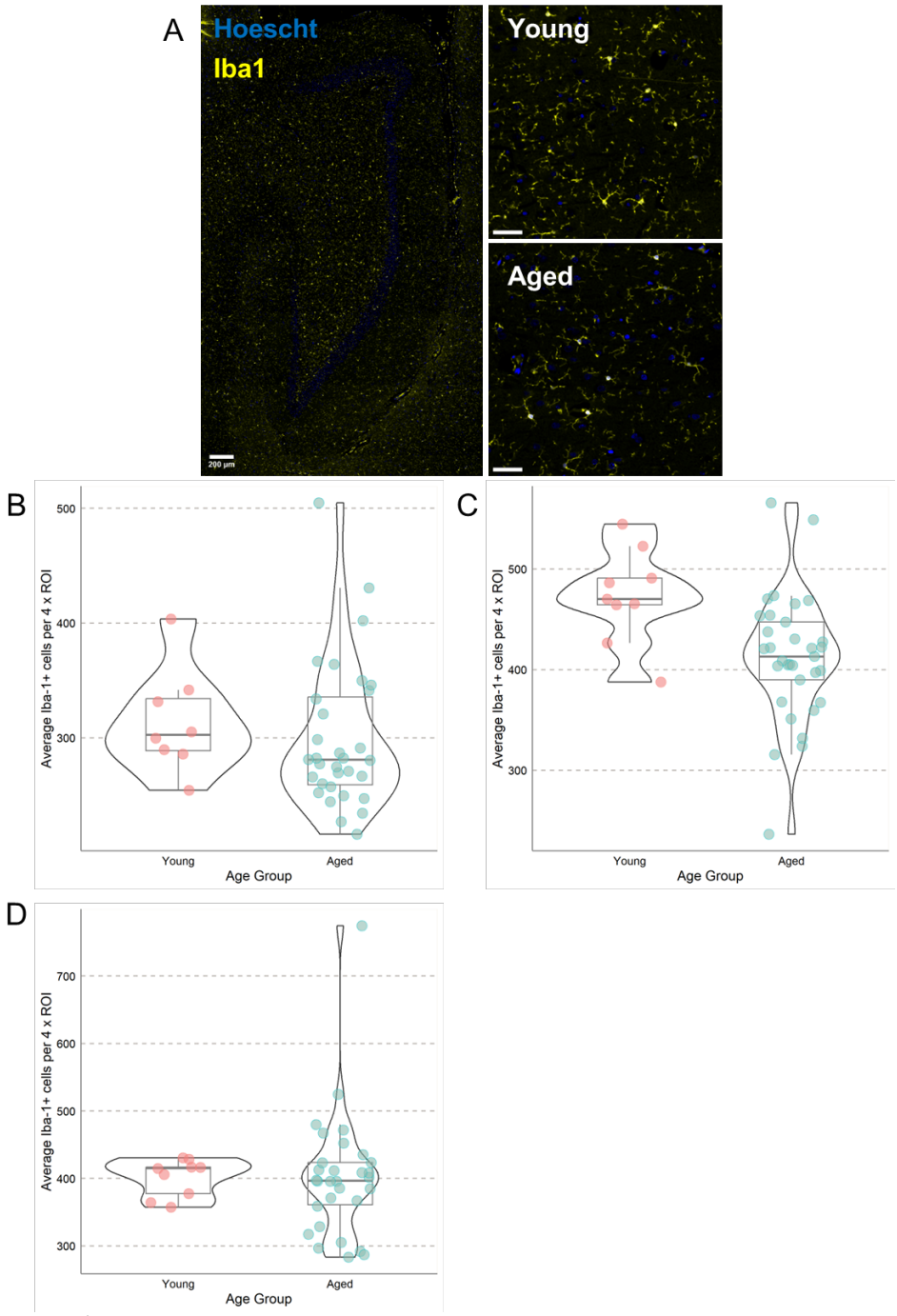

Figure 6.7. Iba1$^+$ microglial cell density is unaffected by age in the cynomolgus macaque hippocampus. (A) Iba1$^+$ microglial cells were identified by immunostaining (yellow) and nuclei were counterstained with Hoechst (blue). Representative images of microglia in the CA1 hippocampal subfield of young (0-5 years; n=3) and aged (13-20 years; n=13) cynomolgus macaques are shown. Quantification of Iba1$^+$ microglial cells was carried out in (B) CA1 (C) CA2/3 and (D) CA4 subfields of the hippocampus. Each data point displayed in the figure represents the average number of Iba1$^+$ cells across 4 ROIs in one tissue section. Measurements were taken from three sequential tissue sections for each cynomolgus macaque in each age group. Statistical analysis between the groups was carried out by fitting a linear mixed model. 95% CI and p-values were computed using a Wald t-distribution approximation. In all regions the effect of age group was found to be statistically non-significant (A: 95% CI [-87.52, 64.79], t(36) = -0.30, p = 0.764; B: 95% CI [-125.01, 6.63], t(38) = -1.82, p = 0.077; C: 95% CI[-84.50, 66.36], t(148) = -0.24, p = 0.812). Scale bar = 50µm unless otherwise specified.

6.2. Discussion

Age is the major risk factor in developing neurodegenerative disease and is associated with inflammageing and pathological changes in the CNS [538-540]. Determining the changes that occur as part of the healthy ageing process, and in the absence of disease, is therefore important.

The histological findings presented in this chapter are considered to represent normal age-related pathology and are not indicative of the presence of neurodegenerative disease. Of note, the observation that neuromelanin is present within neurons in the SN in the aged cohort of the present study, but not young, aligns with what is known about neuromelanin accumulation with age in humans and primates [507, 509].

While haemosiderin and ferritin are distinct iron storage forms, they are often not differentiated, with positive Perls' Prussian blue staining commonly referred to as haemosiderin staining, despite the iron stain reacting with all ferric iron deposits, including iron bound to ferritin. This misconception might stem from the fact that ferritin-bound iron is water-soluble and could leach from samples during staining. However, while Perls' staining may be less sensitive to ferritin deposits (positive ferritin staining has previously been described as having a lighter blue 'blush' compared to the deeper blue of haemosiderin [541]) it is not insensitive.

In this Chapter, a clear distinction between ferritin and haemosiderin was not possible as staining for ferritin was not attempted. Therefore, while most positive Perls' staining showed deep blue, granular deposits suggestive of haemosiderin, I did not attempt to distinguish the iron storage forms. Despite this, it is likely that the areas where haemosiderin is observed in H&E-stained sections corresponding to positive Perls' staining represent significant haemosiderin deposition, even if iron-containing ferritin is also present.

Haemosiderin was a common observation in aged but not young animals. A previous survey of brain histopathology carried out in 76 young cynomolgus macaques (2-8 years) found only one instance of haemosiderin deposition, substantiating my findings in the young cohort [542]. In aged animals, iron deposits in the midbrain and cerebellum, visualised as haemosiderin on H&E-stained sections or as a granular blue pigment in Perls'-stained sections, were frequently located close to or within the perivascular space of blood vessels. This observation aligns with the theory that age-related disruption of the BBB may occur in these regions. However, the limited dispersion of the deposits around vessels indicates that any disruption was mild. The variability in the number of deposits observed in different animals may be linked to previous or current systemic inflammation. A previous study showed that in aged, but not young mice, LPS administration results in increased cerebral microbleeds, indicating that systemic inflammation

increases susceptibility to BBB disruption in aged mice [543]. In the present study, it is plausible that inflammation arising from illness or injury could compromise the BBB, primarily affecting the aged cohort and contributing to the observed deposition.

Significant iron deposition is also evident in the CA1 hippocampal subfield in the majority of aged animals, aligning with the findings of previous studies of ageing humans and NHPs [544-546]. Iron deposition in CA1 is associated with reduced memory performance in cognitively unimpaired older humans using magnetic resonance imaging (MRI) [546]. Behavioural analysis was not feasible in the present study, but a previous study in aged rhesus macaques showed that calorie restriction from middle-age reduces iron accumulation in multiple brain regions, including the hippocampus, in parallel with improved fine motor performance compared to animals with no calorie restriction [544]. These studies suggest that accumulation of iron in the hippocampus is detrimental even in cognitively normal individuals. The findings here indicate that iron also accumulates in the hippocampus, and specifically the CA1 subfield, in cynomolgus macaques, and could provide a suitable model for further studies of iron-associated pathology in the hippocampus.

In the aged cohort iron deposits were more abundant in the SN than in any other region and often present in the neuropil, but not in proximity to blood vessels. The visualisation of ferric iron deposits using Perls' Prussian blue confirms that a substantial amount of stored iron is not chelated by neuromelanin in this brain region. The lack of iron deposits in young animals signifies that ageing is associated with an increase in total iron, as has been observed in the human SN, which may arise due to increased BBB permeability or changes in iron homeostasis [506-508]. The additional iron may then be bound by ferritin, which has also been reported to be upregulated with age in the SN, or haemosiderin [506, 507].

Alternatively, extra-neuronal deposits may accumulate due to the redistribution of iron within the SN in various storage forms. A potential trigger could be intracellular iron levels reaching a level where they exceed the capacity of neuromelanin to efficiently chelate the metal, resulting in an increased amount of intracellular redox-active iron. This would contribute to neuronal stress and eventual cell death, possibly explaining the neuronal loss observed as a feature of normal ageing in elderly subjects [547]. The release of neuromelanin into the extracellular space is, however, associated with microglial activation [548-550]. No significant increase in Iba1 density was observed in the present study in the SN. This suggests that any extracellular neuromelanin, if present, is being efficiently cleared by phagocytic microglia or brain-resident macrophages. This efficient clearance likely prevents the triggering of a pro-inflammatory response but may contribute to these cells becoming over-laden with iron, which may represent the iron deposits observed in H&E and Perls'-stained tissue sections.

The lack of an age-related change in Iba1 density aligns with studies of microglial cell densities in elderly chimpanzees, common marmosets, and rhesus macaques, where no change in total microglial numbers was seen with age in either the SN or hippocampus [529-531]. In contrast, Kodama *et al.* reported an increase in the number of Iba1$^+$ microglial cells in the hippocampus of older cynomolgus macaques when comparing young (3-5 years) and aged (18-19 years) cohorts (Table 6.2) [532]. The discrepancy between the findings of Kodama *et al.* and those presented here may be attributed to several factors. First, different age boundaries; the present study includes animals aged 13-20 years in the aged cohort, whereas Kodama *et al.* focused on 18- and 19-year-old cynomolgus macaques. Second, Kodama *et al.* had a larger young cohort (12 animals compared to 3 in the present study) and an equal number of aged animals.

Table 6. 2. Histological studies investigating the effect of age on microglial cell density in the hippocampus and SN

			Observation	
Study	Species (Cohort size)	Age range (Sex)	Hippocampus	SN
Present study	Cynomolgus macaques (16)	4 – 20 years (MF)	↔* (CA1 – CA4)	↔
Kodama *et al.* [532]	Cynomolgus macaques (24)	3 – 19 years (F)	↑	-
Kanaan, Kordower, and Collier [529]	Rhesus macaques (14)	9 – 29 years (MF)	-	↔
Rodriguez-Callejas, Fuchs, and Perez-Cruz [531]	Common marmosets (11)	1.6 – 18 years† (M)	↔	-
Edler *et al.* [530]	Chimpanzees (20)	37 – 62 years (MF)	↔ (CA1, CA3)	-
DiPatre and Gelman [537]	Human (17)	38 – 72† (not reported)	↑ (CA1 – CA4)	-
Shahidehpour *et al.* [528]	Human (51)	10 – 99 (MF)	↑ (CA1)	-

M, male; F, female; MF; mixed-sex group; SN, substantia nigra; CA, cornu ammonis
* ↔ indicates no change
† Mean age of youngest *vs* oldest groups

Third, methodological differences. Kodama *et al.* did not specify which hippocampal subfields were examined or include technical replicates in their analysis, and they employed a different image analysis procedure.

In contrast, histological human studies have suggested an age-related increase in microglial activation and density, although studies are sparse (Table 6.2). A post-mortem study found microglial density was increased in the CA1-CA4 hippocampus subfields of elderly humans in the absence of neurodegenerative disease when compared to young subjects, and further increased in subjects with AD [537]. The study was, however, limited by small sample sizes. A more recent analysis found that an increase in total microglia was associated with age in the CA1 subfield of the hippocampus [528]. I*n vivo* position electron tomography (PET) imaging to quantify microglial activation in healthy subjects has produced conflicting results. Some studies have shown microglial activation is increased in older subjects in multiple brain regions, including the hippocampus and the cerebellum, while another did not [551-553].

The main drawback of using Iba1 density as a method to assess age-related microglial changes is it's high sensitivity to variations in staining quality and background staining, which can introduce bias when averaging across different image fields [554]. It is also difficult to distinguish increases in cell number versus increases in activation. Another drawback of this study is that microglial morphology was not assessed. Increased numbers of microglia with an activated or dystrophic morphology have been observed in both ageing humans and NHPs [205, 206, 527-531]. In humans, however, one study attributed the increase in the number of dystrophic microglia with age to an age-related increase in the total number of microglia [528]. There is limited visual evidence of differences in microglial morphology between the young and the aged cohorts in the present study. However, since there are no known studies of microglial morphology in cynomolgus macaques, it would be interesting to explore alternative methods, such as skeletal or fractal analysis, for assessing microglial morphology.

Although this study did not find an association between areas with increased iron deposition and microglial activation, previous research has suggested a potential link between dysregulated iron homeostasis and age-related microglial alterations. In humans, genes associated with iron homeostasis are upregulated in ageing- and disease-associated microglia [528]. Among these genes, the enrichment of FTL is particularly notable, as a positive association between FTL and FTH protein concentrations and iron in the SN has been observed throughout the lifespan [507, 528]. FTL^+ microglia have been reported to increase with age in humans, likely in response to elevated intracellular iron concentrations, and are associated with a higher incidence of dystrophic morphology [206]. An increased abundance of dystrophic $Iba1^+FTL^+$ microglia has also been previously observed in AD patients [525].

To further elucidate the links between dysregulated iron homeostasis and dystrophic microglia the use of cynomolgus macaques as an animal model may be beneficial, as the present work suggests a similar age-associated accumulation of iron as seen in humans. Future work would benefit from investigation of ferritin, and especially FTL, expression with age, not performed here due to a lack of known NHP-reactive reagents for this protein, as well as phenotyping and morphological analysis of microglia.

6.2.1. Limitations

The main limitation of the present study is the small number of animals in each cohort. Chronological age does not always equal an individual's immune 'age' [23, 555] and it can be assumed that there is substantial variation in the onset of age-related pathology in the brain. The number of animals included within the present study, or previous studies in NHPs and humans, are therefore insufficient to confidently determine the trajectory of age-related pathology and microglial alterations, or to capture the range of severity that could occur at each age.

Another major limitation is the low number of animals included in the cohort that are of extreme old age. The life span of cynomolgus macaques in captivity is approximately 25-30 years old, however, the animals in the present study were ≤20 years old [556]. The indication that there is some change in microglial density in 18–19-year-old macaques by Kodama *et al.* suggests that more significant pathology and heightened neuroinflammation may be seen at more advanced ages [532]. The wide range of ages included within the aged cohort in the present study may have obscured any age-related alterations.

Other limitations include the use of cross-sectional data to study the longitudinal process of ageing and the use of only one H&E-stained section to assess brain histopathology, as there will likely be considerable variation within individuals depending on the depth the section was taken. The ongoing nature of the present study's sample collection also meant that brain tissues were stored for differing lengths of time, which may affect staining efficiency. One animal in the young cohort had recurring bouts of diarrhoea prior to being culled, while two of the aged animals had high blood sugar prior to being culled, indicative of diabetes. These conditions may have had unknown effects on brain pathology. The present study focused on a small number of brain regions, which does not produce a full picture of age-related brain pathology and neurodegeneration in cynomolgus macaques. Inconsistencies in the depth at which sections were taken for H&E, Perls Prussian Blue, and Iba1 staining between individuals may also have introduced bias, as brain pathology may not be uniform throughout the tissue samples. Finally, the use of Iba1 as a microglial activation marker may not provide sufficient

sensitivity to evaluate age-associated changes in microglial activation. The combined use of Iba1 with other markers, such as MHC-II and CD68, may be beneficial in future work [536].

6.3. Conclusions

The findings presented here highlight that age-related pathology is a common finding in older cynomolgus macaques and that they display the same age-related iron accumulation in the hippocampus and the SN observed in humans. In contrast, it does not provide evidence that iron accumulation or ageing alone is associated with microglial activation in cynomolgus macaques, as previously reported in cynomolgus macaques and humans. This may, however, be a result of the small cohort size and lack of animals of extreme age. To fully determine whether microglia are impacted by ageing in cynomolgus macaques, a detailed assessment of changes in microglial morphology throughout the lifespan in cynomolgus macaques is needed. The similarities in age-associated accumulation of age-related histopathology in cynomolgus macaques to humans shown here makes cynomolgus macaques an attractive option for further study of brain ageing and differentiating the processes preceding disease development.

7.0. Chapter 7: General Discussion

7.1. Summary of thesis outcomes

The physiological similarities between NHPs and humans makes them valuable models for biological research. However, due to their considerable cognitive capabilities and complex behavioural needs, their use in research also raises a number of ethical questions, especially regarding studies which may cause pain, distress, or suffering [49]. For this reason, the use of cynomolgus macaques in research requires careful consideration of behavioural, biological, ethical, and practical factors.

The aim of this thesis was to determine the suitability of cynomolgus macaques as a model for studying human ageing, the microbiome-gut-brain axis and inflammageing. To investigate the presence of age-related physiological declines observed in humans [13-15, 23, 63, 65, 134-139, 162, 164, 166, 170, 197, 203, 205, 206], I characterised the effect of age on the interconnected systems of the brain, intestinal tract, and intestinal microbiome in a cohort of healthy, captive-bred cynomolgus macaques of differing ages. To the best of my knowledge, this study represents the first characterisation of the cynomolgus macaque luminal intestinal microbiome in both the small and the large intestine and as such provides a more relevant and accurate representation of the intestinal microbiome compared to the common and continuing use of faecal samples. Additionally, it represents the first characterisation of the effect of ageing on the intestinal mycobiome in cynomolgus macaques. While there is limited evidence that the intestinal microbiome and intestinal homeostasis are affected by age in this cohort of animals, the work in this thesis has demonstrated that cynomolgus macaques may be valuable models for studying age-related brain pathology. Together, the findings provide a valuable reference for the microbiome-gut-brain axis for an animal model commonly used to model human diseases and determine the safety and efficacy of therapeutic interventions.

The intestinal microbiome represents a source of stimuli that may initiate and drive inflammageing through persistent activation of the immune system [140]. This thesis demonstrated that no age-associated changes in intestinal prokaryotic and fungal taxonomic abundance and/or beta-diversity were seen between different age groups in captive-bred cynomolgus macaques, in contrast with what has been found in previously in human studies based on faecal sampling [13-22, 63, 65]. Region-specific measures of alpha-diversity also did not consistently show a difference between age groups. Additionally, no age-associated changes in microbial metabolic pathways were observed, with the exception of a single pathway, which aligns with the overall lack of age-associated shifts in taxonomy. The general lack of age-associated effects on intestinal microbial taxonomy, diversity, and function were unexpected, especially as previous studies have found age-associated changes to the

intestinal microbiome in captive cynomolgus macaques [57, 64, 70]. As discussed in Chapter 4, a number of factors may explain this discrepancy, including differing co-housing arrangements, cohort size, age range, age distribution, and methodology. Based on my findings, it therefore cannot be concluded that cynomolgus macaques reflect the effects of age on the intestinal microbiome described in humans.

An increase in age-associated brain pathology, particularly related to iron-accumulation, is apparent in the brains of aged cynomolgus macaques, aligning with previous observations in humans and NHPs [503, 504, 507-512]. Notably, iron accumulation was detected in the SN, mirroring that seen in human ageing [506-508]. The mechanisms behind this apparent accumulation of iron are unclear but may be related to age-associated increases in BBB permeability or changes in iron homeostasis [225, 503, 518-523]. Conversely, expression of Iba1, a marker for microglial activation, was not associated with age in the hippocampus and SN, two regions which are heavily impacted in neurodegenerative diseases [506, 557]. These findings suggest that microglial homeostasis, albeit as defined by a single marker, Iba1, is unaffected by age in healthy cynomolgus macaques. The similarities between age-associated brain pathology in cynomolgus macaques and humans supports their use in studies requiring suitable animal models for human brain ageing. However, in the absence of microglial activation and age-associated intestinal dysbiosis, the accumulation of age-associated brain pathology cannot be attributed to age-associated neuroinflammation or changes to the microbiota-gut-brain axis in the cohort of animals studied here.

There is conflicting evidence for an increase in intestinal barrier permeability with age, although it is often cited as a potential cause of inflammageing. While evidence for this theory is supported by animal studies, findings in humans are inconclusive [34, 140, 157-160, 162-166]. In this thesis, I tested associations between increasing age and blood-based surrogate markers of intestinal permeability and systemic inflammation and found that age was significantly and positively associated with blood LBP concentration. Age was also associated with morphological changes in the small and large intestine which may be related to an inflammatory status. These findings indicate that cynomolgus macaques may exhibit an age-associated increase in intestinal permeability and inflammageing independently of any structural changes of the intestinal prokaryome and mycobiome, suggesting that these alterations are not driven by bacterial or fungal alterations. However, as discussed further in the next section, the limited sample size used for these experiments restricts the interpretation of these findings.

The work in this thesis also contributes to the existing field of research relating to the characterisation of the cynomolgus macaque intestinal microbiome. Distinct bacterial communities are apparent in different spatial regions of the intestinal tract. Reference-based

taxonomic profiling reveals species belonging to the genus *Segatella* are the dominant taxa in the caecum and the colon, while *S. ventriculi*, a potential pathobiont, is dominant in the small intestine. Resolution of *Segatella* to species level reveals a dominance of species associated with the human, rather than NHP, intestinal microbiota, reflective perhaps of the influence of regular human (handler) contact and differences in diet and hygiene in this cohort of captive-bred cynomolgus macaques compared to wild populations [374]. In the intestinal mycobiota the yeast *A. pintolopesii* is the dominant species in all intestinal regions profiled and is a putative gut commensal. This diverges from findings in human studies in which genera including *Candida*, *Saccharomyces*, and *Aspergillus* are commonly found to dominate the intestinal mycobiome, highlighting the species-specific differences in the composition of intestinal microbiota [168, 170, 173]. The dominance of a yeast species from the *Arxiozyma* genus (previously *Kazachstania*) does, however, align with previous findings in both wild and captive cynomolgus macaques [174]. This suggests a specific adaption of *Arxiozyma* to the cynomolgus macaque intestinal tract, making its presence more resistant to the influence of captivity. I also identified 108 putative novel bacterial and archaeal SGBs, the identification of which contributes to knowledge of the cynomolgus macaque microbiome and may be a source of previously unrealised microbial diversity.

7.2. Study limitations

7.2.1. Sample collection

The target sample size for this study was 30 cynomolgus macaques, with 10 animals each of the young, adult, and aged age groups. Limitations on the availability of animals due to increased demand during the COVID-19 pandemic were a factor which limited sample collection. Additionally, sample collection was limited to animals to be culled for reasons separate to the study objectives, such as ex-breeder status designation, diagnosis of non-infectious disease or illness, or abnormal or aggressive behaviour. These limits especially restricted sample collection from young animals. As samples were collected on an *ad hoc* basis, sample storage duration also differed between animals and may have impacted inter-individual comparisons. In particular, this may have affected analysis of the intestinal microbiome. Microbial composition profiles are less stable in faecal samples stored without preservation buffer than those which are [558]. In the present study, intestinal content samples were collected from healthy animals and stored at -80 °C with no additive following collection. Differing storage times pre-DNA extraction may therefore have had a disparate impact on microbial community composition. In contrast, faecal samples collected from obese animals and age-matched controls were collected into OMNIgene-GUT tubes, which contain a preservation buffer. This may have had a beneficial effect on taxonomic and functional stability

of the microbiome profiles of these samples, and improves confidence in the comparisons made despite the samples being collected at different times [559, 560].

An additional limitation was the age boundaries established for each age category. Animals within the 'young' age group (0-7 years) ranged from infancy to adolescence. This broad categorisation of age encompasses many developmental stages, from weaning to sexual maturity. For females, who reach sexual maturity at approximately 4 years, compared to 7 years for males, this also encompasses an age at which they can reproduce [561]. The limited number of animals prevented further modification of the age boundaries. Together, these limitations may contribute to the inability to discern significant age-associated effects on the intestinal microbiome, as previous microbiome studies in NHPs using larger sample sizes and/or a more even distribution of ages evaluating age-associated microbial alterations found significant effects [57, 64, 70]. This may also explain the absence of corresponding age-associated effects on brain and intestinal pathology, and systemic markers of inflammageing.

The lack of animals of extreme old age may also contribute to the inability to detect age-associated intestinal microbial alterations. The typical lifespan of cynomolgus macaques in captivity is 25-30 years, with some animals reaching up to 40 years old, although in the wild the median lifespan of macaques is approximately 15 years [260, 562]. The samples used to investigate the intestinal microbiome in this thesis were collected from animals of between 4-20 years old. Within the colony from which these animals came, animals are not typically kept to ages greater than 20 years. Macaques age at around three times the rate of humans [563, 564] with the majority of our animals in the 'aged' category being equivalent to middle-aged humans (45-60 years old). Most studies associate age-associated changes to the intestinal microbiome with older adults [13-22, 63, 65]. However, while a higher variability in the composition of the intestinal microbiota is associated with adults >60 years old, the human intestinal microbiota starts to exhibit increased uniqueness at approximately 50 years of age. These changes positively correlate with microbial metabolic markers associated with immune function, inflammation, and longevity [87]. This suggests that, potentially subtle, microbial alterations begin in middle age in humans. It is possible that the upper limit of the cohorts' age range, in addition to the size of the cohort, was insufficient to capture age-associated effects.

7.2.2. Limitations of characterising the intestinal microbiome

As described in Chapter 4, a limitation of the intestinal prokaryome characterisation is the underrepresentation of NHP-specific intestinal commensals within commonly used reference-based profiling databases [361]. Species-level resolution of the intestinal mycobiome is also restricted by the limited divergence of the ITS region in closely related species, as discussed in Chapter 3 [456, 457]. These constraints limit the characterisation of the bacterial, archaeal,

and fungal fractions of the intestinal microbiota, and therefore the ability to determine age-associated alterations.

Marker gene and shotgun metagenomic sequencing measurements suffer from taxonomic bias because of how different taxa respond to each step in a sequencing protocol. These biases can arise at each step in a given workflow, including taxa-specific variation in DNA extraction efficiency, amplification, sequencing and accuracy of taxonomic assignment [565, 566]. While all samples used for characterisation of the prokaryome and the mycobiome in this study are subjected to the same protocols, respectively, it is possible that taxonomic bias results in variations in relative abundance across samples [567]. As a result, my investigation of the intestinal microbiome in this cohort of cynomolgus macaques may be subject to taxonomic bias, which may affect the accuracy of comparisons between individuals as well as to findings from other studies.

Further bias may have been introduced because of sampling time. Diurnal oscillations in bacterial abundance in the intestinal microbiome are apparent in mice and humans, influenced by factors including food intake and the host's circadian rhythms [354, 568, 569]. The consequence of this is that the composition of the intestinal microbiome will vary depending on the time of day that animals are culled, and sampling carried out. This was not accounted for within this study but may have had an impact on the taxonomic and functional profiles of the intestinal microbiome. Also unaccounted for was the temporal variability of the intestinal microbiome. A previous study in humans found that, day to day, the major faecal bacterial genera can vary in abundance by up to 100-fold. Some of this variation is attributable to differences in diet and stool moisture content, but not to the time of day the samples were collected, suggesting that this variability is independent from the diurnal oscillations of the intestinal microbiome [570]. These findings imply that intra-individual variation may vary over a short time-period as much as inter-individual variation, and that large sample sizes and/or repeat, longitudinal, sampling may be required to account for this variability and distinguish significant effects on microbial composition.

7.2.3. Confounding variables

The animals in this study underwent regular treatment with antibiotics in response to infection or injury. Administration of antibiotics in humans results in compositional changes to the intestinal microbiome, as well as a reduced microbial diversity lasting for several months or longer [571]. Occasionally, antibiotic administration to these animals was followed with probiotic treatment, which can influence microbial taxonomy [572]. These variables are not accounted for within this thesis but may impact measures of intestinal microbial diversity and comparisons between individuals. Additionally, close contact from co-housing can lead to the sharing of

microbes and animals' intestinal microbiomes becoming more similar over time, as described in mice co-housed within cages [419]. Grooming behaviours also promote similarity of the intestinal microbiome [381, 398-400]. These factors may be an influencing factor on intestinal microbiome composition, explaining the similarity of the intestinal microbiome between age groups. Close contact between individuals of differing ages is, however, more reflective of social interactions in humans and wild cynomolgus macaques.

Injury is a common occurrence within the colony due to aggressive interactions with other animals. In mice, skin injury is associated with changes to the intestinal microbiome and intestinal immune homeostasis [573]. Given the link between changes in the intestinal microbiome, disruption of intestinal immune homeostasis, and inflammatory responses in the brain, it's possible that injury can influence microbial taxonomy, inflammatory and intestinal permeability biomarkers, and the accumulation of age-associated brain pathology. The frequency, type, and timing of injuries were not accounted for in this study, making it impossible to rule them out as confounding factors.

7.3. Future Research

To validate the findings of this thesis, a follow-up study with a larger cohort, including animals of more extreme old age (20-30 years old), and an evenly distributed age range should be conducted. Power calculations based on the current results will help determine the optimal number of animals to include in this future study. Previous work in wild macaques found that age-associated shifts in the composition of the intestinal microbiota were specific to male animals [92]. It may therefore also be interesting to incorporate an even sex distribution within this study to investigate potential sex-specific effects of ageing.

Future work should also more comprehensively characterise the intestinal microbiome to determine with certainty whether age-associated changes to the intestinal microbiome of healthy, captive-bred cynomolgus macaques are present. This should include characterisation of the intestinal virome. This was not attempted in this thesis due to the complexities involved in virome characterisation, including the challenges associated with taxonomic annotation of genome sequences resulting from incomplete reference databases [574, 575]. Like bacteria and fungi, viruses, including bacteriophages, interact with the host immune system and aid in maintaining immune homeostasis and disease progression [576]. Previous investigation of the DNA faecal virome in captive cynomolgus macaques revealed significant age-associated shifts in viral, predominantly bacteriophage, taxonomy [577]. It would be interesting to see if this is replicable in this cohort of captive-bred cynomolgus macaques.

Secondly, for further investigation of the metabolic function of the intestinal microbiome, metabolomics and/or metatranscriptomics may be useful tools. Metabolomics provides a direct measure of metabolic activity, while metatranscriptomics captures the active functional profile of a microbial community through messenger RNA (mRNA) sequencing [578]. In contrast, functional inference of the microbiome using WGS data, as carried out in this study, can only imply the functional potential of the microbial community [579]. Metabolomic and metatranscriptomic techniques may reveal further age-related effects on metabolic pathways within this cohort, as well as providing insights into host-microbial interactions that may are not apparent with WGS datasets.

Thirdly, the under-representation of NHP microbiomes in microbial reference databases limits the identification of age-associated alterations in bacterial and archaeal fractions of the intestinal microbiota in this cohort of cynomolgus macaques. To overcome this, further identification and characterisation of novel taxa within the cynomolgus macaque intestinal microbiome is needed. In this thesis, I identified putative novel SGBs and taxonomically assigned them to genus level, partially characterising the fraction of the intestinal prokaryome that remained uncharacterised by reference-based profiling methods. To further characterise the intestinal microbiome in ageing cynomolgus macaques, it would be beneficial to investigate any age-associated effects on abundance and distribution of these SGBs across the cohort.

Finally, it will be of interest to compare the intestinal microbiome of this cohort to wild cynomolgus macaques and human populations to determine their similarity to captive-bred cynomolgus macaques. Previous work has found that the intestinal microbiome of wild cynomolgus macaques changes following translocation to a hygienic, captive environment [60]. My own findings suggests that the intestinal microbiota of captive-bred cynomolgus macaques exhibits similarity to humans, although further work would be required to confirm this. Establishing the effect of captivity on the cynomolgus macaque microbiome may be a valuable reference for future microbiome research in this animal model.

Aside from further characterisation of the intestinal microbiome, future experiments could also improve the characterisation of the effect of age on CNS inflammation and microglia in cynomolgus macaques, as discussed in Chapter 6. This could include morphological phenotyping to identify activated or primed morphology, which has previously been associated with age, and evaluating the expression of microglial activation-associated molecules such as MHC-II and CD68 [205, 206, 208, 213-215]. It could also include evaluation of the expression of the FTL receptor, upregulation of which has been associated with age, dysregulated iron homeostasis, and dystrophic microglia, to further investigate the link between iron deposition and age-related pathology in the brain [206]. Future experiments could also employ

immunofluorescence staining to investigate the effects of ageing on BBB tight junction protein expression. This approach may also help determine whether age-related changes in the BBB contribute to increased brain iron deposition.

7.4. Conclusion

Collectively the findings of this thesis do not support the use of captive cynomolgus macaques aged 20 years or younger as an ideal animal model for human ageing and its association with intestinal dysbiosis. They do, however, provide a basis for further investigation of age-associated brain pathology, intestinal permeability, and inflammageing in this animal model. They also provide a valuable reference for the effect of ageing on healthy, captive-bred cynomolgus macaques.

References

1. Parker, A., S. Fonseca, and S.R. Carding. *Gut microbes and metabolites as modulators of blood-brain barrier integrity and brain health.* Gut Microbes, 2020. **11**(2): p. 135-157. DOI: 10.1080/19490976.2019.1638722.
2. Hooper, L.V. and A.J. Macpherson. *Immune adaptations that maintain homeostasis with the intestinal microbiota.* Nature Reviews Immunology, 2010. **10**(3): p. 159-169. DOI: 10.1038/nri2710.
3. Parker, A., S. James, C. Purse, A. Brion, A. Goldson, A. Telatin, D. Baker, and S. Carding. *Absence of Bacteria Permits Fungal Gut-To-Brain Translocation and Invasion in Germfree Mice but Ageing Alone Does Not Drive Pathobiont Expansion in Conventionally Raised Mice.* Frontiers in Aging Neuroscience, 2022. **14**. DOI: 10.3389/fnagi.2022.828429.
4. James, S.A., A. Parker, C. Purse, A. Telatin, D. Baker, S. Holmes, J. Durham, S.G.P. Funnell, and S.R. Carding. *The Cynomolgus Macaque Intestinal Mycobiome Is Dominated by the Kazachstania Genus and K. pintolopesii Species.* Journal of Fungi, 2022. **8**(10). DOI: 10.3390/jof8101054.
5. United Nations, *World Social Report 2023: Leaving No One Behind in an Ageing World*. 2023, United Nations Fund for Population Activities, https://desapublications.un.org/publications/world-social-report-2023-leaving-no-one-behind-ageing-world.
6. Barnett, K., S.W. Mercer, M. Norbury, G. Watt, S. Wyke, and B. Guthrie. *Epidemiology of multimorbidity and implications for health care, research, and medical education: a cross-sectional study.* Lancet, 2012. **380**(9836): p. 37-43. DOI: 10.1016/S0140-6736(12)60240-2.
7. Partridge, L., J. Deelen, and P.E. Slagboom. *Facing up to the global challenges of ageing.* Nature, 2018. **561**(7721): p. 45-56. DOI: 10.1038/s41586-018-0457-8.
8. Feigin, V.L., T. Vos, E. Nichols, M.O. Owolabi, W.M. Carroll, M. Dichgans, G. Deuschl, P. Parmar, M. Brainin, and C. Murray. *The global burden of neurological disorders: translating evidence into policy.* Lancet Neurol, 2020. **19**(3): p. 255-265. DOI: 10.1016/S1474-4422(19)30411-9.
9. Lamptey, R.N.L., B. Chaulagain, R. Trivedi, A. Gothwal, B. Layek, and J. Singh. *A Review of the Common Neurodegenerative Disorders: Current Therapeutic Approaches and the Potential Role of Nanotherapeutics.* Int J Mol Sci, 2022. **23**(3). DOI: 10.3390/ijms23031851.
10. Loh, J.S., W.Q. Mak, L.K.S. Tan, C.X. Ng, H.H. Chan, S.H. Yeow, J.B. Foo, Y.S. Ong, C.W. How, and K.Y. Khaw. *Microbiota-gut-brain axis and its therapeutic applications in neurodegenerative diseases.* Signal Transduct Target Ther, 2024. **9**(1): p. 37. DOI: 10.1038/s41392-024-01743-1.
11. Sender, R., S. Fuchs, and R. Milo. *Are We Really Vastly Outnumbered? Revisiting the Ratio of Bacterial to Host Cells in Humans.* Cell, 2016. **164**(3): p. 337-40. DOI: 10.1016/j.cell.2016.01.013.
12. Zheng, D.P., T. Liwinski, and E. Elinav. *Interaction between microbiota and immunity in health and disease.* Cell Research, 2020. **30**(6): p. 492-506. DOI: 10.1038/s41422-020-0332-7.
13. Ghosh, T.S., F. Shanahan, and P.W. O'Toole. *The gut microbiome as a modulator of healthy ageing.* Nature Reviews Gastroenterology & Hepatology, 2022. **19**(9): p. 565-584. DOI: 10.1038/s41575-022-00605-x.
14. Ghosh, T.S., F. Shanahan, and P.W. O'Toole. *Toward an improved definition of a healthy microbiome for healthy aging.* Nature Aging, 2022. **2**(11): p. 1054–1069. DOI: 10.1038/s43587-022-00306-9.
15. Odamaki, T., K. Kato, H. Sugahara, N. Hashikura, S. Takahashi, J.Z. Xiao, F. Abe, and R. Osawa. *Age-related changes in gut microbiota composition from newborn to*

centenarian: a cross-sectional study. BMC Microbiol, 2016. **16**: p. 90. DOI: 10.1186/s12866-016-0708-5.
16. Xu, C., H. Zhu, and P. Qiu. *Aging progression of human gut microbiota.* BMC Microbiol, 2019. **19**(1): p. 236. DOI: 10.1186/s12866-019-1616-2.
17. Biagi, E., C. Franceschi, S. Rampelli, M. Severgnini, R. Ostan, S. Turroni, C. Consolandi, S. Quercia, M. Scurti, D. Monti, M. Capri, P. Brigidi, and M. Candela. *Gut Microbiota and Extreme Longevity.* Current Biology, 2016. **26**(11): p. 1480-1485. DOI: 10.1016/j.cub.2016.04.016.
18. Wu, L., T. Zeng, A. Zinellu, S. Rubino, D.J. Kelvin, and C. Carru. *A Cross-Sectional Study of Compositional and Functional Profiles of Gut Microbiota in Sardinian Centenarians.* mSystems, 2019. **4**(4). DOI: 10.1128/mSystems.00325-19.
19. Rampelli, S., M. Soverini, F. D'Amico, M. Barone, T. Tavella, D. Monti, M. Capri, A. Astolfi, P. Brigidi, E. Biagi, C. Franceschi, S. Turroni, and M. Candela. *Shotgun Metagenomics of Gut Microbiota in Humans with up to Extreme Longevity and the Increasing Role of Xenobiotic Degradation.* mSystems, 2020. **5**(2). DOI: 10.1128/mSystems.00124-20.
20. Kong, F., Y. Hua, B. Zeng, R. Ning, Y. Li, and J. Zhao. *Gut microbiota signatures of longevity.* Curr Biol, 2016. **26**(18): p. R832-R833. DOI: 10.1016/j.cub.2016.08.015.
21. Wang, N., R. Li, H.J. Lin, C.W. Fu, X.C. Wang, Y.M. Zhang, M.F. Su, P.X. Huang, J.H. Qian, F. Jiang, H.X. Wang, L.F. Jiang, X. Yu, J.X. Liu, Y. Chen, and Q.W. Jiang. *Enriched taxa were found among the gut microbiota of centenarians in East China.* Plos One, 2019. **14**(10). DOI: 10.1371/journal.pone.0222763.
22. Tuikhar, N., S. Keisam, R.K. Labala, Imrat, P. Ramakrishnan, M.C. Arunkumar, G. Ahmed, E. Biagi, and K. Jeyaram. *Comparative analysis of the gut microbiota in centenarians and young adults shows a common signature across genotypically non-related populations.* Mechanisms of Ageing and Development, 2019. **179**: p. 23-35. DOI: 10.1016/j.mad.2019.02.001.
23. Alpert, A., Y. Pickman, M. Leipold, Y. Rosenberg-Hasson, X. Ji, R. Gaujoux, H. Rabani, E. Starosvetsky, K. Kveler, S. Schaffert, D. Furman, O. Caspi, U. Rosenschein, P. Khatri, C.L. Dekker, H.T. Maecker, M.M. Davis, and S.S. Shen-Orr. *A clinically meaningful metric of immune age derived from high-dimensional longitudinal monitoring.* Nat Med, 2019. **25**(3): p. 487-495. DOI: 10.1038/s41591-019-0381-y.
24. Schaap, L.A., S.M.F. Pluijm, D.J.H. Deeg, T.B. Harris, S.B. Kritchevsky, A.B. Newman, L.H. Colbert, M. Pahor, S.M. Rubin, F.A. Tylavsky, M. Visser, and H.A. Study. *Higher Inflammatory Marker Levels in Older Persons: Associations With 5-Year Change in Muscle Mass and Muscle Strength.* Journals of Gerontology Series a-Biological Sciences and Medical Sciences, 2009. **64**(11): p. 1183-1189. DOI: 10.1093/gerona/glp097.
25. Soysal, P., B. Stubbs, P. Lucato, C. Luchini, M. Solmi, R. Peluso, G. Sergi, A.T. Isik, E. Manzato, S. Maggi, M. Maggio, A.M. Prina, T.D. Cosco, Y.T. Wu, and N. Veronese. *Inflammation and frailty in the elderly: A systematic review and meta-analysis.* Ageing Research Reviews, 2016. **31**: p. 1-8. DOI: 10.1016/j.arr.2016.08.006.
26. Kuo, H.K., J.F. Bean, C.J. Yen, and S.G. Leveille. *Linking C-reactive protein to late-life disability in the National Health and Nutrition Examination Survey (NHANES) 1999-2002.* Journals of Gerontology Series a-Biological Sciences and Medical Sciences, 2006. **61**(4): p. 380-387. DOI: DOI 10.1093/gerona/61.4.380.
27. Ferrucci, L., T.B. Harris, J.M. Guralnik, R.P. Tracy, M.C. Corti, H.J. Cohen, B. Penninx, M. Pahor, R. Wallace, and R.J. Havlik. *Serum IL-6 level and the development of disability in older persons.* Journal of the American Geriatrics Society, 1999. **47**(6): p. 639-646. DOI: 10.1111/j.1532-5415.1999.tb01583.x.
28. Fabbri, E., Y. An, M. Zoli, E.M. Simonsick, J.M. Guralnik, S. Bandinelli, C.M. Boyd, and L. Ferrucci. *Aging and the Burden of Multimorbidity: Associations With Inflammatory and Anabolic Hormonal Biomarkers.* Journals of Gerontology Series a-Biological Sciences and Medical Sciences, 2015. **70**(1): p. 63-70. DOI: 10.1093/gerona/glu127.

29. Xue, Q.L. *The frailty syndrome: definition and natural history.* Clin Geriatr Med, 2011. **27**(1): p. 1-15. DOI: 10.1016/j.cger.2010.08.009.
30. Franceschi, C., M. Bonafe, S. Valensin, F. Olivieri, M. De Luca, E. Ottaviani, and G. De Benedictis. *Inflamm-aging. An evolutionary perspective on immunosenescence.* Ann N Y Acad Sci, 2000. **908**: p. 244-54. DOI: 10.1111/j.1749-6632.2000.tb06651.x.
31. Franceschi, C., P. Garagnani, P. Parini, C. Giuliani, and A. Santoro. *Inflammaging: a new immune-metabolic viewpoint for age-related diseases.* Nat Rev Endocrinol, 2018. **14**(10): p. 576-590. DOI: 10.1038/s41574-018-0059-4.
32. López-Otin, C., M.A. Blasco, L. Partridge, M. Serrano, and G. Kroemer. *Hallmarks of aging: An expanding universe.* Cell, 2023. **186**(2): p. 243-278. DOI: 10.1016/j.cell.2022.11.001.
33. Morais, L.H., H.L.t. Schreiber, and S.K. Mazmanian. *The gut microbiota-brain axis in behaviour and brain disorders.* Nat Rev Microbiol, 2021. **19**(4): p. 241-255. DOI: 10.1038/s41579-020-00460-0.
34. Parker, A., S. Romano, R. Ansorge, A. Aboelnour, G. Le Gall, G.M. Savva, M.G. Pontifex, A. Telatin, D. Baker, E. Jones, D. Vauzour, S. Rudder, L.A. Blackshaw, G. Jeffery, and S.R. Carding. *Fecal microbiota transfer between young and aged mice reverses hallmarks of the aging gut, eye, and brain.* Microbiome, 2022. **10**(1). DOI: 10.1186/s40168-022-01243-w.
35. Lee, J., V.R. Venna, D.J. Durgan, H.N. Shi, J. Hudobenko, N. Putluri, J. Petrosino, L.D. McCullough, and R.M. Bryan. *Young versus aged microbiota transplants to germ-free mice: increased short-chain fatty acids and improved cognitive performance.* Gut Microbes, 2020. **12**(1). DOI: 10.1080/19490976.2020.1814107.
36. D'Amato, A., L.D. Mannelli, E. Lucarini, A.L. Man, G. Le Gall, J.J.V. Branca, C. Ghelardini, A. Amedei, E. Bertelli, M. Regoli, A. Pacini, G. Luciani, P. Gallina, A. Altera, A. Narbad, M. Gulisano, L. Hoyles, D. Vauzour, and C. Nicoletti. *Faecal microbiota transplant from aged donor mice affects spatial learning and memory via modulating hippocampal synaptic plasticity- and neurotransmission-related proteins in young recipients.* Microbiome, 2020. **8**(1). DOI: 10.1186/s40168-020-00914-w.
37. Grabrucker, S., M. Marizzoni, E. Silajdzic, N. Lopizzo, E. Mombelli, S. Nicolas, S. Dohm-Hansen, C. Scassellati, D.V. Moretti, M. Rosa, K. Hoffmann, J.F. Cryan, O.F. O'Leary, J.A. English, A. Lavelle, C. O'Neill, S. Thuret, A. Cattaneo, and Y.M. Nolan. *Microbiota from Alzheimer's patients induce deficits in cognition and hippocampal neurogenesis.* Brain, 2023. **146**(12): p. 4916-4934. DOI: 10.1093/brain/awad303.
38. Sampson, T.R., J.W. Debelius, T. Thron, S. Janssen, G.G. Shastri, Z.E. Ilhan, C. Challis, C.E. Schretter, S. Rocha, V. Gradinaru, M.F. Chesselet, A. Keshavarzian, K.M. Shannon, R. Krajmalnik-Brown, P. Wittung-Stafshede, R. Knight, and S.K. Mazmanian. *Gut Microbiota Regulate Motor Deficits and Neuroinflammation in a Model of Parkinson's Disease.* Cell, 2016. **167**(6): p. 1469-1480. DOI: 10.1016/j.cell.2016.11.018.
39. Zhuang, Z.Q., L.L. Shen, W.W. Li, X. Fu, F. Zeng, L. Gui, Y. Lü, M. Cai, C. Zhu, Y.L. Tan, P. Zheng, H.Y. Li, J. Zhu, H.D. Zhou, X.L. Bu, and Y.J. Wang. *Gut Microbiota is Altered in Patients with Alzheimer's Disease.* Journal of Alzheimers Disease, 2018. **63**(4): p. 1337-1346. DOI: 10.3233/Jad-180176.
40. Vogt, N.M., R.L. Kerby, K.A. Dill-McFarland, S.J. Harding, A.P. Merluzzi, S.C. Johnson, C.M. Carlsson, S. Asthana, H. Zetterberg, K. Blennow, B.B. Bendlin, and F.E. Rey. *Gut microbiome alterations in Alzheimer's disease.* Scientific Reports, 2017. **7**. DOI: 10.1038/s41598-017-13601-y.
41. Liu, P., L. Wu, G. Peng, Y. Han, R. Tang, J. Ge, L. Zhang, L. Jia, S. Yue, K. Zhou, L. Li, B. Luo, and B. Wang. *Altered microbiomes distinguish Alzheimer's disease from amnestic mild cognitive impairment and health in a Chinese cohort.* Brain Behav Immun, 2019. **80**: p. 633-643. DOI: 10.1016/j.bbi.2019.05.008.

42. Qian, Y., X. Yang, S. Xu, C. Wu, Y. Song, N. Qin, S.D. Chen, and Q. Xiao. *Alteration of the fecal microbiota in Chinese patients with Parkinson's disease.* Brain Behav Immun, 2018. **70**: p. 194-202. DOI: 10.1016/j.bbi.2018.02.016.
43. Huang, B., S.W.H. Chau, Y.P. Liu, J.W.Y. Chan, J. Wang, S.L. Ma, J.H. Zhang, P.K.S. Chan, Y.K. Yeoh, Z.G. Chen, L. Zhou, S.H. Wong, V.C.T. Mok, K.F. To, H.M. Lai, S. Ng, C. Trenkwalder, F.K.L. Chan, and Y.K. Wing. *Gut microbiome dysbiosis across early Parkinson's disease, REM sleep behavior disorder and their first-degree relatives.* Nature Communications, 2023. **14**(1). DOI: 10.1038/s41467-023-38248-4.
44. Hill-Burns, E.M., J.W. Debelius, J.T. Morton, W.T. Wissemann, M.R. Lewis, Z.D. Wallen, S.D. Peddada, S.A. Factor, E. Molho, C.P. Zabetian, R. Knight, and H. Payami. *Parkinson's Disease and Parkinson's Disease Medications Have Distinct Signatures of the Gut Microbiome.* Movement Disorders, 2017. **32**(5): p. 739-749. DOI: 10.1002/mds.26942.
45. Unger, M.M., J. Spiegel, K.U. Dillmann, D. Grundmann, H. Philippeit, J. Bürmann, K. Fassbender, A. Schwiertz, and K.H. Schäfer. *Short chain fatty acids and gut microbiota differ between patients with Parkinson's disease and age-matched controls.* Parkinsonism & Related Disorders, 2016. **32**: p. 66-72. DOI: 10.1016/j.parkreldis.2016.08.019.
46. Nuzum, N.D., E.A. Szymlek-Gay, S. Loke, S.L. Dawson, W.P. Teo, A.M. Hendy, A. Loughman, and H. Macpherson. *Differences in the gut microbiome across typical ageing and in Parkinson's disease.* Neuropharmacology, 2023. **235**. DOI: 10.1016/j.neuropharm.2023.109566.
47. Romano, S., G.M. Savva, J.R. Bedarf, I.G. Charles, F. Hildebrand, and A. Narbad. *Meta-analysis of the Parkinson's disease gut microbiome suggests alterations linked to intestinal inflammation.* Npj Parkinsons Disease, 2021. **7**(1). DOI: 10.1038/s41531-021-00156-z.
48. Nagpal, J. and J.F. Cryan. *Microbiota-brain interactions : Moving toward mechanisms in model organisms.* Neuron, 2021. **109**(24): p. 3930-3953. DOI: 10.1016/j.neuron.2021.09.036.
49. Phillips, K.A., K.L. Bales, J.P. Capitanio, A. Conley, P.W. Czoty, B.A. t Hart, W.D. Hopkins, S.L. Hu, L.A. Miller, M.A. Nader, P.W. Nathanielsz, J. Rogers, C.A. Shively, and M.L. Voytko. *Why primate models matter.* Am J Primatol, 2014. **76**(9): p. 801-27. DOI: 10.1002/ajp.22281.
50. Gray, D.T. and C.A. Barnes. *Experiments in macaque monkeys provide critical insights into age-associated changes in cognitive and sensory function.* Proc Natl Acad Sci U S A, 2019. **116**(52): p. 26247-26254. DOI: 10.1073/pnas.1902279116.
51. Lopez-Otin, C., M.A. Blasco, L. Partridge, M. Serrano, and G. Kroemer. *The hallmarks of aging.* Cell, 2013. **153**(6): p. 1194-217. DOI: 10.1016/j.cell.2013.05.039.
52. Claesson, M.J., I.B. Jeffery, S. Conde, S.E. Power, E.M. O'Connor, S. Cusack, H.M. Harris, M. Coakley, B. Lakshminarayanan, O. O'Sullivan, G.F. Fitzgerald, J. Deane, M. O'Connor, N. Harnedy, K. O'Connor, D. O'Mahony, D. van Sinderen, M. Wallace, L. Brennan, C. Stanton, J.R. Marchesi, A.P. Fitzgerald, F. Shanahan, C. Hill, R.P. Ross, and P.W. O'Toole. *Gut microbiota composition correlates with diet and health in the elderly.* Nature, 2012. **488**(7410): p. 178-84. DOI: 10.1038/nature11319.
53. Claesson, M.J., S. Cusack, O. O'Sullivan, R. Greene-Diniz, H. de Weerd, E. Flannery, J.R. Marchesi, D. Falush, T. Dinan, G. Fitzgerald, C. Stanton, D. van Sinderen, M. O'Connor, N. Harnedy, K. O'Connor, C. Henry, D. O'Mahony, A.P. Fitzgerald, F. Shanahan, C. Twomey, C. Hill, R.P. Ross, and P.W. O'Toole. *Composition, variability, and temporal stability of the intestinal microbiota of the elderly.* Proc Natl Acad Sci U S A, 2011. **108**: p. 4586-91. DOI: 10.1073/pnas.1000097107.
54. Gao, L., I. Maidment, F.E. Matthews, L. Robinson, C. Brayne, M.R.C.C. Function, and Ageing Study. *Medication usage change in older people (65+) in England over 20 years: findings from CFAS I and CFAS II.* Age and Ageing, 2018. **47**(2): p. 220-225. DOI: 10.1093/ageing/afx158.

55. Petersen, C. and J.L. Round. *Defining dysbiosis and its influence on host immunity and disease.* Cell Microbiol, 2014. **16**(7): p. 1024-33. DOI: 10.1111/cmi.12308.
56. Lugli, G.A., L. Mancabelli, C. Milani, F. Fontana, C. Tarracchini, G. Alessandri, D. van Sinderen, F. Turroni, and M. Ventura. *Comprehensive insights from composition to functional microbe-based biodiversity of the infant human gut microbiota.* NPJ Biofilms Microbiomes, 2023. **9**(1): p. 25. DOI: 10.1038/s41522-023-00392-6.
57. Yang, Y.P., Y. Lu, P.J. Yu, Q.M. Liu, C.S. Gao, X.T. Zhang, and Q. Sun. *Characterization of gut microbial alterations in cynomolgus macaques during growth and maturation.* Zoological Research, 2022. **43**(2): p. 176-179. DOI: 10.24272/j.issn.2095-8137.2021.304.
58. Yatsunenko, T., F.E. Rey, M.J. Manary, I. Trehan, M.G. Dominguez-Bello, M. Contreras, M. Magris, G. Hidalgo, R.N. Baldassano, A.P. Anokhin, A.C. Heath, B. Warner, J. Reeder, J. Kuczynski, J.G. Caporaso, C.A. Lozupone, C. Lauber, J.C. Clemente, D. Knights, R. Knight, and J.I. Gordon. *Human gut microbiome viewed across age and geography.* Nature, 2012. **486**(7402): p. 222-7. DOI: 10.1038/nature11053.
59. Adriansjach, J., S.T. Baum, E.J. Lefkowitz, W.J. Van Der Pol, T.W. Buford, and R.J. Colman. *Age-Related Differences in the Gut Microbiome of Rhesus Macaques.* J Gerontol A Biol Sci Med Sci, 2020. **75**(7): p. 1293-1298. DOI: 10.1093/gerona/glaa048.
60. Sawaswong, V., P. Chanchaem, T. Kemthong, S. Warit, A. Chaiprasert, S. Malaivijitnond, and S. Payungporn. *Alteration of gut microbiota in wild-borne long-tailed macaques after 1-year being housed in hygienic captivity.* Sci Rep, 2023. **13**(1). DOI: 10.1038/s41598-023-33163-6.
61. Sadoughi, B., D. Schneider, R. Daniel, O. Schulke, and J. Ostner. *Aging gut microbiota of wild macaques are equally diverse, less stable, but progressively personalized.* Microbiome, 2022. **10**(1): p. 95. DOI: 10.1186/s40168-022-01283-2.
62. Human Microbiome Project, C. *Structure, function and diversity of the healthy human microbiome.* Nature, 2012. **486**(7402): p. 207-14. DOI: 10.1038/nature11234.
63. Mariat, D., O. Firmesse, F. Levenez, V. Guimaraes, H. Sokol, J. Dore, G. Corthier, and J.P. Furet. *The Firmicutes/Bacteroidetes ratio of the human microbiota changes with age.* BMC Microbiol, 2009. **9**: p. 123. DOI: 10.1186/1471-2180-9-123.
64. Duan, J.J., B.M. Yin, W. Li, T.J. Chai, W.W. Liang, Y. Huang, X.M. Tan, P. Zheng, J. Wu, Y.F. Li, Y. Li, W. Zhou, and P. Xie. *Age-related changes in microbial composition and function in cynomolgus macaques.* Aging-US, 2019. **11**(24): p. 12080-12096. DOI: 10.18632/aging.102541.
65. Vaiserman, A., M. Romanenko, L. Piven, V. Moseiko, O. Lushchak, N. Kryzhanovska, V. Guryanov, and A. Koliada. *Differences in the gut Firmicutes to Bacteroidetes ratio across age groups in healthy Ukrainian population.* BMC Microbiol, 2020. **20**(1): p. 221. DOI: 10.1186/s12866-020-01903-7.
66. Mann, E.R., Y.K. Lam, and H.H. Uhlig. *Short-chain fatty acids: linking diet, the microbiome and immunity.* Nat Rev Immunol, 2024. **24**(8): p. 577-595. DOI: 10.1038/s41577-024-01014-8.
67. Martin-Gallausiaux, C., L. Marinelli, H.M. Blottiere, P. Larraufie, and N. Lapaque. *SCFA: mechanisms and functional importance in the gut.* Proc Nutr Soc, 2021. **80**(1): p. 37-49. DOI: 10.1017/S0029665120006916.
68. Gurav, A., S. Sivaprakasam, Y.D. Bhutia, T. Boettger, N. Singh, and V. Ganapathy. *Slc5a8, a Na-coupled high-affinity transporter for short-chain fatty acids, is a conditional tumour suppressor in colon that protects against colitis and colon cancer under low-fibre dietary conditions.* Biochemical Journal, 2015. **469**: p. 267-278. DOI: 10.1042/Bj20150242.
69. Korsten, S., H. Vromans, J. Garssen, and L.E.M. Willemsen. *Butyrate Protects Barrier Integrity and Suppresses Immune Activation in a Caco-2/PBMC Co-Culture Model While HDAC Inhibition Mimics Butyrate in Restoring Cytokine-Induced Barrier Disruption.* Nutrients, 2023. **15**(12). DOI: 10.3390/nu15122760.

70. Wei, Z.Y., J.H. Rao, M.T. Tang, G.A. Zhao, Q.C. Li, L.M. Wu, S.Q. Liu, B.H. Li, B.Q. Xiao, X.Y. Liu, and J.H. Chen. *Characterization of Changes and Driver Microbes in Gut Microbiota During Healthy Aging Using A Captive Monkey Model.* Genomics Proteomics Bioinformatics, 2022. **20**(2): p. 350-365. DOI: 10.1016/j.gpb.2021.09.009.
71. Dill-McFarland, K.A., Z.Z. Tang, J.H. Kemis, R.L. Kerby, G. Chen, A. Palloni, T. Sorenson, F.E. Rey, and P. Herd. *Close social relationships correlate with human gut microbiota composition.* Sci Rep, 2019. **9**(1): p. 703. DOI: 10.1038/s41598-018-37298-9.
72. Ross, F.C., D. Patangia, G. Grimaud, A. Lavelle, E.M. Dempsey, R.P. Ross, and C. Stanton. *The interplay between diet and the gut microbiome: implications for health and disease.* Nature Reviews Microbiology, 2024. DOI: 10.1038/s41579-024-01068-4.
73. Weersma, R.K., A. Zhernakova, and J.Y. Fu. *Interaction between drugs and the gut microbiome.* Gut, 2020. **69**(8): p. 1510-1519. DOI: 10.1136/gutjnl-2019-320204.
74. Fishbein, S.R.S., B. Mahmud, and G. Dantas. *Antibiotic perturbations to the gut microbiome.* Nature Reviews Microbiology, 2023. **21**(12): p. 772-788. DOI: 10.1038/s41579-023-00933-y.
75. Ghosh, T.S., S. Rampelli, I.B. Jeffery, A. Santoro, M. Neto, M. Capri, E. Giampieri, A. Jennings, M. Candela, S. Turroni, E.G. Zoetendal, G.D.A. Hermes, C. Elodie, N. Meunier, C.M. Brugere, E. Pujos-Guillot, A.M. Berendsen, L. De Groot, E.J.M. Feskins, J. Kaluza, B. Pietruszka, M.J. Bielak, B. Comte, M. Maijo-Ferre, C. Nicoletti, W.M. De Vos, S. Fairweather-Tait, A. Cassidy, P. Brigidi, C. Franceschi, and P.W. O'Toole. *Mediterranean diet intervention alters the gut microbiome in older people reducing frailty and improving health status: the NU-AGE 1-year dietary intervention across five European countries.* Gut, 2020. **69**(7): p. 1218-1228. DOI: 10.1136/gutjnl-2019-319654.
76. Sun, L., C. Xie, G. Wang, Y. Wu, Q. Wu, X. Wang, J. Liu, Y. Deng, J. Xia, B. Chen, S. Zhang, C. Yun, G. Lian, X. Zhang, H. Zhang, W.H. Bisson, J. Shi, X. Gao, P. Ge, C. Liu, K.W. Krausz, R.G. Nichols, J. Cai, B. Rimal, A.D. Patterson, X. Wang, F.J. Gonzalez, and C. Jiang. *Gut microbiota and intestinal FXR mediate the clinical benefits of metformin.* Nat Med, 2018. **24**(12): p. 1919-1929. DOI: 10.1038/s41591-018-0222-4.
77. Forslund, K., F. Hildebrand, T. Nielsen, G. Falony, E. Le Chatelier, S. Sunagawa, E. Prifti, S. Vieira-Silva, V. Gudmundsdottir, H.K. Pedersen, M. Arumugam, K. Kristiansen, A.Y. Voigt, H. Vestergaard, R. Hercog, P.I. Costea, J.R. Kultima, J. Li, T. Jorgensen, F. Levenez, J. Dore, H.I.T.c. Meta, H.B. Nielsen, S. Brunak, J. Raes, T. Hansen, J. Wang, S.D. Ehrlich, P. Bork, and O. Pedersen. *Disentangling type 2 diabetes and metformin treatment signatures in the human gut microbiota.* Nature, 2015. **528**(7581): p. 262-266. DOI: 10.1038/nature15766.
78. Kazarina, A., J. Kuzmicka, S. Bortkevica, P. Zayakin, J. Kimsis, V. Igumnova, D. Sadovska, L. Freimane, A. Kivrane, A. Namina, V. Capligina, A. Poksane, and R. Ranka. *Oral microbiome variations related to ageing: possible implications beyond oral health.* Arch Microbiol, 2023. **205**(4): p. 116. DOI: 10.1007/s00203-023-03464-5.
79. Ren, Y., M. Chen, Z. Wang, and J.J. Han. *Oral microbiota in aging and diseases.* Life Med, 2024. **3**(3): p. lnae024. DOI: 10.1093/lifemedi/lnae024.
80. Kunath, B.J., C. De Rudder, C.C. Laczny, E. Letellier, and P. Wilmes. *The oral-gut microbiome axis in health and disease.* Nat Rev Microbiol, 2024. **22**(12): p. 791-805. DOI: 10.1038/s41579-024-01075-5.
81. Lopez, R., P.C. Smith, G. Gostemeyer, and F. Schwendicke. *Ageing, dental caries and periodontal diseases.* J Clin Periodontol, 2017. **44 Suppl 18**: p. S145-S152. DOI: 10.1111/jcpe.12683.
82. Arimatsu, K., H. Yamada, H. Miyazawa, T. Minagawa, M. Nakajima, M.I. Ryder, K. Gotoh, D. Motooka, S. Nakamura, T. Iida, and K. Yamazaki. *Oral pathobiont induces systemic inflammation and metabolic changes associated with alteration of gut microbiota.* Sci Rep, 2014. **4**: p. 4828. DOI: 10.1038/srep04828.
83. Feng, Y.K., Q.L. Wu, Y.W. Peng, F.Y. Liang, H.J. You, Y.W. Feng, G. Li, X.J. Li, S.H. Liu, Y.C. Li, Y. Zhang, and Z. Pei. *Oral P. gingivalis impairs gut permeability and mediates*

immune responses associated with neurodegeneration in LRRK2 R1441G mice. J Neuroinflammation, 2020. **17**(1): p. 347. DOI: 10.1186/s12974-020-02027-5.

84. He, Y., W. Wu, H.M. Zheng, P. Li, D. McDonald, H.F. Sheng, M.X. Chen, Z.H. Chen, G.Y. Ji, Z.D. Zheng, P. Mujagond, X.J. Chen, Z.H. Rong, P. Chen, L.Y. Lyu, X. Wang, C.B. Wu, N. Yu, Y.J. Xu, J. Yin, J. Raes, R. Knight, W.J. Ma, and H.W. Zhou. *Regional variation limits applications of healthy gut microbiome reference ranges and disease models.* Nat Med, 2018. **24**(10): p. 1532-1535. DOI: 10.1038/s41591-018-0164-x.
85. Deschasaux, M., K.E. Bouter, A. Prodan, E. Levin, A.K. Groen, H. Herrema, V. Tremaroli, G.J. Bakker, I. Attaye, S.J. Pinto-Sietsma, D.H. van Raalte, M.B. Snijder, M. Nicolaou, R. Peters, A.H. Zwinderman, F. Backhed, and M. Nieuwdorp. *Depicting the composition of gut microbiota in a population with varied ethnic origins but shared geography.* Nat Med, 2018. **24**(10): p. 1526-1531. DOI: 10.1038/s41591-018-0160-1.
86. Badal, V.D., E.D. Vaccariello, E.R. Murray, K.E. Yu, R. Knight, D.V. Jeste, and T.T. Nguyen. *The Gut Microbiome, Aging, and Longevity: A Systematic Review.* Nutrients, 2020. **12**(12). DOI: 10.3390/nu12123759.
87. Wilmanski, T., C. Diener, N. Rappaport, S. Patwardhan, J. Wiedrick, J. Lapidus, J.C. Earls, A. Zimmer, G. Glusman, M. Robinson, J.T. Yurkovich, D.M. Kado, J.A. Cauley, J. Zmuda, N.E. Lane, A.T. Magis, J.C. Lovejoy, L. Hood, S.M. Gibbons, E.S. Orwoll, and N.D. Price. *Gut microbiome pattern reflects healthy ageing and predicts survival in humans.* Nat Metab, 2021. **3**(2): p. 274-286. DOI: 10.1038/s42255-021-00348-0.
88. Han, H., J. Zhu, Z. Zhu, J. Ni, R. Du, Y. Dai, Y. Chen, Z. Wu, L. Lu, and R. Zhang. *p-Cresyl sulfate aggravates cardiac dysfunction associated with chronic kidney disease by enhancing apoptosis of cardiomyocytes.* J Am Heart Assoc, 2015. **4**(6). DOI: 10.1161/JAHA.115.001852.
89. Nemet, I., P.P. Saha, N. Gupta, W. Zhu, K.A. Romano, S.M. Skye, T. Cajka, M.L. Mohan, L. Li, Y. Wu, M. Funabashi, A.E. Ramer-Tait, S.V. Naga Prasad, O. Fiehn, F.E. Rey, W.H.W. Tang, M.A. Fischbach, J.A. DiDonato, and S.L. Hazen. *A Cardiovascular Disease-Linked Gut Microbial Metabolite Acts via Adrenergic Receptors.* Cell, 2020. **180**(5): p. 862-877 e22. DOI: 10.1016/j.cell.2020.02.016.
90. Sang, J., D. Zhuang, T. Zhang, Q. Wu, J. Yu, and Z. Zhang. *Convergent and Divergent Age Patterning of Gut Microbiota Diversity in Humans and Nonhuman Primates.* mSystems, 2022. **7**(4): p. e0151221. DOI: 10.1128/msystems.01512-21.
91. Janiak, M.C., M.J. Montague, C.I. Villamil, M.K. Stock, A.E. Trujillo, A.N. DePasquale, J.D. Orkin, S.E. Bauman Surratt, O. Gonzalez, M.L. Platt, M.I. Martinez, S.C. Anton, M.G. Dominguez-Bello, A.D. Melin, and J.P. Higham. *Age and sex-associated variation in the multi-site microbiome of an entire social group of free-ranging rhesus macaques.* Microbiome, 2021. **9**(1): p. 68. DOI: 10.1186/s40168-021-01009-w.
92. Chen, Z., Y.K. Yeoh, M. Hui, P.Y. Wong, M.C.W. Chan, M. Ip, J. Yu, R.D. Burk, F.K.L. Chan, and P.K.S. Chan. *Diversity of macaque microbiota compared to the human counterparts.* Sci Rep, 2018. **8**(1). DOI: 10.1038/s41598-018-33950-6.
93. Johnson, J.S., D.J. Spakowicz, B.Y. Hong, L.M. Petersen, P. Demkowicz, L. Chen, S.R. Leopold, B.M. Hanson, H.O. Agresta, M. Gerstein, E. Sodergren, and G.M. Weinstock. *Evaluation of 16S rRNA gene sequencing for species and strain-level microbiome analysis.* Nat Commun, 2019. **10**(1). DOI: 10.1038/s41467-019-13036-1.
94. Pallikkuth, S., R. Mendez, K. Russell, T. Sirupangi, D. Kvistad, R. Pahwa, F. Villinger, S. Banerjee, and S. Pahwa. *Age Associated Microbiome and Microbial Metabolites Modulation and Its Association With Systemic Inflammation in a Rhesus Macaque Model.* Front Immunol, 2021. **12**. DOI: 10.3389/fimmu.2021.748397.
95. Leite, G.G.S., S. Weitsman, G. Parodi, S. Celly, R. Sedighi, M. Sanchez, W. Morales, M.J. Villanueva-Millan, G.M. Barlow, R. Mathur, S.K. Lo, L.H. Jamil, S. Paski, A. Rezaie, and M. Pimentel. *Mapping the Segmental Microbiomes in the Human Small Bowel in Comparison with Stool: A REIMAGINE Study.* Dig Dis Sci, 2020. **65**(9): p. 2595-2604. DOI: 10.1007/s10620-020-06173-x.

96. Leite, G., M. Pimentel, G.M. Barlow, C. Chang, A. Hosseini, J. Wang, G. Parodi, R. Sedighi, A. Rezaie, and R. Mathur. *Age and the aging process significantly alter the small bowel microbiome.* Cell Rep, 2021. **36**(13). DOI: 10.1016/j.celrep.2021.109765.
97. Gensollen, T., S.S. Iyer, D.L. Kasper, and R.S. Blumberg. *How colonization by microbiota in early life shapes the immune system.* Science, 2016. **352**(6285): p. 539-544. DOI: 10.1126/science.aad9378.
98. Bauer, H., R.E. Horowitz, S.M. Levenson, and H. Popper. *The response of the lymphatic tissue to the microbial flora. Studies on germfree mice.* Am J Pathol, 1963. **42**(4): p. 471-83. https://www.ncbi.nlm.nih.gov/pubmed/13966929.
99. Umesaki, Y., H. Setoyama, S. Matsumoto, and Y. Okada. *Expansion of Alpha-Beta T-Cell Receptor-Bearing Intestinal Intraepithelial Lymphocytes after Microbial Colonization in Germ-Free Mice and Its Independence from Thymus.* Immunology, 1993. **79**(1): p. 32-37. https://www.webofscience.com/wos/woscc/full-record/WOS:A1993KZ91800005.
100. Hapfelmeier, S., M.A. Lawson, E. Slack, J.K. Kirundi, M. Stoel, M. Heikenwalder, J. Cahenzli, Y. Velykoredko, M.L. Balmer, K. Endt, M.B. Geuking, R. Curtiss, 3rd, K.D. McCoy, and A.J. Macpherson. *Reversible microbial colonization of germ-free mice reveals the dynamics of IgA immune responses.* Science, 2010. **328**(5986): p. 1705-9. DOI: 10.1126/science.1188454.
101. Ivanov, II, L. Frutos Rde, N. Manel, K. Yoshinaga, D.B. Rifkin, R.B. Sartor, B.B. Finlay, and D.R. Littman. *Specific microbiota direct the differentiation of IL-17-producing T-helper cells in the mucosa of the small intestine.* Cell Host Microbe, 2008. **4**(4): p. 337-49. DOI: 10.1016/j.chom.2008.09.009.
102. Yamamoto-Hanada, K., L. Yang, M. Narita, H. Saito, and Y. Ohya. *Influence of antibiotic use in early childhood on asthma and allergic diseases at age 5.* Ann Allergy Asthma Immunol, 2017. **119**(1): p. 54-58. DOI: 10.1016/j.anai.2017.05.013.
103. Russell, S.L., M.J. Gold, M. Hartmann, B.P. Willing, L. Thorson, M. Wlodarska, N. Gill, M.R. Blanchet, W.W. Mohn, K.M. McNagny, and B.B. Finlay. *Early life antibiotic-driven changes in microbiota enhance susceptibility to allergic asthma.* EMBO Rep, 2012. **13**(5): p. 440-7. DOI: 10.1038/embor.2012.32.
104. Christ, A., M. Lauterbach, and E. Latz. *Western Diet and the Immune System: An Inflammatory Connection.* Immunity, 2019. **51**(5): p. 794-811. DOI: 10.1016/j.immuni.2019.09.020.
105. Dwiyanto, J., M.H. Hussain, D. Reidpath, K.S. Ong, A. Qasim, S.W.H. Lee, S.M. Lee, S.C. Foo, C.W. Chong, and S. Rahman. *Ethnicity influences the gut microbiota of individuals sharing a geographical location: a cross-sectional study from a middle-income country.* Sci Rep, 2021. **11**(1): p. 2618. DOI: 10.1038/s41598-021-82311-3.
106. Tyakht, A.V., E.S. Kostryukova, A.S. Popenko, M.S. Belenikin, A.V. Pavlenko, A.K. Larin, I.Y. Karpova, O.V. Selezneva, T.A. Semashko, E.A. Ospanova, V.V. Babenko, I.V. Maev, S.V. Cheremushkin, Y.A. Kucheryavyy, P.L. Shcherbakov, V.B. Grinevich, O.I. Efimov, E.I. Sas, R.A. Abdulkhakov, S.R. Abdulkhakov, E.A. Lyalyukova, M.A. Livzan, V.V. Vlassov, R.Z. Sagdeev, V.V. Tsukanov, M.F. Osipenko, I.V. Kozlova, A.V. Tkachev, V.I. Sergienko, D.G. Alexeev, and V.M. Govorun. *Human gut microbiota community structures in urban and rural populations in Russia.* Nat Commun, 2013. **4**. DOI: 10.1038/ncomms3469.
107. Ren, Y., J. Wu, Y. Wang, L. Zhang, J. Ren, Z. Zhang, B. Chen, K. Zhang, B. Zhu, W. Liu, S. Li, and X. Li. *Lifestyle patterns influence the composition of the gut microbiome in a healthy Chinese population.* Sci Rep, 2023. **13**(1). DOI: 10.1038/s41598-023-41532-4.
108. Johansson, M.E.V., M. Phillipson, J. Petersson, A. Velcich, L. Holm, and G.C. Hansson. *The inner of the two Muc2 mucin-dependent mucus layers in colon is devoid of bacteria.* Proceedings of the National Academy of Sciences of the United States of America, 2008. **105**(39): p. 15064-15069. DOI: 10.1073/pnas.0803124105.

109. Catanzaro, J.R., J.D. Strauss, A. Bielecka, A.F. Porto, F.M. Lobos, A. Urban, W.B. Schofield, and N.W. Palm. *IgA-deficient humans exhibit gut microbiota dysbiosis despite secretion of compensatory IgM.* Scientific Reports, 2019. **9**. DOI: 10.1038/s41598-019-49923-2.
110. Belkaid, Y. and T.W. Hand. *Role of the Microbiota in Immunity and Inflammation.* Cell, 2014. **157**(1): p. 121-141. DOI: 10.1016/j.cell.2014.03.011.
111. Shroff, K.E., K. Meslin, and J.J. Cebra. *Commensal enteric bacteria engender a self-limiting humoral mucosal immune response while permanently colonizing the gut.* Infect Immun, 1995. **63**(10): p. 3904-13. DOI: 10.1128/iai.63.10.3904-3913.1995.
112. Rescigno, M., M. Urbano, B. Valzasina, M. Francolini, G. Rotta, R. Bonasio, F. Granucci, J.P. Kraehenbuhl, and P. Ricciardi-Castagnoli. *Dendritic cells express tight junction proteins and penetrate gut epithelial monolayers to sample bacteria.* Nat Immunol, 2001. **2**(4): p. 361-7. DOI: 10.1038/86373.
113. Niess, J.H., S. Brand, X. Gu, L. Landsman, S. Jung, B.A. McCormick, J.M. Vyas, M. Boes, H.L. Ploegh, J.G. Fox, D.R. Littman, and H.C. Reinecker. *CX3CR1-mediated dendritic cell access to the intestinal lumen and bacterial clearance.* Science, 2005. **307**(5707): p. 254-8. DOI: 10.1126/science.1102901.
114. Hooper, L.V., T.S. Stappenbeck, C.V. Hong, and J.I. Gordon. *Angiogenins: a new class of microbicidal proteins involved in innate immunity.* Nat Immunol, 2003. **4**(3): p. 269-73. DOI: 10.1038/ni888.
115. Cash, H.L., C.V. Whitham, C.L. Behrendt, and L.V. Hooper. *Symbiotic bacteria direct expression of an intestinal bactericidal lectin.* Science, 2006. **313**(5790): p. 1126-30. DOI: 10.1126/science.1127119.
116. Zhao, Y., F. Chen, W. Wu, M. Sun, A.J. Bilotta, S. Yao, Y. Xiao, X. Huang, T.D. Eaves-Pyles, G. Golovko, Y. Fofanov, W. D'Souza, Q. Zhao, Z. Liu, and Y. Cong. *GPR43 mediates microbiota metabolite SCFA regulation of antimicrobial peptide expression in intestinal epithelial cells via activation of mTOR and STAT3.* Mucosal Immunol, 2018. **11**(3): p. 752-762. DOI: 10.1038/mi.2017.118.
117. Rogier, E.W., A.L. Frantz, M.E. Bruno, and C.S. Kaetzel. *Secretory IgA is Concentrated in the Outer Layer of Colonic Mucus along with Gut Bacteria.* Pathogens, 2014. **3**(2): p. 390-403. DOI: 10.3390/pathogens3020390.
118. Dupont, A., L. Heinbockel, K. Brandenburg, and M.W. Hornef. *Antimicrobial peptides and the enteric mucus layer act in concert to protect the intestinal mucosa.* Gut Microbes, 2014. **5**(6): p. 761-5. DOI: 10.4161/19490976.2014.972238.
119. Phalipon, A., A. Cardona, J.P. Kraehenbuhl, L. Edelman, P.J. Sansonetti, and B. Corthesy. *Secretory component: a new role in secretory IgA-mediated immune exclusion in vivo.* Immunity, 2002. **17**(1): p. 107-15. DOI: 10.1016/s1074-7613(02)00341-2.
120. Peterson, D.A., N.P. McNulty, J.L. Guruge, and J.I. Gordon. *IgA response to symbiotic bacteria as a mediator of gut homeostasis.* Cell Host Microbe, 2007. **2**(5): p. 328-39. DOI: 10.1016/j.chom.2007.09.013.
121. Kim, S., S.U. Seo, and M.N. Kweon. *Gut microbiota-derived metabolites tune host homeostasis fate.* Semin Immunopathol, 2024. **46**(1-2): p. 2. DOI: 10.1007/s00281-024-01012-x.
122. Park, J.H., T. Kotani, T. Konno, J. Setiawan, Y. Kitamura, S. Imada, Y. Usui, N. Hatano, M. Shinohara, Y. Saito, Y. Murata, and T. Matozaki. *Promotion of Intestinal Epithelial Cell Turnover by Commensal Bacteria: Role of Short-Chain Fatty Acids.* PLoS One, 2016. **11**(5). DOI: 10.1371/journal.pone.0156334.
123. Wang, H.B., P.Y. Wang, X. Wang, Y.L. Wan, and Y.C. Liu. *Butyrate enhances intestinal epithelial barrier function via up-regulation of tight junction protein Claudin-1 transcription.* Dig Dis Sci, 2012. **57**(12): p. 3126-35. DOI: 10.1007/s10620-012-2259-4.
124. Venkatesh, M., S. Mukherjee, H. Wang, H. Li, K. Sun, A.P. Benechet, Z. Qiu, L. Maher, M.R. Redinbo, R.S. Phillips, J.C. Fleet, S. Kortagere, P. Mukherjee, A. Fasano, J. Le Ven, J.K. Nicholson, M.E. Dumas, K.M. Khanna, and S. Mani. *Symbiotic bacterial*

metabolites regulate gastrointestinal barrier function via the xenobiotic sensor PXR and Toll-like receptor 4. Immunity, 2014. **41**(2): p. 296-310. DOI: 10.1016/j.immuni.2014.06.014.
125. Chang, P.V., L. Hao, S. Offermanns, and R. Medzhitov. *The microbial metabolite butyrate regulates intestinal macrophage function via histone deacetylase inhibition.* Proc Natl Acad Sci U S A, 2014. **111**(6): p. 2247-52. DOI: 10.1073/pnas.1322269111.
126. Schulthess, J., S. Pandey, M. Capitani, K.C. Rue-Albrecht, I. Arnold, F. Franchini, A. Chomka, N.E. Ilott, D.G.W. Johnston, E. Pires, J. McCullagh, S.N. Sansom, C.V. Arancibia-Carcamo, H.H. Uhlig, and F. Powrie. *The Short Chain Fatty Acid Butyrate Imprints an Antimicrobial Program in Macrophages.* Immunity, 2019. **50**(2): p. 432-445. DOI: 10.1016/j.immuni.2018.12.018.
127. Song, X., X. Sun, S.F. Oh, M. Wu, Y. Zhang, W. Zheng, N. Geva-Zatorsky, R. Jupp, D. Mathis, C. Benoist, and D.L. Kasper. *Microbial bile acid metabolites modulate gut RORgamma(+) regulatory T cell homeostasis.* Nature, 2020. **577**(7790): p. 410-415. DOI: 10.1038/s41586-019-1865-0.
128. Campbell, C., P.T. McKenney, D. Konstantinovsky, O.I. Isaeva, M. Schizas, J. Verter, C. Mai, W.B. Jin, C.J. Guo, S. Violante, R.J. Ramos, J.R. Cross, K. Kadaveru, J. Hambor, and A.Y. Rudensky. *Bacterial metabolism of bile acids promotes generation of peripheral regulatory T cells.* Nature, 2020. **581**(7809): p. 475–479. DOI: 10.1038/s41586-020-2193-0.
129. Song, X.Y., H.H. Zhang, Y.B. Zhang, B. Goh, B. Bao, S.S. Mello, X.M. Sun, W. Zheng, F.S. Gazzaniga, M. Wu, F.F. Qu, Q.Z. Yin, M.S. Gilmore, S.F. Oh, and D.L. Kasper. *Gut microbial fatty acid isomerization modulates intraepithelial T cells.* Nature, 2023. **619**(7971): p. 837–843. DOI: 10.1038/s41586-023-06265-4.
130. Shiratori, H., H. Oguchi, Y. Isobe, K.H. Han, A. Sen, K. Yakebe, D. Takahashi, M. Fukushima, M. Arita, and K. Hase. *Gut microbiota-derived lipid metabolites facilitate regulatory T cell differentiation.* Scientific Reports, 2023. **13**(1). DOI: 10.1038/s41598-023-35097-5.
131. Clarke, T.B., K.M. Davis, E.S. Lysenko, A.Y. Zhou, Y. Yu, and J.N. Weiser. *Recognition of peptidoglycan from the microbiota by Nod1 enhances systemic innate immunity.* Nat Med, 2010. **16**(2): p. 228-31. DOI: 10.1038/nm.2087.
132. Zeng, M.Y., D. Cisalpino, S. Varadarajan, J. Hellman, H.S. Warren, M. Cascalho, N. Inohara, and G. Núñez. *Gut Microbiota-Induced Immunoglobulin G Controls Systemic Infection by Symbiotic Bacteria and Pathogens.* Immunity, 2016. **44**(3): p. 647-658. DOI: 10.1016/j.immuni.2016.02.006.
133. Abt, M.C., L.C. Osborne, L.A. Monticelli, T.A. Doering, T. Alenghat, G.F. Sonnenberg, M.A. Paley, M. Antenus, K.L. Williams, J. Erikson, E.J. Wherry, and D. Artis. *Commensal bacteria calibrate the activation threshold of innate antiviral immunity.* Immunity, 2012. **37**(1): p. 158-70. DOI: 10.1016/j.immuni.2012.04.011.
134. Milan-Mattos, J.C., F.F. Anibal, N.M. Perseguini, V. Minatel, P. Rehder-Santos, C.A. Castro, F.A. Vasilceac, S.M. Mattiello, L.H. Faccioli, and A.M. Catai. *Effects of natural aging and gender on pro-inflammatory markers.* Braz J Med Biol Res, 2019. **52**(9). DOI: 10.1590/1414-431X20198392.
135. Tang, Y., P.F. Liang, J.Z. Chen, S. Fu, B. Liu, M. Feng, B.J. Lin, B. Lee, A.P. Xu, and H.Y. Lan. *The baseline levels and risk factors for high-sensitive C-reactive protein in Chinese healthy population.* Immunity & Ageing, 2018. **15**. DOI: 10.1186/s12979-018-0126-7.
136. Kalair, A., M. Pavan, N. Alpert, S. Ghaffari, and E. Taioli. *Blood inflammatory markers and mortality in the US population: A Health and Retirement Survey (HRS) analysis.* PLoS One, 2023. **18**(10). DOI: 10.1371/journal.pone.0293027.
137. Shen-Orr, S.S., D. Furman, B.A. Kidd, F. Hadad, P. Lovelace, Y.W. Huang, Y. Rosenberg-Hasson, S. Mackey, F.A. Grisar, Y. Pickman, H.T. Maecker, Y.H. Chien, C.L. Dekker, J.C. Wu, A.J. Butte, and M.M. Davis. *Defective Signaling in the JAK-STAT*

Pathway Tracks with Chronic Inflammation and Cardiovascular Risk in Aging Humans. Cell Syst, 2016. **3**(4): p. 374-384. DOI: 10.1016/j.cels.2016.09.009.
138. Fulop, T., A. Larbi, N. Douziech, C. Fortin, K.P. Guerard, O. Lesur, A. Khalil, and G. Dupuis. *Signal transduction and functional changes in neutrophils with aging.* Aging Cell, 2004. **3**(4): p. 217-26. DOI: 10.1111/j.1474-9728.2004.00110.x.
139. Hearps, A.C., G.E. Martin, T.A. Angelovich, W.J. Cheng, A. Maisa, A.L. Landay, A. Jaworowski, and S.M. Crowe. *Aging is associated with chronic innate immune activation and dysregulation of monocyte phenotype and function.* Aging Cell, 2012. **11**(5): p. 867-75. DOI: 10.1111/j.1474-9726.2012.00851.x.
140. Thevaranjan, N., A. Puchta, C. Schulz, A. Naidoo, J.C. Szamosi, C.P. Verschoor, D. Loukov, L.P. Schenck, J. Jury, K.P. Foley, J.D. Schertzer, M.J. Larche, D.J. Davidson, E.F. Verdu, M.G. Surette, and D.M.E. Bowdish. *Age-Associated Microbial Dysbiosis Promotes Intestinal Permeability, Systemic Inflammation, and Macrophage Dysfunction.* Cell Host Microbe, 2017. **21**(4): p. 455-466. DOI: 10.1016/j.chom.2017.03.002.
141. Donaldson, D.S., J. Pollock, P. Vohra, M.P. Stevens, and N.A. Mabbott. *Microbial Stimulation Reverses the Age-Related Decline in M Cells in Aged Mice.* iScience, 2020. **23**(6). DOI: 10.1016/j.isci.2020.101147.
142. Stebegg, M., A. Silva-Cayetano, S. Innocentin, T.P. Jenkins, C. Cantacessi, C. Gilbert, and M.A. Linterman. *Heterochronic faecal transplantation boosts gut germinal centres in aged mice.* Nature Communications, 2019. **10**. DOI: 10.1038/s41467-019-10430-7.
143. Bárcena, C., R. Valdés-Mas, P. Mayoral, C. Garabaya, S. Durand, F. Rodríguez, M.T. Fernández-García, N. Salazar, A.M. Nogacka, N. Garatachea, N. Bossut, F. Aprahamian, A. Lucia, G. Kroemer, J.M.P. Freije, P.M. Quirós, and C. López-Otín. *Healthspan and lifespan extension by fecal microbiota transplantation into progeroid mice.* Nature Medicine, 2019. **25**(8): p. 1234–1242. DOI: 10.1038/s41591-019-0504-5.
144. Mogilenko, D.A., I. Shchukina, and M.N. Artyomov. *Immune ageing at single-cell resolution.* Nat Rev Immunol, 2022. **22**(8): p. 484-498. DOI: 10.1038/s41577-021-00646-4.
145. Wiley, C.D. and J. Campisi. *The metabolic roots of senescence: mechanisms and opportunities for intervention.* Nat Metab, 2021. **3**(10): p. 1290-1301. DOI: 10.1038/s42255-021-00483-8.
146. Yoshimoto, S., T.M. Loo, K. Atarashi, H. Kanda, S. Sato, S. Oyadomari, Y. Iwakura, K. Oshima, H. Morita, M. Hattori, K. Honda, Y. Ishikawa, E. Hara, and N. Ohtani. *Obesity-induced gut microbial metabolite promotes liver cancer through senescence secretome.* Nature, 2013. **499**(7456): p. 97-101. DOI: 10.1038/nature12347.
147. Zhang, L., F. Yu, and J. Xia. *Trimethylamine N-oxide: role in cell senescence and age-related diseases.* Eur J Nutr, 2023. **62**(2): p. 525-541. DOI: 10.1007/s00394-022-03011-w.
148. Vogt, N.M., K.A. Romano, B.F. Darst, C.D. Engelman, S.C. Johnson, C.M. Carlsson, S. Asthana, K. Blennow, H. Zetterberg, B.B. Bendlin, and F.E. Rey. *The gut microbiota-derived metabolite trimethylamine N-oxide is elevated in Alzheimer's disease.* Alzheimers Res Ther, 2018. **10**(1): p. 124. DOI: 10.1186/s13195-018-0451-2.
149. Zhou, H., Y. Luo, W. Zhang, F. Xie, C. Deng, W. Zheng, S. Zhu, and Q. Wang. *Causal effect of gut-microbiota-derived metabolite trimethylamine N-oxide on Parkinson's disease: A Mendelian randomization study.* Eur J Neurol, 2023. **30**(11): p. 3451-3461. DOI: 10.1111/ene.15702.
150. Chung, S.J., J.H. Rim, D. Ji, S. Lee, H.S. Yoo, J.H. Jung, K. Baik, Y. Choi, B.S. Ye, Y.H. Sohn, M. Yun, S.G. Lee, and P.H. Lee. *Gut microbiota-derived metabolite trimethylamine N-oxide as a biomarker in early Parkinson's disease.* Nutrition, 2021. **83**. DOI: 10.1016/j.nut.2020.111090.
151. Koeth, R.A., Z. Wang, B.S. Levison, J.A. Buffa, E. Org, B.T. Sheehy, E.B. Britt, X. Fu, Y. Wu, L. Li, J.D. Smith, J.A. DiDonato, J. Chen, H. Li, G.D. Wu, J.D. Lewis, M. Warrier, J.M. Brown, R.M. Krauss, W.H. Tang, F.D. Bushman, A.J. Lusis, and S.L. Hazen.

Intestinal microbiota metabolism of L-carnitine, a nutrient in red meat, promotes atherosclerosis. Nat Med, 2013. **19**(5): p. 576-85. DOI: 10.1038/nm.3145.
152. Wang, Z., E. Klipfell, B.J. Bennett, R. Koeth, B.S. Levison, B. Dugar, A.E. Feldstein, E.B. Britt, X. Fu, Y.M. Chung, Y. Wu, P. Schauer, J.D. Smith, H. Allayee, W.H. Tang, J.A. DiDonato, A.J. Lusis, and S.L. Hazen. *Gut flora metabolism of phosphatidylcholine promotes cardiovascular disease.* Nature, 2011. **472**(7341): p. 57-63. DOI: 10.1038/nature09922.
153. Kawamoto, S., K. Uemura, N. Hori, L. Takayasu, Y. Konishi, K. Katoh, T. Matsumoto, M. Suzuki, Y. Sakai, T. Matsudaira, T. Adachi, N. Ohtani, D.M. Standley, W. Suda, S. Fukuda, and E. Hara. *Bacterial induction of B cell senescence promotes age-related changes in the gut microbiota.* Nat Cell Biol, 2023. **25**(6): p. 865-876. DOI: 10.1038/s41556-023-01145-5.
154. Idda, M.L., W.G. McClusky, V. Lodde, R. Munk, K. Abdelmohsen, M. Rossi, and M. Gorospe. *Survey of senescent cell markers with age in human tissues.* Aging-Us, 2020. **12**(5): p. 4052-4066. DOI: 10.18632/aging.102903.
155. Moorefield, E.C., S.F. Andres, R.E. Blue, L. Van Landeghem, A.T. Mah, M.A. Santoro, and S. Ding. *Aging effects on intestinal homeostasis associated with expansion and dysfunction of intestinal epithelial stem cells.* Aging-US, 2017. **9**(8): p. 1898-1915. DOI: 10.18632/aging.101279.
156. Sharma, R., R. Kumar, A. Sharma, A. Goel, and Y. Padwad. *Long-term consumption of green tea EGCG enhances murine health span by mitigating multiple aspects of cellular senescence in mitotic and post-mitotic tissues, gut dysbiosis, and immunosenescence.* J Nutr Biochem, 2022. **107**. DOI: 10.1016/j.jnutbio.2022.109068.
157. Tran, L. and B. Greenwood-Van Meerveld. *Age-associated remodeling of the intestinal epithelial barrier.* J Gerontol A Biol Sci Med Sci, 2013. **68**(9): p. 1045–1056. DOI: 10.1093/gerona/glt106.
158. Ren, W.Y., K.F. Wu, X. Li, M. Luo, H.C. Liu, S.C. Zhang, and Y. Hu. *Age-related changes in small intestinal mucosa epithelium architecture and epithelial tight junction in rat models.* Aging Clin Exp Res, 2014. **26**(2): p. 183-91. DOI: 10.1007/s40520-013-0148-0.
159. Walker, E.M., N. Slisarenko, G.L. Gerrets, P.J. Kissinger, E.S. Didier, M.J. Kuroda, R.S. Veazey, S.M. Jazwinski, and N. Rout. *Inflammaging phenotype in rhesus macaques is associated with a decline in epithelial barrier-protective functions and increased pro-inflammatory function in CD161-expressing cells.* Geroscience, 2019. **41**(6): p. 739-757. DOI: 10.1007/s11357-019-00099-7.
160. Mitchell, E.L., A.T. Davis, K. Brass, M. Dendinger, R. Barner, R. Gharaibeh, A.A. Fodor, and K. Kavanagh. *Reduced Intestinal Motility, Mucosal Barrier Function, and Inflammation in Aged Monkeys.* J Nutr Health Aging, 2017. **21**(4): p. 354-361. DOI: 10.1007/s12603-016-0725-y.
161. Tran, L. and B. Greenwood-Van Meerveld. *Age-Associated Remodeling of the Intestinal Epithelial Barrier.* Journals of Gerontology Series a-Biological Sciences and Medical Sciences, 2013. **68**(9): p. 1045-+. DOI: 10.1093/gerona/glt106.
162. Man, A.L., E. Bertelli, S. Rentini, M. Regoli, G. Briars, M. Marini, A.J. Watson, and C. Nicoletti. *Age-associated modifications of intestinal permeability and innate immunity in human small intestine.* Clin Sci (Lond), 2015. **129**(7): p. 515-27. DOI: 10.1042/CS20150046.
163. Wilms, E., F.J. Troost, M. Elizalde, B. Winkens, P. de Vos, Z. Mujagic, D. Jonkers, and A.A.M. Masclee. *Intestinal barrier function is maintained with aging - a comprehensive study in healthy subjects and irritable bowel syndrome patients.* Sci Rep, 2020. **10**(1): p. 475. DOI: 10.1038/s41598-019-57106-2.
164. Valentini, L., S. Ramminger, V. Haas, E. Postrach, M. Werich, A. Fischer, M. Koller, A. Swidsinski, S. Bereswill, H. Lochs, and J.D. Schulzke. *Small intestinal permeability in older adults.* Physiol Rep, 2014. **2**(4). DOI: 10.14814/phy2.281.

165. Saweirs, W.M., D.J. Andrews, and T.S. Low-Beer. *The double sugar test of intestinal permeability in the elderly.* Age and Ageing, 1985. **14**(5): p. 312-5. DOI: 10.1093/ageing/14.5.312.
166. Saltzman, J.R., K.V. Kowdley, G. Perrone, and R.M. Russell. *Changes in small-intestine permeability with aging.* J Am Geriatr Soc, 1995. **43**(2): p. 160-4. DOI: 10.1111/j.1532-5415.1995.tb06382.x.
167. Kristoff, J., G. Haret-Richter, D. Ma, R.M. Ribeiro, C. Xu, E. Cornell, J.L. Stock, T. He, A.D. Mobley, S. Ross, A. Trichel, C. Wilson, R. Tracy, A. Landay, C. Apetrei, and I. Pandrea. *Early microbial translocation blockade reduces SIV-mediated inflammation and viral replication.* J Clin Invest, 2014. **124**(6): p. 2802-6. DOI: 10.1172/JCI75090.
168. Nash, A.K., T.A. Auchtung, M.C. Wong, D.P. Smith, J.R. Gesell, M.C. Ross, C.J. Stewart, G.A. Metcalf, D.M. Muzny, R.A. Gibbs, N.J. Ajami, and J.F. Petrosino. *The gut mycobiome of the Human Microbiome Project healthy cohort.* Microbiome, 2017. **5**(1): p. 153. DOI: 10.1186/s40168-017-0373-4.
169. Underhill, D.M. and I.D. Iliev. *The mycobiota: interactions between commensal fungi and the host immune system.* Nat Rev Immunol, 2014. **14**(6): p. 405-16. DOI: 10.1038/nri3684.
170. Lai, S., Y. Yan, Y. Pu, S. Lin, J.G. Qiu, B.H. Jiang, M.I. Keller, M. Wang, P. Bork, W.H. Chen, Y. Zheng, and X.M. Zhao. *Enterotypes of the human gut mycobiome.* Microbiome, 2023. **11**(1): p. 179. DOI: 10.1186/s40168-023-01586-y.
171. Pappas, P.G., M.S. Lionakis, M.C. Arendrup, L. Ostrosky-Zeichner, and B.J. Kullberg. *Invasive candidiasis.* Nat Rev Dis Primers, 2018. **4**. DOI: 10.1038/nrdp.2018.26.
172. Liu, F., Z.D. Hu, A. Yurkov, X.H. Chen, W.J. Bao, Q. Ma, W.N. Zhao, S. Pan, X.M. Zhao, J.H. Liu, Q.M. Wang, and T. Boekhout. *Saccharomycetaceae: delineation of fungal genera based on phylogenomic analyses, genomic relatedness indices and genomics-based synapomorphies.* Persoonia, 2024. **52**: p. 1-21. DOI: 10.3767/persoonia.2024.52.01.
173. Shuai, M., Y. Fu, H.L. Zhong, W. Gou, Z. Jiang, Y. Liang, Z. Miao, J.J. Xu, T. Huynh, M.L. Wahlqvist, Y.M. Chen, and J.S. Zheng. *Mapping the human gut mycobiome in middle-aged and elderly adults: multiomics insights and implications for host metabolic health.* Gut, 2022. **71**(9): p. 1812-1820. DOI: 10.1136/gutjnl-2021-326298.
174. Sawaswong, V., P. Chanchaem, A. Khamwut, K. Praianantathavorn, T. Kemthong, S. Malaivijitnond, and S. Payungporn. *Oral-fecal mycobiome in wild and captive cynomolgus macaques (Macaca fascicularis).* Fungal Genet Biol, 2020. **144**. DOI: 10.1016/j.fgb.2020.103468.
175. Sun, B., Y. Xia, P.A. Garber, K.R. Amato, A. Gomez, X. Xu, W. Li, M. Huang, D. Xia, X. Wang, and J. Li. *Captivity Is Associated With Gut Mycobiome Composition in Tibetan Macaques (Macaca thibetana).* Front Microbiol, 2021. **12**. DOI: 10.3389/fmicb.2021.665853.
176. Jiang, T.T., T.Y. Shao, W.X.G. Ang, J.M. Kinder, L.H. Turner, G. Pham, J. Whitt, T. Alenghat, and S.S. Way. *Commensal Fungi Recapitulate the Protective Benefits of Intestinal Bacteria.* Cell Host Microbe, 2017. **22**(6): p. 809-816. DOI: 10.1016/j.chom.2017.10.013.
177. Wheeler, M.L., J.J. Limon, A.S. Bar, C.A. Leal, M. Gargus, J. Tang, J. Brown, V.A. Funari, H.L. Wang, T.R. Crother, M. Arditi, D.M. Underhill, and I.D. Iliev. *Immunological Consequences of Intestinal Fungal Dysbiosis.* Cell Host Microbe, 2016. **19**(6): p. 865-73. DOI: 10.1016/j.chom.2016.05.003.
178. van Tilburg Bernardes, E., V.K. Pettersen, M.W. Gutierrez, I. Laforest-Lapointe, N.G. Jendzjowsky, J.B. Cavin, F.A. Vicentini, C.M. Keenan, H.R. Ramay, J. Samara, W.K. MacNaughton, R.J.A. Wilson, M.M. Kelly, K.D. McCoy, K.A. Sharkey, and M.C. Arrieta. *Intestinal fungi are causally implicated in microbiome assembly and immune development in mice.* Nat Commun, 2020. **11**(1). DOI: 10.1038/s41467-020-16431-1.
179. Iliev, I.D., V.A. Funari, K.D. Taylor, Q. Nguyen, C.N. Reyes, S.P. Strom, J. Brown, C.A. Becker, P.R. Fleshner, M. Dubinsky, J.I. Rotter, H.L.L. Wang, D.P.B. McGovern, G.D.

Brown, and D.M. Underhill. *Interactions Between Commensal Fungi and the C-Type Lectin Receptor Dectin-1 Influence Colitis.* Science, 2012. **336**(6086): p. 1314-1317. DOI: 10.1126/science.1221789.
180. Chen, Y., Z.J. Chen, R.Y. Guo, N. Chen, H.F. Lu, S.A. Huang, J. Wang, and L.J. Li. *Correlation between gastrointestinal fungi and varying degrees of chronic hepatitis B virus infection.* Diagnostic Microbiology and Infectious Disease, 2011. **70**(4): p. 492-498. DOI: 10.1016/j.diagmicrobio.2010.04.005.
181. Frykman, P.K., A. Nordensköjld, A. Kawaguchi, T.T. Hui, A.L. Granström, Z. Cheng, J. Tang, D.M. Underhill, I. Iliev, V.A. Funari, T. Wester, and H.C.R.G. HCRG. *Characterization of Bacterial and Fungal Microbiome in Children with Hirschsprung Disease with and without a History of Enterocolitis: A Multicenter Study.* Plos One, 2015. **10**(4). DOI: 10.1371/journal.pone.0124172.
182. Alonso, R., D. Pisa, B. Aguado, and L. Carrasco. *Identification of Fungal Species in Brain Tissue from Alzheimer's Disease by Next-Generation Sequencing.* Journal of Alzheimers Disease, 2017. **58**(1): p. 55-67. DOI: 10.3233/Jad-170058.
183. Pisa, D., R. Alonso, A. Juarranz, A. Rabano, and L. Carrasco. *Direct visualization of fungal infection in brains from patients with Alzheimer's disease.* J Alzheimers Dis, 2015. **43**(2): p. 613-24. DOI: 10.3233/JAD-141386.
184. Pisa, D., R. Alonso, A.M. Fernandez-Fernandez, A. Rabano, and L. Carrasco. *Polymicrobial Infections In Brain Tissue From Alzheimer's Disease Patients.* Sci Rep, 2017. **7**(1). DOI: 10.1038/s41598-017-05903-y.
185. Pisa, D., R. Alonso, A. Rabano, I. Rodal, and L. Carrasco. *Different Brain Regions are Infected with Fungi in Alzheimer's Disease.* Sci Rep, 2015. **5**. DOI: 10.1038/srep15015.
186. Alonso, R., D. Pisa, A. Rábano, and L. Carrasco. *Alzheimer's disease and disseminated mycoses.* European Journal of Clinical Microbiology & Infectious Diseases, 2014. **33**(7): p. 1125-1132. DOI: 10.1007/s10096-013-2045-z.
187. Luan, C., L. Xie, X. Yang, H. Miao, N. Lv, R. Zhang, X. Xiao, Y. Hu, Y. Liu, N. Wu, Y. Zhu, and B. Zhu. *Dysbiosis of fungal microbiota in the intestinal mucosa of patients with colorectal adenomas.* Sci Rep, 2015. **5**. DOI: 10.1038/srep07980.
188. van der Velden, W.J., M.G. Netea, A.F. de Haan, G.A. Huls, J.P. Donnelly, and N.M. Blijlevens. *Role of the mycobiome in human acute graft-versus-host disease.* Biol Blood Marrow Transplant, 2013. **19**(2): p. 329-32. DOI: 10.1016/j.bbmt.2012.11.008.
189. Zuo, T., H. Zhan, F. Zhang, Q. Liu, E.Y.K. Tso, G.C.Y. Lui, N. Chen, A. Li, W.Q. Lu, F.K.L. Chan, P.K.S. Chan, and S.C. Ng. *Alterations in Fecal Fungal Microbiome of Patients With COVID-19 During Time of Hospitalization until Discharge.* Gastroenterology, 2020. **159**(4): p. 1302–1310. DOI: 10.1053/j.gastro.2020.06.048.
190. Zhai, B., M. Ola, T. Rolling, N.L. Tosini, S. Joshowitz, E.R. Littmann, L.A. Amoretti, E. Fontana, R.J. Wright, E. Miranda, C.A. Veelken, S.M. Morjaria, J.U. Peled, M.R.M. van den Brink, N.E. Babady, G. Butler, Y. Taur, and T.M. Hohl. *High-resolution mycobiota analysis reveals dynamic intestinal translocation preceding invasive candidiasis.* Nature Medicine, 2020. **26**(1): p. 59–64. DOI: 10.1038/s41591-019-0709-7.
191. Castanheira, M., S.A. Messer, P.R. Rhomberg, and M.A. Pfaller. *Antifungal susceptibility patterns of a global collection of fungal isolates: results of the SENTRY Antifungal Surveillance Program (2013).* Diagn Microbiol Infect Dis, 2016. **85**(2): p. 200-4. DOI: 10.1016/j.diagmicrobio.2016.02.009.
192. Silva, S., M. Negri, M. Henriques, R. Oliveira, D.W. Williams, and J. Azeredo. *Candida glabrata, Candida parapsilosis and Candida tropicalis: biology, epidemiology, pathogenicity and antifungal resistance.* FEMS Microbiol Rev, 2012. **36**(2): p. 288-305. DOI: 10.1111/j.1574-6976.2011.00278.x.
193. Rodrigues Hoffmann, A., M.G. Ramos, R.T. Walker, and L.W. Stranahan. *Hyphae, pseudohyphae, yeasts, spherules, spores, and more: A review on the morphology and pathology of fungal and oomycete infections in the skin of domestic animals.* Vet Pathol, 2023. **60**(6): p. 812-828. DOI: 10.1177/03009858231173715.

194. Moyes, D.L., C. Murciano, M. Runglall, A. Kohli, A. Islam, and J.R. Naglik. *Activation of MAPK/c-Fos induced responses in oral epithelial cells is specific to Candida albicans and Candida dubliniensis hyphae.* Med Microbiol Immunol, 2012. **201**(1): p. 93-101. DOI: 10.1007/s00430-011-0209-y.
195. Richardson, J.P., R. Brown, N. Kichik, S. Lee, E. Priest, S. Mogavero, C. Maufrais, D.N. Wickramasinghe, A. Tsavou, N.K. Kotowicz, O.W. Hepworth, A. Gallego-Cortes, N.O. Ponde, J. Ho, D.L. Moyes, D. Wilson, C. D'Enfert, B. Hube, and J.R. Naglik. *Candidalysins Are a New Family of Cytolytic Fungal Peptide Toxins.* mBio, 2022. **13**(1). DOI: 10.1128/mbio.03510-21.
196. Moyes, D.L., D. Wilson, J.P. Richardson, S. Mogavero, S.X. Tang, J. Wernecke, S. Hofs, R.L. Gratacap, J. Robbins, M. Runglall, C. Murciano, M. Blagojevic, S. Thavaraj, T.M. Forster, B. Hebecker, L. Kasper, G. Vizcay, S.I. Iancu, N. Kichik, A. Hader, O. Kurzai, T. Luo, T. Kruger, O. Kniemeyer, E. Cota, O. Bader, R.T. Wheeler, T. Gutsmann, B. Hube, and J.R. Naglik. *Candidalysin is a fungal peptide toxin critical for mucosal infection.* Nature, 2016. **532**(7597): p. 64-8. DOI: 10.1038/nature17625.
197. Pu, L., S. Pang, W. Mu, X. Chen, Y. Zou, Y. Wang, Y. Ding, Q. Yan, Y. Huang, X. Chen, T. Peng, W. Luo, and S. Wang. *The gut mycobiome signatures in long-lived populations.* iScience, 2024. **27**(8). DOI: 10.1016/j.isci.2024.110412.
198. Powell, N., M.M. Walker, and N.J. Talley. *The mucosal immune system: master regulator of bidirectional gut-brain communications.* Nat Rev Gastroenterol Hepatol, 2017. **14**(3): p. 143-159. DOI: 10.1038/nrgastro.2016.191.
199. Huuskonen, J., T. Suuronen, T. Nuutinen, S. Kyrylenko, and A. Salminen. *Regulation of microglial inflammatory response by sodium butyrate and short-chain fatty acids.* Br J Pharmacol, 2004. **141**(5): p. 874-80. DOI: 10.1038/sj.bjp.0705682.
200. Heneka, M.T. *Microglia take centre stage in neurodegenerative disease.* Nat Rev Immunol, 2019. **19**(2): p. 79-80. DOI: 10.1038/s41577-018-0112-5.
201. Borst, K., A.A. Dumas, and M. Prinz. *Microglia: Immune and non-immune functions.* Immunity, 2021. **54**(10): p. 2194-2208. DOI: 10.1016/j.immuni.2021.09.014.
202. Nimmerjahn, A., F. Kirchhoff, and F. Helmchen. *Resting microglial cells are highly dynamic surveillants of brain parenchyma in vivo.* Science, 2005. **308**(5726): p. 1314-1318. DOI: 10.1126/science.1110647.
203. Edler, M.K., I. Mhatre-Winters, and J.R. Richardson. *Microglia in Aging and Alzheimer's Disease: A Comparative Species Review.* Cells, 2021. **10**(5). DOI: 10.3390/cells10051138.
204. Woodburn, S.C., J.L. Bollinger, and E.S. Wohleb. *The semantics of microglia activation: neuroinflammation, homeostasis, and stress.* Journal of Neuroinflammation, 2021. **18**(1). DOI: 10.1186/s12974-021-02309-6.
205. Streit, W.J., N.W. Sammons, A.J. Kuhns, and D.L. Sparks. *Dystrophic microglia in the aging human brain.* Glia, 2004. **45**(2): p. 208-12. DOI: 10.1002/glia.10319.
206. Lopes, K.O., D.L. Sparks, and W.J. Streit. *Microglial dystrophy in the aged and Alzheimer's disease brain is associated with ferritin immunoreactivity.* Glia, 2008. **56**(10): p. 1048-60. DOI: 10.1002/glia.20678.
207. Torres-Platas, S.G., S. Comeau, A. Rachalski, G. Dal Bo, C. Cruceanu, G. Turecki, B. Giros, and N. Mechawar. *Morphometric characterization of microglial phenotypes in human cerebral cortex.* Journal of Neuroinflammation, 2014. **11**. DOI: 10.1186/1742-2094-11-12.
208. Frank, M.G., R.M. Barrientos, J.C. Biedenkapp, J.W. Rudy, L.R. Watkins, and S.F. Maier. *mRNA up-regulation of MHC II and pivotal pro-inflammatory genes in normal brain aging.* Neurobiol Aging, 2006. **27**(5): p. 717-22. DOI: 10.1016/j.neurobiolaging.2005.03.013.
209. Gyoneva, S., R. Hosur, D. Gosselin, B. Zhang, Z. Ouyang, A.C. Cotleur, M. Peterson, N. Allaire, R. Challa, P. Cullen, C. Roberts, K. Miao, T.L. Reynolds, C.K. Glass, L. Burkly, and R.M. Ransohoff. *Cx3cr1-deficient microglia exhibit a premature aging transcriptome.* Life Sci Alliance, 2019. **2**(6). DOI: 10.26508/lsa.201900453.

210. Sierra, A., A.C. Gottfried-Blackmore, B.S. McEwen, and K. Bulloch. *Microglia derived from aging mice exhibit an altered inflammatory profile.* Glia, 2007. **55**(4): p. 412-24. DOI: 10.1002/glia.20468.
211. Njie, E.G., E. Boelen, F.R. Stassen, H.W. Steinbusch, D.R. Borchelt, and W.J. Streit. *Ex vivo cultures of microglia from young and aged rodent brain reveal age-related changes in microglial function.* Neurobiol Aging, 2012. **33**(1). DOI: 10.1016/j.neurobiolaging.2010.05.008.
212. Niraula, A., J.F. Sheridan, and J.P. Godbout. *Microglia Priming with Aging and Stress.* Neuropsychopharmacology, 2017. **42**(1): p. 318-333. DOI: 10.1038/npp.2016.185.
213. Sheffield, L.G. and N.E.J. Berman. *Microglial expression of MHC class II increases in normal aging of nonhuman primates.* Neurobiology of Aging, 1998. **19**(1): p. 47-55. DOI: 10.1016/S0197-4580(97)00168-1.
214. VanGuilder, H.D., G.V. Bixler, R.M. Brucklacher, J.A. Farley, H. Yan, J.P. Warrington, W.E. Sonntag, and W.M. Freeman. *Concurrent hippocampal induction of MHC II pathway components and glial activation with advanced aging is not correlated with cognitive impairment.* J Neuroinflammation, 2011. **8**: p. 138. DOI: 10.1186/1742-2094-8-138.
215. Godbout, J.P., J. Chen, J. Abraham, A.F. Richwine, B.M. Berg, K.W. Kelley, and R.W. Johnson. *Exaggerated neuroinflammation and sickness behavior in aged mice after activation of the peripheral innate immune system.* Faseb Journal, 2005. **19**(7): p. 1329-31. DOI: 10.1096/fj.05-3776fje.
216. Frank, M.G., R.M. Barrientos, L.R. Watkins, and S.F. Maier. *Aging sensitizes rapidly isolated hippocampal microglia to LPS ex vivo.* J Neuroimmunol, 2010. **226**(1-2): p. 181-4. DOI: 10.1016/j.jneuroim.2010.05.022.
217. Norden, D.M., P.J. Trojanowski, E. Villanueva, E. Navarro, and J.P. Godbout. *Sequential activation of microglia and astrocyte cytokine expression precedes increased Iba-1 or GFAP immunoreactivity following systemic immune challenge.* Glia, 2016. **64**(2): p. 300-16. DOI: 10.1002/glia.22930.
218. Damani, M.R., L.A. Zhao, A.M. Fontainhas, J. Amaral, R.N. Fariss, and W.T. Wong. *Age-related alterations in the dynamic behavior of microglia.* Aging Cell, 2011. **10**(2): p. 263-276. DOI: 10.1111/j.1474-9726.2010.00660.x.
219. Erny, D., A.L. Hrabe de Angelis, D. Jaitin, P. Wieghofer, O. Staszewski, E. David, H. Keren-Shaul, T. Mahlakoiv, K. Jakobshagen, T. Buch, V. Schwierzeck, O. Utermohlen, E. Chun, W.S. Garrett, K.D. McCoy, A. Diefenbach, P. Staeheli, B. Stecher, I. Amit, and M. Prinz. *Host microbiota constantly control maturation and function of microglia in the CNS.* Nat Neurosci, 2015. **18**(7): p. 965-77. DOI: 10.1038/nn.4030.
220. Lynch, C.M.K., C.S.M. Cowan, T.F.S. Bastiaanssen, G.M. Moloney, N. Theune, M. van de Wouw, E. Florensa Zanuy, A.P. Ventura-Silva, M.G. Codagnone, F. Villalobos-Manriquez, M. Segalla, F. Koc, C. Stanton, P. Ross, T.G. Dinan, G. Clarke, and J.F. Cryan. *Critical windows of early-life microbiota disruption on behaviour, neuroimmune function, and neurodevelopment.* Brain Behav Immun, 2023. **108**: p. 309-327. DOI: 10.1016/j.bbi.2022.12.008.
221. Caliskan, G., T. French, S. Enrile Lacalle, M. Del Angel, J. Steffen, M.M. Heimesaat, I. Rita Dunay, and O. Stork. *Antibiotic-induced gut dysbiosis leads to activation of microglia and impairment of cholinergic gamma oscillations in the hippocampus.* Brain Behav Immun, 2022. **99**: p. 203-217. DOI: 10.1016/j.bbi.2021.10.007.
222. Galea, I. *The blood-brain barrier in systemic infection and inflammation.* Cell Mol Immunol, 2021. **18**(11): p. 2489-2501. DOI: 10.1038/s41423-021-00757-x.
223. Wu, D., Q. Chen, X. Chen, F. Han, Z. Chen, and Y. Wang. *The blood-brain barrier: structure, regulation, and drug delivery.* Signal Transduct Target Ther, 2023. **8**(1): p. 217. DOI: 10.1038/s41392-023-01481-w.
224. Marchetti, L. and B. Engelhardt. *Immune cell trafficking across the blood-brain barrier in the absence and presence of neuroinflammation.* Vasc Biol, 2020. **2**(1): p. H1-H18. DOI: 10.1530/VB-19-0033.

225. Haruwaka, K., A. Ikegami, Y. Tachibana, N. Ohno, H. Konishi, A. Hashimoto, M. Matsumoto, D. Kato, R. Ono, H. Kiyama, A.J. Moorhouse, J. Nabekura, and H. Wake. *Dual microglia effects on blood brain barrier permeability induced by systemic inflammation.* Nat Commun, 2019. **10**(1). DOI: 10.1038/s41467-019-13812-z.
226. Urich, E., S.E. Lazic, J. Molnos, I. Wells, and P.O. Freskgard. *Transcriptional profiling of human brain endothelial cells reveals key properties crucial for predictive in vitro blood-brain barrier models.* PLoS One, 2012. **7**(5). DOI: 10.1371/journal.pone.0038149.
227. Hoshi, Y., Y. Uchida, M. Tachikawa, T. Inoue, S. Ohtsuki, and T. Terasaki. *Quantitative atlas of blood-brain barrier transporters, receptors, and tight junction proteins in rats and common marmoset.* J Pharm Sci, 2013. **102**(9): p. 3343-55. DOI: 10.1002/jps.23575.
228. Falcone, C., M. Wolf-Ochoa, S. Amina, T. Hong, G. Vakilzadeh, W.D. Hopkins, P.R. Hof, C.C. Sherwood, P.R. Manger, S.C. Noctor, and V. Martinez-Cerdeno. *Cortical interlaminar astrocytes across the therian mammal radiation.* J Comp Neurol, 2019. **527**(10): p. 1654-1674. DOI: 10.1002/cne.24605.
229. Oberheim, N.A., T. Takano, X. Han, W. He, J.H. Lin, F. Wang, Q. Xu, J.D. Wyatt, W. Pilcher, J.G. Ojemann, B.R. Ransom, S.A. Goldman, and M. Nedergaard. *Uniquely hominid features of adult human astrocytes.* J Neurosci, 2009. **29**(10): p. 3276-87. DOI: 10.1523/JNEUROSCI.4707-08.2009.
230. Braniste, V., M. Al-Asmakh, C. Kowal, F. Anuar, A. Abbaspour, M. Toth, A. Korecka, N. Bakocevic, L.G. Ng, P. Kundu, B. Gulyas, C. Halldin, K. Hultenby, H. Nilsson, H. Hebert, B.T. Volpe, B. Diamond, and S. Pettersson. *The gut microbiota influences blood-brain barrier permeability in mice.* Sci Transl Med, 2014. **6**(263). DOI: 10.1126/scitranslmed.3009759.
231. Matt, S.M., J.M. Allen, M.A. Lawson, L.J. Mailing, J.A. Woods, and R.W. Johnson. *Butyrate and Dietary Soluble Fiber Improve Neuroinflammation Associated With Aging in Mice.* Frontiers in Immunology, 2018. **9**. DOI: 10.3389/fimmu.2018.01832.
232. Hoyles, L., T. Snelling, U.K. Umlai, J.K. Nicholson, S.R. Carding, R.C. Glen, and S. McArthur. *Microbiome-host systems interactions: protective effects of propionate upon the blood-brain barrier.* Microbiome, 2018. **6**. DOI: 10.1186/s40168-018-0439-y.
233. St'astny, F., I. Skultétyová, L. Pliss, and D. Jezová. *Quinolinic acid enhances permeability of rat brain microvessels to plasma albumin.* Brain Research Bulletin, 2000. **53**(4): p. 415-420. DOI: 10.1016/S0361-9230(00)00368-3.
234. Erikson, K., H. Tuominen, M. Vakkala, J.H. Liisanantti, T. Karttunen, H. Syrjala, and T.I. Ala-Kokko. *Brain tight junction protein expression in sepsis in an autopsy series.* Crit Care, 2020. **24**(1): p. 385. DOI: 10.1186/s13054-020-03101-3.
235. Qin, L.H., W. Huang, X.A. Mo, Y.L. Chen, and X.H. Wu. *LPS Induces Occludin Dysregulation in Cerebral Microvascular Endothelial Cells via MAPK Signaling and Augmenting MMP-2 Levels.* Oxid Med Cell Longev, 2015. **2015**. DOI: 10.1155/2015/120641.
236. Cersosimo, M.G. and E.E. Benarroch. *Pathological correlates of gastrointestinal dysfunction in Parkinson's disease.* Neurobiology of Disease, 2012. **46**(3): p. 559-564. DOI: 10.1016/j.nbd.2011.10.014.
237. Schwiertz, A., J. Spiegel, U. Dillmann, D. Grundmann, J. Bürmann, K. Fassbender, K.H. Schäfer, and M.M. Unger. *Fecal markers of intestinal inflammation and intestinal permeability are elevated in Parkinson's disease.* Parkinsonism & Related Disorders, 2018. **50**: p. 104-107. DOI: 10.1016/j.parkreldis.2018.02.022.
238. Elbaz, A., L. Carcaillon, S. Kab, and F. Moisan. *Epidemiology of Parkinson's disease.* Revue Neurologique, 2016. **172**(1): p. 14-26. DOI: 10.1016/j.neurol.2015.09.012.
239. DeTure, M.A. and D.W. Dickson. *The neuropathological diagnosis of Alzheimer's disease.* Molecular Neurodegeneration, 2019. **14**(1): p. 32. DOI: 10.1186/s13024-019-0333-5.
240. Wang, X., G. Sun, T. Feng, J. Zhang, X. Huang, T. Wang, Z. Xie, X. Chu, J. Yang, H. Wang, S. Chang, Y. Gong, L. Ruan, G. Zhang, S. Yan, W. Lian, C. Du, D. Yang, Q.

Zhang, F. Lin, J. Liu, H. Zhang, C. Ge, S. Xiao, J. Ding, and M. Geng. *Sodium oligomannate therapeutically remodels gut microbiota and suppresses gut bacterial amino acids-shaped neuroinflammation to inhibit Alzheimer's disease progression.* Cell Res, 2019. **29**(10): p. 787-803. DOI: 10.1038/s41422-019-0216-x.

241. Cox, L.M., M.J. Schafer, J. Sohn, J. Vincentini, H.L. Weiner, S.D. Ginsberg, and M.J. Blaser. *Calorie restriction slows age-related microbiota changes in an Alzheimer's disease model in female mice.* Scientific Reports, 2019. **9**. DOI: 10.1038/s41598-019-54187-x.
242. Dodiya, H.B., T. Kuntz, S.M. Shaik, C. Baufeld, J. Leibowitz, X. Zhang, N. Gottel, X. Zhang, O. Butovsky, J.A. Gilbert, and S.S. Sisodia. *Sex-specific effects of microbiome perturbations on cerebral Aβ amyloidosis and microglia phenotypes.* Journal of Experimental Medicine, 2019. **216**(7): p. 1542-1560. DOI: 10.1084/jem.20182386.
243. Dodiya, H.B., H.L. Lutz, I.Q. Weigle, P. Patel, J. Michalkiewicz, C.J. Roman-Santiago, C.M. Zhang, Y.X. Liang, A. Srinath, X.L. Zhang, J. Xia, M. Olszewski, X.Q. Zhang, M.J. Schipma, E.B. Chang, R.E. Tanzi, J.A. Gilbert, and S.S. Sisodia. *Gut microbiota-driven brain Aβ amyloidosis in mice requires microglia.* Journal of Experimental Medicine, 2021. **219**(1). DOI: 10.1084/jem.20200895.
244. Harach, T., N. Marungruang, N. Duthilleul, V. Cheatham, K.D. Mc Coy, G. Frisoni, J.J. Neher, F. Fak, M. Jucker, T. Lasser, and T. Bolmont. *Reduction of Abeta amyloid pathology in APPPS1 transgenic mice in the absence of gut microbiota.* Sci Rep, 2017. **7**. DOI: 10.1038/srep41802.
245. Minter, M.R., C. Zhang, V. Leone, D.L. Ringus, X.Q. Zhang, P. Oyler-Castrillo, M.W. Musch, F. Liao, J.F. Ward, D.M. Holtzman, E.B. Chang, R.E. Tanzi, and S.S. Sisodia. *Antibiotic-induced perturbations in gut microbial diversity influences neuro-inflammation and amyloidosis in a murine model of Alzheimer's disease.* Scientific Reports, 2016. **6**. DOI: 10.1038/srep30028.
246. Schrag, A., L. Horsfall, K. Walters, A. Noyce, and I. Petersen. *Prediagnostic presentations of Parkinson's disease in primary care: a case-control study.* Lancet Neurol, 2015. **14**(1): p. 57-64. DOI: 10.1016/S1474-4422(14)70287-X.
247. Chen, S.J., C.C. Chen, H.Y. Liao, Y.T. Lin, Y.W. Wu, J.M. Liou, M.S. Wu, C.H. Kuo, and C.H. Lin. *Association of Fecal and Plasma Levels of Short-Chain Fatty Acids With Gut Microbiota and Clinical Severity in Patients With Parkinson Disease.* Neurology, 2022. **98**(8): p. e848-e858. DOI: 10.1212/WNL.0000000000013225.
248. Aho, V.T.E., M.C. Houser, P.A.B. Pereira, J.J. Chang, K. Rudi, L. Paulin, V. Hertzberg, P. Auvinen, M.G. Tansey, and F. Scheperjans. *Relationships of gut microbiota, short-chain fatty acids, inflammation, and the gut barrier in Parkinson's disease.* Molecular Neurodegeneration, 2021. **16**(1). DOI: 10.1186/s13024-021-00427-6.
249. Nishiwaki, H., J. Ueyama, M. Ito, T. Hamaguchi, K. Takimoto, T. Maeda, K. Kashihara, Y. Tsuboi, H. Mori, K. Kurokawa, M. Katsuno, M. Hirayama, and K. Ohno. *Meta-analysis of shotgun sequencing of gut microbiota in Parkinson's disease.* NPJ Parkinsons Dis, 2024. **10**(1): p. 106. DOI: 10.1038/s41531-024-00724-z.
250. Coimbra, C.G. and V.B. Junqueira. *High doses of riboflavin and the elimination of dietary red meat promote the recovery of some motor functions in Parkinson's disease patients.* Braz J Med Biol Res, 2003. **36**(10): p. 1409-17. DOI: 10.1590/s0100-879x2003001000019.
251. Marashly, E.T. and S.A. Bohlega. *Riboflavin Has Neuroprotective Potential: Focus on Parkinson's Disease and Migraine.* Front Neurol, 2017. **8**: p. 333. DOI: 10.3389/fneur.2017.00333.
252. Lohr, K.M., B. Frost, C. Scherzer, and M.B. Feany. *Biotin rescues mitochondrial dysfunction and neurotoxicity in a tauopathy model.* Proc Natl Acad Sci U S A, 2020. **117**(52): p. 33608-33618. DOI: 10.1073/pnas.1922392117.
253. Sun, M.-F., Y.-L. Zhu, Z.-L. Zhou, X.-B. Jia, Y.-D. Xu, Q. Yang, C. Cui, and Y.-Q. Shen. *Neuroprotective effects of fecal microbiota transplantation on MPTP-induced Parkinson's disease mice: Gut microbiota, glial reaction and TLR4/TNF-α signaling*

pathway. Brain, Behavior, and Immunity, 2018. **70**: p. 48-60. DOI: 10.1016/j.bbi.2018.02.005.
254. Bruggeman, A., C. Vandendriessche, H. Hamerlinck, D. De Looze, D.J. Tate, M. Vuylsteke, L. De Commer, L. Devolder, J. Raes, B. Verhasselt, D. Laukens, R.E. Vandenbroucke, and P. Santens. *Safety and efficacy of faecal microbiota transplantation in patients with mild to moderate Parkinson's disease (GUT-PARFECT): a double-blind, placebo-controlled, randomised, phase 2 trial.* eClinicalMedicine, 2024. **71**. DOI: 10.1016/j.eclinm.2024.102563.
255. DuPont, H.L., J. Suescun, Z.D. Jiang, E.L. Brown, H.T. Essigmann, A.S. Alexander, A.W. DuPont, T. Iqbal, N.S. Utay, M. Newmark, and M.C. Schiess. *Fecal microbiota transplantation in Parkinson's disease-A randomized repeat-dose, placebo-controlled clinical pilot study.* Frontiers in Neurology, 2023. **14**. DOI: 10.3389/fneur.2023.1104759.
256. Cheng, Y., G.H. Tan, Q.H. Zhu, C. Wang, G.C. Ruan, S.H. Ying, J.L. Qie, X.F. Hu, Z.F. Xiao, F.H. Xu, L. Chen, M.J. Chen, Y. Pei, H. Zhang, Y.T. Tian, D.F. Chen, X.Y. Liu, H.Q. Huang, and Y.L. Wei. *Efficacy of fecal microbiota transplantation in patients with Parkinson's disease: clinical trial results from a randomized, placebo-controlled design.* Gut Microbes, 2023. **15**(2). DOI: 10.1080/19490976.2023.2284247.
257. Hazan, S. *Rapid improvement in Alzheimer's disease symptoms following fecal microbiota transplantation: a case report.* Journal of International Medical Research, 2020. **48**(6). DOI: 10.1177/0300060520925930.
258. Imdad, A., N.G. Pandit, M. Zaman, N.Z. Minkoff, E.E. Tanner-Smith, O.G. Gomez-Duarte, S. Acra, and M.R. Nicholson. *Fecal transplantation for treatment of inflammatory bowel disease.* Cochrane Database of Systematic Reviews, 2023(4). DOI: 10.1002/14651858.CD012774.pub3.
259. Hensley-McBain, T., A.S. Zevin, J. Manuzak, E. Smith, J. Gile, C. Miller, B. Agricola, M. Katze, R.K. Reeves, C.S. Kraft, S. Langevin, and N.R. Klatt. *Effects of Fecal Microbial Transplantation on Microbiome and Immunity in Simian Immunodeficiency Virus-Infected Macaques.* J Virol, 2016. **90**(10): p. 4981-4989. DOI: 10.1128/JVI.00099-16.
260. Shively, C.A., A. Lacreuse, B.M. Frye, E.S. Rothwell, and M. Moro. *Nonhuman primates at the intersection of aging biology, chronic disease, and health: An introduction to the American Journal of Primatology Special Issue on aging, cognitive decline, and neuropathology in nonhuman primates.* Am J Primatol, 2021. **83**(11). DOI: 10.1002/ajp.23309.
261. Beckman, D., S. Ott, K. Donis-Cox, W.G. Janssen, E. Bliss-Moreau, P.H. Rudebeck, M.G. Baxter, and J.H. Morrison. *Oligomeric Abeta in the monkey brain impacts synaptic integrity and induces accelerated cortical aging.* Proc Natl Acad Sci U S A, 2019. **116**(52): p. 26239-26246. DOI: 10.1073/pnas.1902301116.
262. Seyhan, A.A. *Lost in translation: the valley of death across preclinical and clinical divide – identification of problems and overcoming obstacles.* Translational Medicine Communications, 2019. **4**(1): p. 18. DOI: 10.1186/s41231-019-0050-7.
263. Azkona, G. and R. Sanchez-Pernaute. *Mice in translational neuroscience: What R we doing?* Prog Neurobiol, 2022. **217**. DOI: 10.1016/j.pneurobio.2022.102330.
264. Estes, J.D., S.W. Wong, and J.M. Brenchley. *Nonhuman primate models of human viral infections.* Nat Rev Immunol, 2018. **18**(6): p. 390-404. DOI: 10.1038/s41577-018-0005-7.
265. Messaoudi, I., R. Estep, B. Robinson, and S.W. Wong. *Nonhuman primate models of human immunology.* Antioxid Redox Signal, 2011. **14**(2): p. 261-73. DOI: 10.1089/ars.2010.3241.
266. Freire-Cobo, C., M.K. Edler, M. Varghese, E. Munger, J. Laffey, S. Raia, S.S. In, B. Wicinski, M. Medalla, S.E. Perez, E.J. Mufson, J.M. Erwin, E.E. Guevara, C.C. Sherwood, J.I. Luebke, A. Lacreuse, M.A. Raghanti, and P.R. Hof. *Comparative neuropathology in aging primates: A perspective.* Am J Primatol, 2021. **83**(11). DOI: 10.1002/ajp.23299.

267. Verdier, J.M., I. Acquatella, C. Lautier, G. Devau, S. Trouche, C. Lasbleiz, and N. Mestre-Frances. *Lessons from the analysis of nonhuman primates for understanding human aging and neurodegenerative diseases.* Front Neurosci, 2015. **9**: p. 64. DOI: 10.3389/fnins.2015.00064.
268. Mattison, J.A. and K.L. Vaughan. *An overview of nonhuman primates in aging research.* Exp Gerontol, 2017. **94**: p. 41-45. DOI: 10.1016/j.exger.2016.12.005.
269. Kishi, N., K. Sato, E. Sasaki, and H. Okano. *Common marmoset as a new model animal for neuroscience research and genome editing technology.* Dev Growth Differ, 2014. **56**(1): p. 53-62. DOI: 10.1111/dgd.12109.
270. Ward, J.M. and E.J. Vallender. *The resurgence and genetic implications of New World primates in biomedical research.* Trends Genet, 2012. **28**(12): p. 586-91. DOI: 10.1016/j.tig.2012.09.003.
271. Tardif, S.D., K.G. Mansfield, R. Ratnam, C.N. Ross, and T.E. Ziegler. *The marmoset as a model of aging and age-related diseases.* ILAR J, 2011. **52**(1): p. 54-65. DOI: 10.1093/ilar.52.1.54.
272. Asadzadeh, M., S. Ahmad, N. Al-Sweih, and Z. Khan. *Rapid and Accurate Identification of Candida albicans and Candida dubliniensis by Real-Time PCR and Melting Curve Analysis.* Med Princ Pract, 2018. **27**(6): p. 543-548. DOI: 10.1159/000493426.
273. Gardes, M. and T.D. Bruns. *ITS primers with enhanced specificity for basidiomycetes--application to the identification of mycorrhizae and rusts.* Mol Ecol, 1993. **2**(2): p. 113-8. DOI: 10.1111/j.1365-294x.1993.tb00005.x.
274. White T.J., B.T.D., Lee S.L., Taylor J.W. , *Amplification and direct sequencing of fungal ribosomal RNA genes for phylogenetics*, in *PCR Protocols: A Guide to Methods and Applications*, G.D.H. Innis M.A., Sninsky J.J., Editor. 1990, Academic Press: San Diego, CA, USA. p. 315-322.
275. Tokuno, H., M. Takada, Y. Kondo, and N. Mizuno. *Laminar organization of the substantia nigra pars reticulata in the macaque monkey, with special reference to the caudato-nigro-tectal link.* Exp Brain Res, 1993. **92**(3): p. 545-8. DOI: 10.1007/BF00229045.
276. Snippert, H.J., A.G. Schepers, G. Delconte, P.D. Siersema, and H. Clevers. *Slide preparation for single-cell-resolution imaging of fluorescent proteins in their three-dimensional near-native environment.* Nat Protoc, 2011. **6**(8): p. 1221-8. DOI: 10.1038/nprot.2011.365.
277. Schindelin, J., I. Arganda-Carreras, E. Frise, V. Kaynig, M. Longair, T. Pietzsch, S. Preibisch, C. Rueden, S. Saalfeld, B. Schmid, J.Y. Tinevez, D.J. White, V. Hartenstein, K. Eliceiri, P. Tomancak, and A. Cardona. *Fiji: an open-source platform for biological-image analysis.* Nature Methods, 2012. **9**(7): p. 676-682. DOI: 10.1038/Nmeth.2019.
278. Ansorge, R., G. Birolo, S.A. James, and A. Telatin. *Dadaist2: A Toolkit to Automate and Simplify Statistical Analysis and Plotting of Metabarcoding Experiments.* Int J Mol Sci, 2021. **22**(10). DOI: 10.3390/ijms22105309.
279. Telatin, A., P. Fariselli, and G. Birolo. *SeqFu: A Suite of Utilities for the Robust and Reproducible Manipulation of Sequence Files.* Bioengineering-Basel, 2021. **8**(5). DOI: 10.3390/bioengineering8050059.
280. Martin, M. *Cutadapt removes adapter sequences from high-throughput sequencing reads.* EMBnet.journal, 2011. **17**(1). DOI: 10.14806/ej.17.1.200.
281. Chen, S., Y. Zhou, Y. Chen, and J. Gu. *fastp: an ultra-fast all-in-one FASTQ preprocessor.* Bioinformatics, 2018. **34**(17): p. i884-i890. DOI: 10.1093/bioinformatics/bty560.
282. Rivers, A.R., K.C. Weber, T.G. Gardner, S. Liu, and S.D. Armstrong. *ITSxpress: Software to rapidly trim internally transcribed spacer sequences with quality scores for marker gene analysis.* F1000Res, 2018. **7**: p. 1418. DOI: 10.12688/f1000research.15704.1.
283. Callahan, B.J., P.J. McMurdie, M.J. Rosen, A.W. Han, A.J. Johnson, and S.P. Holmes. *DADA2: High-resolution sample inference from Illumina amplicon data.* Nat Methods, 2016. **13**(7): p. 581-3. DOI: 10.1038/nmeth.3869.

284. Nilsson, R.H., K.H. Larsson, A.F.S. Taylor, J. Bengtsson-Palme, T.S. Jeppesen, D. Schigel, P. Kennedy, K. Picard, F.O. Glockner, L. Tedersoo, I. Saar, U. Koljalg, and K. Abarenkov. *The UNITE database for molecular identification of fungi: handling dark taxa and parallel taxonomic classifications.* Nucleic Acids Res, 2019. **47**(D1): p. D259-D264. DOI: 10.1093/nar/gky1022.
285. Sievers, F. and D.G. Higgins. *The Clustal Omega Multiple Alignment Package.* Methods Mol Biol, 2021. **2231**: p. 3-16. DOI: 10.1007/978-1-0716-1036-7_1.
286. Price, M.N., P.S. Dehal, and A.P. Arkin. *FastTree: computing large minimum evolution trees with profiles instead of a distance matrix.* Mol Biol Evol, 2009. **26**(7): p. 1641-50. DOI: 10.1093/molbev/msp077.
287. Lagkouvardos, I., S. Fischer, N. Kumar, and T. Clavel. *Rhea: a transparent and modular R pipeline for microbial profiling based on 16S rRNA gene amplicons.* PeerJ, 2017. **5**. DOI: 10.7717/peerj.2836.
288. McMurdie, P.J. and S. Holmes. *phyloseq: an R package for reproducible interactive analysis and graphics of microbiome census data.* PLoS One, 2013. **8**(4). DOI: 10.1371/journal.pone.0061217.
289. Dhariwal, A., J. Chong, S. Habib, I.L. King, L.B. Agellon, and J. Xia. *MicrobiomeAnalyst: a web-based tool for comprehensive statistical, visual and meta-analysis of microbiome data.* Nucleic Acids Res, 2017. **45**(W1): p. W180-W188. DOI: 10.1093/nar/gkx295.
290. Chen, S.F., Y.Q. Zhou, Y.R. Chen, and J. Gu. *fastp: an ultra-fast all-in-one FASTQ preprocessor.* Bioinformatics, 2018. **34**(17): p. 884-890. DOI: 10.1093/bioinformatics/bty560.
291. Blanco-Miguez, A., F. Beghini, F. Cumbo, L.J. McIver, K.N. Thompson, M. Zolfo, P. Manghi, L. Dubois, K.D. Huang, A.M. Thomas, W.A. Nickols, G. Piccinno, E. Piperni, M. Puncochar, M. Valles-Colomer, A. Tett, F. Giordano, R. Davies, J. Wolf, S.E. Berry, T.D. Spector, E.A. Franzosa, E. Pasolli, F. Asnicar, C. Huttenhower, and N. Segata. *Extending and improving metagenomic taxonomic profiling with uncharacterized species using MetaPhlAn 4.* Nat Biotechnol, 2023. **41**(11): p. 1633-1644. DOI: 10.1038/s41587-023-01688-w.
292. Beghini, F., L.J. McIver, A. Blanco-Miguez, L. Dubois, F. Asnicar, S. Maharjan, A. Mailyan, P. Manghi, M. Scholz, A.M. Thomas, M. Valles-Colomer, G. Weingart, Y. Zhang, M. Zolfo, C. Huttenhower, E.A. Franzosa, and N. Segata. *Integrating taxonomic, functional, and strain-level profiling of diverse microbial communities with bioBakery 3.* Elife, 2021. **10**. DOI: 10.7554/eLife.65088.
293. Buchfink, B., C. Xie, and D.H. Huson. *Fast and sensitive protein alignment using DIAMOND.* Nature Methods, 2015. **12**(1): p. 59-60. DOI: 10.1038/nmeth.3176.
294. Uritskiy, G.V., J. DiRuggiero, and J. Taylor. *MetaWRAP-a flexible pipeline for genome-resolved metagenomic data analysis.* Microbiome, 2018. **6**. DOI: 10.1186/s40168-018-0541-1.
295. Li, D.H., R.B. Luo, C.M. Liu, C.M. Leung, H.F. Ting, K. Sadakane, H. Yamashita, and T.W. Lam. *MEGAHIT v1.0: A fast and scalable metagenome assembler driven by advanced methodologies and community practices.* Methods, 2016. **102**: p. 3-11. DOI: 10.1016/j.ymeth.2016.02.020.
296. Gurevich, A., V. Saveliev, N. Vyahhi, and G. Tesler. *QUAST: quality assessment tool for genome assemblies.* Bioinformatics, 2013. **29**(8): p. 1072-1075. DOI: 10.1093/bioinformatics/btt086.
297. Kang, D.W.D., F. Li, E. Kirton, A. Thomas, R. Egan, H. An, and Z. Wang. *MetaBAT 2: an adaptive binning algorithm for robust and efficient genome reconstruction from metagenome assemblies.* Peerj, 2019. **7**. DOI: 10.7717/peerj.7359.
298. Wu, Y.W., B.A. Simmons, and S.W. Singer. *MaxBin 2.0: an automated binning algorithm to recover genomes from multiple metagenomic datasets.* Bioinformatics, 2016. **32**(4): p. 605-607. DOI: 10.1093/bioinformatics/btv638.

299. Alneberg, J., B.S. Bjarnason, I. de Bruijn, M. Schirmer, J. Quick, U.Z. Ijaz, L. Lahti, N.J. Loman, A.F. Andersson, and C. Quince. *Binning metagenomic contigs by coverage and composition.* Nature Methods, 2014. **11**(11): p. 1144-1146. DOI: 10.1038/Nmeth.3103.
300. Olm, M.R., C.T. Brown, B. Brooks, and J.F. Banfield. *dRep: a tool for fast and accurate genomic comparisons that enables improved genome recovery from metagenomes through de-replication.* Isme Journal, 2017. **11**(12): p. 2864-2868. DOI: 10.1038/ismej.2017.126.
301. Parks, D.H., M. Imelfort, C.T. Skennerton, P. Hugenholtz, and G.W. Tyson. *CheckM: assessing the quality of microbial genomes recovered from isolates, single cells, and metagenomes.* Genome Res, 2015. **25**(7): p. 1043-55. DOI: 10.1101/gr.186072.114.
302. Chaumeil, P.-A., A.J. Mussig, P. Hugenholtz, and D.H. Parks. *GTDB-Tk v2: memory friendly classification with the genome taxonomy database.* Bioinformatics, 2022. **38**(23): p. 5315-5316. DOI: 10.1093/bioinformatics/btac672.
303. Parks, D.H., M. Chuvochina, P.-A. Chaumeil, C. Rinke, A.J. Mussig, and P. Hugenholtz. *A complete domain-to-species taxonomy for Bacteria and Archaea.* Nature Biotechnology, 2020. **38**(9): p. 1079-1086. DOI: 10.1038/s41587-020-0501-8.
304. Parks, D.H., M. Chuvochina, D.W. Waite, C. Rinke, A. Skarshewski, P.-A. Chaumeil, and P. Hugenholtz. *A standardized bacterial taxonomy based on genome phylogeny substantially revises the tree of life.* Nature Biotechnology, 2018. **36**(10): p. 996-1004. DOI: 10.1038/nbt.4229.
305. Chaumeil, P.-A., A.J. Mussig, P. Hugenholtz, and D.H. Parks. *GTDB-Tk: a toolkit to classify genomes with the Genome Taxonomy Database.* Bioinformatics, 2019. **36**(6): p. 1925-1927. DOI: 10.1093/bioinformatics/btz848.
306. Lahti, L. and S. Shetty, *Tools for microbiome analysis in R*. 2017, http://microbiome.github.com/microbiome.
307. Pinheiro, J., D. Bates, and R Core Team, *nlme: Linear and Nonlinear Mixed Effects Models*, in *R package version 3.1-166*. 2024, https://CRAN.R-project.org/package=nlme.
308. Dixon, P. *VEGAN, a package of R functions for community ecology.* Journal of Vegetation Science, 2003. **14**(6): p. 927-930. DOI: 10.1111/j.1654-1103.2003.tb02228.x.
309. Martinez Arbizu, P., *pairwiseAdonis: Pairwise multilevel comparison using adonis.* 2020, https://github.com/pmartinezarbizu/pairwiseAdonis.
310. Mallick, H., A. Rahnavard, L.J. McIver, S. Ma, Y. Zhang, L.H. Nguyen, T.L. Tickle, G. Weingart, B. Ren, E.H. Schwager, S. Chatterjee, K.N. Thompson, J.E. Wilkinson, A. Subramanian, Y. Lu, L. Waldron, J.N. Paulson, E.A. Franzosa, H.C. Bravo, and C. Huttenhower. *Multivariable association discovery in population-scale meta-omics studies.* PLoS Comput Biol, 2021. **17**(11). DOI: 10.1371/journal.pcbi.1009442.
311. Komsta, L., *outliers: Tests for Outliers*. 2022 DOI: 10.32614/CRAN.package.outliers.
312. Pohlert, T., *PMCMRplus: Calculate Pairwise Multiple Comparisons of Mean Rank Sums Extended*. 2024 DOI: 10.32614/CRAN.package.PMCMRplus.
313. Bates, D., M. Mächler, B.M. Bolker, and S.C. Walker. *Fitting Linear Mixed-Effects Models Using lme4.* Journal of Statistical Software, 2015. **67**(1): p. 1-48. DOI: 10.18637/jss.v067.i01.
314. Broad, J., V.W.S. Kung, A. Palmer, S. Elahi, A. Karami, T. Darreh-Shori, S. Ahmed, M.A. Thaha, R. Carroll, J. Chin-Aleong, J.E. Martin, M.J. Saffrey, C.H. Knowles, and G.J. Sanger. *Changes in neuromuscular structure and functions of human colon during ageing are region-dependent.* Gut, 2019. **68**(7): p. 1210-1223. DOI: 10.1136/gutjnl-2018-316279.
315. Camilleri, M., J.S. Lee, B. Viramontes, A.E. Bharucha, and E.G. Tangalos. *Insights into the Pathophysiology and Mechanisms of Constipation, Irritable Bowel Syndrome, and Diverticulosis in Older People.* Journal of the American Geriatrics Society, 2000. **48**(9): p. 1142-1150. DOI: 10.1111/j.1532-5415.2000.tb04793.x.

316. Bosco, N. and M. Noti. *The aging gut microbiome and its impact on host immunity.* Genes Immun, 2021. **22**(5-6): p. 289-303. DOI: 10.1038/s41435-021-00126-8.
317. Mabbott, N.A. *A breakdown in communication? Understanding the effects of aging on the human small intestine epithelium.* Clin Sci (Lond), 2015. **129**(7): p. 529-31. DOI: 10.1042/CS20150364.
318. Heston, M.B., K.L. Hanslik, K.R. Zarbock, S.J. Harding, N.J. Davenport-Sis, R.L. Kerby, N. Chin, Y. Sun, A. Hoeft, Y. Deming, N.M. Vogt, T.J. Betthauser, S.C. Johnson, S. Asthana, G. Kollmorgen, I. Suridjan, N. Wild, H. Zetterberg, K. Blennow, F.E. Rey, B.B. Bendlin, and T.K. Ulland. *Gut inflammation associated with age and Alzheimer's disease pathology: a human cohort study.* Sci Rep, 2023. **13**(1). DOI: 10.1038/s41598-023-45929-z.
319. Erben, U., C. Loddenkemper, K. Doerfel, S. Spieckermann, D. Haller, M.M. Heimesaat, M. Zeitz, B. Siegmund, and A.A. Kuhl. *A guide to histomorphological evaluation of intestinal inflammation in mouse models.* Int J Clin Exp Pathol, 2014. **7**(8): p. 4557-76. https://www.ncbi.nlm.nih.gov/pubmed/25197329.
320. Feakins, R., P. Borralho Nunes, A. Driessen, I.O. Gordon, N. Zidar, P. Baldin, B. Christensen, S. Danese, N. Herlihy, M. Iacucci, M.B. Loughrey, F. Magro, A. Mookhoek, M. Svrcek, and F. Rosini. *Definitions of Histological Abnormalities in Inflammatory Bowel Disease: an ECCO Position Paper.* J Crohns Colitis, 2024. **18**(2): p. 175-191. DOI: 10.1093/ecco-jcc/jjad142.
321. Sovran, B., F. Hugenholtz, M. Elderman, A.A. Van Beek, K. Graversen, M. Huijskes, M.V. Boekschoten, H.F.J. Savelkoul, P. De Vos, J. Dekker, and J.M. Wells. *Age-associated Impairment of the Mucus Barrier Function is Associated with Profound Changes in Microbiota and Immunity.* Sci Rep, 2019. **9**(1): p. 1437. DOI: 10.1038/s41598-018-35228-3.
322. Martin, K., T.B. Kirkwood, and C.S. Potten. *Age changes in stem cells of murine small intestinal crypts.* Exp Cell Res, 1998. **241**(2): p. 316-23. DOI: 10.1006/excr.1998.4001.
323. Rosa, E.F., A.C. Silva, S.S. Ihara, O.A. Mora, J. Aboulafia, and V.L. Nouailhetas. *Habitual exercise program protects murine intestinal, skeletal, and cardiac muscles against aging.* J Appl Physiol, 2005. **99**(4): p. 1569-75. DOI: 10.1152/japplphysiol.00417.2005.
324. Suzuki, T., K. Aoki, K. Shimokobe, S. Omiya, C. Funayama, T. Takahashi, and M. Kato. *Age-related morphological and functional changes in the small intestine of senescence-accelerated mouse.* Exp Gerontol, 2022. **163**. DOI: 10.1016/j.exger.2022.111795.
325. Hassan, Z.A., A. Zauszkiewicz-Pawlak, S.A. Abdelrahman, S. Algaidi, M. Desouky, and S.M. Shalaby. *Morphological alterations in the jejunal mucosa of aged rats and the possible protective role of green tea.* Folia Histochem Cytobiol, 2017. **55**(3): p. 124-139. DOI: 10.5603/FHC.a2017.0012.
326. Holt, P.R., R.R. Pascal, and D.P. Kotler. *Effect of aging upon small intestinal structure in the Fischer rat.* J Gerontol, 1984. **39**(6): p. 642-7. DOI: 10.1093/geronj/39.6.642.
327. Lipski, P.S., M.K. Bennett, P.J. Kelly, and O.F. James. *Ageing and duodenal morphometry.* J Clin Pathol, 1992. **45**(5): p. 450-2. DOI: 10.1136/jcp.45.5.450.
328. Corazza, G.R., M. Frazzoni, M.R. Gatto, and G. Gasbarrini. *Ageing and small-bowel mucosa: a morphometric study.* Gerontology, 1986. **32**(1): p. 60-5. DOI: 10.1159/000212766.
329. Webster, S.G. and J.T. Leeming. *The appearance of the small bowel mucosa in old age.* Age and Ageing, 1975. **4**(3): p. 168-74. DOI: 10.1093/ageing/4.3.168.
330. Paone, P. and P.D. Cani. *Mucus barrier, mucins and gut microbiota: the expected slimy partners?* Gut, 2020. **69**(12): p. 2232-2243. DOI: 10.1136/gutjnl-2020-322260.
331. Newton, J.L., N. Jordan, J. Pearson, G.V. Williams, A. Allen, and O.F. James. *The adherent gastric antral and duodenal mucus gel layer thins with advancing age in subjects infected with Helicobacter pylori.* Gerontology, 2000. **46**(3): p. 153-7. DOI: 10.1159/000022151.

332. Elderman, M., B. Sovran, F. Hugenholtz, K. Graversen, M. Huijskes, E. Houtsma, C. Belzer, M. Boekschoten, P. de Vos, J. Dekker, J. Wells, and M. Faas. *The effect of age on the intestinal mucus thickness, microbiota composition and immunity in relation to sex in mice.* PLoS One, 2017. **12**(9). DOI: 10.1371/journal.pone.0184274.
333. Tran, L. and B. Greenwood-Van Meerveld. *Age-associated remodeling of the intestinal epithelial barrier.* J Gerontol A Biol Sci Med Sci, 2013. **68**(9): p. 1045-56. DOI: 10.1093/gerona/glt106.
334. Johnson, A.L., R.I. Keesler, A.D. Lewis, J.R. Reader, and S.T. Laing. *Common and Not-So-Common Pathologic Findings of the Gastrointestinal Tract of Rhesus and Cynomolgus Macaques.* Toxicol Pathol, 2022. **50**(5): p. 638-659. DOI: 10.1177/01926233221084634.
335. Puzianowska-Kuznicka, M., M. Owczarz, K. Wieczorowska-Tobis, P. Nadrowski, J. Chudek, P. Slusarczyk, A. Skalska, M. Jonas, E. Franek, and M. Mossakowska. *Interleukin-6 and C-reactive protein, successful aging, and mortality: the PolSenior study.* Immun Ageing, 2016. **13**: p. 21. DOI: 10.1186/s12979-016-0076-x.
336. Tiainen, K., M. Hurme, A. Hervonen, T. Luukkaala, and M. Jylha. *Inflammatory markers and physical performance among nonagenarians.* J Gerontol A Biol Sci Med Sci, 2010. **65**(6): p. 658-63. DOI: 10.1093/gerona/glq056.
337. Brinkley, T.E., X. Leng, M.E. Miller, D.W. Kitzman, M. Pahor, M.J. Berry, A.P. Marsh, S.B. Kritchevsky, and B.J. Nicklas. *Chronic inflammation is associated with low physical function in older adults across multiple comorbidities.* J Gerontol A Biol Sci Med Sci, 2009. **64**(4): p. 455-61. DOI: 10.1093/gerona/gln038.
338. Ahmadi-Abhari, S., R.N. Luben, N.J. Wareham, and K.T. Khaw. *Distribution and determinants of C-reactive protein in the older adult population: European Prospective Investigation into Cancer-Norfolk study.* Eur J Clin Invest, 2013. **43**(9): p. 899-911. DOI: 10.1111/eci.12116.
339. Meng, L., Z. Song, A. Liu, U. Dahmen, X. Yang, and H. Fang. *Effects of Lipopolysaccharide-Binding Protein (LBP) Single Nucleotide Polymorphism (SNP) in Infections, Inflammatory Diseases, Metabolic Disorders and Cancers.* Front Immunol, 2021. **12**. DOI: 10.3389/fimmu.2021.681810.
340. Seethaler, B., M. Basrai, A.M. Neyrinck, J.A. Nazare, J. Walter, N.M. Delzenne, and S.C. Bischoff. *Biomarkers for assessment of intestinal permeability in clinical practice.* American Journal of Physiology-Gastrointestinal and Liver Physiology, 2021. **321**(1): p. G11-G17. DOI: 10.1152/ajpgi.00113.2021.
341. Stojanovic, O., J. Altirriba, D. Rigo, M. Spiljar, E. Evrard, B. Roska, S. Fabbiano, N. Zamboni, P. Maechler, F. Rohner-Jeanrenaud, and M. Trajkovski. *Dietary excess regulates absorption and surface of gut epithelium through intestinal PPARalpha.* Nat Commun, 2021. **12**(1): p. 7031. DOI: 10.1038/s41467-021-27133-7.
342. Taylor, S.R., S. Ramsamooj, R.J. Liang, A. Katti, R. Pozovskiy, N. Vasan, S.K. Hwang, N. Nahiyaan, N.J. Francoeur, E.M. Schatoff, J.L. Johnson, M.A. Shah, A.J. Dannenberg, R.P. Sebra, L.E. Dow, L.C. Cantley, K.Y. Rhee, and M.D. Goncalves. *Dietary fructose improves intestinal cell survival and nutrient absorption.* Nature, 2021. **597**(7875): p. 263-267. DOI: 10.1038/s41586-021-03827-2.
343. Bauer, S.A., D.L. Pearl, K.E. Leslie, J. Fournier, and P.V. Turner. *Causes of obesity in captive cynomolgus macaques: influence of body condition, social and management factors on behaviour around feeding.* Lab Anim, 2012. **46**(3): p. 193-9. DOI: 10.1258/la.2012.011120.
344. Fuke, N.B., T. Yamashita, S. Shimizu, M. Matsumoto, K. Sawada, S.E. Jung, I. Tokuda, M. Misawa, S. Suzuki, Y. Ushida, T. Mikami, K. Itoh, and H. Suganuma. *Association of Plasma Lipopolysaccharide-Binding Protein Concentration with Dietary Factors, Gut Microbiota, and Health Status in the Japanese General Adult Population: A Cross-Sectional Study.* Metabolites, 2023. **13**(2). DOI: 10.3390/metabo13020250.
345. Gonzalez-Quintela, A., M. Alonso, J. Campos, L. Vizcaino, L. Loidi, and F. Gude. *Determinants of Serum Concentrations of Lipopolysaccharide-Binding Protein (LBP) in*

the Adult Population: The Role of Obesity. Plos One, 2013. **8**(1). DOI: 10.1371/journal.pone.0054600.
346. McFarlane, D., R.F. Wolf, K.A. McDaniel, and G.L. White. *Age-Associated Alteration in Innate Immune Response in Captive Baboons.* Journals of Gerontology Series a-Biological Sciences and Medical Sciences, 2011. **66**(12): p. 1309-1317. DOI: 10.1093/gerona/glr146.
347. Baumann, A., A. Hernandez-Arriaga, A. Brandt, V. Sanchez, A. Nier, F. Jung, R. Kehm, A. Hohn, T. Grune, C. Frahm, O.W. Witte, A. Camarinha-Silva, and I. Bergheim. *Microbiota profiling in aging-associated inflammation and liver degeneration.* Int J Med Microbiol, 2021. **311**(4). DOI: 10.1016/j.ijmm.2021.151500.
348. Kim, K.A., J.J. Jeong, S.Y. Yoo, and D.H. Kim. *Gut microbiota lipopolysaccharide accelerates inflamm-aging in mice.* BMC Microbiol, 2016. **16**: p. 9. DOI: 10.1186/s12866-016-0625-7.
349. Gorman, A. and A.P. Golovanov. *Lipopolysaccharide Structure and the Phenomenon of Low Endotoxin Recovery.* Eur J Pharm Biopharm, 2022. **180**: p. 289-307. DOI: 10.1016/j.ejpb.2022.10.006.
350. Kohman, R.A., B. Crowell, and A.W. Kusnecov. *Differential sensitivity to endotoxin exposure in young and middle-age mice.* Brain Behav Immun, 2010. **24**(3): p. 486-92. DOI: 10.1016/j.bbi.2009.12.004.
351. Tateda, K., T. Matsumoto, S. Miyazaki, and K. Yamaguchi. *Lipopolysaccharide-induced lethality and cytokine production in aged mice.* Infect Immun, 1996. **64**(3): p. 769-74. DOI: 10.1128/iai.64.3.769-774.1996.
352. McKenney, E.A., A.R. Hale, J. Anderson, R. Larsen, C. Grant, and R.R. Dunn. *Hidden diversity: comparative functional morphology of humans and other species.* PeerJ, 2023. **11**. DOI: 10.7717/peerj.15148.
353. Wang, C., L.K. Lutes, C. Barnoud, and C. Scheiermann. *The circadian immune system.* Sci Immunol, 2022. **7**(72). DOI: 10.1126/sciimmunol.abm2465.
354. Heddes, M., B. Altaha, Y. Niu, S. Reitmeier, K. Kleigrewe, D. Haller, and S. Kiessling. *The intestinal clock drives the microbiome to maintain gastrointestinal homeostasis.* Nat Commun, 2022. **13**(1). DOI: 10.1038/s41467-022-33609-x.
355. Biagi, E., L. Nylund, M. Candela, R. Ostan, L. Bucci, E. Pini, J. Nikkila, D. Monti, R. Satokari, C. Franceschi, P. Brigidi, and W. De Vos. *Through ageing, and beyond: gut microbiota and inflammatory status in seniors and centenarians.* PLoS One, 2010. **5**(5). DOI: 10.1371/journal.pone.0010667.
356. Rampelli, S., M. Candela, S. Turroni, E. Biagi, S. Collino, C. Franceschi, P.W. O'Toole, and P. Brigidi. *Functional metagenomic profiling of intestinal microbiome in extreme ageing.* Aging (Albany NY), 2013. **5**(12): p. 902-12. DOI: 10.18632/aging.100623.
357. Cho, S.Y., J. Kim, J.H. Lee, J.H. Sim, D.H. Cho, I.H. Bae, H. Lee, M.A. Seol, H.M. Shin, T.J. Kim, D.Y. Kim, S.H. Lee, S.S. Shin, S.H. Im, and H.R. Kim. *Modulation of gut microbiota and delayed immunosenescence as a result of syringaresinol consumption in middle-aged mice.* Sci Rep, 2016. **6**. DOI: 10.1038/srep39026.
358. Liu, P., L. Wu, G.P. Peng, Y.Q. Han, R.Q. Tang, J.P. Ge, L.J. Zhang, L.F. Jia, S.Q. Yue, K. Zhou, L.J. Li, B.Y. Luo, and B.H. Wang. *Altered microbiomes distinguish Alzheimer's disease from amnestic mild cognitive impairment and health in a Chinese cohort.* Brain Behavior and Immunity, 2019. **80**: p. 633-643. DOI: 10.1016/j.bbi.2019.05.008.
359. Qu, J., F. Yang, T. Zhu, Y. Wang, W. Fang, Y. Ding, X. Zhao, X. Qi, Q. Xie, M. Chen, Q. Xu, Y. Xie, Y. Sun, and D. Chen. *A reference single-cell regulomic and transcriptomic map of cynomolgus monkeys.* Nat Commun, 2022. **13**(1): p. 4069. DOI: 10.1038/s41467-022-31770-x.
360. Li, X., S. Liang, Z. Xia, J. Qu, H. Liu, C. Liu, H. Yang, J. Wang, L. Madsen, Y. Hou, J. Li, H. Jia, K. Kristiansen, and L. Xiao. *Establishment of a Macaca fascicularis gut microbiome gene catalog and comparison with the human, pig, and mouse gut microbiomes.* Gigascience, 2018. **7**(9). DOI: 10.1093/gigascience/giy100.

361. Manara, S., F. Asnicar, F. Beghini, D. Bazzani, F. Cumbo, M. Zolfo, E. Nigro, N. Karcher, P. Manghi, M.I. Metzger, E. Pasolli, and N. Segata. *Microbial genomes from non-human primate gut metagenomes expand the primate-associated bacterial tree of life with over 1000 novel species.* Genome Biol, 2019. **20**(1): p. 299. DOI: 10.1186/s13059-019-1923-9.
362. Ye, S.H., K.J. Siddle, D.J. Park, and P.C. Sabeti. *Benchmarking Metagenomics Tools for Taxonomic Classification.* Cell, 2019. **178**(4): p. 779-794. DOI: 10.1016/j.cell.2019.07.010.
363. Hitch, T.C.A., K. Bisdorf, A. Afrizal, T. Riedel, J. Overmann, T. Strowig, and T. Clavel. *A taxonomic note on the genus Prevotella: Description of four novel genera and emended description of the genera Hallella and Xylanibacter.* Syst Appl Microbiol, 2022. **45**(6). DOI: 10.1016/j.syapm.2022.126354.
364. Lowe, S.E., H.S. Pankratz, and J.G. Zeikus. *Influence of pH extremes on sporulation and ultrastructure of Sarcina ventriculi.* J Bacteriol, 1989. **171**(7): p. 3775-81. DOI: 10.1128/jb.171.7.3775-3781.1989.
365. Chuvochina, M., A.J. Mussig, P.A. Chaumeil, A. Skarshewski, C. Rinke, D.H. Parks, and P. Hugenholtz. *Proposal of names for 329 higher rank taxa defined in the Genome Taxonomy Database under two prokaryotic codes.* FEMS Microbiol Lett, 2023. **370**. DOI: 10.1093/femsle/fnad071.
366. Strong, P.J., S. Xie, and W.P. Clarke. *Methane as a Resource: Can the Methanotrophs Add Value?* Environmental Science & Technology, 2015. **49**(7): p. 4001-4018. DOI: 10.1021/es504242n.
367. Bowers, R.M., N.C. Kyrpides, R. Stepanauskas, M. Harmon-Smith, D. Doud, T.B.K. Reddy, F. Schulz, J. Jarett, A.R. Rivers, E.A. Eloe-Fadrosh, S.G. Tringe, N.N. Ivanova, A. Copeland, A. Clum, E.D. Becraft, R.R. Malmstrom, B. Birren, M. Podar, P. Bork, G.M. Weinstock, G.M. Garrity, J.A. Dodsworth, S. Yooseph, G. Sutton, F.O. Glöckner, J.A. Gilbert, W.C. Nelson, S.J. Hallam, S.P. Jungbluth, T.J.G. Ettema, S. Tighe, K.T. Konstantinidis, W.T. Liu, B.J. Baker, T. Rattei, J.A. Eisen, B. Hedlund, K.D. McMahon, N. Fierer, R. Knight, R. Finn, G. Cochrane, I. Karsch-Mizrachi, G.W. Tyson, C. Rinke, A. Lapidus, F. Meyer, P. Yilmaz, D.H. Parks, A.M. Eren, L. Schriml, J.F. Banfield, P. Hugenholtz, T. Woyke, and G.S. Consortium. *Minimum information about a single amplified genome (MISAG) and a metagenome-assembled genome (MIMAG) of bacteria and archaea.* Nature Biotechnology, 2017. **35**(8): p. 725-731. DOI: 10.1038/nbt.3893.
368. Clayton, J.B., P. Vangay, H. Huang, T. Ward, B.M. Hillmann, G.A. Al-Ghalith, D.A. Travis, H.T. Long, B.V. Tuan, V.V. Minh, F. Cabana, T. Nadler, B. Toddes, T. Murphy, K.E. Glander, T.J. Johnson, and D. Knights. *Captivity humanizes the primate microbiome.* Proc Natl Acad Sci U S A, 2016. **113**(37): p. 10376-81. DOI: 10.1073/pnas.1521835113.
369. Schnorr, S.L., M. Candela, S. Rampelli, M. Centanni, C. Consolandi, G. Basaglia, S. Turroni, E. Biagi, C. Peano, M. Severgnini, J. Fiori, R. Gotti, G. De Bellis, D. Luiselli, P. Brigidi, A. Mabulla, F. Marlowe, A.G. Henry, and A.N. Crittenden. *Gut microbiome of the Hadza hunter-gatherers.* Nat Commun, 2014. **5**. DOI: 10.1038/ncomms4654.
370. Obregon-Tito, A.J., R.Y. Tito, J. Metcalf, K. Sankaranarayanan, J.C. Clemente, L.K. Ursell, Z. Zech Xu, W. Van Treuren, R. Knight, P.M. Gaffney, P. Spicer, P. Lawson, L. Marin-Reyes, O. Trujillo-Villarroel, M. Foster, E. Guija-Poma, L. Troncoso-Corzo, C. Warinner, A.T. Ozga, and C.M. Lewis. *Subsistence strategies in traditional societies distinguish gut microbiomes.* Nat Commun, 2015. **6**. DOI: 10.1038/ncomms7505.
371. De Filippo, C., D. Cavalieri, M. Di Paola, M. Ramazzotti, J.B. Poullet, S. Massart, S. Collini, G. Pieraccini, and P. Lionetti. *Impact of diet in shaping gut microbiota revealed by a comparative study in children from Europe and rural Africa.* Proc Natl Acad Sci U S A, 2010. **107**(33): p. 14691-6. DOI: 10.1073/pnas.1005963107.
372. Pasolli, E., F. Asnicar, S. Manara, M. Zolfo, N. Karcher, F. Armanini, F. Beghini, P. Manghi, A. Tett, P. Ghensi, M.C. Collado, B.L. Rice, C. DuLong, X.C. Morgan, C.D. Golden, C. Quince, C. Huttenhower, and N. Segata. *Extensive Unexplored Human*

Microbiome Diversity Revealed by Over 150,000 Genomes from Metagenomes Spanning Age, Geography, and Lifestyle. Cell, 2019. **176**(3): p. 649-662. DOI: 10.1016/j.cell.2019.01.001.

373. Rinott, E., A.Y. Meir, G. Tsaban, H. Zelicha, A. Kaplan, D. Knights, K. Tuohy, M.U. Scholz, O. Koren, M.J. Stampfer, D.D. Wang, I. Shai, and I. Youngster. *The effects of the Green-Mediterranean diet on cardiometabolic health are linked to gut microbiome modifications: a randomized controlled trial.* Genome Med, 2022. **14**(1): p. 29. DOI: 10.1186/s13073-022-01015-z.
374. Blanco-Miguez, A., E.J.C. Galvez, E. Pasolli, F. De Filippis, L. Amend, K.D. Huang, P. Manghi, T.R. Lesker, T. Riedel, L. Cova, M. Puncochar, A.M. Thomas, M. Valles-Colomer, I. Schober, T.C.A. Hitch, T. Clavel, S.E. Berry, R. Davies, J. Wolf, T.D. Spector, J. Overmann, A. Tett, D. Ercolini, N. Segata, and T. Strowig. *Extension of the Segatella copri complex to 13 species with distinct large extrachromosomal elements and associations with host conditions.* Cell Host Microbe, 2023. **31**(11): p. 1804-1819. DOI: 10.1016/j.chom.2023.09.013.
375. Tett, A., K.D. Huang, F. Asnicar, H. Fehlner-Peach, E. Pasolli, N. Karcher, F. Armanini, P. Manghi, K. Bonham, M. Zolfo, F. De Filippis, C. Magnabosco, R. Bonneau, J. Lusingu, J. Amuasi, K. Reinhard, T. Rattei, F. Boulund, L. Engstrand, A. Zink, M.C. Collado, D.R. Littman, D. Eibach, D. Ercolini, O. Rota-Stabelli, C. Huttenhower, F. Maixner, and N. Segata. *The Prevotella copri Complex Comprises Four Distinct Clades Underrepresented in Westernized Populations.* Cell Host Microbe, 2019. **26**(5): p. 666-679. DOI: 10.1016/j.chom.2019.08.018.
376. Kovatcheva-Datchary, P., A. Nilsson, R. Akrami, Y.S. Lee, F. De Vadder, T. Arora, A. Hallen, E. Martens, I. Bjorck, and F. Backhed. *Dietary Fiber-Induced Improvement in Glucose Metabolism Is Associated with Increased Abundance of Prevotella.* Cell Metab, 2015. **22**(6): p. 971-82. DOI: 10.1016/j.cmet.2015.10.001.
377. Scher, J.U., A. Sczesnak, R.S. Longman, N. Segata, C. Ubeda, C. Bielski, T. Rostron, V. Cerundolo, E.G. Pamer, S.B. Abramson, C. Huttenhower, and D.R. Littman. *Expansion of intestinal Prevotella copri correlates with enhanced susceptibility to arthritis.* Elife, 2013. **2**. DOI: 10.7554/eLife.01202.
378. Rolhion, N., B. Chassaing, M.A. Nahori, J. de Bodt, A. Moura, M. Lecuit, O. Dussurget, M. Berard, M. Marzorati, H. Fehlner-Peach, D.R. Littman, A.T. Gewirtz, T. Van de Wiele, and P. Cossart. *A Listeria monocytogenes Bacteriocin Can Target the Commensal Prevotella copri and Modulate Intestinal Infection.* Cell Host Microbe, 2019. **26**(5): p. 691-701. DOI: 10.1016/j.chom.2019.10.016.
379. Haro, C., S. Garcia-Carpintero, O.A. Rangel-Zuniga, J.F. Alcala-Diaz, B.B. Landa, J.C. Clemente, P. Perez-Martinez, J. Lopez-Miranda, F. Perez-Jimenez, and A. Camargo. *Consumption of Two Healthy Dietary Patterns Restored Microbiota Dysbiosis in Obese Patients with Metabolic Dysfunction.* Mol Nutr Food Res, 2017. **61**(12). DOI: 10.1002/mnfr.201700300.
380. Xiao, X., A. Singh, A. Giometto, and I.L. Brito. *Segatella copri strains adopt distinct roles within a single individual's gut.* bioRxiv, 2024. DOI: 10.1101/2024.05.20.595015.
381. Tung, J., L.B. Barreiro, M.B. Burns, J.C. Grenier, J. Lynch, L.E. Grieneisen, J. Altmann, S.C. Alberts, R. Blekhman, and E.A. Archie. *Social networks predict gut microbiome composition in wild baboons.* Elife, 2015. **4**. DOI: 10.7554/eLife.05224.
382. Debray, R., C.C. Dickson, S.E. Webb, E.A. Archie, and J. Tung. *Shared environments complicate the use of strain-resolved metagenomics to infer microbiome transmission.* Microbiome, 2025. **13**(1): p. 59. DOI: 10.1186/s40168-025-02051-8.
383. Turnbaugh, P.J., M. Hamady, T. Yatsunenko, B.L. Cantarel, A. Duncan, R.E. Ley, M.L. Sogin, W.J. Jones, B.A. Roe, J.P. Affourtit, M. Egholm, B. Henrissat, A.C. Heath, R. Knight, and J.I. Gordon. *A core gut microbiome in obese and lean twins.* Nature, 2009. **457**(7228): p. 480-4. DOI: 10.1038/nature07540.
384. Dong, T.S., M. Guan, E.A. Mayer, J. Stains, C. Liu, P. Vora, J.P. Jacobs, V. Lagishetty, L. Chang, R.L. Barry, and A. Gupta. *Obesity is associated with a distinct brain-gut*

microbiome signature that connects Prevotella and Bacteroides to the brain's reward center. Gut Microbes, 2022. **14**(1). DOI: 10.1080/19490976.2022.2051999.
385. Stanislawski, M.A., D. Dabelea, L.A. Lange, B.D. Wagner, and C.A. Lozupone. *Gut microbiota phenotypes of obesity.* NPJ Biofilms Microbiomes, 2019. **5**(1): p. 18. DOI: 10.1038/s41522-019-0091-8.
386. Ley, R.E., F. Backhed, P. Turnbaugh, C.A. Lozupone, R.D. Knight, and J.I. Gordon. *Obesity alters gut microbial ecology.* Proc Natl Acad Sci USA, 2005. **102**(31): p. 11070-5. DOI: 10.1073/pnas.0504978102.
387. Murphy, E.F., P.D. Cotter, S. Healy, T.M. Marques, O. O'Sullivan, F. Fouhy, S.F. Clarke, P.W. O'Toole, E.M. Quigley, C. Stanton, P.R. Ross, R.M. O'Doherty, and F. Shanahan. *Composition and energy harvesting capacity of the gut microbiota: relationship to diet, obesity and time in mouse models.* Gut, 2010. **59**(12): p. 1635-42. DOI: 10.1136/gut.2010.215665.
388. Palmas, V., S. Pisanu, V. Madau, E. Casula, A. Deledda, R. Cusano, P. Uva, S. Vascellari, A. Loviselli, A. Manzin, and F. Velluzzi. *Gut microbiota markers associated with obesity and overweight in Italian adults.* Sci Rep, 2021. **11**(1). DOI: 10.1038/s41598-021-84928-w.
389. Armougom, F., M. Henry, B. Vialettes, D. Raccah, and D. Raoult. *Monitoring bacterial community of human gut microbiota reveals an increase in Lactobacillus in obese patients and Methanogens in anorexic patients.* PLoS One, 2009. **4**(9). DOI: 10.1371/journal.pone.0007125.
390. Duncan, S.H., G.E. Lobley, G. Holtrop, J. Ince, A.M. Johnstone, P. Louis, and H.J. Flint. *Human colonic microbiota associated with diet, obesity and weight loss.* Int J Obes (Lond), 2008. **32**(11): p. 1720-4. DOI: 10.1038/ijo.2008.155.
391. Schwiertz, A., D. Taras, K. Schafer, S. Beijer, N.A. Bos, C. Donus, and P.D. Hardt. *Microbiota and SCFA in lean and overweight healthy subjects.* Obesity (Silver Spring), 2010. **18**(1): p. 190-5. DOI: 10.1038/oby.2009.167.
392. Walters, W.A., Z. Xu, and R. Knight. *Meta-analyses of human gut microbes associated with obesity and IBD.* FEBS Lett, 2014. **588**(22): p. 4223-33. DOI: 10.1016/j.febslet.2014.09.039.
393. Nagpal, R., C.A. Shively, S.A. Appt, T.C. Register, K.T. Michalson, M.Z. Vitolins, and H. Yadav. *Gut Microbiome Composition in Non-human Primates Consuming a Western or Mediterranean Diet.* Front Nutr, 2018. **5**: p. 28. DOI: 10.3389/fnut.2018.00028.
394. Ley, R.E., P.J. Turnbaugh, S. Klein, and J.I. Gordon. *Microbial ecology: human gut microbes associated with obesity.* Nature, 2006. **444**(7122): p. 1022-3. DOI: 10.1038/4441022a.
395. Turnbaugh, P.J., R.E. Ley, M.A. Mahowald, V. Magrini, E.R. Mardis, and J.I. Gordon. *An obesity-associated gut microbiome with increased capacity for energy harvest.* Nature, 2006. **444**(7122): p. 1027-31. DOI: 10.1038/nature05414.
396. Finucane, M.M., T.J. Sharpton, T.J. Laurent, and K.S. Pollard. *A taxonomic signature of obesity in the microbiome? Getting to the guts of the matter.* PLoS One, 2014. **9**(1). DOI: 10.1371/journal.pone.0084689.
397. Grieneisen, L., M. Dasari, T.J. Gould, J.R. Bjork, J.C. Grenier, V. Yotova, D. Jansen, N. Gottel, J.B. Gordon, N.H. Learn, L.R. Gesquiere, T.L. Wango, R.S. Mututua, J.K. Warutere, L. Siodi, J.A. Gilbert, L.B. Barreiro, S.C. Alberts, J. Tung, E.A. Archie, and R. Blekhman. *Gut microbiome heritability is nearly universal but environmentally contingent.* Science, 2021. **373**(6551): p. 181-186. DOI: 10.1126/science.aba5483.
398. Johnson, K.V.A., K.K. Watson, R.I.M. Dunbar, and P.W.J. Burnet. *Sociability in a non-captive macaque population is associated with beneficial gut bacteria.* Frontiers in Microbiology, 2022. **13**. DOI: 10.3389/fmicb.2022.1032495.
399. Moeller, A.H., S. Foerster, M.L. Wilson, A.E. Pusey, B.H. Hahn, and H. Ochman. *Social behavior shapes the chimpanzee pan-microbiome.* Sci Adv, 2016. **2**(1). DOI: 10.1126/sciadv.1500997.

400. Raulo, A., L. Ruokolainen, A. Lane, K. Amato, R. Knight, S. Leigh, R. Stumpf, B. White, K.E. Nelson, A.L. Baden, and S.R. Tecot. *Social behaviour and gut microbiota in red-bellied lemurs (Eulemur rubriventer): In search of the role of immunity in the evolution of sociality.* J Anim Ecol, 2018. **87**(2): p. 388-399. DOI: 10.1111/1365-2656.12781.
401. Canale-Parola, E. and R.S. Wolfe. *Studies on Sarcina ventriculi. I. Stock culture method.* J Bacteriol, 1960. **79**(6): p. 857-9. DOI: 10.1128/jb.79.6.857-859.1960.
402. Makovska, M., J. Killer, N. Modrackova, E. Ingribelli, A. Amin, E. Vlkova, P. Bolechova, and V. Neuzil-Bunesova. *Species and Strain Variability among Sarcina Isolates from Diverse Mammalian Hosts.* Animals, 2023. **13**(9). DOI: 10.3390/ani13091529.
403. Ushida, K., S. Tsuchida, Y. Ogura, T. Hayashi, A. Sawada, and G. Hanya. *Draft Genome Sequences of Sarcina ventriculi Strains Isolated from Wild Japanese Macaques in Yakushima Island.* Genome Announc, 2016. **4**(1). DOI: 10.1128/genomeA.01694-15.
404. Crowther, J.S. *Sarcina ventriculi in human faeces.* J Med Microbiol, 1971. **4**(3): p. 343-50. DOI: 10.1099/00222615-4-3-343.
405. Marcelino, L.P., D.F. Valentini, S. Machado, P.G. Schaefer, R.C. Rivero, and A.B. Osvaldt. *Sarcina ventriculi a rare pathogen.* Autops Case Rep, 2021. **11**. DOI: 10.4322/acr.2021.337.
406. Tartaglia, D., F. Coccolini, A. Mazzoni, S. Strambi, E. Cicuttin, C. Cremonini, G. Taddei, A.G. Puglisi, C. Ugolini, I. Di Stefano, F. Basolo, and M. Chiarugi. *Sarcina Ventriculi infection: a rare but fearsome event. A Systematic Review of the Literature.* Int J Infect Dis, 2022. **115**: p. 48-61. DOI: 10.1016/j.ijid.2021.11.027.
407. Kastl, A.J., Jr., N.A. Terry, G.D. Wu, and L.G. Albenberg. *The Structure and Function of the Human Small Intestinal Microbiota: Current Understanding and Future Directions.* Cell Mol Gastroenterol Hepatol, 2020. **9**(1): p. 33-45. DOI: 10.1016/j.jcmgh.2019.07.006.
408. Bae, G.S., E.S. Jeon, H.C. Son, P. Kang, K.S. Lim, E.H. Hwang, G. Kim, S.H. Baek, Y.J. An, G.Y. Shim, Y.M. Woo, Y. Kim, T. Oh, S.H. Kim, J. Hong, and B.S. Koo. *Clostridium ventriculi in a cynomolgus monkey with acute gastric dilatation and rupture: A case report.* J Med Primatol, 2024. **53**(1). DOI: 10.1111/jmp.12668.
409. Owens, L.A., B. Colitti, I. Hirji, A. Pizarro, J.E. Jaffe, S. Moittie, K.A. Bishop-Lilly, L.A. Estrella, L.J. Voegtly, J.H. Kuhn, G. Suen, C.L. Deblois, C.D. Dunn, C. Juan-Salles, and T.L. Goldberg. *A Sarcina bacterium linked to lethal disease in sanctuary chimpanzees in Sierra Leone.* Nat Commun, 2021. **12**(1): p. 763. DOI: 10.1038/s41467-021-21012-x.
410. Chibani, C.M., A. Mahnert, G. Borrel, A. Almeida, A. Werner, J.F. Brugère, S. Gribaldo, R.D. Finn, R.A. Schmitz, and C. Moissl-Eichinger. *A catalogue of 1,167 genomes from the human gut archaeome.* Nature Microbiology, 2022. **7**(1): p. 48–61. DOI: 10.1038/s41564-021-01020-9.
411. Horz, H.P. and G. Conrads. *The discussion goes on: What is the role of Euryarchaeota in humans?* Archaea, 2010. **2010**. DOI: 10.1155/2010/967271.
412. Thomas, C.M., E. Desmond-Le Quemener, S. Gribaldo, and G. Borrel. *Factors shaping the abundance and diversity of the gut archaeome across the animal kingdom.* Nat Commun, 2022. **13**(1). DOI: 10.1038/s41467-022-31038-4.
413. Kumpitsch, C., F.P.S. Fischmeister, A. Mahnert, S. Lackner, M. Wilding, C. Sturm, A. Springer, T. Madl, S. Holasek, C. Hogenauer, I.A. Berg, V. Schoepf, and C. Moissl-Eichinger. *Reduced B12 uptake and increased gastrointestinal formate are associated with archaeome-mediated breath methane emission in humans.* Microbiome, 2021. **9**(1): p. 193. DOI: 10.1186/s40168-021-01130-w.
414. Fernandes, J., A. Wang, W. Su, S.R. Rozenbloom, A. Taibi, E.M. Comelli, and T.M. Wolever. *Age, dietary fiber, breath methane, and fecal short chain fatty acids are interrelated in Archaea-positive humans.* J Nutr, 2013. **143**(8): p. 1269-75. DOI: 10.3945/jn.112.170894.

415. Polag, D., O. Leiss, and F. Keppler. *Age dependent breath methane in the German population.* Sci Total Environ, 2014. **481**: p. 582-7. DOI: 10.1016/j.scitotenv.2014.02.086.
416. Cisek, A.A., I. Bak, I. Stefanska, and M. Binek. *Selection and Optimization of High-Yielding DNA Isolation Protocol for Quantitative Analyses of Methanogenic Archaea.* Microorganisms, 2022. **10**(3). DOI: 10.3390/microorganisms10030523.
417. Anders, J.L., M.A.M. Moustafa, W.M.A. Mohamed, T. Hayakawa, R. Nakao, and I. Koizumi. *Comparing the gut microbiome along the gastrointestinal tract of three sympatric species of wild rodents.* Sci Rep, 2021. **11**(1). DOI: 10.1038/s41598-021-99379-6.
418. Bradley, P.H. and K.S. Pollard. *Proteobacteria explain significant functional variability in the human gut microbiome.* Microbiome, 2017. **5**(1): p. 36. DOI: 10.1186/s40168-017-0244-z.
419. Russell, A., J.N. Copio, Y. Shi, S. Kang, C.L. Franklin, and A.C. Ericsson. *Reduced housing density improves statistical power of murine gut microbiota studies.* Cell Rep, 2022. **39**(6): p. 110783. DOI: 10.1016/j.celrep.2022.110783.
420. El Kaoutari, A., F. Armougom, J.I. Gordon, D. Raoult, and B. Henrissat. *The abundance and variety of carbohydrate-active enzymes in the human gut microbiota.* Nat Rev Microbiol, 2013. **11**(7): p. 497-504. DOI: 10.1038/nrmicro3050.
421. Tanes, C., K. Bittinger, Y. Gao, E.S. Friedman, L. Nessel, U.R. Paladhi, L. Chau, E. Panfen, M.A. Fischbach, J. Braun, R.J. Xavier, C.B. Clish, H. Li, F.D. Bushman, J.D. Lewis, and G.D. Wu. *Role of dietary fiber in the recovery of the human gut microbiome and its metabolome.* Cell Host Microbe, 2021. **29**(3): p. 394-407 e5. DOI: 10.1016/j.chom.2020.12.012.
422. Vacca, M., G. Celano, F.M. Calabrese, P. Portincasa, M. Gobbetti, and M. De Angelis. *The Controversial Role of Human Gut Lachnospiraceae.* Microorganisms, 2020. **8**(4). DOI: 10.3390/microorganisms8040573.
423. Tsai, C.-C., M.-H. Chiu, H.-P. Kek, M.-C. Yang, Y.-T. Su, H.-K. Liu, M.-S. Wu, and Y.-T. Yeh. *The Reduced Gut Lachnospira Species Is Linked to Liver Enzyme Elevation and Insulin Resistance in Pediatric Fatty Liver Disease.* International Journal of Molecular Sciences, 2024. **25**(7). DOI: 10.3390/ijms25073640.
424. Notting, F., W. Pirovano, W. Sybesma, and R. Kort. *The butyrate-producing and spore-forming bacterial genus Coprococcus as a potential biomarker for neurological disorders.* Gut Microbiome, 2023. **4**: p. e16. DOI: 10.1017/gmb.2023.14.
425. Nie, K., K. Ma, W. Luo, Z. Shen, Z. Yang, M. Xiao, T. Tong, Y. Yang, and X. Wang. *Roseburia intestinalis: A Beneficial Gut Organism From the Discoveries in Genus and Species.* Front Cell Infect Microbiol, 2021. **11**. DOI: 10.3389/fcimb.2021.757718.
426. Stilling, R.M., M. van de Wouw, G. Clarke, C. Stanton, T.G. Dinan, and J.F. Cryan. *The neuropharmacology of butyrate: The bread and butter of the microbiota-gut-brain axis?* Neurochem Int, 2016. **99**: p. 110-132. DOI: 10.1016/j.neuint.2016.06.011.
427. Chen, L.X., K. Anantharaman, A. Shaiber, A.M. Eren, and J.F. Banfield. *Accurate and complete genomes from metagenomes.* Genome Res, 2020. **30**(3): p. 315-333. DOI: 10.1101/gr.258640.119.
428. Parks, D.H., M. Chuvochina, C. Rinke, A.J. Mussig, P.A. Chaumeil, and P. Hugenholtz. *GTDB: an ongoing census of bacterial and archaeal diversity through a phylogenetically consistent, rank normalized and complete genome-based taxonomy.* Nucleic Acids Research, 2022. **50**(D1): p. D785-D794. DOI: 10.1093/nar/gkab776.
429. Pereira-Marques, J., A. Hout, R.M. Ferreira, M. Weber, I. Pinto-Ribeiro, L.J. van Doorn, C.W. Knetsch, and C. Figueiredo. *Impact of Host DNA and Sequencing Depth on the Taxonomic Resolution of Whole Metagenome Sequencing for Microbiome Analysis.* Front Microbiol, 2019. **10**. DOI: 10.3389/fmicb.2019.01277.
430. Gweon, H.S., L.P. Shaw, J. Swann, N. De Maio, M. AbuOun, R. Niehus, A.T.M. Hubbard, M.J. Bowes, M.J. Bailey, T.E.A. Peto, S.J. Hoosdally, A.S. Walker, R.P. Sebra, D.W. Crook, M.F. Anjum, D.S. Read, N. Stoesser, M. Anjum, L. Barker, H. Brett, K. Chau, D.

Gilson, J. Kavanagh, H. Jones, A.E. Sheppard, R. Smith, E. Stubberfield, N. Woodford, and R. Consortium. *The impact of sequencing depth on the inferred taxonomic composition and AMR gene content of metagenomic samples.* Environmental Microbiome, 2019. **14**(1). DOI: 10.1186/s40793-019-0347-1.

431. Schnoes, A.M., S.D. Brown, I. Dodevski, and P.C. Babbitt. *Annotation error in public databases: misannotation of molecular function in enzyme superfamilies.* PLoS Comput Biol, 2009. **5**(12): p. e1000605. DOI: 10.1371/journal.pcbi.1000605.
432. Wang, W.L., S.Y. Xu, Z.G. Ren, L. Tao, J.W. Jiang, and S.S. Zheng. *Application of metagenomics in the human gut microbiome.* World J Gastroenterol, 2015. **21**(3): p. 803-14. DOI: 10.3748/wjg.v21.i3.803.
433. Ahmed, H., Q. Leyrolle, V. Koistinen, O. Kärkkäinen, S. Layé, N. Delzenne, and K. Hanhineva. *Microbiota-derived metabolites as drivers of gut–brain communication.* Gut Microbes, 2022. **14**(1). DOI: 10.1080/19490976.2022.2102878.
434. Zhang, X., D. Shen, Z. Fang, Z. Jie, X. Qiu, C. Zhang, Y. Chen, and L. Ji. *Human gut microbiota changes reveal the progression of glucose intolerance.* PLoS One, 2013. **8**(8). DOI: 10.1371/journal.pone.0071108.
435. Qin, J., Y. Li, Z. Cai, S. Li, J. Zhu, F. Zhang, S. Liang, W. Zhang, Y. Guan, D. Shen, Y. Peng, D. Zhang, Z. Jie, W. Wu, Y. Qin, W. Xue, J. Li, L. Han, D. Lu, P. Wu, Y. Dai, X. Sun, Z. Li, A. Tang, S. Zhong, X. Li, W. Chen, R. Xu, M. Wang, Q. Feng, M. Gong, J. Yu, Y. Zhang, M. Zhang, T. Hansen, G. Sanchez, J. Raes, G. Falony, S. Okuda, M. Almeida, E. LeChatelier, P. Renault, N. Pons, J.M. Batto, Z. Zhang, H. Chen, R. Yang, W. Zheng, S. Li, H. Yang, J. Wang, S.D. Ehrlich, R. Nielsen, O. Pedersen, K. Kristiansen, and J. Wang. *A metagenome-wide association study of gut microbiota in type 2 diabetes.* Nature, 2012. **490**(7418): p. 55-60. DOI: 10.1038/nature11450.
436. Karlsson, F.H., V. Tremaroli, I. Nookaew, G. Bergstrom, C.J. Behre, B. Fagerberg, J. Nielsen, and F. Backhed. *Gut metagenome in European women with normal, impaired and diabetic glucose control.* Nature, 2013. **498**(7452): p. 99-103. DOI: 10.1038/nature12198.
437. Sato, J., A. Kanazawa, F. Ikeda, T. Yoshihara, H. Goto, H. Abe, K. Komiya, M. Kawaguchi, T. Shimizu, T. Ogihara, Y. Tamura, Y. Sakurai, R. Yamamoto, T. Mita, Y. Fujitani, H. Fukuda, K. Nomoto, T. Takahashi, T. Asahara, T. Hirose, S. Nagata, Y. Yamashiro, and H. Watada. *Gut Dysbiosis and Detection of "Live Gut Bacteria" in Blood of Japanese Patients With Type 2 Diabetes.* Diabetes Care, 2014. **37**(8): p. 2343-2350. DOI: 10.2337/dc13-2817.
438. Zhang, F., D. Aschenbrenner, J.Y. Yoo, and T. Zuo. *The gut mycobiome in health, disease, and clinical applications in association with the gut bacterial microbiome assembly.* Lancet Microbe, 2022. **3**(12): p. e969-e983. DOI: 10.1016/S2666-5247(22)00203-8.
439. Qin, J., R. Li, J. Raes, M. Arumugam, K.S. Burgdorf, C. Manichanh, T. Nielsen, N. Pons, F. Levenez, T. Yamada, D.R. Mende, J. Li, J. Xu, S. Li, D. Li, J. Cao, B. Wang, H. Liang, H. Zheng, Y. Xie, J. Tap, P. Lepage, M. Bertalan, J.M. Batto, T. Hansen, D. Le Paslier, A. Linneberg, H.B. Nielsen, E. Pelletier, P. Renault, T. Sicheritz-Ponten, K. Turner, H. Zhu, C. Yu, S. Li, M. Jian, Y. Zhou, Y. Li, X. Zhang, S. Li, N. Qin, H. Yang, J. Wang, S. Brunak, J. Dore, F. Guarner, K. Kristiansen, O. Pedersen, J. Parkhill, J. Weissenbach, H.I.T.C. Meta, P. Bork, S.D. Ehrlich, and J. Wang. *A human gut microbial gene catalogue established by metagenomic sequencing.* Nature, 2010. **464**(7285): p. 59-65. DOI: 10.1038/nature08821.
440. Gong, Y., C. Li, C. Wang, J. Li, M. Ding, D. Chen, and M. Lao. *Epidemiology and Mortality-Associated Factors of Invasive Fungal Disease in Elderly Patients: A 20-Year Retrospective Study from Southern China.* Infect Drug Resist, 2020. **13**: p. 711-723. DOI: 10.2147/IDR.S242187.
441. Sokol, H., V. Leducq, H. Aschard, H.P. Pham, S. Jegou, C. Landman, D. Cohen, G. Liguori, A. Bourrier, I. Nion-Larmurier, J. Cosnes, P. Seksik, P. Langella, D. Skurnik, M.L.

Richard, and L. Beaugerie. *Fungal microbiota dysbiosis in IBD.* Gut, 2017. **66**(6): p. 1039-1048. DOI: 10.1136/gutjnl-2015-310746.
442. Hoarau, G., P.K. Mukherjee, C. Gower-Rousseau, C. Hager, J. Chandra, M.A. Retuerto, C. Neut, S. Vermeire, J. Clemente, J.F. Colombel, H. Fujioka, D. Poulain, B. Sendid, and M.A. Ghannoum. *Bacteriome and Mycobiome Interactions Underscore Microbial Dysbiosis in Familial Crohn's Disease.* mBio, 2016. **7**(5). DOI: 10.1128/mBio.01250-16.
443. Tsui, C., E.F. Kong, and M.A. Jabra-Rizk. *Pathogenesis of Candida albicans biofilm.* Pathog Dis, 2016. **74**(4). DOI: 10.1093/femspd/ftw018.
444. Govrins, M. and C. Lass-Florl. *Candida parapsilosis complex in the clinical setting.* Nat Rev Microbiol, 2024. **22**(1): p. 46-59. DOI: 10.1038/s41579-023-00961-8.
445. Roberts, K., A. Osme, C. De Salvo, E. Zoli, J. Herrada, T.S. McCormick, M. Ghannoum, F. Cominelli, and L. Di Martino. *Candida tropicalis Affects Candida albicans Virulence by Limiting Its Capacity to Adhere to the Host Intestinal Surface, Leading to Decreased Susceptibility to Colitis in Mice.* J Fungi (Basel), 2024. **10**(4). DOI: 10.3390/jof10040245.
446. Denning, D.W. *Global incidence and mortality of severe fungal disease.* Lancet Infect Dis, 2024. **24**(7): p. e428-e438. DOI: 10.1016/S1473-3099(23)00692-8.
447. Pfaller, M.A., D.J. Diekema, J.D. Turnidge, M. Castanheira, and R.N. Jones. *Twenty Years of the SENTRY Antifungal Surveillance Program: Results for Candida Species From 1997-2016.* Open Forum Infect Dis, 2019. **6**(1): p. S79-S94. DOI: 10.1093/ofid/ofy358.
448. Fernandez, M., E.H. Moylett, D.E. Noyola, and C.J. Baker. *Candidal meningitis in neonates: a 10-year review.* Clin Infect Dis, 2000. **31**(2): p. 458-63. DOI: 10.1086/313973.
449. Lee, B.E., P.Y. Cheung, J.L. Robinson, C. Evanochko, and C.M. Robertson. *Comparative study of mortality and morbidity in premature infants (birth weight, < 1,250 g) with candidemia or candidal meningitis.* Clin Infect Dis, 1998. **27**(3): p. 559-65. DOI: 10.1086/514712.
450. Cohen-Wolkowiez, M., P.B. Smith, B. Mangum, W.J. Steinbach, B.D. Alexander, C.M. Cotten, R.H. Clark, T.J. Walsh, and D.K. Benjamin, Jr. *Neonatal Candida meningitis: significance of cerebrospinal fluid parameters and blood cultures.* J Perinatol, 2007. **27**(2): p. 97-100. DOI: 10.1038/sj.jp.7211628.
451. Seaks, C.E. and D.M. Wilcock. *Infectious hypothesis of Alzheimer disease.* PLoS Pathog, 2020. **16**(11). DOI: 10.1371/journal.ppat.1008596.
452. Arfken, A.M., J.F. Frey, T.G. Ramsay, and K.L. Summers. *Yeasts of Burden: Exploring the Mycobiome-Bacteriome of the Piglet GI Tract.* Front Microbiol, 2019. **10**. DOI: 10.3389/fmicb.2019.02286.
453. Summers, K.L., J.F. Frey, T.G. Ramsay, and A.M. Arfken. *The piglet mycobiome during the weaning transition: a pilot study1.* Journal of Animal Science, 2019. **97**(7): p. 2889-2900. DOI: 10.1093/jas/skz182.
454. Summers, K.L., J. Foster Frey, and A.M. Arfken. *Characterization of Kazachstania slooffiae, a Proposed Commensal in the Porcine Gut.* J Fungi (Basel), 2021. **7**(2). DOI: 10.3390/jof7020146.
455. James, S.A., S. Phillips, A. Telatin, D. Baker, R. Ansorge, P. Clarke, L.J. Hall, and S.R. Carding. *Preterm Infants Harbour a Rapidly Changing Mycobiota That Includes Pathobionts.* Journal of Fungi, 2020. **6**(4). DOI: 10.3390/jof6040273.
456. Kiss, L. *Limits of nuclear ribosomal DNA internal transcribed spacer (ITS) sequences as species barcodes for Fungi.* Proceedings of the National Academy of Sciences of the United States of America, 2012. **109**(27). DOI: 10.1073/pnas.1207143109.
457. Jiang, S.M., Y.F. Chen, S.Y. Han, L.X. Lv, and L.J. Li. *Next-Generation Sequencing Applications for the Study of Fungal Pathogens.* Microorganisms, 2022. **10**(10). DOI: 10.3390/microorganisms10101882.
458. Phaff, H.J., A. Vaughan-Martini, and W.T. Starmer. *Debaryomyces prosopidis sp. nov., a yeast from exudates of mesquite trees.* International Journal of Systematic Bacteriology, 1998. **48**: p. 1419-1424. DOI: 10.1099/00207713-48-4-1419.

459. Suzuki, M., G.S. Prasad, and C.P. Kurtzman, *Debaryomyces Lodder & Kreger-van Rij*. 5th ed. The yeasts: a taxonomic study, ed. C. Kurtzman, J.W. Fell, and T. Boekhout. Vol. 2. 2011: Elsevier.
460. Kurtzman, C.P., C.J. Robnett, J.M. Ward, C. Brayton, P. Gorelick, and T.J. Walsh. *Multigene phylogenetic analysis of pathogenic Candida species in the Kazachstania (Arxiozyma) telluris complex and description of their ascosporic states as Kazachstania bovina sp nov., K-heterogenica sp nov., K-pintolopesii sp nov., and K-slooffiae sp nov.* Journal of Clinical Microbiology, 2005. **43**(1): p. 101-111. DOI: 10.1128/Jcm.43.1.101-111.2005.
461. Flahou, B., T. De Baere, K. Chiers, F. Pasmans, F. Haesebrouck, and R. Ducatelle. *Gastric Infection with Kazachstania heterogenica influences the outcome of a Helicobacter suis infection in Mongolian gerbils.* Helicobacter, 2010. **15**(1): p. 67-75. DOI: 10.1111/j.1523-5378.2009.00736.x.
462. Alvarez-Perez, S., A. Mateos, L. Dominguez, E. Martinez-Nevado, A. Rodriguez-Bertos, J.L. Blanco, and M.E. Garcia. *First isolation of the anamorph of Kazachstania heterogenica from a fatal infection in a primate host.* Med Mycol, 2012. **50**(2): p. 193-6. DOI: 10.3109/13693786.2011.578155.
463. Hoffmann, P., M. Burmester, M. Langeheine, R. Brehm, M.T. Empl, B. Seeger, and G. Breves. *Caco-2/HT29-MTX co-cultured cells as a model for studying physiological properties and toxin-induced effects on intestinal cells.* Plos One, 2021. **16**(10). DOI: 10.1371/journal.pone.0257824.
464. Zhao, H., R. Yan, X. Zhou, F. Ji, and B. Zhang. *Hydrogen sulfide improves colonic barrier integrity in DSS-induced inflammation in Caco-2 cells and mice.* Int Immunopharmacol, 2016. **39**: p. 121-127. DOI: 10.1016/j.intimp.2016.07.020.
465. Wu, Y., S. Du, J.L. Johnson, H.Y. Tung, C.T. Landers, Y. Liu, B.G. Seman, R.T. Wheeler, M. Costa-Mattioli, F. Kheradmand, H. Zheng, and D.B. Corry. *Microglia and amyloid precursor protein coordinate control of transient Candida cerebritis with memory deficits.* Nat Commun, 2019. **10**(1): p. 58. DOI: 10.1038/s41467-018-07991-4.
466. Pande, K., C.B. Chen, and S.M. Noble. *Passage through the mammalian gut triggers a phenotypic switch that promotes commensalism.* Nature Genetics, 2013. **45**(9): p. 1088-1091. DOI: 10.1038/ng.2710.
467. Nagendra, H. *Opposite trends in response for the Shannon and Simpson indices of landscape diversity.* Applied Geography, 2002. **22**(2): p. 175-186. DOI: 10.1016/S0143-6228(02)00002-4.
468. Hallen-Adams, H.E. and M.J. Suhr. *Fungi in the healthy human gastrointestinal tract.* Virulence, 2017. **8**(3): p. 352-358. DOI: 10.1080/21505594.2016.1247140.
469. Schei, K., E. Avershina, T. Oien, K. Rudi, T. Follestad, S. Salamati, and R.A. Odegård. *Early gut mycobiota and mother-offspring transfer.* Microbiome, 2017. **5**(107). DOI: 10.1186/s40168-017-0319-x.
470. Jain, U., A.M. Ver Heul, S.S. Xiong, M.H. Gregory, E.G. Demers, J.T. Kern, C.W. Lai, B.D. Muegge, D.A.G. Barisas, J.S. Leal-Ekman, P. Deepak, M.A. Ciorba, T.C. Liu, D.A. Hogan, P. Debbas, J. Braun, D.P.B. McGovern, D.M. Underhill, and T.S. Stappenbeck. *Debaryomyces is enriched in Crohn's disease intestinal tissue and impairs healing in mice.* Science, 2021. **371**(6534): p. 1154-1159. DOI: 10.1126/science.abd0919.
471. Coker, O.O., G. Nakatsu, R.Z. Dai, W.K.K. Wu, S.H. Wong, S.C. Ng, F.K.L. Chan, J.J.Y. Sung, and J. Yu. *Enteric fungal microbiota dysbiosis and ecological alterations in colorectal cancer.* Gut, 2019. **68**(4): p. 654-662. DOI: 10.1136/gutjnl-2018-317178.
472. Mar, J.S., B.J. LaMere, D.L. Lin, S. Levan, M. Nazareth, U. Mahadevan, and S.V. Lynch. *Disease Severity and Immune Activity Relate to Distinct Interkingdom Gut Microbiome States in Ethnically Distinct Ulcerative Colitis Patients.* Mbio, 2016. **7**(4). DOI: 10.1128/mBio.01072-16.
473. Nakase, T. and M. Suzuki. *Taxonomic Studies on Debaryomyces-Hansenii (Zopf) Lodder Et Kreger-Vanrij and Related Species. 1. Chemotaxonomic Investigations.*

Journal of General and Applied Microbiology, 1985. **31**(1): p. 49-69. DOI: 10.2323/jgam.31.49.
474. Fortman, J.D., T.A. Hewett, and L.C. Halliday, *Important biologic features.* The laboratory nonhuman primate, ed. J.D. Fortman, T.A. Hewett, and L.C. Halliday. 2017: CRC Press.
475. Banjara, N., K.W. Nickerson, M.J. Suhr, and H.E. Hallen-Adams. *Killer toxin from several food-derived Debaryomyces hansenii strains effective against pathogenic Candida yeasts.* International Journal of Food Microbiology, 2016. **222**: p. 23-29. DOI: 10.1016/j.ijfoodmicro.2016.01.016.
476. Buzzini, P. and A. Martini. *Large-scale screening of selected Candida maltosa, Debaryomyces hansenii and Pichia anomala killer toxin activity against pathogenic yeasts.* Med Mycol, 2001. **39**(6): p. 479-82. DOI: 10.1080/mmy.39.6.479.482.
477. Vaughan-Martini, A., M.-A. Lachance, and C.P. Kurtzman, *Kazachstania Zubkova*. 5th ed. The Yeasts: A Taxonomic Study, ed. C. Kurtzman, J.W. Fell, and T. Boekhout. Vol. 2. 2011: Elsevier.
478. Bendová, B., J. Piálek, L. Dureje, L. Schmiedová, D. Cízková, J.F. Martin, and J. Kreisinger. *How being synanthropic affects the gut bacteriome and mycobiome: comparison of two mouse species with contrasting ecologies.* Bmc Microbiology, 2020. **20**(1). DOI: 10.1186/s12866-020-01859-8.
479. Urubschurov, V., K. Büsing, G. Freyer, D.P.R. Herlemann, W.B. Souffrant, and A. Zeyner. *New insights into the role of the porcine intestinal yeast, Kazachstania slooffiae, in intestinal environment of weaned piglets.* Fems Microbiology Ecology, 2017. **93**(2). DOI: 10.1093/femsec/fiw245.
480. Urubschurov, V., P. Janczyk, W.B. Souffrant, G. Freyer, and A. Zeyner. *Establishment of intestinal microbiota with focus on yeasts of unweaned and weaned piglets kept under different farm conditions.* FEMS Microbiol Ecol, 2011. **77**(3): p. 493-502. DOI: 10.1111/j.1574-6941.2011.01129.x.
481. Jenkins, T.P., N. Acs, E.W. Arendrup, A. Swift, A. Duzs, I. Chatzigiannidou, M. Pichler, T. Kittila, L. Peachey, L. Gram, N. Canibe, A.H. Laustsen, S. Brix, and S.W. Thrane. *Protecting the piglet gut microbiota against ETEC-mediated post-weaning diarrhoea using specific binding proteins.* NPJ Biofilms Microbiomes, 2024. **10**(1): p. 42. DOI: 10.1038/s41522-024-00514-8.
482. Raja, H.A., A.N. Miller, C.J. Pearce, and N.H. Oberlies. *Fungal Identification Using Molecular Tools: A Primer for the Natural Products Research Community.* Journal of Natural Products, 2017. **80**(3): p. 756-770. DOI: 10.1021/acs.jnatprod.6b01085.
483. Eichele, D.D. and K.K. Kharbanda. *Dextran sodium sulfate colitis murine model: An indispensable tool for advancing our understanding of inflammatory bowel diseases pathogenesis.* World J Gastroenterol, 2017. **23**(33): p. 6016-6029. DOI: 10.3748/wjg.v23.i33.6016.
484. Allert, S., T.M. Förster, C.M. Svensson, J.P. Richardson, T. Pawlik, B. Hebecker, S. Rudolphi, M. Juraschitz, M. Schaller, M. Blagojevic, J. Morschhäuser, M.T. Figge, I.D. Jacobsen, J.R. Naglik, L. Kasper, S. Mogavero, and B. Hube. *Candida albicans-Induced Epithelial Damage Mediates Translocation through Intestinal Barriers.* Mbio, 2018. **9**(3). DOI: 10.1128/mBio.00915-18.
485. Weide, M.R. and J.F. Ernst. *Caco-2 monolayer as a model for transepithelial migration of the fungal pathogen Candida albicans.* Mycoses, 1999. **42**(S2): p. 61-67. DOI: 10.1111/j.1439-0507.1999.tb00015.x.
486. Bohringer, M., S. Pohlers, S. Schulze, D. Albrecht-Eckardt, J. Piegsa, M. Weber, R. Martin, K. Hunniger, J. Linde, R. Guthke, and O. Kurzai. *Candida albicans infection leads to barrier breakdown and a MAPK/NF-kappaB mediated stress response in the intestinal epithelial cell line C2BBe1.* Cell Microbiol, 2016. **18**(7): p. 889-904. DOI: 10.1111/cmi.12566.
487. Cottier, F. and R.A. Hall. *Face/Off: The Interchangeable Side of Candida Albicans.* Front Cell Infect Microbiol, 2019. **9**: p. 471. DOI: 10.3389/fcimb.2019.00471.

488. Basmaciyan, L., F. Bon, T. Paradis, P. Lapaquette, and F. Dalle. *Candida Albicans Interactions With The Host: Crossing The Intestinal Epithelial Barrier.* Tissue Barriers, 2019. **7**(2). DOI: 10.1080/21688370.2019.1612661.
489. Dalle, F., B. Wachtler, C. L'Ollivier, G. Holland, N. Bannert, D. Wilson, C. Labruere, A. Bonnin, and B. Hube. *Cellular interactions of Candida albicans with human oral epithelial cells and enterocytes.* Cell Microbiol, 2010. **12**(2): p. 248-71. DOI: 10.1111/j.1462-5822.2009.01394.x.
490. James, S.A., A. Parker, C. Purse, A. Telatin, D. Baker, R. Evans, S. Holmes, S.G.P. Funnell, and S.R. Carding. *Draft Genome Sequence of a Primate Isolate of Kazachstania pintolopesii.* Mycopathologia, 2023. **188**(5): p. 821-823. DOI: 10.1007/s11046-023-00772-8.
491. Hiengrach, P., A. Chindamporn, and A. Leelahavanichkul. *Kazachstania pintolopesii in Blood and Intestinal Wall of Macrophage-Depleted Mice with Cecal Ligation and Puncture, the Control of Fungi by Macrophages during Sepsis.* J Fungi, 2023. **9**(12). DOI: 10.3390/jof9121164.
492. Lionakis, M.S., J.K. Lim, C.C. Lee, and P.M. Murphy. *Organ-specific innate immune responses in a mouse model of invasive candidiasis.* J Innate Immun, 2011. **3**(2): p. 180-99. DOI: 10.1159/000321157.
493. Kavanaugh, N.L., A.Q. Zhang, C.J. Nobile, A.D. Johnson, and K. Ribbeck. *Mucins suppress virulence traits of Candida albicans.* mBio, 2014. **5**(6). DOI: 10.1128/mBio.01911-14.
494. Jakobsson, H.E., A.M. Rodriguez-Pineiro, A. Schutte, A. Ermund, P. Boysen, M. Bemark, F. Sommer, F. Backhed, G.C. Hansson, and M.E. Johansson. *The composition of the gut microbiota shapes the colon mucus barrier.* EMBO Rep, 2015. **16**(2): p. 164-77. DOI: 10.15252/embr.201439263.
495. Round, J.L. and S.K. Mazmanian. *The gut microbiota shapes intestinal immune responses during health and disease.* Nature Reviews Immunology, 2009. **9**(5): p. 313-323. DOI: 10.1038/nri2515.
496. Hayes, C.L., J. Dong, H.J. Galipeau, J. Jury, J. McCarville, X. Huang, X.Y. Wang, A. Naidoo, A.N. Anbazhagan, J. Libertucci, C. Sheridan, P.K. Dudeja, D.M.E. Bowdish, M.G. Surette, and E.F. Verdu. *Commensal microbiota induces colonic barrier structure and functions that contribute to homeostasis.* Sci Rep, 2018. **8**(1). DOI: 10.1038/s41598-018-32366-6.
497. Drummond, R.A., J.V. Desai, E.E. Ricotta, M. Swamydas, C. Deming, S. Conlan, M. Quinones, V. Matei-Rascu, L. Sherif, D. Lecky, C.R. Lee, N.M. Green, N. Collins, A.M. Zelazny, D.R. Prevots, D. Bending, D. Withers, Y. Belkaid, J.A. Segre, and M.S. Lionakis. *Long-term antibiotic exposure promotes mortality after systemic fungal infection by driving lymphocyte dysfunction and systemic escape of commensal bacteria.* Cell Host Microbe, 2022. **30**(7): p. 1020-1033. DOI: 10.1016/j.chom.2022.04.013.
498. Koh, A.Y. *Murine models of Candida gastrointestinal colonization and dissemination.* Eukaryot Cell, 2013. **12**(11): p. 1416-22. DOI: 10.1128/EC.00196-13.
499. Gupta, Y., A.L. Ernst, A. Vorobyev, F. Beltsiou, D. Zillikens, K. Bieber, S. Sanna-Cherchi, A.M. Christiano, C.D. Sadik, R.J. Ludwig, and T. Sezin. *Impact of diet and host genetics on the murine intestinal mycobiome.* Nat Commun, 2023. **14**(1): p. 834. DOI: 10.1038/s41467-023-36479-z.
500. Jayasudha, R., T. Das, S. Kalyana Chakravarthy, G. Sai Prashanthi, A. Bhargava, M. Tyagi, P.K. Rani, R.R. Pappuru, and S. Shivaji. *Gut mycobiomes are altered in people with type 2 Diabetes Mellitus and Diabetic Retinopathy.* PLoS One, 2020. **15**(12). DOI: 10.1371/journal.pone.0243077.
501. Van Syoc, E., M.P. Nixon, J.D. Silverman, Y. Luo, F.J. Gonzalez, I. Elbere, J. Klovins, A.D. Patterson, C.J. Rogers, and E. Ganda. *Changes in the type 2 diabetes gut mycobiome associate with metformin treatment across populations.* mBio, 2024. **15**(6). DOI: 10.1128/mbio.00169-24.

502. He, J.L., Y.W. Zhao, J.L. Yang, J.M. Ju, B.Q. Ye, J.Y. Huang, Z.H. Huang, W.Y. Zhao, W.F. Zeng, M. Xia, and Y. Liu. *Enhanced interactions among gut mycobiomes with the deterioration of glycemic control.* Med, 2024. **5**(8): p. 909-925. DOI: 10.1016/j.medj.2024.03.023.
503. Ward, R.J., F.A. Zucca, J.H. Duyn, R.R. Crichton, and L. Zecca. *The role of iron in brain ageing and neurodegenerative disorders.* Lancet Neurol, 2014. **13**(10): p. 1045-60. DOI: 10.1016/S1474-4422(14)70117-6.
504. Ficiarà, E., I. Stura, and C. Guiot. *Iron Deposition in Brain: Does Aging Matter?* Int J Mol Sci, 2022. **23**(17). DOI: 10.3390/ijms231710018.
505. Ndayisaba, A., C. Kaindlstorfer, and G.K. Wenning. *Iron in Neurodegeneration - Cause or Consequence?* Front Neurosci, 2019. **13**: p. 180. DOI: 10.3389/fnins.2019.00180.
506. Zecca, L., A. Stroppolo, A. Gatti, D. Tampellini, M. Toscani, M. Gallorini, G. Giaveri, P. Arosio, P. Santambrogio, R.G. Fariello, E. Karatekin, M.H. Kleinman, N. Turro, O. Hornykiewicz, and F.A. Zucca. *The role of iron and copper molecules in the neuronal vulnerability of locus coeruleus and substantia nigra during aging.* Proc Natl Acad Sci U S A, 2004. **101**(26): p. 9843-8. DOI: 10.1073/pnas.0403495101.
507. Zecca, L., M. Gallorini, V. Schunemann, A.X. Trautwein, M. Gerlach, P. Riederer, P. Vezzoni, and D. Tampellini. *Iron, neuromelanin and ferritin content in the substantia nigra of normal subjects at different ages: consequences for iron storage and neurodegenerative processes.* J Neurochem, 2001. **76**(6): p. 1766-73. DOI: 10.1046/j.1471-4159.2001.00186.x.
508. Zucca, F.A., C. Bellei, S. Giannelli, M.R. Terreni, M. Gallorini, E. Rizzio, G. Pezzoli, A. Albertini, and L. Zecca. *Neuromelanin and iron in human locus coeruleus and substantia nigra during aging: consequences for neuronal vulnerability.* J Neural Transm (Vienna), 2006. **113**(6): p. 757-67. DOI: 10.1007/s00702-006-0453-2.
509. Corey, T.M., O. Illanes, M. Lawrence, S.E. Perez, S. Liddie, and J.J. Callanan. *Naturally occurring histological findings and Alzheimer's-like pathology in the brain of aging African green monkeys (Chlorocebus sabaeus).* J Comp Neurol, 2023. **531**(13): p. 1276-1298. DOI: 10.1002/cne.25494.
510. Del, C.V.H.M., S. Ritchie, A. Glatz, M. Allerhand, S. Munoz Maniega, A.J. Gow, N.A. Royle, M.E. Bastin, J.M. Starr, I.J. Deary, and J.M. Wardlaw. *Brain iron deposits and lifespan cognitive ability.* Age (Dordr), 2015. **37**(5): p. 100. DOI: 10.1007/s11357-015-9837-2.
511. Janaway, B.M., J.E. Simpson, N. Hoggard, J.R. Highley, G. Forster, D. Drew, O.H. Gebril, F.E. Matthews, C. Brayne, S.B. Wharton, P.G. Ince, M.R.C.C. Function, and S. Ageing Neuropathology. *Brain haemosiderin in older people: pathological evidence for an ischaemic origin of magnetic resonance imaging (MRI) microbleeds.* Neuropathol Appl Neurobiol, 2014. **40**(3): p. 258-69. DOI: 10.1111/nan.12062.
512. Uno, H. *Age-related pathology and biosenescent markers in captive rhesus macaques.* Age (Omaha), 1997. **20**(1): p. 1-13. DOI: 10.1007/s11357-997-0001-5.
513. Zucca, F.A., A. Capucciati, C. Bellei, M. Sarna, T. Sarna, E. Monzani, L. Casella, and L. Zecca. *Neuromelanins in brain aging and Parkinson's disease: synthesis, structure, neuroinflammatory, and neurodegenerative role.* IUBMB Life, 2023. **75**(1): p. 55-65. DOI: 10.1002/iub.2654.
514. Haining, R.L. and C. Achat-Mendes. *Neuromelanin, one of the most overlooked molecules in modern medicine, is not a spectator.* Neural Regen Res, 2017. **12**(3): p. 372-375. DOI: 10.4103/1673-5374.202928.
515. Marsden, C.D. *Pigmentation in the nucleus substantiae nigrae of mammals.* J Anat, 1961. **95**(Pt 2): p. 256-61. https://www.ncbi.nlm.nih.gov/pubmed/13767161.
516. Jahns, H., J.J. Callanan, M.C. McElroy, D.J. Sammin, and H.F. Bassett. *Age-related and non-age-related changes in 100 surveyed horse brains.* Vet Pathol, 2006. **43**(5): p. 740-50. DOI: 10.1354/vp.43-5-740.

517. Taylor, E.N., N. Huang, J. Wisco, Y. Wang, K.G. Morgan, and J.A. Hamilton. *The brains of aged mice are characterized by altered tissue diffusion properties and cerebral microbleeds.* J Transl Med, 2020. **18**(1): p. 277. DOI: 10.1186/s12967-020-02441-6.
518. Moller, H.E., L. Bossoni, J.R. Connor, R.R. Crichton, M.D. Does, R.J. Ward, L. Zecca, F.A. Zucca, and I. Ronen. *Iron, Myelin, and the Brain: Neuroimaging Meets Neurobiology.* Trends Neurosci, 2019. **42**(6): p. 384-401. DOI: 10.1016/j.tins.2019.03.009.
519. Martinez-Ramirez, S., S.M. Greenberg, and A. Viswanathan. *Cerebral microbleeds: overview and implications in cognitive impairment.* Alzheimers Research & Therapy, 2014. **6**(3). DOI: 10.1186/alzrt263.
520. Greenberg, S.M., M.W. Vernooij, C. Cordonnier, A. Viswanathan, R. Al-Shahi Salman, S. Warach, L.J. Launer, M.A. Van Buchem, M.M. Breteler, and G. Microbleed Study. *Cerebral microbleeds: a guide to detection and interpretation.* Lancet Neurol, 2009. **8**(2): p. 165-74. DOI: 10.1016/S1474-4422(09)70013-4.
521. Shoamanesh, A., C.S. Kwok, and O. Benavente. *Cerebral microbleeds: histopathological correlation of neuroimaging.* Cerebrovasc Dis, 2011. **32**(6): p. 528-34. DOI: 10.1159/000331466.
522. Knox, E.G., M.R. Aburto, G. Clarke, J.F. Cryan, and C.M. O'Driscoll. *The blood-brain barrier in aging and neurodegeneration.* Mol Psychiatry, 2022. **27**(6): p. 2659-2673. DOI: 10.1038/s41380-022-01511-z.
523. Erickson, M.A. and W.A. Banks. *Age-Associated Changes in the Immune System and Blood(-)Brain Barrier Functions.* Int J Mol Sci, 2019. **20**(7). DOI: 10.3390/ijms20071632.
524. Wilson, D., G. Ambler, K.J. Lee, J.S. Lim, M. Shiozawa, M. Koga, L. Li, C. Lovelock, H. Chabriat, M. Hennerici, Y.K. Wong, H.K.F. Mak, L. Prats-Sanchez, A. Martinez-Domeno, S. Inamura, K. Yoshifuji, E.M. Arsava, S. Horstmann, J. Purrucker, B.Y.K. Lam, A. Wong, Y.D. Kim, T.J. Song, M. Schrooten, R. Lemmens, S. Eppinger, T. Gattringer, E. Uysal, Z. Tanriverdi, N.M. Bornstein, E.B. Assayag, H. Hallevi, J. Tanaka, H. Hara, S.B. Coutts, L. Hert, A. Polymeris, D.J. Seiffge, P. Lyrer, A. Algra, J. Kappelle, R. Al-Shahi Salman, H.R. Jager, G.Y.H. Lip, H.P. Mattle, L.D. Panos, J.L. Mas, L. Legrand, C. Karayiannis, T. Phan, S. Gunkel, N. Christ, J. Abrigo, T. Leung, W. Chu, F. Chappell, S. Makin, D. Hayden, D.J. Williams, M.E. Kooi, D.H.K. van Dam-Nolen, C. Barbato, S. Browning, K. Wiegertjes, A.M. Tuladhar, N. Maaijwee, C. Guevarra, C. Yatawara, A.M. Mendyk, C. Delmaire, S. Kohler, R. van Oostenbrugge, Y. Zhou, C. Xu, S. Hilal, B. Gyanwali, C. Chen, M. Lou, J. Staals, R. Bordet, N. Kandiah, F.E. de Leeuw, R. Simister, A. van der Lugt, P.J. Kelly, J.M. Wardlaw, Y. Soo, F. Fluri, V. Srikanth, D. Calvet, S. Jung, V.I.H. Kwa, S.T. Engelter, N. Peters, E.E. Smith, Y. Yakushiji, D.N. Orken, F. Fazekas, V. Thijs, J.H. Heo, V. Mok, R. Veltkamp, H. Ay, T. Imaizumi, B. Gomez-Anson, K.K. Lau, E. Jouvent, P.M. Rothwell, K. Toyoda, H.J. Bae, J. Marti-Fabregas, D.J. Werring and N. Microbleeds International Collaborative. *Cerebral microbleeds and stroke risk after ischaemic stroke or transient ischaemic attack: a pooled analysis of individual patient data from cohort studies.* Lancet Neurol, 2019. **18**(7): p. 653-665. DOI: 10.1016/S1474-4422(19)30197-8.
525. Kenkhuis, B., A. Somarakis, L. de Haan, O. Dzyubachyk, I.J. ME, N. de Miranda, B.P.F. Lelieveldt, J. Dijkstra, W.M.C. van Roon-Mom, T. Hollt, and L. van der Weerd. *Iron loading is a prominent feature of activated microglia in Alzheimer's disease patients.* Acta Neuropathol Commun, 2021. **9**(1): p. 27. DOI: 10.1186/s40478-021-01126-5.
526. Shaerzadeh, F., L. Phan, D. Miller, M. Dacquel, W. Hachmeister, C. Hansen, A. Bechtle, D. Tu, M. Martcheva, T.C. Foster, A. Kumar, W.J. Streit, and H. Khoshbouei. *Microglia senescence occurs in both substantia nigra and ventral tegmental area.* Glia, 2020. **68**(11): p. 2228-2245. DOI: 10.1002/glia.23834.
527. Robillard, K.N., K.M. Lee, K.B. Chiu, and A.G. MacLean. *Glial cell morphological and density changes through the lifespan of rhesus macaques.* Brain Behav Immun, 2016. **55**: p. 60-69. DOI: 10.1016/j.bbi.2016.01.006.

528. Shahidehpour, R.K., R.E. Higdon, N.G. Crawford, J.H. Neltner, E.T. Ighodaro, E. Patel, D. Price, P.T. Nelson, and A.D. Bachstetter. *Dystrophic microglia are associated with neurodegenerative disease and not healthy aging in the human brain.* Neurobiology of Aging, 2021. **99**: p. 19-27. DOI: 10.1016/j.neurobiolaging.2020.12.003.
529. Kanaan, N.M., J.H. Kordower, and T.J. Collier. *Age-related changes in glial cells of dopamine midbrain subregions in rhesus monkeys.* Neurobiol Aging, 2010. **31**(6): p. 937-52. DOI: 10.1016/j.neurobiolaging.2008.07.006.
530. Edler, M.K., C.C. Sherwood, R.S. Meindl, E.L. Munger, W.D. Hopkins, J.J. Ely, J.M. Erwin, D.P. Perl, E.J. Mufson, P.R. Hof, and M.A. Raghanti. *Microglia changes associated to Alzheimer's disease pathology in aged chimpanzees.* J Comp Neurol, 2018. **526**(18): p. 2921-2936. DOI: 10.1002/cne.24484.
531. Rodriguez-Callejas, J.D., E. Fuchs, and C. Perez-Cruz. *Evidence of Tau Hyperphosphorylation and Dystrophic Microglia in the Common Marmoset.* Front Aging Neurosci, 2016. **8**: p. 315. DOI: 10.3389/fnagi.2016.00315.
532. Kodama, R., X. Yang, Y. Saski, S. Iwashige, Y. Tanigawa, T. Yoshikawa, T. Nagaoka, Y. Kamimura, and H. Maeda. *Age-related lesions in the cerebrum in middle-aged female cynomolgus monkeys.* Toxicol Pathol, 2010. **38**(2): p. 303-11. DOI: 10.1177/0192623309358904.
533. Scheiblich, H., M. Trombly, A. Ramirez, and M.T. Heneka. *Neuroimmune Connections in Aging and Neurodegenerative Diseases.* Trends Immunol, 2020. **41**(4): p. 300-312. DOI: 10.1016/j.it.2020.02.002.
534. Kondo, H., P. Lavenex, and D.G. Amaral. *Intrinsic connections of the macaque monkey hippocampal formation: II. CA3 connections.* J Comp Neurol, 2009. **515**(3): p. 349-77. DOI: 10.1002/cne.22056.
535. Bachstetter, A.D., L.J. Van Eldik, F.A. Schmitt, J.H. Neltner, E.T. Ighodaro, S.J. Webster, E. Patel, E.L. Abner, R.J. Kryscio, and P.T. Nelson. *Disease-related microglia heterogeneity in the hippocampus of Alzheimer's disease, dementia with Lewy bodies, and hippocampal sclerosis of aging.* Acta Neuropathol Commun, 2015. **3**: p. 32. DOI: 10.1186/s40478-015-0209-z.
536. Hopperton, K.E., D. Mohammad, M.O. Trepanier, V. Giuliano, and R.P. Bazinet. *Markers of microglia in post-mortem brain samples from patients with Alzheimer's disease: a systematic review.* Mol Psychiatry, 2018. **23**(2): p. 177-198. DOI: 10.1038/mp.2017.246.
537. DiPatre, P.L. and B.B. Gelman. *Microglial cell activation in aging and Alzheimer disease: partial linkage with neurofibrillary tangle burden in the hippocampus.* J Neuropathol Exp Neurol, 1997. **56**(2): p. 143-9. DOI: 10.1097/00005072-199702000-00004.
538. Hou, Y.J., X.L. Dan, M. Babbar, Y. Wei, S.G. Hasselbalch, D.L. Croteau, and V.A. Bohr. *Ageing as a risk factor for neurodegenerative disease.* Nature Reviews Neurology, 2019. **15**(10): p. 565-581. DOI: 10.1038/s41582-019-0244-7.
539. Barrientos, R.M., M.M. Kitt, L.R. Watkins, and S.F. Maier. *Neuroinflammation in the normal aging hippocampus.* Neuroscience, 2015. **309**: p. 84-99. DOI: 10.1016/j.neuroscience.2015.03.007.
540. Giunta, B., F. Fernandez, W.V. Nikolic, D. Obregon, E. Rrapo, T. Town, and J. Tan. *Inflammaging as a prodrome to Alzheimer's disease.* Journal of Neuroinflammation, 2008. **5**. DOI: 10.1186/1742-2094-5-51.
541. Trump, B.F., J.M. Valigorsky, A.U. Arstila, W.J. Mergner, and T.D. Kinney. *The relationship of intracellular pathways of iron metabolism to cellular iron overload and the iron storage diseases. Cell sap and cytocavitary network pathways in relation to lysosomal storage and turnover of iron macromolecules.* Am J Pathol, 1973. **72**(2): p. 295-336. https://www.ncbi.nlm.nih.gov/pubmed/4579280.
542. Butt, M.T., K.M. Whitney, W. Davis, S. Akella, S. Parker, and G.L. Foley. *Microscopic background changes in brains of cynomolgus monkeys.* Toxicol Pathol, 2015. **43**(4): p. 513-8. DOI: 10.1177/0192623314537723.
543. Sumbria, R.K., M.M. Grigoryan, V. Vasilevko, A. Paganini-Hill, K. Kilday, R. Kim, D.H. Cribbs, and M.J. Fisher. *Aging exacerbates development of cerebral microbleeds in a*

mouse model. J Neuroinflammation, 2018. **15**(1): p. 69. DOI: 10.1186/s12974-018-1092-x.
544. Kastman, E.K., A.A. Willette, C.L. Coe, B.B. Bendlin, K.J. Kosmatka, D.G. McLaren, G. Xu, E. Canu, A.S. Field, A.L. Alexander, M.L. Voytko, T.M. Beasley, R.J. Colman, R.H. Weindruch, and S.C. Johnson. *A calorie-restricted diet decreases brain iron accumulation and preserves motor performance in old rhesus monkeys.* J Neurosci, 2012. **32**(34): p. 11897-904. DOI: 10.1523/jneurosci.2553-12.2012.
545. Rodriguez-Callejas, J.D., D. Cuervo-Zanatta, A. Rosas-Arellano, C. Fonta, E. Fuchs, and C. Perez-Cruz. *Loss of ferritin-positive microglia relates to increased iron, RNA oxidation, and dystrophic microglia in the brains of aged male marmosets.* Am J Primatol, 2019. **81**(2). DOI: 10.1002/ajp.22956.
546. Zhou, J., A. Wearn, J. Huck, C. Hughes, G. Baracchini, J. Tremblay-Mercier, J. Poirier, S. Villeneuve, C.L. Tardif, M.M. Chakravarty, A.M. Daugherty, C.J. Gauthier, G.R. Turner, R.N. Spreng, and P.-A.R. Group. *Iron Deposition and Distribution Across the Hippocampus Is Associated with Pattern Separation and Pattern Completion in Older Adults at Risk for Alzheimer's Disease.* J Neurosci, 2024. **44**(19). DOI: 10.1523/JNEUROSCI.1973-23.2024.
547. Buchman, A.S., J.M. Shulman, S. Nag, S.E. Leurgans, S.E. Arnold, M.C. Morris, J.A. Schneider, and D.A. Bennett. *Nigral pathology and parkinsonian signs in elders without Parkinson disease.* Ann Neurol, 2012. **71**(2): p. 258-66. DOI: 10.1002/ana.22588.
548. Beach, T.G., L.I. Sue, D.G. Walker, L.F. Lue, D.J. Connor, J.N. Caviness, M.N. Sabbagh, and C.H. Adler. *Marked microglial reaction in normal aging human substantia nigra: correlation with extraneuronal neuromelanin pigment deposits.* Acta Neuropathol, 2007. **114**(4): p. 419-24. DOI: 10.1007/s00401-007-0250-5.
549. Wilms, H., P. Rosenstiel, J. Sievers, G. Deuschl, L. Zecca, and R. Lucius. *Activation of microglia by human neuromelanin is NF-kappaB dependent and involves p38 mitogen-activated protein kinase: implications for Parkinson's disease.* FASEB J, 2003. **17**(3): p. 500-2. DOI: 10.1096/fj.02-0314fje.
550. Zhang, W., K. Phillips, A.R. Wielgus, J. Liu, A. Albertini, F.A. Zucca, R. Faust, S.Y. Qian, D.S. Miller, C.F. Chignell, B. Wilson, V. Jackson-Lewis, S. Przedborski, D. Joset, J. Loike, J.S. Hong, D. Sulzer, and L. Zecca. *Neuromelanin activates microglia and induces degeneration of dopaminergic neurons: implications for progression of Parkinson's disease.* Neurotox Res, 2011. **19**(1): p. 63-72. DOI: 10.1007/s12640-009-9140-z.
551. Schuitemaker, A., T.F. van der Doef, R. Boellaard, W.M. van der Flier, M. Yaqub, A.D. Windhorst, F. Barkhof, C. Jonker, R.W. Kloet, A.A. Lammertsma, P. Scheltens, and B.N. van Berckel. *Microglial activation in healthy aging.* Neurobiol Aging, 2012. **33**(6): p. 1067-72. DOI: 10.1016/j.neurobiolaging.2010.09.016.
552. Suridjan, I., P.M. Rusjan, A.N. Voineskos, T. Selvanathan, E. Setiawan, A.P. Strafella, A.A. Wilson, J.H. Meyer, S. Houle, and R. Mizrahi. *Neuroinflammation in healthy aging: a PET study using a novel Translocator Protein 18kDa (TSPO) radioligand, [(18)F]-FEPPA.* Neuroimage, 2014. **84**: p. 868-75. DOI: 10.1016/j.neuroimage.2013.09.021.
553. Gulyas, B., A. Vas, M. Toth, A. Takano, A. Varrone, Z. Cselenyi, M. Schain, P. Mattsson, and C. Halldin. *Age and disease related changes in the translocator protein (TSPO) system in the human brain: positron emission tomography measurements with [11C]vinpocetine.* Neuroimage, 2011. **56**(3): p. 1111-21. DOI: 10.1016/j.neuroimage.2011.02.020.
554. Green, T.R.F., S.M. Murphy, and R.K. Rowe. *Comparisons of quantitative approaches for assessing microglial morphology reveal inconsistencies, ecological fallacy, and a need for standardization.* Sci Rep, 2022. **12**(1). DOI: 10.1038/s41598-022-23091-2.
555. Sayed, N., Y. Huang, K. Nguyen, Z. Krejciova-Rajaniemi, A.P. Grawe, T. Gao, R. Tibshirani, T. Hastie, A. Alpert, L. Cui, T. Kuznetsova, Y. Rosenberg-Hasson, R. Ostan, D. Monti, B. Lehallier, S.S. Shen-Orr, H.T. Maecker, C.L. Dekker, T. Wyss-Coray, C. Franceschi, V. Jojic, F. Haddad, J.G. Montoya, J.C. Wu, M.M. Davis, and D. Furman.

An inflammatory aging clock (iAge) based on deep learning tracks multimorbidity, immunosenescence, frailty and cardiovascular aging. Nat Aging, 2021. **1**: p. 598-615. DOI: 10.1038/s43587-021-00082-y.

556. Choi, K., J. Chang, M.J. Lee, S. Wang, K. In, W.C. Galano-Tan, S. Jun, K. Cho, Y.H. Hwang, S.J. Kim, and W. Park. *Reference values of hematology, biochemistry, and blood type in cynomolgus monkeys from cambodia origin.* Lab Anim Res, 2016. **32**(1): p. 46-55. DOI: 10.5625/lar.2016.32.1.46.
557. Rao, Y.L., B. Ganaraja, B.V. Murlimanju, T. Joy, A. Krishnamurthy, and A. Agrawal. *Hippocampus and its involvement in Alzheimer's disease: a review.* 3 Biotech, 2022. **12**(2): p. 55. DOI: 10.1007/s13205-022-03123-4.
558. Zouiouich, S., D.A. Byrd, X. Hua, S. Karwa, Y. Wan, J. Shi, G.C. Humphrey, G.L. Ackermann, R. Knight, C.C. Abnet, E. Vogtmann, and R. Sinha. *Stability of the Fecal and Oral Microbiome over 2 Years at -80 degrees C for Multiple Collection Methods.* Cancer Epidemiol Biomarkers Prev, 2023. **32**(3): p. 444-451. DOI: 10.1158/1055-9965.EPI-22-0883.
559. Kim, J.H., J.Y. Jeon, Y.J. Im, N. Ha, J.K. Kim, S.J. Moon, and M.G. Kim. *Long-term taxonomic and functional stability of the gut microbiome from human fecal samples.* Sci Rep, 2023. **13**(1): p. 114. DOI: 10.1038/s41598-022-27033-w.
560. Choo, J.M., L.E. Leong, and G.B. Rogers. *Sample storage conditions significantly influence faecal microbiome profiles.* Sci Rep, 2015. **5**: p. 16350. DOI: 10.1038/srep16350.
561. Drevon-Gaillot, E., M.F. Perron-Lepage, C. Clement, and R. Burnett. *A review of background findings in cynomolgus monkeys (Macaca fascicularis) from three different geographical origins.* Experimental and Toxicologic Pathology, 2006. **58**(2-3): p. 77-88. DOI: 10.1016/j.etp.2006.07.003.
562. Johnson, R.L. and E. Kapsalis. *Ageing, infecundity and reproductive senescence in free-ranging female rhesus monkeys.* J Reprod Fertil, 1995. **105**(2): p. 271-8. DOI: 10.1530/jrf.0.1050271.
563. Colman, R.J. *Non-human primates as a model for aging.* Biochim Biophys Acta Mol Basis Dis, 2018. **1864**(9 Pt A): p. 2733-2741. DOI: 10.1016/j.bbadis.2017.07.008.
564. Liu, Y.S., M. Baxi, C.R. Madan, K. Zhan, N. Makris, D.L. Rosene, R.J. Killiany, S. Cetin-Karayumak, O. Pasternak, M. Kubicki, and B. Cao. *Brain age of rhesus macaques over the lifespan.* Neurobiol Aging, 2024. **139**: p. 73-81. DOI: 10.1016/j.neurobiolaging.2024.02.014.
565. Costea, P.I., G. Zeller, S. Sunagawa, E. Pelletier, A. Alberti, F. Levenez, M. Tramontano, M. Driessen, R. Hercog, F.E. Jung, J.R. Kultima, M.R. Hayward, L.P. Coelho, E. Allen-Vercoe, L. Bertrand, M. Blaut, J.R.M. Brown, T. Carton, S. Cools-Portier, M. Daigneault, M. Derrien, A. Druesne, W.M. de Vos, B.B. Finlay, H.J. Flint, F. Guarner, M. Hattori, H. Heilig, R.A. Luna, J. van Hylckama Vlieg, J. Junick, I. Klymiuk, P. Langella, E. Le Chatelier, V. Mai, C. Manichanh, J.C. Martin, C. Mery, H. Morita, P.W. O'Toole, C. Orvain, K.R. Patil, J. Penders, S. Persson, N. Pons, M. Popova, A. Salonen, D. Saulnier, K.P. Scott, B. Singh, K. Slezak, P. Veiga, J. Versalovic, L. Zhao, E.G. Zoetendal, S.D. Ehrlich, J. Dore, and P. Bork. *Towards standards for human fecal sample processing in metagenomic studies.* Nat Biotechnol, 2017. **35**(11): p. 1069-1076. DOI: 10.1038/nbt.3960.
566. McLaren, M.R., A.D. Willis, and B.J. Callahan. *Consistent and correctable bias in metagenomic sequencing experiments.* Elife, 2019. **8**. DOI: 10.7554/eLife.46923.
567. McLaren, M.R., J.T. Nearing, A.D. Willis, K.G. Lloyd, and B.J. Callahan. *Implications of taxonomic bias for microbial differential-abundance analysis.* bioRxiv, 2022: p. 2022.08.19.504330. DOI: 10.1101/2022.08.19.504330.
568. Lopez, D.E.G., L.M. Lashinger, G.M. Weinstock, and M.S. Bray. *Circadian rhythms and the gut microbiome synchronize the host's metabolic response to diet.* Cell Metabolism, 2021. **33**(5): p. 873-887. DOI: 10.1016/j.cmet.2021.03.015.

569. Penny, H.A., R.G. Domingues, M.Z. Krauss, F. Melo-Gonzalez, M.A.E. Lawson, S. Dickson, J. Parkinson, M. Hurry, C. Purse, E. Jegham, C. Godinho-Silva, M. Rendas, H. Veiga-Fernandes, D.A. Bechtold, R.K. Grencis, K.M. Toellner, A. Waisman, J.R. Swann, J.E. Gibbs, and M.R. Hepworth. *Rhythmicity of intestinal IgA responses confers oscillatory commensal microbiota mutualism.* Science Immunology, 2022. **7**(75). DOI: 10.1126/sciimmunol.abk2541.
570. Vandeputte, D., L. De Commer, R.Y. Tito, G. Kathagen, J. Sabino, S. Vermeire, K. Faust, and J. Raes. *Temporal variability in quantitative human gut microbiome profiles and implications for clinical research.* Nat Commun, 2021. **12**(1): p. 6740. DOI: 10.1038/s41467-021-27098-7.
571. Anthony, W.E., B. Wang, K.V. Sukhum, A.W. D'Souza, T. Hink, C. Cass, S. Seiler, K.A. Reske, C. Coon, E.R. Dubberke, C.D. Burnham, G. Dantas, and J.H. Kwon. *Acute and persistent effects of commonly used antibiotics on the gut microbiome and resistome in healthy adults.* Cell Rep, 2022. **39**(2): p. 110649. DOI: 10.1016/j.celrep.2022.110649.
572. Oh, B., B.S. Kim, J.W. Kim, J.S. Kim, S.J. Koh, B.G. Kim, K.L. Lee, and J. Chun. *The Effect of Probiotics on Gut Microbiota during the Helicobacter pylori Eradication: Randomized Controlled Trial.* Helicobacter, 2016. **21**(3): p. 165-74. DOI: 10.1111/hel.12270.
573. Dokoshi, T., Y. Chen, K.J. Cavagnero, G. Rahman, D. Hakim, S. Brinton, H. Schwarz, E.A. Brown, A. O'Neill, Y. Nakamura, F. Li, N.H. Salzman, R. Knight, and R.L. Gallo. *Dermal injury drives a skin to gut axis that disrupts the intestinal microbiome and intestinal immune homeostasis in mice.* Nat Commun, 2024. **15**(1): p. 3009. DOI: 10.1038/s41467-024-47072-3.
574. Wang, D. *5 challenges in understanding the role of the virome in health and disease.* PLoS Pathog, 2020. **16**(3): p. e1008318. DOI: 10.1371/journal.ppat.1008318.
575. Li, J., F. Yang, M. Xiao, and A. Li. *Advances and challenges in cataloging the human gut virome.* Cell Host Microbe, 2022. **30**(7): p. 908-916. DOI: 10.1016/j.chom.2022.06.003.
576. Cao, Z.R., N. Sugimura, E. Burgermeister, M.P. Ebert, T. Zuo, and P. Lan. *The gut virome: A new microbiome component in health and disease.* Ebiomedicine, 2022. **81**. DOI: 10.1016/j.ebiom.2022.104113.
577. Tan, X.M., T.J. Chai, J.J. Duan, J. Wu, H.P. Zhang, Y.F. Li, Y. Huang, X. Hu, P. Zheng, J.L. Song, P. Ji, X. Jin, H.M. Zhang, and P. Xie. *Dynamic changes occur in the DNA gut virome of female cynomolgus macaques during aging.* Microbiologyopen, 2021. **10**(2). DOI: 10.1002/mbo3.1186.
578. Aguiar-Pulido, V., W. Huang, V. Suarez-Ulloa, T. Cickovski, K. Mathee, and G. Narasimhan. *Metagenomics, Metatranscriptomics, and Metabolomics Approaches for Microbiome Analysis.* Evol Bioinform Online, 2016. **12**(Suppl 1): p. 5-16. DOI: 10.4137/EBO.S36436.
579. Emerson, J.B., R.I. Adams, C.M.B. Roman, B. Brooks, D.A. Coil, K. Dahlhausen, H.H. Ganz, E.M. Hartmann, T. Hsu, N.B. Justice, I.G. Paulino-Lima, J.C. Luongo, D.S. Lymperopoulou, C. Gomez-Silvan, B. Rothschild-Mancinelli, M. Balk, C. Huttenhower, A. Nocker, P. Vaishampayan, and L.J. Rothschild. *Schrodinger's microbes: Tools for distinguishing the living from the dead in microbial ecosystems.* Microbiome, 2017. **5**(1): p. 86. DOI: 10.1186/s40168-017-0285-3.

Appendices

Appendix 1. Redacted copy of the original study plan

Study Plan: 6189

VERSION: 20NOV2020

STUDY TITLE: Assessment of ageing on the innervation of gut and status of critical brain regions in cynomolgus and rhesus macaques (QIB1)

SPONSOR	TEST FACILITY
Quadram Institute Biosciences Norwich Research Park Norwich NR47UQ	Public Health England NIS Laboratories Research Porton Down, Salisbury Wiltshire SP4 0JG UK

OPERATIONAL DATES:
Planned start date: 26 June 2019
Planned completion date: 25 June 2022

STUDY PLAN APPROVED BY STUDY MANAGER:
Name: [redacted] Position: Study Manager

Signed: [redacted] Date: 07 Dec 2020

STUDY PLAN APPROVED BY SCIENTIFIC LEAD:
Name: [redacted] Position: Research Lead

Signed: [redacted] Date: 07 Dec 2020

STUDY PLAN APPROVED BY TEST FACILITY MANAGEMENT:
Name: [redacted] Position:

Signed: [redacted] Date: 07 Dec 2020

1. OBJECTIVES

To investigate the differences in innervation of different regions of the gut and brain between young, middle aged and older cynomolgus macaques.

2. BACKGROUND

In work completed at Quadram, murine tissue examination suggests that there are marked age-related differences in innervation and epithelial composition of the gut. Work by others also finds altered immune activation status of the gut and brain with ageing. This study seeks to determine whether these finding are replicated in the cynomolgus macaque.

3. MANAGEMENT OF STUDY

PHE Porton Down:
Study manager:
Test facility manager:
Project Licence Holder:
Named Animal Care AND Welfare Officer:
Named Veterinary Surgeon:
Sample oversight
Sample Analysis: PHE (as identified), QIB, UCL and UofS

Sponsor: QIB

4. TEST SYSTEM

Justification:
Dementia is a priority for the NHS and PHE as deaths resulting from it have now exceeeded those of acute respiratory infection. The mechanisms of accelerated ageing on dementia patients is poorly understood. Model systems that accurately reflect the process in man are required to both understand these changes and potentially to treat or reverse early onset decline. Terminal exsangination will be conducted under the authority of Home Office licence number [redacted]

4.1 Cynomolgus Macaques

Species: Macaca fascicularis
Health Status: Conventional colony free of herpes B-virus, TB, SIV, STLV
Source of supply: [redacted]
Number required:
Sex: 15 male, 15 female. Three groups each of 5 x male and 5 x female animals if possible.
Age: Adult

Identification of Test System
Each animal will have been identified by a permanent tattoo using a unique number.

Location

The animals will be sourced from the [redacted] breeding facility. Animals may have been housed with non-study animals.

4.2 Rhesus Macaques
Species: Macaca mulatta
Health Status: Conventional colony free of herpes B-virus, TB, SIV, STLV
Source of supply: [redacted]
Number required:
Sex: 15 male, 15 female. Three groups each of 5 x male and 5 x female animals if possible.
Age: Adult

Identification of Test System
Each animal will have been identified by a permanent tattoo using a unique number.

Location
The animals will be sourced from the [redacted] breeding facility. Animals may have been housed with non-study animals.

5. ALLOCATION TO GROUPS:

In order to examine differences in age, three age groups have been identified (**Table 1**). It is anticipated that 10 animals in each age-group would generate enough tissue for QIB to assess age-related changes.

Table 1. Group age structure of study macaques

Group	Species	Individual	Individual	Age range
1	Cyno	1-10	1-10	1-4 years
2	Cyno	11-20	11-20	4-8 years
3	Cyno	21-30	21-30	8 or more
4	Rhesus	1-10	1-10	1-4 years
5	Rhesus	11-20	11-20	4-8 years
6	Rhesus	21-30	21-30	8 or more

Individuals will be identified by the number tattooed onto its body. This identification number will be recorded onto the appropriate worksheets associated with sample requests (BIG SOP 143) and necropsy (BIG SOP 173).

6. EXSANGUINATION

Terminal sample procedure

1. Sedated animals will be transferred to the procedures room, weighed and rectal temperature taken (SOP BIG/020 Sedation of Primates for Procedures). During sedation, it would be preferable for each subject to undertake a hearing assessment using an OAE device. This may not be possible without an adequate seal inside the hearing canal and may require adaptation of the sealing grommets. The hearing test is non-invasive so no extra justification required under a project licence and will be under terminal anaesthesia. Hearing assessment and retina scanning will be included once the process for performing them has been worked up.

2. Anaesthesia will be continued and animals will be exsanguinated. (SOP BIG/021 Anaesthesia of primates for terminal procedures)

3. After exsanguination, animals will be euthanised by injection of a lethal dose of barbiturate.

4. Once euthanasia is complete and the brain removed, the euthanised subject's brain blood will be flushed through. Details for flushing will be supplied by used of a SPA. (**Brain**).

5. At necropsy (SOP BIG/173 Necropsy) brain and gut samples will be obtained as described in the following section.

6. A full post–mortem for the collection of abnormal tissue samples will only be performed if there are signs of ill health.

7. SAMPLE COLLECTION AND STORAGE

This study does not exclude the possibility that other samples will be taken for use in other studies. These tissue samples will be handled on an *ad hoc* basis. The information of tissue sample and requesting scientist's name will be recorded in the necropsy record.

Samples for this study to be collected will include:

Table 2. sample overview

Sample	Tube/pot	Storage temp when collected	Storage temperature long term (if applicable)	Ship samples to:	recipient
Blood - serum	BD Vacutainer SST II, amber lid	ambient	-20 °C	QIB at -20 °C	Aimee
Blood - Plasma	BD Vacutainer K3E, lilac lid	ambient	-20 °C	QIB at -20 °C	Aimee
Duodenum – snap frozen	Large Eppendorf tube	Dry ice	-80 °C	QIB on dry ice	Aimee
Duodenum – NBF	Bijoux of NBF	ambient	Swap to 70% EtOH after 24h then 4°C	QIB ambient	Aimee
Duodenum stool – Omnigene	Omnigene tubes	ambient	ambient	QIB ambient	Aimee
Duodenum stool – frozen	Large Eppendorf tube	Dry ice	-80 °C	QIB on dry ice	Aimee
Jejunum – snap frozen	Large Eppendorf tube	Dry ice/	-80 °C	QIB on dry ice	Aimee
Jejunum – NBF	Bijoux of NBF	ambient	Swap to 70% EtOH after 24h then 4°C	QIB ambient	Aimee
Jejunum stool – Omnigene	Omnigene tubes	ambient	ambient	QIB ambient	Aimee

Jejunum stool – frozen	Large Eppendorf tube	Dry ice	-80 °C	QIB on dry ice	Aimee
Ileum – snap frozen	Large Eppendorf tube	Dry ice	-80 °C	QIB on dry ice	Aimee
Ilieum – NBF	Bijoux of NBF	ambient	Swap to 70% EtOH after 24h then 4°C	QIB ambient	Aimee
Ilieum stool – Omnigene	Omnigene tubes	ambient	ambient	QIB ambient	Aimee
Ilieum stool – frozen	Large Eppendorf tube	Dry ice	-80 °C	QIB on dry ice	Aimee
Caecal stool – frozen	Large Eppendorf tube	Dry ice	-80 °C	QIB on dry ice	Aimee
Proximal colon – snap frozen	Large Eppendorf tube	Dry ice	-80 °C	QIB on dry ice	Aimee
Proximal colon – NBF	Bijoux of NBF	ambient	Swap to 70% EtOH after 24h then 4°C	QIB ambient	Aimee
Proximal colon stool – Omnigene	Omnigene tubes	ambient	ambient	QIB ambient	Aimee
Distal colon stool – frozen	Large Eppendorf tube	Dry ice	-80 °C	QIB on dry ice	Aimee
Distal colon – snap frozen	Large Eppendorf tube	Dry ice	-80 °C	QIB on dry ice	Aimee
Distal colon – NBF	Bijoux of NBF	ambient	Swap to 70% EtOH after 24h then 4°C	QIB ambient	Aimee
Distal colon stool – Omnigene	Omnigene tubes	ambient	ambient	QIB ambient	Aimee
Distal colon stool – frozen	Large Eppendorf tube	Dry ice/	-80 °C	QIB on dry ice	Aimee
Brain	Large NBF tub	ambient	Swap to 70% EtOH after 5 days then 4°C	QIB ambient	Aimee
Eyes*	Tubes supplied by Glen	Dissected retina (Glen) Snap frozen	-80 °C	UCL	Glen
	Tubes supplied by Glen	Fixed in NBF/PFA 1 h then swapped to PBS-azide and stored 4°C	After 1h, NBF/PFA swapped to PBS-azide and stored 4°C	UCL	Glen

* If staff not confident with dissection, place both eyes into NBF. Glen may be in attendance and may override the process described for eyes.

7.2 Blood

7.2.1 Serum

Tube 1. Serum: BD Vacutainer SST II, amber lid

1. Collect 4 mL blood SST II vacutainer tube.
2. Allow to clot undisturbed at RT (usually takes 15–30 minutes).
3. Centrifuge at 1,000–2,000 x g for 10 minutes in a refrigerated centrifuge.
4. Transfer the supernatant (serum) into clean Eppendorfs (~0.25 ml aliquots) and freeze.
5. Store and transport at –20°C or lower.

Tube 2. Plasma: BD Vacutainer K3E, lilac lid

1. Collect 2 mL blood into vacutainer EDTA tube.
2. Centrifuge at 1,000–2,000 x g for 10 minutes in a refrigerated centrifuge.
3. Transfer the supernatant (serum) into clean Eppendorfs (~0.25 ml aliquots) and freeze.
4. Store and transport at –20°C or lower.

Each aliquot will be labelled with the study number, animal ID, date taken and aliquot number.

7.3 Gut tissues samples and stools samples;

Two samples to be taken from each of five regions of the intestinal tract. These regions are;

- Duodenum* see below for sampling specifics.
- Jejenum
- Ileum
- Proximal colon and
- Distal colon.

See **Appendix 1** for a diagram showing how the tissue sections should be dissected. The following should be prepared:

NB- When sampling tissues, be consistent- always sample from the same location in an organ or tissue in each animal. Ensure that tissue sections for fixing are immersed in a sufficient volume of fixative to ensure complete fixation (a minimum one volume of tissue to 10 volumes of fixative).

7.3.1 Procedure for collecting tissue samples and faecal material.

1. Collect two circular cross sections of tissue approx. 5 mm wide from the intestinal tract. Flush gently with PBS to remove large faecal matter. Do not scrape mucosal surface.
2. Cut the rings of tissue into two semi-circular pieces of tissue to give 4 semicircles.
3. One of each of the two samples will be frozen by snap frozen (e.g. in a tube, into dry ice/isopentane).

4. One of each will go into 10% neutral buffered formalin for 24 hrs, to be replaced with 70% ethanol the following day.
5. Detailed instructions of how to use the omnigene tubes are found in **Appendix 2** and must be read before use.
6. Collect faecal material adjacent from each of the five intestinal identified below in the gut sample section (PLUS a sample from caecum) for microbiome analysis.

**Duodenal region: Avoiding the pylorus and duodenal bulb and below the hepatopancreatic sphincter eg sample from area boxed in blue.*

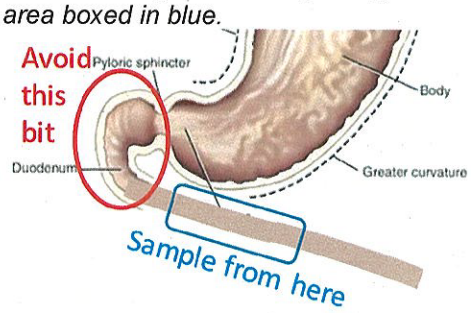

7.4 Brain

1. Whole brain will be removed, flushed through with protease inhibitor flushing buffer, first with cold protease inhibitor buffer, then with cold 4% NBF.
2. Separate the hemispheres. Placed both halves into 10% NBF pot for 5 days before dispatch.

(Protease inhibitor flushing buffer: AEBSF 2.0 mM, Aprotinin 0.3 µM, Bestatin 130 µM, EDTA 1.0 mM, E-64 14 µM, Leupeptin 1.0 µM, Sodium Fluoride 2.0 mM, Sodium Pyrophosphate 10 mM. All prepared in Phosphate buffered saline, stored at between 4 °C and 0 °C and held in an ice-bath before use.)

7.5 Eyes

1. Eye 1: retina dissected and snap frozen. (if not feasible, do both as per Eye 2).
2. Eye 2: pierce sclera with a needle to allow fixative to permeate Fix in 4% PFA (or NBF) 1h. Swap to PBS-azide and store at 4 degrees.

Note: This procedure may be over-ridden by that of [redacted] if he is in attendance and taking eye tissue for subsequent supply to QIB.

8. SAMPLE COLLECTION AND STORAGE

All samples will be transferred to PHE main site by dispatch for further processing. The study manager will be responsible for ensuring that the relevant samples are dispatched. See Table 2

Samples should be sent:

Attention of [redacted]
Quadram Institute Bioscience

Norwich Research Park
Colney Lane
Norwich, NR4 7UQ

9. DISPOSAL OF TEST SYSTEM

Remaining tissues of the animals culled during the course of the study or on termination of the study will be disposed of in accordance with current BIG procedures and SOPs.

10. SOPs utilised in the study

BIG 136, BIG 143, BIG 173
Histology HPC-001,

Appendix 1. Guidance notes for gut tissue collections

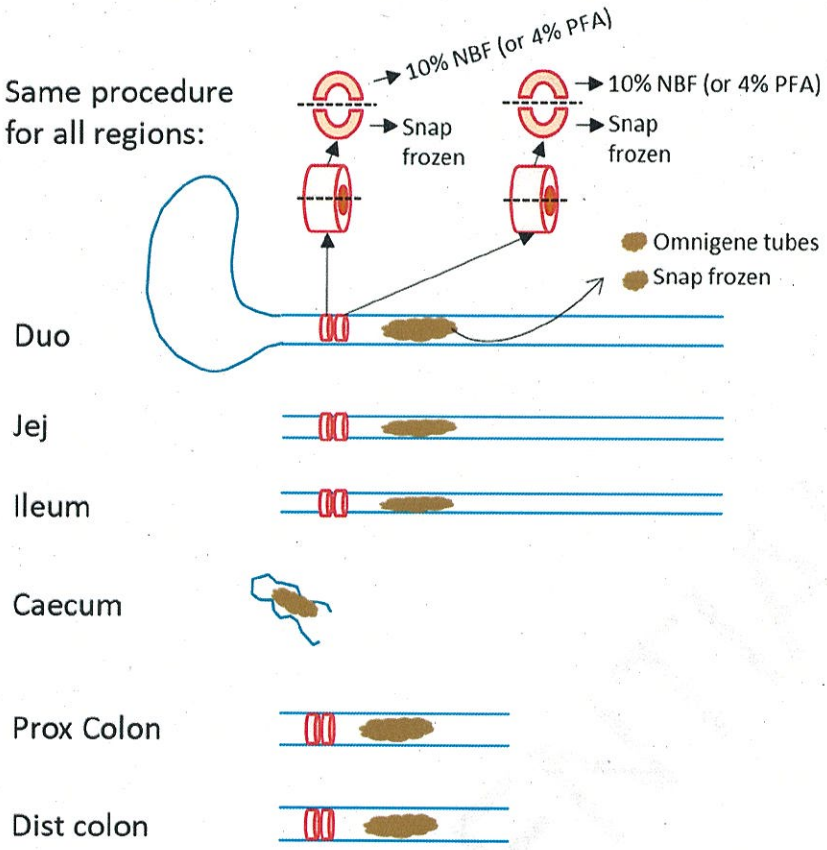

Appendix 3. Sample collection method of OMNIgene GUT OMR-200

1. 

Unscrew the purple cap from the collection device and set it aside for later use.

2. 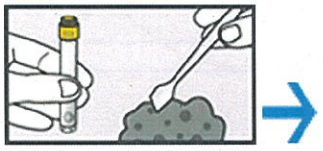

Use the stick to collect a small amount of faecal sample.

3. 

Transfer the faecal sample into the yellow tube top Repeat until the sample reaches the top and fills it completely.

4. 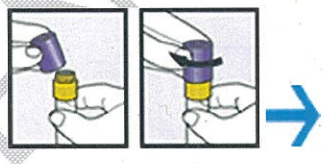

Screw the purple cap back onto the yellow tube top until tightly closed.

5. 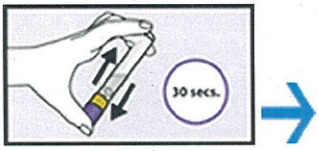

Shake the sealed tube as hard and fast as possible in a back and forth motion for a minimum of 30 seconds.

6. 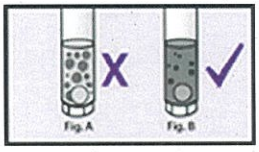

The faecal sample will be mixed with the stabilizing liquid in the tube; not all particles will dissolve.

Study 6189 Sample collection worksheet

Date: .....

Animal information	
Species (rhesus, cyno (Mauritian/Indonesian)	
ID	
D.O.B	
Age	
Reason for cull: Ex breeder, sustained ill health or other (please provide details)	

(Tick to indicate samples collected)

sample	Tube/sample description	Laboratory Records of procedure Worksheet ref: (Tick for yes, X for no, if no fill in comments box at bottom for reason)
Serum	Collect 4 ml into BD vacutainer SST II vacutainer, amber lid	
Plasma	Collect 2 ml into BD Vacutainer EDTA, lilac lid	
Duodenum	2 half semicircles samples snap frozen on dry ice.	
	2 half semi-circle places into 10% NBF	
	Duodenum stool into Omnigene -Gut tube ambient	
	Duodenum stool into large universal -large Eppendorf tube frozen	

Jejunum	2 half semi-circles samples snap frozen 2 on dry ice.	
	2 half semi-circle places into 10% NBF	
	Duodenum stool into Omnigene -Gut tube ambient	
	Duodenum stool into large universal -large Eppendorf tube frozen	
Ileum	2 half semi-circle samples snap frozen on dry ice.	
	2 half semi-circle places into 10% NBF	
	Ileum stool into Omnigene - Gut tube ambient	
	Ileum stool into large universal -large Eppendorf tube frozen	
Caecal content	Caecal stool into large universal large Eppendorf tube frozen	
Proximal colon	2 half semicircles samples snap frozen on dry ice.	
	2 half semi-circle places into 10% NBF	
	Proximal colon stool into Omnigene -Gut tube ambient	
	Proximal colon stool into large universal -large Eppendorf tube frozen	
Distal colon	2 half semicircles samples snap frozen on dry ice.	
	2 half semi-circle places into 10% NBF	
	Distal colon stool into Omnigene -Gut tube ambient	
	Distal colon stool into large universal -large Eppendorf tube frozen	

Brain (after flushing)	Separate hemisphere, place both hemispheres into NBF.	
Eyes	One retina to be fixed 1h then transferred to PBS-azide	
	One retina to be snap frozen	
Total number of samples	36	

Reason for failure to collect sample.

Operator/date.....

Appendix 2. FIJI/ImageJ macro to analyse Iba1^{+} cell density using 4 ROIs

```
// 20X Iba1 microglial density macro

// MAKE SURE THERE IS NOTHING IN YOUR IMAGE_FOLDER EXCEPT THE IMAGES YOU
WANT TO ANALYSE
// OTHER FILES, FOLDERS, ETC. WILL BE INCLUDED IN THE LOOP AND CREATE
DUPLICATES OF YOUR ANALYSIS

//Prompts you to select your 20X image folder .tif files
image_folder = getDirectory("Select your image folder");
output_folder = getDirectory("Select your output folder for processed
images.");

//RETRIEVES THE LIST OF IMAGE FILES AND BEGINS MACRO LOOP
imageList = getFileList(image_folder);
n = image_folder.length;
//Batch Mode
setBatchMode(false);
for(i = 0;i<n;i++){
      open(image_folder+imageList[i]);

      // Clear the ROI Manager
      roiManager("reset");

      filename = getInfo("image.filename");
      selectWindow(filename);
      run("Duplicate...", " ");
      run("Enhance Contrast", "saturated=0.35");
      run("Apply LUT");
      run("Despeckle");
      setAutoThreshold("Default dark");

      // Set threshold
//    run("Threshold...");         // uncomment this section the 1st time
the macro is run to set threshold manually
//    title = "WaitForUserDemo";
//    msg = "If necessary, use the \"Threshold\" tool to\nadjust the
threshold, then click \"OK\".";
//    waitForUser(title, msg);
      setThreshold(12000, 65535);
      setOption("BlackBackground", false);
      run("Convert to Mask");
      run("Despeckle");

      // CREATE ROIs
      makeOval(3563, 7886, 2000, 2000);
      roiManager("Add");
      makeOval(4247, 6650, 2000, 2000);
      roiManager("Add");
      makeOval(4379, 5438, 2000, 2000);
      roiManager("Add");
      makeOval(4259, 4130, 2000, 2000);
      roiManager("Add");

      // Display ROIs and wait for user interaction to move them
```

```
      roiManager("Show All");
      title = "WaitForUserROI";
      msg = "Move ROIs if necessary, then click \"OK\".";
      waitForUser(title, msg);

      // Perform particle analysis on each ROI separately
      //roiManager("Select All");
      //run("Analyze Particles...", "size=20-Infinity pixel
circularity=5.00-1.00 display summarize add");
      //run("Clear Results");

      // Set common properties for each ROI after particle analysis
      RoiManager.setGroup(0);
      RoiManager.setPosition(0);
      roiManager("Set Color", "blue");
      roiManager("Set Line Width", 0);

      // Analyse particles

      roiManager("Select", 0);
      run("Analyze Particles...", "size=20-Infinity pixel
circularity=5.00-1.00 display summarize add");
      roiManager("Select", 1);
      run("Clear Results");
      run("Analyze Particles...", "size=20-Infinity pixel
circularity=5.00-1.00 display summarize add");
      roiManager("Select", 2);
      run("Analyze Particles...", "size=20-Infinity pixel
circularity=5.00-1.00 display summarize add");
      roiManager("Select", 3);
      run("Analyze Particles...", "size=20-Infinity pixel
circularity=5.00-1.00 display summarize add");


      //save file
      saveAs("jpeg",output_folder+File.separator+"Density_"+filename);
      // Close the image
      close();
}

// Set Batch Mode back to true after the loop
setBatchMode(true);
```

Appendix 3. Overview of samples included within the analysis in Chapter 4

ID	Age Group	Age (Years)	Sex	Sample Region	Health Status
037KJC	Young	4	M	PC	Healthy
037KJC	Young	4	M	DC	Healthy
037KJC	Young	4	M	Duodenum	Healthy
037KJC	Young	4	M	Jejunum	Healthy
M293ID	Young	4	F	Caecum	Healthy
M293ID	Young	4	F	Ileum	Healthy
M293ID	Young	4	F	Duodenum	Healthy
M293ID	Young	4	F	Jejunum	Healthy
M293ID	Young	4	F	PC	Healthy
BD566GDH	Young	5	M	Caecum	Healthy
BD566GDH	Young	5	M	PC	Healthy
BD566GDH	Young	5	M	Ileum	Healthy
BD566GDH	Young	5	M	Jejunum	Healthy
BD566GDH	Young	5	M	DC	Healthy
BD566GDH	Young	5	M	Duodenum	Healthy
BD566GDH	Young	5	M	Faecal	Healthy
M838DC	Young	6	M	Caecum	Healthy
M838DC	Young	6	M	DC	Healthy
M838DC	Young	6	M	Duodenum	Healthy
M838DC	Young	6	M	Ileum	Healthy
M497BF	Adult	8	F	Ileum	Healthy
M497BF	Adult	8	F	Jejunum	Healthy
M497BF	Adult	8	F	PC	Healthy
M497BF	Adult	8	F	DC	Healthy
M497BF	Adult	8	F	Duodenum	Healthy
I050DF	Adult	9	F	Caecum	Healthy
I050DF	Adult	9	F	Ileum	Healthy
I050DF	Adult	9	F	Duodenum	Healthy
I320FC	Adult	10	F	Ileum	Healthy
I321BH	Adult	10	F	Caecum	Healthy
I321BH	Adult	10	F	PC	Healthy
Z672D	Adult	10	F	Caecum	Healthy
Z672D	Adult	10	F	Duodenum	Healthy
Z672D	Adult	10	F	Jejunum	Healthy
M972H-A*	Adult	10	F	Faecal	Obese
M972H-B*	Adult	10	F	Faecal	Obese
G30 - F1	Adult	10	F	Faecal	Healthy
G30 - F2	Adult	10	F	Faecal	Healthy
I321BG	Adult	11	F	Duodenum	Healthy
I321BG	Adult	11	F	Jejunum	Healthy
BD556GE	Aged	13	F	Caecum	Healthy

BD556GE	Aged	13	F	PC	Healthy
BD556GE	Aged	13	F	DC	Healthy
BD556GE	Aged	13	F	Duodenum	Healthy
BD556GE	Aged	13	F	Ileum	Healthy
I153CE	Aged	13	F	Caecum	Diabetic
I153CE	Aged	13	F	DC	Diabetic
I153CE	Aged	13	F	Ileum	Diabetic
I153CE	Aged	13	F	Duodenum	Diabetic
I153CE	Aged	13	F	Jejunum	Diabetic
M139F	Aged	13	F	Caecum	Healthy
M139F	Aged	13	F	PC	Healthy
M139F	Aged	13	F	DC	Healthy
M139F	Aged	13	F	Duodenum	Healthy
M139F	Aged	13	F	Ileum	Healthy
M139F	Aged	13	F	Jejunum	Healthy
M1116D	Aged	14	F	Caecum	Healthy
M1116D	Aged	14	F	PC	Healthy
M1116D	Aged	14	F	DC	Healthy
M1116D	Aged	14	F	Duodenum	Healthy
M1116D	Aged	14	F	Ileum	Healthy
M1116D	Aged	14	F	Jejunum	Healthy
M139E	Aged	14	M	Caecum	Healthy
M139E	Aged	14	M	Ileum	Healthy
M139E	Aged	14	M	PC	Healthy
M139E	Aged	14	M	Duodenum	Healthy
M139E	Aged	14	M	Jejunum	Healthy
M1464F	Aged	14	M	Caecum	Diabetic
M1464F	Aged	14	M	PC	Diabetic
M1464F	Aged	14	M	DC	Diabetic
M1464F	Aged	14	M	Duodenum	Diabetic
M1464F	Aged	14	M	Ileum	Diabetic
M1464F	Aged	14	M	Jejunum	Diabetic
M736G	Aged	14	F	PC	Healthy
M736G	Aged	14	F	Ileum	Healthy
M736G	Aged	14	F	DC	Healthy
M736G	Aged	14	F	Duodenum	Healthy
M7012E	Aged	15	F	Caecum	Healthy
M7012E	Aged	15	F	DC	Healthy
M7012E	Aged	15	F	Duodenum	Healthy
M871C	Aged	15	F	Caecum	Healthy
M871C	Aged	15	F	PC	Healthy
M871C	Aged	15	F	DC	Healthy
M895BA	Aged	15	F	Caecum	Healthy
M895BA	Aged	15	F	PC	Healthy
M895BA	Aged	15	F	DC	Healthy

M895BA	Aged	15	F	Duodenum	Healthy
M895BA	Aged	15	F	Ileum	Healthy
M895BA	Aged	15	F	Jejunum	Healthy
I007CB	Aged	16	F	Caecum	Healthy
I007CB	Aged	16	F	DC	Healthy
I007CB	Aged	16	F	Ileum	Healthy
I007CB	Aged	16	F	Jejunum	Healthy
I007CB	Aged	16	F	Duodenum	Healthy
I142BD	Aged	16	F	Caecum	Healthy
I142BD	Aged	16	F	PC	Healthy
I142BD	Aged	16	F	DC	Healthy
I142BD	Aged	16	F	Duodenum	Healthy
I142BD	Aged	16	F	Jejunum	Healthy
I150E	Aged	17	F	Caecum	Healthy
I150E	Aged	17	F	PC	Healthy
I150E	Aged	17	F	Duodenum	Healthy
I150E	Aged	17	F	Jejunum	Healthy
I150E	Aged	17	F	Ileum	Healthy
I150E	Aged	17	F	DC	Healthy
I150E	Aged	17	F	Faecal	Healthy
M224C	Aged	18	F	Caecum	Healthy
M224C	Aged	18	F	PC	Healthy
M224C	Aged	18	F	DC	Healthy
M224C	Aged	18	F	Duodenum	Healthy
M972-A*	Aged	19	F	Faecal	Obese
M972-B*	Aged	19	F	Faecal	Obese
M224	Aged	20	F	Caecum	Healthy
M224	Aged	20	F	PC	Healthy
M224	Aged	20	F	Ileum	Healthy
M224	Aged	20	F	Jejunum	Healthy
M224	Aged	20	F	DC	Healthy
MHC2 - F1	Aged	15-16	F	Faecal	Healthy
MHC2 - M1	Aged	15-16	M	Faecal	Healthy

* Duplicate samples

PC – Proximal Colon; DC – Distal Colon

Appendix 4. WGS reads pre- and post- removal of reads mapping to the NHP genome

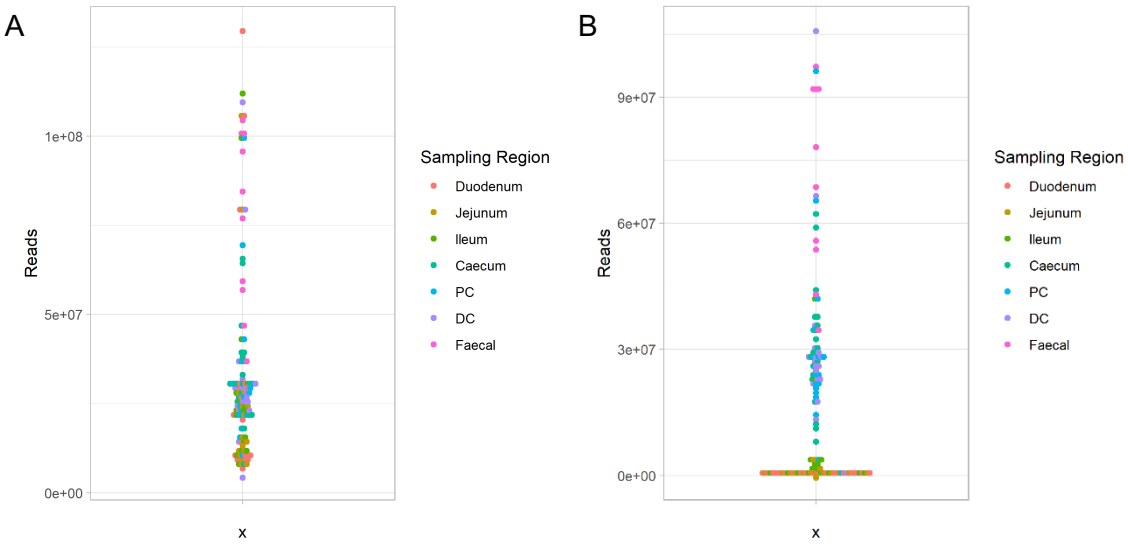

Appendix 4. Number of WGS reads per metagenomic sample (A) pre- and (B) post- removal of reads mapping to the host genome.

Appendix 5. Prokaryotic species-level alpha diversity across different age groups

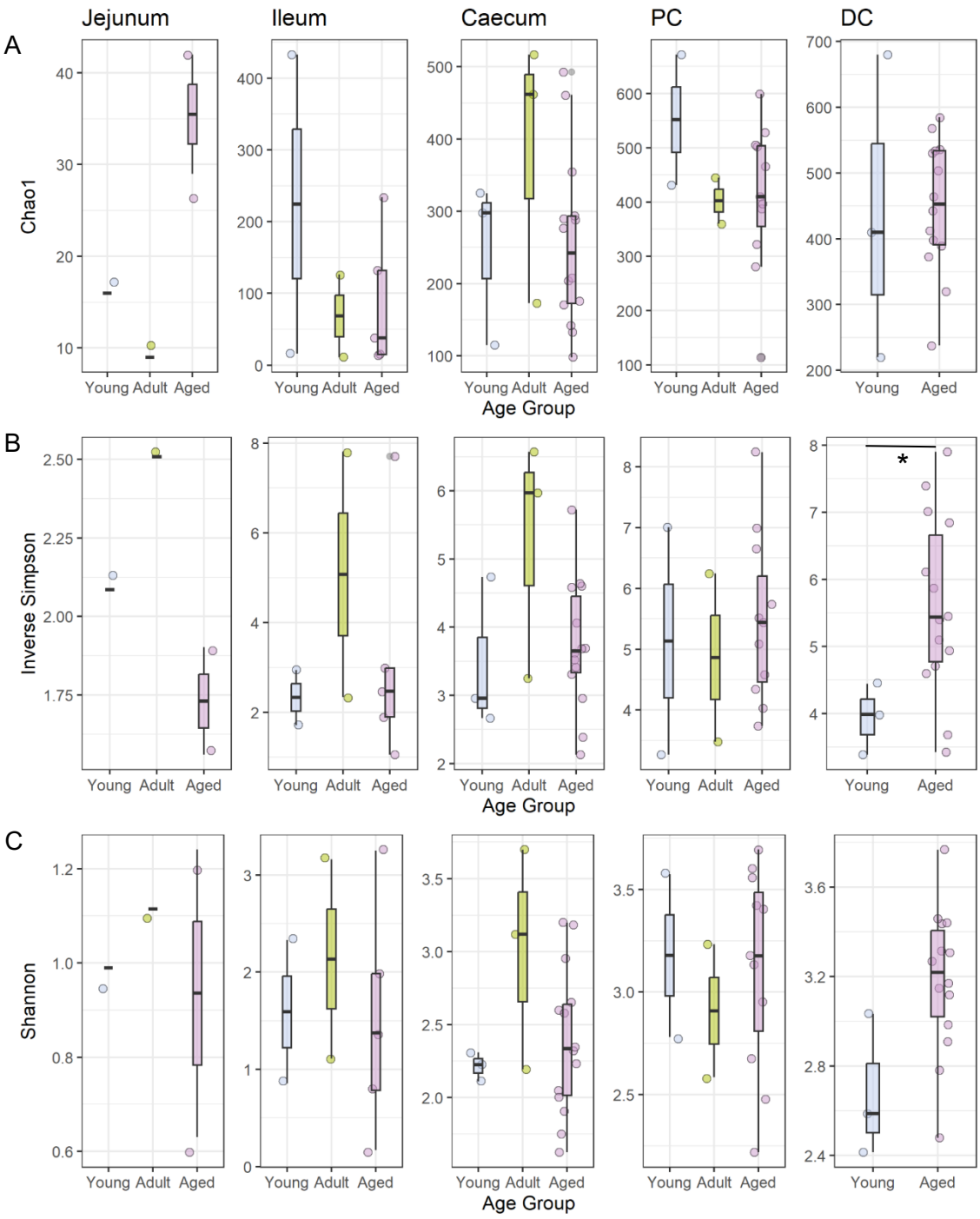

Appendix 5. Species-level alpha diversity measures of the intestinal microbiota across different regions of the intestinal tract in healthy cynomolgus macaques of varying ages. Alpha diversity is assessed using three metrics: (A) Chao1 index (B) Inverse Simpson's index (C) Shannon's index. Age groups are defined as 4-7 years (Young), 8-12 years (Adult) and 13-20 years (Aged). Statistical differences between groups were assessed by Kruskal-Wallis test for comparisons among three age groups and unpaired two-samples Wilcoxon test for comparisons between two age groups. Significance was determined at $p < 0.05$. * denotes a significant difference between groups. Proximal Colon, PC; Distal Colon, DC.

Appendix 6. Summary of statistical tests applied to region-specific assessments of the effect of age on intestinal prokaryotic alpha diversity

A. Chao1

Test	Region	Chi_squared	df	W_statistic	p_value	Significant
Kruskal-Wallis	J	2.7	2	NA	0.2592	
Kruskal-Wallis	I	1.2	2	NA	0.5488	
Kruskal-Wallis	C	1.7844	2	NA	0.4098	
Kruskal-Wallis	PC	1.5227	2	NA	0.467	
Wilcoxon	DC	NA	NA	19	0.85	

B. Inverse Simpson

Test	Region	Chi_squared	df	W_statistic	p_value	Significant
Kruskal-Wallis	J	2.7	2	NA	0.2592	
Kruskal-Wallis	I	0.89333	2	NA	0.6398	
Kruskal-Wallis	C	2.2381	2	NA	0.3266	
Kruskal-Wallis	PC	0.32273	2	NA	0.851	
Wilcoxon	DC	NA	NA	4	0.03764	*

C. Shannon

Test	Region	Chi_squared	df	W_statistic	p_value	Significant
Kruskal-Wallis	J	0.3	2	NA	0.8607	
Kruskal-Wallis	I	0.37333	2	NA	0.8297	
Kruskal-Wallis	C	2.0748	2	NA	0.3544	
Kruskal-Wallis	PC	0.51818	2	NA	0.7718	
Wilcoxon	DC	NA	NA	5	0.05084	

Test: The type of test performed (Kruskal-Wallis or unpaired two-samples Wilcoxon test)

Region: The region assessed for each test (Duodenum, D; Jejunum, J; Caecum, C, Proximal Colon, PC; Distal Colon, DC)

Chi_squared: The Kruskal-Wallis chi-squared statistic (NA for Wilcoxon test)

df: Degrees of freedom for Kruskal-Wallis test (NA for Wilcoxon test)

W_statistic: The W statistic for the Wilcoxon test (NA for Kruskal-Wallis tests)

p_value: The p-value for each test

Appendix 6. Summary of the statistical test results applied to the region-specific assessments of species-level alpha diversity in the intestinal microbiota of healthy cynomolgus macaques across different age groups. Alpha diversity was assessed using three metrics: (A) Chao1 index, (B) Inverse Simpson's index, (C) Shannon's index. Significance was determined at $p < 0.05$. Duodenum, D; Jejunum, J; Caecum, C, Proximal Colon, PC; Distal Colon, DC.

Appendix 7. Summary of statistical tests applied to assessments of prokaryotic alpha diversity across different intestinal regions

A

Chao1			
Comparison	Value	p-value	Significant
C-DC	182.4902	9.48E-07	*
C-I	-202.049	1.09E-05	*
C-J	-257.092	3.88E-05	*
C-PC	157.3409	2.67E-05	*
DC-C	-182.49	9.48E-07	*
DC-I	-384.54	3.08E-11	*
DC-J	-439.582	1.70E-09	*
DC-PC	-25.1493	0.460394	
I-C	202.0494	1.09E-05	*
I-DC	384.5395	3.08E-11	*
I-J	-55.0425	0.347396	
I-PC	359.3902	2.57E-10	*
J-C	257.0919	3.88E-05	*
J-DC	439.582	1.70E-09	*
J-I	55.04252	0.347396	
J-PC	414.4327	7.58E-09	*
PC-C	-157.341	2.67E-05	*
PC-DC	25.14931	0.460394	
PC-I	-359.39	2.57E-10	*
PC-J	-414.433	7.58E-09	*

B

Inverse Simpson			
Comparison	Value	p-value	Significant
C-DC	1.446509	0.001717	*
C-I	-0.50946	0.351832	
C-J	-1.28235	0.094536	
C-PC	1.533441	0.001557	*
DC-C	-1.44651	0.001717	*
DC-I	-1.95597	0.001271	*
DC-J	-2.72885	0.000891	*
DC-PC	0.086933	0.851891	
I-C	0.509457	0.351832	
I-DC	1.955966	0.001271	*
I-J	-0.77289	0.335388	
I-PC	2.042898	0.000976	*
J-C	1.282345	0.094536	
J-DC	2.728854	0.000891	*
J-I	0.772888	0.335388	
J-PC	2.815787	0.000695	*
PC-C	-1.53344	0.001557	*
PC-DC	-0.08693	0.851891	
PC-I	-2.0429	0.000976	*
PC-J	-2.81579	0.000695	*

C

Shannon			
Comparison	Value	p-value	Significant
C-DC	0.670645	0.000126	*
C-I	-0.85187	0.000122	*
C-J	-1.24415	5.92E-05	*
C-PC	0.680508	0.000196	*
DC-C	-0.67064	0.000126	*
DC-I	-1.52251	8.41E-09	*
DC-J	-1.9148	3.67E-08	*
DC-PC	0.009863	0.953887	
I-C	0.851866	0.000122	*
I-DC	1.522511	8.41E-09	*
I-J	-0.39229	0.184806	
I-PC	1.532374	1.04E-08	*
J-C	1.244152	5.92E-05	*
J-DC	1.914797	3.67E-08	*
J-I	0.392286	0.184806	
J-PC	1.92466	3.80E-08	*
PC-C	-0.68051	0.000196	*
PC-DC	-0.00986	0.953887	
PC-I	-1.53237	1.04E-08	*
PC-J	-1.92466	3.80E-08	*

Appendix 7. Summary of the statistical test results applied to assessments of species-level alpha diversity in the intestinal microbiota of healthy cynomolgus macaques across different intestinal regions. Alpha diversity was assessed using three metrics: (A) Chao1 index, (B) Inverse Simpson's index, (C) Shannon's index. Statistical analysis was carried out using linear-mixed effect models and significance was determined at $p < 0.05$. p-values were adjusted using BH corrections for multiple comparisons. Duodenum, D; Jejunum, J; Caecum, C, Proximal Colon, PC; Distal Colon, DC.

Appendix 8. Summary of PERMANOVA pairwise comparisons of Bray-Curtis dissimilarity of the prokaryotic component of the intestinal microbiota

A

Comparison	p.value	Significant
Young-Aged	1	
Young-Adult	1	
Aged-Adult	1	

B

Comparison	p.value	Significant
DC-PC	1	
DC-C	0.001	*
DC-I	0.001	*
DC-J	0.003	*
PC-C	0.003	*
PC-I	0.001	*
PC-J	0.001	*
C-I	0.001	*
C-J	0.001	*
I-J	0.455	

Appendix 8. Summary of PERMANOVA pairwise comparisons of Bray-Curtis dissimilarity in the intestinal microbiota of healthy cynomolgus macaques. Results show the effect of (A) age-group and (B) intestinal region on microbial community composition. P-values were adjusted using BH correction for multiple comparisons. Significance was determined at $p < 0.05$. Age groups are defined as 4-7 years (Young), 8-12 years (Adult) and 13-20 years (Aged). Duodenum, D; Jejunum, J; Caecum, C, Proximal Colon, PC; Distal Colon, DC.

Appendix 9. Overview of samples included within the analysis in Chapter 5

ID	Age Group	Age (Years)	Sex	Sample Region	Health Status
037KJC	Young	4	M	Duodenum	Healthy
037KJC	Young	4	M	Jejunum	Healthy
037KJC	Young	4	M	Caecum	Healthy
037KJC	Young	4	M	Proximal Colon	Healthy
037KJC	Young	4	M	Distal Colon	Healthy
M293ID	Young	4	F	Duodenum	Healthy
M293ID	Young	4	F	Jejunum	Healthy
M293ID	Young	4	F	Ileum	Healthy
M293ID	Young	4	F	Caecum	Healthy
M293ID	Young	4	F	Proximal Colon	Healthy
M293ID	Young	4	F	Distal Colon	Healthy
M838DC	Young	6	M	Caecum	Healthy
M497BF	Adult	8	F	Caecum	Healthy
M497BF	Adult	8	F	Proximal Colon	Healthy
I050DF	Adult	9	F	Duodenum	Healthy
I050DF	Adult	9	F	Ileum	Healthy
I050DF	Adult	9	F	Caecum	Healthy
I320FC	Adult	10	F	Duodenum	Healthy
I320FC	Adult	10	F	Jejunum	Healthy
I320FC	Adult	10	F	Caecum	Healthy
I321BH	Adult	10	F	Caecum	Healthy
I321BH	Adult	10	F	Proximal Colon	Healthy
Z672D	Adult	10	F	Duodenum	Healthy
Z672D	Adult	10	F	Jejunum	Healthy
Z672D	Adult	10	F	Ileum	Healthy
Z672D	Adult	10	F	Caecum	Healthy
Z672D	Adult	10	F	Proximal Colon	Healthy
Z672D	Adult	10	F	Distal Colon	Healthy
I321BG	Adult	11	F	Duodenum	Healthy
I321BG	Adult	11	F	Jejunum	Healthy
BD566GE	Aged	13	F	Caecum	Healthy
BD566GE	Aged	13	F	Proximal Colon	Healthy
BD566GE	Aged	13	F	Distal Colon	Healthy
I153CE	Aged	13	F	Jejunum	Diabetic
I153CE	Aged	13	F	Ileum	Diabetic
I153CE	Aged	13	F	Distal Colon	Diabetic
M139F	Aged	13	F	Caecum	Healthy
M139F	Aged	13	F	Proximal Colon	Healthy
M139F	Aged	13	F	Distal Colon	Healthy
M139E	Aged	14	M	Duodenum	Healthy
M139E	Aged	14	M	Ileum	Healthy

M139E	Aged	14	M	Caecum	Healthy
M139E	Aged	14	M	Proximal Colon	Healthy
M139E	Aged	14	M	Distal Colon	Healthy
M1464F	Aged	14	M	Caecum	Diabetic
M1464F	Aged	14	M	Proximal Colon	Diabetic
M1464F	Aged	14	M	Distal Colon	Diabetic
M736G	Aged	14	F	Duodenum	Healthy
M736G	Aged	14	F	Jejunum	Healthy
M736G	Aged	14	F	Ileum	Healthy
M736G	Aged	14	F	Proximal Colon	Healthy
M224	Aged	20	F	Jejunum	Healthy
M224	Aged	20	F	Ileum	Healthy
M224	Aged	20	F	Caecum	Healthy
M224	Aged	20	F	Proximal Colon	Healthy
M224	Aged	20	F	Distal Colon	Healthy

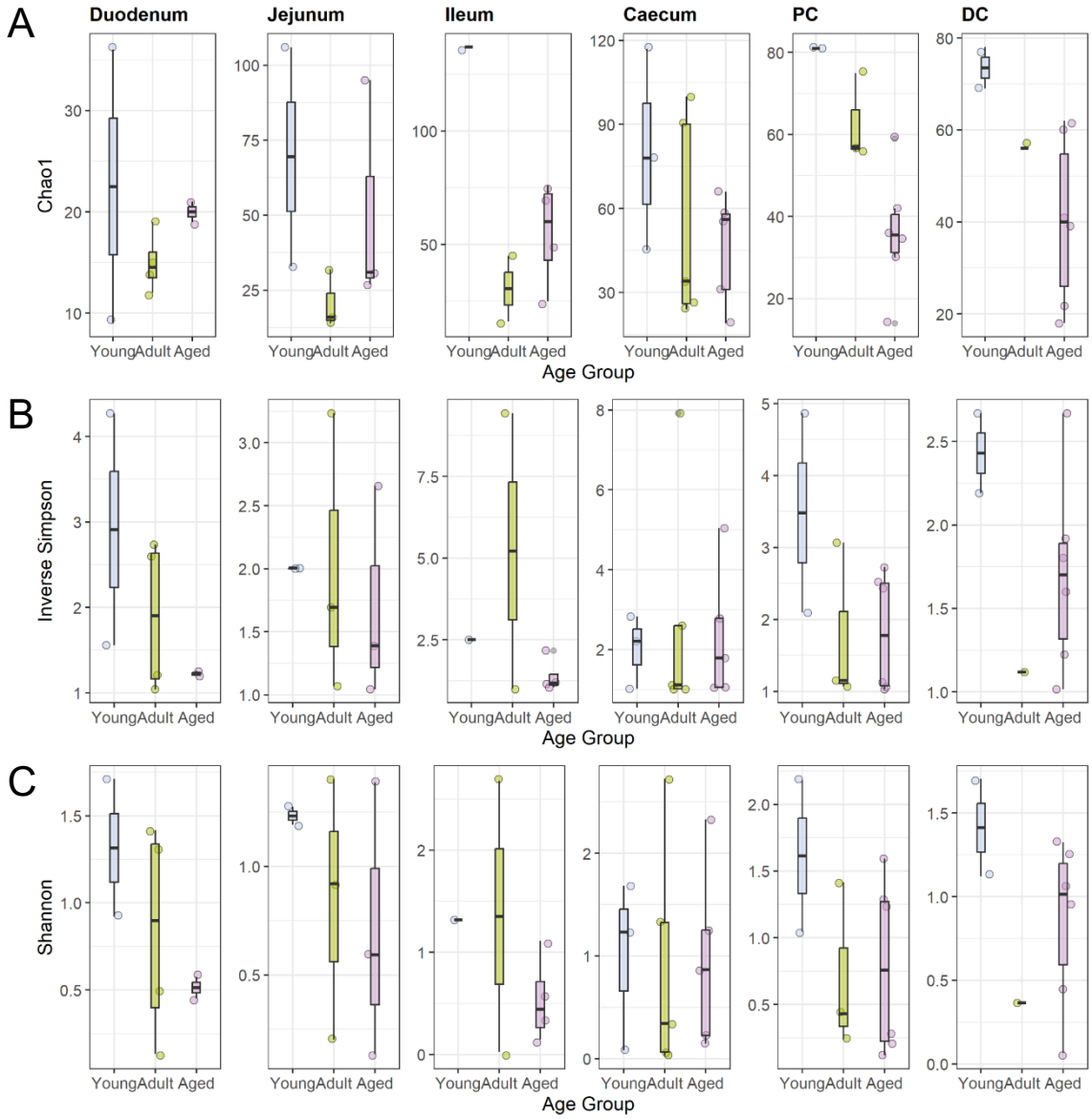

Appendix 10. Species-level alpha diversity measures of the intestinal mycobiota across different regions of the intestinal tract in healthy cynomolgus macaques of varying ages. Alpha diversity is assessed using three metrics: (A) Chao1 index (B) Inverse Simpson's index (C) Shannon's index. Age groups are defined as 4-7 years (Young), 8-12 years (Adult) and 13-20 years (Aged). Statistical differences between groups were assessed by Kruskal-Wallis test for comparisons among three age groups, * = $p<0.05$. Multiple pairwise comparisons were performed using Wilcoxon rank sum test with BH corrections for multiple comparisons where necessary.

Appendix 11. Summary of statistical tests applied to assessments of fungal alpha diversity across different intestinal regions

A

Chao1			
Comparison	Value	p-value	Significant
C-DC	-7.1007	0.425748	
C-D	-40.4501	0.000122	*
C-I	-0.56214	0.954466	
C-J	-13.8144	0.153468	
C-PC	-6.68752	0.419481	
DC-C	7.100696	0.425748	
DC-D	-33.3494	0.00236	*
DC-I	6.538552	0.52923	
DC-J	-6.71368	0.507473	
DC-PC	0.413181	0.963694	
D-C	40.45014	0.000122	*
D-DC	33.34944	0.00236	*
D-I	39.888	0.000559	*
D-J	26.63576	0.011727	*
D-PC	33.76262	0.001391	*
I-C	0.562143	0.954466	
I-DC	-6.53855	0.52923	
I-D	-39.888	0.000559	*
I-J	-13.2522	0.215228	
I-PC	-6.12537	0.544645	
J-C	13.81438	0.153468	
J-DC	6.713679	0.507473	
J-D	-26.6358	0.011727	*
J-I	13.25223	0.215228	
J-PC	7.12686	0.468513	
PC-C	6.687515	0.419481	
PC-DC	-0.41318	0.963694	
PC-D	-33.7626	0.001391	*
PC-I	6.125372	0.544645	
PC-J	-7.12686	0.468513	

B

Inverse Simpson			
Comparison	Value	p-value	Significant
C-DC	-0.39649	0.386181	
C-D	-0.62894	0.201356	
C-I	0.273723	0.590068	
C-J	-0.25954	0.599392	
C-PC	-0.05801	0.890492	
DC-C	0.396495	0.386181	
DC-D	-0.23244	0.659901	
DC-I	0.670218	0.21165	
DC-J	0.136957	0.791889	
DC-PC	0.338486	0.467108	
D-C	0.628935	0.201356	
D-DC	0.23244	0.659901	
D-I	0.902658	0.101881	
D-J	0.369398	0.474382	
D-PC	0.570926	0.262791	
I-C	-0.27372	0.590068	
I-DC	-0.67022	0.21165	
I-D	-0.90266	0.101881	
I-J	-0.53326	0.32751	
I-PC	-0.33173	0.523402	
J-C	0.259538	0.599392	
J-DC	-0.13696	0.791889	
J-D	-0.3694	0.474382	
J-I	0.533261	0.32751	
J-PC	0.201529	0.690393	
PC-C	0.058009	0.890492	
PC-DC	-0.33849	0.467108	
PC-D	-0.57093	0.262791	
PC-I	0.331732	0.523402	
PC-J	-0.20153	0.690393	

C

Shannon			
Comparison	Value	p-value	Significant
C-DC	-0.02076	0.893736	
C-D	-0.11114	0.506674	
C-I	-0.00084	0.996122	
C-J	0.019192	0.909756	
C-PC	-0.00853	0.95263	
DC-C	0.020763	0.893736	
DC-D	-0.09037	0.617263	
DC-I	0.01992	0.912338	
DC-J	0.039956	0.821795	
DC-PC	0.012234	0.938259	
D-C	0.111135	0.506674	
D-DC	0.090372	0.617263	
D-I	0.110292	0.550931	
D-J	0.130328	0.458316	
D-PC	0.102607	0.554465	
I-C	0.000844	0.996122	
I-DC	-0.01992	0.912338	
I-D	-0.11029	0.550931	
I-J	0.020036	0.913453	
I-PC	-0.00769	0.965408	
J-C	-0.01919	0.909756	
J-DC	-0.03996	0.821795	
J-D	-0.13033	0.458316	
J-I	-0.02004	0.913453	
J-PC	-0.02772	0.872877	
PC-C	0.008529	0.95263	
PC-DC	-0.01223	0.938259	
PC-D	-0.10261	0.554465	
PC-I	0.007685	0.965408	
PC-J	0.027721	0.872877	

Appendix 11. Summary of the statistical test results applied to assessments of species-level alpha diversity in the intestinal mycobiota of healthy cynomolgus macaques across different intestinal regions. Alpha diversity was assessed using three metrics: (A) Chao1 index, (B) Inverse Simpson's index, (C) Shannon's index. Statistical analysis was carried out using linear-mixed effect models and significance was determined at $p < 0.05$. p-values were adjusted using BH corrections for multiple comparisons. Duodenum, D; Jejunum, J; Caecum, C, Proximal Colon, PC; Distal Colon, DC.

Appendix 12. Images of *C. albicans* cells in both yeast and hyphal form

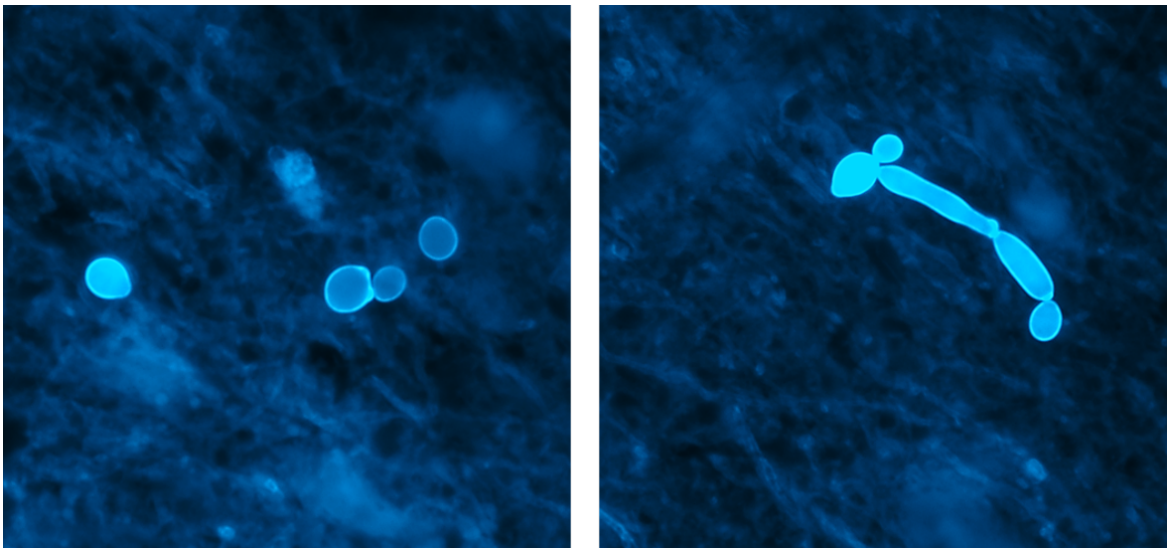

Appendix 12. *C. albicans* cells in both yeast and hyphal form in brain samples spiked with live *C. albicans* cultures are stained cyan by calcofluor white. No such yeast cells or hyphae were detected in brain sections of untreated GF or young or aged untreated SPF mice. This figure also appeared in Parker, James *et al.* (2022) and is reproduced with permission.

James, S.A., A. Parker, C. Purse, A. Telatin, D. Baker, S. Holmes, J. Durham, S.G.P. Funnell, and S.R. Carding, *The Cynomolgus Macaque Intestinal Mycobiome Is Dominated by the Kazachstania Genus and K. pintolopesii Species.* Journal of Fungi, 2022. **8**(10). DOI: 10.3390/jof8101054.

Parker, A., S. James, C. Purse, A. Brion, A. Goldson, A. Telatin, D. Baker, and S. Carding, *Absence of Bacteria Permits Fungal Gut-To-Brain Translocation and Invasion in Germfree Mice but Ageing Alone Does Not Drive Pathobiont Expansion in Conventionally Raised Mice.* Frontiers in Aging Neuroscience, 2022. **14**. DOI: 10.3389/fnagi.2022.828429.

James, S.A., A. Parker, C. Purse, A. Telatin, D. Baker, R. Evans, S. Holmes, S.G.P. Funnell, and S.R. Carding, *Draft Genome Sequence of a Primate Isolate of Kazachstania pintolopesii.* Mycopathologia, 2023. **188**(5): p. 821-823. DOI: 10.1007/s11046-023-00772-8.

Journal of *Fungi*

MDPI

Article

The Cynomolgus Macaque Intestinal Mycobiome Is Dominated by the *Kazachstania* Genus and *K. pintolopesii* Species

Steve A. James [1], Aimee Parker [1], Catherine Purse [1], Andrea Telatin [1], David Baker [1], Sandy Holmes [2], James Durham [2], Simon G. P. Funnell [1,2] and Simon R. Carding [1,3,*]

[1] Gut Microbes and Health, Quadram Institute Bioscience, Norwich Research Park, Norwich NR4 7UQ, UK
[2] UK Health Security Agency, Porton Down, Salisbury SP4 0JG, UK
[3] Norwich Medical School, University of East Anglia, Norwich NR4 7TJ, UK
* Correspondence: simon.carding@quadram.ac.uk

Abstract: The cynomolgus macaque, *Macaca fascicularis*, is a non-human primate (NHP) widely used in biomedical research as its genetics, immunology and physiology are similar to those of humans. They may also be a useful model of the intestinal microbiome as their prokaryome resembles that of humans. However, beyond the prokaryome relatively little is known about other constituents of the macaque intestinal microbiome including the mycobiome. Here, we conducted a region-by-region taxonomic survey of the cynomolgus intestinal mycobiota, from duodenum to distal colon, of sixteen captive animals of differing age (from young to old). Using a high-throughput ITS1 amplicon sequencing-based approach, the cynomolgus gut mycobiome was dominated by fungi from the Ascomycota phylum. The budding yeast genus *Kazachstania* was most abundant, with the thermotolerant species *K. pintolopesii* highly prevalent, and the predominant species in both the small and large intestines. This is in marked contrast to humans, in which the intestinal mycobiota is characterised by other fungal genera including *Candida* and *Saccharomyces*, and *Candida albicans*. This study provides a comprehensive insight into the fungal communities present within the captive cynomolgus gut, and for the first time identifies *K. pintolopesii* as a candidate primate gut commensal.

Keywords: mycobiome; gastrointestinal tract; cynomolgus macaque; non-human primate; fungi; pathobiont; yeast; *Kazachstania pintolopesii*

Citation: James, S.A.; Parker, A.; Purse, C.; Telatin, A.; Baker, D.; Holmes, S.; Durham, J.; Funnell, S.G.P.; Carding, S.R. The Cynomolgus Macaque Intestinal Mycobiome Is Dominated by the *Kazachstania* Genus and *K. pintolopesii* Species. *J. Fungi* **2022**, *8*, 1054. https://doi.org/10.3390/jof8101054

Academic Editors: David S. Perlin and Soo Chan Lee

Received: 27 July 2022
Accepted: 30 September 2022
Published: 8 October 2022

1. Introduction

The cynomolgus macaque (*Macaca fascicularis*), also known as the long-tailed or crab-eating macaque, is a cercopithecine primate indigenous to mainland Southeast Asia, as well as the maritime islands of Borneo, Java, and Sumatra, and islands of the Philippines. Like its close relative the rhesus macaque (*Macaca mulatta*), the cynomolgus macaque shares behavioural, immunological, and physiological similarities, as well as a close evolutionary relationship with humans, making this non-human primate (NHP) an important animal model for biomedical research [1]. These similarities appear to extend to the intestinal microbiota, with some bacterial taxa being common to both humans and non-human primates. The phyla Bacteroidetes, Firmicutes and Proteobacteria are prominent members of the prokaryome of both the human [2–4], and macaque gastrointestinal tract (GIT) [5–8]. Furthermore, a recent comparative metagenomic survey has shown that the gastrointestinal (GI) microbiota of cynomolgus macaques is more like that of humans than that of either mice or pigs [6]. Hence, these non-human primates represent a more suitable animal model for studying biological processes such as human ageing, and how age shapes the composition (and function) of the GI microbiota, and how this in turn affects GI physiology and host health [9,10].

Beyond the GI prokaryome however, relatively little is known of other constituents of the cynomolgus macaque GI microbiome and in particular, the fungal microbiome

(mycobiome). Whilst typically present in low abundance [11], enteric fungi nevertheless interact with both the prokaryome as well as host cells to alter host immunity, and can exacerbate the severity of several human diseases, including inflammatory bowel disease (IBD) and colorectal cancer [12–19]. A recent study characterising the oral and faecal mycobiomes of wild and captive Thai cynomolgus macaques, represents the first and only such study to date [20], revealing wild macaques have a significantly higher fungal alpha diversity than their captive counterparts. Overall, most fungi in the faecal (and oral) mycobiome, which is a surrogate of the intestinal mycobiome, of these primates belonged to the Ascomycota phylum, with the cynomolgus faecal mycobiota dominated by the budding yeast genus *Kazachstania*. Thermotolerant members of this genus and those belonging to the *K. telluris* species complex (incl. *K. bovina*, *K. pintolopesii*, *K. slooffiae* and *K. telluris*), are often found in the GIT of cows, pigs and rodents [21–26].

In the present study, we employed a high-throughput internal transcribed spacer region 1 (ITS1) amplicon sequencing approach, using an established ITS1 primer set [27,28], to conduct a comprehensive region-by-region taxonomic survey of the cynomolgus macaque intestinal mycobiota, from duodenum to distal colon, in a cohort of young, adult, and aged captive animals. Our goal was to gain a better insight into the composition and diversity of the fungal communities populating the GIT of this biomedically important NHP species, investigate how they change with age and identify candidate fungal GIT commensals.

2. Materials and Methods

2.1. Animals

Sixteen clinically healthy cynomolgus macaques were included in the study. The animals ranged from 4 to 20 years in age and were categorized into young (<7 years), adult (8 to 12 years), or aged (13 years or older) (see Table S1). All animals housed and bred at the UKHSA facility are derived from either Mauritian or South East Asia origin. No new animals have been introduced to these colonies since 2004. The colonies are licensed by the UK Home Office to breed, supply and use macaques for scientific research (Establishment license no. XBF9440B0). The breeding colonies are maintained to the highest standard in terms of animal welfare, health status, genetic profile, and behavioural compatibility, compliant with the UK Home Office Code of Practice for the Housing, and Care of Animals Bred, Supplied or Used for Scientific Purposes, 2014. This is achieved through facilities that provide an enriched and complex environment which meets the behavioural needs of the animals. The cynomolgus macaques are held in either harem breeding groups, or single sex, age matched holding groups. Their accommodation is a climate controlled, multiple room, solid floor caging system. Most groups also have access to an external 'extension' pen that is not climate controlled and open to the elements. All larger rooms have complex enrichment. Deep litter bedding is provided in the largest of these rooms. Water and a complete primate diet is provided ad lib. Fresh fruits, vegetables and pulses are provided daily as enrichment.

2.2. Sample Collection and DNA Extraction

All animals used in this study were required to be euthanized as part of normal colony management needs and requirements. Identified animals were initially sedated with ketamine hydrochloride at a dose of 10 mg/kg before exsanguination and euthanasia via intracardial injection with sodium pentobarbital at a dose of 80 mg/kg for elderly and 120–160 mg/kg for younger NHPs. All procedures were conducted under the authority and in compliance with a UK Homes Office project license. Luminal contents were collected from each GIT region of each animal and immediately frozen prior to transfer on dry ice to the laboratory for storage at −70 °C prior to processing. Total microbial DNA was extracted from ~200 mg of lumen content using the QIAamp PowerFecal Pro DNA kit (QIAGEN) and following the manufacturer's protocol. In addition, all samples were homogenized using a FastPrep-24 benchtop tissue homogenizer (MP Bio) at 6.0 m/s for 1 min. This step was included to aid fungal cell wall disruption to improve fungal DNA recovery. Extracted

DNA was quantified, and quality checked using the Qubit 3.0 fluorometer and associated Qubit dsDNA BR Assay Kit (Invitrogen). DNA samples were stored at −20 °C prior to further analysis.

2.3. ITS1 Amplification, Library Preparation and Sequencing

The fungal ITS1 region was amplified from 100 ng of template DNA by PCR using the ITS1F and ITS2 primer set [29,30], with each primer modified at the 5′ end to include an Illumina adapter tail using the following amplification conditions: 94 °C for 5 min; 35 cycles of 92 °C for 30 s, 55 °C for 30 s, and 72 °C for 45 s; and a final extension of 72 °C for 5 min. Amplification reactions were set up in duplicate for each faecal DNA sample, and positive and negative controls were also included in each PCR run (see Section 2.5). Following ITS1 PCR, a 0.7× SPRI purification using KAPA Pure Beads (Roche, Wilmington, MA, USA) was performed and the purified DNA was eluted in 20 µL of EB buffer (10 mM Tris-HCl). In a second PCR, library index primers were added using a Nextera XT Index Kit v2 (Illumina, Cambridge, UK) and amplified using the following conditions: 95 °C for 5 min: 10 cycles of 95 °C for 30 s, 55 °C for 30 s, and 72 °C for 30 s; and a final extension of 72 °C for 5 min. Following PCR, libraries were quantified using the Invitrogen™ Quant-iT dsDNA high sensitivity assay kit (Thermo Fisher, Waltham, MA, USA) and run on a FLUOstar Optima plate reader (BMG Labtech, Aylesbury, UK). Libraries were pooled following quantification in equal quantities. The final pool was SPRI cleaned using 0.7× KAPA Pure Beads, quantified on a Qubit 3.0 fluorometer and run on a High Sensitivity D1000 ScreenTape (Agilent Inc, Santa Clara, CA, USA) using the Agilent Tapestation 4200 to calculate the final library pool molarity. The pool was then run at a final concentration of 8 pM, on an Illumina MiSeq instrument using the MiSeq® v3 (2× 300 bp) Kit (Illumina) at at the Quadram Institute Bioscience, Norwich. The raw data were analysed using MiSeq reporter. A mean sequence depth of 123,710 reads/sample was achieved; samples with fewer than 10,000 filtered sequences were excluded from further analysis (see Table S2).

2.4. Mycobiome Characterization

Illumina MiSeq reads were analysed using the automated pipeline Dadaist2, a dedicated workflow for ITS profiling [31]. The quality profile of the raw reads (in FASTQ format) was assessed using SeqFu 1.9.3 [32], followed by primer removal using Cutadapt 3.5 [33] and quality filtering via Fastp 0.20.0 [34]. Locus-specific primers and conserved flanking regions were removed using ITSxpress [35]. The identification of representative sequences was performed using DADA2 [36], to produce a set of amplicon sequence variants (ASVs), and their taxonomic assignment was determined using the UNITE Fungal ITS database (release 8.3) [37]. The multiple alignment of the representative sequences was performed using ClustalO [38] and the guide tree was produced using FastTree [39]. Data normalization and diversity were produced using the Rhea scripts [40]. The output feature table, taxonomic classification, phylogeny and metafiles were exported and further analysed using PhyloSeq [41], MicrobiomeAnalyst [42], and the built-in plotting provided by Dadaist2 (via MultiQC [43]).

The raw Illumina ITS1 sequence data produced by the present study have been deposited at the European Nucleotide Archive (EBI), under the Project accession number PRJEB54860. Metadata and supporting scripts are available from the GitHub repository https://github.com/quadram-institute-bioscience/nhp-gut (22 July 2022).

2.5. Inclusion of Controls

Controls were included at each stage of the study. During DNA extraction, an empty bead-beating tube was included and treated the same as tubes containing luminal content and was quantified similarly. This extraction control was included in the initial amplicon PCR to assess that no ITS1 amplicon was produced. Negative (microbial DNA-free H_2O) and positive controls (50 ng *K. telluris* DNA) were included in each PCR run. Libraries were also prepared from the DNA extraction control and from single fungal species

DNAs (*C. albicans* and *K. telluris*) and were used as pipeline controls in the downstream bioinformatic analyses.

3. Results

3.1. Ascomycetous Fungi Dominate the Captive Cynomolgus Gastrointestinal Tract (GIT) Mycobiome

Fungal community profiling of the luminal contents of the duodenum to distal colon of a cohort of 16 captive macaques (NHP1 to NHP16) was performed using high-throughput internal transcribed spacer 1 (ITS1) amplicon sequencing and a DNA extraction protocol we developed and optimised to characterise the preterm infant GIT mycobiome [44]. The macaques ranged from 4 to 20 years in age and categorized into young (<7 years), adult (8 to 12 years), or aged (≥13 years) (Table S1). A total of 6,927,777 quality trimmed ITS1 reads were obtained from 56 lumen samples, ranging from 14,599 (NHP 1, distal colon) to 248,538 (NHP7, caecum), with a sample average of 123,710 reads (Table S2). Over 700 unique amplicon sequence variants (ASVs) were identified, although only 134 ASVs had a relative abundance of 0.01% or more. Collectively, this set of ASVs accounted for 99% of all ITS1 reads and was selected for subsequent taxonomic analyses to determine the composition and relative abundance of the fungal microbiota (mycobiota) in the separate intestinal sites of each macaque. The number of ASVs detected in each macaque ranged from 12 (NHP9) to 68 (NHP2), with over a quarter of ASVs specific to a single animal (36/134; 26.9%).

One hundred and thirty fungal taxa were classified to phylum level (97%), with the majority (95%) resolved to the genus level, and seventy-six of these (57%) to the species level. Four taxa could not be assigned at the phylum level or below and were classified as 'Unidentified' (Table S3). At the phylum level, >99% of fungi belonged to either Ascomycota or Basidiomycota, with a single taxon assigned to the Mucormycota subphylum (Figure 1a), with Ascomycota the predominant phylum accounting for 83% of all fungal reads (Figure 1a). In all, 85 taxa were ascomycetes, 44 were basidiomycetes, and one was identified as a mucormycete (*Mucor saturninus*) (Table S3).

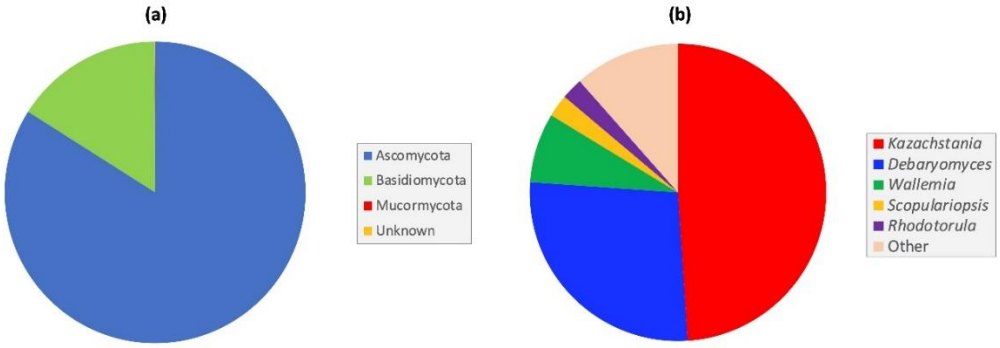

Figure 1. Most abundant fungi in the captive cynomolgus macaque GIT at (**a**) phylum, and (**b**) genus level.

At the genus level, *Kazachstania* and *Debaryomyces* were the dominant genera, accounting for 76% of all ITS1 reads (Figure 1b). Both ascomycetous genera were detected, with varying abundance, in all macaque samples, irrespective of age. Overall, *Kazachstania* was the predominant genus, accounting for 49.0% of all ITS1 reads, and was present in varying abundance in all intestinal samples. Other notable, but less abundant genera included *Wallemia* (7.6%), *Scopulariopsis* (2.4%), and *Rhodotorula* (2.3%) (Figure 1b). Among the ten most abundant genera found in the macaque GIT, seven were yeast genera (*Candida*, *Cystobasidium*, *Debaryomyces*, *Filobasidium*, *Kazachstania*, *Rhodotorula* and *Symmetrospora*) (Table S4).

3.2. Fungal Community Analysis and Identification of a Core NHP Gut Mycobiome

The 134 ASVs were also used to conduct a community analysis of the fungi present in each NHP age group. Specifically, to identify taxa (ASVs) that were specific to or found predominantly in a particular macaque age group, as well as those shared between two or more age groups. The analysis was restricted to those ASVs detected in at least 50% of animals in a particular age group (51/134; Table S5). A Venn diagram was produced from the resulting dataset (Figure 2). In total, seventeen ASVs were found predominantly in the young macaques, seven in the adults, and one in the aged animals. Interestingly, a core set of thirteen ASVs, representing twelve different fungal taxa, were shared between all three age groups (Figure 2). Using type strain ITS1 sequences, ten taxa were resolved to species level and were identified as *Candida albicans*, *C. parapsilosis*, *Cutaneotrichosporon cutaneum*, *Debaryomyces hansenii*, *Filobasidium uniguttulatum*, *Kazachstania pintolopesii*, *Pichia fermentans*, *Rhodotorula mucilaginosa*, *Vishniacozyma carnescens* and *Wallemia muriae* (Table S5). Amongst these fungi, only *C. albicans*, *C. parapsilosis*, *K. pintolopesii* and *P. fermentans* are known to grow at 37 °C (or above), and thus represent candidate cynomolgus gut commensals. Overall, two species, namely *D. hansenii* and *K. pintolopesii*, were found in every single macaque, irrespective of animal age (Table S5).

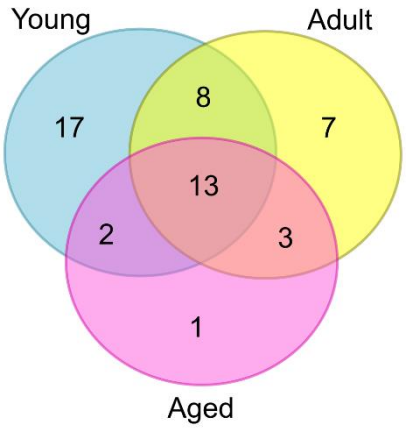

Figure 2. Venn diagram showing the number of fungal taxa (ASVs) found predominantly in each macaque age group (diagram produced using web-based software at: https://www.vanderpeerlab.org/?q=tools/venn-diagram (16 September 2022).

3.3. Kazachstania pintolopesii and Debaryomyces hansenii Are Prevalent throughout the Cynomolgus GIT

Within the enteric fungal communities, two yeast species, *Kazachstania pintolopesii* and *Debaryomyces hansenii* (*Candida famata*) dominated and were present throughout the macaque GIT. Both species were present in all macaque samples irrespective of age, and with varying abundance (Figure 3). Overall, *K. pintolopesii*, a thermotolerant yeast species [22] dominated most GIT samples of adult and aged macaques (72.7%), and caecum of one young macaque (NHP9) (Figure 3). In contrast, *D. hansenii*, a yeast widespread in nature [45], dominated the GIT of two young macaques (NHP11 and NHP12) and most intestinal samples (9/11) of three aged animals (NHP1, NHP7 and NHP10) (Figure 3).

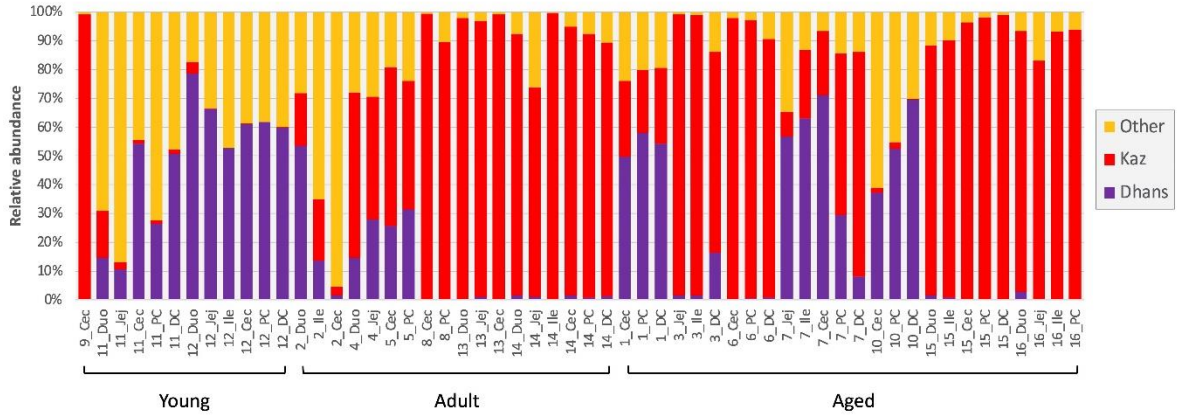

Figure 3. Prevalence and abundance of *K. pintolopesii* (Kaz) and *D. hansenii* (Dhans) in macaque GIT samples.

Although luminal samples could not be obtained from each intestinal region of every animal, samples (40) from nine animals (2 young, 3 adult and 4 aged) were used to conduct a comparative analysis of the most abundant fungi in the small and large intestine. Duodenum-, jejunum- and ileum-derived samples were pooled for taxonomic profiling of the small intestine, while the caecal and colon content samples were likewise pooled for the large intestine analysis. Overall, the two fungal profiles were broadly similar, with *K. pintolopesii* and *D. hansenii* being the most abundant species in both intestinal regions (Figure 4). Two other fungi present in both intestinal regions, but in lower abundance, were the basidiomycetes *Wallemia muriae* and *Rhodotorula mucilaginosa*. Notable differences between the two intestinal regions included the presence of *Scopulariopis brevicaulis*, a soil saprotroph, in the small intestine (Figure 4a), and presence of an *Aspergillus piperis*-like species in the large intestine (Figure 4b).

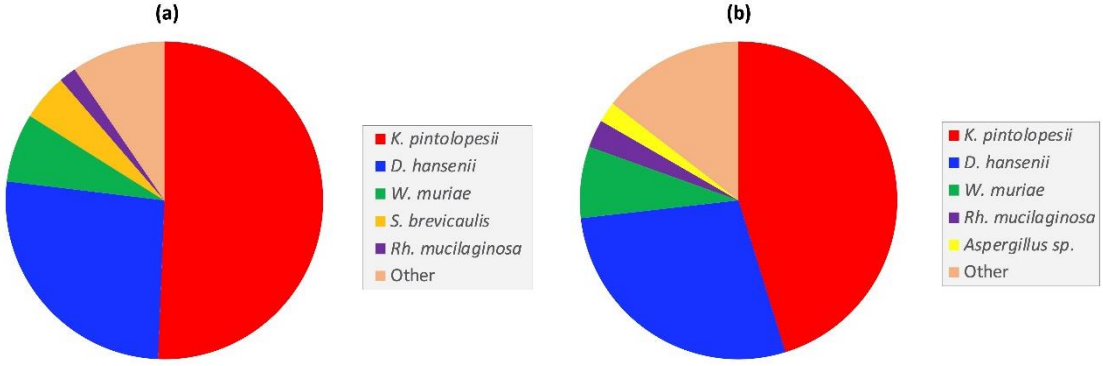

Figure 4. Comparison of the most abundant fungal taxa in the captive macaque (**a**) small- and, (**b**) large intestines.

The caecum provided the most samples (13/16 macaques) (Table S2), enabling a detailed comparative characterization of the fungal communities of this section of the macaque GIT. Three distinct profiles (C1–3) were identified based upon the presence and relative abundance of *D. hansenii* and *K. pintolopesii* (Figure 5). In the majority (C1; 7/13 macaques), *K. pintolopesii* was the predominant species. The second commonest (C2; 5/13) was *D. hansenii*, with a third profile (C3) characterized by the presence of basidiomycetous taxa (e.g., *Cystobasidium pallidum* and *Rh. mucilaginosa*). The C3 profile was atypical and restricted to a single adult female (NHP2) (Figure 5). In this animal, this species profile was caecum-specific, and was not replicated in either of the other two intestinal sites analysed, *D. hansenii* being predominant in the duodenum and *K. pintolopesii* in the ileum (Figure 3).

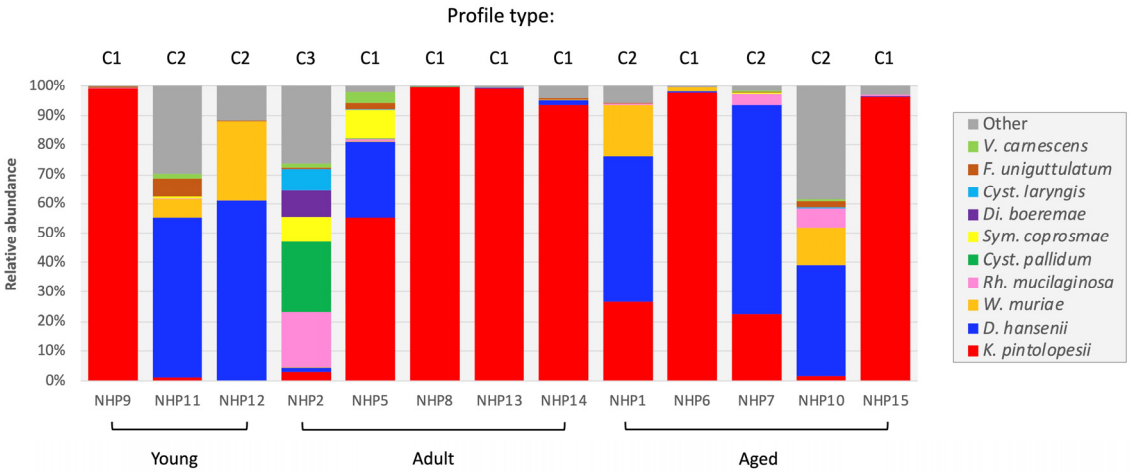

Figure 5. Comparison of the caecal mycobiome of 13 captive macaques of differing age (young, adult or aged).

3.4. Prevalence of Human-Associated Fungi

Candida such as *C. albicans* and *C. parapsilosis* are frequent members of the human GIT mycobiota [44,46–48]. In our captive macaque cohort this genus accounted for <1% of all fungal reads (Table S4). A total of eight *Candida* species were identified, including *C. albicans*, *C. parapsilosis* and *C. tropicalis*, all of which are fungal pathobionts [49]. In contrast, *C. anglica*, *C. freidrichii*, *C. oleophila*, *C. saitoana* and *C. sake* were considered GI transients based on their inability to grow above 30 °C [49].

Candida parapsilosis was the most prevalent *Candida* sp. and except for NHP8 was detected in all animals. *C. albicans*, while less prevalent (12/16) was present in all age groups (Figure 6). For those animals for which multiple intestinal samples were available (Table S6) these two *Candida* were not restricted to one region of the GIT (e.g., *C. albicans* in NHP14; *C. parapsilosis* in NHP12) (Figure 6). In contrast, *C. tropicalis* was detected in only 4 GIT samples of three aged animals (NHP7, NHP15 and NHP16; Figure 6).

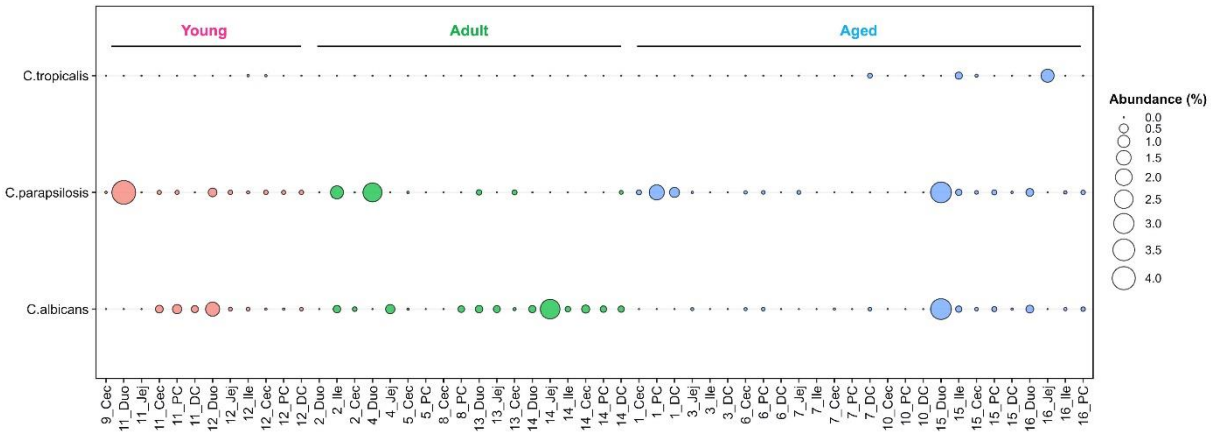

Figure 6. Prevalence and abundance of *Candida* pathobionts in the captive macaque GIT.

Saccharomyces cerevisiae frequently found in the human GIT [47], acquired via diet rather than by vertical transmission [50], accounted for less than 0.2% of all ITS1 reads in NHP samples. This species was detected in varying abundance (0.02 to 4.2%; Table S6) in only seven macaques; two young (NHP9 and NHP12), two adult (NHP2 and NHP13) and three aged (NHP7, NHP10 and NHP15). Like *Candida* spp., *S. cerevisiae* was not restricted to one GI region and in NHP12 was detected in all three small intestinal sites, as well as the caecum.

Debaryomyces hansenii, a food-borne (dairy) yeast commonly detected in the human GIT [45,47] was the most prevalent and abundant human-associated fungus identified in this study. This yeast was detected in all macaques and was present in moderate to high abundance in five macaques; two young (NHP11 and NHP12) and three aged (NHP1, NHP7 and NHP 10) (Figure 3; Table S6).

4. Discussion

Non-human primates, such as cynomolgus macaques represent important animal models in microbiome research, not least for the unprecedented opportunity they offer for gaining better insights into the biological processes (e.g., ageing) and factors (e.g., diet) that influence and shape the human microbiome. To date, much of this research has concentrated on the NHP prokaryome, with relatively little attention given to the other constituents, including intestinal fungi which are typically present in the GIT in much lower abundance than their bacterial counterparts [11]. To begin addressing this shortfall, we used a high-throughput ITS1 amplicon sequencing approach, that we first developed and used to profile the preterm infant GIT mycobiome [44], to characterize the enteric mycobiota in lumen contents collected from six intestinal sites of a cohort of captive macaques of differing age (i.e., from young to old). The results revealed that the cynomolgus GIT, from duodenum to distal colon, is populated by more than 50 genera, almost exclusively from the Ascomycota and Basidiomycota phyla, with Ascomycota the predominant phylum. This dominance, in both the macaque small- and large intestine, was largely due to the presence of taxa from the budding yeast genera *Debaryomyces* and *Kazachstania*, which together accounted for >70% of fungal reads in each intestinal region.

Kazachstania is the predominant genus in our captive macaque cohort, accounting for >72% of all fungal reads, and was found with varying abundance in every animal, and across all age groups. The dominance of this ascomycetous genus was due almost exclusively to one species, *K. pintolopesii*. While *K. telluris*, a close relative, was found in a limited number of macaques from each age group, it was typically present in very low abundance (<1.0%). In contrast, *K. pintolopesii* was highly prevalent throughout the small- and large intestines of each macaque. Furthermore, it was frequently the predominant fungus, and in a third of all GIT samples, *K. pintolopesii* abundancy exceeds 90%.

Kazachstania is a large and diverse yeast genus comprising more than 40 species [51]. Within the genus, *K. pintolopesii* is closely related to *K. bovina*, *K. heterogenica*, *K. slooffiae* and *K. telluris*. Collectively, these five comprise the *K. telluris* species complex, a phylogenetically distinct group of yeasts characterized by their ability to grow at elevated temperature (i.e., 37 °C) [22]. Some representatives of *K. pintolopesii* can survive and grow at temperatures as high as 42 °C [22], a physiological trait rare in yeasts. To date, most strains from this thermotolerant species complex have been isolated from the nasal passages and GIT of birds and mammals [21–25]. Prior to this study, the principal hosts of *K. pintolopesii* appeared to be mice (captive and wild) and rats [21,22,25] with the only member of the *K. telluris* species complex previously found in NHPs being *K. heterogenica*, which was limited to a single strain from a young female white-handed gibbon (*Hylobates lar*) [52].

Debaryomyces hansenii is also highly prevalent in the captive macaque cohort. Distributed throughout the cynomolgus GIT it was the predominant fungus in both the young and elderly animals, albeit to a lesser extent than *K. pintolopesii*. Despite having a lower optimum growth temperature than *K. pintolopesii* [22,45], this halotolerant food-borne (dairy) yeast is a frequent member of the human GI mycobiome [44,48,53,54] and can be cultured from human faeces, and is associated with ulcerative colitis (UC), Crohn's Disease (CD) and colorectal cancer [19,55,56]. *D. hansenii* produces mycocins that kill *C. albicans* [57] and it was interesting to note that in three macaques where this yeast was in high abundance, *C. albicans* was absent. However, given the low abundance (<1.0%) of *C. albicans* in the macaque GIT it is difficult to draw any significance from these observations.

The human GIT like that of the cynomolgus macaque, is largely dominated by fungi from the Ascomycota and Basidiomycota phyla [20,46,48,53,58,59]. However, despite this

similarity, our study has revealed distinct differences at both the genus and species levels between the intestinal mycobiota in humans and cynomolgus macaques. Most notable is the predominance of the *Kazachstania* genus in the cynomolgus gut, with *K. pintolopesii*, a fungus rarely found in humans, the dominant species throughout the cynomolgus GIT (this study; [20]). In contrast, *Candida* and *Saccharomyces* are prominent genera in the human intestinal mycobiome [46,48,53,58,59], often attributed to the presence of the fungal pathobiont *C. albicans* and the food-borne yeast *S. cerevisiae* [46,48,53,58,59]. Despite being rare in the environment [60], *C. albicans* is a common commensal of both the human GIT and oral cavity, and of the vaginal mycobiome [44,48,53,61–63]. Although human-associated fungi were detected in the cynomolgus GIT, most in low abundance (e.g., *C. albicans, C. parapsilosis* and *S. cerevisiae*) with the exception of *D. hansenii*, which was highly prevalent in the macaque cohort, and the predominant intestinal fungus in some of the young and aged animals. In addition to its use as a dairy yeast [45], *D. hansenii* is ubiquitous in nature, and frequently isolated from soil [45,64]. Thus, the presence of this ascomycete in the cynomolgus GIT may be of environmental origin but not from the primate diet. In contrast, the presence of *P. fermentans*, which was detected in many of the macaques, albeit in low abundance, is most likely due to diet. This yeast is frequently found in food and fruit juices [65], and so was most likely acquired from the daily supplement of fresh fruits and vegetables given to the animals. Two basidiomycetous yeasts that were also frequently detected were *Cutaneotrichosporon cutaneum* and *Filobasidium uniguttulatum*. *Cut. cutaneum*, like other members of this genus, is a common colonizer of animal skin [66], and its presence and prevalence could be as the result of skin-oral contact (i.e., grooming) within the colony. Indeed, in Thai cynomolgus macaque, Sawaswong and colleagues found *Cutaneotrichosporon* to be the prominent fungal genus of the oral microbiome of captive macaques [20], providing further support for social grooming as an additional route of fungal acquisition and transmission between primates. *F. uniguttulatum*, like *Cut. cutaneum*, is unable to grow at elevated temperature (i.e., 37 °C), and although its natural habitat remains unknown, it has been isolated previously from animal bedding [67]. Thus, given that the macaques are provided with deep litter bedding this may explain why this basidiomycete was detected in many of the animals. In addition to diet and environment, other factors that may contribute to help shape the enteric fungal communities in cynomolgus macaques and humans, include differing GI physiology and normal core body temperature (i.e., humans, 37.0 °C; macaques, 37.0 to 39.5 °C) [68].

The persistence of *K. pintolopesii* throughout the GIT in young, adult as well as elderly cynomolgus macaques coupled with an innate ability to grow at and above 37 °C [21], suggests that *K. pintolopesii* represents a plausible primate GI commensal. If proven then this raises the question as to what role it performs in the cynomolgus GIT. Insights into its potential role(s) may come from *K. slooffiae*, a close relative, and the predominant fungus in the post-weaning porcine gut [21,23,24,69]. This member of the *K. telluris* species complex [21,22] provides amino acids as an energy source for microbial and piglet growth and is an important source of health promoting micronutrients including vitamin C and formic acid [23,26,69]. Furthermore, a strong (positive) correlation has been identified between *K. slooffiae* and beneficial intestinal bacteria, including *Lactobacillus* and *Prevotella* [24]. In the human GIT, *C. albicans* can interact directly with *Lactobacillus* spp. [70,71], leading to the proposal that *K. slooffiae* may behave similarly to commensal *Candida* spp. in humans [24]. Given the paucity of human-associated *Candida* (e.g., *C. albicans* and *C. parapsilosis*) in these macaques, coupled with the prevalence and abundance of *Prevotella* and *Lactobacillus* spp., including *L. acidophilus* and *L. reuteri*, in the cynomolgus GIT [6], it is conceivable that *K. pintolopesii* performs an equivalent role to that of *K. slooffiae* in pigs. However, this remains to be established in future cynomolgus microbiome studies encompassing both the mycobiome and bacteriome.

Finally, *C. albicans* is a common member of the normal human microbiome, and in healthy individuals, it can remain a lifelong benign commensal. However, under certain circumstances (e.g., immunosuppression, broad-spectrum antibiotic treatment) it can cause

infections ranging from superficial infections of mucosal surfaces to life-threatening systemic candidiasis [62,72,73]. *C. albicans* outgrowth in the human GIT can also compound pre-existing CD and UC [18,74]. Thus, given the pathobiont nature of *C. albicans* (in humans), future research is needed to investigate the pathogenic potential of *K. pintolopesii* in the cynomolgus macaque, and factors that may trigger a transitional shift from harmless commensal to pathogen. This is especially pertinent given that *K. pintolopesii* causes gastric infections in laboratory mice, which can prove fatal [21]. Moreover, *K. heterogenica*, another member of the *K. telluris* species complex and close relative of *K. pintolopesii* [22], can exacerbate *Helicobacter suis*-associated gastric infection in Mongolian gerbils [75], and has been linked to a fatal infection in a young female white-handed gibbon, the first documented case of its kind [52].

5. Conclusions

Our study identified a diverse array of fungi throughout the cynomolgus GIT, with Ascomycota and Basidiomycota the dominant phyla. A characteristic feature is the prominence of the ascomycetous yeast *K. pintolopesii*, a member of the *K. telluris* species complex, which we propose represents a credible primate intestinal commensal. This study paves the way for further investigations, firstly to confirm that *K. pintolopesii* is a primate GIT commensal, and if proven then establish what function it performs in the cynomolgus macaque GIT.

Supplementary Materials: The following supporting information can be downloaded at: https://www.mdpi.com/article/10.3390/jof8101054/s1, Table S1: Details of the captive cynomolgus macaques included in this study, Table S2: Quality-trimmed fungal ITS1 reads per GIT luminal sample, Table S3: Fungal ASVs with a relative abundance of 0.01% or more, Table S4: Most abundant fungal genera in the captive macaque GIT, Table S5: Fungal community analysis. ASVs (fungal taxa) specific/predominantly found in one or more NHP age groups, Table S6:Prevalence and abundance of human-associated fungi in the captive macaque GIT.

Author Contributions: Conceptualization, S.R.C., S.G.P.F., A.P. and S.A.J.; methodology, S.A.J., A.P., C.P., A.T., S.H., J.D. and D.B.; software, A.T.; validation, S.A.J. and A.T.; formal analysis, A.T. and S.A.J.; resources, S.H., J.D. and S.G.P.F.; data curation, A.T.; writing—original draft preparation, S.A.J.; writing—review and editing, S.R.C. and S.A.J.; supervision, S.R.C.; project administration, S.R.C.; funding acquisition, S.R.C. All authors have read and agreed to the published version of the manuscript.

Funding: The authors gratefully acknowledge the support of the Biotechnology and Biological Sciences Research Council (BBSRC), this research was funded by BBSRC Core Capability Grant BB/CCG1860/1, and BBSRC Institute Strategic Programme Grant Gut Microbes and Health (BB/R012490/1) and constituent project BBS/E/F/000PR10353. Additional support was provided by a BBSRC NRP DTP Studentship Grant BB/T008717/1 (C.P.).

Institutional Review Board Statement: All procedures were conducted under the authority and in compliance with UK Home Office project license number PD28B8ED5 and were approved by Porton Committee for the Animal Welfare and Ethical Review Body.

Data Availability Statement: The raw Illumina ITS1 sequence data used in this study have been deposited at the European Nucleotide Archive (EBI), under the Project accession number PRJEB54860. Metadata and supporting scripts are available from the GitHub repository https://github.com/quadram-institute-bioscience/nhp-gut, accessed on 22 July 2022.

Acknowledgments: The authors would like to thank Sumeet Tiwari from the Quadram Institute Bioscience for his rendering of Figure 5. We thank all staff of the specialized UK Health Security Agency (UKHSA) primate facility at Porton and in particular, Caroline Cruttwell, for animal husbandry, and ensuring animal welfare and for maximizing the use of tissues that would otherwise have been discarded. UKHSA also acknowledges funding from the UK Department of Health for funding for the maintenance and operation of the primate facility. Bioinformatics analyses were performed on CLIMB-BIG-DATA computing infrastructure (funded by the UK's Medical Research

Council through grant MR/T030062/1) and the Norwich BioScience Institute Partnership "Research Computing" team (for High Performance Computing resources).

Conflicts of Interest: The authors declare no conflict of interest. The funders had no role in the design of the study; in the collection, analyses, or interpretation of data; in the writing of the manuscript, or in the decision to publish the results.

References

1. Carlsson, H.E.; Schapiro, S.J.; Farah, I.; Hau, J. Use of primates in research: A global overview. *Am. J. Primatol.* **2004**, *63*, 225–237. [CrossRef] [PubMed]
2. Eckburg, P.B.; Bik, E.M.; Bernstein, C.N.; Purdom, E.; Dethlefsen, L.; Sargent, M.; Gill, S.R.; Nelson, K.E.; Relman, D.A. Diversity of the human intestinal microbial flora. *Science* **2005**, *308*, 1635–1638. [CrossRef] [PubMed]
3. Qin, J.J.; Li, R.Q.; Raes, J.; Arumugam, M.; Burgdorf, K.S.; Manichanh, C.; Nielsen, T.; Pons, N.; Levenez, F.; Yamada, T.; et al. A human gut microbial gene catalogue established by metagenomic sequencing. *Nature* **2010**, *464*, 59–65. [CrossRef] [PubMed]
4. Vemuri, R.; Gundamaraju, R.; Shastri, M.D.; Shukla, S.D.; Kalpurath, K.; Ball, M.; Tristram, S.; Shankar, E.M.; Ahuja, K.; Eri, R. Gut Microbial Changes, Interactions, and Their Implications on Human Lifecycle: An Ageing Perspective. *Biomed Res. Int.* **2018**, *2018*, 4178607. [CrossRef]
5. Yasuda, K.; Oh, K.; Ren, B.Y.; Tickle, T.L.; Franzosa, E.A.; Wachtman, L.M.; Miller, A.D.; Westmoreland, S.V.; Mansfield, K.G.; Vallender, E.J.; et al. Biogeography of the Intestinal Mucosal and Lumenal Microbiome in the Rhesus Macaque. *Cell Host Microbe* **2015**, *17*, 385–391. [CrossRef]
6. Li, X.P.; Liang, S.S.; Xia, Z.K.; Qu, J.; Liu, H.; Liu, C.; Yang, H.M.; Wang, J.; Madsen, L.; Hou, Y.; et al. Establishment of a Macaca fascicularis gut microbiome gene catalog and comparison with the human, pig, and mouse gut microbiomes. *Gigascience* **2018**, *7*, giy100. [CrossRef]
7. Cui, Y.F.; Wang, F.J.; Yu, L.; Ye, H.H.; Yang, G.B. Metagenomic comparison of the rectal microbiota between rhesus macaques (*Macaca mulatta*) and cynomolgus macaques (*Macaca fascicularis*). *Zool. Res.* **2019**, *40*, 89–93. [CrossRef] [PubMed]
8. Chen, Z.G.; Yeoh, Y.K.; Hui, M.M.; Wong, P.Y.; Chan, M.C.W.; Ip, M.; Yu, J.; Burk, R.D.; Chan, F.K.L.; Chan, P.K.S. Diversity of macaque microbiota compared to the human counterparts. *Sci. Rep.* **2018**, *8*, 15573. [CrossRef]
9. Didier, E.S.; MacLean, A.G.; Mohan, M.; Didier, P.J.; Lackner, A.A.; Kuroda, M.J. Contributions of Nonhuman Primates to Research on Aging. *Vet. Pathol.* **2016**, *53*, 277–290. [CrossRef]
10. Duan, J.J.; Yin, B.M.; Li, W.; Chai, T.J.; Liang, W.W.; Huang, Y.; Tan, X.M.; Zheng, P.; Wu, J.; Li, Y.F.; et al. Age-related changes in microbial composition and function in cynomolgus macaques. *Aging* **2019**, *11*, 12080–12096. [CrossRef]
11. Huffnagle, G.B.; Noverr, M.C. The emerging world of the fungal microbiome. *Trends Microbiol.* **2013**, *21*, 334–341. [CrossRef] [PubMed]
12. Underhill, D.M.; Lliev, L.D. The mycobiota: Interactions between commensal fungi and the host immune system. *Nat. Rev. Immunol.* **2014**, *14*, 405–416. [CrossRef] [PubMed]
13. Iliev, I.D.; Funari, V.A.; Taylor, K.D.; Nguyen, Q.; Reyes, C.N.; Strom, S.P.; Brown, J.; Becker, C.A.; Fleshner, P.R.; Dubinsky, M.; et al. Interactions Between Commensal Fungi and the C-Type Lectin Receptor Dectin-1 Influence Colitis. *Science* **2012**, *336*, 1314–1317. [CrossRef] [PubMed]
14. Luan, C.G.; Xie, L.L.; Yang, X.; Miao, H.F.; Lv, N.; Zhang, R.F.; Xiao, X.; Hu, Y.F.; Liu, Y.L.; Wu, N.; et al. Dysbiosis of Fungal Microbiota in the Intestinal Mucosa of Patients with Colorectal Adenomas. *Sci. Rep.* **2015**, *5*, 7980. [CrossRef]
15. Suhr, M.J.; Hallen-Adams, H.E. The human gut mycobiome: Pitfalls and potentials-a mycologist's perspective. *Mycologia* **2015**, *107*, 1057–1073. [CrossRef]
16. Hoarau, G.; Mukherjee, P.K.; Gower-Rousseau, C.; Hager, C.; Chandra, J.; Retuerto, M.A.; Neut, C.; Vermeire, S.; Clemente, J.; Colombel, J.F.; et al. Bacteriome and Mycobiome Interactions Underscore Microbial Dysbiosis in Familial Crohn's Disease. *Mbio* **2016**, *7*, e01250-16. [CrossRef]
17. Iliev, I.D.; Leonardi, I. Fungal dysbiosis: Immunity and interactions at mucosal barriers. *Nat. Rev. Immunol.* **2017**, *17*, 635–646. [CrossRef]
18. Sokol, H.; Leducq, V.; Aschard, H.; Pham, H.P.; Jegou, S.; Landman, C.; Cohen, D.; Liguori, G.; Bourrier, A.; Nion-Larmurier, I.; et al. Fungal microbiota dysbiosis in IBD. *Gut* **2017**, *66*, 1039–1048. [CrossRef]
19. Jain, U.; Ver Heul, A.M.; Xiong, S.S.; Gregory, M.H.; Demers, E.G.; Kern, J.T.; Lai, C.W.; Muegge, B.D.; Barisas, D.A.G.; Leal-Ekman, J.S.; et al. Debaryomyces is enriched in Crohn's disease intestinal tissue and impairs healing in mice. *Science* **2021**, *371*, 1154–1159. [CrossRef]
20. Sawaswong, V.; Chanchaem, P.; Khamwut, A.; Praianantathavorn, K.; Kemthong, T.; Malaivijitnond, S.; Payungporn, S. Oral-fecal mycobiome in wild and captive cynomolgus macaques (*Macaca fascicularis*). *Fungal Genet. Biol.* **2020**, *144*, 103468. [CrossRef]
21. Kurtzman, C.P.; Robnett, C.J.; Ward, J.M.; Brayton, C.; Gorelick, P.; Walsh, T.J. Multigene phylogenetic analysis of pathogenic Candida species in the Kazachstania (Arxiozyma) telluris complex and description of their ascosporic states as *Kazachstania bovina* sp nov., *K-heterogenica* sp nov., *K-pintolopesii* sp nov., and *K-slooffiae* sp nov. *J. Clin. Microbiol.* **2005**, *43*, 101–111. [CrossRef] [PubMed]

22. Vaughan-Martini, A.; Lachance, M.-A.; Kurtzman, C.P. Kazachstania Zubkova (1971). In *The Yeasts: A Taxonomic Study*, 5th ed.; Kurtzman, C.P., Fell, J.W., Boekhout, T., Eds.; Elsevier: Amsterdam, The Netherlands, 2011; Volume 2, pp. 439–470.
23. Urubschurov, V.; Busing, K.; Freyer, G.; Herlemann, D.P.R.; Souffrant, W.B.; Zeyner, A. New insights into the role of the porcine intestinal yeast, Kazachstania slooffiae, in intestinal environment of weaned piglets. *FEMS Microbiol. Ecol.* **2017**, *93*, fiw245. [CrossRef] [PubMed]
24. Arfken, A.M.; Frey, J.F.; Ramsay, T.G.; Summers, K.L. Yeasts of Burden: Exploring the Mycobiome-Bacteriome of the Piglet GI Tract. *Front. Microbiol.* **2019**, *10*, 2286. [CrossRef] [PubMed]
25. Bendova, B.; Pialek, J.; Dureje, L.; Schmiedova, L.; Cizkova, D.; Martin, J.F.; Kreisinger, J. How being synanthropic affects the gut bacteriome and mycobiome: Comparison of two mouse species with contrasting ecologies. *BMC Microbiol.* **2020**, *20*, 194. [CrossRef]
26. Summers, K.L.; Frey, J.F.; Arfken, A.M. Characterization of Kazachstania slooffiae, a Proposed Commensal in the Porcine Gut. *J. Fungi* **2021**, *7*, 146. [CrossRef]
27. Huseyin, C.E.; Rubio, R.C.; O'Sullivan, O.; Cotter, P.D.; Scanlan, P.D. The Fungal Frontier: A Comparative Analysis of Methods Used in the Study of the Human Gut Mycobiome. *Front. Microbiol.* **2017**, *8*, 1432. [CrossRef]
28. Thompson, L.R.; Sanders, J.G.; McDonald, D.; Amir, A.; Ladau, J.; Locey, K.J.; Prill, R.J.; Tripathi, A.; Gibbons, S.M.; Ackermann, G.; et al. A communal catalogue reveals Earth's multiscale microbial diversity. *Nature* **2017**, *551*, 457–463. [CrossRef]
29. White, T.J.; Bruns, T.D.; Lee, S.L.; Taylor, J.W. Amplification and direct sequencing of fungal ribosomal RNA genes for phylogenetics. In *PCR Protocols: A Guide to Methods and Applications*; Innis, M.A., Gelfand, D.H., Sninsky, J.J., Eds.; Academic Press: San Diego, CA, USA, 1990; pp. 315–322.
30. Gardes, M.; Bruns, T.D. ITS primers with enhanced specificity for basidiomycetes–application to the identification of mycorrhizae and rusts. *Mol. Ecol.* **1993**, *2*, 113–118. [CrossRef]
31. Ansorge, R.; Birolo, G.; James, S.A.; Telatin, A. Dadaist2: A Toolkit to Automate and Simplify Statistical Analysis and Plotting of Metabarcoding Experiments. *Int. J. Mol. Sci.* **2021**, *22*, 5309. [CrossRef]
32. Telatin, A.; Fariselli, P.; Birolo, G. SeqFu: A Suite of Utilities for the Robust and Reproducible Manipulation of Sequence Files. *Bioengineering* **2021**, *8*, 59. [CrossRef]
33. Martin, M. Cutadapt removes adapter sequences from high-throughput sequencing reads. *EMBnet. J.* **2011**, *17*, 10–12. [CrossRef]
34. Chen, S.F.; Zhou, Y.Q.; Chen, Y.R.; Gu, J. fastp: An ultra-fast all-in-one FASTQ preprocessor. *Bioinformatics* **2018**, *34*, 884–890. [CrossRef] [PubMed]
35. Rivers, A.R.; Weber, K.C.; Gardner, T.G.; Liu, S.; Armstrong, S. ITSxpress: Software to rapidly trim internally transcribed spacer sequences with quality scores for marker gene analysis. *F1000Research* **2018**, *7*, 1418. [CrossRef] [PubMed]
36. Callahan, B.J.; McMurdie, P.J.; Rosen, M.J.; Han, A.W.; Johnson, A.J.A.; Holmes, S.P. $DADA_2$: High-resolution sample inference from Illumina amplicon data. *Nat. Methods* **2016**, *13*, 581–583. [CrossRef]
37. Nilsson, R.H.; Larsson, K.H.; Taylor, A.F.S.; Bengtsson-Palme, J.; Jeppesen, T.S.; Schigel, D.; Kennedy, P.; Picard, K.; Glockner, F.O.; Tedersoo, L.; et al. The UNITE database for molecular identification of fungi: Handling dark taxa and parallel taxonomic classifications. *Nucleic Acids Res.* **2019**, *47*, D259–D264. [CrossRef]
38. Sievers, F.; Higgins, D.G. The Clustal Omega Multiple Alignment Package. In *Multiple Sequence Alignment: Methods and Protocols*; Katoh, K.W., Walker, J.M., Eds.; Methods in Molecular Biology; Humana Press: Totowa, NJ, USA, 2021; Volume 2231, pp. 3–16.
39. Price, M.N.; Dehal, P.S.; Arkin, A.P. FastTree: Computing Large Minimum Evolution Trees with Profiles instead of a Distance Matrix. *Mol. Biol. Evol.* **2009**, *26*, 1641–1650. [CrossRef]
40. Lagkouvardos, I.; Fischer, S.; Kumar, N.; Clavel, T. Rhea: A transparent and modular R pipeline for microbial profiling based on 16S rRNA gene amplicons. *Peerj* **2017**, *5*, e2836. [CrossRef]
41. McMurdie, P.J.; Holmes, S. phyloseq: An R Package for Reproducible Interactive Analysis and Graphics of Microbiome Census Data. *PLoS ONE* **2013**, *8*, e61217. [CrossRef]
42. Dhariwal, A.; Chong, J.; Habib, S.; King, I.L.; Agellon, L.B.; Xia, J.G. MicrobiomeAnalyst: A web-based tool for comprehensive statistical, visual and meta-analysis of microbiome data. *Nucleic Acids Res.* **2017**, *45*, W180–W188. [CrossRef]
43. Ewels, P.; Magnusson, M.; Lundin, S.; Kaller, M. MultiQC: Summarize analysis results for multiple tools and samples in a single report. *Bioinformatics* **2016**, *32*, 3047–3048. [CrossRef]
44. James, S.A.; Phillips, S.; Telatin, A.; Baker, D.; Ansorge, R.; Clarke, P.; Hall, L.J.; Carding, S.R. Preterm Infants Harbour a Rapidly Changing Mycobiota That Includes Candida Pathobionts. *J. Fungi* **2020**, *6*, 273. [CrossRef] [PubMed]
45. Suzuki, M.; Prasad, G.S.; Kurtzman, C.P. Debaryomyces Lodder & Kreger-van Rij (1952). In *The Yeasts: A Taxonomic Study*, 5th ed.; Kurtzman, C.P., Fell, J.W., Boekhout, T., Eds.; Elsevier: Amsterdam, The Netherlands, 2011; Volume 2, pp. 361–372.
46. Hoffmann, C.; Dollive, S.; Grunberg, S.; Chen, J.; Li, H.Z.; Wu, G.D.; Lewis, J.D.; Bushman, F.D. Archaea and Fungi of the Human Gut Microbiome: Correlations with Diet and Bacterial Residents. *PLoS ONE* **2013**, *8*, e66019. [CrossRef]
47. Hallen-Adams, H.E.; Kachman, S.D.; Kim, J.; Legge, R.M.; Martinez, I. Fungi inhabiting the healthy human gastrointestinal tract: A diverse and dynamic community. *Fungal Ecol.* **2015**, *15*, 9–17. [CrossRef]
48. Nash, A.K.; Auchtung, T.A.; Wong, M.C.; Smith, D.P.; Gesell, J.R.; Ross, M.C.; Stewart, C.J.; Metcalf, G.A.; Muzny, D.M.; Gibbs, R.A.; et al. The gut mycobiome of the Human Microbiome Project healthy cohort. *Microbiome* **2017**, *5*, 153. [CrossRef]
49. Lachance, M.-A.; Boekhout, T.; Scorzetti, G.; Fell, J.W.; Kurtzman, C.P. Candida Berkhout (1923). In *The Yeasts: A Taxonomic Study*, 5th ed.; Kurtzman, C.P., Fell, J.W., Boekhout, T., Eds.; Elsevier: Amsterdam, The Netherlands, 2011; Volume 2, pp. 987–1278.

50. Bliss, J.M.; Basavegowda, K.P.; Watson, W.J.; Sheikh, A.U.; Ryan, R.M. Vertical and horizontal transmission of Candida albicans in very low birth weight infants using DNA fingerprinting techniques. *Pediatr. Infect. Dis. J.* **2008**, *27*, 231–235. [CrossRef] [PubMed]
51. Ke, T.; Zhai, Y.C.; Yan, Z.L.; Hui, F.L. *Kazachstania jinghongensis* sp. nov. and *Kazachstania menglunensis* f.a., sp. nov., two yeast species isolated from rotting wood. *Int. J. Syst. Evol. Microbiol.* **2019**, *69*, 3623–3628. [CrossRef]
52. Alvarez-Perez, S.; Mateos, A.; Dominguez, L.; Martinez-Nevado, E.; Rodriguez-Bertos, A.; Blanco, J.L.; Garcia, M.E. First isolation of the anamorph of Kazachstania heterogenica from a fatal infection in a primate host. *Med. Mycol.* **2012**, *50*, 193–196. [CrossRef]
53. Hallen-Adams, H.E.; Suhr, M.J. Fungi in the healthy human gastrointestinal tract. *Virulence* **2017**, *8*, 352–358. [CrossRef]
54. Schei, K.; Avershina, E.; Øien, T.; Rudi, K.; Follestad, T.; Salamati, S.; Ødegard, R.A. Early gut mycobiota and mother-offspring transfer. *Microbiome* **2017**, *5*, 107. [CrossRef]
55. Mar, J.S.; LaMere, B.J.; Lin, D.L.; Levan, S.; Nazareth, M.; Mahadevan, U.; Lynch, S.V. Disease Severity and Immune Activity Relate to Distinct Interkingdom Gut Microbiome States in Ethnically Distinct Ulcerative Colitis Patients. *Mbio* **2016**, *7*, e01072-16. [CrossRef]
56. Coker, O.O.; Nakatsu, G.; Dai, R.Z.; Wu, W.K.K.; Wong, S.H.; Ng, S.C.; Chan, F.K.L.; Sung, J.J.Y.; Yu, J. Enteric fungal microbiota dysbiosis and ecological alterations in colorectal cancer. *Gut* **2019**, *68*, 654–662. [CrossRef] [PubMed]
57. Banjara, N.; Nickerson, K.W.; Suhr, M.J.; Hallen-Adams, H.E. Killer toxin from several food-derived Debaryomyces hansenii strains effective against pathogenic Candida yeasts. *Int. J. Food Microbiol.* **2016**, *222*, 23–29. [CrossRef] [PubMed]
58. Sam, Q.H.; Chang, M.W.; Chai, L.Y.A. The Fungal Mycobiome and Its Interaction with Gut Bacteria in the Host. *Int. J. Mol. Sci.* **2017**, *18*, 330. [CrossRef] [PubMed]
59. Raimondi, S.; Amaretti, A.; Gozzoli, C.; Simone, M.; Righini, L.; Candeliere, F.; Brun, P.; Ardizzoni, A.; Colombari, B.; Paulone, S.; et al. Longitudinal Survey of Fungi in the Human Gut: ITS Profiling, Phenotyping, and Colonization. *Front. Microbiol.* **2019**, *10*, 1575. [CrossRef]
60. Bensasson, D.; Dicks, J.; Ludwig, J.M.; Bond, C.J.; Elliston, A.; Roberts, I.N.; James, S.A. Diverse Lineages of Candida albicans Live on Old Oaks. *Genetics* **2019**, *211*, 277–288. [CrossRef]
61. Sobel, J.D. Vulvovaginal candidosis. *Lancet* **2007**, *369*, 1961–1971. [CrossRef]
62. Brown, G.D.; Denning, D.W.; Gow, N.A.R.; Levitz, S.M.; Netea, M.G.; White, T.C. Hidden Killers: Human Fungal Infections. *Sci. Transl. Med.* **2012**, *4*, 165rv13. [CrossRef]
63. Moran, G.; Coleman, D.; Sullivan, D. An introduction to the medically important Candida species. In *Candida and Candidiasis*, 2nd ed.; Calderone, R.A., Clancy, C.J., Eds.; ASM Press: Washington, DC, USA, 2012; pp. 11–25.
64. Breuer, U.; Harms, H. Debaryomyces hansenii—An extremophilic yeast with biotech nological potential. *Yeast* **2006**, *23*, 415–437. [CrossRef]
65. Kurtzman, C.P.; Pichia, E.C. Hansen (1904). In *The Yeasts: A Taxonomic Study*, 5th ed.; Kurtzman, C.P., Fell, J.W., Boekhout, T., Eds.; Elsevier: Amsterdam, The Netherlands, 2011; Volume 2, pp. 685–707.
66. Sugita, T. Trichosporon Behrend (1890). In *The Yeasts: A Taxonomic Study*, 5th ed.; Kurtzman, C.P., Fell, J.W., Boekhout, T., Eds.; Elsevier: Amsterdam, The Netherlands, 2011; Volume 3, pp. 2015–2061.
67. Kwon-Chung, K. Filobasidium Olive (1968). In *The Yeasts: A Taxonomic Study*, 5th ed.; Kurtzman, C.P., Fell, J.W., Boekhout, T., Eds.; Elsevier: Amsterdam, The Netherlands, 2011; Volume 3, pp. 1457–1465.
68. Laffins, M.M.; Mellal, N.; Almlie, C.L.; Regalia, D.E. Evaluation of Infrared Thermometry in Cynomolgus Macaques (*Macaca fascicularis*). *J. Am. Assoc. Lab. Anim. Sci.* **2017**, *56*, 84–89.
69. Summers, K.L.; Frey, J.F.; Ramsay, T.G.; Arfken, A.M. The piglet mycobiome during the weaning transition: A pilot study. *J. Anim. Sci.* **2019**, *97*, 2889–2900. [CrossRef]
70. Mason, K.L.; Downward, J.R.E.; Mason, K.D.; Falkowski, N.R.; Eaton, K.A.; Kao, J.Y.; Young, V.B.; Huffnagle, G.B. Candida albicans and Bacterial Microbiota Interactions in the Cecum during Recolonization following Broad-Spectrum Antibiotic Therapy. *Infect. Immun.* **2012**, *80*, 3371–3380. [CrossRef] [PubMed]
71. Allonsius, C.N.; van den Broek, M.F.L.; De Boeck, I.; Kiekens, S.; Oerlemans, E.F.M.; Kiekens, F.; Foubert, K.; Vandenheuvel, D.; Cos, P.; Delputte, P.; et al. Interplay between Lactobacillus rhamnosus GG and Candida and the involvement of exopolysaccharides. *Microb. Biotechnol.* **2017**, *10*, 1753–1763. [CrossRef] [PubMed]
72. Mayer, F.L.; Wilson, D.; Hube, B. Candida albicans pathogenicity mechanisms. *Virulence* **2013**, *4*, 119–128. [CrossRef] [PubMed]
73. Kumamoto, C.A.; Gresnigt, M.S.; Hube, B. The gut, the bad and the harmless: Candida albicans as a commensal and opportunistic pathogen in the intestine. *Curr. Opin. Microbiol.* **2020**, *56*, 7–15. [CrossRef]
74. Richard, M.L.; Lamas, B.; Liguori, G.; Hoffmann, T.W.; Sokol, H. Gut Fungal Microbiota: The Yin and Yang of Inflammatory Bowel Disease. *Inflamm. Bowel Dis.* **2015**, *21*, 656–665. [CrossRef]
75. Flahou, B.; De Baere, T.; Chiers, K.; Pasmans, F.; Haesebrouck, F.; Ducatelle, R. Gastric Infection with Kazachstania heterogenica Influences the Outcome of a Helicobacter suis Infection in Mongolian Gerbils. *Helicobacter* **2010**, *15*, 67–75. [CrossRef]

frontiers | Frontiers in Aging Neuroscience

ORIGINAL RESEARCH
published: 18 July 2022
doi: 10.3389/fnagi.2022.828429

Absence of Bacteria Permits Fungal Gut-To-Brain Translocation and Invasion in Germfree Mice but Ageing Alone Does Not Drive Pathobiont Expansion in Conventionally Raised Mice

Aimée Parker[1]†, Steve A. James[1†], Catherine Purse[1], Arlaine Brion[1], Andrew Goldson[1], Andrea Telatin[1], David Baker[1] and Simon R. Carding[2]*

[1] Gut Microbes and Health Research Programme, Quadram Institute, Norwich, United Kingdom, [2] Norwich Medical School, University of East Anglia, Norwich, United Kingdom

OPEN ACCESS

Edited by:
George Tetz,
Human Microbiology Institute,
United States

Reviewed by:
Adrienne M. Antonson,
University of Illinois
at Urbana-Champaign, United States
Anthony John Hannan,
University of Melbourne, Australia

***Correspondence:**
Aimée Parker
aimee.parker@quadram.ac.uk

† These authors have contributed equally to this work

Specialty section:
This article was submitted to Alzheimer's Disease and Related Dementias, a section of the journal Frontiers in Aging Neuroscience

Received: 03 December 2021
Accepted: 20 June 2022
Published: 18 July 2022

Citation:
Parker A, James SA, Purse C, Brion A, Goldson A, Telatin A, Baker D and Carding SR (2022) Absence of Bacteria Permits Fungal Gut-To-Brain Translocation and Invasion in Germfree Mice but Ageing Alone Does Not Drive Pathobiont Expansion in Conventionally Raised Mice. Front. Aging Neurosci. 14:828429. doi: 10.3389/fnagi.2022.828429

Age-associated changes in the structure of the intestinal microbiome and in its interaction with the brain via the gut-brain axis are increasingly being implicated in neurological and neurodegenerative diseases. Intestinal microbial dysbiosis and translocation of microbes and microbial products including fungal species into the brain have been implicated in the development of dementias such as Alzheimer's disease. Using germ-free mice, we investigated if the fungal gut commensal, *Candida albicans*, an opportunistic pathogen in humans, can traverse the gastrointestinal barrier and disseminate to brain tissue and whether ageing impacts on the gut mycobiome as a predisposing factor in fungal brain infection. *C. albicans* was detected in different regions of the brain of colonised germ-free mice in both yeast and hyphal cell forms, often in close association with activated (Iba-1$^+$) microglial cells. Using high-throughput ITS1 amplicon sequencing to characterise the faecal gut fungal composition of aged and young SPF mice, we identified several putative gut commensal fungal species with pathobiont potential although their abundance was not significantly different between young and aged mice. Collectively, these results suggest that although some fungal species can travel from the gut to brain where they can induce an inflammatory response, ageing alone is not correlated with significant changes in gut mycobiota composition which could predispose to these events. These results are consistent with a scenario in which significant disruptions to the gut microbiota or intestinal barrier, beyond those which occur with natural ageing, are required to allow fungal escape and brain infection.

Keywords: ***Candida albicans*, gut-brain, ITS1 sequencing, mycobiome, pathobiont, dementia, ageing**

INTRODUCTION

Ageing is the dominant risk factor associated with the development of neurodegenerative dementias. Altered intestinal microbiota structure and function (microbial dysbiosis) with age is considered a contributing factor in the development of age-associated chronic low-grade systemic and tissue inflammation, termed inflammageing (Boulangé et al., 2016;

Fransen et al., 2017; Thevaranjan et al., 2017; Boehme et al., 2021; Parker et al., 2021) which contributes to neuroinflammation and neurodegenerative disease (Scott et al., 2017; Boehme et al., 2019). Whilst bacterial community diversity, composition, and function changes significantly with age in both animal models and in humans (Claesson et al., 2011; Yatsunenko et al., 2012; Langille et al., 2014; Clark et al., 2015; O'Toole and Jeffery, 2015), comparatively little is known about the impact of ageing upon other members of the intestinal microbiota, including viruses, archaea, and fungi. Fungal diversity in the gut microbiome is decreased in adults compared to infants and children, with fungal richness being higher in females than males regardless of age (Strati et al., 2016). However, little is known of the intestinal fungal composition of elderly versus young adults, or whether fungal composition is altered due to ageing *per se*, or results from changes in behaviour and lifestyle, which occur concomitantly with ageing.

Fungi account for a relatively small fraction of the total human faecal microbiota (10^5–10^6 cells/g faecal matter compared with 10^{11} bacterial cells/g) (Huseyin et al., 2017) and for around 0.1% of the faecal microbiota gene content (Qin et al., 2010; Li et al., 2014; Sender et al., 2016). However, this is likely to be an underestimate of the true fungal intestinal load due to the comparatively smaller number of fungal reference genomes currently available, bias in microbiome analyses introduced by extraction and sequencing methods sub-optimal for mycobiome characterisation (Richard and Sokol, 2019), and the issue that faecal sampling is unlikely to accurately reflect fungal load throughout the GI tract and at the epithelial surface.

Fungal pathogens acquired externally to the host, and reactivation of latent infections, can lead to systemic fungal infection, resulting in significant pathology and mortality (Brown et al., 2012). In some circumstances, fungal species within the gut microbiota, which are normally well tolerated, may disseminate via the circulation to other sites including the brain. For example, cryptococcal meningoencephalitis can occur in immunocompromised individuals or those undergoing specific drug treatment, as well as in premature infants of very low birth weight (Gottfredsson and Perfect, 2000). Invasive candidiasis is a potentially life-threatening fungal infection caused by several *Candida* species, the most common being *Candida albicans*, a dimorphic fungus, which is a common human gut commensal (Brown et al., 2012). When able to penetrate the body's barrier sites, *C. albicans* can cause superficial mucosal infections, and in some cases severe systemic sepsis with associated mortality exceeding 70% (Brown et al., 2012; Allert et al., 2018).

Increased risk of developing Alzheimer's disease (AD) has been associated with infections of the central nervous system (CNS), potentially via impacting innate immune mechanisms and/or protein misfolding (Mawanda and Wallace, 2013). Viral, bacterial, and fungal species have been investigated in this context (Hammond et al., 2010; Huang et al., 2014; Fung et al., 2017; Dominy et al., 2019; Tetz et al., 2020); however, no single infectious agent has to date been demonstrated to be causative in AD onset. Fungal antigens from a variety of species have been detected in the serum of AD patients, including *C. albicans* and a number of other *Candida* species (Pisa et al., 2015b; Alonso et al., 2018). In addition, analysis of post-mortem brain tissue from AD patients and healthy controls identified genetic material from multiple fungal species (including *Candida*), fungal proteins, and fungal cell bodies unique to the brains of AD patients (Alonso et al., 2014; Pisa et al., 2015a,b).

Despite these findings, the concept of a brain-associated microbiota remains highly controversial, and there is no compelling evidence of microbial representation in the CNS of normal healthy hosts. More plausible is that microbes, including fungi, escape confinement in the gut or elsewhere and disseminate more widely when barrier sites and/or the immune system have been seriously compromised. In ageing, declining immune function (immunosenescence), inflammageing, intestinal microbial dysbiosis, and the high incidence of co-morbidities create an environment more permissive to microbial translocation to the circulatory system and dissemination to tissues beyond the gastrointestinal tract (GIT).

Animal studies of the mycobiome and fungal infection can control for or eliminate most of the confounding factors which complicate interpretation of fungal changes in ageing human populations. Mice, for example, harbour many of the same fungal taxa which inhabit the human gut, with a characteristic feature of both the murine and human gut mycobiome being the dominance of the Ascomycota and Basidiomycota phyla (Hallen-Adams et al., 2015; Nash et al., 2017; Ward et al., 2018; Doron et al., 2019; James et al., 2020; Mims et al., 2021). *C. albicans* is frequently present in the healthy human gut as a benign commensal (Brown et al., 2012; Nash et al., 2017; James et al., 2020) and can also be found in captive-bred mice (Doron et al., 2019; Mims et al., 2021), although it may be absent in wild murine species (Bendová et al., 2020).

Multiple *Candida* species can colonise mouse models and persist in the GIT (Prieto and Pla, 2015). Systemic dissemination and candidiasis is evident in immunocompromised mice, however, this often requires high initial inoculums for non-*albicans Candida* species (Conti et al., 2014; Segal and Frenkel, 2018). *C. albicans* can also stably colonise mice and has been used to study fungal intestinal colonisation and dissemination in neonatal mice, antibiotic- or chemotherapy-treated adult mice, and germ-free mice (Field et al., 1981; Kinneberg et al., 1999; Mellado et al., 2000; Wiesner et al., 2001; Schofield et al., 2005; Koh et al., 2008; Koh, 2013). When administered intravenously, *C. albicans* can infect the mouse brain and cause localised cerebritis (Wu et al., 2019).

Here we assessed whether fungal cells could traverse the intestinal barrier and disseminate to the brain by colonising C57BL/6 germ-free mice with a human-derived isolate of *C. albicans* by oral gavage, using confocal microscopy to assess fungal cell dissemination throughout the brain (a graphical overview is shown in **Figure 1**). High-throughput amplicon sequencing of the fungal internal transcribed spacer 1 (ITS1) region was used to investigate the effect of ageing on the composition and diversity of the murine gut mycobiome, and to identify potential fungal pathobionts.

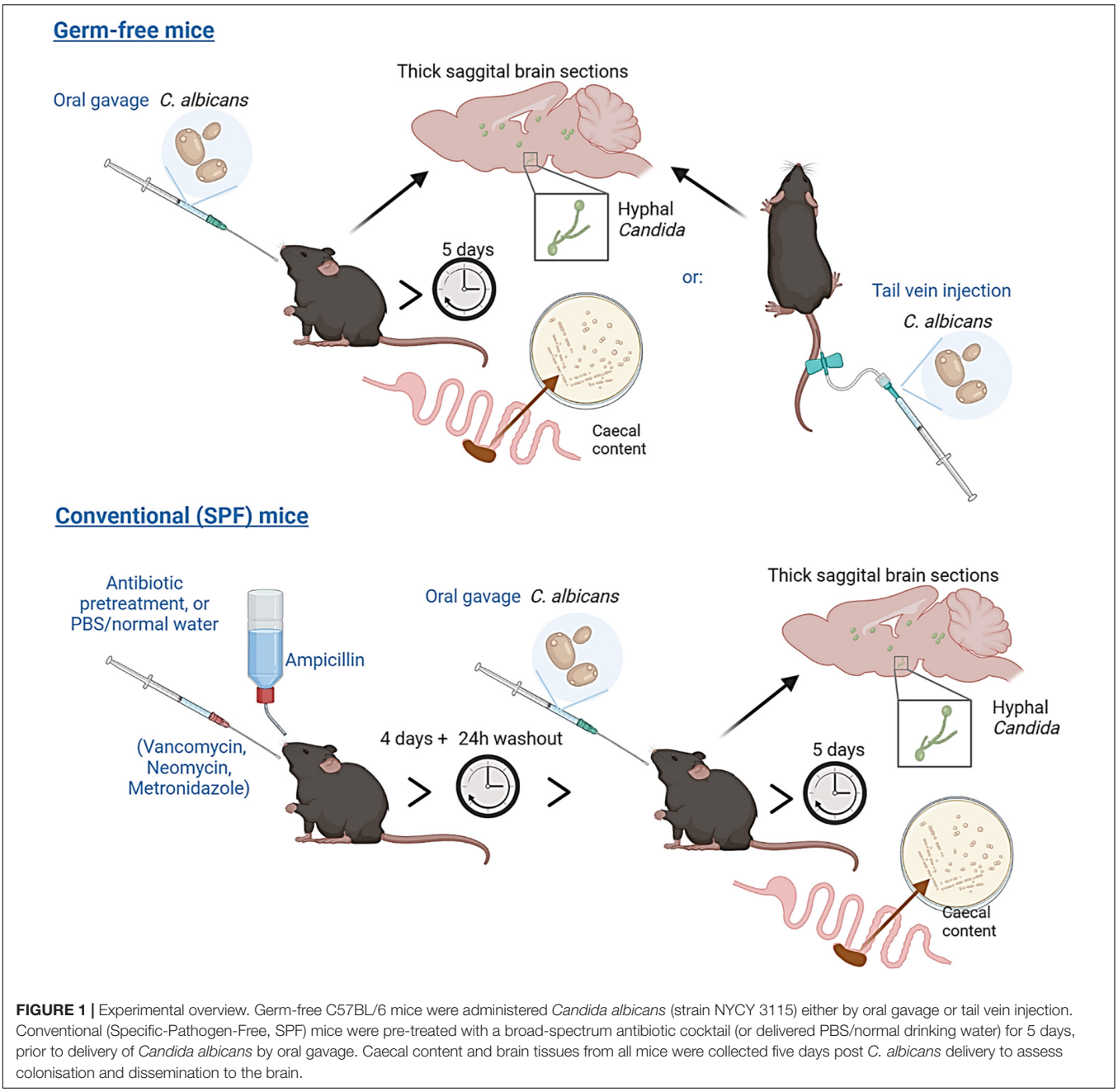

FIGURE 1 | Experimental overview. Germ-free C57BL/6 mice were administered *Candida albicans* (strain NYCY 3115) either by oral gavage or tail vein injection. Conventional (Specific-Pathogen-Free, SPF) mice were pre-treated with a broad-spectrum antibiotic cocktail (or delivered PBS/normal drinking water) for 5 days, prior to delivery of *Candida albicans* by oral gavage. Caecal content and brain tissues from all mice were collected five days post *C. albicans* delivery to assess colonisation and dissemination to the brain.

MATERIALS AND METHODS

Yeast Strain and Growth Conditions

Candida albicans strain (NCYC 3115) is a human clinical isolate from patient faeces collected in a United Kingdom hospital and was provided by the National Collection of Yeast Cultures (Norwich, United Kingdom). For inoculum preparation, stocks were cultured in YM liquid medium (10g/L glucose, 3g/L malt extract, 5g/L peptone, 3g/L yeast extract) at 30°C for 48h with shaking (200 rpm). Cells were collected by low-speed centrifugation (3,000 rpm, 5 min), washed twice in sterile phosphate buffered saline (PBS) and re-suspended in PBS prior to delivery to mice. Fungal colonisation was assessed by measuring CFUs (colony forming units) of *C. albicans* present in the caecum of each mouse. Caecal contents, collected five days post-delivery, were mechanically homogenised in PBS to 100 mg/mL then serially diluted and spread plated onto YM medium. All agar plates were incubated aerobically at 37°C, and colony counts measured after 2 days incubation. Colony morphology was also assessed (and counts determined) by visual inspection, with colonies of differing morphology (morphotypes) selected and stocked for additional phenotyping. YM broth cultures derived from two, post-passaged, colony morphotypes (white and domed vs. darker and flattened) were incubated at 37°C, without

agitation, and examined after 3 days by standard light microscopy for the presence/absence of hyphal and pseudohyphal cells. Species identity was confirmed by standard colony PCR using *C. albicans*-specific primers (Asadzadeh et al., 2018), and by ITS1 sequencing (White et al., 1990; Gardes and Bruns, 1993). Details of all fungal primers used in this study are provided in **Supplementary Figure 4**.

Animal Experiments

All experiments involving animals were performed in accordance with EU and United Kingdom Home Office Legislation and local Animal Welfare and Ethical Review Body approval. Male and female specific pathogen-free (C57BL/6 -SPF) mice aged 3 months or 24 months, and male germ-free (C57BL/6-GF) mice aged 3 months, were maintained in individually ventilated cages (SPF) or in sterile isolators (GF) in adjacent rooms of the Quadram Institute Germ-Free mouse facility within the University of East Anglia Disease Modelling Unit. All mice received autoclaved water and were fed RM3 (SPF) or RM3-(Autoclavable) (GF) diet (Special Diets Services). All mice were maintained under 12-h light-dark cycle. A dose of 2.5×10^5 ($n = 5$) or 5×10^5 ($n = 5$) *C. albicans* cells re-suspended in 200 μL PBS was administered to germ-free animals by oral gavage, whilst a lower dose of 2.5×10^4 cells in 100 μL of PBS was used for tail vein injection control mice. SPF mice ($n = 16$, 8 females and 8 males) were pre-treated for four days with either PBS ($n = 8$) or a cocktail of broad-spectrum antibiotics (VMNA, 0.5 mg/mL vancomycin, 1 mg/mL metronidazole and 1 mg/mL neomycin delivered in 200 μL sterile water by daily oral gavage, and 1 mg/mL ampicillin delivered via drinking water, available *ad libitum*), $n = 8$. Following a 24 h washout period 5×10^5 *C. albicans* cells re-suspended in 200 μL PBS were administered by oral gavage. Mice were then maintained in individually ventilated cages until sacrifice. Brains and caecal content were harvested at day 5 post-inoculation and used for downstream analysis.

Formalin-fixed paraffin-embedded brains were sectioned at 5 μm. Sagittal vibratome sections of 100 μm thickness were prepared from PFA-fixed whole brains embedded in low-melt agarose, a method adapted from Snippert et al. (2011) and were cleared post-staining and prior to mounting using RapiClear (CamBioscience, Cambridge, United Kingdom). *C. albicans* was visualised in sections using a rabbit polyclonal anti-*C. albicans* antibody (NB100-64750 Novus Biologicals, 1:100), and for activated microglia/macrophages using rabbit anti-Iba-1 (ab178846, Abcam, 1:100) for single staining or Abcam ab150167 (1:100) for co-stains. Secondary antibodies used were goat anti-rabbit IgG Alexa Fluor-594 (Invitrogen, 1:100), Goat Anti-Rat Alexa-647 (ab150167, Abcam, 1:500) or donkey anti-rabbit IgG Alexa Fluor 488 (Invitrogen, 1:500). Nuclei were stained with Hoechst 33258. Images were collected and analysed using a Zeiss LSM880 confocal microscope and ZEN 2010 software, and FIJI/ImageJ v2.1.0 (Schindelin et al., 2012). *C. albicans* cells were quantified from 100 μm sagittal vibratome sections taken starting from the midline of the left hemisphere of the brain, five sections were taken from each brain sample from *C. albicans*-colonised germ-free mice ($n = 5$ mice), non-colonised control germ-free mice ($n = 3$ mice) and from *C. albicans*-colonised SPF mice receiving either antibiotic or PBS only pre-treatment ($n = 8$ mice/group). Cells were not included in counts if they were obviously within vessels, or were on the periphery of the section and therefore considered to not be truly within the brain tissue.

Genomic DNA Extraction

Faecal pellets were collected from temporarily singly housed SPF mice using sterile picks and sterile RNA-DNA-free microtubes and were stored at −70°C prior to processing and DNA extraction. For fungal DNA amplification, total microbial DNA was extracted from ∼50 mg of faeces from each animal using the QIAamp PowerFecal Pro DNA kit (QIAGEN, Hilden, Germany) and following the manufacturer's protocol. In addition, all samples were homogenised using a FastPrep-24 benchtop instrument (MP Biomedicals, Irvine, CA, United States) at 6.0 m/s for 1 min. Extracted DNA was quantified and quality checked using the Qubit 3.0 fluorometer and associated Qubit dsDNA BR Assay Kit (Thermo Fisher, Waltham, MA, United States). DNA samples were stored at −20°C prior to further analysis.

Internal Transcribed Spacer 1 Amplification and Sequencing

The fungal ITS1 region was amplified from 100 ng of faecal DNA by using the pan-fungal ITS1F and ITS2 primer set (White et al., 1990; Gardes and Bruns, 1993), with each primer modified at the 5' end to include an Illumina adapter tail, using KAPA2G Robust DNA polymerase (Kapa Biosystems, Wilmington, MA, United States). Amplification was performed at 94°C (5 min) with 35 cycles of 92°C (30 s), 55°C (30 s), 72°C (45 s), and a final extension of 72°C (5 min). Amplification reactions were set up in duplicate for each DNA sample, and negative (PCR dH_2O) and positive controls (0.01 ng of *C. albicans* DNA) were included in each PCR run. Following ITS1 PCR, a 0.7x SPRI purification using KAPA Pure Beads (Roche, Wilmington, MA, United States) was performed and the purified DNA was eluted in 20 μl of 10 mM Tris-HCl. In a second PCR, library index primers were added using a Nextera XT Index Kit v2 (Illumina, Cambridge, United Kingdom) and amplification was performed at 95°C (5 min) with 10 cycles of 95°C (30 s), 55°C (30 s), 72°C (30 s), and a final extension of 72°C (5 min). Following PCR, libraries were quantified using the Invitrogen™ Quant-iT dsDNA high sensitivity assay kit (Thermo Fisher) and run on a FLUOstar Optima plate reader (BMG Labtech, Aylesbury, United Kingdom). Libraries were pooled following quantification in equal quantities. The final pool was SPRI cleaned using 0.7x KAPA Pure Beads, quantified on a Qubit 3.0 fluorometer and run on a High Sensitivity D1000 ScreenTape (Agilent Inc., Santa Clara, CA, United States) using the Agilent Tapestation 4200 to calculate the final library pool molarity. The pool was run at a final concentration of 8 pM on an Illumina MiSeq instrument using the MiSeq© v3 (2 × 300 bp) Kit (Illumina). All sequencing

was performed at Quadram Institute Bioscience, Norwich. The raw data were analysed locally on the MiSeq instrument using MiSeq reporter.

Mycobiome Characterisation

Illumina MiSeq reads were analysed using the automated pipeline Dadaist2, a dedicated workflow for ITS profiling (Ansorge et al., 2021). The quality profile of the raw reads (in FASTQ format) was assessed using *Fastp* 0.20.0 (Chen et al., 2018), which was also used to remove reads with ambiguous bases. Locus-specific primers were removed using *SeqFu* 1.8 (Telatin et al., 2021). The identification of representative sequences was performed using DADA2 (Callahan et al., 2016), to produce a set of amplicon sequence variants (ASVs), and their taxonomic assignment was determined using the UNITE Fungal ITS database (release 8.2) (Nilsson et al., 2019). The multiple alignment of the representative sequences was performed using ClustalO (Sievers and Higgins, 2021) and the guide tree was produced using FastTree (Price et al., 2009). Data normalization and diversity were produced using the Rhea scripts (Lagkouvardos et al., 2017). The output feature table, taxonomic classification, phylogeny and metadata files were exported and further analysed using MicrobiomeAnalyst (Dhariwal et al., 2017) and the built-in plotting provided by Dadaist2. Every ASV with a zero count in all samples was removed to assess alpha diversity measures.

Statistical Analysis

Three alpha-diversity measures were used to estimate fungal taxa richness (Chao1) as well as taxa richness and evenness (Shannon and Simpson) using MicrobiomeAnalyst (Dhariwal et al., 2017). Data was not rarefied, was scaled by total sum scaling, was non-transformed, and statistical significance was assessed by Student's *t*-test (threshold for significance $P < 0.05$). For comparison of specific taxa, data were CLR-transformed prior to comparison between two groups by *t*-test.

Other Software

Figure 1 was created using BioRender illustration software: https://biorender.com/.

RESULTS

Candida albicans Translocates From Gut to Brain in Monocolonised Germ-Free Mice and Induces an Inflammatory Response in the Brain

Candida albicans (NCYC 3115) was administered by oral gavage to two groups of germ-free adult C57BL/6 mice, in doses of either 2.5×10^5 or 5×10^5 cells. A third group were administered an inoculum of 2.5×10^4 cells by tail vein injection, a dose previously shown to result in fungal translocation to the brain with no lethality (Wu et al., 2019). Control mice received PBS alone by gavage. Both delivery routes, oral or intravenous, resulted in successful colonisation of the GIT, as measured by CFU recovered from caecal content five days post-delivery (**Figure 2A**). Oral administration of 2.5×10^5 cells resulted in caecal counts ranging from 1×10^5 to 1×10^7 CFU, whereas administration of the higher dose of 5×10^5 cells resulted in caecal counts ranging from 6.2×10^6 to 2.2×10^7 CFU. Mice receiving yeast cells intravenously had lower caecal CFU counts of $8 \times 10^5 - 3 \times 10^6$. Caecal content from control mice receiving PBS alone yielded no fungal colonies. Species identity of colonies was confirmed by standard colony PCR using *C. albicans*-specific primers (Asadzadeh et al., 2018).

Two types of post-passage *C. albicans* colonies were cultured from the caecal contents (**Figures 2B–E**), a white and domed morphotype (as per the wild-type), and a darker and flattened morphotype, chromatically and morphologically resembling the previously described Gastrointestinally indUced Transition (GUT) phenotype (Pande et al., 2013). Approximately 66% of colonies recovered from the caecal content of mice in the present study were of this 'GUT'-like phenotype, suggesting substantial adaptation of the administered wild-type *C. albicans* to the C57BL/6 germ-free gut. Cultures derived from this phenotype failed to produce hyphae, either on solid or in liquid media, when grown at 37°C. This was in marked contrast to white phenotype-derived cultures which readily produced hyphae (and pseudohyphae) when grown at this elevated temperature (data not shown).

In mice receiving *C. albicans* orally of either lower (2.5×10^5) or higher dose (5×10^5) inoculum, and in mice receiving the inoculum intravenously, *C. albicans* cells were detected in brain tissue five days post-colonisation by immunostaining with an anti-*C. albicans* antibody (**Figures 3A–F**). Individual *C. albicans* cells and cell clusters were found throughout the brain, in the ventricular spaces, cerebellum, hypothalamus, midbrain and cortex. Clusters and individual *C. albicans* cells were confirmed to be within the plane of the brain tissue by imaging of z-stacks (**Figure 3A**). Individual *C. albicans* cells and cell clusters were frequently found in, or adjacent to, vessels within the brain tissue (**Figure 3B**), and within the ventricular spaces, including the cerebral aqueduct (**Figure 3C**). *Candida albicans* cells were frequently surrounded by Iba-1^+ cells resembling both resident microglia and infiltrating macrophages within or exiting vessels (**Figures 3D,E**), indicating induction of an inflammatory microglial/macrophage response. In one mouse, striking granuloma-like clusters of fungal and Iba-1^+cells were seen in the posterior parietal cortex (**Figure 3D**), which plays a key role in spatial representation of objects for action planning and control. Less frequently hyphae were detected within brain tissue samples (**Figure 3F**) indicating *C. albicans* cells were viable and in an invasive form. No fungal cells or similar microglial clusters were observed in PBS control germ-free mouse brain samples. As mice were not transcardially perfused before brain harvest, we cannot completely rule out that a small number of counted *C. albicans* cells may have been within vessels/capillaries that were sectioned or optically sliced in such a way that we did not identify the vessels. However, the identification of hyphal forms within the brain tissue, and clusters of microglia identified surrounding *C. albicans* cells strongly suggests active invasion of the brain tissue as opposed to circulating yeast

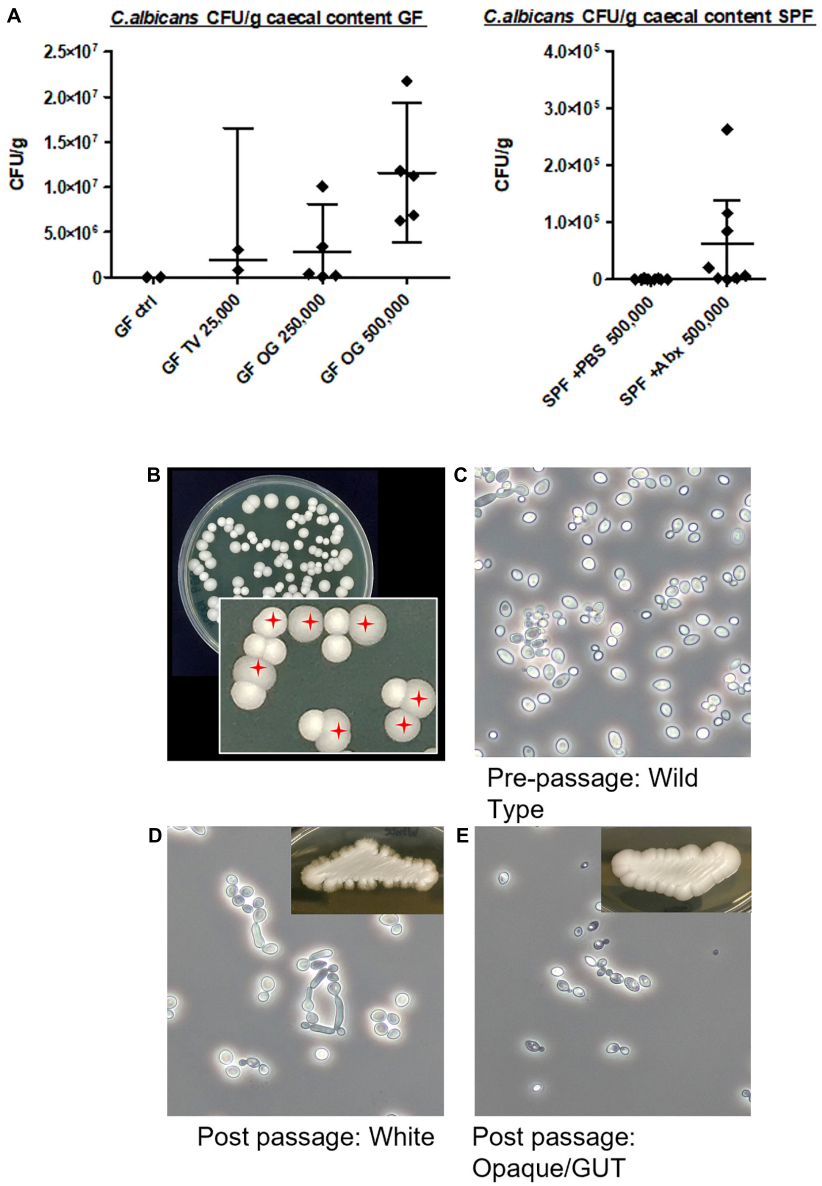

FIGURE 2 | Colonisation of the caecum by *Candida albicans* NCYC 3115 following tail vein injection or oral gavage. **(A)** Colony-forming units (CFU) recovered from caecal content following delivery of *C. albicans* NCYC 3115 to germ-free mice (left) or SPF mice (right). No colonies were present in the caecal content of germ-free control mice administered PBS alone (GF ctrl). TV, tail vein; OG, oral gavage. Numbers on x-axis labels denote amount of *C. albicans* cells administered, error bars denote 95% CI. **(B)** Example YM agar plate with zoom inset showing two phenotypically distinct *C. albicans* colony morphotypes recovered from caecal contents. White and domed morphotype and darker and flattened/Gastrointestinally indUced Transition (GUT) morphotype (red crosshairs). **(C–E)** Photomicrographs of pre-passage wild type cells **(C)**, post-passage white phenotype cells **(D)**, and post-passage darker/GUT phenotype cells **(E)**, all grown at 37°C for 3 days in YM broth.

cells in dissemination form (Gow et al., 2011; Noble et al., 2016).

Short-Term Depletion of Gut Bacteria in Conventional Mice Permits Expansion of *Candida albicans* in the Caecum

To test whether depletion of the gut bacterial community in conventional mice would also allow for fungal expansion and dissemination, we pre-treated SPF mice with a short course of broad-spectrum antibiotics (VMNA), or PBS, prior to *C. albicans* delivery by oral gavage (**Figure 1**). Colony counts from caecal content (**Figure 2A**) showed increased caecal colonisation in antibiotic-pre-treated SPF mice (SPF + Abx) compared with PBS-pre-treated SPF controls, but at much lower levels compared to *C. albicans*-colonised germ-free mice (mean 1.15×10^7 cells/g caecal content in colonised germ-free versus 6.15×10^4 in colonised SPF + Abx). On analysing the brains of the SPF

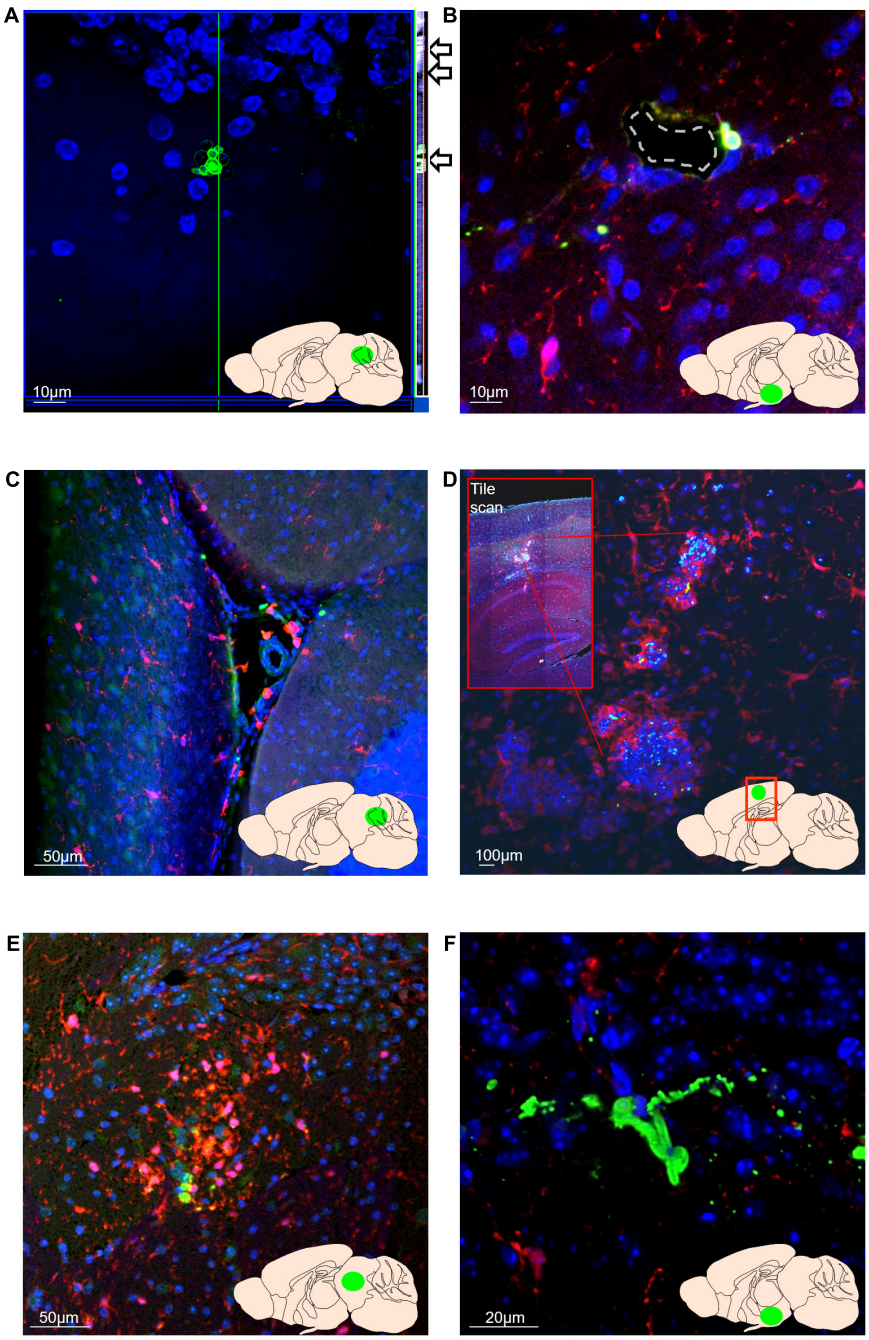

FIGURE 3 | *Candida albicans* can disseminate from the gut to the brain and can grow in the invasive hyphal form within brain tissue. In all images, blue = nuclei (Hoechst), green = *C. albicans*, red = Iba-1-positive microglia/macrophages. Green area in inset brain schematic indicates approximate position of image. **(A)** *C. albicans* cells are detectable within cerebellar brain tissue at 5 days post-colonisation. Z-stack orthogonal view (side bar and arrows) shows *C. albicans* cells are in the same plane as brain cell nuclei. Orthogonal side bar brightness and contrast has been enhanced here for visibility. **(B)** *C. albicans* cells in proximity to a hypothalamic blood vessel (dashed outline). **(C)** *C. albicans* cells and Iba-1 positive macrophages within the cerebral aqueduct (lobule II granule layer visible as dense Hoechst-stained area bottom right of image). **(D)** Foci of clustered Iba-1$^+$ cells (red) around *C. albicans* cells (green) within the posterior parietal association area of the cortex. Inset box shows overview tile scan of the cortex and hippocampus. **(E)** Cluster of Iba-1 + cells around *C. albicans* cells within the midbrain **(F)** Entwined hyphal *C. albicans* hyphae within the hypothalamus.

mice, we found no evidence of fungal cells, either in yeast or hyphal form, within brain sections of either PBS control or antibiotic pre-treated colonised mice, either by staining specifically for *Candida*, or by using a non-specific fungal cell wall stain (example expected staining of positive control shown in **Supplementary Figure 1B**).

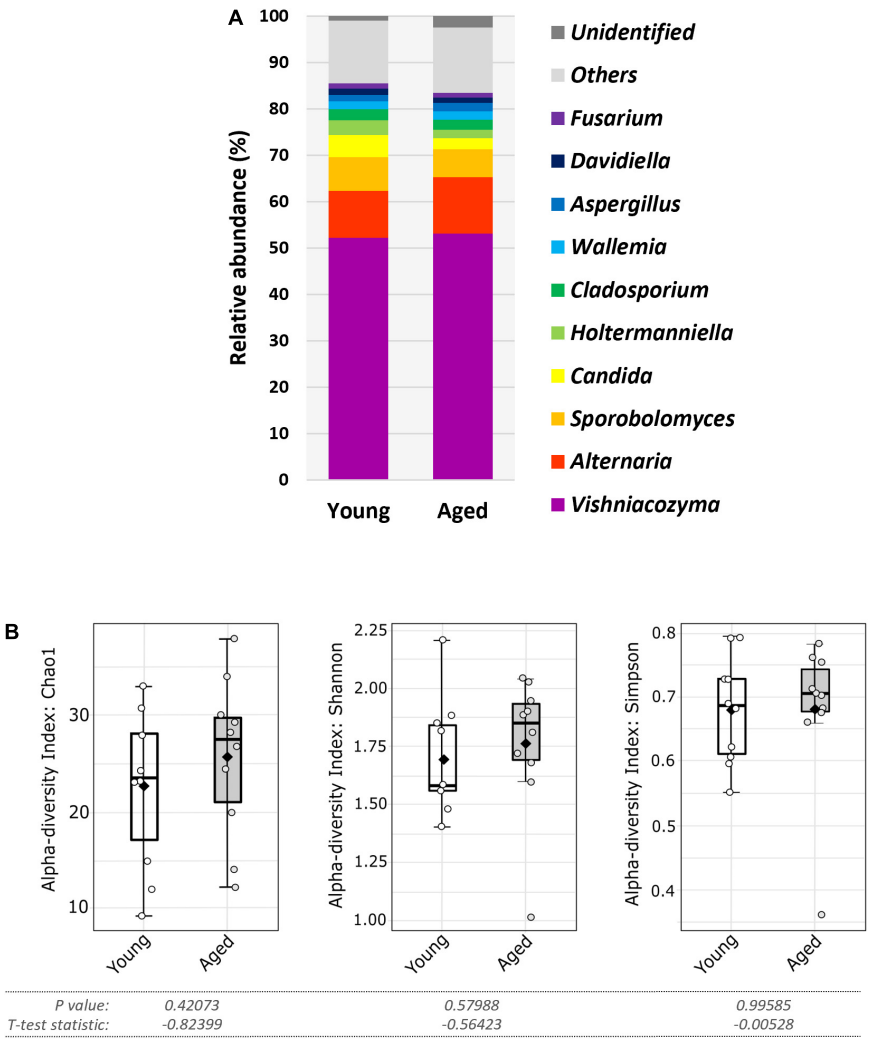

FIGURE 4 | Faecal fungal diversity and top ten genera in aged vs. young SPF mice. **(A)** Top ten most abundant genera (percentage mean relative abundance) in faecal samples of young vs. aged SPF mice (*n* = 10/group). **(B)** Alpha diversity (L-R: Chao1, Shannon, and Simpson indices) of faecal fungal composition of young vs. aged SPF mice (*n* = 10/group), whiskers show spread of data across all mice, solid black dot indicates the mean, horizontal line indicates the median.

Our data shows that disruption of the intestinal environment by antibiotic treatment permits increased fungal colonisation of the intestinal tract, but suggest that short term-antibiotic treatment is not sufficient to promote dissemination to the brain. On the other hand, recent data show that long-term chronic administration of antibiotics can promote systemic dissemination of both fungi and bacteria (Drummond et al., 2022). Advanced age is also associated with changing gut bacterial composition, as well as depleted barrier integrity promoting chronic systemic inflammageing (Fransen et al., 2017; Thevaranjan et al., 2017; Parker et al., 2022). Therefore, we next investigated whether the composition of the enteric mycobiota is altered in aged animals, and whether any fungal species detected are potential pathobionts/opportunistic pathogens with the capacity to cause serious infection.

Ageing Alone Is Not Sufficient to Select for or Drive Pathobiont Expansion in Specific Pathogen-Free Mice

High-throughput internal transcribed spacer 1 (ITS1) amplicon sequencing was used to characterise the faecal fungal communities in young (3-month) and aged (24-month) SPF mice. A total of 1,471,212 quality-trimmed ITS1 reads were obtained, ranging from 14,913 (A7, aged cohort) to 100,384 (Y2, young cohort), with a sample average of 73,560 reads (**Supplementary Figure 2A**). Over 2,000 amplicon sequence variants (ASVs) were used to determine the composition of the fungal microbiota in the young and aged mice at different taxonomic levels.

At the phylum level, most identified fungi in each age group belonged to either the Ascomycota or Basidiomycota

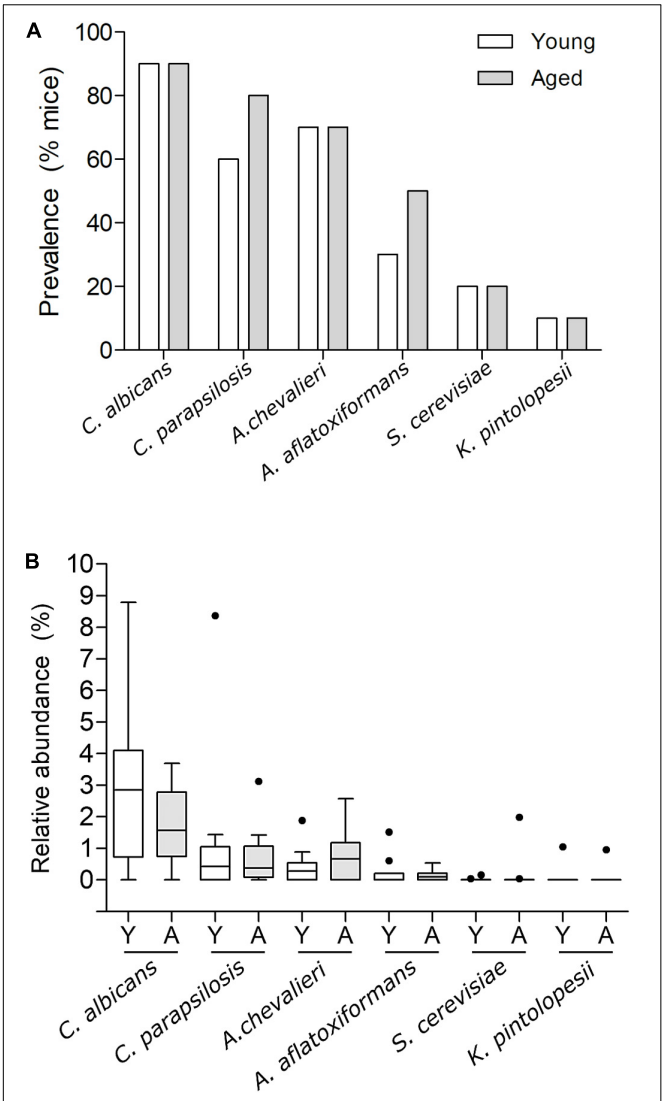

FIGURE 5 | Prevalence and relative abundance of putative gut commensal fungal species in faecal samples of young vs. aged SPF mice. **(A)** Prevalence of putative gut commensal fungal species *Candida albicans*, *Candida parapsilosis, Aspergillus chevalieri*, *Aspergillus aflatoxiformans*, *Saccharomyces cerevisiae*, and *Kazachstania pintolopesii* in faecal samples from groups of young and aged SPF mice (n = 10/group), percentage of mice harbouring each species displayed as % prevalence. **(B)** Percentage relative abundance of those same species in faecal samples from aged (A) vs. young (Y) mice (n = 10/group), Tukey whiskers, horizontal bars show the mean, outliers displayed as round points.

(**Supplementary Figure 2B**). A characteristic feature of the gut mycobiome of our C57BL/6 colony, irrespective of age, was the predominance of the Basidiomycota. At the genus level, when analyses were restricted to the most abundant genera (i.e., those with a relative abundance of 1% or more), which accounted for over 80% of all ITS1 reads, both age groups had broadly similar taxonomic profiles, with *Vishniacozyma* the predominant genus (**Figure 4A**). This basidiomycetous yeast genus had a mean relative abundancy of over 50% in each age group (young, 52.1%; aged, 53.1%). Other notable genera included *Alternaria*, *Sporobolomyces*, *Candida*, *Holtermanniella,* and *Cladosporium* (**Figure 4A**). Whilst most genera displayed comparable mean relative abundancies in both age groups (**Supplementary Figure 2B**), *Sporobolomyces*, *Candida* and *Holtermanniella* were all nominally less abundant, albeit not reaching statistical significance, in the aged mice (**Figure 4A** and **Supplementary Figure 2B**). At the genus level, there was no significant compositional change in alpha diversity between the two age groups ($p > 0.05$ in all three indices) (**Figure 4B**).

For taxa resolved to species level most were categorised as environmental fungi, typically found in soil and/or plant associated. This included *Vishniacozyma victoriae*, the most abundant taxon and a species present in every sample (**Supplementary Figure 3**). Six species were identified as candidate gut colonisers based on their ability to survive and proliferate at 37°C. These were *Aspergillus aflatoxiformans*, *Aspergillus chevalieri*, *Candida albicans*, *Candida parapsilosis*, *Kazachstania pintolopesii,* and *Saccharomyces cerevisiae*. Among these, *C. albicans* was the most prevalent in both age groups (**Figure 5A**), albeit at lower nominal relative abundance in the elderly mice compared to young mice (**Figure 5B** and **Supplementary Figure 3**), (young, 2.9%; aged 1.7%), although this was not statistically significant ($p > 0.05$) (**Figure 5B**, and **Supplementary Figure 3**). In contrast, *A. chevalieri,* which displayed similar prevalence in both cohorts (70%), was present at nominally higher relative abundance in the aged mice (young, 0.42%; aged, 0.77%), although this was also not statistically significant ($p > 0.05$) (**Figure 5B** and **Supplementary Figure 3**). *K. pintolopesii* a common rodent-associated yeast species (Kurtzman et al., 2005; Bendová et al., 2020) was found in only two of the mice (one from the 3-month-old group and one from the 24-month-old group), and at relatively low abundance (∼1%).

In summary, although the overall enteric mycobiota profiles of young and aged mice were broadly similar at the genus level, subtle differences in both the prevalence and abundance were evident at the species level. These differences were evident within a small group of putative commensal fungi, which included three opportunistic pathogens.

DISCUSSION

There is growing interest in the concept that intestinal microbial dysbiosis, as well as microbial infection, contributes to neuroinflammation and neurodegenerative disease, including dementias (Fung et al., 2017; Vogt et al., 2017). The majority of such studies have focused almost exclusively on the prokaryome, with only a small number investigating the mycobiome and implicating fungi in neurological disorders and AD (Alonso et al., 2014; Pisa et al., 2015a,b; Fung et al., 2017; Forbes et al., 2018; Ling et al., 2020). Gut-resident *C. albicans* populations represent the principal source of life-threatening disseminated candidiasis (Bougnoux et al., 2006; Gouba and Drancourt, 2015). In the gut, pathological invasion of *C. albicans* across the epithelial barrier and into the bloodstream occurs via hyphal penetration of cells,

hyphal production of a cytolytic peptide toxin (candidalysin), enterocyte necrosis and subsequent loss of epithelial barrier integrity (Dalle et al., 2010; Allert et al., 2018). Here, using oral delivery of *C. albicans* cells to the GIT of germ-free C57BL/6 mice, we demonstrate that *C. albicans* can traverse both the intestinal and blood-brain barriers and produce hyphae within the brain. We also observed clusters of Iba-1^+ activated immune cells surrounding *C. albicans* cells, in accordance with prior reports of gliosis in mouse models of candidiasis (Lionakis et al., 2011; Wu et al., 2019). Hyphae were not found within the brains of SPF C57BL/6 mice administered *C. albicans* via intravenous injection (Wu et al., 2019), which may reflect the use of different isolates of *C. albicans* between studies, or differences in SPF vs. germ-free mice.

We also found that while short-term antibiotic pre-treatment allowed for increased expansion of *C. albicans* in colonised SPF mice, compared to PBS pre-treated controls, no fungal cells, either in yeast or hyphal form, were detected in the brains of the colonised mice. Drummond and colleagues (Drummond et al., 2022) have recently shown that chronic exposure to antibiotics (>4 weeks in mice or >7 days in humans) can promote fungal and bacterial dissemination to other organs, however, brains were not assessed for fungal cell staining in the mouse studies so it is unclear whether a longer antibiotic regimen might allow for dissemination into the brain tissues. SPF mice may be resistant to brain infection by *C. albicans*, as intestinal mucins can inhibit hyphal formation by *C. albicans* (Kavanaugh et al., 2014) and the mucus layer differs in composition between SPF and germ-free mice (Johansson et al., 2014; Jakobsson et al., 2015). Furthermore, differences in immune responses between *C. albicans* cells and macrophages (Erwig and Gow, 2016) in germ-free versus SPF mice may also affect hyphal formation and persistence.

Considering that fungal processes can contribute to intestinal barrier damage and that age-related intestinal dysbiosis may increase the likelihood of gut-to-brain translocation of microbes in older hosts, we compared the fungal mycobiome of young and aged mice. Within the mycobiota of young mice three species, namely *C. albicans*, *C. parapsilosis* and *K. pintolopesii*, are recognised opportunistic pathogens of humans and mice, and are capable of causing life-threatening systemic infections (Kurtzman et al., 2005; Pfaller and Diekema, 2007). However, the relative abundances of these species were not significantly different in aged mice, nor was there any evidence of significant fungal dysbiosis in aged mice. This suggests that ageing alone is not a major driver of fungal composition in the mouse gut microbiota. In mice at least, it is more likely that other environmental factors including dietary changes, medications (antibiotics), infections and/or changes in host defence mechanisms and immune status might be required to permit fungal gut-brain translocation in aged, but otherwise healthy, hosts.

There is limited available data on the mycobiota profile of aged healthy human adults (Strati et al., 2016), although some studies have sequenced the mycobiota of patients with metabolic or neurodegenerative disease (Ahmad et al., 2020; Jayasudha et al., 2020; Ling et al., 2020; Nagpal et al., 2020). The gut microbiome in patients with mild cognitive impairment (MCI) and those with AD is reported to differ from healthy controls (Vogt et al., 2017; Zhuang et al., 2018; Saji et al., 2019). A study of patients from a United States cohort with MCI for example, found a higher proportion of the fungal genera *Botrytis, Kazachstania*, *Phaeoacremonium*, and *Cladosporium* but a reduced proportion of *Meyerozyma* compared to controls (Nagpal et al., 2020). A study of the faecal mycobiome of a Chinese cohort of AD patients reported increased abundance of the species *C. tropicalis*, *Trametes versicolor*, *Schizophyllum commune*, *Davidiella tassiana*, *Exophiala dermatitidis,* and *Erythrobasidium hasegawianum* compared to controls, but found no significant differences in the most prevalent C*andida* species, including *C. albicans* (Ling et al., 2020). In both the MCI and AD cohorts, no significant change in fungal alpha or beta diversity was seen compared to controls (Ling et al., 2020; Nagpal et al., 2020). With no evident overlap between studies of shared taxa with altered relative abundance, it is currently not possible to identify specific fungi (e.g., pathobionts) which may be associated with the development of these neurodegenerative disorders.

A major difficulty in attributing causality in MCI or AD development to an altered microbiome or mycobiome is identifying and measuring confounding factors, in particular the impact of age-associated changes in lifestyle, diet, behaviour, and co-morbidities. For example, many prescribed orally administered drugs including antibiotics, antidepressants and anti-inflammatory compounds, can significantly impact microbiota composition and function (Maier et al., 2018, 2021; Vich Vila et al., 2020), as can behavioural changes and shifts in diet or living conditions (Auchtung et al., 2018; Raimondi et al., 2019). These factors are of relevance to patients with MCI or AD. Such co-variables are minimised in animal models kept under environmentally controlled conditions and maintained on defined diets. However, when using transgenic mouse models of AD for example, it is often unclear what effects the genetic modifications may have on host immune, neural, or other responses that create an altered intestinal environment which is permissive for particular microbes and pathobionts. Whilst these considerations may help explain conflicting results between human studies, and when comparing results of animal and patient studies, it remains to be determined whether altered microbiota and mycobiota composition is a contributing factor in the development of dementias, or is merely a symptomatic or correlative phenomenon.

CONCLUSION

Here we show that in the absence of other enteric microbes, orally delivered *C. albicans* can translocate from the gut to the brain and induce cerebral inflammation. Furthermore, we also show that ageing alone did not alter the overall composition of the gut mycobiota in specific pathogen-free mice. This indicates that ageing alone is not sufficient to induce mycobiome dysbiosis and cerebral fungal infection, and that other disruptions to the gut microbiota and/or the intestinal barrier may be needed to permit gut fungal pathobiont escape and infection of the brain.

DATA AVAILABILITY STATEMENT

The datasets presented in this study can be found in online repositories. The names of the repository/repositories and accession number(s) can be found below: https://www.ncbi.nlm.nih.gov/, PRJEB49148.

ETHICS STATEMENT

The animal study was reviewed and approved by local (University of East Anglia) Animal Welfare and Ethical Review Body approval. All experiments involving animals were performed in accordance with EU and United Kingdom Home Office Legislation, revised Animals (Scientific Procedures) Act 1986 United Kingdom.

AUTHOR CONTRIBUTIONS

AP and SJ: conceptualization, methodology, investigation, formal analysis, data visualization, manuscript original draft, and review and editing. CP: investigation, formal analysis, data visualization, and manuscript content and review. AB, AG, and DB: methodology and investigation. AT: methodology, investigation, and formal analysis. SC: supervision, resources, funding, project administration, and manuscript review and editing. All authors contributed to the article and approved the submitted version.

FUNDING

The authors gratefully acknowledge the support of the Biotechnology and Biological Sciences Research Council (BBSRC), this research was funded by BBSRC Core Capability (Grant: BB/CCG1860/1 and Project Grant: BB/N000250/1), BBSRC Institute Strategic Programme Grant Gut Microbes and Health (BB/R012490/1), and its constituent projects (BBS/E/F/000PR10353 and BBS/E/F/000PR10355).

ACKNOWLEDGMENTS

We thank the staff of the Disease Modelling Unit at the University of East Anglia for animal husbandry and ensuring animal welfare.

SUPPLEMENTARY MATERIAL

The Supplementary Material for this article can be found online at: https://www.frontiersin.org/articles/10.3389/fnagi.2022.828429/full#supplementary-material

REFERENCES

Ahmad, H. F., Mejia, J. L. C., Krych, L., Khakimov, B., Kot, W., Bechshøft, Rasmus L., et al. (2020). Gut Mycobiome Dysbiosis Is Linked to Hypertriglyceridemia among Home Dwelling Elderly Danes. *BioRxiv* . [Epub ahead of print]. doi: 10.1101/2020.04.16.044693

Allert, S., Förster, T. M., Svensson, C. M., Richardson, J. P., Pawlik, T., Hebecker, B., et al. (2018). Candida Albicans-Induced Epithelial Damage Mediates Translocation through Intestinal Barriers. *MBio* 9:e915–e918. doi: 10.1128/MBIO.00915-18/SUPPL_FILE/MBO003183909SF5.TIF

Alonso, R., Pisa, D., Fernández-Fernández, A. M., and Carrasco, L. (2018). Infection of Fungi and Bacteria in Brain Tissue From Elderly Persons and Patients With Alzheimer's Disease. *Front. Aging Neurosci.* 10:159. doi: 10.3389/fnagi.2018.00159

Alonso, R., Pisa, D., Marina, A. I., Morato, E., Rábano, A., and Carrasco, L. (2014). Fungal Infection in Patients with Alzheimer's Disease. *J. Alzheimer's Dis.* 41, 301–311. doi: 10.3233/JAD-132681

Ansorge, R., Birolo, G., James, S. A., and Telatin, A. (2021). Dadaist2: A Toolkit to Automate and Simplify Statistical Analysis and Plotting of Metabarcoding Experiments. *Int. J. Mol. Sci.* 22:5309. doi: 10.3390/IJMS22105309

Asadzadeh, M., Ahmad, S., Al-Sweih, N., and Khan, Z. (2018). Rapid and Accurate Identification of Candida Albicans and Candida Dubliniensis by Real-Time PCR and Melting Curve Analysis. *Med. Princ. Pract.* 27, 543–548. doi: 10.1159/000493426

Auchtung, T. A., Fofanova, T. Y., Stewart, C. J., Nash, A. K., Wong, M. C., Gesell, J. R., et al. (2018). Investigating Colonization of the Healthy Adult Gastrointestinal Tract by Fungi. *MSphere* 3:e92–e18. doi: 10.1128/mSphere.00092-18

Bendová, B., Piálek, J., Ďureje, Ľ, Schmiedová, L., Čížková, D., Martin, J. F., et al. (2020). How Being Synanthropic Affects the Gut Bacteriome and Mycobiome: Comparison of Two Mouse Species with Contrasting Ecologies. *BMC Microbiol.* 20:194. doi: 10.1186/s12866-020-01859-8

Boehme, M., Guzzetta, K. E., Bastiaanssen, T. F. S., Bastiaanssen Gerard, M. M., Andreu Gual-Grau, S. S., et al. (2021). Microbiota from Young Mice Counteracts Selective Age-Associated Behavioral Deficits. *Nat. Aging* 1, 666–676. doi: 10.1038/s43587-021-00093-9

Boehme, M., van de Wouw, M., Bastiaanssen, T. F. S., Olavarría-Ramírez, L., Lyons, K., Fouhy, F., et al. (2019). Mid-Life Microbiota Crises: Middle Age Is Associated with Pervasive Neuroimmune Alterations That Are Reversed by Targeting the Gut Microbiome. *Mol. Psychiatry* 25, 2567–2583. doi: 10.1038/s41380-019-0425-1

Bougnoux, M. E., Diogo, D., François, N., Sendid, B., Veirmeire, S., Colombel, J. F., et al. (2006). Multilocus Sequence Typing Reveals Intrafamilial Transmission and Microevolutions of Candida Albicans Isolates from the Human Digestive Tract. *J. Clin. Microbiol.* 44, 1810–1820. doi: 10.1128/JCM.44.5.1810-1820.2006

Boulangé, C. L., Neves, A. L., Chilloux, J., Nicholson, J. K., and Dumas, M. E. (2016). Impact of the Gut Microbiota on Inflammation, Obesity, and Metabolic Disease. *Genome Med.* 8:42. doi: 10.1186/s13073-016-0303-2

Brown, G. D., Denning, D. W., Gow, N. A., Levitz, S. M., Netea, M. G., and White, T. C. (2012). Hidden Killers: Human Fungal Infections. *Sci. Transl. Med.* 4:165rv13. doi: 10.1126/SCITRANSLMED.3004404

Callahan, B. J., McMurdie, P. J., Rosen, M. J., Han, A. W., Johnson, A. J., and Holmes, S. P. (2016). DADA2: High-Resolution Sample Inference from Illumina Amplicon Data. *Nat. Methods* 13, 581–583. doi: 10.1038/NMETH.3869

Chen, S., Zhou, Y., Chen, Y., and Gu, J. (2018). Fastp: An Ultra-Fast All-in-One FASTQ Preprocessor. *Bioinformatics* 34:i884–i890. doi: 10.1093/BIOINFORMATICS/BTY560

Claesson, M. J., Cusack, S., O'Sullivan, O., Greene-Diniz, R., de Weerd, H., Flannery, E., et al. (2011). Composition, Variability, and Temporal Stability of the Intestinal Microbiota of the Elderly. *Proc.Nat. Acad. Sci. U.S.A.* 108, 4586–4591. doi: 10.1073/pnas.1000097107

Clark, R. I., Salazar, A., Yamada, R., Fitz-Gibbon, S., Morselli, M., Alcaraz, J., et al. (2015). Distinct Shifts in Microbiota Composition during Drosophila Aging Impair Intestinal Function and Drive Mortality. *Cell Rep.* 12, 1656–1667. doi: 10.1016/j.celrep.2015.08.004

Conti, H. R., Huppler, A. R., Whibley, N., and Gaffen, S. L. (2014). Animal Models for Candidiasis. *Curr. Protoco. Immunol.* 105, 19.6.1-19.6.17. doi: 10.1002/0471142735.IM1906S105

Dalle, F., Wächtler, B., L'Ollivier, C., Holland, G., Bannert, N., Wilson, D., et al. (2010). Cellular Interactions of Candida Albicans with Human Oral Epithelial Cells and Enterocytes. *Cell. Microbiol* 12, 248–271. doi: 10.1111/J.1462-5822.2009.01394.X

Dhariwal, A., Chong, J., Habib, S., King, I. L., Agellon, L. B., and Xia, J. (2017). MicrobiomeAnalyst: A Web-Based Tool for Comprehensive Statistical, Visual and Meta-Analysis of Microbiome Data. *Nucleic Acids Res.* 45:W180–W188. doi: 10.1093/NAR/GKX295

Dominy, S. S., Lynch, C., Ermini, F., Benedyk, M., Marczyk, A., Konradi, A., et al. (2019). *Porphyromonas gingivalis* in Alzheimer's disease brains: evidence for disease causation and treatment with small-molecule inhibitors. *Sci. Adv.* 5:eaau3333. doi: 10.1126/sciadv.aau3333

Doron, I., Leonardi, I., and Iliev, I. D. (2019). Profound Mycobiome Differences between Segregated Mouse Colonies Do Not Influence Th17 Responses to a Newly Introduced Gut Fungal Commensal. *Fungal Genet. Biol.?* 127:45. doi: 10.1016/J.FGB.2019.03.001

Drummond, R. A., Desai, J. V., Ricotta, E. E., Swamydas, M., Deming, C., Conlan, S., et al. (2022). Long-Term Antibiotic Exposure Promotes Mortality after Systemic Fungal Infection by Driving Lymphocyte Dysfunction and Systemic Escape of Commensal Bacteria. *Cell Host Microbe*. [Epub ahead of print]. doi: 10.1016/J.CHOM.2022.04.013

Erwig, L. P., and Gow, N. A. (2016). Interactions of Fungal Pathogens with Phagocytes. *Nat. Rev. Microbiol.* 14, 163–176. doi: 10.1038/NRMICRO.2015.21

Field, L. H., Pope, L. M., Cole, G. T., Guentzel, M. N., and Berry, L. J. (1981). Persistence and Spread of Candida Albicans after Intragastric Inoculation of Infant Mice. *Infect. Immun.* 31, 783–791. doi: 10.1128/IAI.31.2.783-791.1981

Forbes, J. D., Bernstein, C. N., Tremlett, H., Van Domselaar, G., and Knox, N. C. (2018). A Fungal World: Could the Gut Mycobiome Be Involved in Neurological Disease? *Front. Microbiol.* 9:3249. doi: 10.3389/FMICB.2018.03249

Fransen, F., van Beek, A. A., Borghuis, T., Aidy, S. E., Hugenholtz, F., van der Gaast-de Jongh, C., et al. (2017). Aged Gut Microbiota Contributes to Systemical Inflammaging after Transfer to Germ-Free Mice. *Front. Immunol.* 8:1385. doi: 10.3389/fimmu.2017.01385

Fung, T. C., Olson, C. A., and Hsiao, E. Y. (2017). Interactions between the Microbiota, Immune and Nervous Systems in Health and Disease. *Nat. Neurosci.* 20, 145–155. doi: 10.1038/nn.4476

Gardes, M., and Bruns, T. D. (1993). ITS Primers with Enhanced Specificity for Basidiomycetes–Application to the Identification of Mycorrhizae and Rusts. *Mol. Ecol.* 2, 113–118. doi: 10.1111/J.1365-294X.1993.TB00005.X

Gottfredsson, M., and Perfect, J. R. (2000). Fungal Meningitis. *Semin. Neurol.* 20, 307–322. doi: 10.1055/S-2000-9394/ID/40

Gouba, N., and Drancourt, M. (2015). Digestive Tract Mycobiota: A Source of Infection. *Med. Mal. Infect.* 45, 9–16. doi: 10.1016/J.MEDMAL.2015.01.007

Gow, N. A., van de Veerdonk, F. L., Brown, A. J., and Netea, M. G. (2011). Candida Albicans Morphogenesis and Host Defence: Discriminating Invasion from Colonization. *Nat. Rev. Microbiol.* 10, 112–122. doi: 10.1038/nrmicro2711

Hallen-Adams, H. E., Kachman, S. D., Kim, J., Legge, R. M., and Martínez, I. (2015). Fungi Inhabiting the Healthy Human Gastrointestinal Tract: A Diverse and Dynamic Community. *Fungal Ecol.* 15, 9–17. doi: 10.1016/J.FUNECO.2015.01.006

Hammond, C. J., Hallock, L. R., Howanski, R. J., Appelt, D. M., Little, C. S., and Balin, B. J. (2010). Immunohistological Detection of Chlamydia Pneumoniae in the Alzheimer's Disease Brain. *BMC Neurosci.* 11:121. doi: 10.1186/1471-2202-11-121

Huang, W. S., Yang, T. Y., Shen, W. C., Lin, C. L., Lin, M. C., and Kao, C. H. (2014). Association between *Helicobacter Pylori* Infection and Dementia. *J. Clin. Neurosci.* 21, 1355–1358. doi: 10.1016/J.JOCN.2013.11.018

Huseyin, C. E., Rubio, R. C., O'Sullivan, O., Cotter, P. D., and Scanlan, P. D. (2017). The Fungal Frontier: A Comparative Analysis of Methods Used in the Study of the Human Gut Mycobiome. *Front. Microbiol.* 8:1432. doi: 10.3389/fmicb.2017.01432

Jakobsson, H. E., Rodríguez-Piñeiro, A. M., Schütte, A., Ermund, A., Boysen, P., Bemark, M., et al. (2015). The Composition of the Gut Microbiota Shapes the Colon Mucus Barrier. *EMBO Rep.* 16, 164–177. doi: 10.15252/EMBR.201439263

James, S. A., Phillips, S., Telatin, A., Baker, D., Ansorge, R., Clarke, P., et al. (2020). Preterm Infants Harbour a Rapidly Changing Mycobiota That Includes Candida Pathobionts. *J. Fungi* 6:273. doi: 10.3390/JOF6040273

Jayasudha, R., Das, T., Kalyana Chakravarthy, S., Sai Prashanthi, G., Bhargava, A., Tyagi, M., et al. (2020). Gut Mycobiomes Are Altered in People with Type 2 Diabetes Mellitus and Diabetic Retinopathy. *PLoS One* 15:e0243077. doi: 10.1371/JOURNAL.PONE.0243077

Johansson, M. E., Gustafsson, J. K., Holmén-Larsson, J., Jabbar, K. S., Xia, L., Xu, H., et al. (2014). Bacteria Penetrate the Normally Impenetrable Inner Colon Mucus Layer in Both Murine Colitis Models and Patients with Ulcerative Colitis. *Gut* 63, 281–291. doi: 10.1136/GUTJNL-2012-303207/-/DC1

Kavanaugh, N. L., Zhang, A. Q., Nobile, C. J., Johnson, A. D., and Ribbeck, K. (2014). Mucins Suppress Virulence Traits of Candida Albicans. *MBio* 5, 1911–1925. doi: 10.1128/MBIO.01911-14/SUPPL_FILE/MBO005142043S1.DOCX

Kinneberg, K. M., Bendel, C. M., Jechorek, R. P., Cebelinski, E. A., Gale, C. A., Berman, J. G., et al. (1999). Effect of INT1 Gene on Candida Albicans Murine Intestinal Colonization. *J. Surgical Res.* 87, 245–251. doi: 10.1006/JSRE.1999.5755

Koh, A. Y. (2013). Murine Models of Candida Gastrointestinal Colonization and Dissemination. *Eukaryot. Cell* 12, 1416–1422. doi: 10.1128/EC.00196-13

Koh, A. Y., Köhler, J. R., Coggshall, K. T., Van Rooijen, N., and Pier, G. B. (2008). Mucosal Damage and Neutropenia Are Required for Candida Albicans Dissemination. *PLoS Pathogens* 4:e35. doi: 10.1371/journal.ppat.0040035

Kurtzman, C. P., Robnett, C. J., Ward, J. M., Brayton, C., Gorelick, P., and Walsh, T. J. (2005). Multigene Phylogenetic Analysis of Pathogenic Candida Species in the Kazachstania (Arxiozyma) Telluris Complex and Description of Their Ascosporic States as Kazachstania Bovina Sp. Nov., K. Heterogenica Sp. Nov., K. Pintolopesii Sp. Nov., and K. Slooffiae Sp. Nov. *J. Clin. Microbiol.* 43, 101–111. doi: 10.1128/JCM.43.1.101-111.2005

Lagkouvardos, I., Fischer, S., Kumar, N., and Clavel, T. (2017). Rhea: A Transparent and Modular R Pipeline for Microbial Profiling Based on 16S RRNA Gene Amplicons. *PeerJ* 5:e2836. doi: 10.7717/PEERJ.2836

Langille, M. G., Meehan, C. J., Koenig, J. E., Dhanani, A. S., Rose, R. A., Howlett, S. E., et al. (2014). Microbial Shifts in the Aging Mouse Gut. *Microbiome* 2:50. doi: 10.1186/s40168-014-0050-9

Li, J., Jia, H., Cai, X., Zhong, H., Feng, Q., Sunagawa, S., et al. (2014). An Integrated Catalog of Reference Genes in the Human Gut Microbiome. *Nat. Biotechnol.* 32, 834–841. doi: 10.1038/NBT.2942

Ling, Z., Zhu, M., Liu, X., Shao, L., Cheng, Y., Yan, X., et al. (2020). Fecal Fungal Dysbiosis in Chinese Patients With Alzheimer's Disease. *Front. Cell Dev. Biol.* 8:631460. doi: 10.3389/FCELL.2020.631460

Lionakis, M. S., Lim, J. K., Lee, C. C., and Murphy, P. M. (2011). Organ-Specific Innate Immune Responses in a Mouse Model of Invasive Candidiasis. *J. Innate Immunity* 3:180. doi: 10.1159/000321157

Maier, L., Goemans, C. V., Wirbel, J., Kuhn, M., Eberl, C., Pruteanu, M., et al. (2021). Unravelling the collateral damage of antibiotics on gut bacteria. *Nature* 599, 120–124. doi: 10.1038/s41586-021-03986-2

Maier, L., Pruteanu, M., Kuhn, M., Zeller, G., Telzerow, A., Anderson, E. E., et al. (2018). Extensive Impact of Non-Antibiotic Drugs on Human Gut Bacteria. *Nature* 555, 623–628. doi: 10.1038/nature25979

Mawanda, F., and Wallace, R. (2013). Can infections cause Alzheimer's disease? *Epidemiol Rev.* 35, 161–180. doi: 10.1093/epirev/mxs007

Mellado, E., Cuenca-Estrella, M., Regadera, J., González, M., Díaz-Guerra, T. M., and Rodríguez-Tudela, J. L. (2000). Sustained Gastrointestinal Colonization and Systemic Dissemination by Candida Albicans, Candida Tropicalis and Candida Parapsilosis in Adult Mice. *Diagn. Microbiol. Infect. Dis.* 38, 21–28. doi: 10.1016/S0732-8893(00)00165-6

Mims, T. S., Abdallah, Q. A., Stewart, J. D., Watts, S. P., White, C. T., Rousselle, T. V., et al. (2021). The Gut Mycobiome of Healthy Mice Is Shaped by the Environment and Correlates with Metabolic Outcomes in Response to Diet. *Commun. Biol.* 4:281. doi: 10.1038/s42003-021-01820-z

Nagpal, R., Neth, B. J., Wang, S., Mishra, S. P., Craft, S., and Yadav, H. (2020). Gut Mycobiome and Its Interaction with Diet, Gut Bacteria and Alzheimer's Disease Markers in Subjects with Mild Cognitive Impairment: A Pilot Study. *EBioMedicine* 59:102950. doi: 10.1016/j.ebiom.2020.102950

Nash, A. K., Stewart, C. J., Smith, D. P., Muzny, D. M., Metcalf, G. A., Gesell, J. R., et al. (2017). The Gut Mycobiome of the Human Microbiome Project Healthy Cohort. *Microbiome* 5:53. doi: 10.1186/s40168-017-0373-4

Nilsson, R. H., Larsson, K. H., Taylor, A. F. S., Bengtsson-Palme, J., Jeppesen, T. S., Schigel, D., et al. (2019). The UNITE Database for Molecular Identification of Fungi: Handling Dark Taxa and Parallel Taxonomic Classifications. *Nucleic Acids Res.* 47:D259–D264. doi: 10.1093/NAR/GKY1022

Noble, S. M., Gianetti, B. A., and Witchley, J. N. (2016). Candida Albicans Cell-Type Switching and Functional Plasticity in the Mammalian Host. *Nat. Rev. Microbiol.* 15, 96–108. doi: 10.1038/NRMICRO.2016.157

O'Toole, P. W., and Jeffery, I. B. (2015). Gut Microbiota and Aging. *Science* 350, 1214–1215. doi: 10.1126/science.aac8469

Pande, K., Chen, C., and Noble, S. M. (2013). Passage through the Mammalian Gut Triggers a Phenotypic Switch That Promotes Candida Albicans Commensalism. *Nat. Genet.* 45:1088. doi: 10.1038/NG.2710

Parker, A., Boloko, L., Moolla, M. S., Ebrahim, N., Ayele, B. T., Broadhurst, A. G. B., et al. (2021). Heterochronic fecal microbiota transfer reverses hallmarks of the aging murine gut, eye and brain. *SSRN Electron. J.* doi: 10.2139/SSRN.3811833

Parker, A., Boloko, L., Moolla, M. S., Ebrahim, N., Ayele, B. T., Broadhurst, A. G. B., et al. (2022). Fecal Microbiota Transfer between Young and Aged Mice Reverses Hallmarks of the Aging Gut, Eye, and Brain. *Microbiome* 10:68 . doi: 10.1186/S40168-022-01243-W

Pfaller, M. A., and Diekema, D. J. (2007). Epidemiology of Invasive Candidiasis: A Persistent Public Health Problem. *Clin. Microbiol. Rev.* 20, 133–163. doi: 10.1128/CMR.00029-06

Pisa, D., Alonso, R., Juarranz, A., Rábano, A., and Carrasco, L. (2015a). Direct Visualization of Fungal Infection in Brains from Patients with Alzheimer's Disease. *J. Alzheimer's Dis.* 43, 613–624. doi: 10.3233/JAD-141386

Pisa, D., Alonso, R., Rábano, A., Rodal, I., and Carrasco, L. (2015b). Different Brain Regions Are Infected with Fungi in Alzheimer's Disease. *Sci. Rep.* 5:15015. doi: 10.1038/srep15015

Price, M. N., Dehal, P. S., and Arkin, A. P. (2009). FastTree: Computing Large Minimum Evolution Trees with Profiles Instead of a Distance Matrix. *Mol. Biol. Evol.*26, 1641–1650. doi: 10.1093/MOLBEV/MSP077

Prieto, D., and Pla, J. (2015). Distinct Stages during Colonization of the Mouse Gastrointestinal Tract by Candida Albicans. *Front. Microbiol.* 6:792. doi: 10.3389/FMICB.2015.00792

Qin, J., Li, R., Raes, J., Arumugam, M., Burgdorf, K. S., Manichanh, C., et al. (2010). A Human Gut Microbial Gene Catalogue Established by Metagenomic Sequencing. *Nature* 464, 59–65. doi: 10.1038/NATURE08821

Raimondi, S., Amaretti, A., Gozzoli, C., Simone, M., Righini, L., Candeliere, F., et al. (2019). Longitudinal Survey of Fungi in the Human Gut: ITS Profiling, Phenotyping, and Colonization. *Front. Microbiol.* 10:1575. doi: 10.3389/FMICB.2019.01575/BIBTEX

Richard, M. L., and Sokol, H. (2019). The Gut Mycobiota: Insights into Analysis, Environmental Interactions and Role in Gastrointestinal Diseases. *Nat. Rev. Gastroenterol. Hepatol.* 16, 331–345. doi: 10.1038/s41575-019-0121-2

Saji, N., Murotani, K., Hisada, T., Tsuduki, T., Sugimoto, T., Kimura, A., et al. (2019). The Relationship between the Gut Microbiome and Mild Cognitive Impairment in Patients without Dementia: A Cross-Sectional Study Conducted in Japan. *Sci. Rep.* 9:19227. doi: 10.1038/S41598-019-55851-Y

Schindelin, J., Arganda-Carreras, I., Frise, E., Kaynig, V., Longair, M., Pietzsch, T., et al. (2012). Fiji: An Open-Source Platform for Biological-Image Analysis. *Nat. Methods* 9, 676–682. doi: 10.1038/nmeth.2019

Schofield, D. A., Westwater, C., and Balish, E. (2005). Short Communication Correspondence Divergent Chemokine, Cytokine and â-Defensin Responses to Gastric Candidiasis in Immunocompetent C57BL/6 and BALB/c Mice. *J. Med. Microbiol.* 54, 87–92. doi: 10.1099/jmm.0.45755-0

Scott, K. A., Ida, M., Peterson, V. L., Prenderville, J. A., Moloney, G. M., Izumo, T., et al. (2017). Revisiting Metchnikoff: Age-Related Alterations in Microbiota-Gut-Brain Axis in the Mouse. *Brain Behav. Immunity* 65, 20–32. doi: 10.1016/j.bbi.2017.02.004

Segal, E., and Frenkel, M. (2018). Experimental In Vivo Models of Candidiasis. *J. Fungi* 4:21. doi: 10.3390/JOF4010021

Sender, R., Fuchs, S., and Milo, R. (2016). Revised Estimates for the Number of Human and Bacteria Cells in the Body. *PLoS Biol.* 14:21. doi: 10.1371/JOURNAL.PBIO.1002533

Sievers, F., and Higgins, D. G. (2021). The Clustal Omega Multiple Alignment Package. *Methods Mol. Biol.* 2231, 3–16. doi: 10.1007/978-1-0716-1036-7_1

Snippert, H. J., Schepers, A. G., Delconte, G., Siersema, P. D., and Clevers, H. (2011). Slide Preparation for Single-Cell–Resolution Imaging of Fluorescent Proteins in Their Three-Dimensional near-Native Environment. *Nat. Protoc.* 6, 1221–1228. doi: 10.1038/nprot.2011.365

Strati, F., Di Paola, M., Stefanini, I., Albanese, D., Rizzetto, L., Lionetti, P., et al. (2016). Age and Gender Affect the Composition of Fungal Population of the Human Gastrointestinal Tract. *Front. Microbiol.* 7:1227. doi: 10.3389/FMICB.2016.01227/BIBTEX

Telatin, A., Fariselli, P., and Birolo, G. (2021). SeqFu: A Suite of Utilities for the Robust and Reproducible Manipulation of Sequence Files. *Bioengineering* 8:59. doi: 10.3390/bioengineering8050059

Tetz, G., Pinho, M., Pritzkow, S., Mendez, N., Soto, C., and Tetz, V. (2020). Bacterial DNA promotes tau aggregation. *Sci. Rep.* 10:2369. doi: 10.1038/s41598-020-59364-x

Thevaranjan, N., Puchta, A., Schulz, C., Naidoo, A., Szamosi, J. C., Verschoor, C. P., et al. (2017). Age-Associated Microbial Dysbiosis Promotes Intestinal Permeability, Systemic Inflammation, and Macrophage Dysfunction. *Cell Host Microbe* 21:455–466.e4. doi: 10.1016/j.chom.2017.03.002

Vich Vila, A., Collij, V., Sanna, S., Sinha, T., Imhann, F., Bourgonje, A. R., et al. (2020). . Impact of Commonly Used Drugs on the Composition and Metabolic Function of the Gut Microbiota. *Nat. Commun.* 11:362. doi: 10.1038/s41467-019-14177-z

Vogt, N. M., Kerby, R. L., Dill-McFarland, K. A., Harding, S. J., Merluzzi, A. P., Johnson, S. C., et al. (2017). Gut Microbiome Alterations in Alzheimer's Disease. *Sci. Rep.* 7:13537. doi: 10.1038/S41598-017-13601-Y

Ward, T. L., Dominguez-Bello, M. G., Heisel, T., Al-Ghalith, G., Knights, D., and Gale, C. A. (2018). Development of the Human Mycobiome over the First Month of Life and across Body Sites. *MSystems* 3:e00140-17. doi: 10.1128/MSYSTEMS.00140-17

White, T. J., Bruns, T., Lee, S., and Taylor, J. (1990). "Amplification And Direct Sequencing Of Fungal Ribosomal Rna Genes For Phylogenetics," in *PCR Protocols: a Guide to Methods and Applications*, eds M. A. Innis, D. H. Gelfand, J. J. Sninsky, and T. J. White (New York, N.Y: Academic Press, Inc), 315–322.

Wiesner, S. M., Jechorek, R. P., Garni, R. M., Bendel, C. M., and Wells, C. L. (2001). Gastrointestinal Colonization by Candida Albicans Mutant Strains in Antibiotic-Treated Mice. *Clin. Diagnostic Lab. Immunol.* 8, 192–195. doi: 10.1128/CDLI.8.1.192-195.2001

Wu, Y., Du, S., Johnson, J. L., Tung, H. Y., Landers, C. T., Liu, Y., et al. (2019). Microglia and Amyloid Precursor Protein Coordinate Control of Transient Candida Cerebritis with Memory Deficits. *Nat. Commun.*10:58. doi: 10.1038/s41467-018-07991-4

Yatsunenko, T., Rey, F. E., Manary, M. J., Trehan, I., Dominguez-Bello, M. G., Contreras, M., et al. (2012). Human Gut Microbiome Viewed across Age and Geography. *Nature* 486, 222–227. doi: 10.1038/nature11053

Zhuang, Z. Q., Shen, L. L., Li, W. W., Fu, X., Zeng, F., Gui, L., et al. (2018). Gut Microbiota Is Altered in Patients with Alzheimer's Disease. *J. Alzheimer's Dis.?* 63, 1337–1346. doi: 10.3233/JAD-180176

Conflict of Interest: The authors declare that the research was conducted in the absence of any commercial or financial relationships that could be construed as a potential conflict of interest.

Publisher's Note: All claims expressed in this article are solely those of the authors and do not necessarily represent those of their affiliated organizations, or those of the publisher, the editors and the reviewers. Any product that may be evaluated in this article, or claim that may be made by its manufacturer, is not guaranteed or endorsed by the publisher.

Mycopathologia (2023) 188:821–823
https://doi.org/10.1007/s11046-023-00772-8

Draft Genome Sequence of a Primate Isolate of *Kazachstania pintolopesii*

Received: 23 May 2023 / Accepted: 3 July 2023 / Published online: 17 August 2023

Abstract *Kazachstania pintolopesii* is an opportunistic mammalian pathobiont from the *K. telluris* species complex. No draft genomes of this species are currently available. Here, we report the first draft genome sequence of a primate isolate of *K. pintolopesii* (NCYC 4417).

Keywords *Kazachstania pintolopesii* · Draft genome · Non-human primate · Cynomolgus macaque · Fungal pathobiont · Gut mycobiota

Kazachstania pintolopesii is an ascomycetous yeast and relative of *K. bovina*, *K. heterogenica*, *K. slooffiae* and *K. telluris* [1]. Collectively, these species constitute the *K. telluris* complex, a phylogenetically distinct group of thermotolerant yeasts able to grow at 37 °C and above [1, 2]. They are widely distributed [1], but are found predominantly in the gastrointestinal (GI) tracts and nasal passages of birds and mammals [1–3]. Rodents are the principal hosts for *K. pintolopesii* [1, 2, 4] with a recent study extending its host range to include cynomolgus macaques [5]. These fungi are also considered pathobionts causing infections in rodents, primates, and less frequently in humans [2, 6, 7]. *K. pintolopesii* is in addition to being a gut commensal also associated with fatal infections in laboratory mice [2], and with ankylosing spondylitis in cynomolgus macaques [8]. Draft genomes for three members of the complex have been published [9–11], but despite its potential significance as a pathobiont no *K. pintolopesii* genomes have been published to date.

Here, we have combined short- and long-read sequencing to obtain the genome sequence of *K. pintolopesii* NCYC 4417, a faeces-derived isolate from a captive adult macaque. A faecal homogenate was prepared in sterile phosphate-buffered saline (PBS) and cultured onto Sabouraud dextrose (SD) agar plates containing penicillin (25 U/mL) and streptomycin (25 U/mL) at 37 °C. Species identity, from single colonies, was determined by PCR amplification and Sanger sequencing of the ribosomal DNA internal transcribed spacer 1 (ITS1) region of the ribosomal DNA locus using primers ITS1F [12] and ITS2 [13]. The ITS1 sequence of strain NCYC 4417 (GenBank accession number PRJEB63679) is 99.7% identical to that of the *K. pintolopesii* type strain CBS 2985 (GenBank accession number NR_155233).

For short- and long-read sequencing, total genomic DNA was extracted from a stationary phase SD culture using a MasterPure Yeast DNA Purification Kit (Cambio, Cambridge, UK). Short-read Illumina sequencing was performed using a modified 20-fold dilution of DNA Prep (Flex) reagent and run on a NextSeq 500 sequencer, producing 9,108,736 paired-end 150-bp reads (∼ 186 × coverage). Nanopore sequencing was performed using a MinION sequencer (Oxford Nanopore Technologies, ONT), ligation sequencing kit SQK-LSK109 (ONT) and flow cell FLO-MIN106 R9.4.1 (ONT). This produced a total of 437,446 reads with an average read length of 4,069 bases (∼ 127 × coverage).

Base calling was performed using Guppy v.6.1.2 (basecall_model_version_id = 2021–05-17_dna_r9.4.1_minion_384_d37a2ab9). Raw short- and long-read polishing, including the removal of adapters and low-quality bases, was performed using SeqFu 1.16 [14] and fastp 0.23 [15]. The genome was assembled using Flye 2.9.1 [16] and polished with one round of Pilon 1.24 [17]. The genome assembly comprised of 34 contigs with the largest being 1,738,127 bp in length. The total size of the genome was 13,992,981 bp, the N_{50} value was 947 kb, and the G + C content was 30.63%. In addition, a putative 8-nt telomeric repeat was identified (5'-WGTATGGG-3'), similar in sequence to the canonical eukaryotic telomere motif [18], and present in 50–100 tandem copies at one or both termini of 13 contigs. Augustus v.3.3.3 [19] predicted 4884 protein-coding genes using the *Saccharomyces cerevisiae* (S288C) training data set, and 196 tRNA genes were detected using tRNAscan-SE 2.0 [20]. Genome completeness was estimated as 91.0% using BUSCO v5.4.4 [21]. Dependencies and scripts are available at https://github.com/quadram-institute-bioscience/ont-candida.

Author Contributions All authors contributed to the study conception and design. Material preparation, data collection and analysis were performed by SAJ, AP, CP, AT, DB, RH, SH, SGPF and SRC. The first draft of the manuscript was written by SAJ and SRC, and all authors commented on previous versions of the manuscript. All authors read and approved the final manuscript.

Funding This research was funded in part by a Biotechnology and Biological Sciences Research Council (BBSRC) awarded Core Capability Grant BB/CCG1860/1, project grant BB/N000250/1, and Institute Strategic Programme Grant Gut Microbes and Health (BB/R012490/1) and its constituent projects BBS/E/F/000PR10353, BBS/E/F/000PR10355.

Data availability This whole-genome shotgun project has been deposited at DDJB/ENA/Genbank (Biosample Number SAMEA112953918, BioProject Number PRJEB61520, and Assembly Accession Number GCA_950065675.1). The version described in this paper is version 1. The raw reads were deposited at SRA (Accession Numbers ERR11267923 and ERR11267961).This article was written according to MycopathologiaGENOMES checklist requirements [22].

Declarations

Conflict of interest The authors have no relevant financial or non-financial interests to disclose.

Ethics Approval This article does not include human participants, or any procedures carried out on animals.

Author names and affiliations

[1]Steve A. James
[1]Aimee Parker
[1]Catherine Purse
[1]Andrea Telatin
[1]David Baker
[1]Rhiannon Evans
[2]Sandy Holmes
[1,2]Simon G. P. Funnell
[1,3]Simon R. Carding

[1]Food, Microbiome and Health, Quadram Institute Bioscience, Norwich, UK
e-mail: steve.james@quadram.ac.uk

[2]UK Health Security Agency, Porton Down, Salisbury, UK

[3]Norwich Medical School, University of East Anglia, Norwich, UK

References

1. Vaughan-Martini A, Lachance M-A, Kurtzman CP. Kazachstania Zubkova (1971), p 439–470. *In* Kurtzman CP, Fell JW, Boekhout T (ed), The yeasts: A taxonomic study, 5 ed, vol 2. Elsevier, Amsterdam, 2021.
2. Kurtzman CP, Robnett CJ, Ward JM, Brayton C, Gorelick P, Walsh TJ. Multigene phylogenetic analysis of pathogenic Candida species in the Kazachstania (Arxiozyma) telluris complex and description of their ascosporic states as Kazachstania bovina sp nov., K-heterogenica sp nov., K-pintolopesii sp nov., and K-slooffiae sp nov. J Clin Microbiol. 2005;43:101–11. https://doi.org/10.1128/JCM.43.1.101-111.2005.
3. Arfken AM, Frey JF, Ramsay TG, Summers KL. Yeasts of burden: Exploring the Mycobiome-Bacteriome of the Piglet GI Tract. Front Microbiol. 2019;10:2286. https://doi.org/10.3389/fmicb.2019.02286.

4. Bendova B, Pialek J, Dureje L, Schmiedova L, Cizkova D, Martin JF, Kreisinger J. How being synanthropic affects the gut bacteriome and mycobiome: comparison of two mouse species with contrasting ecologies. BMC Microbiol. 2020;20:194. https://doi.org/10.1186/s12866-020-01859-8.
5. James SA, Parker A, Purse C, Telatin A, Baker D, Holmes S, Durham J, Funnell SGP, Carding SR. The Cynomolgus Macaque intestinal mycobiome is dominated by the Kazachstania Genus and K. pintolopesii species. J Fungi. 2022; 8:1054. https://doi.org/10.3390/jof8101054.
6. Alvarez-Perez S, Mateos A, Dominguez L, Martinez-Nevado E, Rodriguez-Bertos A, Blanco JL, Garcia ME. First isolation of the anamorph of Kazachstania heterogenica from a fatal infection in a primate host. Med Mycol. 2012;50:193–6. https://doi.org/10.3109/13693786.2011.578155.
7. Brunet K, Minoza A, Rammaert B, Portet-Sulla V, Hubert F, Lorenzo JC, Rodier MH, Cateau E. Invasive Candida bovina infection, France. Emerging Infect Dis. 2020;26:626–7. https://doi.org/10.3201/eid2603.191371.
8. Zhang HT, Wei Y, Jia HH, Chen DL, Tang XC, Wang J, Chen ML, Guo YR. Immune activation of characteristic gut mycobiota Kazachstania pintolopesii on IL-23/IL-17R signaling in ankylosing spondylitis. Front Cellular Infection Microbiol. 2022;12:1035366. https://doi.org/10.3389/fcimb.2022.1035366.
9. Morio F, O'Brien CE, Butler G. Draft genome sequence of the yeast Kazachstania telluris CBS 16338 isolated from forest soil in Ireland. Mycopathologia. 2020;185:587–90. https://doi.org/10.1007/s11046-020-00449-6.
10. Davies CP, Arfken AM, Frey JF, Summers KL. Draft genome sequence of Kazachstania slooffiae, isolated from post-weaning piglet feces. Microbiol Resource Announce. 2021;10:e00198-e221. https://doi.org/10.1128/MRA.00198-21.
11. Deroche L, Buyck J, Cateau E, Rammaert B, Marchand S, Brunet K. Draft genome sequence of Kazachstania bovina yeast isolated from human infection. Mycopathologia. 2022;187:413–5. https://doi.org/10.1007/s11046-022-00639-4.
12. Gardes M, Bruns TD. ITS primers with enhanced specificity for basidiomycetes–application to the identification of mycorrhizae and rusts. Mol Ecol. 1993;2:113–8. https://doi.org/10.1111/j.1365-294x.1993.tb00005.x.
13. White TJ, Bruns TD, Lee SL, Taylor JW. Amplification and direct sequencing of fungal ribosomal RNA genes for phylogenetics. In: Innis MA, Gelfand DH, Sninsky JJ, editors. PCR protocols: a guide to methods and applications. San Diego: Academic Press; 1990. p. 315–22.
14. Telatin A, Fariselli P, Birolo G. SeqFu: A Suite of Utilities for the Robust and Reproducible Manipulation of Sequence Files. Bioeng-Basel 2021;8:59. https://doi.org/10.3390/bioengineering8050059.
15. Chen SF, Zhou YQ, Chen YR, Gu J. fastp: an ultra-fast all-in-one FASTQ preprocessor. Bioinformatics. 2018;34:i884–90. https://doi.org/10.1093/bioinformatics/bty560.
16. Kolmogorov M, Yuan J, Lin Y, Pevzner PA. Assembly of long, error-prone reads using repeat graphs. Nat Biotechnol. 2019;37:540–6. https://doi.org/10.1038/s41587-019-0072-8.
17. Walker BJ, Abeel T, Shea T, Priest M, Abouelliel A, Sakthikumar S, Cuomo CA, Zeng QD, Wortman J, Young SK, Earl AM. Pilon: an integrated tool for comprehensive microbial variant detection and genome assembly improvement. Plos One. 2014;9:e112963. https://doi.org/10.1371/journal.pone.0112963.
18. Cervenak F, Sepsiova R, Nosek J, Tomaska L. Step-by-step evolution of telomeres: Lessons from yeasts. Genome Biol Evolut. 2021;13:evaa268. https://doi.org/10.1093/gbe/evaa268.
19. Stanke M, Diekhans M, Baertsch R, Haussler D. Using native and syntenically mapped cDNA alignments to improve de novo gene finding. Bioinformatics. 2008;24:637–44. https://doi.org/10.1093/bioinformatics/btn013.
20. Lowe TM, Eddy SR. tRNAscan-SE: A program for improved detection of transfer RNA genes in genomic sequence. Nucleic Acids Res. 1997;25:955–64. https://doi.org/10.1093/nar/25.5.955.
21. Manni M, Berkeley MR, Seppey M, Simao FA, Zdobnov EM. BUSCO update: Novel and streamlined workflows along with broader and deeper phylogenetic coverage for scoring of eukaryotic, prokaryotic, and viral genomes. Mol Biol Evol. 2021;38:4647–54. https://doi.org/10.1093/molbev/msab199.
22. Mac Aogain M, Chaturvedi V, Chotirmall SH. MycopathologiaGENOMES: The New 'Home' for the publication of fungal genomes. Mycopathologia. 2019;184:551–4. https://doi.org/10.1007/s11046-019-00366-3.